OMICS-BASED ANALYSIS ON THE INTERACTION BETWEEN MICROBE AND AGRICULTURAL ANIMALS

EDITED BY: Wei Zhang, Jing Wang, Chang Guangjun, Xudong Sun, Haidong Yao and Fabiana Quoos Mayer

PUBLISHED IN: Frontiers in Microbiology, Frontiers in Veterinary Science and Frontiers in Genetics

frontiers Research Topics

ISSN 1664-8714
ISBN 978-2-88974-627-9
DOI 10.3389/978-2-88974-627-9

About Frontiers

Frontiers is more than just an open-access publisher of scholarly articles: it is a pioneering approach to the world of academia, radically improving the way scholarly research is managed. The grand vision of Frontiers is a world where all people have an equal opportunity to seek, share and generate knowledge. Frontiers provides immediate and permanent online open access to all its publications, but this alone is not enough to realize our grand goals.

Frontiers Journal Series

The Frontiers Journal Series is a multi-tier and interdisciplinary set of open-access, online journals, promising a paradigm shift from the current review, selection and dissemination processes in academic publishing. All Frontiers journals are driven by researchers for researchers; therefore, they constitute a service to the scholarly community. At the same time, the Frontiers Journal Series operates on a revolutionary invention, the tiered publishing system, initially addressing specific communities of scholars, and gradually climbing up to broader public understanding, thus serving the interests of the lay society, too.

Dedication to Quality

Each Frontiers article is a landmark of the highest quality, thanks to genuinely collaborative interactions between authors and review editors, who include some of the world's best academicians. Research must be certified by peers before entering a stream of knowledge that may eventually reach the public - and shape society; therefore, Frontiers only applies the most rigorous and unbiased reviews.
Frontiers revolutionizes research publishing by freely delivering the most outstanding research, evaluated with no bias from both the academic and social point of view. By applying the most advanced information technologies, Frontiers is catapulting scholarly publishing into a new generation.

What are Frontiers Research Topics?

Frontiers Research Topics are very popular trademarks of the Frontiers Journals Series: they are collections of at least ten articles, all centered on a particular subject. With their unique mix of varied contributions from Original Research to Review Articles, Frontiers Research Topics unify the most influential researchers, the latest key findings and historical advances in a hot research area! Find out more on how to host your own Frontiers Research Topic or contribute to one as an author by contacting the Frontiers Editorial Office: frontiersin.org/about/contact

OMICS-BASED ANALYSIS ON THE INTERACTION BETWEEN MICROBE AND AGRICULTURAL ANIMALS

Topic Editors:
Wei Zhang, Beijing Academy of Agricultural and Forestry Sciences, China
Jing Wang, Beijing Academy of Agricultural and Forestry Sciences, China
Chang Guangjun, Nanjing Agricultural University, China
Xudong Sun, Heilongjiang Bayi Agricultural University, China
Haidong Yao, Karolinska Institutet (KI), Sweden
Fabiana Quoos Mayer, Desidério Finamor Veterinary Research Institute (IPVDF), Brazil

Citation: Zhang, W., Wang, J., Guangjun, C., Sun, X., Yao, H., Mayer, F. Q., eds. (2022). Omics-based Analysis on the Interaction Between Microbe and Agricultural Animals. Lausanne: Frontiers Media SA. doi: 10.3389/978-2-88974-627-9

Table of Contents

frontiers in Microbiology

ORIGINAL RESEARCH
published: 11 January 2021
doi: 10.3389/fmicb.2020.617800

Caeca Microbial Variation in Broiler Chickens as a Result of Dietary Combinations Using Two Cereal Types, Supplementation of Crude Protein and Sodium Butyrate

*Daniel Borda-Molina[1], Gábor Mátis[2], Máté Mackei[2], Zsuzsanna Neogrády[2], Korinna Huber[1], Jana Seifert[1] and Amélia Camarinha-Silva[1]**

[1]*Institute of Animal Science, University of Hohenheim, Stuttgart, Germany,* [2]*Division of Biochemistry, Department of Physiology and Biochemistry, University of Veterinary Medicine, Budapest, Hungary*

OPEN ACCESS

Edited by:
Jing Wang,
Beijing Academy of Agriculture and Forestry Sciences, China

Reviewed by:
Richard Ducatelle,
Ghent University, Belgium
Robert J. Moore,
RMIT University, Australia

***Correspondence:**
Amélia Camarinha-Silva
amelia.silva@uni-hohenheim.de

Specialty section:
This article was submitted to Systems Microbiology, a section of the journal Frontiers in Microbiology

Received: *15 October 2020*
Accepted: *14 December 2020*
Published: *11 January 2021*

Citation:
Borda-Molina D, Mátis G, Mackei M, Neogrády Z, Huber K, Seifert J and Camarinha-Silva A (2021) Caeca Microbial Variation in Broiler Chickens as a Result of Dietary Combinations Using Two Cereal Types, Supplementation of Crude Protein and Sodium Butyrate. Front. Microbiol. 11:617800. doi: 10.3389/fmicb.2020.617800

The intestinal microbiome can influence the efficiency and the health status of its host's digestive system. Indigestible non-starch polysaccharides (NSP) serve as substrates for bacterial fermentation, resulting in short-chain fatty acids like butyrate. In broiler's nutrition, dietary crude protein (CP) and butyrate's presence is of particular interest for its impact on intestinal health and growth performance. In this study, we evaluated the effect on the microbial ecology of the ceca of dietary supplementations, varying the cereal type (maize and wheat), adequate levels of CP and supplementation of sodium butyrate on broiler chickens with 21 days. The overall structure of bacterial communities was statistically affected by cereal type, CP, and sodium butyrate ($p = 0.001$). Wheat in the diet promoted the presence of Lactobacillaceae, Bifidobacteriaceae and *Bacteroides xylanisolvens*, which can degrade complex carbohydrates. Maize positively affected the abundance of *Bacteroides vulgatus*. The addition of CP promoted the family Rikenellaceae, while sodium butyrate as feed supplement was positively related to the family Lachnospiraceae. Functional predictions showed an effect of the cereal type and a statistical significance across all supplementations and their corresponding interactions. The composition of diets affected the overall structure of broilers' intestinal microbiota. The source of NSP as a substrate for bacterial fermentation had a stronger stimulus on bacterial communities than CP content or supplementation of butyrate.

Keywords: broiler chickens, microbiota, non-starch polysaccharides, butyrate, functional prediction

INTRODUCTION

Diet composition has a significant impact on poultry due to its influence on digestibility, gut wall morphology, and microbial structure, which might affect the health status, carcass composition and meat quality (Teirlynck et al., 2009). Maize-based (MB) diets have a higher positive impact on broilers' performance than other cereals, which is attributed to the low presence of non-starch

polysaccharides (NSP). NSPs have adverse effects on nutrient digestion and absorption (Meng et al., 2004; Lentle and Janssen, 2008; Teirlynck et al., 2009). Other cereal-based diets with higher amounts of NSPs, such as wheat, are supplemented with additive enzymes like xylanase and glucanase. This facilitates the degradation of NSPs and the release of carbon sources that promote a favorable bacterial population in the gastrointestinal tract (GIT; Lentle and Janssen, 2008). Fermentation products, like short-chain fatty acids (SCFA), are essential for the host metabolism and have positive effects on gut health.

Growth parameters in broiler chicks are also influenced by the dietary concentration of crude protein (CP), which might affect carcass yield and breast meat yield and causes a decrease in pancreas weight (Alleman et al., 2000; Lentle and Janssen, 2008; Abbasi et al., 2014). Moreover, in the intestines, an adequate protein concentration is required to maintain its viability, mass and amount of energy, where low levels resulted in the reduction of jejunal villus height and crypt depth (Abbasi et al., 2014).

The addition of butyrate in the form of sodium butyrate is seen as an alternative to promote broiler chickens' development. This compound is solid, stable and is associated with the improvement of body weight, feed conversion ratio and the development of gut wall tissues by increasing villus height and crypt depth ratio of duodenum and jejunum (Leeson et al., 2005; Jiang et al., 2015; Ahsan et al., 2016). Furthermore, it modifies immune and inflammatory responses by decreasing the production of pro-inflammatory cytokines and mitigates the increase of corticosterone concentration, which is present during stress conditions (Zhang et al., 2011; Jiang et al., 2015). Regarding gut intestinal microbiota, butyrate is associated with increased beneficial bacterial populations while the colonization of harmful species is reduced (Ahsan et al., 2016).

To analyze the effects of dietary treatments in poultry, one of the most studied sections in the GIT is the ceca, where most fermentation processes occur, leading to the assimilation of complex substrates. This assimilation is facilitated by metabolic activities of the genera *Ruminococcus, Streptococcus, Faecalibacterium, Lactobacillus*, and *Clostridium* cluster IV, XIVa and XIVb (Borda-Molina et al., 2016; Volf et al., 2016), which colonize and maintain fermentation processes, together with the production of SCFA including butyrate.

This study aimed to describe the influence of two types of dietary cereals, two different crude protein contents, and butyrate supplementation on the cecal microbiota and its central metabolic functions in broiler chickens with 21 days.

MATERIALS AND METHODS

Birds and Experimental Procedures

The experiment was conducted in the Research Institute for Animal Breeding, Nutrition and Meat Science at Herceghalom, Hungary. All procedures regarding animal handling and treatments were approved by the Government Office of Pest County, Food Chain Safety, Plant Protection and Soil Conservation Directorate, Budapest, Hungary (permission number: PEI/001/1430-4/2015).

A total of 240 male one-day-old Ross 308 broiler chicks were obtained from a commercial hatchery (Gallus Poultry Farming and Hatching Ltd., Devecser, Hungary) and randomly allocated to eight dietary groups (n = 30 per group). Specific details for experimental design have been previously published (Petrilla et al., 2018). Four of the diets consisted of maize (MB) as the cereal type and the other four were assigned to wheat [wheat-based diet (WB)] as the cereal type, supplemented with xylanase-glucanase enzyme mixture. Crude protein content was set to an appropriate dietary phase [normal protein (NP)] or reduced by 15% [low protein (LP)], the latter supplemented with essential amino acids. The feed was formulated considering the presence of sodium butyrate (But) or its absence (Ctr; **Supplementary Tables 1A,B**). At 21 days, 10 chickens per group were randomly selected and slaughtered by decapitation after carbon dioxide anesthesia without any starving period before sampling. Samples from cecal digesta were immediately collected and shock-frozen in liquid nitrogen and stored at −80°C until analysis.

DNA Extraction, Illumina Amplicon Sequencing and Bioinformatic Analysis

DNA was extracted from approximately 250 mg of each digesta sample using FastDNA™ SPIN Kit for the soil from MP Biomedicals (Solon, OH, United States) following the manufacturer's instructions. The quality and concentration of DNA were assessed through NanoDrop 2000 Spectrophotometer (Thermo Scientific, Waltham, MA, United States), and DNA was stored until use at −20°C. The V1-2 region of the 16S rRNA gene was amplified to produce Illumina sequencing library. The protocol followed the same methodology as Kaewtapee et al. (Kaewtapee et al., 2017). Briefly, 1 µl of DNA was used in a 20 µl reaction containing PrimeSTAR Hot Start DNA polymerase (2.5 U, Clontech Laboratories, Mountain View, CA, United States), 2.5 mM dNTP mixture, and 0.2 µM primers; an initial denaturation at 95°C for 3 min was followed by 20 cycles of denaturation at 98°C for 10 s, subsequent annealing at 59°C for 10 s, extension step at 72°C for 45 s and a final extension for 2 min at 72°C; 1 µl from the resultant product was taken to perform the second PCR with the aforementioned conditions in a 50 µl reaction for 15 cycles. Amplicons were verified by agarose gel electrophoresis, purified and normalized using SequalPrep Normalization Kit (Invitrogen Inc., Carlsbad, CA, United States). Samples were pooled and sequenced using 250 bp paired-end sequencing chemistry on an Illumina MiSeq platform.

Raw reads were quality filtered, assembled, and aligned using Mothur pipeline (Kozich et al., 2013). Sequences were excluded if they had any primer or barcode mismatch and an N character. A total of 5.314.942 reads were obtained, checked for chimeras using UCHIME, and clustered at 97% identity into 1,284 operative taxonomic units (OTU). Only OTUs presenting on average, an abundance higher than 0.0001% and with a sequence length > 250 bp were considered for further analysis. The closest representative was manually identified with RDP's

seqmatch function (Wang et al., 2007) and a species name was given if >97% similarity was observed with the closest representative sequence. Sequences were submitted to European Nucleotide Archive under the accession number PRJEB40780. Functional predictions were obtained with the R package Tax4Fun, which relies on the SILVA database (Quast et al., 2013). The biom table to assign this functionality was obtained from the mothur pipeline.

Correlation network analysis was done based on the SparCC algorithm (Friedman and Alm, 2012; Chong et al., 2020), making log ratio transformations and including multiple iterations to exclude taxa pairs outliers. The algorithm determines the co-abundance and co-exclusion of bacteria present in the absolute abundance (Zhang et al., 2018). The permutation was settled at 100 with a threshold value of p as 0.05 and a correlation threshold as 0.3 at the genus taxonomical level. Nodes indicated the genus and were colored based on their abundance for each treatment, while edges represented the correlations' strength.

Statistical Analysis

Datasets were analyzed with the multivariate software PRIMER (version 7.0.9, PRIMER-E, Plymouth Marine Laboratory, Plymouth, United Kingdom; Clarke and Warwick, 1994). Data were standardized by total, and similarity matrixes were created using the Bray-Curtis coefficient (Bray and Curtis, 1957). PERMANOVA analysis, using a permutation method under a reduced model, was used to study the significant differences between the dietary treatments and was considered significantly different if $p \leq 0.05$. The community similarity structure was depicted through Principal Coordinates Analysis (PCoA). Similarity percentage (SIMPER) analysis was used to identify the OTUs responsible for the differences between the groups (Clarke and Warwick, 1994). Correlations were estimated with the Spearman coefficient using PRISM 6 (GraphPad Software, CA) and were considered significantly different if $p < 0.05$. Diversity indices (Shannon diversity and Pielou's evenness) were calculated based on abundance data with PRIMER software.

An univariate approach within the program JMP (JMP® Pro 15.0.0, Cary, NC, United States) was used to test for individual effects on each output (OTU assignation, family assignation, or predicted function at the third KEGG level). Calculations were based on ANOVA and multiple comparisons based on the least-squares mean estimates and followed the model:

$$\begin{aligned} y_{ijkl} = \mu + cereal\ type_i + crude\ protein_j + \\ sodium\ butyrate_k + \left(cereal\ type_i \times crude\ protein_j\right) + \\ \left(cereal\ type_i \times sodium\ butyrate_k\right) + \\ \left(crude\ protein_j \times cereal\ type_k\right) + \\ \left(cereal\ type_i \times crude\ protein_j \times sodium\ butyrate_k\right) + \\ block_l + e_{ijkl} \end{aligned}$$

RESULTS

Notwithstanding that the present trial was not designed to study the animals' growth performance, it should be addressed that the growth of the broilers matched the standards of the Ross 308 breed. Body weight and average daily body weight gain data are presented in [**Supplementary Table 2**; according to (Petrilla et al., 2018)]. The applied dietary strategies can effectively contribute to better growth performance and carcass characteristics of broilers. The body weight of the chickens increased significantly with the low protein diet with essential amino acid supplementation during the entire trial (**Supplementary Table 2**).

Taxonomical Distribution Based on Dietary Supplementations

A significant interaction between the type of cereal, the normal or decreased content of crude protein, and the presence or absence of sodium butyrate (CeXCPxSo) was found in the caecal microbial communities (p = 0.001; **Supplementary Table 3**). Furthermore, pairwise comparisons showed that the microbial communities differed from each other in all diets ($p \leq 0.05$; **Supplementary Table 3**). The sample average similarity ranged between 59% (NP MB Ctr) and 43% (LP WB But). A clustering of the caecal microbiota samples based on maize or wheat was observed sharing 54% similarity. (**Figure 1** and **Supplementary Figures 1, 2A**). Even if significant differences were confirmed for the CP and sodium butyrate supplementation (**Supplementary Table 3**), there was no apparent clustering based on those criteria (**Supplementary Figures 2B,C**). Shannon diversity index did not show significant statistical differences between the different diets, which confirms the abundance of species as the driving factor for the variations (**Supplementary Figure 3**).

The most predominant phylum in all treatments was Firmicutes accounting for 57–71% of the total community and higher abundances were detected in diets with LP content (**Supplementary Figure 4**). Bacteroidetes was the second most abundant phylum (21–32%) with lower relative abundances in the WB diets than the maize and diets with LP contents. On the third position, Proteobacteria were 5 to 10% abundant, showing higher fractions with normal CP levels. Actinobacteria was promoted when WB diet was fed, with abundances ranging from 2 to 4% compared to 0.2–0.4% in maize-based diets. Furthermore, diets NP WB But and LP WB But, with butyrate supplementation, had more OTUs affiliated to the phylum Actinobacteria (**Supplementary Figure 4**).

The abundance of Bifidobacteriaceae and Lactobacillaceae increased for the WB diets (**Supplementary Figure 5A**). Rikenellaceae was more abundant in diets with a normal level of CP content, whereas Ruminococcaceae was promoted in the diet with low CP content (**Supplementary Figure 5A** and **Supplementary Table 4**). Additionally, sodium butyrate supplementation increased the presence of Lachnospiraceae (**Supplementary Table 4**). The abundance of Bacteroidaceae was affected by the interaction of CP content and sodium butyrate. This family was detected in higher abundance in the diet with normal CP and without sodium butyrate supplementation (**Supplementary Table 4**).

Thirty-two OTUs were the most important contributors to the differences observed across all diets. OTU1, closely

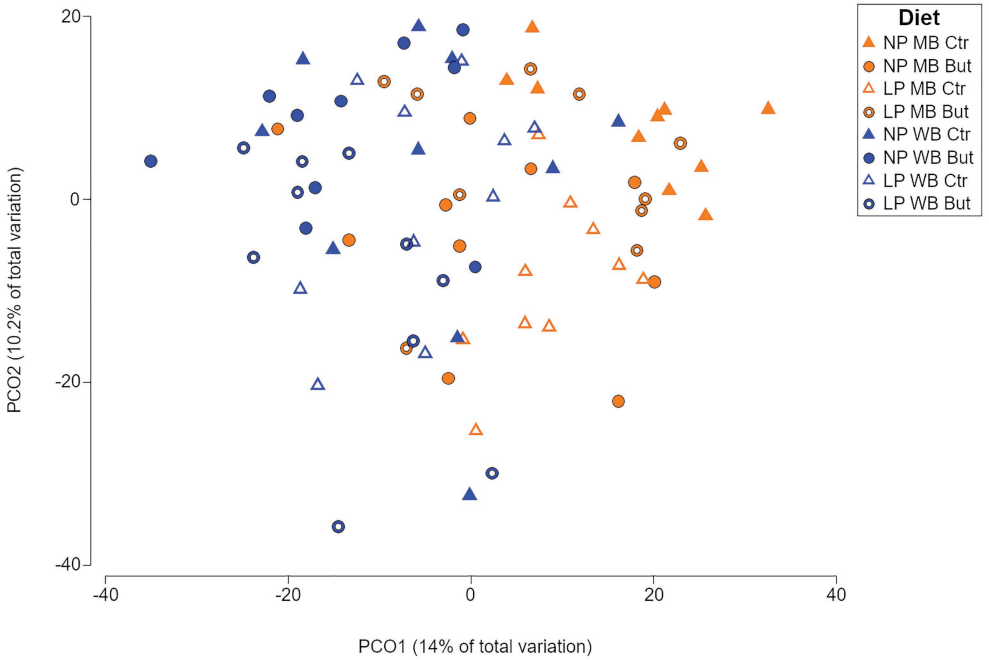

FIGURE 1 | Principal coordinate analysis showing the microbial community distribution of the eight dietary treatments. NP, normal protein diet; LP, low protein diet; MB, maize based diet, WB, wheat based diet; But, sodium butyrate; Ctr, no sodium butyrate.

related to *Bacteroides vulgatus*, was detected in higher abundance in MB NP Ctr (23%), and in lower abundance in LP WB But (8%; **Figure 2**). It was significantly affected by all three factors and promoted by maize as the cereal type ($p < 0.0001$), and no sodium butyrate supplementation ($p = 0.0008$; **Supplementary Table 5**). OTU1 showed negative interactions with several other OTUs (**Supplementary Table 6**). *Bacteroides xylanisolvens* (OTU 3) was more abundant in case of diets LP WB But and LP MB Ctr (11 and 10%, respectively), whereas it was found with 4% abundance in diets NP MB Ctr, NP WB But, and LP WB Ctr (**Figure 2**). OTU3 was affected by the interaction of the three factors ($p = 0.0008$): maize as cereal type, low CP, and no sodium butyrate supplementation (**Supplementary Table 5**). OTU8 assigned to an uncultured *Ruminococcus* registered the highest abundance in LP MB Ctr (10%; **Figure 2**) with a tendency to be promoted by the wheat as the cereal type ($p = 0.07$) and positive correlations to other OTUs (**Supplementary Table 6**).

The genus *Lactobacillus*, represented by OTU2 – *Lactobacillus crispatus* and OTU11 – *Lactobacillus vaginalis*, showed a positive correlation with body weight (**Figure 3**). OTU2 was more abundant in WB diets such as in NP WB But (14%), while an average abundance of 6% was registered for MB diets (**Figure 2**). It is influenced by the interaction of crude protein level and sodium butyrate ($p = 0.03$), and a tendency was detected for the cereal type and CP ($p = 0.07$; **Supplementary Table 5**). OTU2 showed positive interactions with other OTUs assigned to *Lactobacillus* (**Supplementary Table 6**). OTU4, assigned to *Lactobacillus salivarius*, was registered in higher abundance NP MB Ctr (on average 7%) while it was detected in lower abundance in NP WB Ctr (in av. 3%). OTU4 was affected by the interaction of the three supplementations ($p = 0.011$). *L. vaginalis* (OTU11) was more abundant when wheat was used as a cereal with highest abundance in diet LP WB But (4%). This result was supported by the significant effect found with the cereal type ($p = 0.048$; **Supplementary Table 5**).

Streptococcus alactolyticus (OTU36) was 2% abundant in the LP MB Ctr diet, while the other registered percentages were lower than one. The interaction of cereal type and CP content was significant ($p = 0.02$) for this OTU. In diets with maize and wheat supplementation and normal CP (NP MB Ctr and NP WB Ctr), an uncultured *Parasutterella* (OTU6) was found in higher abundance (4%) when compared to other diets. This OTU was significantly affected by crude protein ($p = 0.003$) and sodium butyrate supplementation ($p = 0.007$; **Supplementary Table 5**). The cereal type had a significant effect on *Bifidobacterium pseudolongum* (OTU22; $p = 0.0002$; **Supplementary Table 5**) with registered abundances lower than 1% in maize cereal diets, while 1.9% (NP WB Ctr), 3.6% (NP WB But), 1.4% (LP WB Ctr), and 3.5% (LP WB But) were detected in WB diets.

The connectivity level was further inspected by a network analysis based on the differences observed between maize and wheat. The approach was followed by estimating correlation values, restricting the components to the genus level, and decreasing compositional effects. A higher quantity of significant edges was observed with wheat as a cereal type (**Figure 4**). More connections to the Lactobacillus and Bacteroides genera were observed compared to the MB diet.

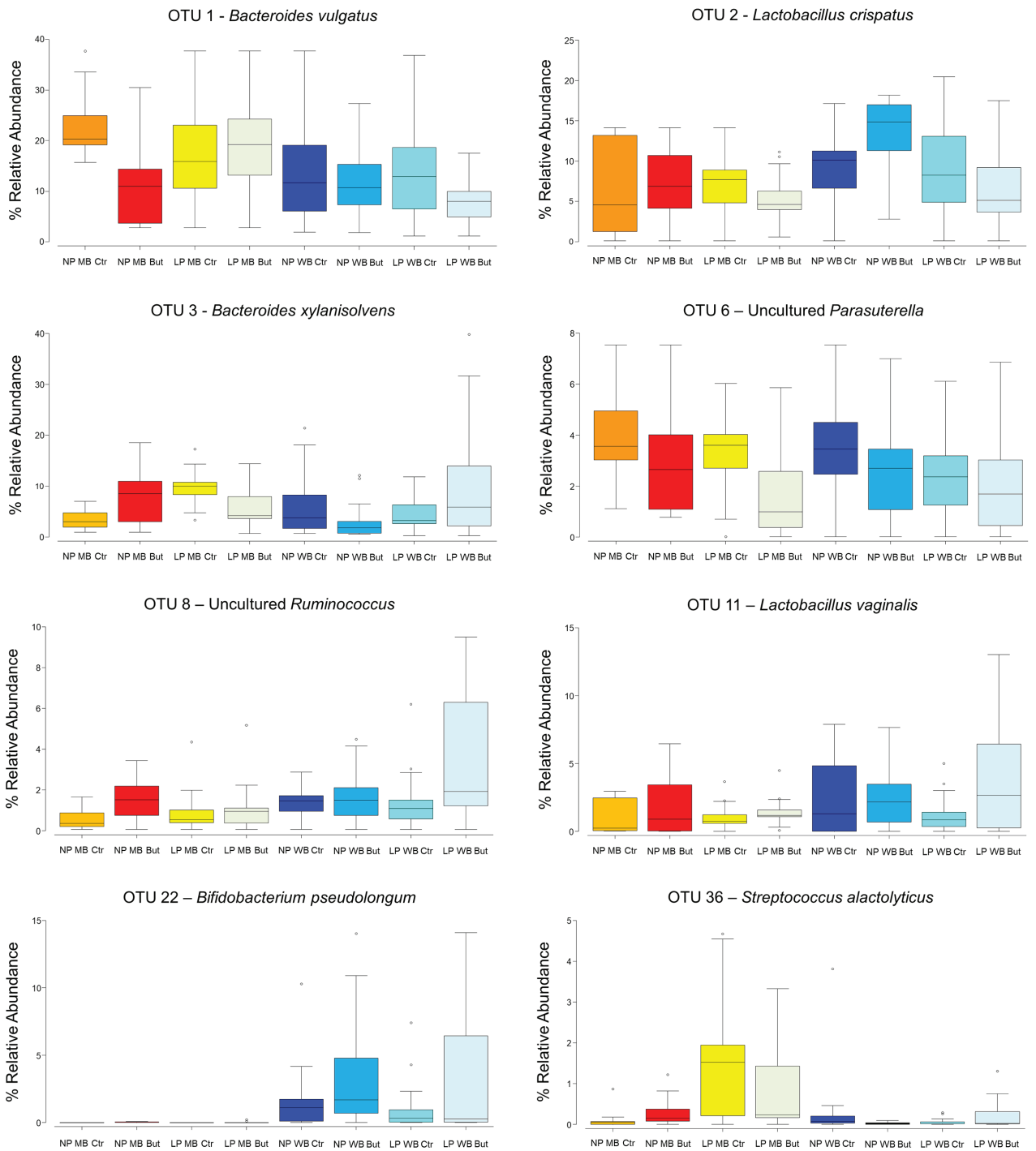

FIGURE 2 | Box-plots of the most relevant operative taxonomic units (OTUs) in the eight dietary treatments.

Functional Prediction of the Microbial Communities Influenced by the Diets

Functional predictions showed the strongest effect of the cereal type (**Supplementary Table 7**) and other statistical significances across all supplementations and their corresponding interactions ($p \leq 0.05$; **Supplementary Table 8**). The influence of the cereal type was also observed in the microbial community composition (**Supplementary Figure 1A**). The pairwise comparison demonstrated that significant differences were present mainly when the cereal type changed. The broad categories of amino

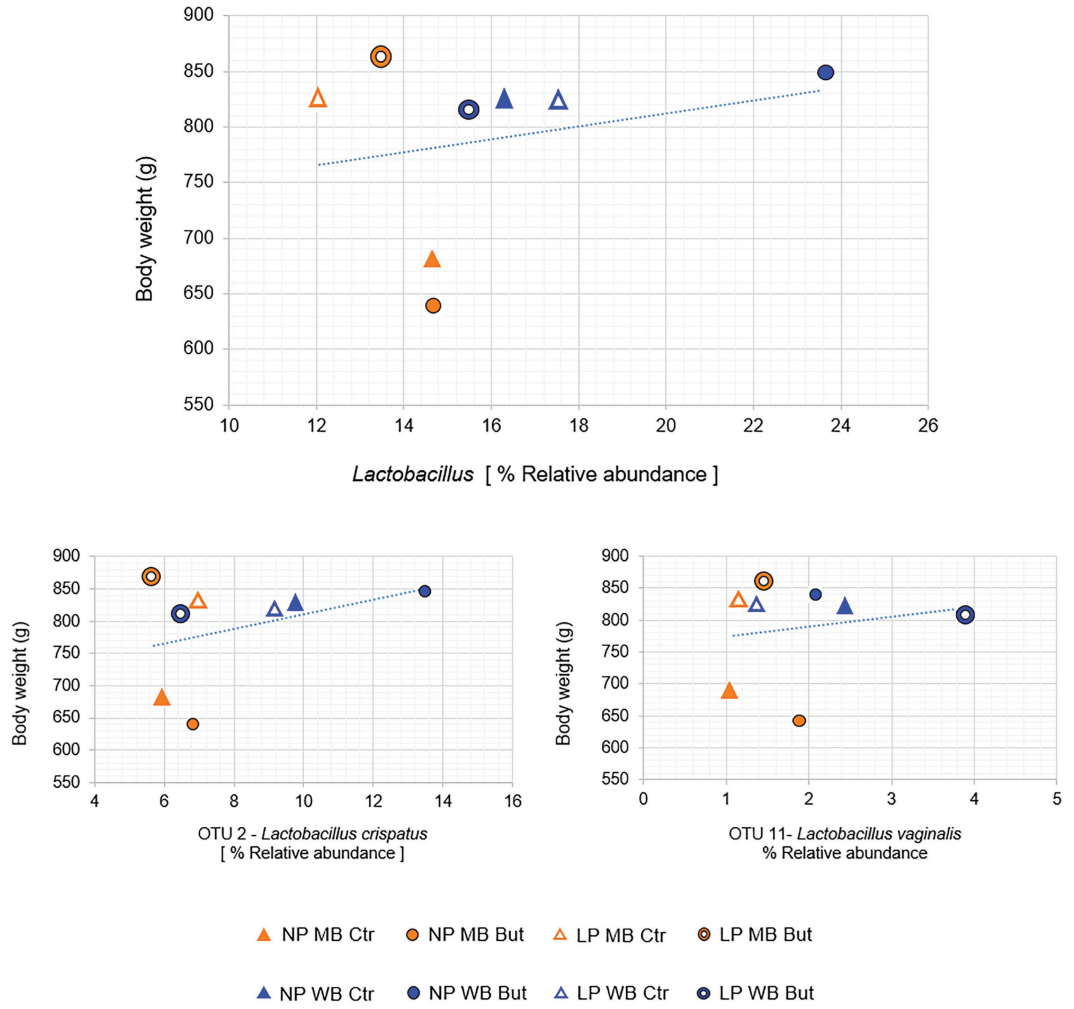

FIGURE 3 | Positive correlations between body and the genus *Lactobacillus*, OTU 2 and OUT 11. (Spearman correlation resulted in positive value and $p \leq 0.05$).

acid metabolism, carbohydrate metabolism, biosynthesis of other secondary metabolites, protein export, lipid metabolism, membrane transport were identified as the cause of the changes in predicted functions between the cereal types (**Supplementary Table 8**). Moreover, maize influenced a higher abundance of the predicted functions of the carbohydrate metabolism and biosynthesis of other secondary metabolites ($p \leq 0.05$; **Figure 5**).

Some functions within amino acid metabolism differed significantly with sodium butyrate supplementation. Specifically, glycine, serine, and threonine metabolism had more abundance of genes in the absence of butyrate, while cysteine and methionine metabolism and lysine biosynthesis were higher in the presence of butyrate (**Supplementary Table 8**).

Crude protein content was significantly different for lysine degradation (amino acid metabolism) and galactose metabolism (Carbohydrate metabolism), where normal levels induced a higher abundance of genes (**Supplementary Table 8**).

DISCUSSION

Cereal type, CP levels, and presence/absence of sodium butyrate have a decisive impact on the gut microbial structure. Diet is one of the main contributors that influence both the host and its microbes (Borda-Molina et al., 2018; Makki et al., 2018). Therefore, different studies focused on the impact of cereal types on the gut microbiota (Maesschalck et al., 2019; Paraskeuas and Mountzouris, 2019), different levels of CP (Apajalahti and Vienola, 2016; Cesare et al., 2019) and different concentrations of sodium butyrate (Bortoluzzi et al., 2017; Wu et al., 2018). However, until now, there was no study testing the influence of these three essential dietary components in the same experimental trial.

In this work, the main contributor to differences in the community structure was the cereal supplementation. Wheat-based diets contain a high concentration of non-digestible polysaccharides, causing the need for supplementing enzymes

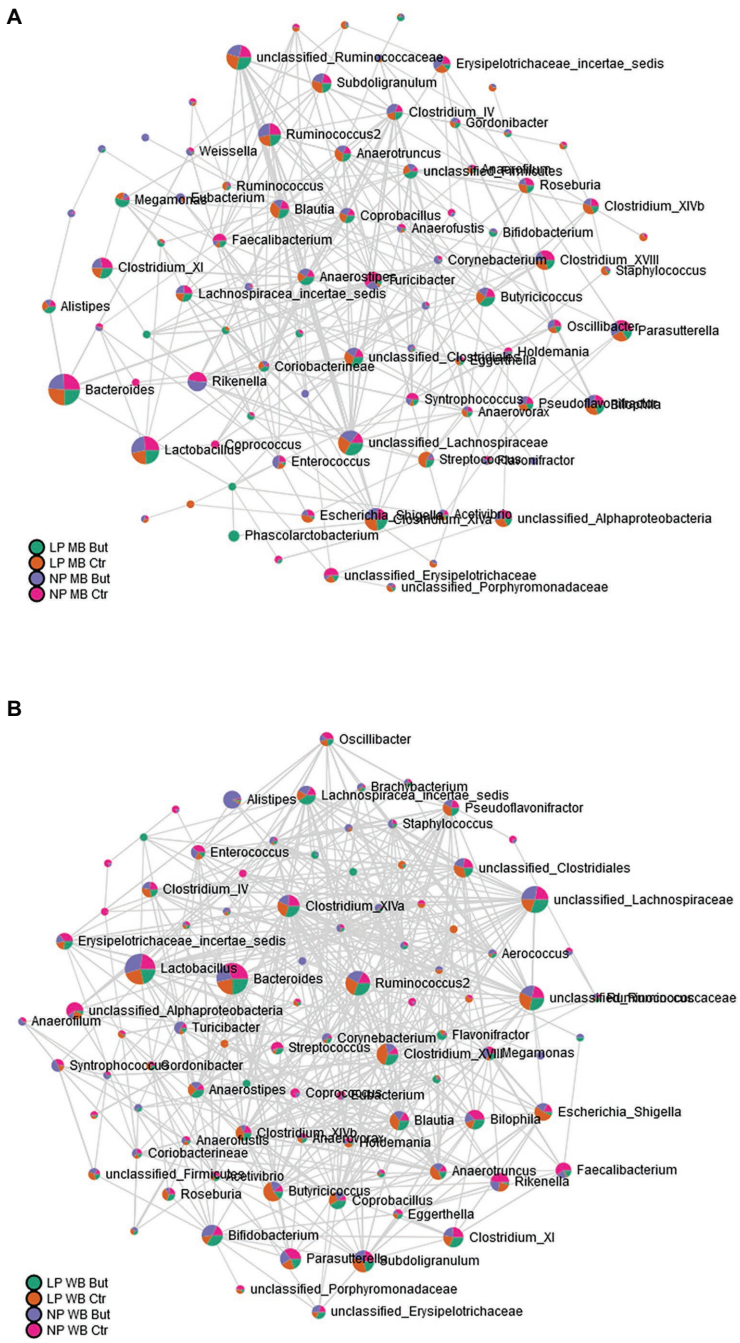

FIGURE 4 | Microbial network at genus level based on correlation analysis. **(A)** MB diets and **(B)** WB diets.

like xylanase-glucanase mixtures to improve digestibility (Keyser et al., 2016). This could influence the activities and the composition of the microbial structure. *Bacteroides vulgatus* is a common colonizer of the chicken cecum (Torok et al., 2011), and it is known to metabolize starch (McCarthy et al., 1988). The lower dominance of *B. vulgatus* in wheat diets could be determined for possible effects on variations in apparent metabolizable energy (Crisol-Martínez et al., 2017).

Bacteroides xylanisolvens was promoted in the presence of WB diets. In the polysaccharides presented in cereals, there is a high content of xylans, which can be degraded to glucoronoarabinoxylans and arabinoxylans, through the xylanolytic activity exerted by *B. xylanisolvens* (Despres et al., 2016). Xylans and their derived compounds are considered to be prebiotic substrates that promote the presence of well-described beneficial bacteria *Lactobacillus* and *Bifidobacteria*

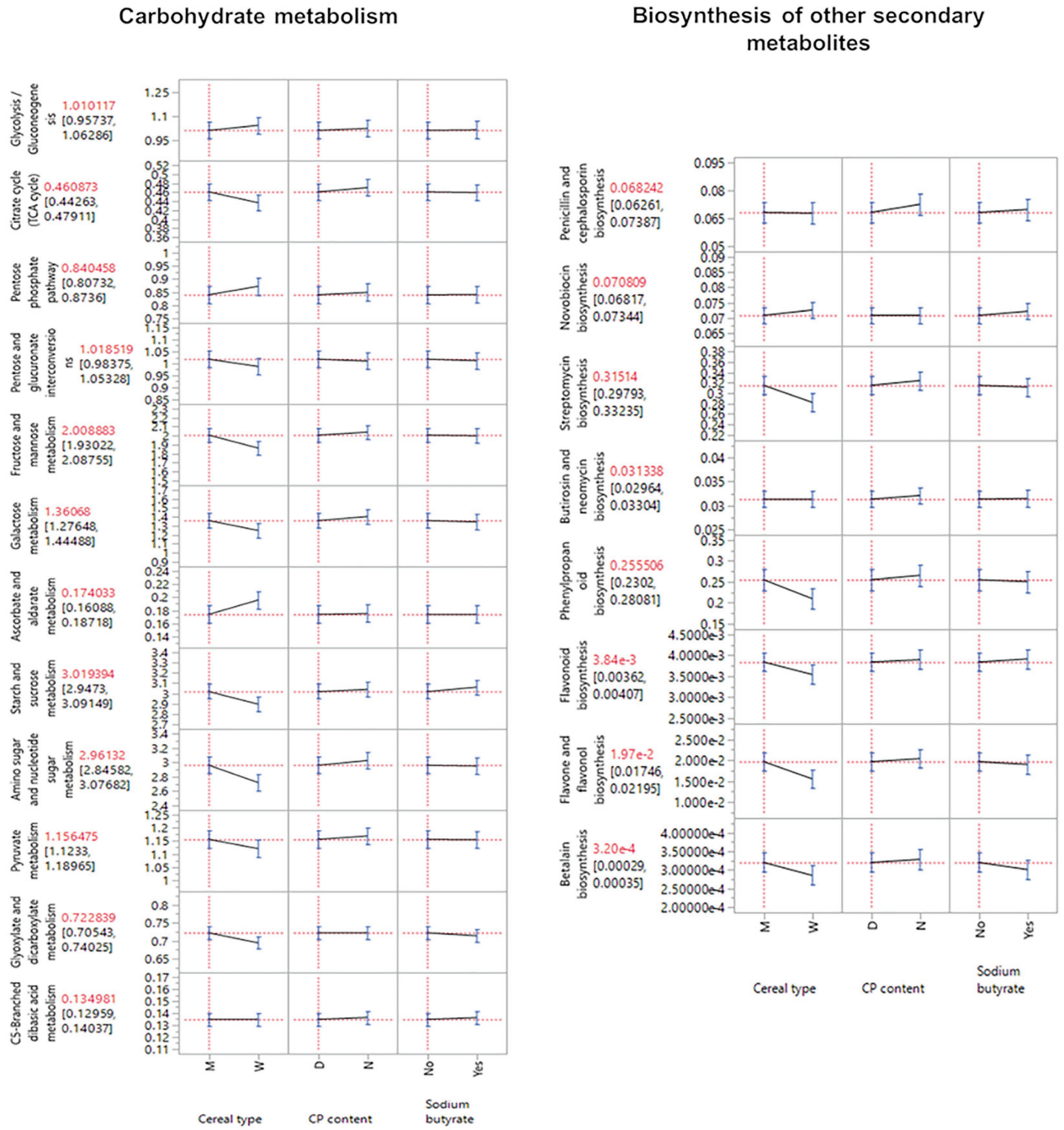

FIGURE 5 | Predicted function for the categories carbohydrate metabolism and biosynthesis of other secondary metabolism. Only statistically significant features were included ($p \leq 0.05$).

(Despres et al., 2016). In this study, wheat promoted the presence of *Bifidobacterium pseudolongum*. *Bifidobacterium* spp. have been previously reported in higher levels in WB diets (Paraskeuas and Mountzouris, 2019). These species can use oligosaccharides from complex plant cell wall substrates due to the high glycosidase activity (van Laere et al., 2000). Lactobacillaceae is also known to develop fermentative activities with xylan and its compounds (Ratnadewi et al., 2020), which is in line with this study's findings. Two of the most abundant OTUs (2 and 11) related to *Lactobacillus* species were also more abundant in WB diets.

Co-occurrence patterns investigated through network analysis are used to depict the microbes' co-existence and maintenance in a determined environment (Williams et al., 2014).

In this study, wheat promotes more neighborhood connectivity in comparison to MB diets. It is suggested that high interactions are promoted in more stable communities (Cardona et al., 2016). Therefore, it is interesting to observe that in wheat diets, *Lactobacillus, Bacteroides*, and unclassified Lachnospiraceae behave like keystone genera (Cardona et al., 2016) since they are detected in higher abundances and also have the more increased connectivity based on the microbial network analysis. Furthermore, *Lactobacillus* positively correlates with the birds' body weight, and simultaneously high abundances were observed in those animals fed with WB diets.

Predicted functions determined cereal type as the most influencing factor. Biosynthesis of secondary metabolites and carbohydrate metabolites displayed more gene abundance for MB diets, which can be associated with the high nutritional value and the dietary preference in chickens for this cereal type (Kiarie et al., 2014). Maize has high concentrations of starch and lower contents of water-soluble NSP, antinutrient components that are much present in wheat (Ranjitkar et al., 2016). This could imply that more intense interactions need to be established to degrade complex substrates present in wheat, while more metabolic activities can be followed in easily degradable substrates present in maize cereals.

This study showed the influence of CP content on the microbial structure. Crude protein is essential in chicken metabolism since it constitutes the source of amino acids that are further absorbed and transformed into body proteins (Nakphaichit, 2014). Family Ruminococcaceae, recognized as a late colonizer of the chicken caeca (Richards et al., 2019), and family Lachnospiraceae were more abundant in the low level CP diets. Both families are major members of the phylum Firmicutes in the ceca; however, Ruminococcaceae is more abundant in birds with low feed conversion ratios (Singh et al., 2012) that can be associated in the present study to the lower levels of CP. The responses obtained by these family members confirm microbiota's significant impact on feed digestion and assimilation of dietary components (Nakphaichit, 2014).

Butyrate is a source of energy to the intestinal epithelium, modulates the immune system, affects metabolism, and its depletion might cause the emergence of diseases by establishing enteric pathogens (Nicholson et al., 2012; Smith et al., 2013; Vital et al., 2017). Species of the family Bacteroidaceae have a large genome, which favors their adaptation to different environmental factors. The presence of carbohydrate-degrading enzymes allows the digestion of substrates from plant, algae, or animal sources. Together with the high tolerance to bile salts in the gut, these conditions influence a beneficial relationship with the host (Wexler, 2014). In this study, this family was affected by sodium butyrate and CP as an indicator of the microbes' response to gut environmental conditions.

The present study showed the close interactions between microbial community composition, including the predicted functions and the complex feedstuff ingredients. It was observed that higher impacts were observed for maize as the main dietary cereal type promoting more abundant species. At the same time, wheat was associated with a higher abundance of well-recognized beneficial microorganisms belonging to Lactobacillaceae and Bifidobacteriaceae. Predicted functions demonstrated that maize could be considered the most potent cereal to promote the metabolism and biosynthesis of secondary metabolites. At the same time, genera in the WB diets have more interactions based on network connectivity due to the higher complexity of this cereal type.

DATA AVAILABILITY STATEMENT

The datasets presented in this study can be found in online repositories. The names of the repository/repositories and accession number(s) can be found at: https://www.ebi.ac.uk/ena, PRJEB40780.

ETHICS STATEMENT

The animal study was reviewed and approved by Government Office of Pest County, Food Chain Safety, Plant Protection and Soil Conservation Directorate, Budapest, Hungary.

AUTHOR CONTRIBUTIONS

GM, ZN, KH, JS, and AC-S: conceptualization. DB-M, MM: methodology. DB-M, GM, and MM: performed the experiment. DB-M, JS, and AC-S: formal analysis. DB-M, GM, MM, ZN, KH, JS, and AC-S: writing—review and editing. ZN and AC-S: funding acquisition. All authors contributed to the article and approved the submitted version.

FUNDING

The study was supported by the Hungarian Scientific Research Fund – OTKA, grant No 114033. AC-S would like to acknowledge the Ellrichshausen'sche Stiftung and JS acknowledge the Carl Zeiss Stiftung for the financial support. AC-S was supported by the European Social Fund and by the Ministry of Science, Research and Arts of Baden-Württemberg.

ACKNOWLEDGMENTS

The authors acknowledge support by the High Performance and Cloud Computing Group at the Zentrum für Datenverarbeitung of the University of Tübingen, the state of Baden-Württemberg through bwHPC.

SUPPLEMENTARY MATERIAL

The Supplementary Material for this article can be found online at: https://www.frontiersin.org/articles/10.3389/fmicb.2020.617800/full#supplementary-material

REFERENCES

Abbasi, M. A., Mahdavi, A. H., Samie, A. H., and Jahanian, R. (2014). Effects of different levels of dietary crude protein and threonine on performance, humoral immune responses and intestinal morphology of broiler chicks. *Rev. Bras. Cienc. Avic.* 16, 35–44. doi: 10.1590/S1516-635X2014000100005

Ahsan, U., Cengiz, Ö., Raza, I., Kuter, E., Chacher, M. F. A., Iqbal, Z., et al. (2016). Sodium butyrate in chicken nutrition: the dynamics of performance, gut microbiota, gut morphology, and immunity. *World Poultry Sci J.* 72, 265–275. doi: 10.1017/S0043933916000210

Alleman, F., Michel, J., Chagneau, A. M., and Leclercq, B. (2000). The effects of dietary protein independent of essential amino acids on growth and body composition in genetically lean and fat chickens. *Br. Poult. Sci.* 41, 214–218. doi: 10.1080/713654902

Apajalahti, J., and Vienola, K. (2016). Interaction between chicken intestinal microbiota and protein digestion. *Anim. Feed Sci. Technol.* 221, 323–330. doi: 10.1016/j.anifeedsci.2016.05.004

Borda-Molina, D., Seifert, J., and Camarinha-Silva, A. (2018). Current perspectives of the chicken gastrointestinal tract and its microbiome. *Comput. Struct. Biotechnol. J.* 16, 131–139. doi: 10.1016/j.csbj.2018.03.002

Borda-Molina, D., Vital, M., Sommerfeld, V., Rodehutscord, M., and Camarinha-Silva, A. (2016). Insights into broilers' gut microbiota fed with phosphorus, calcium, and Phytase supplemented diets. *Front. Microbiol.* 7:2033. doi: 10.3389/fmicb.2016.02033

Bortoluzzi, C., Pedroso, A. A., Mallo, J. J., Puyalto, M., Kim, W. K., and Applegate, T. J. (2017). Sodium butyrate improved performance while modulating the cecal microbiota and regulating the expression of intestinal immune-related genes of broiler chickens. *Poult. Sci.* 96, 3981–3993. doi: 10.3382/ps/pex218

Bray, J. R., and Curtis, J. T. (1957). An ordination of the upland forest communities of southern Wisconsin. *Ecol. Monogr.* 27, 325–349. doi: 10.2307/1942268

Cardona, C., Weisenhorn, P., Henry, C., and Gilbert, J. A. (2016). Network-based metabolic analysis and microbial community modeling. *Curr. Opin. Microbiol.* 31, 124–131. doi: 10.1016/j.mib.2016.03.008

Chong, J., Liu, P., Zhou, G., and Xia, J. (2020). Using MicrobiomeAnalyst for comprehensive statistical, functional, and meta-analysis of microbiome data. *Nat. Protoc.* 15, 799–821. doi: 10.1038/s41596-019-0264-1

Clarke, K. R., and Warwick, R. M. (1994). *Change in marine communities: An approach to statistical analysis and interpretation*. Plymouth, UK: PRIMER-E Ltd.

Crisol-Martínez, E., Stanley, D., Geier, M. S., Hughes, R. J., and Moore, R. J. (2017). Sorghum and wheat differentially affect caecal microbiota and associated performance characteristics of meat chickens. *PeerJ* 5:e36071. doi: 10.7717/peerj.3071

de Cesare, A., Faria do Valle, Ì., Sala, C., Sirri, F., Astolfi, A., Castellani, G., et al. (2019). Effect of a low protein diet on chicken ceca microbiome and productive performances. *Poult. Sci.* 98, 3963–3976. doi:10.3382/ps/pez132

de Keyser, K., Kuterna, L., Kaczmarek, S., Rutkowski, A., and Vanderbeke, E. (2016). High dosing NSP enzymes for total protein and digestible amino acid reformulation in a wheat/corn/soybean meal diet in broilers. *J. Appl. Poult. Res.* 25, 239–246. doi:10.3382/japr/pfw006

de Maesschalck, C., Eeckhaut, V., Maertens, L., de Lange, L., Marchal, L., Daube, G., et al. (2019). Amorphous cellulose feed supplement alters the broiler caecal microbiome. *Poult. Sci.* 98, 3811–3817. doi:10.3382/ps/pez090

Despres, J., Forano, E., Lepercq, P., Comtet-Marre, S., Jubelin, G., Chambon, C., et al. (2016). Xylan degradation by the human gut Bacteroides xylanisolvens XB1A(T) involves two distinct gene clusters that are linked at the transcriptional level. *BMC Genomics* 17:326. doi: 10.1186/s12864-016-2680-8

Friedman, J., and Alm, E. J. (2012). Inferring correlation networks from genomic survey data. *PLoS Comput. Biol.* 8:e1002687. doi: 10.1371/journal.pcbi.1002687

Jiang, Y., Zhang, W., Gao, F., and Zhou, G. (2015). Effect of sodium butyrate on intestinal inflammatory response to lipopolysaccharide in broiler chickens. *Can. J. Anim. Sci.* 95, 389–395. doi: 10.4141/cjas-2014-183

Kaewtapee, C., Burbach, K., Tomforde, G., Hartinger, T., Camarinha-Silva, A., Heinritz, S., et al. (2017). Effect of *Bacillus subtilis* and *Bacillus licheniformis* supplementation in diets with low- and high-protein content on ileal crude protein and amino acid digestibility and intestinal microbiota composition of growing pigs. *J. Anim. Sci. Biotechnol.* 8:37. doi: 10.1186/s40104-017-0168-2

Kiarie, E., Romero, L. F., and Ravindran, V. (2014). Growth performance, nutrient utilization, and digesta characteristics in broiler chickens fed corn or wheat diets without or with supplemental xylanase. *Poult. Sci.* 93, 1186–1196. doi: 10.3382/ps.2013-03715

Kozich, J. J., Westcott, S. L., Baxter, N. T., Highlander, S. K., and Schloss, P. D. (2013). Development of a dual-index sequencing strategy and curation pipeline for analyzing amplicon sequence data on the MiSeq Illumina sequencing platform. *Appl. Environ. Microbiol.* 79, 5112–5120. doi: 10.1128/AEM.01043-13

Leeson, S., Namkung, H., Antongiovanni, M., and Lee, E. H. (2005). Effect of butyric acid on the performance and carcass yield of broiler chickens. *Poult. Sci.* 84, 1418–1422. doi: 10.1093/ps/84.9.1418

Lentle, R. G., and Janssen, P. W. M. (2008). Physical characteristics of digesta and their influence on flow and mixing in the mammalian intestine: a review. *J. Comp. Physiol. B Biochem. Syst. Environ. Physiol.* 178, 673–690. doi: 10.1007/s00360-008-0264-x

Makki, K., Deehan, E. C., Walter, J., and Bäckhed, F. (2018). The impact of dietary fiber on gut microbiota in host health and disease. *Cell Host Microbe* 23, 705–715. doi: 10.1016/j.chom.2018.05.012

McCarthy, R. E., Pajeau, M., and Salyers, A. A. (1988). Role of starch as a substrate for *Bacteroides vulgatus* growing in the human colon. *Appl. Environ. Microbiol.* 54, 1911–1916.

Meng, X., Slominski, B. A., and Guenter, W. (2004). The effect of fat type, carbohydrase, and lipase addition on growth performance and nutrient utilization of young broilers fed wheat-based diets. *Poult. Sci.* 83, 1718–1727. doi: 10.1093/ps/83.10.1718

Nakphaichit, M. (2014). Effect of increasing dietary protein from soybean meal on intestinal microbiota and their fatty acids production in broiler chicken. *Adv. Anim. Vet. Sci.* 2, 337–343. doi: 10.14737/journal.aavs/2014/2.6.337.343

Nicholson, J. K., Holmes, E., Kinross, J., Burcelin, R., Gibson, G., Jia, W., et al. (2012). Host-gut microbiota metabolic interactions. *Science* 336, 1262–1267. doi: 10.1126/science.1223813

Paraskeuas, V., and Mountzouris, K. C. (2019). Broiler gut microbiota and expressions of gut barrier genes affected by cereal type and phytogenic inclusion. *Anim. Nutr.* 5, 22–31. doi: 10.1016/j.aninu.2018.11.002

Petrilla, J., Mátis, G., Kulcsár, A., Talapka, P., Bíró, E., Mackei, M., et al. (2018). Effect of dietary cereal type, crude protein and butyrate supplementation on metabolic parameters of broilers. *Acta Vet. Hung.* 66, 408–452. doi: 10.1556/004.2018.037

Quast, C., Pruesse, E., Yilmaz, P., Gerken, J., Schweer, T., Yarza, P., et al. (2013). The SILVA ribosomal RNA gene database project: improved data processing and web-based tools. *Nucleic Acids Res.* 41, D590–D596. doi: 10.1093/nar/gks1219

Ranjitkar, S., Karlsson, A. H., Petersen, M. A., Bredie, W. L. P., Petersen, J. S., and Engberg, R. M. (2016). The influence of feeding crimped kernel maize silage on broiler production, nutrient digestibility and meat quality. *Br. Poult. Sci.* 57, 93–104. doi: 10.1080/00071668.2015.1115468

Ratnadewi, A. A. I., Amaliyah Zain, M. H., Nara Kusuma, A. N., Handayani, W., Nugraha, A. S., and Siswoyo, T. A. (2020). Lactobacillus casei fermentation towards xylooligosaccharide (XOS) obtained from coffee peel enzymatic hydrolysate. *Biocatal. Agric. Biotechnol.* 23:101446. doi: 10.1016/j.bcab.2019.101446

Richards, P., Fothergill, J., Bernardeau, M., and Wigley, P. (2019). Development of the caecal microbiota in three broiler breeds. *Front. Vet. Sci.* 6:201. doi: 10.3389/fvets.2019.00201

Singh, K. M., Shah, T., Deshpande, S., Jakhesara, S. J., Koringa, P. G., Rank, D. N., et al. (2012). High through put 16S rRNA gene-based pyrosequencing analysis of the fecal microbiota of high FCR and low FCR broiler growers. *Mol. Biol. Rep.* 39, 10595–10602. doi: 10.1007/s11033-012-1947-7

Smith, P. M., Howitt, M. R., Panikov, N., Michaud, M., Gallini, C. A., Bohlooly-Y, M., et al. (2013). The microbial metabolites, short-chain fatty acids, regulate colonic treg cell homeostasis. *Science* 341, 569–573. doi: 10.1126/science.1241165

Teirlynck, E., Bjerrum, L., Eeckhaut, V., Huygebaert, G., Pasmans, F., Haesebrouck, F., et al. (2009). The cereal type in feed influences gut wall morphology and intestinal immune cell infiltration in broiler chickens. *Br. J. Nutr.* 102, 1453–1461. doi: 10.1017/S0007114509990407

Torok, V. A., Hughes, R. J., Mikkelsen, L. L., Perez-Maldonado, R., Balding, K., MacAlpine, R., et al. (2011). Identification and characterization of potential

performance-related gut microbiotas in broiler chickens across various feeding trials. *Appl. Environ. Microbiol.* 77, 5868–5878. doi: 10.1128/AEM.00165-11

van Laere, K. M., Hartemink, R., Bosveld, M., Schols, H. A., and Voragen, A. G. (2000). Fermentation of plant cell wall derived polysaccharides and their corresponding oligosaccharides by intestinal bacteria. *J. Agric. Food Chem.* 48, 1644–1652. doi: 10.1021/jf990519i

Vital, M., Karch, A., and Pieper, D. H. (2017). Colonic butyrate-producing communities in humans: an overview using omics data. *mSystems* 2, e00130–e00147. doi: 10.1128/mSystems.00130-17

Volf, J., Polansky, O., Varmuzova, K., Gerzova, L., Sekelova, Z., Faldynova, M., et al. (2016). Transient and prolonged response of chicken cecum mucosa to colonization with different gut microbiota. *PLoS One* 11:e0163932. doi: 10.1371/journal.pone.0163932

Wang, Q., Garrity, G. M., Tiedje, J. M., and Cole, J. R. (2007). Naive Bayesian classifier for rapid assignment of rRNA sequences into the new bacterial taxonomy. *Appl. Environ. Microbiol.* 73, 5261–5267. doi: 10.1128/AEM.00062-07

Wexler, H. M. (2014). "The genus Bacteroides" in *The prokaryotes: Other major lineages of bacteria and the archaea*. eds. E. Rosenberg, E. F. DeLong, S. Lory, E. Stackebrandt and F. Thompson (Berlin, Heidelberg: Springer Berlin Heidelberg; Imprint: Springer), 459–484.

Williams, R. J., Howe, A., and Hofmockel, K. S. (2014). Demonstrating microbial co-occurrence pattern analyses within and between ecosystems. *Front. Microbiol.* 5:358. doi: 10.3389/fmicb.2014.00358

Wu, W., Xiao, Z., An, W., Dong, Y., and Zhang, B. (2018). Dietary sodium butyrate improves intestinal development and function by modulating the microbial community in broilers. *PLoS One* 13:e0197762. doi: 10.1371/journal.pone.0197762

Zhang, W. H., Jiang, Y., Zhu, Q. F., Gao, F., Dai, S. F., Chen, J., et al. (2011). Sodium butyrate maintains growth performance by regulating the immune response in broiler chickens. *Br. Poult. Sci.* 52, 292–301. doi: 10.1080/00071668.2011.578121

Zhang, L., Wu, W., Lee, Y. -K., Xie, J., and Zhang, H. (2018). Spatial heterogeneity and co-occurrence of mucosal and luminal microbiome across swine intestinal tract. *Front. Microbiol.* 9:48. doi: 10.3389/fmicb.2018.00048

Conflict of Interest: The authors declare that the research was conducted in the absence of any commercial or financial relationships that could be construed as a potential conflict of interest.

frontiers in Microbiology

ORIGINAL RESEARCH
published: 05 February 2021
doi: 10.3389/fmicb.2020.630280

Metagenomics Reveals That Intravenous Injection of Beta-Hydroxybutyric Acid (BHBA) Disturbs the Nasopharynx Microflora and Increases the Risk of Respiratory Diseases

*Jiancheng Qi[1], Dongjie Cai[1], Yaocheng Cui[1], Tianyu Tan[1], Huawei Zou[2], Wei Guo[3], Yue Xie[1], Hongrui Guo[1], Shi-Yi Chen[4], Xiaoping Ma[1], Liping Gou[1], Hengmin Cui[1], Yi Geng[1], Ming Zhang[4], Gang Ye[1], Zhijun Zhong[1], Zhihua Ren[1], Yanchun Hu[1], Ya Wang[1], Junliang Deng[1], Shumin YU[1], Suizhong Cao[1], Metha Wanapat[5], Jing Fang[1], Zhisheng Wang[2] and Zhicai Zuo[1]**

[1] College of Veterinary Medicine, Sichuan Agricultural University, Chengdu, China, [2] Institute of Animal Nutrition, Sichuan Agricultural University, Chengdu, China, [3] Department of Clinical Laboratory, Chengdu Medical College, Chengdu, China, [4] College of Animal Science and Technology, Sichuan Agricultural University, Chengdu, China, [5] Tropical Feed Resources Research and Development Center (TROFREC), Department of Animal Science, Faculty of Agriculture, Khon Kaen University, Khon Kaen, Thailand

OPEN ACCESS

Edited by:
Xudong Sun,
Heilongjiang Bayi Agricultural University, China

Reviewed by:
Jianzhu Liu,
Shandong Agricultural University, China
Guowen Liu,
Jilin University, China

***Correspondence:**
Zhicai Zuo
zzcjl@126.com

Specialty section:
This article was submitted to Systems Microbiology, a section of the journal Frontiers in Microbiology

Received: 17 November 2020
Accepted: 21 December 2020
Published: 05 February 2021

Citation:
Qi J, Cai D, Cui Y, Tan T, Zou H, Guo W, Xie Y, Guo H, Chen S-Y, Ma X, Gou L, Cui H, Geng Y, Zhang M, Ye G, Zhong Z, Ren Z, Hu Y, Wang Y, Deng J, YU S, Cao S, Wanapat M, Fang J, Wang Z and Zuo Z (2021) Metagenomics Reveals That Intravenous Injection of Beta-Hydroxybutyric Acid (BHBA) Disturbs the Nasopharynx Microflora and Increases the Risk of Respiratory Diseases. Front. Microbiol. 11:630280. doi: 10.3389/fmicb.2020.630280

It is widely accepted that maintenance of microbial diversity is essential for the health of the respiratory tract; however, there are limited reports on the correlation between starvation and respiratory tract microbial diversity. In the present study, saline/β-hydroxybutyric acid (BHBA) intravenous injection after dietary restriction was used to imitate different degrees of starvation. A total of 13 healthy male yaks were imposed to different dietary restrictions and intravenous injections, and their nasopharyngeal microbiota profiles were obtained by metagenomic shotgun sequencing. In healthy yaks, the main dominant phyla were *Proteobacteria* (33.0%), *Firmicutes* (22.6%), *Bacteroidetes* (17.2%), and *Actinobacteria* (13.2%); the most dominated species was *Clostridium botulinum* (10.8%). It was found that 9 days of dietary restriction and 2 days of BHBA injection (imitating severe starvation) significantly decreased the microbial diversity and disturbed its structure and functional composition, which increased the risk of respiratory diseases. This study also implied that oral bacteria played an important role in maintaining nasopharynx microbial homeostasis. In this study, the correlation between starvation and nasopharynx microbial diversity and its potential mechanism was investigated for the first time, providing new ideas for the prevention of respiratory diseases.

Keywords: starvation, nasopharynx microbiota, respiratory tract, microbial diversity, metagenomics, yak

INTRODUCTION

Yak (*Bos grunniens*) is semidomesticated herbivore livestock on the Qinghai-Tibet Plateau (Qiu et al., 2012). In the cold seasons, yaks often suffer from severe starvation, weight loss, high morbidity, and mortality due to long-time lack of pasturage (Xue et al., 2005). Recently, it is widely accepted that this high prevalence of diseases was associated with the harsh environment in the cold

seasons (Xue et al., 2005). However, it is unclear whether starvation affects the respiratory system and then results in the high prevalence of diseases.

The respiratory tract is an important part of the respiratory system, which harbors various microbial communities in every ecological niche (Dickson et al., 2016). The respiratory tract microbiome is highly dynamic and affected by many factors. For instance, Woldehiwet et al. (1990) found that the upper respiratory tract microbiota of calves was affected by individual differences, age, and environmental temperature; Anand and Mande (2018) summarized that diet could affect respiratory microbiota, whereas Bosch et al. (2016) indicated that upper respiratory tract microbiota in infancy was affected by delivery mode. It was thought that these factors affected the proliferation ability of certain bacteria and immunity of the host (Man et al., 2017). In recent years, the correlations between microbiota and the healthy of respiratory tract has attracted lots of attention. Man and Wypych both believed that airway-related diseases of both humans and cattle are caused by the disturbance of the microbiome (Man et al., 2017; Wypych et al., 2019), and Mohamed summarized that the mucosal microbiota had substantial effects on the bovine respiratory health (Zeineldin et al., 2019). Collectively, it is recognized that maintaining the respiratory tract microbiota homeostasis played a vital role in keeping the airway healthy (Man et al., 2017). There are also many reports on the microbiota differences along the respiratory tract. Bassis et al. (2015) and Nicola et al. (2017) found that the microbiome of the lower respiratory tract was closely associated with that of the upper respiratory tract. Charlson et al. (2011) and Zeineldin et al. (2017) found that the microbiota in the nasopharynx could affect the health of the entire respiratory tract. The nasopharynx is the overlapping area of the oral cavity, nasal cavity, and trachea, which explains why the nasopharyngeal microbiota has a considerable overlap microbial composition of anterior nares, nasopharynx, oropharynx, and trachea, including *Moraxella*, *Dolosigranulum*, *Staphylococcus*, *Corynebacterium*, etc. (Dickson et al., 2017; Man et al., 2017). Therefore, the microbial community profiles of the nasopharynx can reflect the comprehensive situation of the entire respiratory tract (McMullen et al., 2020).

Traditional bacterial culture technology, 16S RNA sequencing, etc., were once used to study nasopharyngeal microbial communities, but these tools have their disadvantages; for example, many bacteria are uncultivable, and 16S RNA sequencing is not deep enough to be accurate to species level. In the past decades, with the advances in the next-generation sequencing technologies, metagenomics-based studies have been widely applied to determine the composition of various microbiomes and to analyze their functions at the DNA and RNA levels (Wang et al., 2015; Gilbert et al., 2016). Metagenomics can accurately detect all the species and their relative abundance in a sample and allow us to precisely analyze and predict the structure and function of the microbial community.

Previous research showed that the main features of starvation are lower blood glucose and elevated blood ketones [acetone, acetoacetate, and especially β-hydroxybutyric acid (BHBA)] due to the fulsome catabolism of fat (Whiting et al., 2012; Dhatariya et al., 2020). BHBA, the most primary (>70%) end products of lipid decomposition, provides energy for animals when animals suffer excessive starvation (Belkhou et al., 1991; Cahill, 2006; Dhatariya et al., 2020).

Hence, to explore the correlation between starvation and nasopharyngeal microbiota, we imitated mild and excessive starvation state by fasting and BHBA solution intravenous infusion. The nasopharyngeal microbiome was sampled and sequenced, and their differences in diversity, structure, and function among the experimental and control groups were analyzed using a metagenomic shotgun sequencing approach. Until now, there are limited studies on the correlation between starvation and respiratory tract microbiome; our study will fill this knowledge gap, enrich our understanding of the microbiota of the respiratory tract, and provide new prevention and treatment strategies for respiratory diseases.

MATERIALS AND METHODS

Experimental Animals

Before the experiment, 13 healthy (with no macroscopic symptoms) and well-grown (with similar weights, 237.97 ± 11.75 kg) 2.5-year-old male Jiulong yaks were adaptively fed (without any antibacterial agents) for 2 months in independent cowsheds. All cowsheds were cleaned with insect repellant and sanitizer every week. All fodder and water were prepared according to Zou et al.s' (2020) study. After adaptively feeding, all yaks (n = 13) were randomly divided into three groups: control group (n = 3), mild dietary restriction (DR) group (n = 5), and excessive DR (n = 5) group. Yaks in the control group were numbered Z1–Z3, yaks in the mild DR group were numbered G1–G5, and yaks in the excessive DR group were numbered GB1–GB5. Yaks in the mild DR group and excessive DR group were starved (without any fodder) for 9 days. The 9 days of dietary restriction time was determined according to previous work (Zarrin et al., 2013; Zou et al.s', 2020) to ensure that yaks were in the state of negative energy balance without health threatening. Yaks in the control group were free to access fodder within the synchronous 9 days. All yaks received a continuous 48 hours of intravenous infusion from 9:00 AM on the seventh day to 9:00 AM on the ninth day. Yaks in the control group and mild DR group were infused with 0.9% saline, whereas yaks in the excessive DR group were infused with BHBA solution (1.7 mmol/L). The experiment flow before sampling is visualized in **Supplementary Figure 1B**.

BHBA Infusion

The BHBA solution was prepared following the previous study (Zarrin et al., 2013). BHBA acid sodium salt (Sigma, United States) was solvated into ultrapure water to the concentration of 1.7 mmol/L. The pH value of this solution was adjusted to 7.4 by HCl followed by autoclaving at 131°C, 100 kPa for 50 min. Then, the prepared solution was stored at 4°C as soon as being filtered through the 0.22-μm filter. The indwelling intravenous catheters (Jinhuan

Medical Supplies, China) were fitted on both of the ear veins of each yak on day 7. The infusion was through the left-side catheters of yaks by a peristaltic pump (Haoke Medical Instrument, China). The initial infusion dose was calculated based on the bodyweight of yaks (8.5 μmol/Kg/min). During the first 2 h of infusion, the blood samples were collected through the right-side catheters every 15 min and then determined the BHBA concentration immediately using a blood ketone meter (Dizhun Biotechnology, China). BHBA infusion rate was instantly adjusted to maintain the blood BHBA concentration between 1.5 and 2.0 mmol/L, whose aim was to avoid ketosis caused by excess high BHBA concentration. The yaks in the control group and mild DR group were infused into 0.9% saline solution with the same infusion time and rate. More details could be found in Zou et al.s' (2020) work.

Sample Collection, DNA Extraction, Sequencing, and Quality Control

When the intravenous infusion stopped, microbiota samples were collected using 20-cm sterile deep nasopharyngeal swabs (Merlin Technology, China) from the nasopharynx mucosa and immediately stored in a dry icebox. DNA was extracted using the MO BIO PowerSoil DNA Isolation Kit (MO BIO Laboratories, United States) according to Earth Microbiome Project standard protocols (Marotz et al., 2017). DNA concentrations of all samples was detected by NanoDrop (Thermo Scientific, United States), and the results ranged from 15.2 to 75.4 ng/μL. DNA samples' quality was estimated on agarose gel electrophoresis. Only samples that meet the following criteria were used for library construction: (1) DNA concentration is >15 ng/μL; (2) the total weight of DNA is >6 μg; (3) DNA band that was visualized on agarose gel electrophoresis must be clear and of good quality. Finally, 1 μg DNA of each sample was pooled to an equimolar concentration to construct the DNA libraries (DNA was sheared to 350 bp) using the Illumina DNA Sample Preparation Kit according to the manufacturer's instructions. Amplified libraries were sequenced on Illumina HiSeq 2500 platform (2 × 250 bp). Adaptor contamination was removed using Cutadapt 1.3 (Martin, 2011) with parameters "-o 4 -e 0.1." Quality control was performed using a sliding window (5-bp bases) in Trimmomatic (Bolger et al., 2014) with the following criteria: (1) cutting once the average quality within the window falls below Q 20; (2) clean reads do not contain any N bases; (3) trimming is applied to the 3' end of reads, dropping those reads that were of less than 50-bp length; (4) only paired-end reads were retained for downstream analyses. To contigs and scaffolds, the obtained paired-end clean reads of each sample were performed *de novo* assembly using Megahit with the parameter "K-mer∼ [27, 127]" (Li et al., 2010). Detailed contigs/scaffolds statistical information was shown in **Supplementary Table 8** (Sheet 2).

The metagenome dataset used in this study was deposited into the National Centre for Biotechnology Information's Sequence Read Archive (SRA; http://www.ncbi.nlm.nih.gov/sra) under accession bioproject number: PRJNA681085 (SRA: SAMN16932244-SAMN16932256)[1].

Species Annotation

To analyze the species composition, the scaffolds/scaftigs of each sample were subjected to BLASTN ("E < 0.00001") against the bacterial, archaeal, fungal, and virus sequences in the NCBI-NT database (National Centre for Biotechnology Information–Nucleotide Collection, v2016-6-19). Because each target sequence could match different reference sequences that belong to a different taxon, we performed the Lowest Common Ancestor algorithm (Huson et al., 2018) using MEGAN5 (MEta Genome Analyzer) (Huson et al., 2011) software to increase the preciseness and dependability without loss of biological significance. In brief, we classified the last level of common classification before the reference sequences branched into different species as the annotation information of species classification of the target sequences. Then the relative abundance of each taxon at every classification level was obtained by combining the relative abundance of these scaffolds/scaftigs sequences in each sample using Quantitative Insights Into Microbial (QIIME) software (Caporaso et al., 2010). To analyze the significance of species relative abundance difference, we performed a two-tailed *t*-test against the average relative abundance using the SciPy database (Virtanen et al., 2020) in Python software and controlled the false discovery rate (FDR) using the Benjamini-Hochberg method (Benjamini and Hochberg, 1995). In brief, we calculated the fold change value of every functional group between each sample and demonstrated them using Log_2 (fold-change value). Only those functional groups with both | Log2 (fold-change value) | > 1 and $p < 0.05$ were considered having significant difference. According to the composition structure of each sample at each classification level and their relative abundance, we visualized them in heat map using R software package. Through randomly sampling a certain number of sequences in each sample, we predicted the possible species total number and their relative abundance within a set of given sequencing depths and drawn rarefaction curve (Heck et al., 1975) using QIIME software. To analyze the distribution of species abundance, the taxon of each sample at species level was arranged from high to low according to their relative abundance, and the relative abundance value was transformed into vertical ordinate by Log_2, then we drew the rank abundance curve using R software. We also calculated the Spearman rank correlation coefficient (Sedgwick, 2014) of the top 50 species with the highest relative abundance using Mothur software (Schloss et al., 2009) and drew the connection networks (Faust and Raes, 2012) of species ($|\rho| > 0.8$, $p < 0.01$) and visualized them using Cytoscape software (Shannon et al., 2003). To compare the diversity of different samples and correct the diversity difference caused by the sequencing depth, we randomly sampled the bottom functional group abundance spectrum of all samples in each functional database or the species-level composition spectrum according to the lowest sequencing depth.

[1]https://www.ncbi.nlm.nih.gov/bioproject/PRJNA681085

And then we obtained the alpha diversity (including Chao1 index, ACE index, Shannon index, and Simpson index) of each sample by QIIME software. To analyze the unsupervised β diversity, principal complement analysis (Euclidean distance) (Ramette, 2007) was performed on the abundance spectrum of the bottom functional groups and species-level composition spectrum annotated by each functional database in each sample using QIIME software and R software. At last, to find a biomarker, we performed linear discriminant analysis effect size (LEfSe) analysis (Segata et al., 2011) by submitting the composition spectrum data at species level to Galaxy online analysis platform (huttenhower.sph.harvard.edu/galaxy/).

Function Annotation

Scaffolds/scaftigs sequences with more than 200 bp of each sample were selected to predict genes at the MetaGeneMark database (Zhu et al., 2010), and then we identified the open reading frames and obtained the predicted protein sequences. CD-HIT (Cluster Database at High Identity With Tolerance) (Fu et al., 2012) was used to classify the obtained protein sequences based on 90% sequence similarity and to remove redundancy, and the longest sequence was selected as the representative sequence to obtain the non-redundant protein sequence sets. We used Soap.coverage (soap.genomics.org.cn/) to determine the relative abundance of each protein of each sample. By comparing the protein sequence sets with the Kyoto Encyclopedia of Genes and Genomes (KEGG) Pathway Database (Kanehisa et al., 2004), the proteins predicted by the MetaGeneMark database could be annotated and classified. In brief, the non-redundant protein sequence sets were uploaded to KEGG Automatic Annotation Server for functional annotation (in "GENES data set," partially select "for Prokaryotes"; the rest of the parameters are default), and the returned annotation results were summarized so that the annotation results at each classification level and their corresponding relative abundance were obtained. And then we obtained the relative abundance distribution of each functional classification level at each sample in the KEGG database using QIIME software. The enrichment analysis results were obtained by hypergeometric distribution in the SciPy by a two-tailed *t*-test against KEGG Orthology (KO) functional groups, and the FDR was controlled.

Statistical Analysis

Relative abundances of the non-eukaryotic KO gene were calculated by normalizing all the KOs of each sample to sum to 1. Observation matrix tables containing relative abundance information of KOs were used to calculate Euclidean distance based on UPGMA algorithm, and principal coordinates analysis plot was built using the R data analysis package. The entire visualized figures were drawn by an R package. The test of significance based on a two-tailed *t*-test was performed to determine whether there was a significant difference in abundance of the gene between different diet groups by using GraphPad Prism 5 software (GraphPad Software, Inc., United States).

RESULTS

Data Quality and Diversity Analysis

All DNA samples of 13 nasopharyngeal swab samples were qualified to be added to Illumina HiSeq 2500 high-throughput sequencing platform. Then, the total metagenomic DNA was randomly interrupted into short clips, which were subjected to paired-end sequencing (2×250 bp) for library construction. A total of 678,219,000 raw paired-end reads were generated, and the average proportion of these sequences with high-quality reads in each sample was 99.86 ± 0.01. Quality control analysis showed that the assembled sequences were of high accuracy, which made subsequent analysis results reliable enough. The detailed indexes of quality control are shown in **Supplementary Table 1A**.

In the rarefaction curve, before reaching 18,000, the rarefaction curves of 13 samples all fractured and trended to flatten out, indicating that the sequencing depth was sufficient to reveal their microorganism composition (**Figure 1A**). We performed principal component analysis (PCA, Euclidean distance) against all species of 13 samples. It was found that although there were differences among the 13 samples, they could be roughly clustered into two populations (pink and reseda areas) (**Figure 1B**). A similar result was also found in the PCA of KO analysis (**Supplementary Figure 1A**).

Then, we calculated the Shannon diversity index of all 13 samples and visualized the average means of each group using an R package (**Supplementary Table 1B** and **Figure 1C**). There was no significant difference between the control group and mild DR group ($p > 0.05$); the Shannon index of the control group was significantly higher than that of the excessive DR group ($p < 0.05$), and the Shannon index of the mild DR group was extremely higher than the excessive DR group ($p < 0.01$). The detailed statistical data of diversity indexes are shown in **Supplementary Table 1B**. We also analyzed the rank abundance curves of all 13 samples (**Figure 1D**). Unlike what the Shannon index indicated, it was found that both the richness and evenness of the control group were higher than those of the mild DR group ($p < 0.05$).

Functional Annotation Analysis

The predicted relative abundance of all KOs of each sample is shown in **Supplementary Table 2**. We visualized the top 20 KOs with the highest average abundance of each group using the R software. In the control group, K07316 (mod, adenine-specific DNA methyltransferase) was the most dominant KO followed by K03168 (top A, DNA topoisomerase I); in the mild DR group, the abundance of K03168 increased and became the most abundant, whereas the abundance K07316 decreased; in the excessive DR group, the abundance of K07316 and K03168 both significantly increased; K07316 became the most abundant KO again and followed by K03168 (**Supplementary Figure 2**). Then we compared the average relative abundance of the same KOs among different groups. The relative abundance of K07316 and K03168 significantly changed ($p < 0.05$), whereas the other KOs (within the top 20) did not significantly change ($p > 0.05$) (**Figure 2A**). The detailed data of the predicted

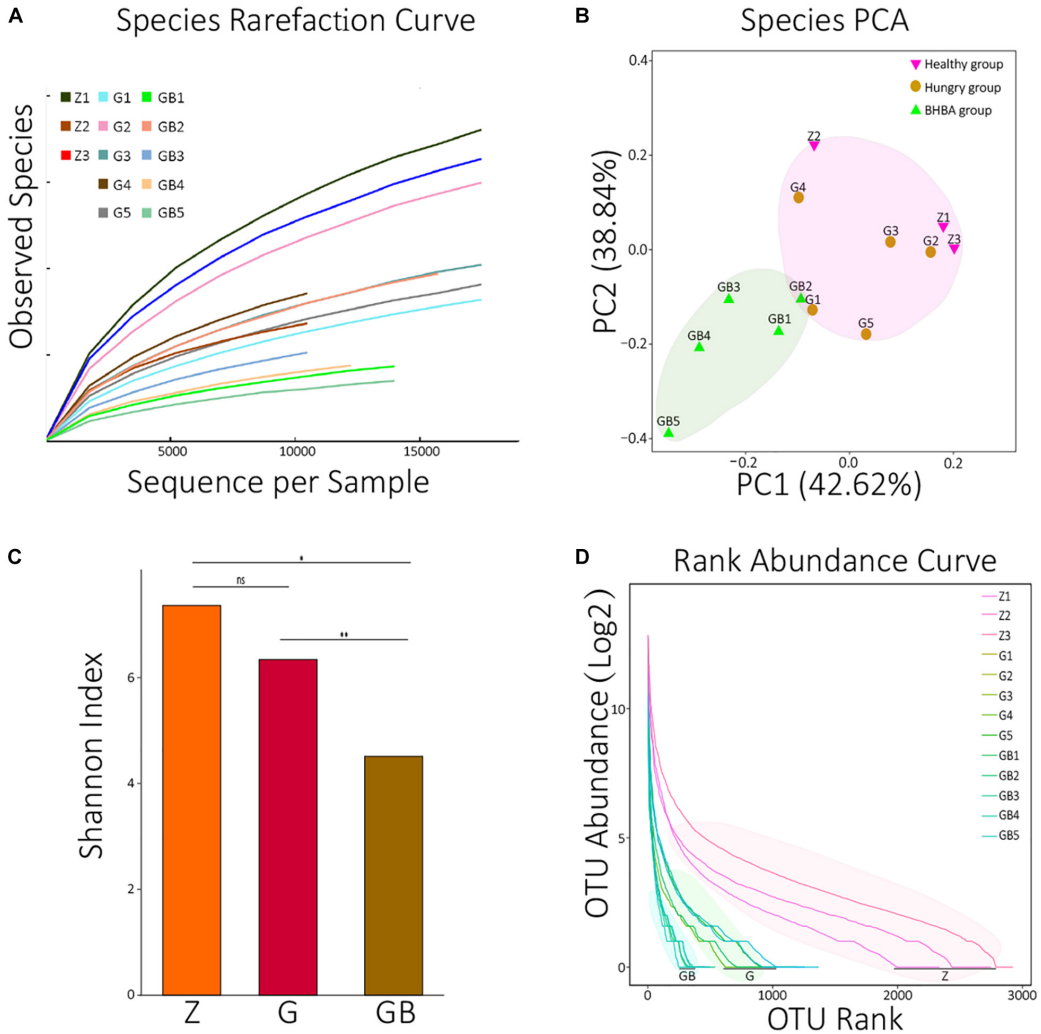

FIGURE 1 | Data processing and diversity analyses. **(A)** Species rarefaction curves of 13 samples. X: number of randomly selected sequences in each sample, Y: species number observed at corresponding depth. The curvature of the curve represents the possibility that observes new species, the smoother curves, the lower probability of observing new species, and the deeper sequencing depth. **(B)** PCA (principal component analysis) of species in each sample. The distance between the two samples represents the significance of the difference between them. **(C)** The average means of Shannon diversity index of each group. ns: non-significant, $p > 0.05$; *$0.01 < p < 0.05$; **$p < 0.01$. **(D)** The rank abundance curves of each sample at the species level. X: taxon arranged in the order of abundance at the species level, Y: the Log2 means which translated from the relative abundance of each species in the corresponding sample. The length of the curve represents the richness of each sample; the curvature of the curve represents the evenness of each sample. OTUs: operational taxonomic units; two sequences with >97% similarity at the species level were defined as the same OTU.

relative abundance of all KEGG third-level pathways of each sample are shown in **Supplementary Table 3**. We also visualized the top 20 KEGG third-level pathways with the highest average abundance of each group using an R software (**Figure 2B**), and it is difficult to sum up the changing patterns induced by DR among the three groups at KEGG third-level pathways. Then KEGG enrichment analysis was also performed to analyze the differences of KEGG second-level pathways among the groups. We obtained six enriched third-level pathways between the control group and the mild DR group, eight enriched third-level pathways between the mild DR group and the excessive DR group, and 11 enriched third-level pathways between the control group and the excessive DR group ($p < 0.05$) (**Table 1**). At last, we also visualized the average abundance of 6 KEGG first-level pathways of each group (**Figure 2C**). Interestingly, the average abundance of the disease pathway of the excessive DR group was significantly higher than the mild DR group ($p < 0.05$), but other pathways did not significantly change ($p > 0.05$).

Species Composition Annotation Analysis

At the species level, 4,271 microbial taxa were detected in all three groups, and the detailed relative abundance data at the species level in each sample are shown in **Supplementary Table 4**. We counted the average number of detected species in each group

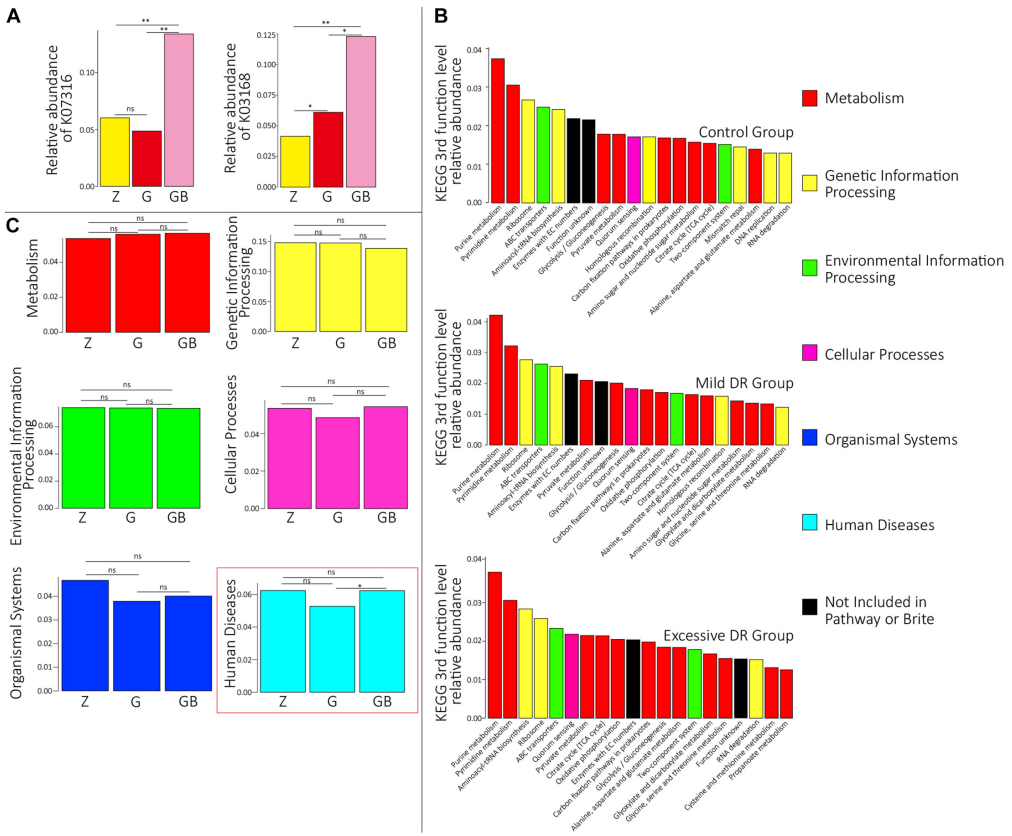

FIGURE 2 | Protein functional annotation analysis. **(A)** KOs with a significant difference in the relative abundance between groups. *Z* for the control group, G for the mild DR group, GB for the excessive DR group. ns: non-significant, *0.01 < p < 0.05, **p < 0.01. **(B)** The top 20 KEGG third-level pathways with the highest average relative abundance of each group, different colors in the legend indicate different KEGG first-function-level pathways. **(C)** The difference of relative abundance of each of six KEGG first-function-level pathways among groups. *Z* for the control group, G for the mild DR group, GB for the excessive DR group. ns: non-significant, $p > 0.05$; *0.01 < p < 0.05.

and found that the number of detected species was significantly lower in the excessive DR group than in the other two groups ($p < 0.05$) and the species number of the mild DR group also significantly lower than in the control group ($p < 0.05$) (**Figure 3A**). At the phylum level, the top four phyla with the highest average relative abundance in each group were identified (**Figure 3B**), and their variations among the groups were analyzed (**Figure 3C**). In the control group, *Proteobacteria* was the most dominant phylum, followed by *Firmicutes*, *Bacteroidetes*, and *Actinobacteria*; in the mild DR group and excessive DR group, *Proteobacteria* was also the most dominant phylum and followed by *Firmicutes*, *Actinobacteria*, and *Bacteroidetes*. It is found that the abundance of *Bacteroidetes* varied most significantly ($p < 0.05$), the abundance of *Proteobacteria* showed a trend of variation ($p < 0.07$) between the control group and excessive DR group, and the abundance of *Firmicutes* and *Actinobacteria* did not differ significantly among groups ($p > 0.05$). The detailed relative abundance data of each sample are shown in **Supplementary Table 5**. To analyze the species composition more intuitively, we visualized the top 20 species with the highest relative abundance of each group (**Figures 3B,E**). *Clostridium botulinum* was the most dominant species in the control group and mild DR group, whereas *Photorhabdus laumondii* was the most dominant species in the excessive DR group (**Figures 3B,E**). The abundance of other species was distinctly decreased in the mild DR group (G: 45% vs. Z: 69%) and excessive DR group (GB: 25% vs. Z: 69%) (**Figure 3E**). And to analyze the difference in species composition among groups, we compared the average relative abundance of the same species among different groups (a total of 34 different kinds of top 20 abundant species in all three groups) (**Supplementary Figure 3A**). We identified five species, which significantly changed among three groups: *P. laumondii*, *Avibacterium paragallinarum*, *Babesia bigemina*, *Pseudomonas stutzeri*, and *Neisseria* sp. 10022 (**Supplementary Figure 3A**); 7 of these 34 species were at present in all three groups of top 20 abundant species: *C. botulinum*, *P. laumondii*, *Corynebacterium maris*, *Bacteroides heparinolyticus*, *Neisseria* sp. 10022, *Corynebacterium vitaeruminis*, and *Moraxella bovoculi* (**Figure 4B** and **Supplementary Figure 3B**), which might be "the core bacteria" for the yak nasopharynx microbial community. We also detected the species number of viruses in each group and their average relative abundance (**Supplementary Table 6** and **Figure 3D**). The average species number of viruses detected in the mild DR group and excessive DR group was much lower than that

in the control group (8, 9, and 23, respectively) (**Supplementary Table 6**). However, the average relative abundance of detected virus in the mild DR group was extremely lower than that in the control group ($p < 0.01$), and the average relative abundance of the excessive DR group was extremely higher than that in the mild DR group ($p < 0.01$), whereas the average relative abundance in the excessive DR group was significantly higher than that in the control group ($p < 0.05$) (**Supplementary Table 6** and **Figure 3D**). Meanwhile, to analyze the abundance variation among groups more generally, we also performed a cluster analysis for the top 50 species with the highest significance ($p < 0.05$) of variation and drew a heat map to visualize the results (**Figure 3F** and **Supplementary Table 7**). Against the control group, mild DR significantly altered 18 species (4 were decreased, 14 were increased); against the control group, excessive DR significantly decreased 47 of the 50 species and significantly increased the other 3 of them, and against the mild DR group, excessive DR significantly decreased 44 of the 50 species and increased the other 6 of them. It is worth noting that there were two alteration patterns: one is that the species alteration induced by 7 days of DR quickly recovered after 2 days of BHBA intravenous injection treatment (P1 and P2 in **Supplementary Figure 3A**); the other one is that the species alteration induced by 7 days of DR was further enhanced after

TABLE 1 | The results of KEGG enrichment analysis.

Group	Pathway	Pathway name	KEGG level 1	KEGG level 2
Control group vs. mild DR group	ko99984	Nucleotide	Not included in pathway or BRITE	Unclassified: metabolism
	ko00965	Betalain biosynthesis	Metabolism	Biosynthesis of other secondary metabolites
	ko04614	Renin-angiotensin system	Organismal Systems	Endocrine system
	ko00240	Pyrimidine metabolism	Metabolism	Nucleotide metabolism
	ko04622	RIG-I–like receptor signaling pathway	Organismal Systems	Immune system
	ko00910	Nitrogen metabolism	Metabolism	Energy metabolism
Mild DR group vs. excessive DR group	ko00010	Glycolysis/gluconeogenesis	Metabolism	Carbohydrate metabolism
	ko00750	Vitamin B6 metabolism	Metabolism	Metabolism of cofactors and vitamins
	ko00520	Amino sugar and nucleotide sugar metabolism	Metabolism	Carbohydrate metabolism
	ko00350	Tyrosine metabolism	Metabolism	Amino acid metabolism
	ko00340	Histidine metabolism	Metabolism	Amino acid metabolism
	ko99997	Function	Not included in pathway or BRITE	Poorly characterized
	ko00780	Biotin metabolism	Metabolism	Metabolism of cofactors and vitamins
	ko99976	Replication	Not included in pathway or BRITE	Unclassified: gene□c information processing
Control group vs. excessive DR group	ko00760	Nicotinate and nicotinamide metabolism	Metabolism	Metabolism of cofactors and vitamins
	ko00590	Arachidonic acid metabolism	Metabolism	Lipid metabolism
	ko04918	Thyroid hormone synthesis	Organismal Systems	Endocrine system
	ko05133	Pertussis	Diseases	Infectious diseases: bacterial
	ko00523	Polyketide sugar unit biosynthesis	Metabolism	Metabolism of terpenoids and polyketides
	ko00520	Amino sugar and nucleotide sugar metabolism	Metabolism	Carbohydrate metabolism
	ko00521	Streptomycin biosynthesis	Metabolism	Biosynthesis of other secondary metabolites
	ko00051	Fructose and mannose metabolism	Metabolism	Carbohydrate metabolism
	ko00480	Glutathione metabolism	Metabolism	Metabolism of other amino acids
	ko00720	Carbon fixation pathways in prokaryotes	Metabolism	Energy metabolism
	ko00020	Citrate cycle (TCA cycle)	Metabolism	Carbohydrate metabolism

DR, dietary restriction; KO, KEGG Orthology.

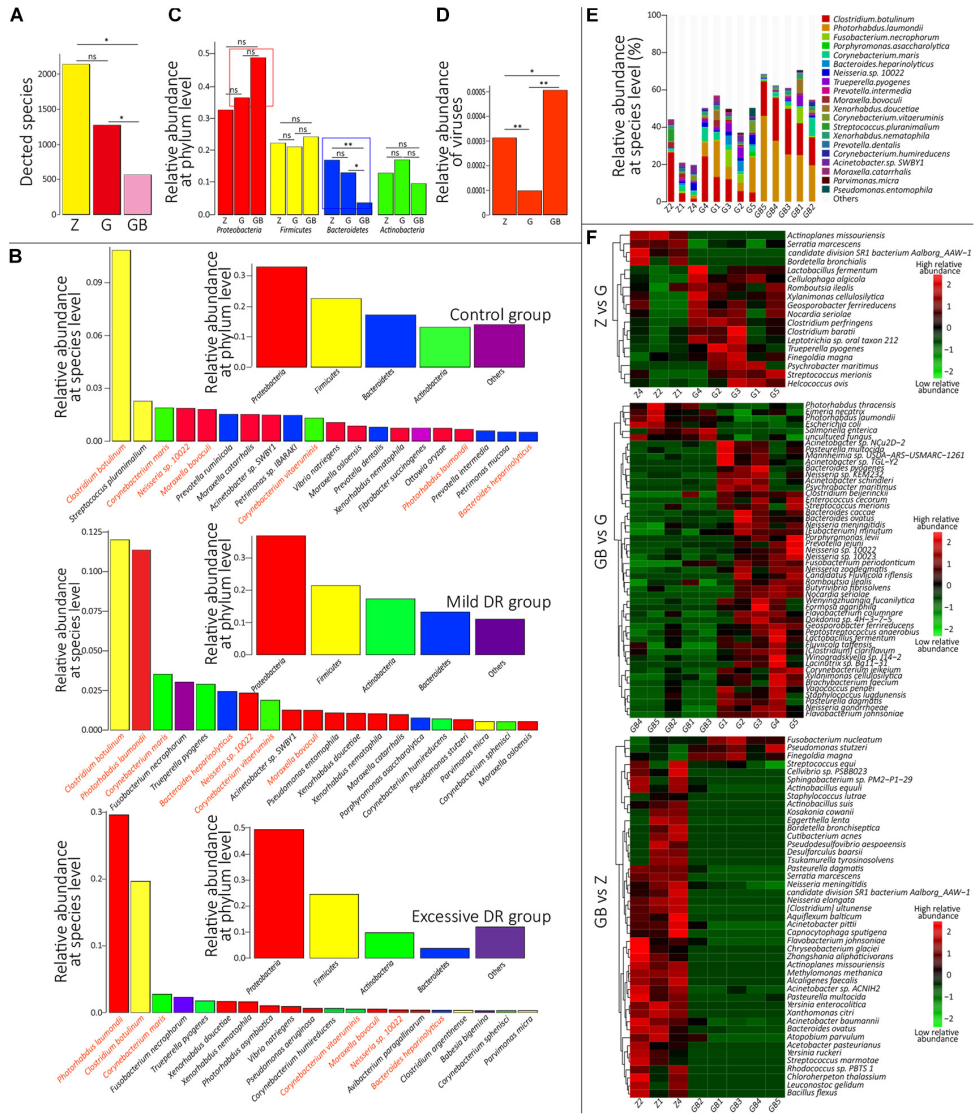

FIGURE 3 | Species annotation analysis. **(A)** The average detected species number of each group. *Z* for the control group, G for the mild DR group, GB for the excessive DR group. ns: non-significant, $p > 0.05$; *$0.01 < p < 0.05$. **(B)** Inner: Top four dominant phyla with the highest average relative abundance in each group. Outer: The top 20 dominant species with the highest average relative abundance in each group. Species with the same color belong to the phyla with the corresponding color. Species name marked by orange means "core species." **(C)** The difference of average relative abundance of each of four dominant phyla in each group. *Z* for the control group, G for the mild DR group, GB for the excessive DR group. ns: non-significant, *$0.01 < p < 0.05$; **$p < 0.01$. **(D)** The difference of average relative abundance of the detected virus number in each group. *Z* for the control group, G for the mild DR group, GB for the excessive DR group. ns: non-significant, *$0.01 < p < 0.05$; **$p < 0.01$. **(E)** The top 20 dominant species with the highest average relative abundance in each sample and their percentages, *Z* for the control group, G for the mild DR group, GB for the excessive DR group. **(F)** Heat map shows the top 50 species with the highest significance among groups. *Z* for the control group, G for the mild DR group, GB for the excessive DR group. Red indicates that the species has higher relative abundance, whereas green indicates that the species has lower relative abundance. The value is the result of the *Z* scoring of species relative abundance; the bigger value of color, the higher relative abundance.

2 days of BHBA intravenous injection treatment (P3 and P4 in **Supplementary Figure 3A**).

Microbial Interactions Prediction Analysis

To understand the interrelationships among these microorganisms in each group, we constructed co-connection networks of the top 50 species with the most dominant abundance in each group, and the results showed that the species interconnection within the control group was tighter than the mild DR group or excessive DR group (**Figure 4A**). Interestingly, most of these species had a positive correlation with each other (red line), whereas only a few of these species had a negative correlation with other species (green line). In the control group, there were four dominant teams (marked

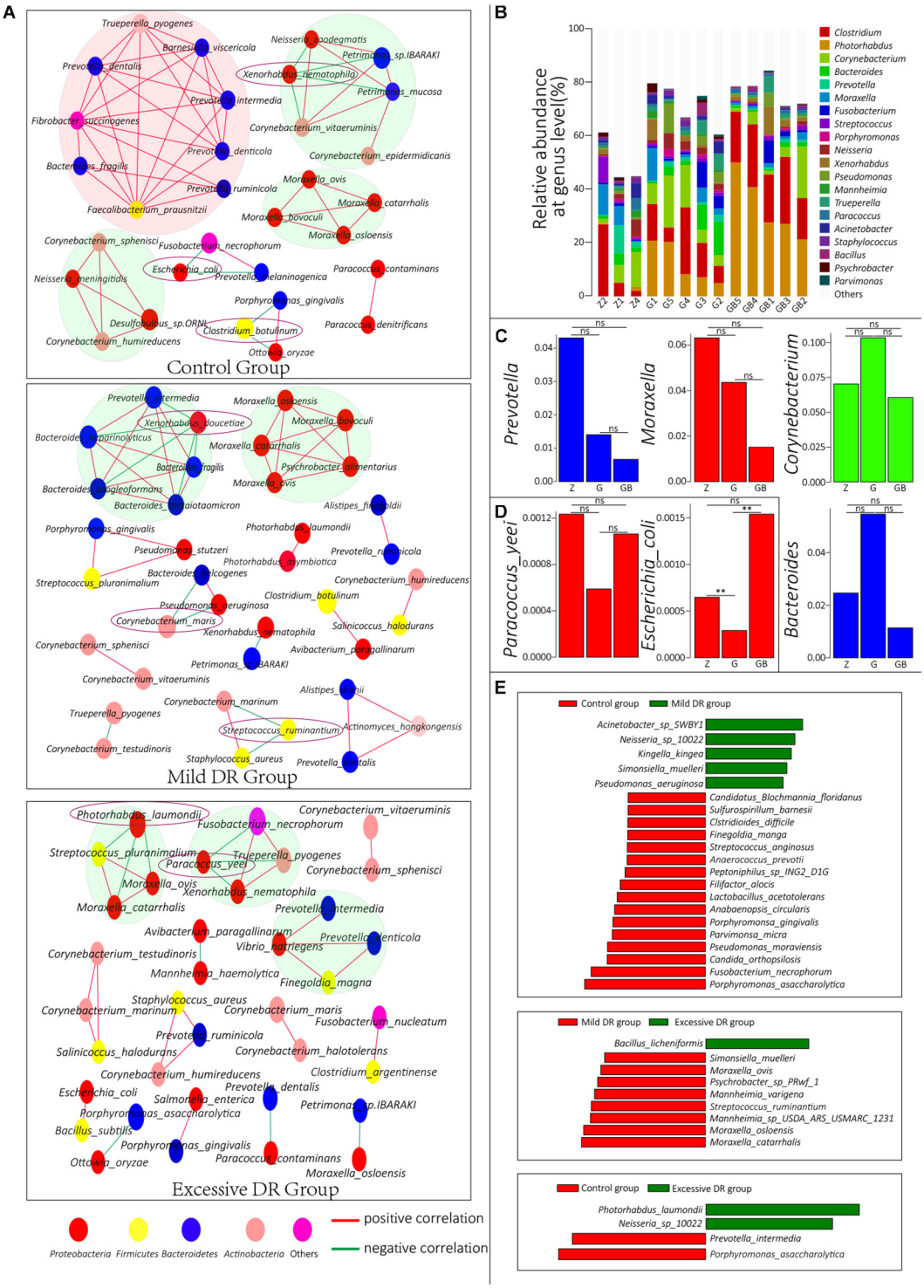

FIGURE 4 | (A) Co-correlation network of the top 50 species with the highest average relative abundance in each group. One circle indicates one species, and the species with the same color belong to a phylum with the corresponding color. **(B)** The top 20 dominant phyla with the highest average relative abundance in each sample and their percentages, *Z* for the control group, G for the mild DR group, GB for the excessive DR group. **(C,D)** The difference of average relative abundance of some key species and genus in each group, *Z* for the control group, G for the mild DR group, GB for the excessive DR group. ns: non-significant; $^{*}0.01 < p < 0.05$; $^{**}p < 0.01$. **(E)** Linear discriminant analysis (LDA) effect size (LEfSe) analysis between groups. The red square indicates that the relative abundance increased, and the green square indicates that the relative abundance decreased. The length of the square indicates the magnitude of significance.

by big circles), which mainly consisted of genus *Prevotella*, *Moraxella*, and *Corynebacterium*. Within these 50 species, *Xenorhabdus nematophila*, *Escherichia coli*, and *C. botulinum* had a negative correlation with other species and could be regarded as "key species." In the mild DR group, similarly, there were two dominant teams, which were mainly composed of genus *Bacteroides* and *Moraxella*. *Xenorhabdus doucetiae*, *C. maris*, and *Streptococcus ruminantium* were the "key species." In the excessive DR group, there were three dominant teams (no major genera); *P. laumondii* and *Paracoccus yeei* were the "key species." We also counted and visualized the top 20 genera with the highest relative abundance of each sample. It was found that *Clostridium* was the most dominant genus in the control group, whereas *Photorhabdus* was the most dominant genus in the mild DR group and excessive DR group (**Figure 4B**). Then, we compared the average relative abundance of the same genus (**Figure 4C**) and the "key species" (**Supplementary Figure 3A** and **Figure 4D**), which was mentioned previously. It was found that these major genera did not significantly change ($p > 0.05$) among groups, but two kinds of "key species" had been significantly changed ($p < 0.05$) among groups: *P. laumondii* and *E. coli*. The detailed data are shown in **Supplementary Table 8** (Sheet 1). And finally, to find a biomarker species of each group, we performed a LEfSe analysis between groups and identified the five species with the most significant relative abundance difference as the biomarker species: *Acinetobacter* sp. SWBY1, *Porphyromonas asaccharolytica*, *Bacillus licheniformis*, *Moraxella catarrhalis*, and *P. laumondii* (**Figure 4E**).

DISCUSSION

In the present study, the influence of starvation on the nasopharyngeal microbiome was explored, and its potential mechanism was discussed. Metagenomic sequencing identified the four most dominant phyla: *Proteobacteria*, *Firmicutes*, *Bacteroidetes*, and *Actinobacteria*; five most dominant genera: *Clostridium*, *Bacteroides*, *Prevotella*, *Moraxella*, and *Streptococcus*; and the most dominant species: *C. botulinum*. From a protein perspective, starvation mainly affected K07316 and K03168, which were once discussed by Desirazu et al. (Rao et al., 2014) and Giovanni et al. (Capranico et al., 2017), respectively. From a species perspective, starvation mainly affected *Proteobacteria* and *Bacteroidetes* at the phyla level. Whereas mild DR affected some KOs and species but had no significant influence on the nasopharyngeal microbiota community, excessive DR significantly decreased the diversity of the community by affecting oral microorganisms, and disturbed their composition and structure, implying a higher risk of respiratory tract diseases.

Intravenous Injection of BHBA Simulates Severe DR

The 9 days of DR group (G) and BHBA intravenous injection group (GB) represented short-term mild DR and long-time excessive DR, respectively. Generally, animals would go through three stages as the degree of starvation increases. First, when an animal cannot take sufficient food in, it will use stored glycogen or synthesize glucose by gluconeogenesis to maintain a certain concentration of blood glucose that supplies the necessary energy for some essential physiological functions. Yu et al. (2016) and Zou et al. (2019) found that in the first 9 days of starvation, the blood glucose concentration in the yak would significantly decrease immediately and then remains stable. Second, when the stored glycogen runs out, the animal body will break fat down to provide energy. BHBA, the main product of fat catabolism, is preferentially utilized by the brain and nervous system (Prince et al., 2013). Zou et al.s' (2020) had confirmed that BHBA intake after 7 days of starvation significantly increased the blood BHBA concentration in yaks. For instance, in the perinatal period, cows often experience ketoacidosis due to large amounts of fat catabolism induced by severe nutrient deficiency (Suthar et al., 2013). The main characteristics of ketoacidosis are the high concentration of BHBA and low concentration of blood glucose (Frise et al., 2013; Jezek et al., 2017; McIntyre et al., 2019). Third, when the fat runs out, proteins in the animal tissues will begin to be degraded, which can lead to serious consequences, even death. Hence, BHBA intravenous injection treatment was performed using the same procures as Zou et al.s' (2020) experiment of Zou and was similar to that induced by long-term starvation or lactation.

Mild Starvation Slightly Affects the Microbial Community of the Nasopharynx Probably by Altering the Oral Microbiota and Mucosal Mucins

Because we controlled environmental factors, the mucosal immune system of the host and available energy resources are the two major internal factors that determine the homeostasis of the nasopharyngeal microbial community (Brugman and Nieuwenhuis, 2010; David et al., 2014). The enrichment analysis results showed that the expression level of the immune system, nucleotide metabolism, and secondary metabolites pathways in the mild DR group were significantly down-regulated when compared with the control group, indicating that mild DR affected the proliferation and metabolism of the community. And the changes in energy metabolism also indicated that their energy source had changed (**Table 1**). Besides there was a more complex network consisting of *Prevotella* in the control group (**Figure 4A**). *Prevotella* mainly exists in the digestive system and absorbs nutrients by breaking down cellulose (Suthar et al., 2013; Kovatcheva-Datchary et al., 2015). But this network faded away gradually as the DR level increased (**Figure 4A**). Although it is insignificant, the relative abundance of genus *Prevotella* was decreased in both the mild DR group and excessive DR group when compared to the control group (**Figure 4C**).

Because of the topographical continuity between the oral cavity and nasopharynx, the microorganisms of the oral cavity can spread to the nasopharynx (Charlson et al., 2011). Considering the main nutrient source of *Prevotella*

is fiber (Kovatcheva-Datchary et al., 2015), which comes from fodder, we speculated that the decrease of *Prevotella* relative abundance in the oral cavity induced by DR led to its decrease in the nasopharynx. When yaks cannot take in fodder or pasture, *Prevotella* in the oral cavity cannot obtain fiber, leading to the abundance of oral *Prevotella* decrease, and so does the nasopharynx *Prevotella*. Also, *P. asaccharolytica*, the common oral cavity bacteria, was the common biomarker (**Figure 4E**) for the control group against both the mild DR group and excessive DR group, also indicating that oral microorganisms had a tighter connection with nasopharyngeal bacteria.

It was also shown that the relative abundance of some other species increased in the mild DR group, such as *Clostridium* and *Photorhabdus*, which are resident bacteria in cattle respiratory tracts (Holman et al., 2015; Lima et al., 2016). In the mild DR group, the blood glucose concentration was very low, indicating a decrease in mucosal mucin secretion and insufficient mucosal immune function to manage the microbiota (Marcos et al., 2003). Frenkel and Ribbeck (2017) found that salivary mucins affected the bacterial viability by promoting a less competitive growth mode, and Flynn et al. (2016) confirmed that *Pseudomonas aeruginosa* could degrade mucins into nutrients, and mucins are essential for some pathogens. Therefore, we thought that the decrease of normal fiber-degrading oropharynx bacteria would empty the ecological niche in the nasopharynx. The empty ecological niche could provide suitable proliferation resources for those mucin-degrading bacteria and pathogens, resulting in those already decreased mucins being further consumed. Finally, the homeostasis of the nasopharyngeal microbial community would be destroyed.

The co-connection network results also showed that DR mainly affected the team in the pink big circle. *Faecalibacterium prausnitzii*, which is a widely accepted probiotic for humans (Ferreira-Halder et al., 2017; Lopez-Siles et al., 2017), and the five other commensal oral fiber-degrading bacteria: *Prevotella dentalis*, *Fibrobacter succinogenes*, *Prevotella ruminicola*, *Prevotella denticola*, and *Prevotella intermedia* (Kobayashi et al., 2008), consisting of the main team in the control group. And the three biomarkers species, *Acinetobacter* sp. SWBY1, *P. asaccharolytica*, and *B. licheniformis*, also were common oral bacteria.

Taking all these evidence into account, two change patterns were concluded. First, oropharynx-derived microorganisms and their collaborators have decreased. Second, microorganisms competing for the ecological niche with oropharyngeal microbiota and microorganisms inhibited by mucins have increased.

Excessive DR Significantly Altered the Homeostasis of the Nasopharyngeal Microbial Community Because of the Presence of BHBA

BHBA treatment significantly decreased the diversity and affected the homeostasis of the nasopharyngeal microbial community. Compared with the control group, the pathways of energy metabolism, secondary metabolites biosynthesis, and carbon fixation in the excessive DR group were changed in a wider range than those in the mild DR group (**Table 1**), indicating that excessive DR had a stronger influence on the community function. By combining the data of both the mild DR group and excessive DR group, we concluded four alteration patterns: after 2 days of BHBA intravenous injection treatment, the increase and decrease that induced by 7 days of DR were recovered or were further enhanced (**Supplementary Figure 3A**). Yaks in the mild DR group and excessive DR group were treated with the same operations, except that those in the excessive DR group were treated with intravenous infusion of BHBA instead of normal saline. Therefore, we speculated that the presence of BHBA was the reason for the diversity decreasing and homeostasis alteration in the excessive DR group. Like subclinical ketosis, BHBA treatment increased not only the glucose concentration but also the BHBA concentration in blood (Andersson, 1988; Sturm et al., 2020) and resulted in increased ketone bodies in the exhalant gas (Dobbelaar et al., 1996), which could be used as nutrients by some bacteria. Schulz et al. (2015) found that cows with subclinical ketosis showed an enhanced immune response when compared with metabolically healthy individuals. Zou et al.s' (2020) study also confirmed that BHBA treatment recovered the concentration of blood sugar. This enhanced immune response and recovered blood glucose indicated that BHBA treatment recovered the immune system and the secretion of mucosal mucins, inhibiting those bacteria without mucin resistance. Because the lack of fodder and pasture doesn't recover, the decrease of normal oropharynx fiber-degrading bacteria continuous, and then this empty ecological niche would be occupied by those bacteria which could utilize mucins or ketone bodies as energy resources. Ketones and mucins improved the proliferation of some bacteria, while the enhanced immune response inhibited the proliferation of some others, which resulted in these four alteration patterns mentioned previously (**Supplementary Figure 3A**). Therefore, BHBA, which is a more efficient energy resource, replenished the energy needs of the DR yaks and enhanced the immune system, but did not alter the lack of normal oropharynx bacteria, finally resulting in the extremely complex alterations and these significant influences.

Excessive DR Increased the Risk of Respiratory Diseases

From a protein perspective, excessive DR down-regulated the biosynthesis metabolism of streptomycin, which has a powerful antibacterial effect (Schatz et al., 2005). Otherwise, excessive DR up-regulated bacterial infection-related pathways such as pertussis (de Gouw et al., 2011), which is a common bovine respiratory disease, and the up-regulated KEGG first-level pathway in the diseases (KEGG BRITE: 08402) (**Figure 2C**). All these results indicated that BHBA treatment increased the risk of diseases including respiratory tract diseases. The same conclusion can be drawn from the view of observed species alteration. Excessive DR treatment significantly decreased the microbial diversity, which means the risks of respiratory flora disorders

and respiratory diseases were increased (Koppen et al., 2015; Dickson et al., 2016; Man et al., 2017; Zeineldin et al., 2019). BHBA treatment also increased the relative abundance of *Proteobacteria* (**Figure 3C**), which is considered as a common factor of inflammation and lung diseases (Rizzatti et al., 2017). Correlation network analysis (**Figure 4A**) results showed that excessive DR destroyed the microbial community interrelationship in the control group, and this disorder was thought to contribute to respiratory diseases (Koppen et al., 2015; Zeineldin et al., 2019). Our results showed that BHBA treatment increased the relative abundance of *Pseudomonas Acinetobacter*, *Bacillus*, *Bacteroides*, *Clostridium*, and *Enterococcus*, which are common bovine respiratory pathogens (Klima et al., 2019). Moreover, BHBA treatment significantly increased the relative abundance of viruses (including bacteriophage) and decreased their kind number (**Supplementary Table 6**), indicating that BHBA treatment increased the risk of respiratory diseases. All these evidences indicated that BHBA treatment could increase the risk of respiratory diseases.

Furthermore, those "key species" negatively correlated with most of the other species (within the top 50); it was speculated that these species might play an important role in maintaining the homeostasis of the nasopharyngeal microbial community. *F. prausnitzii* and other *Prevotella* bacteria, which formed the biggest connection network in the control group, were considered to be probiotics by some researchers (Ley, 2016; Lopez-Siles et al., 2017). They and those biomarkers of the control group might be useful in the prevention and treatment of bovine respiratory diseases. Nevertheless, further evidence is still needed.

CONCLUSION

In summary, although we simulated excessive DR by using BHBA intravenous injection treatment instead of really testing excessive starvation, the present study was sufficient to confirm that starvation would affect the composition, function, and diversity of the yak nasopharyngeal microbial community. Starvation mainly affected *Bacteroidetes* and *Proteobacteria* at the phylum level, whereas *P. laumondii*, *A, paragallinarum*, *B. bigemina*, *P. stutzeri*, and *Neisseria* sp. 10022 at the species level. The influence of mild starvation was insignificant. Excessive starvation affected the oral microorganisms and mucosal mucins, and significantly disturbed the nasopharynx microbiome, and increased the risk of respiratory diseases. These results could enrich our knowledge of the respiratory tract microenvironment and provide us with new strategies for respiratory disease prevention and treatment. However, because of the lack of longitudinally following these yaks, physiological data, and the limitation of sample size, further experiments are still required.

DATA AVAILABILITY STATEMENT

The datasets presented in this study can be found in online repositories. The names of the repository and accession number can be found below: NCBI SRA database; accession number is PRJNA681085.

ETHICS STATEMENT

The animal study was reviewed and approved by Institutional Animal Care and Use Committee of Sichuan Agricultural University.

AUTHOR CONTRIBUTIONS

JQ, ZW, and ZZ conceived and designed the experiments. JQ, HZ, ZZ, and YC performed the experiments. JQ, YC, ZZ, and DC analyzed the data and wrote the manuscript. All authors critically reviewed the manuscript.

FUNDING

This work was supported by the National Key Research and Development Project (2018YFD0501800), Sichuan Science and Technology Program (2018NZ0002 and 2019YFQ0012), and the Sichuan Beef Cattle Innovation Team of National Modern Agricultural Industry Technology System (No. DKYB20100805). The authors thank Dr. Siyuan Zhang for their help with the supporting of R software technique and graphics beautification.

SUPPLEMENTARY MATERIAL

The Supplementary Material for this article can be found online at: https://www.frontiersin.org/articles/10.3389/fmicb.2020.630280/full#supplementary-material

Supplementary Figure 1 | (A) The PCA (principal component analysis) of KEGG Orthology (KO). Fifteen samples can be roughly clustered into two groups (pink and reseda) like species PCA. **(B)** The flowchart of procedures in the experiment before sampling.

Supplementary Figure 2 | The average relative abundance of top 20 KOs with the highest relative abundance in each group.

Supplementary Figure 3 | (A) The difference of average relative abundance of 34 top 20 species, which occurred in all three groups. Species with the same color belong to the phyla with the corresponding color like Figure 4. Z for the control group, G for the mild DR group, GB for the excessive DR group. ns: non-significant, $p > 0.05$; *$0.01 < p < 0.05$. Marking by the red square means the difference was significant. The yellow line divided these 34 species into four groups according to their changing rule. P1: pattern 1, BHBA treatment enhanced the increase of relative abundance; P2: pattern 2, BHBA treatment enhanced the decrease of relative abundance; P3: pattern 3, BHBA recovered the decrease of relative abundance; P4, pattern 4, BHBA treatment recovered the increase of relative abundance. **(B)** Venn diagram analysis of 34 top 20 species of three groups. Red words indicate that the relative abundance of this species increased; purple words indicate that the relative abundance of this species decreased. The overlapping parts of the circles represent the species that are shared in corresponding groups.

Supplementary Table 1 | (A) Statistical table of reads data. N (%): the ratio of fuzzy bases to total bases; GC (%): the ratio of G and C bases to total bases; Q20 (%): the proportion of bases with accuracy above 99% to total bases; Q30 (%): the proportion of bases with accuracy above 99.9% to total bases; HQ reads (%): the percentage of high-quality sequences in the raw sequences; HQ data (%): the percentage of bases in high quality-sequences to the bases in raw sequences.

(B) The detailed Simpson index, Chao1 index, ACE index, and Shannon index of each sample and their average means of each group.

Supplementary Table 2 | Detailed relative abundance of KOs of each sample.

Supplementary Table 3 | Detailed relative abundance of all KEGG third-level pathways of each sample.

Supplementary Table 4 | Detailed relative abundance of every species of each sample.

Supplementary Table 5 | Detailed relative abundance data at the phyla level of each sample.

Supplementary Table 6 | Detailed relative abundance data of detected viruses of each group.

Supplementary Table 7 | Detailed relative abundance data of top 50 species significantly changed species.

Supplementary Table 8 | (A) Detailed relative abundance data at the genus level of each sample. **(B)** Detailed statistical information of contigs/scaffolds. Length of N20/50/90: arranges all the assembled contigs/scaffolds sequences in order of length from long to short and then added from long to short. When the addition length reaches 20%/50%/90% of the total length of contigs/scaffolds sequences, the corresponding length of the last series will be the length of N20/50/90.

REFERENCES

Anand, S., and Mande, S. S. (2018). Diet, microbiota and gut-lung connection. *Front*. Microbiol. 9: 214. doi: 10.3389/fmicb.2018.02147

Andersson, L. (1988). Subclinical ketosis in dairy cows. *Vet. Clin. North Am. Food Anim. Pract.* 4, 233–251. doi: 10.1016/s0749-0720(15)31046-x

Bassis, C. M., Erb-Downward, J. R., Dickson, R. P., Freeman, C. M., Schmidt, T. M., Young, V. B., et al. (2015). Analysis of the upper respiratory tract microbiotas as the source of the lung and gastric microbiotas in healthy individuals. *mBio* 6:e00037-15. doi: 10.1128/mBio.00037-15

Belkhou, R., Cherel, Y., Heitz, A., Robin, J.-P., and Le Maho, Y. (1991). Energy contribution of proteins and lipids during prolonged fasting in the rat. *Nutr. Res.* 11, 365–374. doi: 10.1016/s0271-5317(05)80312-4

Benjamini, Y., and Hochberg, Y. (1995). Controlling the false discovery rate–a practical and powerful approach to multiple testing. *J. R. Stat. Soc. Series B (Methodological)* 57, 289–300. doi: 10.2307/2346101

Bolger, A. M., Lohse, M., and Usadel, B. (2014). Trimmomatic: a flexible trimmer for Illumina sequence data. *Bioinformatics* 30, 2114–2120. doi: 10.1093/bioinformatics/btu170

Bosch, A., Levin, E., van Houten, M. A., Hasrat, R., Kalkman, G., Biesbroek, G., et al. (2016). Development of upper respiratory tract microbiota in infancy is affected by mode of delivery. *EBioMedicine* 9, 336–345. doi: 10.1016/j.ebiom.2016.05.031

Brugman, S., and Nieuwenhuis, E. E. (2010). Mucosal control of the intestinal microbial community. *J. Mol. Med. (Berl)* 88, 881–888. doi: 10.1007/s00109-010-0639-9

Cahill, G. F. Jr. (2006). Fuel metabolism in starvation. *Annu. Rev. Nutr.* 26, 1–22.

Caporaso, J. G., Kuczynski, J., Stombaugh, J., Bittinger, K., Bushman, F. D., Costello, E. K., et al. (2010). QIIME allows analysis of high-throughput community sequencing data. *Nat. Methods* 7, 335–336. doi: 10.1038/nmeth.f.303

Capranico, G., Marinello, J., and Chillemi, G. (2017). Type I DNA topoisomerases. *J. Med. Chem.* 60, 2169–2192. doi: 10.1021/acs.jmedchem.6b00966

Charlson, E. S., Bittinger, K., Haas, A. R., Fitzgerald, A. S., Frank, I., Yadav, A., et al. (2011). Topographical continuity of bacterial populations in the healthy human respiratory tract. *Am. J. Respir. Crit. Care Med.* 184, 957–963. doi: 10.1164/rccm.201104-0655OC

David, L. A., Maurice, C. F., Carmody, R. N., Gootenberg, D. B., Button, J. E., Wolfe, B. E., et al. (2014). Diet rapidly and reproducibly alters the human gut microbiome. *Nature* 505, 559–563. doi: 10.1038/nature12820

de Gouw, D., Diavatopoulos, D. A., Bootsma, H. J., Hermans, P. W., and Mooi, F. R. (2011). Pertussis: a matter of immune modulation. *FEMS Microbiol. Rev.* 35, 441–474. doi: 10.1111/j.1574-6976.2010.00257.x

Dhatariya, K. K., Glaser, N. S., Codner, E., and Umpierrez, G. E. (2020). Diabetic ketoacidosis. *Nat. Rev. Dis. Primers* 6:40. doi: 10.1038/s41572-020-0165-1

Dickson, R. P., Erb-Downward, J. R., Freeman, C. M., McCloskey, L., Falkowski, N. R., Huffnagle, G. B., et al. (2017). Bacterial topography of the healthy human lower respiratory tract. *mBio* 8:e02287-16. doi: 10.1128/mBio.02287-16

Dickson, R. P., Erb-Downward, J. R., Martinez, F. J., and Huffnagle, G. B. (2016). The Microbiome and the respiratory tract. *Annu. Rev. Physiol.* 78, 481–504.

Dobbelaar, P., Mottram, T., Nyabadza, C., Hobbs, P., Elliott-Martin, R. J., and Schukken, Y. H. (1996). Detection of ketosis in dairy cows by analysis of exhaled breath. *Vet. Q.* 18, 151–152. doi: 10.1080/01652176.1996.9694638

Faust, K., and Raes, J. (2012). Microbial interactions: from networks to models. *Nat. Rev. Microbiol.* 10, 538–550. doi: 10.1038/nrmicro2832

Ferreira-Halder, C. V., Faria, A. V. S., and Andrade, S. S. (2017). Action and function of *Faecalibacterium prausnitzii* in health and disease. *Best Pract. Res. Clin. Gastroenterol.* 31, 643–648. doi: 10.1016/j.bpg.2017.09.011

Flynn, J. M., Niccum, D., Dunitz, J. M., and Hunter, R. C. (2016). Evidence and role for bacterial mucin degradation in cystic fibrosis airway disease. *PLoS Pathog.* 12:e1005846. doi: 10.1371/journal.ppat.1005846

Frenkel, E. S., and Ribbeck, K. (2017). Salivary mucins promote the coexistence of competing oral bacterial species. *ISME J.* 11, 1286–1290. doi: 10.1038/ismej.2016.200

Frise, C. J., Mackillop, L., Joash, K., and Williamson, C. (2013). Starvation ketoacidosis in pregnancy. *Eur. J. Obstet. Gynecol. Reprod. Biol.* 167, 1–7. doi: 10.1016/j.ejogrb.2012.10.005

Fu, L., Niu, B., Zhu, Z., Wu, S., and Li, W. (2012). CD-HIT: accelerated for clustering the next-generation sequencing data. *Bioinformatics* 28, 3150–3152. doi: 10.1093/bioinformatics/bts565

Gilbert, J. A., Quinn, R. A., Debelius, J., Xu, Z. Z., Morton, J., Garg, N., et al. (2016). Microbiome-wide association studies link dynamic microbial consortia to disease. *Nature* 535, 94–103. doi: 10.1038/nature18850

Heck, K. L., van Belle, G., and Simberloff, D. (1975). Explicit calculation of the rarefaction diversity measurement and the determination of sufficient sample size. *Ecology* 56, 1459–1461. doi: 10.2307/1934716

Holman, D. B., Timsit, E., and Alexander, T. W. (2015). The nasopharyngeal microbiota of feedlot cattle. *Sci. Rep.* 5:15557.

Huson, D. H., Albrecht, B., Bagci, C., Bessarab, I., Gorska, A., Jolic, D., et al. (2018). MEGAN-LR: new algorithms allow accurate binning and easy interactive exploration of metagenomic long reads and contigs. *Biol. Direct.* 13:6. doi: 10.1186/s13062-018-0208-7

Huson, D. H., Mitra, S., Ruscheweyh, H. J., Weber, N., and Schuster, S. C. (2011). Integrative analysis of environmental sequences using MEGAN4. *Genome Res.* 21, 1552–1560. doi: 10.1101/gr.120618.111

Jezek, J., Cincovic, M. R., Nemec, M., Belic, B., Djokovic, R., Klinkon, M., et al. (2017). Beta-hydroxybutyrate in milk as screening test for subclinical ketosis in dairy cows. *Pol. J. Vet. Sci.* 20, 507–512. doi: 10.1515/pjvs-2017-0061

Kanehisa, M., Goto, S., Kawashima, S., Okuno, Y., and Hattori, M. (2004). The KEGG resource for deciphering the genome. *Nucleic Acids Res. (Database)* 32, D277–D280.

Klima, C. L., Holman, D. B., Ralston, B. J., Stanford, K., Zaheer, R., Alexander, T. W., et al. (2019). Lower respiratory tract microbiome and resistome of bovine respiratory disease mortalities. *Microb Ecol.* 78, 446–456. doi: 10.1007/s00248-019-01361-3

Kobayashi, Y., Shinkai, T., and Koike, S. (2008). Ecological and physiological characterization shows that *Fibrobacter succinogenes* is important in rumen fiber digestion - review. *Folia Microbiol. (Praha)* 53, 195–200. doi: 10.1007/s12223-008-0024-z

Koppen, I. J. N., Bosch, A., Sanders, E. A. M., van Houten, M. A., and Bogaert, D. (2015). The respiratory microbiota during health and disease: a paediatric perspective. *Pneumonia (Nathan)* 6, 90–100.

Kovatcheva-Datchary, P., Nilsson, A., Akrami, R., Lee, Y. S., De Vadder, F., Arora, T., et al. (2015). Dietary fiber-induced improvement in glucose metabolism is associated with increased abundance of prevotella. *Cell Metab.* 22, 971–982. doi: 10.1016/j.cmet.2015.10.001

Ley, R. E. (2016). Gut microbiota in 2015: prevotella in the gut: choose carefully. *Nat. Rev. Gastroenterol. Hepatol.* 13, 69–70. doi: 10.1038/nrgastro.2016.4

Li, R., Zhu, H., Ruan, J., Qian, W., Fang, X., Shi, Z., et al. (2010). De novo assembly of human genomes with massively parallel short read sequencing. *Genome Res.* 20, 265–272. doi: 10.1101/gr.097261.109

Lima, S. F., Teixeira, A. G., Higgins, C. H., Lima, F. S., and Bicalho, R. C. (2016). The upper respiratory tract microbiome and its potential role in bovine respiratory disease and otitis media. *Sci. Rep.* 6:29050.

Lopez-Siles, M., Duncan, S. H., Garcia-Gil, L. J., and Martinez-Medina, M. (2017). *Faecalibacterium prausnitzii*: from microbiology to diagnostics and prognostics. *ISME J.* 11, 841–852. doi: 10.1038/ismej.2016.176

Man, W. H., de Steenhuijsen Piters, W. A., and Bogaert, D. (2017). The microbiota of the respiratory tract: gatekeeper to respiratory health. *Nat. Rev. Microbiol.* 15, 259–270. doi: 10.1038/nrmicro.2017.14

Marcos, A., Nova, E., and Montero, A. (2003). Changes in the immune system are conditioned by nutrition. *Eur. J. Clin. Nutr.* 57(Suppl. 1), S66–S69.

Marotz, C., Amir, A., Humphrey, G., Gaffney, J., Gogul, G., and Knight, R. (2017). DNA extraction for streamlined metagenomics of diverse environmental samples. *Biotechniques* 62, 290–293. doi: 10.2144/000114559

Martin, M. (2011). Cutadapt removes adapter sequences from high-throughput sequencing reads. *EMBnet J.* 17:3. doi: 10.14806/ej.17.1.200

McIntyre, H. D., Catalano, P., Zhang, C., Desoye, G., Mathiesen, E. R., and Damm, P. (2019). Gestational diabetes mellitus. *Nat. Rev. Dis. Primers* 5:47. doi: 10.1038/s41572-019-0098-8

McMullen, C., Alexander, T. W., Leguillette, R., Workentine, M., and Timsit, E. (2020). Topography of the respiratory tract bacterial microbiota in cattle. *Microbiome* 8:91. doi: 10.1186/s40168-020-00869-y

Nicola, I., Cerutti, F., Grego, E., Bertone, I., Gianella, P., D'Angelo, A., et al. (2017). Characterization of the upper and lower respiratory tract microbiota in Piedmontese calves. *Microbiome* 5:152. doi: 10.1186/s40168-017-0372-5

Prince, A., Zhang, Y., Croniger, C., and Puchowicz, M. (2013). Oxidative metabolism: glucose versus ketones. *Adv. Exp. Med. Biol.* 789, 323–328.

Qiu, Q., Zhang, G., Ma, T., Qian, W., Wang, J., Ye, Z., et al. (2012). The yak genome and adaptation to life at high altitude. *Nat. Genet.* 44, 946–949. doi: 10.1038/ng.2343

Ramette, A. (2007). Multivariate analyses in microbial ecology. *FEMS Microbiol. Ecol.* 62, 142–160. doi: 10.1111/j.1574-6941.2007.00375.x

Rao, D. N., Dryden, D. T., and Bheemanaik, S. (2014). Type III restriction-modification enzymes: a historical perspective. *Nucleic Acids Res.* 42, 45–55. doi: 10.1093/nar/gkt616

Rizzatti, G., Lopetuso, L. R., Gibiino, G., Binda, C., and Gasbarrini, A. (2017). *Proteobacteria*: a common factor in human diseases. *Biomed. Res. Int.* 2017:9351507.

Schatz, A., Bugie, E., and Waksman, S. A. (2005). Streptomycin, a substance exhibiting antibiotic activity against gram-positive and gram-negative bacteria. 1944. *Clin. Orthop. Relat. Res.* 437, 3–6. doi: 10.1097/01.blo.0000175887.98112.fe

Schloss, P. D., Westcott, S. L., Ryabin, T., Hall, J. R., Hartmann, M., Hollister, E. B., et al. (2009). Introducing mothur: open-source, platform-independent, community-supported software for describing and comparing microbial communities. *Appl. Environ. Microbiol.* 75, 7537–7541. doi: 10.1128/AEM.01541-09

Schulz, K., Frahm, J., Kersten, S., Meyer, U., Reiche, D., Sauerwein, H., et al. (2015). Effects of elevated parameters of subclinical ketosis on the immune system of dairy cows: in vivo and in vitro results. *Arch. Anim. Nutr.* 69, 113–127. doi: 10.1080/1745039X.2015.1013666

Sedgwick, P. (2014). Spearman's rank correlation coefficient. *BMJ* 349:g7327. doi: 10.1136/bmj.g7327

Segata, N., Izard, J., Waldron, L., Gevers, D., Miropolsky, L., Garrett, W. S., et al. (2011). Metagenomic biomarker discovery and explanation. *Genome Biol.* 12:R60. doi: 10.1186/gb-2011-12-6-r60

Shannon, P., Markiel, A., Ozier, O., Baliga, N. S., Wang, J. T., Ramage, D., et al. (2003). Cytoscape: a software environment for integrated models of biomolecular interaction networks. *Genome Res.* 13, 2498–2504. doi: 10.1101/gr.1239303

Sturm, V., Efrosinin, D., Ohlschuster, M., Gusterer, E., Drillich, M., and Iwersen, M. (2020). Combination of sensor data and health monitoring for early detection of subclinical ketosis in dairy cows. *Sensors (Basel)* 20:1484. doi: 10.3390/s20051484

Suthar, V. S., Canelas-Raposo, J., Deniz, A., and Heuwieser, W. (2013). Prevalence of subclinical ketosis and relationships with postpartum diseases in European dairy cows. *J. Dairy Sci.* 96, 2925–2938. doi: 10.3168/jds.2012-6035

Virtanen, P., Gommers, R., Oliphant, T. E., Haberland, M., Reddy, T., Cournapeau, D., et al. (2020). SciPy 1.0: fundamental algorithms for scientific computing in Python. *Nat. Methods* 17, 261–272. doi: 10.1038/s41592-019-0686-2

Wang, W. L., Xu, S. Y., Ren, Z. G., Tao, L., Jiang, J. W., and Zheng, S. S. (2015). Application of metagenomics in the human gut microbiome. *World J. Gastroenterol.* 21, 803–814. doi: 10.3748/wjg.v21.i3.803

Whiting, T. L., Postey, R. C., Chestley, S. T., and Wruck, G. C. (2012). Explanatory model of cattle death by starvation in Manitoba: forensic evaluation. *Can. Vet. J.* 53, 1173–1180.

Woldehiwet, Z., Mamache, B., and Rowan, T. G. (1990). The effects of age, environmental temperature and relative humidity on the bacterial flora of the upper respiratory tract in calves. *Br. Vet. J.* 146, 211–218. doi: 10.1016/s0007-1935(11)80004-7

Wypych, T. P., Wickramasinghe, L. C., and Marsland, B. J. (2019). The influence of the microbiome on respiratory health. *Nat. Immunol.* 20, 1279–1290. doi: 10.1038/s41590-019-0451-9

Xue, B., Zhao, X. Q., and Zhang, Y. S. (2005). Seasonal changes in weight and body composition of yak grazing on alpine-meadow grassland in the Qinghai-Tibetan plateau of China. *J. Anim. Sci.* 83, 1908–1913. doi: 10.2527/2005.8381908x

Yu, X., Peng, Q., Luo, X., An, T., Guan, J., and Wang, Z. (2016). Effects of starvation on lipid metabolism and gluconeogenesis in yak. *Asian-Australas J. Anim. Sci.* 29, 1593–1600. doi: 10.5713/ajas.15.0868

Zarrin, M., De Matteis, L., Vernay, M. C., Wellnitz, O., van Dorland, H. A., and Bruckmaier, R. M. (2013). Long-term elevation of beta-hydroxybutyrate in dairy cows through infusion: effects on feed intake, milk production, and metabolism. *J. Dairy Sci.* 96, 2960–2972. doi: 10.3168/jds.2012-6224

Zeineldin, M., Lowe, J., and Aldridge, B. (2019). Contribution of the mucosal microbiota to bovine respiratory health. *Trends Microbiol.* 27, 753–770. doi: 10.1016/j.tim.2019.04.005

Zeineldin, M. M., Lowe, J. F., Grimmer, E. D., de Godoy, M. R. C., Ghanem, M. M., Abd El-Raof, Y. M., et al. (2017). Relationship between nasopharyngeal and bronchoalveolar microbial communities in clinically healthy feedlot cattle. *BMC Microbiol.* 17:138. doi: 10.1186/s12866-017-1042-2

Zhu, W., Lomsadze, A., and Borodovsky, M. (2010). Ab initio gene identification in metagenomic sequences. *Nucleic Acids Res.* 38:e132. doi: 10.1093/nar/gkq275

Zou, H., Hu, R., Dong, X., Shah, A. M., Wang, Z., Ma, J., et al. (2020). Lipid catabolism in starved yak is inhibited by intravenous infusion of beta-hydroxybutyrate. *Animals (Basel)* 10:E136. doi: 10.3390/ani10010136

Zou, H., Hu, R., Wang, Z., Shah, A. M., Zeng, S., Peng, Q., et al. (2019). Effects of nutritional deprivation and re-alimentation on the feed efficiency, blood biochemistry, and rumen microflora in yaks (*Bos grunniens*). *Animals (Basel)* 9:E807. doi: 10.3390/ani9100807

Conflict of Interest: The authors declare that the research was conducted in the absence of any commercial or financial relationships that could be construed as a potential conflict of interest.

frontiers in Microbiology

ORIGINAL RESEARCH
published: 04 March 2021
doi: 10.3389/fmicb.2021.630605

The Rumen Bacterial Community in Dairy Cows Is Correlated to Production Traits During Freshening Period

*Shuai Huang[1], Shoukun Ji[2], Garret Suen[3], Feiran Wang[1] and Shengli Li[1]**

[1] State Key Laboratory of Animal Nutrition, Beijing Engineering Technology Research Center of Raw Milk Quality and Safety Control, College of Animal Science and Technology, China Agricultural University, Beijing, China, [2] College of Animal Science and Technology, Hebei Agricultural University, Baoding, China, [3] Department of Bacteriology, University of Wisconsin-Madison, Madison, WI, United States

The rumen microbiome plays a vital role in providing nutrition to the host animal, thereby influencing ruminant production. Despite its importance, it is not fully understood how variation in the ruminal bacteria community composition influences dry matter intake (DMI), milk yield and ruminal fermentative parameters in dairy cows, especially during freshening period. Here, we hypothesized that during early lactation, high DMI cows having a different ruminal microbiota than low DMI cows, and that this difference persists over time. To test this, we enrolled 65 fresh and determinzed their DMI using an auto-feed intake recording system. Fourteen days after calving, the 10 animals with the lowest (LFI) and the 10 animals with the highest (HFI)-average DMI were selected for further analysis. Rumen fluid was collected from these two cohorts at 1 (Fresh1d) and 14 days (Fresh14d) after calving and their ruminal microbiota were assessed using 16S rRNA sequencing. Volatile fatty acid (VFA) concentrations were also quantified. Comparison of the ruminal microbiotas between Fresh1d and Fresh14d showed that Fresh14d cows had a significantly higher relative abundance of VFA—producing microbes ($P < 0.05$), such as *Prevotella_7* and *Succinivibrionaceae_UCG-001*. This was commensurate with the concentrations of acetate, propionate, butyrate, valerate and total VFAs, were also significantly ($P < 0.05$) increased in Fresh14d cows. We also found that the differences in the ruminal microbiota between LFI and HFI cows was limited, but DMI significantly altered ($P < 0.05$) the relative proportion of bacteria in the families *Coriobacteriaceae*, and *Succinivibrionaceae*. Furthermore, specific operational taxonomic units belonging to the *Anaeroplasma* was significantly ($P < 0.05$) correlated with DMI and milk yield. Taking together, our findings provide a framework for future studies of freshening period cow that seek to better understand the role of the ruminal microbiota during this critical period in the lactation cycle.

Keywords: ruminal bacteria, fresh cows, dry matter intake, production traits, 16S rRNA sequencing

Abbreviations: ADF, Acid detergent fiber; AP, acetate-to-propionate ratio; DDGS, Dried distillers grains with soluble; DM, Dry matter; DMI, Dry matter intake; Fresh1d, 1 day after calving of fresh cows; Fresh14d, 14 days after calving of fresh cows; HFI, high average feed intake from the fresh cows; LFI, low average feed intake from the fresh cows; NDF, Neutral detergent fiber; NMDS, Non-Metric Multidimensional Scaling; OTUs, Operational Taxonomic Units; TVFAs, total of volatile fatty acids.

OPEN ACCESS

Edited by:
Xudong Sun, Heilongjiang Bayi Agricultural University, China

Reviewed by:
Min Wang, Chinese Academy of Sciences, China
Xiliang Du, Jilin University, China

****Correspondence:***
Shengli Li
lisheng0677@163.com

Specialty section:
This article was submitted to Systems Microbiology, a section of the journal Frontiers in Microbiology

Received: *18 November 2020*
Accepted: *11 February 2021*
Published: *04 March 2021*

Citation:
Huang S, Ji S, Suen G, Wang F and Li S (2021) The Rumen Bacterial Community in Dairy Cows Is Correlated to Production Traits During Freshening Period. Front. Microbiol. 12:630605. doi: 10.3389/fmicb.2021.630605

INTRODUCTION

Dairy cows are important global contributors to agriculture as sources of milk and milk products. A critical stage in the dairy cow production lifecycle is the transition period, which occurs between lactation cycles and spans from 3 weeks before to 3 weeks after calving. During this period, cows undergo dramatic changes in host physiology and nutrient metabolism, which can result in health disorders, reduced dry matter intake (DMI), and lower milk yield. Previous works has documented the influence of diet on host metabolism and physiology during the transition period, but far less is known regarding the impact of the ruminal microbiome, which is a known driver of host production (Weimer, 2015). Importantly, ruminal microbes ferment plant polysaccharides into VFAs, including acetate, propionate, and butyrate, which serve as the major energy source for the cow (Reynolds et al., 1988; Flint et al., 2008). Recent studies reported the difference of rumen microbiota under the different feed intake of lactating dairy cows (Li et al., 2020) and yaks (Shi et al., 2020). However, there are no studies focused on the difference of rumen microbiota between low and high feed intake in dairy cows during the freshening period.

Recently, studies have shown that the rumen microbiota undergoes dramatic and distinct shifts from gestation to lactation. Lima et al. (2015) described these shifts in 115 Holstein dairy cows (67 multiparous and 48 primiparous) from 1 week before postpartum to 1 week after postpartum. Dynamic changes in the structure of the metabolically active rumen bacterial communities were found over the transition period (parturition ± 3 weeks), likely in response to the dramatic changes in physiology and nutritional factors like DMI and feed composition (Zhu et al., 2017). These findings were supported by another study of 10 primiparous Holstein dairy cows during the transition period, which also found distinct changes in the rumen bacterial composition in response to dietary changes (Zhu et al., 2018). In contrast, a study by Pitta et al. (2014) showed no difference in the dominant ruminal bacterial phyla, families and genera in both primiparous and multiparous cows 1–3 d post-calving and 4 weeks into lactation.

Given this paucity of data, it is clear that more work is required to better understand the influence of the ruminal microbiota during the transition period. In particular, a deeper understanding of the freshening period (2 weeks after parturition) is necessary, as ∼50% of all cows experience low DMI during this period, resulting in a state of negative energy balance (Ferguson, 2001). Increasing evidence showed that improving DMI of fresh cows can alleviate the negative energy balance and increased the downstream milk production of dairy cows (Roche et al., 2013).

Here, we hypothesized that the rumen microbiota of low DMI cows is significantly different from high DMI cows, and that this difference persists over time. To address this, we conducted a study to explore the dynamics of the ruminal microbial community during the freshening period in dairy cows. Specifically, we compared the ruminal microbiota of low DMI fresh cows to high DMI fresh cows in order to identify potential relationships between the ruminal bacteria and DMI. Understanding the differences between these groups will provide a framework for fresh cows and thereby achieve improved lactation efficiency while reducing the risk for the adverse outcomes that usually persist in low DMI fresh cows.

MATERIALS AND METHODS

Animals Care and Management

Sixty-five fresh (2.40 ± 0.50 parity, body condition score 3.58 ± 0.12, body weight 612.13 ± 11.40 kg) Holstein dairy cows were selected after calving from a commercial dairy farm herd (Beijing, China). All cows were cohoused and kept in a free stall barn. No drugs or antibiotics were used 3 months prior to the study. All cows had *ad libitum* access to fresh water and were fed three times daily (07:30, 14:30, and 19:00) with a total mixed ration, as shown in **Table 1**.

Daily Milk Yield and Dry Matter Intake Data Collection

Individual feed intake was measured by a roughage intake control system (Insentec B.V., Marknesse, Netherlands). Cows were milked thrice daily (07:00, 14:00, and 22:00) by farm staff. Milk

TABLE 1 | Composition and chemical components of the diet used in this study.

Items[1]	Pre-partum	Fresh
Ingredients, kg		
Oat grass	4.83	1.20
Alfalfa hay	–	3.00
Whole corn silage	8.62	11.20
Flaked corn	0.87	2.00
Corn pellets	0.87	1.18
Soybean meal	1.84	2.97
Soybean hull	0.50	2.00
Sprayed corn husk	1.40	0.18
DDGS	1.20	1.50
5% premix	0.75	0.65
Cottonseed	–	0.50
5% anion premix	0.13	–
Yeast culture XP	0.15	0.20
Molasses	–	0.50
Contents,%		
Dry matter as fed	53.39	49.32
Crude protein	14.23	16.56
Crude fat	2.04	3.40
ADF	20.37	20.58
NDF	40.84	34.63
NEL[2](MCal/kg)	1.58	1.72
Ca	0.80	0.70
P	0.35	0.33

[1]DDGS dried distillers grains with solubles, DM dry matter, NDF neutral detergent fiber, ADF acid detergent fiber, NFC non-fiber carbohydrates, Ca calcium, P phosphorus.

[2]NE_L: Nutrients contents was measured value and NE_L was calculated value with model from NRC (2001).

yield was recorded by a milking machine (2 × 48, BouMatic Company, Madison, WI, United States) for each cow.

Grouping and Sampling Period

All cows were transferred to a new barn from 10 days before calving to allow the animals to acclimate to their new surroundings. The experimental period was from 1 d to 14 d after calving. During this period, the 10 cows with the lowest average DMI (LFI) and the 10 cows with highest average DMI (HFI) were selected from the 65 fresh cows. We note that a previous study found that characterizing the ruminal microbiota of 16 cows maintained on the same diet is sufficient to determine meaningful differences within their microbial communities (Jami and Mizrahi, 2012). Therefore, our selection of 20 disparate DMI cows from a cohort of 65 early lactation cows is likely sufficient to detect differences inthe their ruminal microbiotas as it relates to host phenotype. Once lactation began, the LFI and HFI cows were sampled at 1 (Fresh1d, $n = 20$) and 14 (Fresh14d, $n = 20$) days after calving.

Blood Samples Collection and Measurement

Blood samples were collected from each cow via tail vein before morning feeding. Samples were centrifuged at 3,000 × g for 10 min to obtain serum and stored at −20°C untile subsequent analysis of glucose, non-esterified fatty acid (NEFA), and β-hydroxybutyrate (BHBA). Serum samples were analyzed for NEFA and BHBA using a colorimetric kit (Nanjing Jiancheng, Jiangsu, China), and glucose by a GF-D200 automatic biochemical analyzer (Caihong, Shandong, China).

Rumen Fluid Collection and Processing

Rumen fluid samples were collected from each cow using an oral gastric tube (Ancitech, Winnipeg, MB, Canada) prior to morning feeding (07:00). The sampling device was cleaned thoroughly with fresh warm water after each sampling to avoid cow-to-cow contamination and the first 200 mL of collected rumen fluid was discarded to avoid saliva contamination. Subsequent rumen fluid was collected and filtered through four layers of cheesecloth. Samples were placed into sterile 50 mL plastic tubes on wet ice and immediately transported back to the farm office and frozen at −80°C until DNA extraction was performed.

An additional 30 mL of rumen fluid was transferred into a centrifuge tube and stored at −20°C until VFA analysis. VFA determination was conducted as follows. Rumen fluid was centrifuged at 8, 000 × g at 4°C for 15 min to obtain the supernatant, which was then quantified using gas chromatography as described by Erwin et al. (1961).

Genomic DNA Extraction, Amplification, and Sequencing

Total genomic DNA was extracted from 1 mL rumen fluid samples using an OMEGA DNA kit (Omega Bio-Tek, Norcross, GA, United States) according to the manufacturer's specifications. The quality of DNA was confirmed by 1% agarose gel electrophoresis. The amplicon library preparation was performed by PCR amplification of the V3-V4 region of the 16S rRNA gene using the primers 338F (5′-ACTCCTACGGGAGGCAGCAG-3′) and 806R (5′-GGACTACNNGGGTATCTAAT-3′) including NEBNext adapters sequences, indices and Taq DNA Polymerase as well as AMPure XP Beads (New England Biolabs Inc., Ipswich, MA, United States) (Ren et al., 2017). PCR conditions are as follows: 5 min of denaturation at 95°C, followed by 28 cycles of 45 s for denaturation at 95°C, 50 s for annealing at 55°C and 45 s for elongation at 72°C with a final extension at 72°C for 10 min. PCRs were performed in triplicate 25 μL mixture containing 12.5 μL KAPA 2G Robust Hot Start Ready Mix (Kapa Biosystems, Wilmington, MA, United States), 1 μL of each primer (5 μM), 5 μL template DNA (6 ng/uL) and 5.5 uL ddH_2O. The amplified PCR products were purified using an Agencourt AMPure XP Kit (Beckman Coulter Genomics, Indianapolis, IN, United States), and quantified using PCR (ABI 9700, Thermo Fisher Scientific, Waltham, MA, United States). Purified PCR products were pooled in equimolar amounts and sequenced on an Illumina MiSeq (Illumina, San Diego, CA, United States) (Caporaso et al., 2012) using a 2 × 250 bp sequencing kit.

Quality Control and Sequencing Data Analysis

Low quality (score ≤ 20) short reads (<200 bp) and reads containing ambiguous bases or unmatched to primer sequences and barcode tags were filtered out from dataset using QIIME 1.8 (Caporaso et al., 2010). The resulting reads were merged using PEAR 0.9.6 (Zhang et al., 2014) and demultiplexed using FLASH 1.20 (Magoc and Salzberg, 2011). Reads with merged length less than 230 bp and chimeric sequences were removed by UCHIME (UCHIME Algorithm) (Edgar et al., 2011). In order to reduce the error caused by the different sequencing depths of the samples, all samples were subsampled to equal size of 23,902 sequences for downstream alpha and beta diversity analysis. To ensure the comparability of the species diversity between the samples, standardized OTU documents were used to analyze the species and diversity indexes.

The remaining sequences were clustered into operational taxonomic units (OTUs) at a 97% similarity using the Ribosomal Database Project classifier (Cole et al., 2009) with a confidence threshold of 0.70 and compared against the SILVA 128 database (Release September 29, 2016) (Quast et al., 2013). All were removed using UCLUST (Edgar, 2010) to generate a representative OTU table.

The OTU level alpha diversity of bacterial communities was determined using Shannon and Chao1 indices and calculated using procedures within QIIME 1.8 and visualized using the "ggplot2" package in R (version 3.6.1) (Wickham, 2009). The non-metric multidimensional scaling (NMDS) ordination was performed on Bray-Curtis dissimilarity distances calculated in R. Analysis of similarities (ANOSIM) (999 permutations) using Bray-Curtis distances were performed to compare the similarity of microbial community among the observed microbial profiles

based on different groups and sample time using the "vegan" package in R (Oksanen et al., 2015).

Sequence and Statistics Analysis

Data on DMI, milk yield, rumen fermentation parameters and serum biochemical parameters were analyzed using the linear mixed models procedure of SAS 9.4 (Cary, North Carolina, United States). Alpha-diversity indices, the significance of the pairwise comparison between LFI and HFI groups and between Fresh1d and Fresh14d groups were analyzed using the Wilcoxon rank test using the "dplyr" package[1] (author, H. Wickham, R. François, L. Henry, K. Müller; published date, 2018; version, 0.7.6) in R. Spearman's rank correlation was used to identify the relationship between the relative abundance of OTUs and production traits of LFI and HFI cows using the "Psych" package[2] (author, W Revelle; published date, 2016; version, 1.6.9) and visualized using the "corrplot" package[3] (author, Taiyun Wei; published date, 2017; version, 0.84) in R. All *P*-value was corrected using a false discovery rate of 0.05 as described by Benjamini and Hochberg (1995) and false discovery rate corrected $P < 0.05$ were considered significant.

RESULTS

Measurement of Production Traits, Rumen Fermentative Parameters, and Blood Metabolites in Fresh Cows

DMI and milk yield for all cows across the entire trial period are shown in **Table 1**. The levels of acetate, propionate, butyrate, valerate and total VFAs were significantly ($P < 0.05$) higher in Fresh14d compared to Fresh1d, whereas the acetate:propionate (AP) ratio and serum glucose was significantly ($P < 0.05$) lower in Fresh14d groups. We found that DMI increased and significantly differed ($P < 0.05$) between LFI and HFI groups (**Table 2**). No significant differences ($P > 0.05$) in milk yield, DMI/milk yield, acetate, propionate, butyrate, valerate, isovalerate, total VFAs, AP, NEFA, BHBA and glucose were observed between LFI and HFI groups.

Sequencing Metrics for the Ruminal Microbiota of Fresh Cows

A total of 1,087,457 raw sequences were generated with an average of 27,186 ± 745 (mean ± *SD*) per sample, respectively. An average of 1,532 ± 258 OTUs across all samples was identified at 97% sequence similarity. Rarefaction curves showed a smaller number of new OTU identification as the number of sequences per sample increased (**Supplementary Figure S1**), implying the adequate sampling depth for covering the rumen bacterial composition that we tested. Good's coverage for the fresh cow samples was determined with a mean value of 0.982 across all 40 samples, indicating sufficient sequence coverage for all samples. The mean Shannon's diversity and Chao1's richness for all fresh cow samples was 8.38 ± 0.64 and 1963.94 ± 285.88, respectively.

The most highly abundant phyla for all fresh cow samples included the *Bacteroidetes* (52.60%), *Firmicutes* (34.90%), *Proteobacteria* (6.21%), with less contributions from the *Fibrobacteres* (1.24%) and *Spirochaetes* (1.23%) (**Figures 1A,B**). Within these phyla, the most abundant families included the *Prevotellaceae* (40.17%), *Lachnospiraceae* (12.19%), *Ruminococcaceae* (9.63%) and *Succinivibrionaceae* (5.39%, **Figures 1A,B**). At the genus level, 8 genera had >2% relative abundance: *Prevotella_1* (31.29%), *Succiniclasticum* (4.37%), *Christensenellaceae_R-7_group* (2.78%), *Rikenellaceae_RC9_gut_group* (2.69%), *Prevotella_7* (2.53%), *Succinivibrionaceae_UCG-001* (2.22%), *Succinivibrionaceae_UCG-002* (2.04%), and *Ruminococcus_1* (2.03%, **Figures 1A,B**).

Defining a Core Microbiota for Fresh Cows and DMI Cows

We then sought to determine the core microbiota across all fresh cows in our study and found 2,737 OTUs shared among all fresh cow samples (**Figure 2A**). These included bacterial families with >1% total relative abundance: *Prevotellaceae* (26.39%), *Lachnospiraceae* (6.23%), *Ruminococcaceae* (4.26%), *Acidaminococcaceae* (4.19%), *Bacteroidales_S24-7_group* (3.01%), *Veillonellaceae* (2.61%), *Christensenellaceae* (1.85%), and *Fibrobacteraceae* (1.05%, **Supplementary Table S1**). The shared genera among all samples >1% of the total relative abundance were the *Prevotella_1* (23.39%), *Succiniclasticum* (4.19%), *unclassified_Bacteroidales_S24-7_group* (3.01%), *Christensenellaceae_R-7_group* (1.85%), *Ruminocroccaceae_NK4A214_group* (1.27%), *Lachnospiraceae_NK3A20_group* (1.11%), *Selenomonas_1* (1.06%), and *Fibrobacter* (1.05%).

We then determined the core set of OTUs shared between the LFI and HFI cows and found 2,392 OTUs shared across LFI and HFI samples (**Figure 2B**). More unique OTUs were found in the HFI group, relative to the LFI group. The LFI and HFI groups shared 80% of the total number of identified OTUs. Of the 2,392 OTUs shared across both DMI groups, most of them belonged to the genera *Prevotella_1* (33.26%), *unclassified_c_WCHB1-41* (21.80%), *Prevotella_7* (4.96%), *Succinivibrionaceae_UCG-001* (4.45%), *unclassified_Bacteroidales_S24-7_group* (4.20%), *Succiniclasticum* (4.05%), *unclassified_Lachnospiraceae* (2.69%), and *Ruminococcus_1* (2.32%, **Supplementary Table S1**).

The Ruminal Bacterial Community in Fresh Cows Differs Between Days 1 and 14 After Calving

To determine if differences exist between the ruminal microbiota of fresh cows at Fresh1d and Fresh14d, we performed a Bray-Curtis dissimilarity analysis and visualized this using an NMDS plot as shown in **Figure 3A**. We found that the ruminal microbiota differed between both groups upon visual inspection. We then analyzed these data in greater detail using ANOSIM and confirmed that these two groups were statistically different ($R^2 = 0.65$, $P = 0.001$). Moreover, we found that the ruminal

[1]https://cran.r-project.org/package/dplyr

[2]http://cran.r-project.org/web/packages/psych

[3]https://cran.r-project.org/web/packages/corrplot/

TABLE 2 | DMI, milk yield, rumen fermentative parameters and blood metabolites.

Item[1]	Freshening period		SEM	*P*-value	DMI		SEM	*P*-value
	Fresh1d (*n* = 20)	Fresh14d (*n* = 20)			LFI (*n* = 10)	HFI (*n* = 10)		
DMI, kg	6.43	15.36	0.60	< 0.001	16.52	19.57	0.59	0.023
Milk yield, kg	20.47	36.41	1.45	< 0.001	34.64	36.07	1.00	0.382
DMI/milk yield	0.74	0.50	0.05	< 0.001	0.53	0.61	0.03	0.586
Fermentation								
Acetate, mmol/L	45.18	61.31	4.18	0.015	61.50	61.13	2.96	0.668
Propionate, mmol/L	10.96	20.22	1.63	0.002	20.74	19.64	1.75	0.781
Butyrate, mmol/L	5.77	10.25	0.75	< 0.001	10.34	10.14	0.64	0.884
Valerate, mmol/L	0.53	1.01	0.06	< 0.001	1.10	0.90	0.08	0.225
Isovalerate, mmol/L	2.10	2.05	0.12	0.779	2.18	1.92	0.12	0.269
TVFAs, mmol/L	63.14	94.20	6.89	0.005	93.86	94.74	4.95	0.936
AP	5.32	3.26	0.32	< 0.001	3.24	3.29	0.16	0.883
Metabolites								
NEFA, mmol/L	0.20	0.21	0.002	0.058	0.21	0.20	0.005	0.170
BHBA, mmol/L	1.26	1.28	0.03	0.602	1.30	1.27	0.04	0.765
Glucose, mmol/L	3.65	3.11	0.12	0.025	3.14	3.08	0.12	0.815

[1] *TVFAs, total of VFAs; AP, the acetate-to-propionate raito; NEFA, non-esterified fatty acid; BHBA, β-hydroxybutyrate.*

microbiota of the Fresh14d cows had a significantly ($P < 0.001$) lower number of OTUs, relative to Fresh1d cows, which was further supported by significant differences in the Chao1 richness and Shannon diversity index ($P < 0.001$) values for the two groups (**Supplementary Figure S2A**).

At the phylum level, the relative abundance of phyla *Bacteroidetes*, *Firmicutes* and *Proteobacteria* showed no significant ($P > 0.05$) difference between Fresh1d and Fresh14d. In contrast, the phyla *Actinobacteria* and *Tenericutes* were significantly ($P < 0.05$) decreased (**Table 3**). At the family level, the predominant family *Ruminococcaceae*, *Bacteroidales_BS11_gut_group*, *Christensenellaceae* and *Rikenellaceae* were significantly ($P < 0.05$) decreased from Fresh1d to Fresh14 (**Table 3**). The relative abundance of the families *Prevotellaceae* and *Veillonellaceae* were significantly ($P < 0.05$) higher in Fresh14d compared to Fresh1d (**Table 3**). At the genus level, the relative abundance of some genera changed more than 10-fold, including *Prevotella_7* (increasing 83.33-fold, $P < 0.001$), *Erysipelotrichaceae_UCG-002* (increasing 3827.75-fold, $P = 0.001$), and *Succinivibrionaceae_UCG-001* (increasing 42,380.95-fold, $P < 0.001$, **Table 4**).

Differences in the Ruminal Bacterial Community Between LFI and HFI Cows Is Limited

Considering the importance of DMI for the fresh group, we compared LFI and HFI cows from the fresh cow group at 14d to determine if differences exist between these cows. First, we performed a Bray-Curtis dissimilarity analysis of the microbiota for LFI and HFI cows and visualized this using an NMDS plot as shown in **Figure 3B**. We found that the ruminal microbiota was similar as both groups did not show a clear separation, and this was also confirmed using ANOSIM analysis ($R^2 = 0.006$, $P = 0.355$). In addition, we found that the ruminal microbiota from those two groups had no significant differences in the Shannon diversity index ($P = 0.529$), Chao1 richness ($P = 0.684$), and number of OTUs ($P = 0.481$) for the two groups (**Supplementary Figure S2B**).

We then quantified the difference between the community composition of the LFI and HFI groups using the Wilcoxon test on the relative abundances for all samples at the phylum and family level. We found that phyla *Proteobacteria* was significantly ($P = 0.043$) enriched in the LFI group relative to the HFI group (**Table 3**). At the family level, *Coriobacteriaceae* (phylum *Actinobacteria*), and *Succinivibrionaceae* (phylum *Proteobacteria*) were significantly ($P < 0.05$) different between groups (**Table 3**). A higher relative abundance of *Erysipelotrichaceae_UCG-002* in the LFI group, relative to the HFI group (**Table 4**). The relative abundance of *Christensenellaceae_R-7_group* and *Ruminococcaceae_UCG-010* were tended to higher ($0.05 < P < 0.1$) and the relative abundance of *Lachnospira* was tended to lower ($0.05 < P < 0.1$) in the HFI group relative to the LFI group (**Table 4**).

Correlation of Ruminal Bacteria With Production and Rumen Fermentative Parameters in LFI and HFI Cows

To explore the potential roles of ruminal bacteria on production and fermentation, we analyzed the relationship between DMI, milk yield, DMI/milk yield, VFAs (acetate, propionate, butyrate, valerate, isovalerate, total VFAs and AP) and the relative abundance of OTUs using Spearman's rank correlations. All OTUs with relative abundances <0.01% of all samples were removed from this analysis. The relationship between OTUs and production and fermentation traits were visualized in a heatmap,

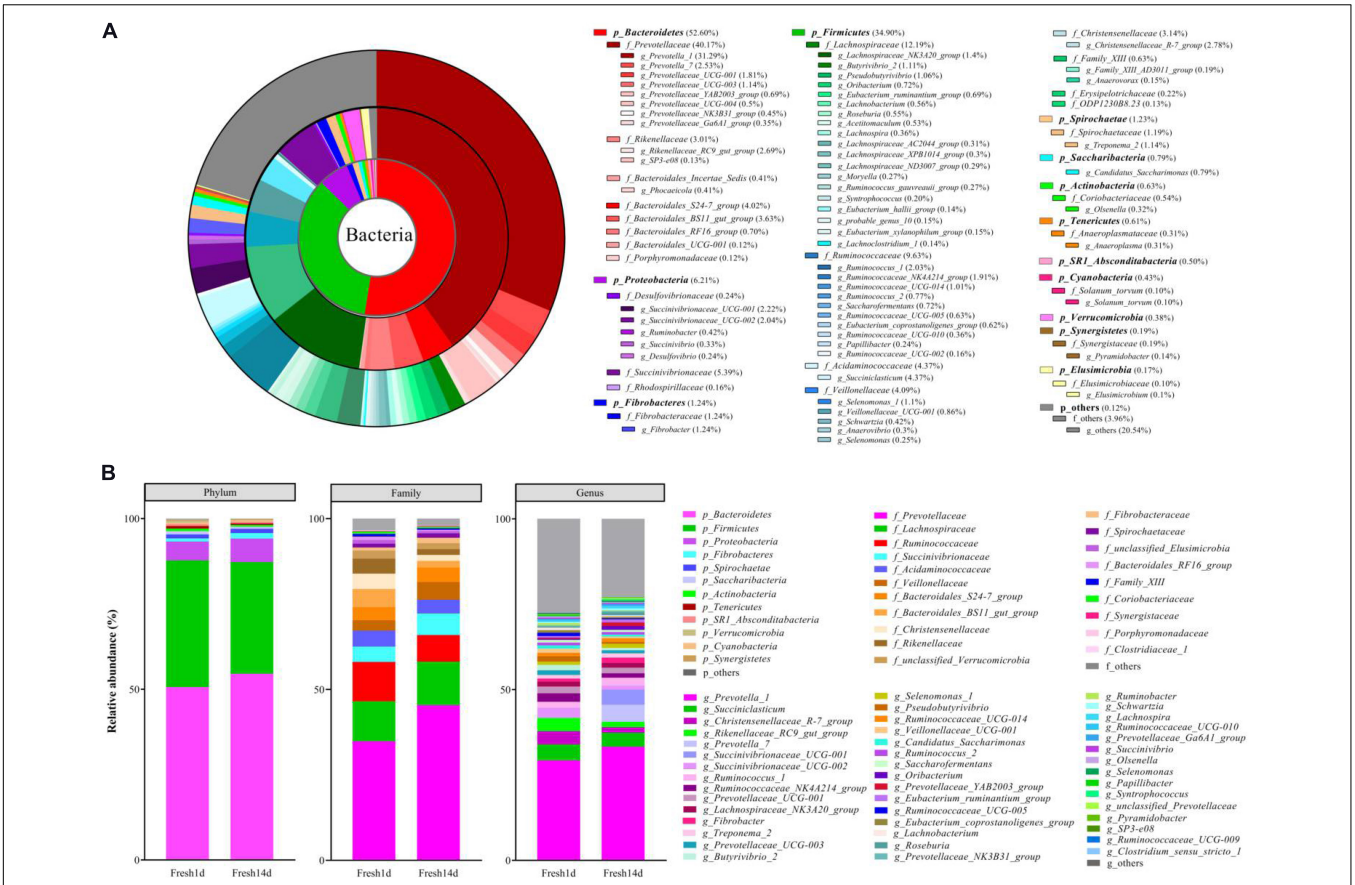

FIGURE 1 | The ruminal bacterial composition of fresh cows. **(A)** Relative distribution of the most dominant bacterial phyla, family and genera (relative abundance >0.1% for all samples) for fresh cow samples. The pie chart inner ring represents the genus level, the middle ring represents the family level and the outer ring represents the phylum level. Different shades of color represent different bacteria. Numbers in brackets denote the average relative abundance of the bacteria across 40 samples. **(B)** Stacked bar graphs of the average relative abundances of phyla, family and genus (relative abundance >0.1% at least one sample) for fresh cow on d1 and d14 after calving.

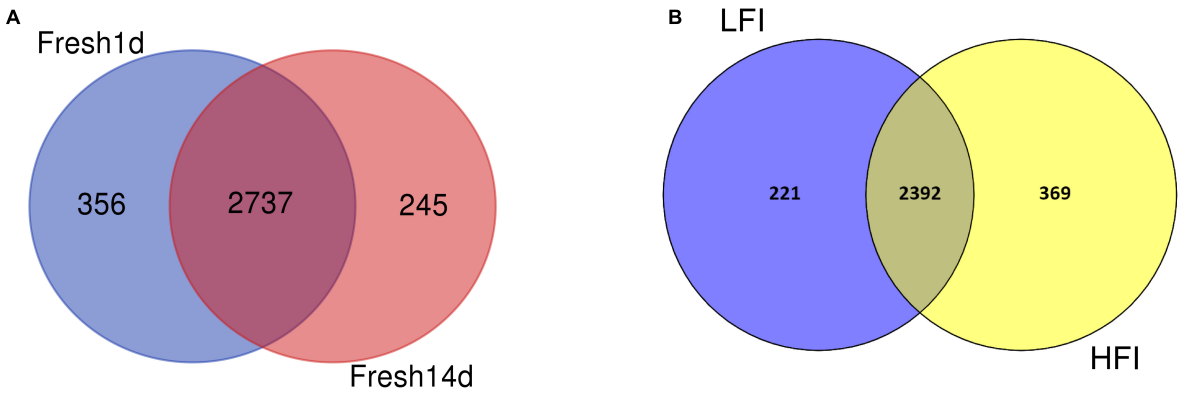

FIGURE 2 | (A) Venn diagram plot of fresh cow samples. The core community for all fresh cow is defined as those OTUs present in all fresh animals cows for all sampling time. **(B)** Venn diagram plot of LFI and HFI cow samples. The core community for LFI and HFI cows is defined as those OTUs present in LFI and HFI cow at 14d after calving.

as showed in **Figure 4**. We found a total of 24 OTUs that were significantly ($P < 0.05$) correlated with DMI; of them, 8 OTUs negatively correlated with DMI, 4 of which were in the genus *Prevotella_1* ($P < 0.05$) and 3 of which were in the family *Bacteroidales_S24-7_group* ($P < 0.05$). There were 15 OTUs positively correlated with DMI, of which 3 were

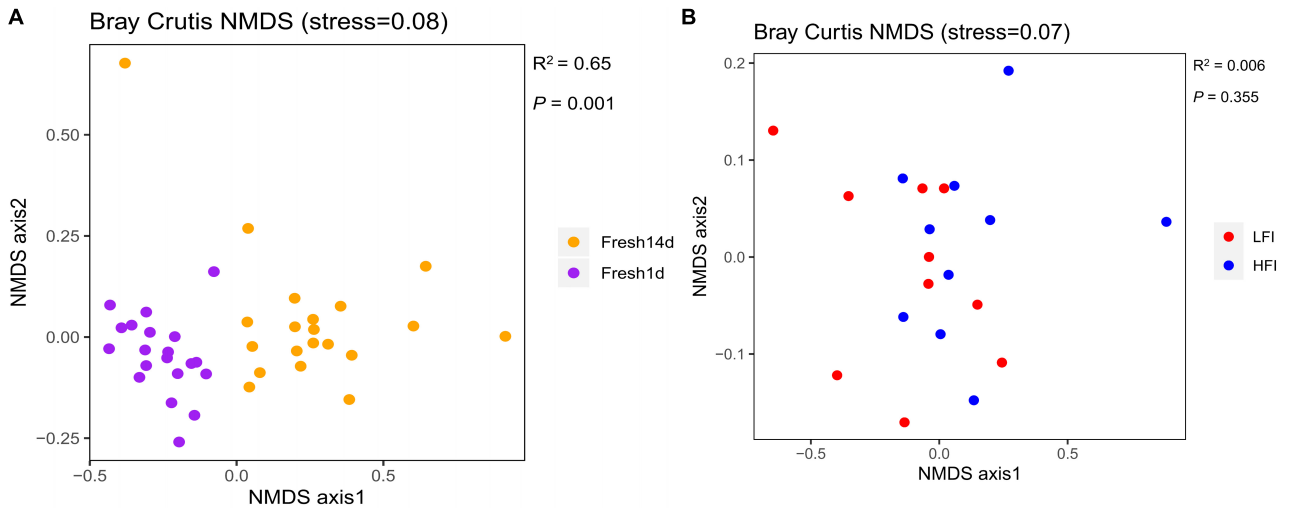

FIGURE 3 | (A) NMDS plots of the bacterial communities of fresh cows samples on 1 d (n = 20) and 14 d (n = 20) after calving. Fresh1d: fresh cows on 1d after calving; Fresh14d: fresh cows on 14 d after calving. **(B)** NMDS plots of the ruminal bacterial communities of LFI (n = 10) and HFI (n = 10) cows based on Bray-Curtis distance. LFI, low feed intake fresh cow group; HFI, high feed intake fresh cow group.

TABLE 3 | Significantly different phyla and families (relative abundance > 0.1%) within the rumen microbiota by lactation period and DMI as determined by the Wilcoxon test.

Phylum/Family	Lactation		SEM	*P*-value	DMI		SEM	*P*-value
	Fresh1	Fresh14d			LFI	HFI		
Actinobacteria	0.74	0.51	0.06	0.040	0.39	0.63	0.07	0.089
Coriobacteriaceae	0.66	0.43	0.05	0.011	0.32	0.54	0.06	0.045
Bacteroidetes	50.65	54.56	1.17	0.210	52.04	57.07	1.68	0.143
Bacteroidales_BS11_gut_group	5.30	1.95	0.42	< 0.001	1.57	2.34	0.27	0.280
Bacteroidales_Incertae_Sedis	0.55	0.27	0.03	0.002	0.23	0.30	0.03	0.315
Bacteroidales_RF16_group	1.00	0.40	0.08	0.006	0.33	0.47	0.09	0.406
Bacteroidales_UCG-001	0.17	0.08	0.02	0.035	0.04	0.11	0.02	0.256
Marinilabiaceae	0.12	4.18E-03	0.02	0.002	2.09E-03	6.28E-03	1.49E-03	0.087
Porphyromonadaceae	0.21	0.02	0.04	0.002	7.53E-03	0.04	0.02	0.516
Prevotellaceae	34.89	45.45	1.70	0.002	44.07	46.82	2.07	0.315
Rikenellaceae	4.35	1.68	0.32	< 0.001	1.27	2.09	0.29	0.315
Firmicutes	37.11	32.69	1.47	0.054	34.16	31.22	1.40	0.481
Christensenellaceae	4.53	1.76	0.32	0.002	1.30	2.22	0.35	0.063
Clostridiales_vadinBB60_group	0.11	0.03	0.01	0.010	0.02	0.04	8.91E-03	0.092
Family_XIII	0.80	0.46	0.04	0.002	0.46	0.46	0.03	0.791
ODP1230B8.23	0.17	0.08	0.03	0.011	0.02	0.13	0.05	0.140
Ruminococcaceae	11.49	7.77	0.55	0.007	7.96	7.58	0.53	0.796
Veillonellaceae	3.03	5.16	0.34	0.003	5.46	4.86	0.45	0.529
Proteobacteria	5.53	6.90	1.17	0.840	9.36	4.43	1.23	0.043
Desulfovibrionaceae	0.34	0.14	0.03	< 0.001	0.13	0.15	0.02	0.940
Succinivibrionaceae	4.49	6.30	0.73	0.610	8.89	3.71	1.25	0.043
Synergistetes	0.18	0.19	0.08	0.005	0.10	0.28	0.09	0.186
Synergistaceae	0.18	0.19	0.04	0.060	0.10	0.28	0.09	0.186
Tenericutes	0.75	0.47	0.06	0.005	0.44	0.50	0.06	0.880
Anaeroplasmataceae	0.39	0.24	0.03	0.049	0.19	0.28	0.04	0.344

in the *Treponema_2* ($P < 0.05$) and 2 were in the family *Prevotellaceae* ($P < 0.05$). There was one OTUs identified as belonging to the *Defluviitaleaceae_UCG-011* that was negatively ($P < 0.05$) associated with DMI. In addition, OTUs within the *Prevotellaceae_UCG-001*, *Lachnobacterium,* and *Olsenella* were significantly and positively ($P < 0.05$) correlated with DMI.

TABLE 4 | Significantly different genera (relative abundance > 0.1%) within the rumen microbiota by lactation period and DMI as determined by the Wilcoxon test.

Genera	Lactation		SEM	*P*-value	DMI		SEM	*P*-value
	Fresh1d	Fresh14d			LFI	HFI		
Phocaeicola	0.55	0.27	0.03	< 0.001	0.23	0.30	0.03	0.315
Prevotella_7	0.06	5.00	1.02	< 0.001	7.80	2.19	1.90	0.344
Prevotellaceae_Ga6A1_group	0.22	0.49	0.04	0.003	0.41	0.58	0.06	0.290
Prevotellaceae_UCG-003	1.37	0.91	0.09	0.017	0.70	1.13	0.12	0.112
Prevotellaceae_YAB2003_group	0.32	1.07	0.10	< 0.001	1.13	1.00	0.15	0.912
Rikenellaceae_RC9_gut_group	3.84	1.54	0.28	< 0.001	1.19	1.88	0.24	0.315
SP3-e08	0.20	0.06	0.03	< 0.001	0.01	0.11	0.05	0.494
Anaerotruncus	0.14	0.04	0.01	< 0.001	0.05	0.03	0.01	1.000
Anaerovorax	0.20	0.09	0.01	< 0.001	0.10	0.09	0.01	0.677
Butyrivibrio_2	1.57	0.66	0.10	< 0.001	0.65	0.68	0.06	0.971
Christensenellaceae_R-7_group	3.90	1.66	0.28	< 0.001	1.20	2.11	0.34	0.070
Coprococcus_2	0.02	0.06	0.01	0.003	0.07	0.06	0.01	0.426
Erysipelotrichaceae_UCG-002	2.09E-04	0.08	0.02	0.001	0.14	0.01	0.03	0.038
Eubacterium_coprostanoligenes_group	0.79	0.45	0.05	0.003	0.42	0.48	0.03	0.406
Eubacterium_hallii_group	0.16	0.12	0.01	0.018	0.09	0.14	0.02	0.173
Eubacterium_ruminantium_group	0.47	0.91	0.07	0.008	1.01	0.81	0.11	0.529
Eubacterium_uniforme	6.28E-04	0.10	0.02	< 0.001	0.13	0.08	0.03	0.344
Lachnoclostridium_1	0.11	0.17	0.01	0.006	0.18	0.15	0.01	0.344
Lachnoclostridium_12	0.03	0.09	0.01	0.017	0.10	0.07	0.02	0.384
Lachnospira	0.05	0.67	0.09	< 0.001	0.92	0.41	0.16	0.075
Lachnospiraceae_ND3007_group	0.39	0.18	0.04	0.001	0.21	0.16	0.05	0.850
Lachnospiraceae_NK4A136_group	0.13	0.07	0.01	0.013	0.08	0.06	0.01	0.449
Lachnospiraceae_XPB1014_group	0.47	0.14	0.03	< 0.001	0.10	0.17	0.03	0.256
Lactobacillus	0.01	0.07	0.01	0.002	0.10	0.04	0.03	0.677
Megasphaera	0.01	0.11	0.02	< 0.001	0.14	0.08	0.03	0.363
Moryella	0.31	0.22	0.02	0.010	0.22	0.23	0.02	0.970
Oribacterium	0.32	1.13	0.14	< 0.001	1.42	0.84	0.25	0.529
Papillibacter	0.42	0.06	0.05	< 0.001	0.05	0.07	0.01	0.384
probable_genus_10	0.18	0.11	0.01	0.039	0.12	0.11	0.02	0.850
Pseudobutyrivibrio	1.59	0.53	0.14	< 0.001	0.46	0.59	0.06	0.353
Ruminococcaceae_NK4A214_group	2.51	1.30	0.14	< 0.001	1.21	1.39	0.12	0.481
Ruminococcaceae_UCG-002	0.21	0.11	0.02	0.013	0.11	0.12	0.02	0.496
Ruminococcaceae_UCG-005	0.95	0.31	0.10	0.002	0.30	0.32	0.07	0.393
Ruminococcaceae_UCG-010	0.59	0.13	0.06	< 0.001	0.11	0.16	0.03	0.054
Schwartzia	0.32	0.52	0.04	0.004	0.53	0.51	0.04	0.623
Selenomonas	4.81E-03	0.50	0.07	< 0.001	0.65	0.35	0.13	0.315
Selenomonas_3	0.00	0.10	0.02	< 0.001	0.15	0.07	0.03	0.103
Veillonellaceae_UCG-001	1.24	0.47	0.09	< 0.001	0.44	0.50	0.05	0.473
Desulfovibrio	0.33	0.14	0.03	< 0.001	0.13	0.15	0.02	0.910
Ruminobacter	0.68	0.17	0.09	< 0.001	0.18	0.15	0.06	0.520
Succinivibrionaceae_UCG-001	1.05E-03	4.45	0.71	< 0.001	6.48	2.42	1.24	0.162
Succinivibrionaceae_UCG-002	2.92	1.16	0.36	0.005	1.59	0.72	0.40	0.472
Candidatus_Saccharimonas	0.98	0.60	0.06	0.005	0.57	0.63	0.05	0.529
Pyramidobacter	0.13	0.15	0.03	0.018	0.09	0.21	0.06	0.186
Anaeroplasma	0.39	0.24	0.03	0.036	0.19	0.28	0.04	0.344

We also found 11 OTUs that were significantly correlated with milk yield; of them, 6 OTUs were significantly and negatively ($P < 0.05$) associated with milk yield, and belonged to the genera *Lachnospiraceae_NK3A20_group*, *Coprococcus_1*, *Oribacterium*, *Mogibacterium* and family *Bacteroidales_BS11_gut_group* and *Prevotellaceae*. There were 5 OTUs significantly and positively ($P < 0.05$) correlated with milk yield and belonged to the genera *Prevotella_1*, *Anaeroplasma*, *Treponema_2,* and *Eubacterium_coprostanoligenes_group*. Additionally, we identified a significant and negative correlation

between DMI/milk yield and the relative abundance of OTUs within *Prevotella_1* and the family *Bacteroidales_S24-7_group* ($P < 0.05$).

For VFAs, we found that acetate concentration was postively correlated with the relative abundance of OTU2072 (*Anaeroplasma*, $r = 0.578$, $P = 0.007$) and OTU587 (*Treponema_2*, $r = 0.550$, $P = 0.012$). We also found that propionate concentration was negatively correlated with the relative abundance of four OTUs, including OTU2019 (*Butyrivibrio_2*, $r = -0.654$, $P = 0.003$), OTU742 (*Prevotella_1*, $r = -0.469$, $P = 0.049$), OTU928 (*Prevotella_1*, $r = -0.523$, $P = 0.026$), and OTU2499 (*Christensenellaceae_R-7_group*, $r = -0.476$, $P = 0.046$). The butyrate concentration was negatively and significantly ($P < 0.05$) correlated with OTUs within *Butyrivibrio_2*, *Candidatus_Saccharimonas,* and *Prevotella_1*. OTUs within *Anaeroplasma* and the family *Bacteroidales_S24-7_group* were significantly and positively ($P < 0.05$) correlated with valerate concentration, while OTUs within *Acetitomaculum*, *Butyrivibrio_2*, *Candidatus_Saccharimonas,* and *Christensenellaceae_R-7_group* were significantly and negatively ($P < 0.05$) correlated with valerate concentration. The isovalerate concentration was positively correlated with OTU1731 (Fibrobacter, $r = 0.522$, $P = 0.018$). The AP ratio was positively correlated with the relative abundances of OTU2019 (*Butyrivibrio_2*, $r = 0.571$, $P = 0.013$), OTU2297 (*Christensenellaceae_R-7_group*, r = 0.514, $P = 0.029$), OTU2499 (*Christensenellaceae_R-7_group*, $r = 0.491$, $P = 0.038$), OTU2457 (*Mogibacterium*, $r = 0.502$, $P = 0.034$) and OTU928 (*Prevotella_1*, $r = 0.504$, $P = 0.033$).

DISCUSSION

The objective of this study was to characterize the ruminal microbiota during the freshening period and to determine the impact of DMI in shaping its dynamics. We designed this experiment to follow the rumen microbiota within the first 14 days after calving in a group of fresh cows and to compare low and high DMI cows from this group. Given that low DMI in fresh cows is known to result in reduced lactation efficiency and increased risk for host metabolic syndromes, understanding the dynamics of the ruminal microbiota during this period may provide a framework for managing this critical transition period.

Consistent with the known changes in both host metabolism and the endocrine system across gestation and lactation, it is perhaps not surprising that we observed significant differences in the ruminal bacterial community and rumen fermentation index in fresh cows between days 1 and 14. This is also likely due to the significant differences in the diet fed to transition animals, which differs substantially from the beginning to the end of this period. Recently it was shown that lactation has a far greater impact in shaping the ruminal microbiota in dairy cows than host genetics (Bainbridge et al., 2016). Additionally, Pitta et al. (2014) found that the ruminal microbiota of lactation cows 1–3 days after calving was most similar to the ruminal microbiota of prepartum cows. Thus, the shifts in the ruminal bacterial community of fresh cows from 1 to 14 days observed here is likely due to the interaction of lactation and diet.

Compared to Fresh1d cows, the Fresh14d cows harbored a higher relative abundance of *Prevotellaceae*, *Veillonellaceae*, and bacteria within these families are known to degrade and ferment carbohydrates into VFAs (Zhang et al., 2018). We also found significantly higher relative abundances of *Succinivibrionaceae_UCG-001*, which was increased more than 4,000-fold in Fresh14d cows. This is in agreement with observations indicating that members of this genera utilize hydrogen to produce succinate, which can be converted to propionate (McCabe et al., 2015). This purported in propionate may contribute to the observed decrease in AP. Moreover, we found higher levels of acetate, propionate, valerate, total VFAs, and a lower AP ratio in the rumen from Fresh14d cows, relative to Fresh1d cows, which likely reflects a stronger fermentation capacity of the Fresh14d ruminal microbiota.

In addition to our findings on the temporal dynamics of the rumen microbiota in fresh cows, our study also considered the impact of DMI on the rumen microbiota of fresh cows. Here, we found that increased DMI was associated with lower relative abundances of *Erysipelotrichaceae_UCG-002*, within the family *Erysipelotrichaceae*, and higher relative abundances of *Ruminococcaceae_UCG-010*, within the family *Ruminococcaceae*. These findings are in accordance with a previous study of low, medium, and high feed intake cows during early lactation which found decreased numbers of *Erysipelotrichaceae* and increased numbers of *Ruminococcaceae* in high feed intake cows (Li et al., 2020). More recently, a study on the feed efficiency of dairy cows found that increased milk production was associated with higher relative abundances of bacteria in the *Bacteroidales*, *Lachnospiraceae*, *Ruminococcaceae*, and *Prevotella* (Shabat et al., 2016).

Given the effect of DMI on the rumen bacterial community, it is not surprising that specific bacterial species are strongly correlated with DMI. Here, we observed a strong correlation between DMI and bacteria in the families *Prevotellaceae*, *Ruminnococcaceae*, *unclassified_Bacteroidales_S11_gut_group*, and *Lachnospiraceae*. This is in accordance with other studies that also found a strong correlation between DMI and bacteria in the families *Prevotellaceae* and *Ruminnococcaceae* (Jami et al., 2014). Other work demonstrating the heritability of OTUs within the *Succinivibrionaceae*, *Megasphaera*, *Selenonmonas*, *Oscillospira,* and unclassified *BS11*, as it relates to DMI in beef cattle (Li et al., 2019), also support our findings. Related to this, our study also found that OTUs associated with high DMI fresh cows were the core microbiota in LFI and HFI cows. We note that many of these are consistent with previously reported OTUs found to be heritable in high DMI beef cattle, including bacteria in the *Prevotella* and *Lanchnospirraceae* (Sasson et al., 2017). In our study, we also found a strong and positive correlation between milk yield and OTUs within *Prevotella_1*, *Anaeroplasm* and *Treponema_2*. This is in accordance with other studies which also found that *Prevotella*, *unclassified_Bacteroidales_S24-7* and *Succinivibrionaceae* were strongly and positively correlated with milk yield in lactating dairy cows (Indugu et al., 2017). Given

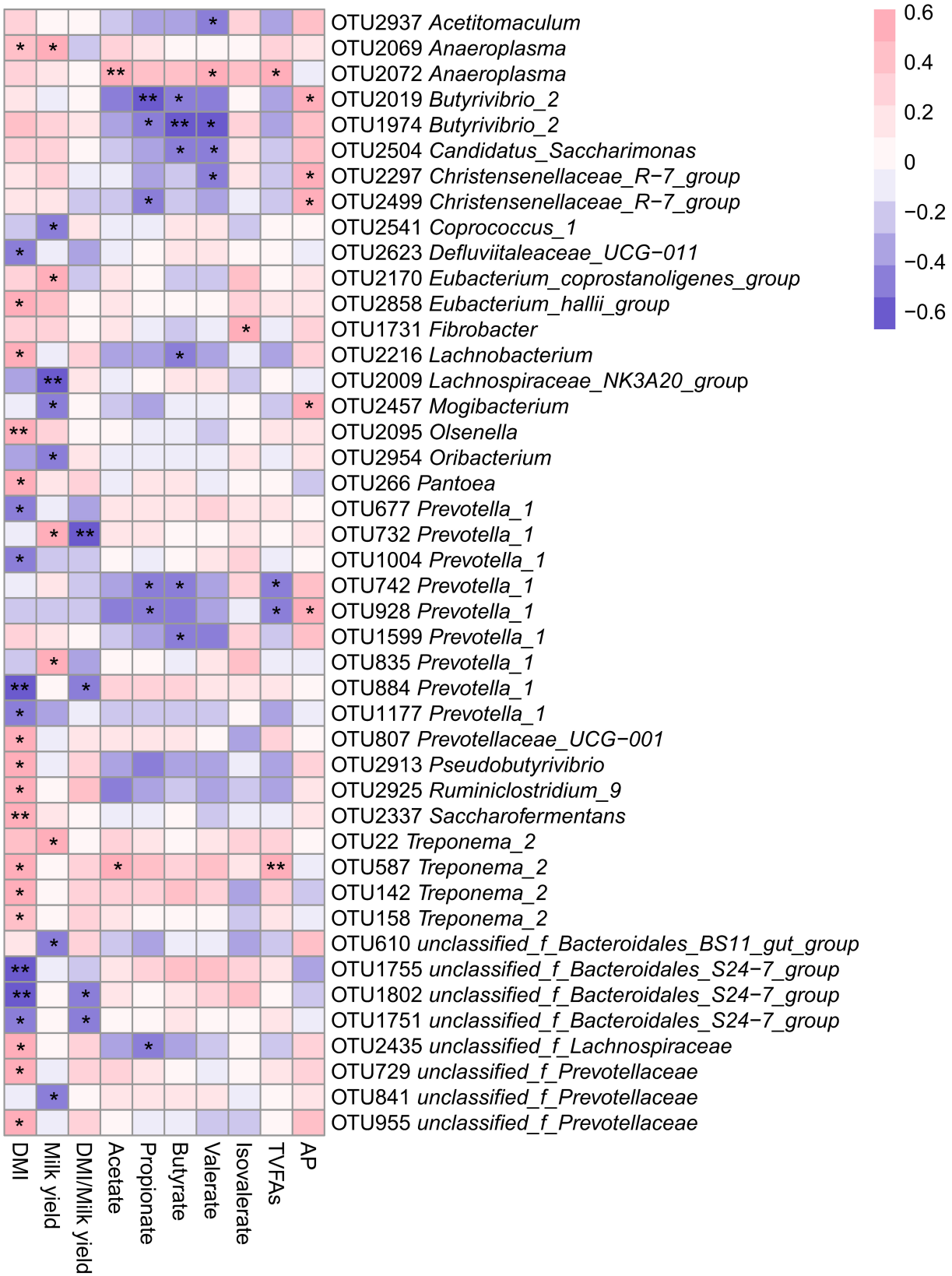

FIGURE 4 | Heatmap of OTUs (relative abundance >0.01% in at all samples) significantly associated with production and rumen fermentative parameters in LFI and HFI cows, as determined by Spearman's correlation analysis. *$0.01 < P < 0.05$, **$0.001 < P < 0.01$.

these findings future work should further investigate these bacteria as potential targets for improving DMI in fresh cows.

Considering the essential role of the rumen bacteria in fermenting plant material into VFAs (Kittelmann et al., 2013), which have a direct effect on milk production (Hurtaud et al., 1995; Brulc et al., 2009), documenting the rumen microbiota in early lactation may help in better understanding the impact of the rumen microbiota on production traits. Moreover, the rumen microbiota during the freshening period may serve as a predictor of future production and may allow for manipulation in order to improve long term milk production. The results presented here have identified a number of specific bacterial taxa associated with both low and high DMI in fresh cows over time, and many of these may serve as potential targets for mitigating the challenges associated with low DMI cows during the freshening period. However, future work using more functional approaches, such as metagenomics and metatranscriptomics, should be conducted to better understand the interaction between rumen microbiome and DMI in fresh cows.

CONCLUSION

In summary, the results of this study provide novel evidence for an alteration of the microbiome in the rumen of fresh cows from 1 to 14 days after calving. We found that the ruminal microbiota and its associated fermentation patterns differed during this period and that the relative abundance of many VFA—producing microbes within the *Prevotellaceae*, *Lactobacillaceae,* and *Veillonellaceae* were dramatically increased in Fresh14d cows compared with Fresh1d cows. These findings indicate a potential stronger ability to ferment dietary substrates by the rumen microbiota of Fresh14d cows than that of Fresh1d cows. Additionally, we found limited differences between the ruminal microbiota of LFI and HFI groups, thereby reflecting the limited role of DMI on shaping the rumen microbiota during the freshening period. Furthermore, a strong relationship between the relative abundances of specific OTUs and host production traits suggests the possibility to predict downstream host production using the rumen microbiota. This could lead to approaches for manipulating the rumen microbiota to improve DMI and milk production in dairy cows during the transition period. Future studies should investigate the relationship between the rumen microbiota and DMI across different environments in an integrative manner that incorporates both host genetics and functional metagenomics in the rumen.

DATA AVAILABILITY STATEMENT

The datasets presented in this study can be found in online repositories. The names of the repository/repositories and accession number(s) can be found below: https://www.ncbi.nlm.nih.gov/, PRJNA599409.

ETHICS STATEMENT

The animal experiments and study protocols described in this study were approved by the Institutional Animal Care and Use Committee of the College of Animal Science and Technology (Project number 31772628) at China Agricultural University, Beijing, China.

AUTHOR CONTRIBUTIONS

SJ, SL, and SH conceived and designed the study. SH and FW collected all samples used in this study. SH performed the data analysis and wrote the manuscript with contributions from GS. All authors read and approved the final manuscript.

FUNDING

This research was supported by the Key Research and Development Project of Ningxia Hui Autonomous Region grant numbers 2018BBF33006 and 2018YFD0501600 from the National Key Research and Development Program of China. GS was supported by a US Department of Agriculture National Institute of Food and Agriculture Hatch project WIS02007.

ACKNOWLEDGMENTS

We would like to thank the staff at the Zhongdi Breeding Stock Co., Ltd., for daily animal care. We also thank all members of the Li laboratory for their support and help in collecting samples. Finally, we thank Jie Huang from Yangzhou Univerisity, Yangzhou, China, for collecting samples and feeding animals.

SUPPLEMENTARY MATERIAL

The Supplementary Material for this article can be found online at: https://www.frontiersin.org/articles/10.3389/fmicb.2021.630605/full#supplementary-material

REFERENCES

Bainbridge, M. L., Cersosimo, L. M., Wright, A. D., and Kraft, J. (2016). Rumen bacterial communities shift across a lactation in Holstein, Jersey and Holstein x Jersey dairy cows and correlate to rumen function, bacterial fatty acid composition and production parameters. *FEMS Microbiol. Ecol.* 92:fiw059. doi: 10.1093/femsec/fiw059

Benjamini, Y., and Hochberg, Y. (1995). Controlling the false discovery rate: a practical and powerful approach to multiple testing. *J. R. Statis. Soc.* 57, 289–300. doi: 10.1111/j.2517-6161.1995.tb02031.x

Brulc, J. M., Antonopoulos, D. A., Miller, M. E., Wilson, M. K., Yannarell, A. C., Dinsdale, E. A., et al. (2009). Gene-centric metagenomics of the fiber-adherent bovine rumen microbiome reveals forage specific glycoside hydrolases. *Proc. Nalt. Acad. Sci. U.S.A.* 106, 1948–1953. doi: 10.1073/pnas.0806191105

Caporaso, J. G., Kuczynski, J., Stombaugh, J., Bittinger, K., Bushman, F. D., Costello, E. K., et al. (2010). QIIME allows analysis of highthroughput community sequencing data. *Nat. Methods* 7, 335–336. doi: 10.1038/nmeth0510-335

Caporaso, J. G., Lauber, C. L., Walters, W. A., Berg-Lyons, D., Huntley, J., Fierer, N., et al. (2012). Ultra-high-throughput microbial community analysis on the Illumina HiSeq and MiSeq platforms. *ISME J.* 6, 1621–1624. doi: 10.1038/ismej.2012.8

Cole, J. R., Wang, Q., Cardenas, E., Fish, J., Chai, B., Farris, R. J., et al. (2009). The Ribosomal database project: improved alignments and new tools for rRNA analysis. *Nucleic Acids Res.* 37, D141–D145. doi: 10.1093/nar/gkn879

Edgar, R. C. (2010). Search and clustering orders of magnitude faster than BLAST. *Bioinformatics* 26, 2460–2461. doi: 10.1093/bioinformatics/btq461

Edgar, R. C., Haas, B. J., Clemente, J. C., Quince, C., and Knight, R. (2011). UCHIME improves sensitivity and speed of chimera detection. *Bioinformatics* 27, 2194–2200. doi: 10.1093/bioinformatics/btr381

Erwin, E., Marco, G., and Emery, E. (1961). Volatile fatty acid analyses of blood and rumen. *J. Dairy Sci.* 44, 1768–1771.

Ferguson, J. D. (2001). *Milk Urea Nitrogen*. 2681–2692. Available online at: http://cahpwww.vet.upenn.edu/doku.php/dairycattle:mun. (accessed July 28, 2014).

Flint, H. J., Bayer, E. A., Rincon, M. T., Lamed, R., and White, B. A. (2008). Polysaccharide utilization by gut bacteria: potential for new insights from genomic analysis. *Nat. Rev. Microbiol.* 6, 121–131. doi: 10.1038/nrmicro1817

Hurtaud, C., Rulquin, H., and Verite, R. (1995). Effect of infused volatile fatty acids and caseinate on milk composition and coagulation in dairy cows. *J. Dairy Sci.* 76, 3011–3020. doi: 10.3168/jds.S0022-0302(93)77640-7

Indugu, N., Vecchiarelli, B., Baker, L. D., Ferguson, J. D., Vanamala, J. K. P., and Pitta, D. W. (2017). Comparison of rumen bacterial communities in dairy herds of different production. *BMC Microbiol.* 17:190. doi: 10.1186/s12866-017-1098-z

Jami, E., and Mizrahi, I. (2012). Composition and similarity of bovine rumen microbiota across individual animals. *PLoS One* 7:e33306. doi: 10.1371/journal.pone.0033306.g001

Jami, E., White, B. A., and Mizrahi, I. (2014). Potential role of the bovine rumen microbiome in modulating milk composition and feed efficiency. *PLoS One* 9:e85423. doi: 10.1371/journal.pone.0085423

Kittelmann, S., Seedorf, H., Walters, W. A., Clemente, J. C., Knight, R., Gordon, J. I., et al. (2013). Simultaneous amplicon sequencing to explore co-occurrence patterns of bacterial, archaeal and eukaryotic microorganisms in rumen microbial communities. *PLoS One* 8:e47879. doi: 10.1371/journal.pone.0047879

Li, F., Li, C., Chen, Y., Liu, J., Zhang, C., Irving, B., et al. (2019). Host genetics influence the rumen microbiota and heritable rumen microbial features associate with feed efficiency in cattle. *Microbiome* 7:92. doi: 10.1186/s40168-019-0699-1

Li, Y. Q., Xi, Y. M., Wang, Z. D., Zeng, H. F., and Han, Z. (2020). Combined signature of rumen microbiome and metabolome in dairy cows with different feed intake levels. *J. Anim. Sci.* 98, 1–15. doi: 10.1093/jas/skaa070

Lima, F. S., Oikonomou, G., Lima, S. F., Bicalho, M. L., Ganda, E. K., Filho, J. C., et al. (2015). Prepartum and postpartum rumen fluid microbiomes: characterization and correlation with production traits in dairy cows. *Appl. Environ. Microbiol.* 81, 1327–1337. doi: 10.1128/AEM.03138-14

Magoc, T., and Salzberg, S. L. (2011). FLASH: fast length adjustment of short reads to improve genome assemblies. *Bioinformatics* 27, 2957–2963. doi: 10.1093/bioinformatics/btr507

McCabe, M. S., Cormican, P., Keogh, K., O'Connor, A., O'Hara, E., Palladino, R. A., et al. (2015). Illumina MiSeq phylogenetic amplicon sequencing shows a large reduction of an uncharacterised *Succinivibrionaceae* and an Increase of the *Methanobrevibacter gottschalkii Clade* in feed restricted cattle. *PLoS One* 10:e0133234. doi: 10.1371/journal.pone.0133234

Oksanen, J., Blanchet, F. G., Kindt, R., Legendre, P., Minchin, P. R., O'Hara, R. B., et al. (2015). *Vegan: Community Ecology Package*. R Package Version 2.2-1.

Pitta, D. W., Kumar, S., Vecchiarelli, B., Shirley, D. J., Bittinger, K., and Baker, L. D. (2014). Temporal dynamics in the ruminal microbiome of dairy cows during the transition period. *J. Anim. Sci.* 92, 4014–4022. doi: 10.2527/jas2014-7621

Quast, C., Pruesse, E., Yilmaz, P., Gerken, J., Schweer, T., Yarza, P., et al. (2013). The SILVA ribosomal RNA gene database project: improved data processing and web-based tools. *Nucleic Acids Res.* 41, D590–D596. doi: 10.1093/nar/gks1219

Ren, W., Wang, P., Yan, J., Liu, G., Zeng, B., Hussain, T., et al. (2017). Melatonin alleviates weanling stress in mice: involvement of intestinal microbiota. *J. Pineal. Res.* 64:e12448. doi: 10.1111/jpi.12448

Reynolds, C. K., Huntington, G. B., Tyrrell, H. F., and Reynolds, P. J. (1988). Net Metabolism of volatile fatty acids, d-β-hydroxybutyrate, nonesterified fatty acids, and blood gasses by portal-drained viscera and liver of lactating holstein cows. *J. Dairy Sci.* 71, 2395–2405. doi: 10.3168/jds.s0022-0302(88)79824-0

Roche, J. R., Bell, A. W., Overton, T. R., and Loor, J. J. (2013). Nutritional management of the transition cow in the 21st century-a paradigm shift in thinking. *Anim. Prod. Sci.* 53, 1000–1023. doi: 10.1071/an12293

Sasson, G., Kruger Ben-Shabat, S., Seroussi, E., Doron-Faigenboim, A., Shterzer, N., Yaacoby, S., et al. (2017). Heritable bovine rumen bacteria are phylogenetically related and correlated with the cow's capacity to harvest energy from its feed. *mBio* 8, e703–e717. doi: 10.1128/mBio.00703-17

Shabat, S. K., Sasson, G., Doron-Faigenboim, A., Durman, T., Yaacoby, S., Berg Miller, M. E., et al. (2016). Specific microbiome-dependent mechanisms underlie the energy harvest efficiency of ruminants. *ISME J.* 10, 2958–2972. doi: 10.1038/ismej.2016.62

Shi, F. Y., Guo, N., Degen, A. A., Niu, J. H., Wei, H. Y., Jing, X. P., et al. (2020). Effects of level of feed intake and season on digestibility of dietary components, efficiency of microbial protein synthesis, rumen fermentation and ruminal microbiota in yaks. *Anim. Feed Sci. Technol.* 259:114359. doi: 10.1016/j.anifeedsci.2019.114359

Weimer, P. J. (2015). Redundancy, resilience, and host specificity of the ruminal microbiota: implications for engineering improved ruminal fermentations. *Front. Microbiol.* 6:296. doi: 10.3389/fmicb.2015.00296

Wickham, H. (2009). *ggplot2: Elegant Graphics for Data Analysis*. New York, NY: Springer-Verlag.

Zhang, J. J., Kobert, K., Flouri, T., and Stamatakis, A. (2014). PEAR: a fast and accurate Illumina Paired-End reAd mergeR. *Bioinformatics* 30, 614–620. doi: 10.1093/bioinformatics/btt593

Zhang, L., Wu, W., Lee, Y. K., Xie, J., and Zhang, H. (2018). Spatial heterogeneity and co-occurrence of mucosal and luminal microbiome across swine intestinal tract. *Front. Microbiol.* 9:48. doi: 10.3389/fmicb.2018.00048

Zhu, Z., Kristensen, L., Difford, G. F., Poulsen, M., Noel, S. J., Abu Al-Soud, W., et al. (2018). Changes in rumen bacterial and archaeal communities over the transition period in primiparous Holstein dairy cows. *J. Dairy Sci.* 101, 9847–9862. doi: 10.3168/jds.2017-14366

Zhu, Z., Noel, S. J., Difford, G. F., Al-Soud, W. A., Brejnrod, A., Sorensen, S. J., et al. (2017). Community structure of the metabolically active rumen bacterial and archaeal communities of dairy cows over the transition period. *PLoS One* 12:e0187858. doi: 10.1371/journal.pone.0187858

Conflict of Interest: The authors declare that the research was conducted in the absence of any commercial or financial relationships that could be construed as a potential conflict of interest.

frontiers in Genetics

DATA REPORT
published: 04 March 2021
doi: 10.3389/fgene.2021.645401

Transcriptome Analysis of Selenium-Treated Porcine Alveolar Macrophages Against Lipopolysaccharide Infection

*Jia-Xuan Liu, Xin-Yu Chao, Peng Chen, Yi-Ding Wang, Tong-Jian Su, Meng Li, Ru-Yu Xu and Qiong Wu**

Animal Science and Technology College, Beijing University of Agriculture, Beijing, China

Keywords: transcriptome (RNA-seq), selenium, porcine alveolar macrophage, lipopolysaccharide, differentially expressed genes

OPEN ACCESS

Edited by:
Jing Wang,
Beijing Academy of Agriculture and Forestry Sciences, China

Reviewed by:
Haoyu Liu,
Uppsala University, Sweden
Yongxia Liu,
Shandong Agricultural University, China

****Correspondence:***
Qiong Wu
wuqiongbua@163.com

Specialty section:
This article was submitted to Livestock Genomics, a section of the journal Frontiers in Genetics

Received: *23 December 2020*
Accepted: *02 February 2021*
Published: *04 March 2021*

Citation:
Liu J-X, Chao X-Y, Chen P, Wang Y-D, Su T-J, Li M, Xu R-Y and Wu Q (2021) Transcriptome Analysis of Selenium-Treated Porcine Alveolar Macrophages Against Lipopolysaccharide Infection. Front. Genet. 12:645401. doi: 10.3389/fgene.2021.645401

INTRODUCTION

Several Gram-negative bacteria, including *Actinobacillus pleuropneumoniae* and *Haemophilus parasuis*, are responsible for respiratory diseases and cause huge economic losses to the swine industry worldwide. Lipopolysaccharide (LPS) is a cell outer membrane component of Gram-negative bacteria and serves as a major pro-inflammatory stimulus binding to pattern recognition receptor Toll-like receptor 4 (TLR4) (Ciesielska et al., 2020). LPS is ubiquitous in nature and exists in high concentrations in air pollution, soil, and organic dust. Inhalation of LPS is involved in the pathogenesis of lung inflammation (Kaelberer et al., 2020).

Alveolar macrophages (AMs) are the predominant immune cells located at the air-surface interface of alveoli. Resident AMs that arise during embryogenesis and recruited AMs that originate postnatally from circulating monocytes coexist in the inflamed lung. Once infection occurs, AMs move between alveoli to sense and phagocytose inhaled bacteria before they can induce harmful lung inflammation (Neupane et al., 2020). Meanwhile, the Gram-negative bacterial LPS binding to the TLR4 of AMs initiates multiple intracellular signaling pathways and induces the production of some pro-inflammatory cytokines, such as interleukin 1β (IL-1β) (Li et al., 2017). These pro-inflammatory cytokines induce superfluous neutrophil recruitment, leading to continuous lung inflammation and injury. The activation states of AMs are divided into classically activated (M1) and alternatively activated (M2). M1-type AMs generally induced by TLR signaling and interferon-gamma (IFN-γ) secrete pro-inflammatory cytokines, and M2-type AMs generally induced by interleukin-4 (IL-4) are anti-inflammatory and typically express the transforming growth factor-β (TGF-β) (Hussell and Bell, 2014). However, the gene reprogramming and polarization states of macrophages are also affected by stimulation intensity and tissue origin. A meta-analysis of *in vitro* differentiated macrophages showed that macrophages display distinguishing activation states even after early (2–4 h) or late (18–24 h) LPS infection (Chen et al., 2019). In M1-type AMs, increased levels of reactive oxygen species, such as hydrogen peroxide, superoxide, and hydroxyl, are implicated in DNA damage and membrane dysfunction (Riazanski et al., 2020). Therefore, the cellular antioxidant capacity of AMs is indispensable for controlling the homeostasis of intracellular oxidative stress and maintaining immune defense.

Selenium (Se) is considered as a functional element of thioredoxin reductase, glutathione peroxidase, and other Se-containing enzymes and protects against oxidative injury (Silvestrini et al., 2020). LPS infection impairs Se metabolism and leads to dysregulation of selenoprotein expression in the spleen, thymus, and lymph node of pigs (Sun et al., 2017). An animal study using a chicken model of Se deficiency has demonstrated the negative correlation between

Se deficiency and inflammation-related gene expression in skeletal muscles (Wu et al., 2014). Se supplementation can attenuate inflammatory response and lung injury induced by a variety of stimuli, including virus (Liu et al., 2015), bacteria (Xu et al., 2020), and heavy metal (Ghorbel et al., 2017). It was also reported that supplementation of Se to macrophages ameliorates the pro-inflammatory response induced by LPS (Vunta et al., 2008). However, the potential molecular mechanism of the anti-inflammatory function of Se is still unclear. Transcriptome sequencing is proven to be a powerful tool to comprehensively view the immune response of porcine AMs (PAMs) to bacterial or viral infection (Kim et al., 2019; Park et al., 2020). In this study, we performed transcriptome sequencing to deepen the understanding of the mechanism of Se protecting PAMs against LPS infection.

MATERIALS AND METHODS

Cell Culture and Treatment

The porcine lung alveolar macrophage cell line 3D4/31 (ATCC CRL-2844) was cultured in RPMI 1640 medium (Invitrogen, Carlsbad, CA, USA) supplemented with 10% heat-inactivated fetal calf serum, 100 U/ml of penicillin, 100 μg/ml of streptomycin, and 1 mM of sodium pyruvate. Confluent cell monolayers were treated under three different conditions: (i) RPMI 1640 medium alone (CON group), (ii) LPS from *Escherichia coli* O111:B4 (1 μg/ml, 3 ml) infection alone (LPS group), and (iii) pretreatment with Se as sodium selenite containing 0.1 μM for 6 h followed by LPS infection (1 μg/ml) (SeL group).

RNA Extraction, Library Construction, and Sequencing

At 12 h after LPS infection, total RNA was extracted, and the RNA integrity number was further assessed using an RNA 6000 Nano kit (Agilent Technologies, Santa Clara, CA, USA). PCR amplification was performed to obtain the final libraries. The constructed library was quantified and pooled in the flow cell. After cBot clustering, the RNA-seq libraries were sequenced using Illumina high-throughput sequencing Novaseq 6000 platform, with a paired-end read length of 150 base pairs (bp).

Genome Alignment and Gene Annotation

The clean reads were mapped to the pig reference genome Sscrofa11 using TopHat v2.1.1. The mapped reads were assembled into transcripts using StringTie v1.3.3b. The genes were annotated by BLAST based on the Cluster of Orthologous Groups of proteins (COG), Gene Ontology (GO), and Kyoto Encyclopedia of Genes and Genomes (KEGG) databases.

Analysis of Gene Expression Levels and Identification of Differentially Expressed Genes

The expression of genes was calculated and normalized to fragments per kilobases per million reads (FPKM) using RSEM v1.3.1. Differentially Expressed Genes (DEGs) were identified using DESeq2 v1.24.0. The p-value was adjusted using Benjamini and Hochberg's (BH) approach for controlling the false discovery rate. Genes with an adjusted p-value < 0.05 and fold change (FC) > 1.5 were assigned as DEGs.

Enrichment, Venn, and Protein–Protein Interaction Analysis of DEGs

GO enrichment analysis based on Fisher's exact test was carried out to specify the potential roles of DEGs using Goatools v0.6.5. The p-value was adjusted by BH, and GO terms with adjusted p-value < 0.05 were considered significantly enriched. KEGG enrichment analysis was performed to evaluate significantly enriched signal transduction or metabolic pathways using KOBAS v2.1.1. A Venn diagram was generated using the R package Venndiagram. The protein–protein interaction (PPI) analysis of DEGs was based on the Search Tool for the Retrieval of Interacting Genes/Proteins (STRING) database v11.0, and the minimum STRING score was set at 1,000. The interaction with a combined score >0.4 was considered to be significant. The protein network was visualized using NetworkX.

Data Accession Number

The raw transcriptome data have been deposited in the US National Center for Biotechnology Information Sequence Read Archive database under accession no. SRR13277478–SRR13277486.

RESULTS AND DISCUSSION

Quality Control and Transcriptome Assembly

A raw dataset consisting of 487.3 million reads (∼73.6 Gbps) was yielded. After filtering low-quality reads, adaptor or ambiguous sequences, and removal of contamination, 51.9 (98.73%, the percentage of clean reads), 57.1 (98.81%), and 51.9 (98.77%) million clean reads from the CON groups, 52 (98.82%), 49.2 (98.88%), and 58.3 (99.18%) million clean reads from the LPS group, and 51.2 (99.21%), 56.3 (99.24%), and 54.7 (99.29%) million clean reads from the SeL group were retained. The average of Q30 of clean reads was >94.64%, indicating that the obtained clean reads were of high quality (**Supplementary Table 1**). The saturation curve of sequencing showed that the FPKM values of ∼22.18% of genes from the CON, LPS, and SeL groups were expressed between 0.3 and 3.5, and that only a few of 6.53% of genes were highly expressed with an FPKM value >60. Most genes with medium or above expression level (i.e., the genes with FPKM value >3.5) were nearly saturated at 40% of the sequencing reads (ordinate value tended to 1), indicating that the sequencing quantity can cover most of the expressed genes (**Supplementary Table 2**; **Supplementary Figure 1**).

Analysis of Gene Expression

A total of 27,576 genes were found across all samples, including 25,880 (93.85%) annotated genes and 1,696 (6.15%) unannotated novel genes. Among 63,606 transcripts

identified, there were 14,158 novel transcripts, including 538 transcripts with exonic overlap with reference on the opposite strand, 666 transcripts with transfrag falling entirely within a reference intron, 10,491 transcripts with potentially novel isoform: at least one splice junction was shared with a reference transcript, 2,058 unknown transcripts, and intergenic transcripts, and 405 transcripts with generic exonic overlap with a reference transcript (**Supplementary Figure 2**).

A total of 964 (57.72%) novel transcripts and 12,473 (90.04%) novel genes were successfully annotated by BLAST, with 437 transcripts and 7,437 genes in the GO database, 91 and 7,664 in the KEGG database, 331 and 11,080 in the COG database, 955 and 12,451 in the NR database, 366 and 11,199 in the Swiss-Prot database, and 192 and 10,015 in the Pfam database, respectively (**Supplementary Table 3**). According to GO analysis, catalytic activity (259 genes) in molecular function, membrane (190 genes) and membrane part (186 genes) in the cellular component, and cellular process (122 genes) in the biological process were the most enriched ontology terms (**Supplementary Figure 3A**). A total of 91 novel genes were classified into 110 KEGG pathways involving 32 KEGG functional categories, mainly functioning in signal transduction, endocrine system, immune system, digestive system, translation, and environmental adaptation (**Supplementary Figure 3B**). The COG analysis showed that 37 novel genes were assigned into 13 COG functional categories (**Supplementary Figure 3C**), mainly including "intracellular trafficking, secretion, and vesicular transport" (Class U; 12 genes), "posttranslational modification, protein turnover, chaperones" (Class O; 9 genes), and "chromatin structure and dynamics" (Class B; 8 genes).

Analysis of DEGs

In the CON relative to the LPS group (CON_LPS), a total of 223 DEGs, including 28 up-regulated and 195 down-regulated DEGs, were identified (**Supplementary Figure 4A**; **Supplementary Table 4**). The top 10 known up-regulated genes were RF00030, CTF1, CCDC103, STMN3, WIPI1, RELB, PHLDA1, FLT3, CHCHD10, EXOSC6, HSD17B10, OTUD1, PPP1R14B, YRDC, GMIP, SCLY, CEBPB, and SESN2. The top 10 down-regulated genes were VMAC, ECM2, TMOD1, C17orf78, IGSF6, COCH, NAALADL1, MILR1, GSDMC, and SV2A. Out of 58 identified DEGs in LPS relative to the SeL group (LPS_SeL), 25 DEGs were up-regulated, and 33 DEGs were down-regulated (**Supplementary Figure 4B**; **Supplementary Table 5**). Se treatment induced the expression of anti-apoptosis protein BCL-2 and antioxidant defense-related glutathione peroxidase 1 (GPX1) and selenoprotein H and P (SELENOP). Se acts as a rare amino acid selenocysteine through incorporation into selenoproteins. It was reported that Se supplementation protects against apoptosis induced by reactive oxygen species or toxic heavy metal lead in a BCL-2-dependent manner (Khera et al., 2017; Wang et al., 2018). In CON relative to the SeL group (CON_SeL), out of 252 identified DEGs, 27 DEGs were up-regulated, and 225 DEGs were down-regulated (**Supplementary Figure 4C**; **Supplementary Table 6**).

Enrichment Analysis of DEGs

KEGG enrichment analysis of DEGs was performed. The DEGs in the CON_LPS group were enriched in the IL-17 signaling pathway, tumor necrosis factor (TNF) signaling pathway, cytokine–cytokine receptor interaction, lysine degradation, and graft-versus-host disease (**Figure 1A**). The "TGF-β signaling pathway" possessed the highest rich factor in the up-regulated DEGs in the CON_LPS group. TGF-β could skew LPS-stimulated M1-type macrophage polarization toward the M2 phenotype *via* the Akt/FoxO1 pathway and reduce inflammatory reactions in sepsis (Liu et al., 2019). In a previous study, IFN-γ at a concentration of 50 ng/ml and LPS at a concentration of 100 ng/ml classically induce M1 activation of PAMs, accompanied by enriched TNF pathway and down-regulated TGF-β signaling pathway (Liu et al., 2018). LPS stimulation intensity could significantly affect the gene expression profile and polarization state of macrophages. Compared with short exposure (2–4 h) to LPS, short exposure (18–24 h) to LPS increases the expression of M2-related genes, including the tyrosine protein kinase MER and arginase in macrophages (Chen et al., 2019). Further study is needed to explore the regulatory effect of a high concentration of LPS on the polarization state of PAMs. Among the down-regulated DEGs in the CON_LPS group, the enriched KEGG pathways were related to "graft-versus-host disease," followed by "endocrine resistance" and "IL-17 signaling pathway," and "cytokine–cytokine receptor interaction" had the most DEGs. Consistent with the transcriptome analysis of PAMs activated by LPS, down-regulated genes involving cytokine–cytokine receptor interaction suggested their important role in cellular activation (Liu et al., 2018). In contrary to this study, co-infection of *Mycoplasma gallisepticum* and *E. coli* leads to inflammatory damage of chicken lung involving the enriched IL-17 signaling pathway (Wu et al., 2019). Both genes encoding matrix metallopeptidase 9 (MMP9, $Log_2FC = -1.44$) and CCAAT enhancer binding protein beta (CEBPβ, $Log_2FC = 0.60$) were involved in the IL-17 signaling pathway and TNF signaling pathway (**Supplementary Figure 5A**). The DEGs in the LPS_SeL group were highly related to categories including protein digestion and absorption, AGE–RAGE signaling pathway in diabetic complications, TGF-β signaling pathway, thyroid hormone synthesis, relaxin signaling pathway, amoebiasis, glutathione metabolism, PI3K–Akt signaling pathway, and arachidonic acid metabolism (**Figure 1A**). The "tryptophan metabolism" and "phototransduction" pathway possessed the highest rich factor in the up-regulated and down-regulated DEGs in the LPS_SL group, respectively. LPS and IFN-γ-stimulated RAW264.7 macrophages cultured in tryptophan-deficient medium exhibit a significant reduction in iNOS expression involved in pathogen killing (Poormasjedi-Meibod et al., 2013). The expression of proteins involved in tryptophan metabolism indoleamine 2,3-dioxygenase and kynurenic acid is activated in pig bone marrow-derived macrophages infected with LPS (Kapetanovic et al., 2012). The metabolomic analysis also showed

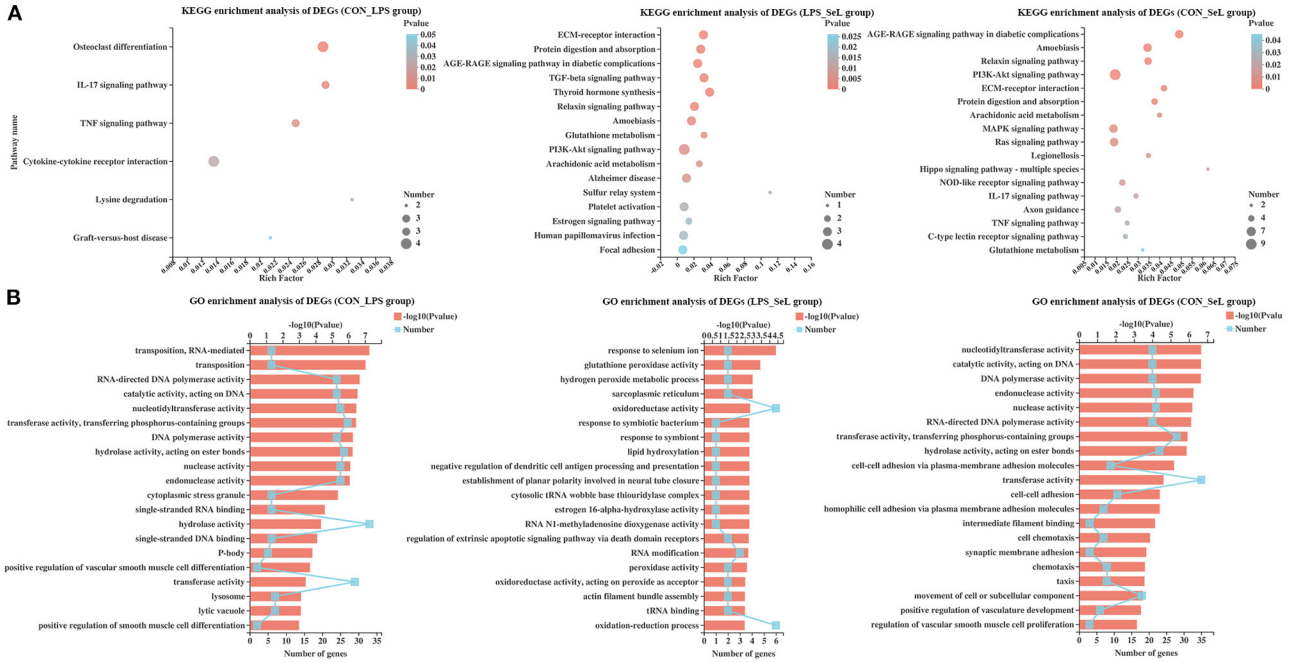

FIGURE 1 | KEGG and GO enrichment analysis of DEGs. Enriched bubble chart showing the enrichment of the KEGG pathway in the CON_LPS, LPS_SeL, and CON-SeL groups **(A)**. X-axis represented the enrichment ratio, and Y-axis represented the top 20 KEGG pathways. Number: bubble size represented the number of genes annotated to a KEGG pathway. Pvalue: color indicated the enriched *p*-value. Enriched bar chart showing the enrichment of the GO pathway in the CON_LPS, LPS_SeL, and CON-SeL groups **(B)**. The length of the X-axis column represents the *p*-value. The value of the box on the fold line above X is the number of DEGs annotated to the GO terms.

that LPS stimulation reprograms metabolomic profiling of the human M1-type AMs and induces tryptophan degradation in tryptophan metabolism (Fall et al., 2020).

Compared with the LPS challenge, Se treatment up-regulated the expression of GPX1 ($Log_2FC = 2.12$) expression and down-regulated the expression of GPX2 ($Log_2FC = -0.72$), which participated in thyroid hormone synthesis, glutathione metabolism, and arachidonic acid metabolism (**Supplementary Figure 5B**). The presence of prostaglandin E2 (PGE2), a main arachidonic acid derivative, is necessary to the LPS-induced production of the pro-inflammatory cytokine IL-1β (Zaslona et al., 2017). Up-regulated thrombospondin 1 (THBS1, $Log_2FC = 0.64$) was involved in the TGF-β signaling pathway and PI3K–Akt signaling pathway. The enriched KEGG pathways for the CON_SeL group, out of 252 DEGs, were very similar to the CON_LPS group, but ranked differently: amoebiasis, relaxin signaling pathway, PI3K–Akt signaling pathway, extracellular matrix (ECM)–receptor interaction, protein digestion and absorption, arachidonic acid metabolism, MAPK signaling pathway, Ras signaling pathway, and Legionellosis, which had many genes in common, including up-regulated genes [GPX1, TLR4, nuclear factor kappa-B (NF-κB) subunit RELβ, chemokine C-X-C motif ligand 2 (CXCL2), platelet-derived growth factor subunit B (PDGFB), GRB2-associated binding protein 1 (GAB1), etc.] and down-regulated genes [phospholipase A2 group 1β (PLA2G1β), MMP9, muscle RAS (MRAS), ephrin A2 (EFNA2), GPX2, etc.] (**Figure 1A**; **Supplementary Figure 5C**). The main limitation of this study was that the Se alone treatment group was not included, which was limited to assess the effect of Se treatment on the gene expression profile of PAMs. Se supplementation was proven to attenuate the levels of oxidative stress and pro-inflammatory gene expression in macrophages (Vunta et al., 2008; Ghorbel et al., 2017). A comprehensive gene expression profile of Se-treated PAMs is needed in further study.

GO enrichment analysis was performed. Among the DEGs in the CON_LPS group, RNA-mediated transposition and transposition classified into biological process class occupied the strongest enrichment degree. The molecular function class was the most abundant function groups, mainly including some enzyme activity, such as polymerase activity, catalytic activity, nucleotidyltransferase activity, transferase activity, hydrolase activity, nuclease activity, and endonuclease activity. The cytoplasmic stress granule was the main type in cellular component (**Figure 1B**). The presence of CEBPB and CD28 was directly related to the positive regulation of IL-4 production (**Supplementary Figure 6A**). The DEGs in the LPS_SeL group were predicted to be involved in the response to Se ion, followed by a response to the symbiotic bacterium, regulation of extrinsic apoptotic signaling pathway *via* death domain receptors, and some oxidative stress-related functional terms, including hydrogen peroxide metabolic process, glutathione peroxidase activity, oxidation–reduction process, oxidoreductase activity, peroxidase activity, and oxidoreductase activity acting on peroxide as acceptor (**Figure 1B**). Up-regulated GPX1 ($Log_2FC = 2.12$) and SELENOP ($Log_2FC = 0.61$) were related to the

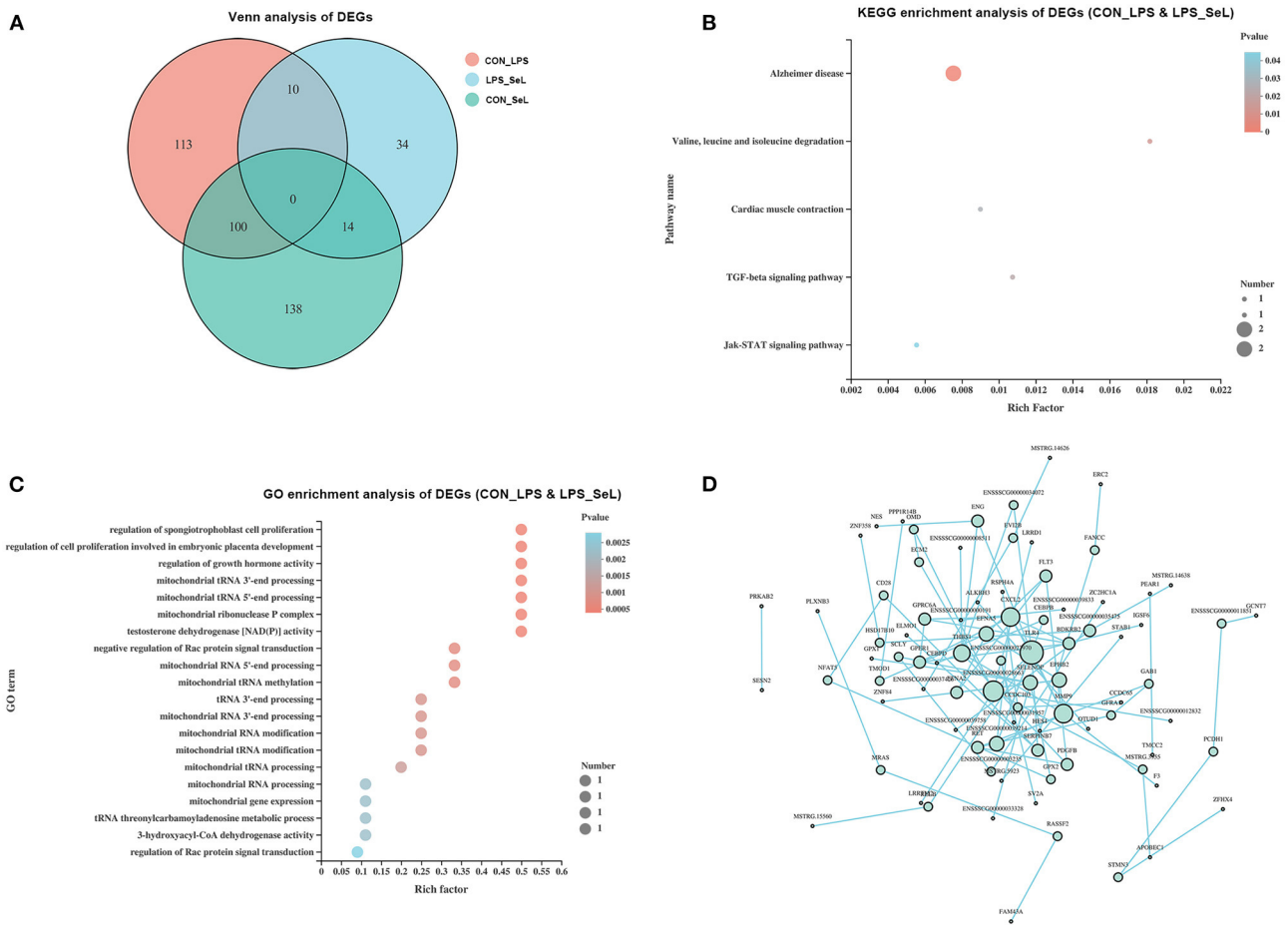

FIGURE 2 | Functional annotation of DEGs affected by both Se treatment and LPS infection. Venn diagram presenting co-expressed and uniquely expressed DEGs in the CON_LPS, LPS_SeL, and CON_SeL groups **(A)**. The KEGG **(B)** and GO **(C)** enrichment analysis of DEGs affected by both Se treatment and LPS infection was indicated. PPI was performed to generate interaction analysis **(D)**. Node color from white to green represents the lowest to highest betweenness centrality. The size of each node corresponded to the number of connections (degree).

response to Se ion (**Supplementary Figure 6B**). Cytochrome P450 1A1 (CYP1A1, $Log_2FC = 2.47$), GPX1, GPX2 ($Log_2FC = -0.72$), and hydroxysteroid 17-beta dehydrogenase 10 (HSD17B10, $Log_2FC = -0.69$) were related to oxidative stress-related function. THBS1 ($Log_2FC = 0.64$) was related to the regulation of extrinsic apoptotic signaling pathway *via* death domain receptors. The DEGs in the CON_SeL group were found to be involved in the significant enrichment of GO biological terms including enzyme activity and cell adhesion function (**Figure 1B**; **Supplementary Figure 6C**).

Functional Annotation of DEGs Affected by Both Se and LPS

According to the Venn analysis, a total of 113, 34, and 138 genes were specifically expressed in the CON_LPS, LPS_SeL, and CON_SeL groups, respectively (**Figure 2A**). A total of 14 and 100 genes were shared by the LPS_SeL and CON_SeL groups and the CON_LPS and CON_SeL groups, respectively. Moreover, only 10 DEGs were shared by the CON_LPS and LPS_SeL groups. The KEGG enrichment analysis showed that the 10 DEGs shared by the CON_LPS and LPS_SeL groups were enriched in Alzheimer disease; valine, leucine, and isoleucine degradation; cardiac muscle contraction; TGF-β signaling pathway; and Jak–STAT signaling pathway (**Figure 2B**). Among the top 20 GO terms identified by enrichment analysis based on 10 DEGs, the first three topmost enriched were regulation of spongiotrophoblast cell proliferation, regulation of cell proliferation involving embryonic placenta development, and regulation of growth hormone activity (**Figure 2C**). The other GO terms were involved in mitochondrial RNA processing and modification.

Interaction Analysis of DEGs

The main protein interaction cluster derived from 409 DEGs contained 84 nodes, each representing 1 protein and connected by 84 edges (**Figure 2D**). TLR4, CXCL2, MMP9, and THBS1, followed by SELENOP, had the highest scores for betweenness centrality, indicating that they accounted for many direct and indirect interactions within the network of PPI. TLR4,

MMP9, CXCL2, and THBS1 had the highest number of direct connections (degree). TLR4 and CXCL2 represented the immune response of M1-type PAMs to LPS infection (Herrera-Uribe et al., 2020).

In this study, most DEGs in PAMs infected with LPS compared with the control group are enriched in the IL-17 signaling pathway, TNF signaling pathway, and cytokine–cytokine receptor interaction. LPS promotes the early activation of TLR4 and CXCL2. Se treatment enhances the antioxidant and anti-inflammatory responses to LPS through integrating GPX1, GPX2, SELENOP, CYP1A1, HSD17B10, and THBS1 genes. These findings provide an important view of the mechanism of Se protecting the host against infection. The study also suggests that dietary Se supply to pigs may help prevent respiratory infection.

DATA AVAILABILITY STATEMENT

The raw transcriptome data have been deposited in the US National Center for Biotechnology Information Sequence Read Archive database under the accession no. SRR13277478–SRR13277486.

AUTHOR CONTRIBUTIONS

QW and J-XL: conceived and designed the experiments and prepared the manuscript. J-XL, X-YC, PC, Y-DW, T-JS, ML, and R-YX: Performed the RNA extraction. QW, J-XL, X-YC, and PC: Performed the analysis of data. All authors contributed to the article and approved the submitted version.

FUNDING

This work was supported financially by the National Key R&D Program of China (Project no. 2017YFD0502200), Undergraduate Scientific Research Project of Cross Training Program of High Level Talents in Beijing Universities (Project no. PXM2020_014207_000009), Research Project for Youth Teachers of Beijing University of Agriculture (Project no. SXQN201904), General Projects of Beijing Municipal Education Commission Science and Technology Plan (Project no. KM202010020009), and Undergraduate Scientific Research Training Project of BUA (Project no. kx2019008).

SUPPLEMENTARY MATERIAL

The Supplementary Material for this article can be found online at: https://www.frontiersin.org/articles/10.3389/fgene.2021.645401/full#supplementary-material

Supplementary Figure 1 | Saturation curve of sequencing of each sample. Each color line represented the saturation curve of gene expression at different expression levels in the sample.

Supplementary Figure 2 | Classification of new transcripts. New transcripts were classified according to the overlapping relationship between spliced transcripts and known transcripts. The percentage of new transcripts were shown.

Supplementary Figure 3 | Annotation analysis of identified novel genes. The novel genes were annotated using based on GO **(A)**, KEGG **(B)**, and COG **(C)** databases.

Supplementary Figure 4 | DEGs in PAMs in response to Se treatment or LPS infection. Volcano plots displaying DEGs in the CON_LPS **(A)**, CON-SeL **(B)**, and LPS_SeL **(C)** groups. The longitudinal dashed lines indicated an expression level of $|FC| \geq 1.5$. The horizontal dashed lines indicated an expression level with a p-value < 0.05. Blue dots (up) represented significantly up-regulated genes; gray dots (down) represented significantly down-regulated genes; red dots (no significance) represented insignificantly DEGs.

Supplementary Figure 5 | KEGGChord plot of top 20 ranked KEGG terms. Chords indicated a detailed relationship between the expression levels of DEGs (left semicircle perimeter) in the CON_LPS **(A)**, LPS_SeL **(B)**, and CON-SeL **(C)** groups and their enriched KEGG pathways (right semicircle perimeter). The genes were linked to their annotated KEGG terms via colored ribbons. Genes were ordered according to $\log_2$FC.

Supplementary Figure 6 | GOChord plot of top 20 ranked GO terms. Chords indicated a detailed relationship between the expression levels of DEGs (left semicircle perimeter) in the CON_LPS **(A)**, LPS_SeL **(B)**, and CON-SeL **(C)** groups and their enriched KEGG pathways (right semicircle perimeter). The genes are linked to their annotated terms via colored ribbons.

REFERENCES

Chen, H. J., Li Yim, A. Y. F., Griffith, G. R., de Jonge, W. J., Mannens, M. M. A. M., Ferrero, E., et al. (2019). Meta-analysis of *in vitro*-differentiated macrophages identifies transcriptomic signatures that classify disease macrophages *in vivo*. *Front. Immunol.* 10:2887. doi: 10.3389/fimmu.2019.02887

Ciesielska, A., Matyjek, M., and Kwiatkowska, K. (2020). TLR4 and CD14 trafficking and its influence on LPS-induced pro-inflammatory signaling. *Cell. Mol. Life Sci.* 78, 1233–1261. doi: 10.1007/s00018-020-03656-y

Fall, F., Lamy, E., Brollo, M., Naline, E., Lenuzza, N., Thévenot, E., et al. (2020). Metabolic reprograming of LPS-stimulated human lung macrophages involves tryptophan metabolism and the aspartate-arginosuccinate shunt. *PLoS ONE* 15:e0230813. doi: 10.1371/journal.pone.0230813

Ghorbel, I., Elwej, A., Chaabane, M., Jamoussi, K., Mnif, H., Boudawara, T., et al. (2017). Selenium alleviates oxidative stress and lung damage induced by aluminum chloride in adult rats: biochemical and histological approach. *Biol. Trace Elem. Res.* 176, 181–191. doi: 10.1007/s12011-016-0818-9

Herrera-Uribe, J., Liu, H., Byrne, K. A., Bond, Z. F., Loving, C. L., and Tuggle, C.K. (2020). Changes in H3K27ac at gene regulatory regions in porcine alveolar macrophages following LPS or PolyIC exposure. *Front. Genet.* 11:817. doi: 10.3389/fgene.2020.00817

Hussell, T., and Bell, T. J. (2014). Alveolar macrophages: plasticity in a tissue-specific context. *Nat. Rev. Immunol.* 14, 81–93. doi: 10.1038/nri3600

Kaelberer, M., Caceres, A., and Jordt, S. E. (2020). Activation of a nerve injury transcriptional signature in airway-innervating sensory neurons after lipopolysaccharide-induced lung inflammation. *Am. J. Physiol. Lung Cell. Mol. Physiol.* 318, L953–L964. doi: 10.1152/ajplung.00403.2019

Kapetanovic, R., Fairbairn, L., Beraldi, D., Sester, D. P., Archibald, A. L., Tuggle, C. K., et al. (2012). Pig bone marrow-derived macrophages resemble human macrophages in their response to bacterial lipopolysaccharide. *J. Immunol.* 188, 3382–3394. doi: 10.4049/jimmunol.1102649

Khera, A., Vanderlelie, J. J., Holland, O., and Perkins, A. V. (2017). Overexpression of endogenous anti-oxidants with selenium supplementation protects trophoblast cells from reactive oxygen species-induced apoptosis in a Bcl-2-dependent manner. *Biol. Trace Elem. Res.* 177, 394–403. doi: 10.1007/s12011-016-0870-5

Kim, S., Oh, M. W., Bin, P. W., and Yoo, H. S. (2019). Global gene networks in 3D4/31 porcine alveolar macrophages treated with antigenic epitopes of *Actinobacillus pleuropneumoniae* ApxIA, IIA, and IVA. *Sci. Rep.* 9:5269. doi: 10.1038/s41598-019-41748-3

Li, B., Fang, J., Zuo, Z., Yin, S., He, T., Yang, M., et al. (2017). Activation of porcine alveolar macrophages by *Actinobacillus pleuropneumoniae* lipopolysaccharide

via the Toll-like Receptor 4/NF-κB-mediated pathway. *Infect. Immun.* 86, e00642–e00617. doi: 10.1128/IAI.00642-17

Liu, F., Qiu, H., Xue, M., Zhang, S., Zhang, X., Xu, J., et al. (2019). MSC-secreted TGF-β regulates lipopolysaccharide-stimulated macrophage M2-like polarization via the Akt/FoxO1 pathway. *Stem Cell Res. Ther.* 10:345. doi: 10.1186/s13287-019-1447-y

Liu, G., Yang, G., Guan, G. P., Zhang, Y. Z., Ren, W. K., Yin, J., et al. (2015). Effect of dietary selenium yeast supplementation on porcine circovirus type 2 (PCV2) infections in mice. *PLoS ONE* 10:e0115833. doi: 10.1371/journal.pone.0115833

Liu, Q., Zhang, Y. L., Hu, W., Hu, S. P., Zhang, Z., Cai, X. H., et al. (2018). Transcriptome of porcine alveolar macrophages activated by interferon-gamma and lipopolysaccharide. *Biochem. Biophys. Res. Commun.* 503, 2666–2672. doi: 10.1016/j.bbrc.2018.08.021

Neupane, A. S., Willson, M., Chojnacki, A. K., Vargas E Silva Castanheira, F., Morehouse, C., Carestia, A., et al. (2020). Patrolling alveolar macrophages conceal bacteria from the immune system to maintain homeostasis. *Cell* 183, 110–125. doi: 10.1016/j.cell.2020.08.020

Park, I. B., Choi, Y. C., Lee, K. T., and Chun, T. (2020). Transcriptome analysis of pig macrophages expressing porcine reproductive and respiratory syndrome virus non-structural protein 1. *Vet. Immunol. Immunopathol.* 231:110147. doi: 10.1016/j.vetimm.2020.110147

Poormasjedi-Meibod, M. S., Jalili, R. B., Hosseini-Tabatabaei, A., Hartwell, R., and Ghahary, A. (2013). Immuno-regulatory function of indoleamine 2,3 dioxygenase through modulation of innate immune responses. *PLoS ONE* 8:e71044. doi: 10.1371/journal.pone.0071044

Riazanski, V., Sui, Z., and Nelson, D. J. (2020). Kinetic separation of oxidative and non-oxidative metabolism in single phagosomes from alveolar macrophages: impact on bacterial killing. *iScience* 23:101759. doi: 10.1016/j.isci.2020.101759

Silvestrini, A., Mordente, A., Martino, G., Bruno, C., Vergani, E., Meucci, E., et al. (2020). The role of selenium in oxidative stress and in nonthyroidal illness syndrome (NTIS): an overview. *Curr. Med. Chem.* 27, 423–449. doi: 10.2174/0929867325666180201111159

Sun, L. H., Pi, D. A., Zhao, L., Wang, X. Y., Zhu, L. Y., Qi, D. S., et al. (2017). Response of selenium and selenogenome in immune tissues to LPS-induced inflammatory reactions in pigs. *Biol. Trace Elem. Res.* 177, 90–96. doi: 10.1007/s12011-016-0863-4

Vunta, H., Belda, B. J., Arner, R. J., Reddy, C. C., Heuvel, J. P. V., and Prabhu, K. S. (2008). Selenium attenuates pro-inflammatory gene expression in macrophages. *Mol. Nutr. Food Res.* 52, 1316–1323. doi: 10.1002/mnfr.200700346

Wang, X., An, Y., Jiao, W., Zhang, Z., Han, H., Gu, X., et al. (2018). Selenium protects against lead-induced apoptosis via endoplasmic reticulum stress in chicken kidneys. *Biol. Trace Elem. Res.* 182, 354–363. doi: 10.1007/s12011-017-1097-9

Wu, Q., Yao, H. D., Tan, S. R., Zhang, Z. W., Zhu, Y. H., and Xu, S. (2014). Possible correlation of selenoprotein W with inflammation factors in chicken skeletal muscles. *Biol. Trace Elem. Res.* 161, 167–172. doi: 10.1007/s12011-014-0092-7

Wu, Z. Y., Ding, L. J., Bao, J. X., Liu, Y. H., Zhang, Q. M., Wang, J., et al. (2019). Co-infection of *Mycoplasma gallisepticum* and *Escherichia coli* triggers inflammatory injury involving the IL-17 signaling pathway. *Front. Microbiol.* 10:2615. doi: 10.3389/fmicb.2019.02615

Xu, J. Y., Jia, W., Hu, C. X., Nie, M., Ming, J. J., Cheng, Q., et al. (2020). Selenium as a potential fungicide could protect oilseed rape leaves from *Sclerotinia sclerotiorum* infection. *Environ. Pollut.* 257:113495. doi: 10.1016/j.envpol.2019.113495

Zaslona, Z., Palsson-McDermott, E. M., Menon, D., Haneklaus, M., Flis, E., Prendeville, H., et al. (2017). The induction of pro-IL-1beta by lipopolysaccharide requires endogenous prostaglandin E2 production. *J. Immunol.* 198, 3558–3564. doi: 10.4049/jimmunol.1602072

Conflict of Interest: The authors declare that the research was conducted in the absence of any commercial or financial relationships that could be construed as a potential conflict of interest.

frontiers in Veterinary Science

ORIGINAL RESEARCH
published: 04 March 2021
doi: 10.3389/fvets.2021.646839

RNA-Seq Analysis Reveals the Role of Omp16 in *Brucella*-Infected RAW264.7 Cells

Dong Zhou[1,2†], *Feijie Zhi*[1,2†], *Jiaoyang Fang*[1,2], *Weifang Zheng*[1,2], *Junmei Li*[1,2], *Guangdong Zhang*[1,2], *Lei Chen*[1,2], *Yaping Jin*[1,2] *and Aihua Wang*[1,2*]

[1] College of Veterinary Medicine, Northwest A&F University, Yangling, China, [2] Key Laboratory of Animal Biotechnology of the Ministry of Agriculture, Northwest A&F University, Yangling, China

Brucellosis is an endemic zoonotic infectious disease in the majority of developing countries, which causes huge economic losses. As immunogenic and protective antigens at the surface of *Brucella* spp., outer membrane proteins (Omps) are particularly attractive for developing vaccine and could have more relevant role in host–pathogen interactions. Omp16, a homolog to peptidoglycan-associated lipoproteins (Pals), is essential for *Brucella* survival *in vitro*. At present, the functions of Omp16 have been poorly studied. Here, the gene expression profile of RAW264.7 cells infected with *Brucella suis* vaccine strain 2 (*B. suis* S2) and ΔOmp16 was analyzed by RNA-seq to investigate the cellular response immediately after *Brucella* entry. The RNA-sequence analysis revealed that a total of 303 genes were significantly regulated by *B. suis* S2 24 h post-infection. Of these, 273 differentially expressed genes (DEGs) were upregulated, and 30 DEGs were downregulated. These DEGs were mainly involved in innate immune signaling pathways, including pattern recognition receptors (PRRs), proinflammatory cytokines, and chemokines by Kyoto Encyclopedia of Genes and Genomes (KEGG) analysis. In ΔOmp16-infected cells, the expression of 52 total cells genes was significantly upregulated and that of 9 total cells genes were downregulated compared to *B. suis* S2-infected RAW264.7 cells. The KEGG pathway analysis showed that several upregulated genes were proinflammatory cytokines and chemokines, such as interleukin (IL)-6, IL-11, IL-12β, C–C motif chemokine (CCL2), and CCL22. All together, we clearly demonstrate that ΔOmp16 can alter macrophage immune-related pathways to increase proinflammatory cytokines and chemokines, which provide insights into illuminating the *Brucella* pathogenic strategies.

Keywords: *B. suis* S2, Omp16, RAW264.7, RNA-seq, interactions

OPEN ACCESS

Edited by:
Wei Zhang,
Beijing Academy of Agricultural and Forestry Sciences, China

Reviewed by:
Qing Yin,
Moffitt Cancer Center, United States
Huanan Wang,
Zhejiang University, China

***Correspondence:**
Aihua Wang
aihuawang1966@163.com

[†]These authors have contributed equally to this work

Specialty section:
This article was submitted to Livestock Genomics, a section of the journal Frontiers in Veterinary Science

Received: *28 December 2020*
Accepted: *26 January 2021*
Published: *04 March 2021*

Citation:
Zhou D, Zhi F, Fang J, Zheng W, Li J, Zhang G, Chen L, Jin Y and Wang A (2021) RNA-Seq Analysis Reveals the Role of Omp16 in Brucella-Infected RAW264.7 Cells. Front. Vet. Sci. 8:646839. doi: 10.3389/fvets.2021.646839

INTRODUCTION

As zoonotic pathogens, *Brucella* spp. cause a serious infection known as brucellosis that results in animal reproductive diseases and human chronic debilitating diseases (1, 2). A diverse array of land and aquatic mammals, including swine, cattle, goats, sheep, dogs, and dolphins, are known to serve as hosts for *Brucella* (1). It infects millions of livestock and more than half a million people annually, causing economic loss and a public health burden (2). Although brucellosis causes abortion and sterility in their hosts, the human disease is principally characterized by recurrent

fever and osteoarticular complications during the chronic stage of the infection (3). In animals, live attenuated vaccines, including *Brucella abortus* S19 and *Brucella melitensis* Rev. 1, still have some disadvantages, such as serodiagnostic interference and residual pathogenicity (4–6). In China, live attenuated *Brucella suis* bv. 1 str. S2 vaccine (*B. suis* S2) is an essential and critical component in the control of brucellosis and also exhibits potential virulence reversion (7). Based on the lack of licensed human vaccines to protect against *Brucella*, safer and better vaccines need to be developed (4, 8).

Brucella outer membrane proteins (Omps) are important components of the cell wall (9). According to molecular weight of Omps, the *Brucella* cell Omps contains three major proteins ranging from 25 to 27, 31 to 34, and 36 to 38 kDa (10). At present, some experiments have shown that Omp10, Omp19, Omp25, and Omp31 are involved in *Brucella* virulence (11–13). The *Brucella* Omp19, Omp25, and Omp31 mutant were attenuated in cellular models and in mice, indicating that Omp19 and Omp25 were important for bacterial survival *in vitro* and *in vivo* (11, 14–17). Furthermore, Omp25 and Omp31 disrupt the immune response by regulating the secretion of tumor necrosis factor alpha (TNF-α) expression and apoptosis in porcine and murine macrophages infected models (18, 19). As the homolog of peptidoglycan-associated lipoproteins (Pals), Omp16 plays a vital role in the maintenance of membrane integrity and the import of certain organic molecules (20–22). Some experiments have shown that Omp16 was involved in *Brucella*-mediated immune response and can also be used as a protective antigen (23–26). However, attempt to directly delete Omp16 was unsuccessful, which also indicated that Omp16 is a vital gene for *Brucella* and plays an important role in the maintenance of membrane integrity and *Brucella* survival. In our previous study using an indirect method to tightly control Omp16 expression, *Brucella* cells lacking Omp16 presented defects in growth, outer membrane integrity, and intracellular survival (20). However, the role of Omp16 in *Brucella*–host interaction has not been well-studied.

In the present study, we identified 303 differentially expressed genes (DEGs) using RNA-seq in *B. suis* S2-infected RAW 264.7 cells compared to uninfected cells. In DEGs, most upregulated genes were involved in the immune system and cytokines, while downregulated genes were related to metabolism and cell cycle. On the basis of ATc-induced conditional complementation strain of the *B. suis* S2 Omp16, 61 DEGs were observed using RNA-seq in ΔOmp16-infected RAW 264.7 cells compared to *B. suis* S2-infected cells. The 52 upregulated genes were involving in pattern recognition receptors (PRRs) signaling pathway, including nucleotide oligomerization domain (NOD)-like receptor signaling pathway, chemokines, and cytokines, while 9 downregulated genes were related to metabolism. Real-time quantitative reverse transcription PCR (qRT-PCR) analysis further verified DEGs. The results presented here are expected to reveal the Omp16 roles during the *Brucella* infection process of RAW 264.7 cells and generate a new insight to explore the pathogenic mechanism of *Brucella*.

MATERIALS AND METHODS

Bacteria Strains and Culture

In the present study, wild-type *B. suis* S2 (CVCC reference number, CVCC70502) bacteria strains were used. *B. suis* S2 ΔOmp16 have been constructed as described previously (20). Wild-type *B. suis* S2 and its derivatives were grown on tryptic soy agar (TSA; Sigma) for 72 h at 37°C or in tryptic soy broth (TSB) with shaking overnight to late-log growth phase. When indicated, bacteria cultures were treated with 50 μg/ml gentamicin and 50 μg/ml ampicillin. Then, wild-type *B. suis* S2 and its derivatives were collected by centrifugation, and the number of bacteria was confirmed using a 10-gradient dilution.

Mammalian Cell Culture and Infection

RAW264.7 macrophage cells were cultured to monolayer in 6- or 24-well plates in Dulbecco's modified Eagle's medium (DMEM; Gibco; 1 g/L glucose) supplemented with 10% fetal bovine serum (FBS, Gibco) at 37°C with 5% CO_2. For infection, RAW264.7 cells were seeded at 1×10^6 cells/well (6-well plate) or 2×10^5 cells/well (24-well plates) in complete medium 12 h before infection, then infected with wild-type *B. suis* S2 and its derivatives at the multiplicity of infection (MOI) of 200:1 for 4 h. Following 4 h of incubation at 37°C in 5% CO_2, RAW264.7 cells were washed three times with 37°C phosphate-buffered saline (PBS) to remove extracellular *Brucella* and incubated for 1 h with medium supplemented with 50 μg/ml kanamycin to kill the remaining extracellular bacteria. Afterward, RAW264.7 cells were cultured in medium supplemented with 25 μg/ml kanamycin to avert continuous infection. This time was considered 0 h. RAW264.7 cells were collected for experiments at specific times.

Collection of RAW264.7 Cells Samples for Transcription Analysis

B. suis S2 and ΔOmp16 were collected at late-log growth phase by centrifugation at 6,000 rpm for 5 min. The collected bacteria were washed three times with PBS, then suspended in PBS. The number of bacteria was confirmed using a 10-gradient dilution. RAW264.7 cells were infected with *B. suis* S2 or ΔOmp16 at MOI of 200:1; then, RAW264.7 cells were collected after 24 h with TRIzol RNA isolation reagent (Invitrogen, Inc., Carlsbad, CA, USA) for total RNA extraction.

RNA-Seq Analysis

Total RNA was prepared as described. Using the Illumina Hiseq 2500 sequencer, RNA were sequenced separately. The reference genome data were downloaded from the National Center for Biotechnology Information (NCBI) database. Raw sequencing reads were cleaned by removing low-quality reads, reads containing poly-N sequences, and adaptor sequences. Then, clean reads were aligned to the reference genome using HISAT40. Using RESM software, the relative transcript abundance was calculated in fragments in reads per kilobase of exon sequence per million mapped sequence reads (FPKM). The $P \leq 0.05$ and the absolute value of log2

ratio ≥1 were used to identify DEGs. The Gene Ontology (GO) database and KEGG database was used to analyze the pathway.

Isolation of RNA From RAW264.7

According to the manufacturer's protocol, total RNA was extracted from *B. suis* S2- or ΔOmp16-infected RAW264.7 cells using TRIzol RNA isolation reagent (Invitrogen, Inc., Carlsbad, CA, USA). Total RNA quality and quantity were evaluated using the NanoDrop ND-1000 spectrophotometer (Thermo Scientific). RNA integrity was assessed by standard denaturing 1% agarose gel electrophoresis.

TABLE 1 | Major characteristics of mRNA libraries and database generated by RNA-seq.

Sample	Raw bases (G)	Raw reads	Clean reads	Total mapped (%)
Control-1	6.72	44779952	42686754	92.68
Control-2	8.58	57180964	54654018	92.81
Control-3	7.62	50818606	48638136	92.31
B. suis. S2-1	6.51	43430156	41599652	93.16
B. suis. S2-2	9.27	61783014	58951842	92.92
B. suis. S2-3	7.72	51497980	48974982	92.26
ΔDnaA <DnaA>-1	5.83	38846290	37181292	92.33
ΔDnaA <DnaA>-2	6.99	46600322	44546310	92.83
ΔDnaA <DnaA>-3	6.49	43256424	41389296	92.29

Quantitative Real-Time PCR

To validate the data generated from the RNA-seq experiment, 13 pathway genes were selected to further analyze via quantitative real-time PCR (qRT-PCR). Total RNA were prepared as described. Briefly, RNA was reverse transcribed into complementary DNA (cDNA) using Maxima First-Strand cDNA synthesis kit (Thermo Fisher Scientific) according to the manufacturer's protocol. qRT-PCR was performed using SYBR Premix Ex Taq™ (Vazyme) and an ABI 7500 Sequencing Detection System. Using the $2^{-\Delta\Delta Ct}$ method, qRT-PCR data were normalized, and glyceraldehyde 3-phosphate dehydrogenase gene (GAPDH) was used an as internal control. All the primers was designed according to mouse messenger RNAs (mRNAs) and are listed in **Supplementary Table 1**.

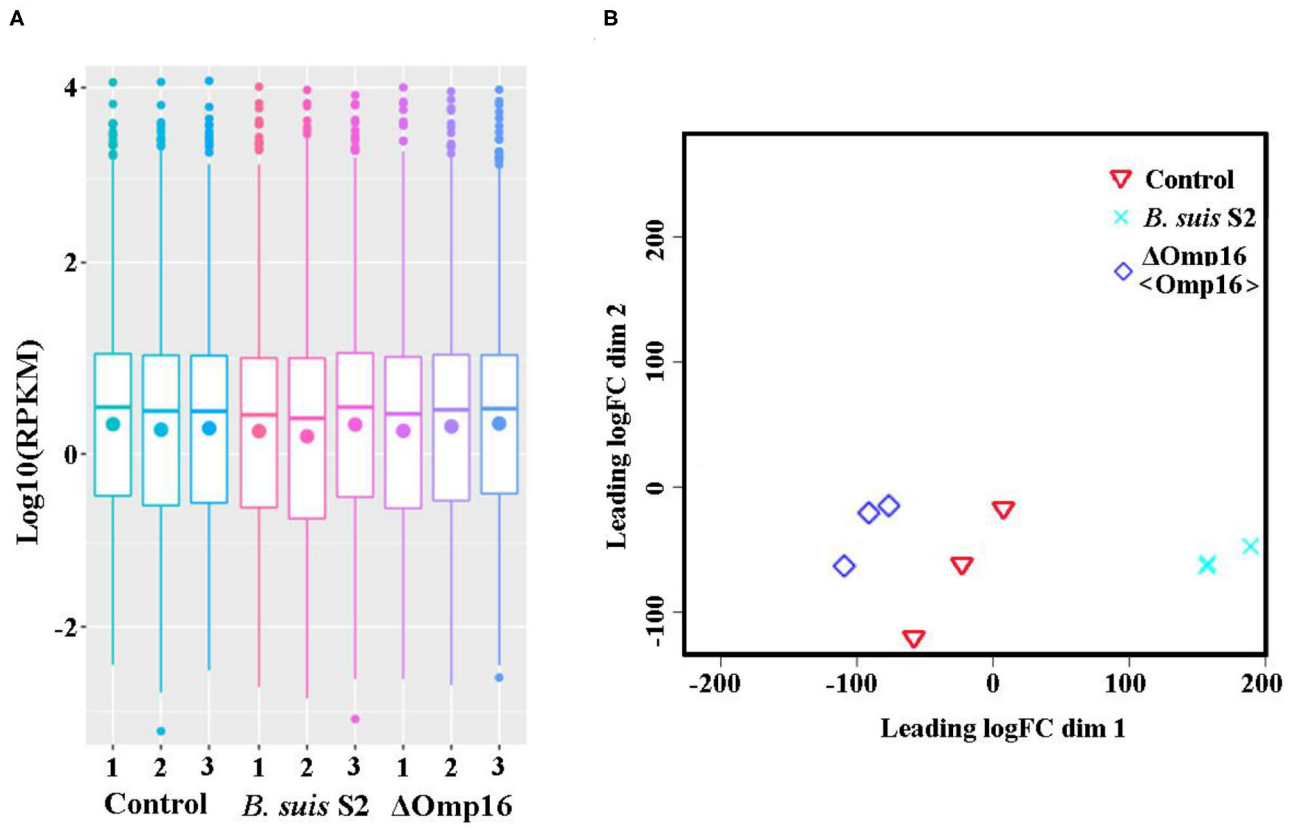

FIGURE 1 | Assessment of gene data quality of all samples. **(A)** A box plot used to compared the intensity distribution of all bacterial samples. The distributions of $\log_{10}$ [reads per kilobase per million mapped reads (RPKM)] ratios among bacterial samples are nearly the same; **(B)** similarities visualized among bacterial samples using an multidimensional scaling (MDS) analysis. Red: uninfected RAW 264.7 cells. Green: *B. suis* S2-infected RAW 264.7 cells. Blue: ΔOmp16-infected RAW 264.7 cells.

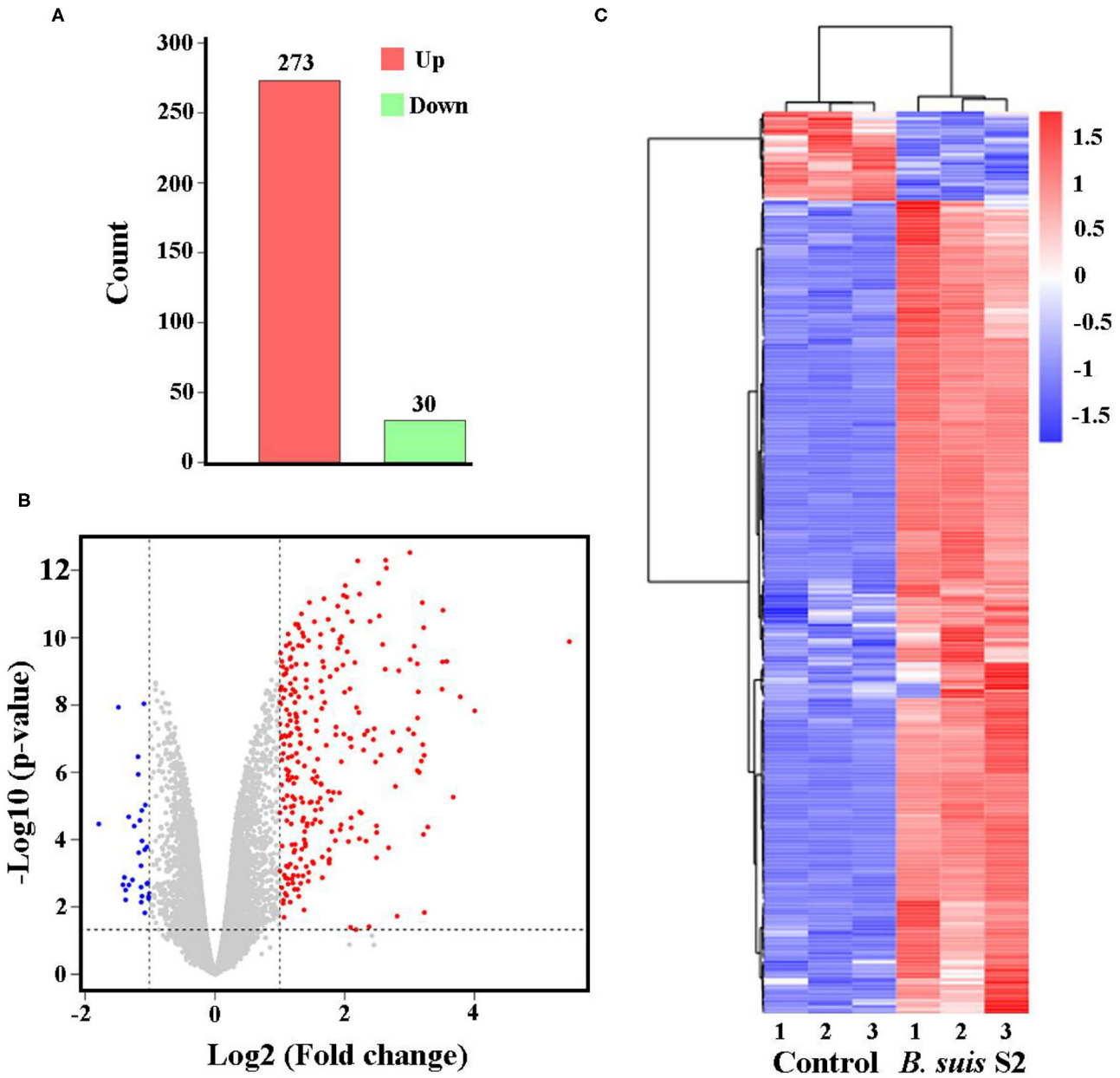

FIGURE 2 | Expression of differentially expressed genes (DEGs) between the uninfected and *B. suis* S2-infected cells. **(A)** Histogram shows the number of DEGs and non-regulated genes between the between the uninfected and *B. suis* S2-infected cells. **(B)** Scatter plot of coexpressed genes between the between the uninfected and *B. suis* S2-infected cells. The red, blue, and gray colors denote upregulated, downregulated, and non-regulated genes, respectively, in the *B. suis* S2-infected cells compared with the uninfected cells based on the following criteria: absolute log2 (fold change) ≥1 and adjusted $P \leq 0.05$. **(C)** The heatmap shows the expression levels of DEGs between the uninfected and *B. suis* S2-infected cells.

Statistical Analysis

SPSS software was used for all statistical analyses (version 22; SPSS, Inc., Chicago, IL). All results were repeated at least three times and are presented as the means ± standard deviations (SDs). An unpaired, two-tailed Student's *t*-test or one-way analysis with group comparisons was used. A probability (*P*) value of ≤0.05 was considered significant.

RESULTS

RNA Quality Analysis and Global Array Data

RNA integrity was determined via denatured agarose gel electrophoresis. Purity and concentration were measured using a spectrophotometer. Electrophoresis showed distinct three bands

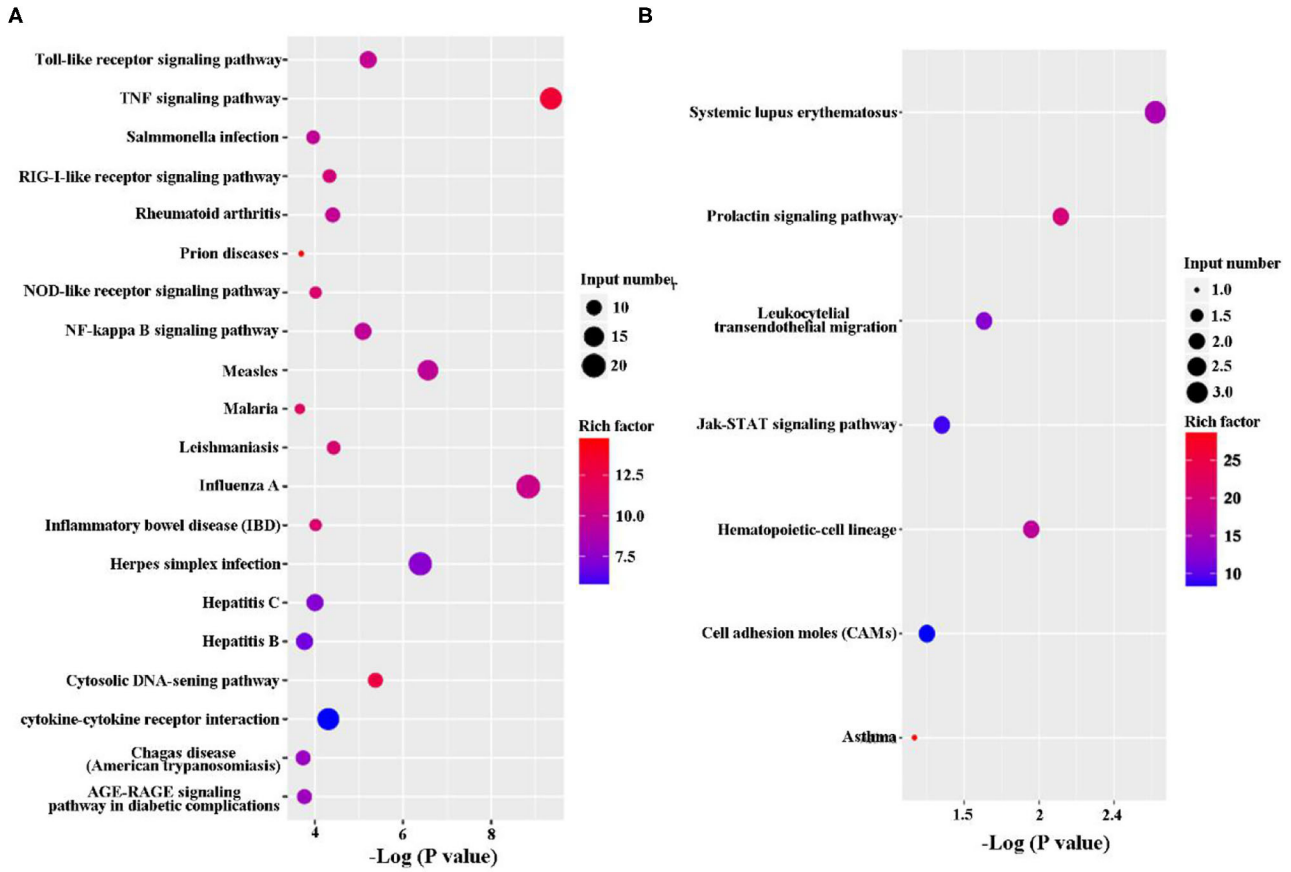

FIGURE 3 | Kyoto Encyclopedia of Genes and Genomes (KEGG) classification of differentially expressed genes (DEGs) between the uninfected and *B. suis* S2-infected cells. The rich factor represents the ratio of **(A)** upregulated genes and **(B)** downregulated genes differentially expressed gene numbers annotated in this pathway term to all gene numbers annotated with this pathway term. A greater rich factor indicates a greater degree of pathway enrichment. The *Q*-value represents the corrected *P*-value and ranges from 0 to 1, and a lower value indicates greater pathway enrichment.

of 5S, 16S, and 23S ribosomal RNA (rRNA), indicating that the total RNA of RAW 264.7 cells were intact. Spectrophotometric RNA analysis revealed an OD_{260}/OD_{280} ratio of >1.8, indicating superior quality of the RNA samples suitable for the RNA-seq analysis.

Using RNA-seq, we conduct a comprehensive comparative transcriptomic analysis of the gene expression profiles of the uninfected, *B. suis* S2-infected-, and ΔOmp16-infected-RAW 264.7 cells. The major characteristics of these libraries for each group are presented in **Table 1**. The box plot was used to evaluate the intensity distribution of all samples. The distributions of $\log_{10}$ (reads per kilobase per million mapped reads, RPKM) among the uninfected, *B. suis* S2-infected-, and ΔOmp16-infected-RAW 264.7 cells were similar (**Figure 1A**). In addition, the multidimensional scaling (MDS) analysis was used to evaluate the biological repetition of all samples, indicating that three groups samples have a high reproducibility of the data (**Figure 1B**).

Determination of DEGs Between in Uninfected Cells and *B. suis* S2-Infected Cells

The gene expression profiles were compared between uninfected and *B. suis* S2-infected RAW 264.7 cells, and the whole gene expression levels were analyzed by Illumina HiSeq^{TM} 2500. Our comparative transcriptomic analysis revealed 303 DEGs [false discovery rate (FDR) <0.05, fold change ≥2]. Of the 303 DEGs, 273 genes were upregulated and 30 genes were downregulated in *B. suis* S2-infected RAW 264.7 cells compared to uninfected RAW 264.7 cells (**Figure 2A** and **Supplementary Datasheet 1**). Furthermore, 303 DEGs were shown via Volcano Plot between uninfected and *B. suis* S2-infected RAW 264.7 cells (**Figure 2B**). To analyze gene expression data, hierarchical clustering is widely used. On the basis of their expression levels, cluster analysis arranges samples into groups to elucidate possible relationships among samples. In our study, DEGs were analyzed by cluster analysis. A heatmap of these DEGs was presented (**Figure 2C**).

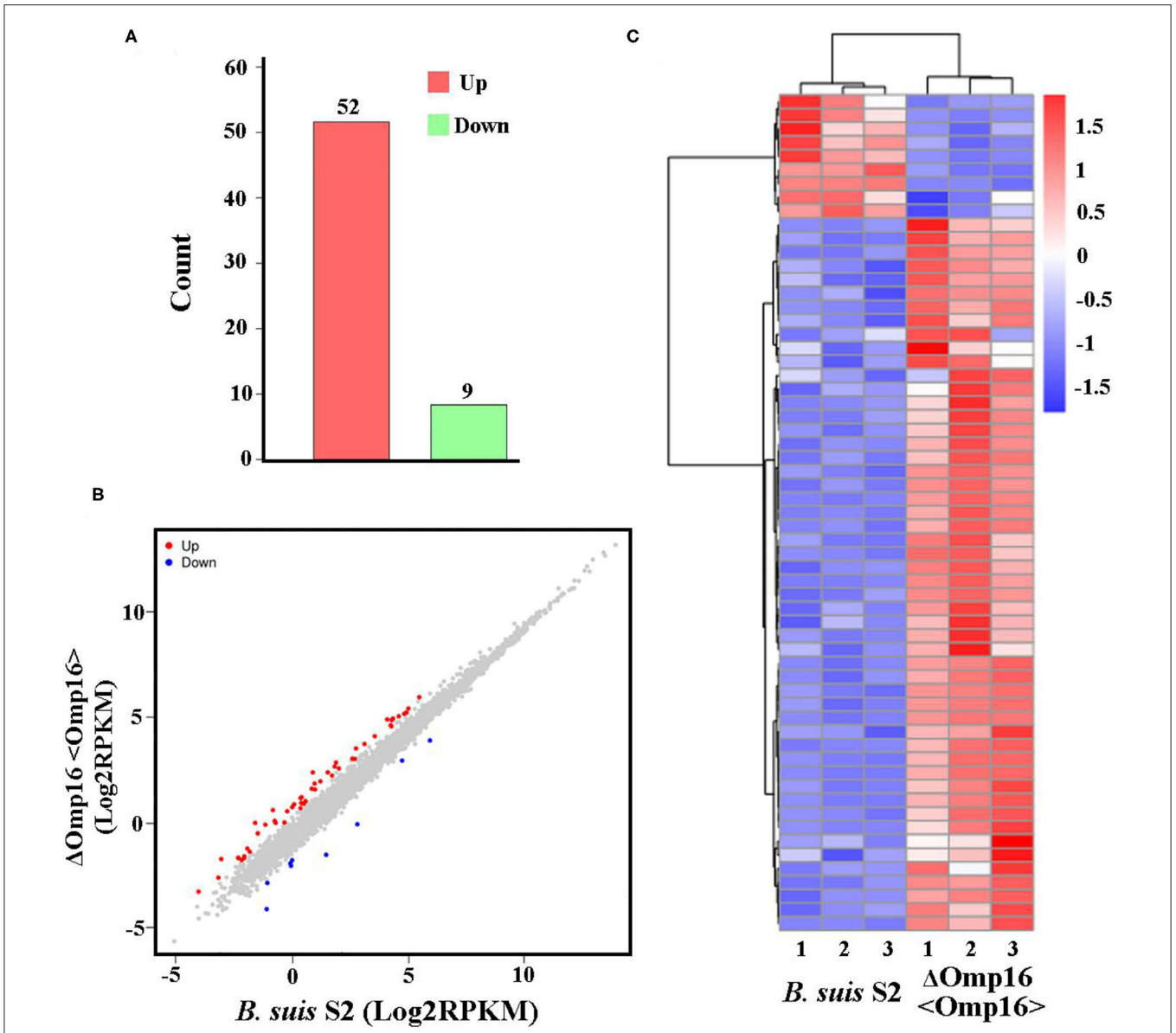

FIGURE 4 | Expression of differentially expressed genes (DEGs) between *B. suis* S2-infected and ΔOmp16-infected cells. **(A)** Histogram shows the number of DEGs and non-regulated genes between *B. suis* S2-infected and ΔOmp16-infected cells. **(B)** Scatter plot of coexpressed genes between the between *B. suis* S2-infected and ΔOmp16-infected cells. The red, blue, and gray colors denote upregulated, downregulated, and non-regulated genes, respectively, in the *B. suis* S2-infected cells compared with the uninfected cells based on the following criteria: absolute log2 (fold change) ≥1 and adjusted $P \leq 0.05$. **(C)** The heatmap shows the expression levels of DEGs between the between *B. suis* S2-infected and ΔOmp16-infected cells.

The KEGG pathway enrichment analysis was performed to analyze DEGs. Based on KEGG pathway enrichment analysis, a majority of the most upregulated genes were involved in immune response, including PRRs (Toll-like receptor signaling pathway and NOD-like receptor signaling pathway), cytokines (IL-1, IL-6, IL-23, and Cfs3), and chemokines (Ccl2, Ccl3, Ccl4, Ccl5, and Ccl10; **Figure 3A** and **Supplementary Datasheet 2**). In addition, apoptosis-related genes, such as TNF, Traf1, Nfkbia, Bcl2, and Gadd45b, were upregulated (**Figure 3A** and **Supplementary Datasheet 2**). However, the major downregulated genes were involved in metabolism and proliferation, including Rapgef3, St6gal1, Cd109, Cish, Gm17041, and Cd24a (**Figure 3B** and **Supplementary Datasheet 2**).

Determination of DEGs Between in *B. suis* S2-Infected Cells and ΔOmp16-Infected Cells

Multiple attempts to delete Omp16 were unsuccessful in *Brucella ovis* PA (13). We also made several attempts to delete Omp16

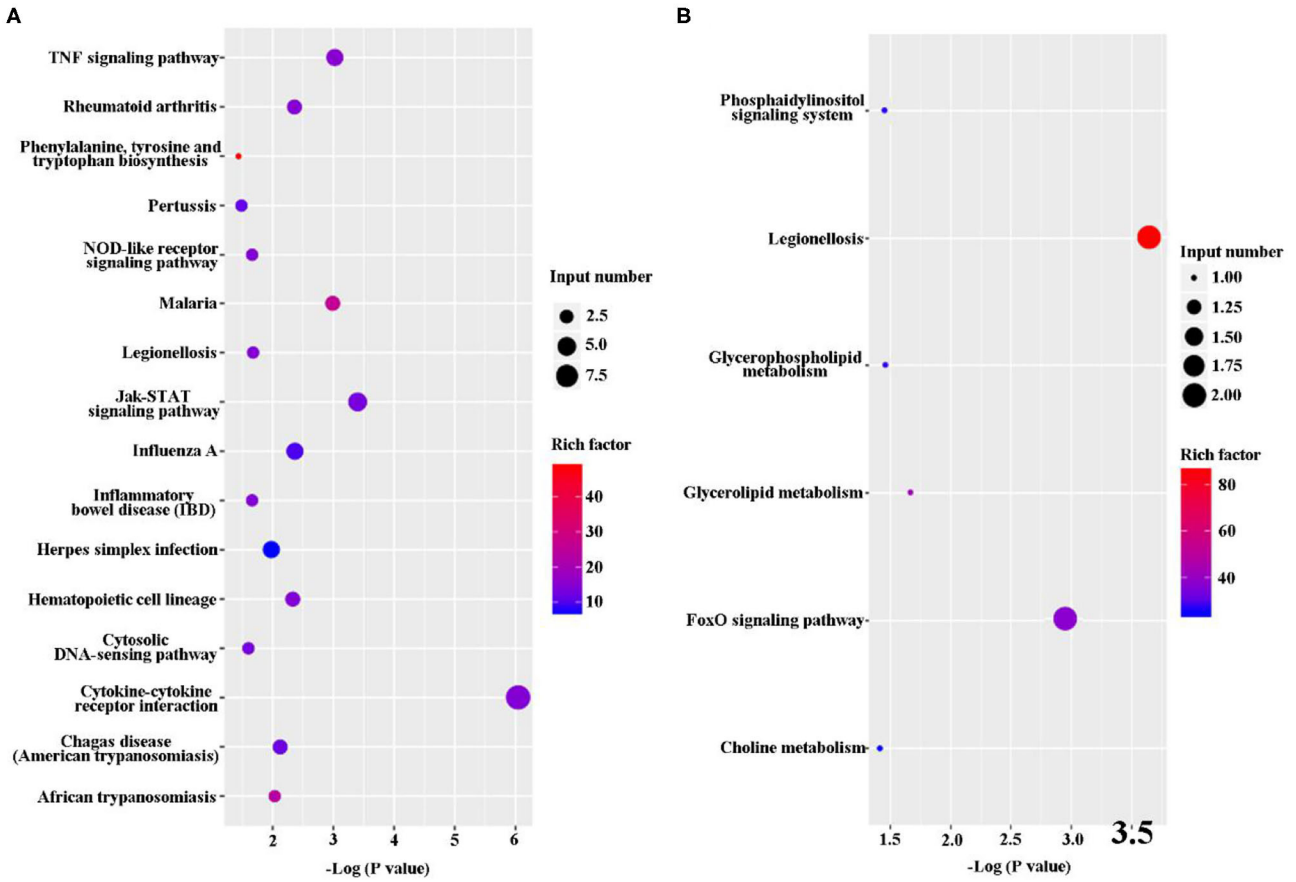

FIGURE 5 | Kyoto Encyclopedia of Genes and Genomes (KEGG) classification of differentially expressed genes (DEGs) between *B. suis* S2-infected and ΔOmp16-infected cells. The rich factor represents the ratio of **(A)** upregulated genes and **(B)** downregulated genes differentially expressed gene numbers annotated in this pathway term to all gene numbers annotated with this pathway term. A greater rich factor indicates a greater degree of pathway enrichment. The *Q*-value represents the corrected *P*-value and ranges from 0 to 1, and a lower value indicates greater pathway enrichment.

in *B. suis* S2 strain but were unsuccessful, which indicated that Omp16 could be a vital gene. Therefore, we obtained ΔOmp16 strain via conditional complementation using tetracycline-induced gene expression system (20). On the basis of ΔOmp16 strain, the gene expression profiles were compared between *B. suis* S2-infected RAW 264.7 cells and ΔOmp16-infected RAW 264.7 cells, and the whole gene expression levels were analyzed by Illumina HiSeq^{TM} 2500. We revealed 61 DEGs (FDR <0.05, fold change ≥ 2) via RNA-seq. Compared to *B. suis* S2-infected RAW 264.7 cells, 52 genes were upregulated and 9 genes were downregulated among the 61 DEGs in ΔOmp16-infected RAW 264.7 cells (**Figure 4A** and **Supplementary Datasheet 3**). Moreover, 61 DEGs were shown via Volcano Plot between *B. suis* S2- and ΔOmp16-infected RAW 264.7 cells (**Figure 4B**). In addition, a heatmap of the DEGs was drawn to directly observe the DEGs expression (**Figure 4C**).

The DEGs were analyze via KEGG pathway enrichment analysis. On the one hand, a majority of the upregulated genes, including Tnfrsf8, Ccl2, IL-12β, IL-11, Ccl22, Csf3, Lif, Tnfrsf1b, and IL-6, were related to immune response, such as TNF signaling pathway, NOD-like receptor signaling pathway, Jak-STAT signaling pathway, cytosolic DNA-sensing pathway, and cytokine–cytokine receptor interaction (**Figure 5A** and **Supplementary Datasheet 4**). On the other hand, the downregulated genes, such Bnip3 Gm45507 and Dgkg, were involved in phosphatidylinositol signaling system, legionellosis, glycerophospholipid metabolism, glycerolipid metabolism, FoxD signaling pathway, and choline metabolism (**Figure 5B** and **Supplementary Datasheet 4**).

qRT-PCR Verification of the RNA-Seq Results

In order to validate the RNA-seq data and ensure technical reproducibility, we selected and evaluated expression of 11 upregulated genes (Gdnf, Ccl2, IL-12β, IL-11, Ccl22, Csf3, Lif, Tnfrsf1b, Tnfrsf8, Slamf7, and IL-6) and 2 downregulated genes (Dgkg and Bnip3) from ΔOmp16-infected RAW 264.7 cells by qRT-PCR. The expressions of these genes obtained using qRT-PCR were in good agreement with the RNA-seq results (**Figures 6A**,**B**).

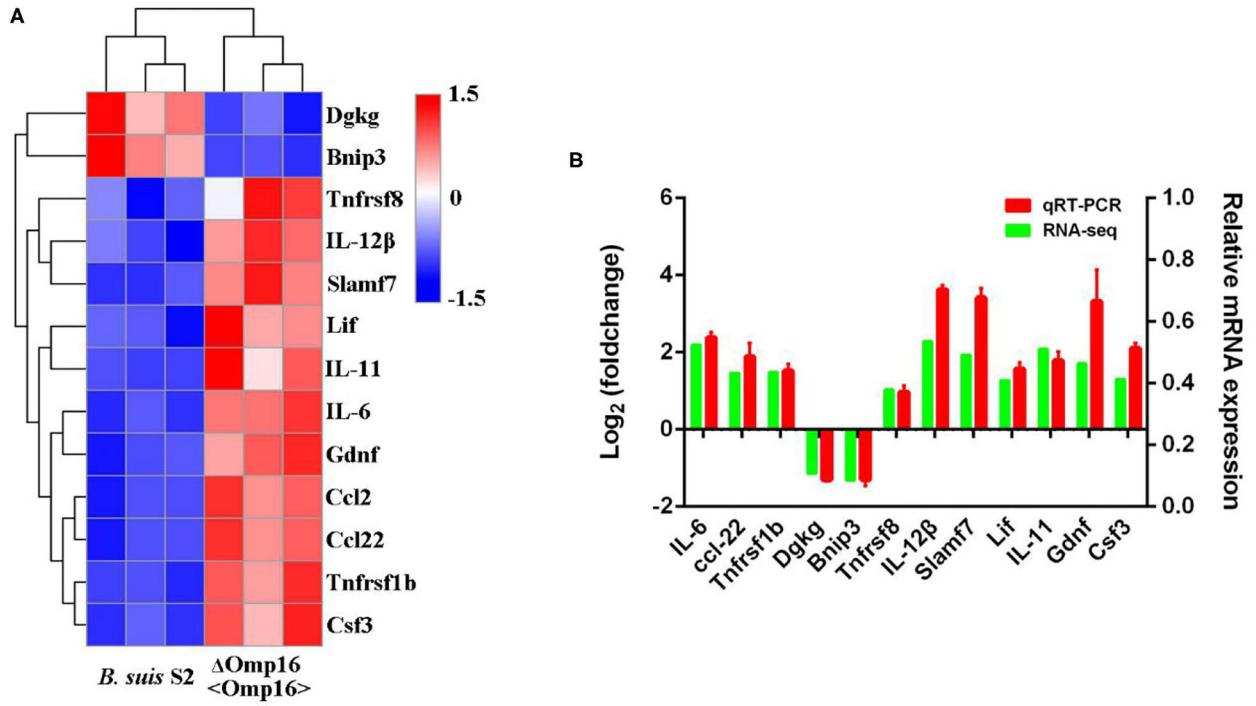

FIGURE 6 | Differentially expressed genes (DEGs) were evaluated by quantitative reverse transcription PCR (qRT-PCR) assays between *B. suis* S2-infected and ΔOmp16-infected cells. **(A)** The heatmap shows the expression levels of 13 DEGs between the between *B. suis* S2-infected and ΔOmp16-infected cells. **(B)** The 10 DEGs expression levels were further detected by qRT-PCR. The results at each time point are expressed as the means ± standard deviations from at least three independent experiments.

DISCUSSION

It has long been recognized that *Brucella* interaction with macrophages is the key aspect of its pathogenesis (2). *Brucella* can elude initial innate immune recognition through modifications of virulence factors such as lipopolysaccharide (LPS) and flagellin, resulting in a mild proinflammatory response that leads to bacterial persistence (2). However, the effects of Omps on host–pathogen interactions have not been fully understood.

In this study, we conducted a comparative transcriptomic analysis among uninfected, *B. suis* S2-infected, or ΔOmp16-infected RAW 264.7 cells to reveal the role of Omp16 during *Brucella*-infected RAW 264.7 cells. After being challenged with *B. suis* S2, we found that a majority of the most upregulated genes were involved in immune response, including PRRs (Toll-like receptor signaling pathway and NOD-like receptor signaling pathway), cytokines (IL-1, IL-6, IL-23, and Cfs3), and chemokines (Ccl2, Ccl3, Ccl4, Ccl5, and Ccl10), but the major downregulated genes were involved in metabolic and proliferation, including Rapgef3, St6gal1, Cd109, Cish, Gm17041, and Cd24. On this basis, we used ΔOmp16 that were previously constructed via conditional complementation by ATc. Compared to *B. suis* S2-infected RAW 264.7 cells, 61 DGEs were found in ΔOmp16-infected RAW 264.7 cells. Surprisingly, some immune-function-related genes were upregulated and were involved in multiple signaling pathways, such as TNF signaling pathway, NOD-like receptor signaling pathway, Jak-STAT signaling pathway, cytosolic DNA-sensing pathway, and cytokine–cytokine receptor interaction. In conclusion, these data provided evidence that Omp16 plays an important role in *Brucella*-induced immune response during infection.

During infection, the host is able to quickly detect invading pathogens to induce immune response to remove invasive pathogens, including initial inflammatory response (2, 3, 27). As a facultative intracellular pathogen, *Brucella* uses multiple strategies to escape immune defense mechanism of the host for survival, such as evading detection by pathogen-associated molecular patterns (PAMPs) (2, 28), inhibiting apoptosis, downregulating antigen presentation, and so on (29). In RNA-seq data, some upregulated genes were involved in PRR signaling pathway, including Toll-like receptor signaling pathway (TLRs) and NOD-like receptor signaling pathway (NLRs), indicating that *Brucella* can activate the host's innate immune response. However, the activation was very weak. *Brucella*, a chronic pathogen, has developed special mechanisms to evade TLR and NLR detection to maintain persistent infection. *Brucella* limits the cell's TLR4 detection of LPS with a longer fatty-acid chain, resulting in a mild proinflammatory response (30). *Brucella*-regulated flagellin synthesis to limit TLR5 detection is the stealthy strategy of *Brucella* toward the innate immune system (31). In addition, *Brucella* is able to degrade MyD88 adaptor-like (MAL) by secreting effector proteins that contain a Toll-interleukin-1 receptor (TIR) domain, such as BtpA and BtpB (1, 32, 33).

The intracellular nature of *Brucella* spp. makes it difficult to eliminate these bacteria by antimicrobial response drugs (29, 34). Thus, several cytokines and chemokines are key players against brucellosis, inducing innate and adaptive immune responses (3). The adaptive immune response to *Brucella* spp. is characterized by elevated levels of proinflammatory cytokines linked to Th1 responses, such as IL-1β and IL-6 (2, 3). In RNA-seq, compared to uninfected group, the Th1-responses-related cytokines, including IL-1 and IL-6, were increased in *B. suis* S2-infected cells, indicating that *Brucella* was able to activate RAW 264.7 macrophage cells to produce Th1 response-related cytokines. In addition, NF-kB, a central transcription factor, was responsible for controlling about 150 target genes expression, including multiple cytokines, chemokines, and receptors required for immune recognition (35). Thus, the NF-kB signaling pathway plays an important role in resistance to *Brucella* infection. In RNA-seq, KEGG pathway enrichment analysis shows that upregulated gene is enriched in the NF-kB signaling pathway, indicating that NF-kB signaling pathway is involved in eliminating intracellular *Brucella*.

Brucella spp. Omps have been broadly characterized as immunogenic and protective antigens (36, 37). Omp16, a homolog to Pals, is vital for *Brucella* survival *in vivo* or *in vitro* (13, 20). Compared to *B. suis* S2-infected RAW 264.7 cells, some inflammatory cytokines were upregulated, including IL-6, IL-11, and IL-12β, indicating that Omp16 could inhibit some inflammatory cytokines to promote *Brucella* intracellular survival. The mRNA expression of IL-6 was enhanced in ΔOmp16-infected RAW 264.7 cells compared to *B. suis* S2-infected RAW 264.7 cells (20). These results are consistent with the RNA-seq results. In previous studies, IL-6 contributes to increasing susceptibility during infection (38, 39). *Brucella* have some Omps that inhibit several cytokine secretions to contribute to intracellular survival. In porcine and murine macrophages, *Brucella* Omp25 inhibited TNF-α expression to promote intracellular survival via regulating different microRNA (18).

Interestingly, metabolic and proliferation-related genes are downregulated in RNA-seq, indicating that the activity of RAW 264.7 cells is decreased during *Brucella* infection. In the past, studies were mainly focused on the pathogen intracellular survival, inflammation response, immune response, and apoptosis. Thus, exploring the role of metabolic and proliferation-related genes is required.

CONCLUSION

The RNA-sequence analysis revealed that 303 genes were significantly regulated by *B. suis* S2, and these DEGs were mainly involved in innate immune signaling pathways, including PRRs and proinflammatory cytokines and chemokines. In ΔOmp1-infected RAW 264.7 cells, the expressions of 52 total cell genes were significantly upregulated and that of 9 total cells genes were downregulated. The KEGG pathway analysis showed that several upregulated genes were proinflammatory cytokines and chemokines. All together, we clearly demonstrate that ΔOmp16 can alter macrophage immune-related pathways to increase proinflammatory cytokines and chemokines. Further deep understanding of the regulation mechanisms of Omp16 in *Brucella*-infected macrophage may help to provide insights into illuminating the *Brucella* pathogenic strategies.

DATA AVAILABILITY STATEMENT

The datasets presented in this study can be found in online repositories. The names of the repository/repositories and accession number(s) can be found below: Dryad doi: 10.5061/dryad.tqjq2bvxv.

AUTHOR CONTRIBUTIONS

AW contributed to the conception and design of the work. FZ, JF, JL, GZ, and LC executed the experiments. DZ and FZ contributed to the analysis and interpretation of the data and drafted the manuscript. YJ and AW contributed to the final approval of the version for publication. All authors have read and agreed to the published version of the manuscript.

FUNDING

This research was funded by the National Key R&D Program of China (2018YFD0500900) and the National Natural Science Foundation of China (31672584).

SUPPLEMENTARY MATERIAL

The Supplementary Material for this article can be found online at: https://www.frontiersin.org/articles/10.3389/fvets.2021.646839/full#supplementary-material

Supplementary Table 1 | A list of all primers used in qRT-PCR.

Supplementary Datasheet 1 | The DEGs between the uninfected and *B. suis* S2-infected cells.

Supplementary Datasheet 2 | The DEGs KEGG classification between the uninfected and *B. suis* S2-infected cells.

Supplementary Datasheet 3 | The DEGs between *B. suis* S2-infected and ΔOmp16-infected cells.

Supplementary Datasheet 4 | The DEGs KEGG classification between *B. suis* S2-infected and ΔOmp16-infected cells.

REFERENCES

1. Glowacka P, Zakowska D, Naylor K, Niemcewicz M, Bielawska-Drozd A. Brucella - virulence factors, pathogenesis and treatment. *Pol J Microbiol.* (2018) 67:151–61. doi: 10.21307/pjm-2018-029
2. Byndloss MX, Tsolis RM. Brucella spp. virulence factors and immunity. *Annu Rev Anim Biosci.* (2016) 4:111–27. doi: 10.1146/annurev-animal-021815-111326
3. de Figueiredo P, Ficht TA, Rice-Ficht A, Rossetti CA, Adams LG. Pathogenesis and immunobiology of Brucellosis review of brucella-host interactions. *Am J Pathol.* (2015) 185:1505–17. doi: 10.1016/j.ajpath.2015.03.003

4. Lalsiamthara J, Lee JH. Development and trial of vaccines against Brucella. *J Vet Sci.* (2017) 18:281–90. doi: 10.4142/jvs.2017.18.S1.281
5. Schurig GG, Sriranganathan N, Corbel MJ. Brucellosis vaccines: past, present and future. *Vet Microbiol.* (2002) 90:479–96. doi: 10.1016/S0378-1135(02)00255-9
6. E.Dorneles MS, Sriranganathan N, Lage AP. Recent advances in *Brucella abortus* vaccines. *Vet Res.* (2015) 46:76. doi: 10.1186/s13567-015-0199-7
7. Zhu LQ, Feng Y, Zhang G, Jiang H, Zhang Z, Wang N, et al. *Brucella suis* strain 2 vaccine is safe and protective against heterologous Brucella spp. infections. *Vaccine.* (2016) 34:395–400. doi: 10.1016/j.vaccine.2015.09.116
8. Avila-Calderon ED, Lopez-Merino A, Sriranganathan N, Boyle S, Contreras-Rodriguez A. A history of the development of Brucella vaccines. *BioMed Res Int.* (2013) 2013:743509. doi: 10.1155/2013/743509
9. Tibor A, Decelle B, Letesson JJ. Outer membrane proteins Omp10, Omp16, and Omp19 of Brucella spp. are lipoproteins. *Infect Immun.* (1999) 67:4960–2. doi: 10.1128/IAI.67.9.4960-4962.1999
10. Tibor A, Weynants V, Denoel P, Lichtfouse B, De Bolle X, Saman E, et al. Molecular cloning, nucleotide sequence, and occurrence of a 16.5-kilodalton outer membrane protein of *Brucella abortus* with similarity to pal lipoproteins. *Infect. Immun.* (1994) 62:3633–9. doi: 10.1128/IAI.62.9.3633-3639.1994
11. Tibor A, Wansard V, Bielartz V, Delrue RM, Danese I, Michel P, et al. Effect of omp10 or omp19 deletion on *Brucella abortus* outer membrane properties and virulence in mice. *Infect Immun.* (2002) 70:5540–6. doi: 10.1128/IAI.70.10.5540-5546.2002
12. Li TS, Huang ML, Wang Z, Guo F, Zhang H, Chen CF. Construction and characteristic analysis of Omp10 deletion mutant of *Brucella abortus*. *Pak J Zool.* (2017) 49:1809–16. doi: 10.17582/journal.pjz/2017.49.5.1809.1816
13. Sidhu-Munoz RS, Sancho P, Vizcaino N. *Brucella ovis* PA mutants for outer membrane proteins Omp10, Omp19, SP41, and BepC are not altered in their virulence and outer membrane properties. *Vet. Microbiol.* (2016) 186:59–66. doi: 10.1016/j.vetmic.2016.02.010
14. Pasquevich KA, Carabajal MV, Guaimas FF, Bruno L, Roset MS, Coria LM, et al. Omp19 enables *Brucella abortus* to evade the antimicrobial activity from host's proteolytic defense system. *Front. Immunol.* (2019) 10:436. doi: 10.3389/fimmu.2019.01436
15. Edmonds MD, Cloeckaert A, Elzer PH, Brucella species lacking the major outer membrane protein Omp25 are attenuated in mice and protect against *Brucella melitensis* and *Brucella ovis*. *Vet. Microbiol.* (2002) 88:205–21. doi: 10.1016/S0378-1135(02)00110-4
16. Edmonds MD, Cloeckaert A, Booth NJ, Fulton T, Hagius SD, Walker JV, et al. Attenuation of a *Brucella abortus* mutant lacking a major 25 kDa outer membrane protein in cattle. *Am J Vet Res.* (2001) 62:1461–6. doi: 10.2460/ajvr.2001.62.1461
17. Verdiguel-Fernandez L, Oropeza-Navarro R, Ortiz A, Robles-Pesina MG, Ramirez-Lezama J, Castaneda-Ramirez A, et al. *Brucella melitensis* omp31 mutant is attenuated and confers protection against virulent *Brucella melitensis* challenge in BALB/c mice. *J Microbiol Biotechnol.* (2020) 30:497–504. doi: 10.4014/jmb.1908.08056
18. Luo X, Zhang X, Wu X, Yang X, Han C, Wang Z, et al. Brucella downregulates tumor necrosis factor-alpha to promote intracellular survival via Omp25 regulation of different microRNAs in porcine and murine macrophages. *Front Immunol.* (2017) 8:2013. doi: 10.3389/fimmu.2017.02013
19. Zhang K, Wang H, Guo F, Yuan L, Zhang WJ, Wang YZ et al. OMP31 of *Brucella melitensis* 16M impairs the apoptosis of macrophages triggered by TNF-α. *Exp Ther Med.* (2016) 12:2783–9. doi: 10.3892/etm.2016.3655
20. Zhi FJ, Zhou D, Li JM, Tian LL, Zhang GD, Jin YP, et al. Omp16, a conserved peptidoglycan-associated lipoprotein, is involved in Brucella virulence *in vitro*. *J Microbiol.* (2020) 58:793–804. doi: 10.1007/s12275-020-0144-y
21. Hirakawa H, Suzue K, Kurabayashi K, Tomita H. The Tol-Pal system of uropathogenic *Escherichia coli* is responsible for optimal internalization into and aggregation within bladder epithelial cells, colonization of the urinary tract of mice, and bacterial motility. *Front. Microbiol.* (2019) 10:1827. doi: 10.3389/fmicb.2019.01827
22. Walburger A, Lazdunski C, Corda Y. The Tol/Pal system function requires an interaction between the C-terminal domain of TolA and the N-terminal domain of TolB. *Mol Microbiol.* (2002) 44:695–708. doi: 10.1046/j.1365-2958.2002.02895.x
23. Prusty BR, Tabassum R, Chaudhuri P, Saini M, Chaturvedi VK, Mishra BP, et al. Expression of Omp16 and L7/L12 *Brucella abortus* protective antigens as secretory fusion proteins in mammalian cells. *Indian J Biotechnol.* (2017) 16:289–95. Available online at: http://nopr.niscair.res.in/handle/123456789/43344
24. Pasquevich KA, Garcia Samartino C, Coria LM, Estein SM, Zwerdling A, Ibanez AE, et al. The protein moiety of *Brucella abortus* outer membrane protein 16 is a new bacterial pathogen-associated molecular pattern that activates dendritic cells *in vivo*, induces a Th1 immune response, and is a promising self-adjuvanting vaccine against systemic and oral acquired brucellosis. *J Immunol.* (2010) 184:5200–12. doi: 10.4049/jimmunol.0902209
25. Pasquevich KA, Estein SM, Garcia Samartino C, Zwerdling A, Coria LM, Barrionuevo P, et al. Immunization with recombinant Brucella species outer membrane protein Omp16 or Omp19 in adjuvant induces specific CD4+ and CD8+ T cells as well as systemic and oral protection against *Brucella abortus* infection. *Infect Immun.* (2009) 77:436–45. doi: 10.1128/IAI.01151-08
26. Luo D, Ni B, Li P, Shi W, Zhang S, Han Y, et al. Protective immunity elicited by a divalent DNA vaccine encoding both the L7/L12 and Omp16 genes of *Brucella abortus* in BALB/c mice. *Infect Immun.* (2006) 74:2734–41. doi: 10.1128/IAI.74.5.2734-2741.2006
27. Elfaki MG, Alaidan AA, Al-Hokail AA. Host response to Brucella infection: review and future perspective. *J Infect Dev Countr.* (2015) 9:697–701. doi: 10.3855/jidc.6625
28. Celli J. Surviving inside a macrophage: the many ways of Brucella. *Res Microbiol.* (2006) 157:93–8. doi: 10.1016/j.resmic.2005.10.002
29. Skendros P, Pappas G, Boura P. Cell-mediated immunity in human brucellosis. *Microbes Infect.* (2011) 13:134–42. doi: 10.1016/j.micinf.2010.10.015
30. Cardoso PG, Macedo GC, Azevedo V, Oliveira SC. Brucella spp noncanonical LPS: structure, biosynthesis, and interaction with host immune system. *Microb Cell Fact.* (2006) 5:13. doi: 10.1186/1475-2859-5-13
31. Terwagne M, Ferooz J, Rolan HG, Sun YH, Atluri V, Xavier MN, et al. Innate immune recognition of flagellin limits systemic persistence of Brucella. *Cell Microbiol.* (2013) 15:942–60. doi: 10.1111/cmi.12088
32. Dehio C, Tsolis RM. Type IV effector secretion and subversion of host functions by Bartonella and Brucella species. *Curr Top Microbiol Immunol.* (2017) 413:269–95. doi: 10.1007/978-3-319-75241-9_11
33. de Jong MF, Tsolis RM. Brucellosis and type IV secretion. *Fut Microbiol.* (2012) 7:47–58. doi: 10.2217/fmb.11.136
34. Skalsky K, Yahav D, Bishara J, Pitlik S, Leibovici L, Paul M. Treatment of human brucellosis: systematic review and meta-analysis of randomised controlled trials. *Brit Med J.* (2008) 336:701–4. doi: 10.1136/bmj.39497.500903.25
35. Baldwin AS. The NF-kappa B and I kappa B proteins: new discoveries and insights. *Annu Rev Immunol.* (1996) 14:649–83. doi: 10.1146/annurev.immunol.14.1.649
36. Bowden RA, Estein SM, Zygmunt MS, Dubray G, Cloeckaert A. Identification of protective outer membrane antigens of *Brucella ovis* by passive immunization of mice with monoclonal antibodies. *Microbes infect.* (2000) 2:481–8. doi: 10.1016/S1286-4579(00)00317-8
37. Cloeckaert A, Tibor A, Zygmunt MS. Brucella outer membrane lipoproteins share antigenic determinants with bacteria of the family Rhizobiaceae. *Clin Diagn Lab Immunol.* (1999) 6:627–9.doi: 10.1128/CDLI.6.4.627-629.1999
38. Karaoglan I, Pehlivan S, Namiduru M, Pehlivan M, Kilincarslan C, Balkan Y, et al. TNF-alpha, TGF-beta, IL-10, IL-6 and IFN-gamma gene polymorphisms as risk factors for brucellosis. *New Microbiol.* (2009) 32:173–8.
39. Budak F, Goral G, Heper Y, Yilmaz E, Aymak F, Basturk B, et al. IL-10 and IL-6 gene polymorphisms as potential host susceptibility factors in Brucellosis. *Cytokine.* (2007) 38:32–36. doi: 10.1016/j.cyto.2007.04.008

Conflict of Interest: The authors declare that the research was conducted in the absence of any commercial or financial relationships that could be construed as a potential conflict of interest.

frontiers in Genetics

ORIGINAL RESEARCH
published: 08 March 2021
doi: 10.3389/fgene.2021.627623

Whole-Blood Transcriptome Analysis of Feedlot Cattle With and Without Bovine Respiratory Disease

*Janelle Jiminez[1], Edouard Timsit[2,3,4], Karin Orsel[2], Frank van der Meer[5], Le Luo Guan[1] and Graham Plastow[1]**

[1] Department of Agricultural, Food and Nutritional Science, Livestock Gentec, University of Alberta, Edmonton, AB, Canada, [2] Department of Production Animal Health, Faculty of Veterinary Medicine, University of Calgary, Calgary, AB, Canada, [3] Simpson Ranch Chair in Beef Cattle Health and Wellness, University of Calgary, Calgary, AB, Canada, [4] Ceva Santé Animale, Libourne, France, [5] Department of Ecosystem and Public Health, Faculty of Veterinary Medicine, University of Calgary, Calgary, AB, Canada

Bovine respiratory disease (BRD) is one of the main factors leading to morbidity and mortality in feedlot operations in North America. A complex of viral and bacterial pathogens can individually or collectively establish BRD in cattle, and to date, most disease characterization studies using transcriptomic techniques examine bronchoalveolar and transtracheal fluids, lymph node, and lung tissue as well as nasopharyngeal swabs, with limited studies investigating the whole-blood transcriptome. Here, we aimed to identify differentially expressed (DE) genes involved in the host immune response to BRD using whole blood and RNA sequencing. Samples were collected from heifers (average arrival weight = 215.0 ± 5.3 kg) with (n = 25) and without (n = 18) BRD at a commercial feedlot in Western Canada. RNAseq analysis showed a distinct whole-blood transcriptome profile between BRD and non-BRD heifers. Further examination of the DE genes revealed that those involved in the host inflammatory response and infectious disease pathways were enriched in the BRD animals, while gene networks associated with metabolism and cell growth and maintenance were downregulated. Overall, the transcriptome profile derived from whole blood provided evidence that a distinct antimicrobial peptide-driven host immune response was occurring in the animals with BRD. The blood transcriptome of the BRD animals shows similarities to the transcriptome profiles obtained from lung and bronchial lymph nodes in other studies. This suggests that the blood transcriptome is a potential diagnostic tool for the identification of biomarkers of BRD infection and can be measured in live animals and used to further understand infection and disease in cattle. It may also provide a useful tool to increase the understanding of the genes involved in establishing BRD in beef cattle and be used to investigate potential therapeutic applications.

Keywords: bovine respiratory disease, differentially expressed genes (DEGs), host immune response, innate immunity, RNA sequencing

OPEN ACCESS

Edited by:
Fabiana Quoos Mayer, Institute of Veterinary Research Desidério Finamor (IPVDF), Brazil

Reviewed by:
Ricardo Zanella, The University of Passo Fundo, Brazil
Jose Vargas, The University of Passo Fundo, Brazil

***Correspondence:**
Graham Plastow
plastow@ualberta.ca

Specialty section:
This article was submitted to Livestock Genomics, a section of the journal Frontiers in Genetics

Received: *09 November 2020*
Accepted: *08 February 2021*
Published: *08 March 2021*

Citation:
Jiminez J, Timsit E, Orsel K, van der Meer F, Guan LL and Plastow G (2021) Whole-Blood Transcriptome Analysis of Feedlot Cattle With and Without Bovine Respiratory Disease. Front. Genet. 12:627623. doi: 10.3389/fgene.2021.627623

INTRODUCTION

Bovine respiratory disease (BRD) is one of the main causes of morbidity and mortality in beef cattle in North America (USDA, 2011). Beef cattle of all ages can be affected with BRD; however, they are most affected on or soon after entry into the feedlot (Babcock et al., 2010). This timing of infection is most likely due to the animal's exposure to a wide range of pathogens that takes place at a time when various stressors (weaning, transportation, and commingling) negatively affect their immune system (Caswell, 2014; Timsit et al., 2016).

Although respiratory pathogens (mainly viruses and bacteria) and factors predisposing cattle to BRD are relatively well understood (Taylor et al., 2010), the host response and its relationship with disease outcomes to BRD, such as the host's ability to maintain performance regardless of pathogen burden, needs to be further investigated (Van Eenennaam et al., 2014; Mulder and Rashidi, 2017). For instance, in cattle infected with respiratory pathogens, it is currently difficult to determine which cattle will exhibit visual and clinical signs of BRD or even require an antimicrobial treatment (Timsit et al., 2011b; Wolfger et al., 2015). Transcriptome analysis can lead to insights into disease processes, and biomarkers to assess disease states, progression, and prognosis. Thus far, transcriptomic techniques have examined bronchoalveolar fluids, lung tissue, and sputum samples of cattle with or without BRD (Aich et al., 2009; Rai et al., 2015; Behura et al., 2017; Johnston et al., 2019), but there is much less information on the whole-blood transcriptome (Lindholm-Perry et al., 2018; Sun et al., 2020). In comparison with lung tissue biopsies, blood is easier to obtain and can be collected repeatedly throughout the production period and can give real-time results, instead of postmortem conclusions. Furthermore the host immune response detected in the blood can reflect those responses occurring at the site of infection (Kawayama et al., 2016; Vinther et al., 2016).

Therefore, the objective of this study was to use RNA sequencing to analyze the whole-blood transcriptome of feedlot cattle with or without BRD. We hypothesized that animals exhibiting BRD would show a specific pattern of response in their blood transcriptome and that such patterns will provide further insight into the host immune response. Furthermore, variation in the blood transcriptome of animals with and without BRD could potentially provide markers of resistance or resilience markers for future application in breeding or management.

Abbreviations: ADG, average daily gain; ALAS, aminolevulinic acid synthase; BoHV-1, bovine herpes virus-1; BRD, bovine respiratory disease; BRSV, bovine respiratory syncytial virus; BVDV, bovine viral diarrhea virus; CATH, cathelicidin; CFB, complement factor B; CPM, counts per million; DE, differentially expressed; DEFB, beta-defensin; DOF, days on feed; EBD, enteric beta defensin; FDR, false discovery rate; GLM, general linear model; GZM, granzyme; HB, globin; HP, haptoglobin; IL, interleukin; LCN, lipocalin; LTF, lactoferrin; MHC, major histocompatibility complex; MMP, matrix metallopeptidase; NB, non-BRD; PCA, principal component analysis; PCR, polymerase chain reaction; PI3V, bovine parainfluenza-3; RIN, RNA integrity value; SERPINB, serpin peptidase inhibitor; S100A, S100 calcium-binding protein; TLR, toll-like receptor; TMM, trimmed mean of *M*-values; TNFAIP, tumor necrosis factor alpha induced protein; WC, workshop cluster.

MATERIALS AND METHODS

Ethics Statement

This study was conducted in accordance to the Canadian Council of Animal Care (2009) guidelines and recommendations (CCAC, 2009). All experimental procedures were reviewed and approved by the University of Calgary Veterinary Sciences Animal Care Committee (AC15-0109).

Animals

Mixed-breed beef heifers at high risk of developing BRD (i.e., recently weaned, commingled, and auction-market derived) were enrolled between November 2015 and January 2016 at a commercial feedlot in Southern Alberta, Canada. At on-arrival processing, heifers received a subcutaneous injection of a long-acting macrolide (tulathromycin, Draxxin, 2.5 mg/kg, Zoetis, Kirkland, QC, Canada) and were weighed and vaccinated against infectious bovine herpes virus-1 (BoHV-1), bovine viral diarrhea virus (BVDV) (types I and II), bovine parainfluenza-3 (PI3V), bovine respiratory syncytial virus (BRSV), *Mannheimia haemolytica*, *Histophilus somni*, and clostridial pathogens. They were also dewormed with a pour-on ivermectin solution. In addition, they received a prostaglandin F2α analog to induce abortion, as per standard feedlot procedure. Heifers were fed in large outdoor dirt-floor pens with approximately 250–300 animals per pen. They were fed twice daily, a concentrate barley-based receiving/growing diet formulated to meet or exceed nutrient requirements. This diet contained 25 ppm of monensin (Rumensin 200, Elanco, Guelph, ON, Canada) and 35 ppm of chlortetracycline (Aureomycin 220, Zoetis). Each morning before feeding, bunks were visually inspected, and feed deliveries were adjusted to ensure that sufficient feed was available for *ad libitum* consumption. At approximately 30 days after arrival, cattle received another vaccination against infectious BoHV-1, BVDV types I and II, PI3V, BRSV, and a growth implant. Finally, cattle were individually weighed at approximately 120 days on feed (DOF). Average daily gain (ADG) was calculated using the difference between arrival weight and weight at blood sampling, divided by the DOF.

Case Definition

Animals were retrospectively identified as BRD positive based on clinical examination and serum haptoglobin concentration. Heifers with at least one visual BRD sign, a rectal temperature $\geq$40°C, abnormal lung sounds detected at auscultation, a serum haptoglobin concentration $\geq$0.25 g/L, and no prior treatment against BRD or other diseases during the feeding period (i.e., first BRD occurrence) were defined as BRD cases. Heifers that had no visual signs of BRD, a rectal temperature <40°C, no abnormal lung sounds detected at auscultation, a serum haptoglobin concentration <0.25 g/L, and no history of treatment against BRD or other disease during the feeding period were treated as

healthy controls, which were classified as non-BRD (NB) animals for transcriptome analysis.

Study Design

Heifers were observed daily by experienced pen checkers for detection of clinical illness during the first 60 days from entry. Cattle with one or more visual signs of BRD (e.g., depression, nasal or ocular discharge, cough, tachypnea, or dyspnea) were removed from the pens by pen checkers and, if not previously treated for BRD or another disease during the feeding period, were clinically examined by an experienced veterinarian (ET) and a blood sample collected. For every heifer suspected of having BRD, one or two visually healthy cattle (no visual signs of BRD or other disease) were selected as pen-matched contemporary controls (for convenience, these animals were close to the gate or to the apparently sick animal, etc.) examined as for the BRD animals (if not previously treated for BRD or another disease during the feeding period).

Clinical examinations included assessment of visual signs of respiratory disease (cf. above), determination of respiratory rate and rectal temperature, and a complete lung auscultation using a conventional stethoscope to detect abnormal lung sounds (e.g., increased bronchial sounds, crackles, and wheezes). Two blood samples from each animal were collected at the same time by jugular vein puncture to determine (i) serum haptoglobin concentration [plastic serum tubes; Becton Dickinson, ON (Timsit et al., 2011a)] and (ii) the whole-blood transcriptome (Tempus tubes; Thermo Fisher Scientific, ON). Heifers with at least one visual BRD sign and a rectal temperature $\geq$40°C received an antibiotic treatment intramuscularly in combination with non-steroidal anti-inflammatory drugs (e.g., 40 mg/kg of florfenicol and 2.2 mg/kg of flunixin, 2 ml/15 kg, Resflor, Merck Animal Health) after sample collection, in accordance with feedlot treatment protocols.

Determination of Serum Haptoglobin Concentration

Serum haptoglobin concentrations were determined in duplicate using a commercially available kit (Tridelta Phase Range Haptoglobin assay, Tridelta Development) as described (Timsit et al., 2011a). The working range was 0.0–2.5 g/L.

Total RNA Isolation and mRNA Library Preparation

Total RNA was isolated from bovine blood using a Preserved Blood RNA Purification Kit (Norgen Biotek Corp, Thorold, ON, Canada), and the quality of RNA was measured using the 2200 RNA ScreenTape TapeStation System (Agilent Technologies Inc., Cedar Creek, TX, United States) producing RNA integrity (RIN) values ranging from 8.0 to 9.8. To prepare the mRNA cDNA libraries, 1.0 μg of total RNA was used from each sample using the TruSeq RNA Library Preparation kit v2 (Illumina, San Diego, CA, United States). Poly A-containing mRNA was enriched from the total RNA using poly-T oligo attached beads and fragmented for first-strand cDNA synthesis, followed by second-strand synthesis. The ends were repaired, and 3′ end adenylation and adapter ligation were performed for each library. Following these steps, libraries were polymerase chain reaction (PCR) amplified, validated using the Bioanalyzer (Agilent Technologies Inc., Cedar Creek, TX, United States), and finally normalized and pooled. Unique indices were used for all samples, and libraries were pooled and sequenced paired end (2 × 100 bp) on four separate lanes on a HiSeq 4000 platform, and sequencing was performed at McGill University and Genome Quebec Innovation Center (Montreal, QC, Canada). In total, 43 samples were used to generate paired-end sequences, and their raw reads were used for downstream analyses.

Transcriptome Data Analysis

Raw reads were analyzed for quality and adapter sequence presence using FastQC (v0.11.8), and adapter sequences were removed using Trimmomatic (v0.39). These cleaned-up sequences were mapped and aligned to the *Bos taurus* reference genome (ARS-UCD1.2.98) using STAR (v2.7.1a) with default settings (Dobin et al., 2013), and read counts were generated using FeatureCounts (SubRead v1.6.4). The counts were then analyzed using the Bioconductor packages EdgeR and DESeq in the R (v3.5.2) software environment. Counts per million (CPM) was used to evaluate expression, and transcripts with CPM $>$ 2 were considered as expressed.

Differential Gene Expression Analysis

Differential gene expression results were obtained using EdgeR to compare animals with BRD (n = 25) with NB (n = 18) using the following parameters: P-value $<$ 0.05 were adjusted to a 0.01 cutoff (P-adj), with a log fold change (Log2FC) $>$ 2, with log CPM $>$ 2. The data were also filtered with the "keep" command to keep samples with CPM $\geq$ 2 in at least 18 samples, as the number of samples in the NB group was 18 (Robinson et al., 2010). This value represents genes that are expressed in all the samples measured, and the dataset was normalized with the trimmed mean of M-values (TMM) normalization. To test for differential expression between the BRD and NB animals, the factors of "brd" and "pen" were used to test the difference in expression between the animals. The NB animals were set as the reference in this design model, and the read count data were fitted to a negative binomial general linear model (GLM) representing the design. Prior to fitting the model, the "Common," "Trended," and "Tagwise" negative binomial dispersion were estimated, and the biological coefficient of variation was calculated at 78% with a dispersion ratio of 0.61. Statistical tests were then performed for the coefficient relating to the BRD animals, and the top differentially expressed (DE) genes (DEGs) between the BRD and NB samples were ranked by P-value and absolute log2FC. In total, three different DEG analyses were performed: the total DEGs with read counts from both the BRD and NB animals (total DEGs, n = 43, coef = pen); BRD DEGs (n = 25, coef = cluster); and NB DEGs (n = 18, coef = pen). A "cluster" coefficient was also added for the BRD animals representing the three subgroups of the BRD samples differentiated by principal component analysis (PCA) determination of clustered samples (Cluster; n = 3).

Ingenuity Pathway Analysis

Network and pathway analyses were analyzed using Ingenuity Pathway Analysis (IPA)[1] (Qiagen, 2000–2019) software. This core analysis tool was used to identify gene pathways, disease, and networks using the gene expression data calculated by EdgeR. Input files of expression data included DEGs from all animals ($n = 43$) and the BRD-only animals ($n = 25$).

Statistical Analyses

Statistical analysis used the R software package. P-values ≤ 0.05 were used to indicate significance, while false discovery rate (FDR) values were set at 0.05 for the adjusted P-values, unless otherwise stated. Both EdgeR and IPA incorporate statistical analyses into their analysis packages, and those values were reported. For ADG, rectal temperatures, and DOF, a Wilcoxon rank sum test with continuity correction was used to compare the BRD and NB animal values in the Dplyr package.

RESULTS

Confirmation of Disease Status

Forty-four heifers (average arrival weight = 215.0 ± 5.3 kg) were enrolled to the study and were clinically examined and sampled between November 11 and December 11, 2015. Of these, 25 were classified as BRD positive and 18 were classified as NB based on clinical examination and serum haptoglobin concentration. One control heifer was removed from the study, as it had a serum haptoglobin concentration of 3.6 g/L (i.e., ≥0.25 g/L). Heifers with BRD had higher ($P < 0.001$) average rectal temperatures of 40.6 ± 0.03°C, than NB heifers averaging 39.3 ± 0.14°C (**Supplementary Table 1**). Furthermore, the ADG in the NB heifers was considerably higher ($P < 0.001$) than in the BRD heifers, which on average gained less weight ($P < 0.001$) from the time they arrived to the feedlot to the time they were enrolled in the study (**Supplementary Table 1**).

Total Gene Expression Data Summary of All Bovine Respiratory Disease Animals Compared With All Non-bovine Respiratory Disease Animals

A total of 1.51 billion raw reads were generated for the mRNA libraries, and after trimming, an average of 31 M reads per sample was used for alignment (**Supplementary Table 2**). The read-mapping rates ranged from 75.27 to 92.09%, and on average approximately 25 M reads were uniquely mapped per sample (**Supplementary Table 3**). In total, EdgeR analysis identified 11,966 genes, with 3,075 downregulated and 3,236 upregulated when comparing the BRD with NB samples ($n = 43$) using BRD as the coefficient to determine DEGs; 6,311 total DEG, log2FC > 2, P-adj < 0.05. To explore the difference between the expression profiles of the NB and BRD samples, PCA was used to analyze the differences and similarities between the samples. The PCA showed that whole-blood transcriptome profiles of BRD cattle were separated from the NB profiles with 54% of the variation attributed to PC1 (**Figure 1**). Four samples appear as outliers in the PCA plot: two BRD samples and two NB samples (**Figure 1**). As might be expected from this result, the number of DEGs in the NB group was relatively small ($n = 33$ DEGs; total transcripts = 11, 787), whereas thousands of DEGs were identified within the BRD samples, which had a total of 13,404 transcripts identified.

Identification of the Differentially Expressed Genes Between Bovine Respiratory Disease and Non-bovine Respiratory Disease Animals

To investigate the host response due to BRD infection, the top ranked DEGs were identified by comparing the DEGs between the NB and BRD samples. **Table 1** shows the genes with the highest logFC values using the NB animal expression as the reference. Major immune genes such as *interleukin* (*IL*)*1 receptor 2* (*IL1R2*), *complement factor B* (*CFB*), and *IL3 receptor subunit alpha* (*IL3RA*) were identified in the top 10 upregulated DEGs, with *TNF alpha induced protein 6* (*TNFAIP6*) and *IL12B* evident in the top 30 upregulated DEGs. Furthermore, *haptoglobin* (*HP*), *lipocalin* (*LCN2*), *serpin peptidase inhibitor* (*SERPINB4*), and *S100 calcium-binding proteins* (*S100A9* and *S100A8*) were also among the top expressed genes in the BRD animals (**Table 1**). The top downregulated DEGs when comparing the BRD with NB animals (**Table 2**) belonged to hemoglobin synthesis pathways, including *alpha globin* (*HBA*), *beta globin* (*HBB*), *mu globin* (*HBM*), and *aminolevulinic acid synthase* (*ALAS2*). The enriched genes (upregulated in the BRD animals) belong to immune response pathways, as well as gastrointestinal, inflammatory, infectious, and respiratory disease pathways (not shown).

Analysis of Bovine Respiratory Disease Clusters and Differentially Expressed Genes

As the BRD samples were more dispersed in the PCA than those from NB (**Figure 1**), gene expression in the 25 BRD animals was investigated further. Three distinct subsets or clusters were identified within the BRD samples (**Figure 2**). These clusters were not associated with serum haptoglobin level or rectal temperature at clinical examination (**Supplementary Table 1**).

Differentially expressed gene values were calculated within the BRD samples ($n = 25$) and compared with one another for DEG profile, with cluster used as the coefficient to determine DEGs; log2FC > 2, P-adj < 0.05. A total of 13,404 DEGs were identified in these samples (**Table 2**). As Cluster A appeared to be the most distinct, Cluster A read counts were compared with those in Clusters B and C. With the use of logFC > 2, P-value < 0.05, P-adj < 0.01, when compared with A, 109 DEGs common to Clusters B and C were identified (34 upregulated and 74 downregulated). There were 273 DEGs unique to Cluster C and 18 to Cluster B when compared with Cluster A. The top upregulated genes unique to Cluster B included *multidrug resistance protein 4*, *duodenase-1*, and *trefoil factor 2*, while the top downregulated genes were all from

[1] http://www.ingenuity.com

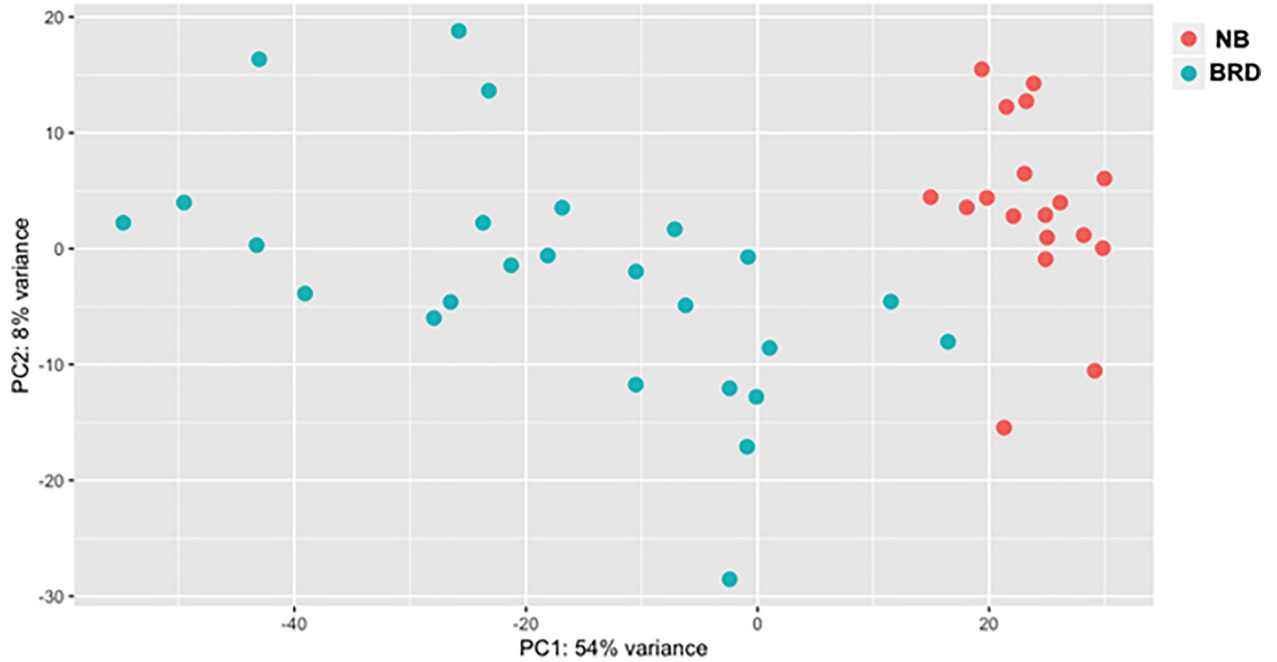

FIGURE 1 | Principal component analysis (PCA) plot comparing differences in total differentially expressed (DE) gene populations between bovine respiratory disease (BRD) and non-BRD (NB) animals. PCA plot displaying differing clustering patterns between heifers displaying clinical signs of BRD (blue) and non-BRD animals (red). Plot was designed using normalized counts (n = 43), using the variable stabilization transformation for the PlotPCA tool in DEGSeq.

TABLE 1 | Top enriched total differentially expressed (DE) genes identified when comparing all bovine respiratory disease (BRD) with all non-BRD (NB) animals.

Gene name	Gene description	LogFC	*P*-Adjust
LRG1	Leucine-rich alpha-2-glycoprotein 1 [Source: VGNC Symbol; Acc: VGNC:30980]	7.84	5.55E-29
SERPINB4	*Bos taurus* serpin peptidase inhibitor, clade B like (LOC786410), mRNA. [Source: RefSeq mRNA; Acc:NM_001206713]	6.14	1.18E-19
IL1R2	Interleukin 1 receptor type 2 [Source: VGNC Symbol; Acc: VGNC:30132]	5.82	2.71E-20
EREG	Epiregulin [Source: VGNC Symbol; Acc: VGNC:28575]	5.37	3.14E-22
THY1	thy-1 cell surface antigen [Source: VGNC Symbol; Acc: VGNC:35856]	5.26	8.05E-20
CFB	Complement factor B [Source: NCBI gene; Acc: 514076]	4.74	1.05E-28
DCSTAMP	Dendrocyte expressed seven transmembrane protein [Source: VGNC Symbol; Acc: VGNC:27925]	4.25	1.80E-22
BMX	BMX non-receptor tyrosine kinase [Source: VGNC Symbol; Acc: VGNC:26529]	4.14	2.65E-30
DPYS	Dihydropyrimidinase [Source: VGNC Symbol; Acc: VGNC:28194]	4.11	9.58E-19
IL3RA	Interleukin 3 receptor subunit alpha [Source: NCBI gene; Acc: 100299249]	4.10	1.17E-31
ADGRG3	Adhesion G protein-coupled receptor G3 [Source: VGNC Symbol; Acc: VGNC:25667]	4.01	8.40E-37
TNFAIP6	TNF alpha induced protein 6 [Source: VGNC Symbol; Acc: VGNC:36156]	3.64	7.16E-17
MMP9	Matrix metallopeptidase 9 [Source: VGNC Symbol; Acc: VGNC:31531]	3.58	1.94E-14
CLEC1B	C-type lectin domain family 1 member B [Source: VGNC Symbol; Acc: VGNC:58366]	3.50	3.98E-13
PLA2G4F	Phospholipase A2 group IVF [Source: VGNC Symbol; Acc: VGNC:32962]	3.47	3.30E-25
LCN2	Lipocalin 2 [Source: VGNC Symbol; Acc: VGNC:30814]	3.45	2.62E-15
IL12B	Interleukin 12B [Source: VGNC Symbol; Acc: VGNC:30111]	3.45	1.44E-19
S100A9	S100 calcium-binding protein A9 [Source: VGNC Symbol; Acc: VGNC:34247]	3.42	2.30E-21
S100A8	S100 calcium-binding protein A8 [Source: VGNC Symbol; Acc: VGNC:34246]	3.42	2.11E-19
RAB20	RAB20, member RAS oncogene family [Source: NCBI gene; Acc: 615760]	3.33	3.22E-32
HP	Haptoglobin [Source: NCBI gene; Acc: 280692]	3.29	2.42E-15
DEFB10	Beta-defensin 10 [Source: NCBI gene; Acc: 100141457]	3.28	2.52E-14
HBB	Hemoglobin, beta [Source: NCBI gene; Acc: 280813]	−3.74	9.97E-25
ALAS2	5′-Aminolevulinate synthase 2 [Source: VGNC Symbol; Acc: VGNC:25804]	−3.80	3.14E-32
HBA2	Hemoglobin, alpha 2 [Source: NCBI gene; Acc: 512439]	−4.86	3.14E-22
HBA1	Hemoglobin, alpha 1 [Source: NCBI gene; Acc: 100140149]	−4.88	2.13E-22

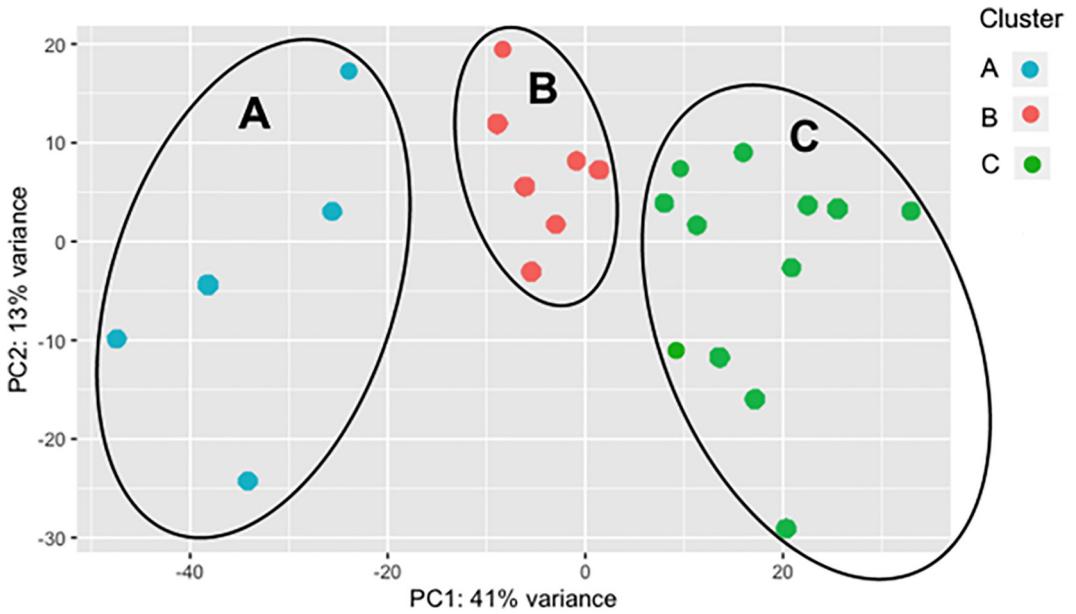

FIGURE 2 | Principal component analysis (PCA) displaying clustering of bovine respiratory disease (BRD) samples. Cluster dendrogram identifying groups in the BRD population (n = 25) that are similar to one another based on gene expression. The BRD data is further subdivided into three distinct clusters.

TABLE 2 | Summary of differentially expressed (DE) genes between bovine respiratory disease (BRD) clusters.

	Cluster comparison[1]		
Item	***B–A**	***C–A**	***C–B**
Total transcripts	13,404	13,404	13,404
↑ Expression	1,739	3,806	581
↓ Expression	1,670	3,464	1,472
Total DEG	3,409	7,270	2,053
No significant changes	9,995	6,134	11,351

[1]*Cluster with (*) annotation is upregulated compared with opposite cluster. Transcripts in B upregulated compared with A. Transcripts in C upregulated when compared with A. Transcripts in C upregulated when compared with B.*

the keratin family (**Table 3**). For Cluster C, upregulated genes included *cornifin B-like*, *solute carrier family 6*, and *serine protease 50*, while *thy-1 cell surface antigen* and *leucine-rich alpha-2-glycoproteins* were downregulated (**Table 3**). When compared with animals in Cluster B and C, animals in Cluster A showed increased expression of genes encoding bovine antimicrobial peptides. Specifically, *cathelicidin-2* (*CATH2*), *CATH3*, *CATH5*, and *CATH6* were upregulated in Cluster A (**Table 4**). These genes had high logFC values (>log2), and genes for other antimicrobial peptides such as *enteric beta defensin* (*EBD*) and *beta-defensin 4A* (*DEFB4*) were also upregulated in Cluster A, when compared with those in B and C. Genes downregulated in Cluster A when compared with Cluster B and C are shown in **Table 5**. Further analysis using the core analysis function in IPA shows the pathway involved in viral infection as one of the top disease pathways according to z-score in the comparison between Cluster A animals with Clusters B and C (**Figure 3**). The highly activated genes in this comparison include *LCN2*, *S1008A*, and *CFB*, with *bovine cathelicidin antimicrobial peptide* (*CAMP*) having the highest experimental log ratio value as identified through IPA (**Table 6**).

Comparison With Related Studies

In order to determine the validity of our results, finding similarities in gene expression to related studies was also a goal of our analysis. Three studies in particular also investigated gene expression in response to cattle with BRD using the blood and bronchial lymph node transcriptome. The work done by Johnston et al. (2019) showed similarities to our work in the clear separation observed when plotting the gene expression pattern between control and infected animals, and also in the identification of genes related to acute phase protein expression (**Supplementary Table 4**). Additionally, Sun et al. (2020) identified enriched expression of genes belonging to heme biosynthesis, acute phase response signaling, and granzyme B signaling, which was also observed in our results (**Supplementary Table 4**). Finally, Scott et al. (2020), who also investigated the blood transcriptome, found similarities with the highly upregulated genes found here including *CATH2*, *LRG1*, and *CFB*, as well as decreased expression of *ALOX15* and *GZMB*.

DISCUSSION

Most previous studies investigating BRD have used fluids and tissues located at the main sites of infection for BRD pathogens, such as bronchial lymph nodes (Tizioto et al., 2015; Johnston et al., 2019), lung tissue (Rai et al., 2015; Chen et al., 2016; Behura et al., 2017), and lymph fluid (Gershwin et al., 2015), and

TABLE 3 | Unique genes of interest in Clusters B and C.

Cluster B		Cluster C	
Upregulated	**Downregulated**	**Upregulated**	**Downregulated**
LOC521568: Multidrug resistance associated protein 4	*KRT85: Keratin 85*	*LOC507527: Cornifin-B-like*	*THY1: thy-1 cell surface antigen*
LOC508858: Duodenase 1	*KRT83: Keratin 83*	*SLC6A15: Solute carrier family 6*	*LOC51110: Serpin peptidase inhibitor, clade B like*
SV2C: Synaptic vesicle glycoprotein	*KRT33B: Keratin, type 1 cuticular Ha3-I-like*	*ANK1: Ankyrin 1*	*PLIN5: Perilipin 5*
VSIG2: V-set and immunoglobulin domain containing 2	*KRT33A: Keratin 33A*	*KRT25: Keratin 25*	*ALPL: Alkaline phosphatase, biomineralization associated*
TFF2: Trefoil factor 2	*KRT86: Keratin 86*	*PRSS50: Serine protease 50*	*LRG1: Leucine-rich alpha-2-glycoprotein*
		BOLA-DQB: Major histocompatibility complex, class II, DQ beta	

TABLE 4 | Top enriched bovine respiratory disease (BRD) differentially expressed (DE) genes in Cluster A compared with Clusters B and C.

Gene name	Gene description	LogFC	*P*-Adjust
CATHL2	Cathelicidin 2 [Source: NCBI gene; Acc: 282165]	8.91	1.03E-33
CD177	CD177 molecule [Source: VGNC Symbol; Acc: VGNC:27006]	8.35	1.17E-34
CATHL6	Cathelicidin 6 [Source: NCBI gene; Acc: 317651]	7.71	2.28E-33
CATHL3	Cathelicidin 1 [Source: NCBI gene; Acc: 282164]	7.37	2.77E-26
CATHL5	Cathelicidin 5 [Source: NCBI gene; Acc: 282167]	7.04	1.48E-28
NGP	Neutrophilic granule protein-like [Source: NCBI gene; Acc: 788112]	5.77	1.12E-13
LTF	Lactotransferrin [Source: VGNC Symbol; Acc: VGNC:31077]	5.57	1.01E-30
MS4A3	Membrane spanning 4-domains A3 [Source: VGNC Symbol; Acc: VGNC:58392]	5.54	1.49E-16
EBD	Enteric beta-defensin [Source: NCBI gene; Acc: 281743]	5.42	4.90E-20
ORM1	Orosomucoid 1 [Source: NCBI gene; Acc: 497200]	5.10	2.85E-23
DEFB4A	Defensin, beta 4A [Source: NCBI gene; Acc: 286836]	5.01	4.34E-20
PGLYRP1	Peptidoglycan recognition protein 1 [Source: VGNC Symbol; Acc: VGNC:32791]	5.01	6.43E-29
MMP8	Matrix metallopeptidase 8 [Source: VGNC Symbol; Acc: VGNC:31530]	5.00	2.50E-18
CCL14	Chemokine (C-C motif) ligand 14 [Source: NCBI gene; Acc: 616723]	4.57	1.16E-22
FLT4	fms related tyrosine kinase 4 [Source: VGNC Symbol; Acc: VGNC:29044]	4.51	9.30E-13
EFNB2	Ephrin B2 [Source: VGNC Symbol; Acc: VGNC:28360]	4.34	2.04E-23
IL1R2	Interleukin 1 receptor type 2 [Source: VGNC Symbol; Acc: VGNC:30132]	4.32	8.21E-16
MMP27	Matrix metallopeptidase 27 [Source: VGNC Symbol; Acc: VGNC:54886]	4.25	8.38E-08
RETN	Resistin [Source: VGNC Symbol; Acc: VGNC:33877]	4.13	1.63E-18
FOLR3	Folate receptor 3 [Source: NCBI gene; Acc: 516067]	4.07	6.08E-07
HSPG2	Heparan sulfate proteoglycan 2 [Source: VGNC Symbol; Acc: VGNC:29988]	3.82	2.72E-22
LCN2	Lipocalin 2 [Source: VGNC Symbol; Acc: VGNC:30814]	3.75	6.71E-18
MMP9	Matrix metallopeptidase 9 [Source: VGNC Symbol; Acc: VGNC:31531]	3.65	2.20E-12
TMEM217	Transmembrane protein 217 [Source: VGNC Symbol; Acc: VGNC:36039]	3.53	2.21E-16
LBP	Lipopolysaccharide-binding protein [Source: VGNC Symbol; Acc: VGNC:56192]	3.48	4.27E-10
RAB3IL1	RAB3A interacting protein like 1 [Source: VGNC Symbol; Acc: VGNC:33655]	3.46	2.11E-09
ALOX5	Arachidonate 5-lipoxygenase [Source: VGNC Symbol; Acc: VGNC:25844]	3.34	3.28E-13
SERPINB2	Serpin family B member 2-like [Source: NCBI gene; Acc: 281376]	3.29	7.61E-11
BPI	Bactericidal permeability increasing protein [Source: NCBI gene; Acc: 280734]	3.20	6.12E-08
CCL24	C-C motif chemokine ligand 24 [Source: VGNC Symbol; Acc: VGNC:26950]	3.18	5.34E-10
ITGA9	Integrin subunit alpha 9 [Source: VGNC Symbol; Acc: VGNC:30320]	3.18	4.25E-13
RGL1	Ral guanine nucleotide dissociation stimulator like 1 [Source: VGNC Symbol; Acc: VGNC:33903]	3.13	1.13E-19
EREG	Epiregulin [Source: VGNC Symbol; Acc: VGNC:28575]	3.11	6.57E-12
SERPINB4	*Bos taurus* serpin peptidase inhibitor, clade B like (LOC786410), mRNA. [Source: RefSeq mRNA; Acc: NM_001206713]	3.07	1.15E-06

have reported various immune-related genes enriched at each site of infection. In addition, these studies have collected these fluids and tissues at postmortem examination. Only a few studies (Lindholm-Perry et al., 2018; Scott et al., 2020) use RNA extracted from blood for gene expression analysis despite the relative ease of its sampling from live animals. We therefore applied

TABLE 5 | Genes downregulated in Cluster A when compared with Clusters B and C.

Gene name	Gene description	LogFC	*P*-Adjust
TAC3	Tachykinin 3 [Source: VGNC Symbol; Acc: VGNC:35556]	−5.16	7.22E-08
LOC100139881	Mast cell protease 2 [Source: NCBI gene; Acc: 100139881]	−3.76	4.82E-05
FOLH1B	Folate hydrolase 1B [Source: NCBI gene; Acc: 505865]	−3.52	5.78E-03
LOC100847119	Immunoglobulin lambda-1 light chain-like [Source: NCBI gene; Acc: 100847119]	−3.48	4.12E-04
NRIP3	Nuclear receptor interacting protein 3 [Source: VGNC Symbol; Acc: VGNC:32264]	−3.30	4.99E-04
LARP6	La ribonucleoprotein domain family member 6 [Source: VGNC Symbol; Acc: VGNC:30793]	−3.06	3.09E-07
BREH1	Retinyl ester hydrolase type 1 [Source: NCBI gene; Acc: 497207]	−2.95	1.30E-08
GABRD	Gamma-aminobutyric acid type A receptor delta subunit [Source: VGNC Symbol; Acc: VGNC:29198]	−2.91	2.94E-05
SEMA3G	Semaphorin 3G [Source: VGNC Symbol; Acc: VGNC:34432]	−2.82	1.72E-09
KLHDC8A	Kelch domain containing 8A [Source: VGNC Symbol; Acc: VGNC:30639]	−2.79	1.07E-08
ADGRA1	Adhesion G protein-coupled receptor A1 [Source: VGNC Symbol; Acc: VGNC:55933]	−2.79	2.59E-06
PRG3	Proteoglycan 3 [Source: NCBI gene; Acc: 617374]	−2.75	1.68E-02
WNT5A	Wnt family member 5A [Source: VGNC Symbol; Acc: VGNC:36960]	−2.73	2.99E-06
GATA2	GATA-binding protein 2 [Source: VGNC Symbol; Acc: VGNC:29266]	−2.68	1.51E-04
GZMB	Granzyme B (granzyme 2, cytotoxic T-lymphocyte-associated serine esterase 1) [Source: NCBI gene; Acc: 281731]	−2.65	7.07E-04
KCNIP3	Potassium voltage-gated channel interacting protein 3 [Source: NCBI gene; Acc: 513316]	−2.61	2.09E-12
WC1.1	Antigen WC1.1 [Source: NCBI gene; Acc: 786796]	−2.59	1.58E-06
GCSAML	Germinal center associated signaling and motility like [Source: HGNC Symbol; Acc: HGNC:29583]	−2.56	3.99E-04
PRRS50	Serine protease 50 [Source: NCBI gene; Acc: 518845]	−2.49	2.03E-05
CD163L1	CD163 molecule-like 1 [Source: NCBI gene; Acc: 338056]	−2.49	9.03E-11
TGFB2	Transforming growth factor beta 2 [Source: VGNC Symbol; Acc: VGNC:35802]	−2.48	7.07E-04
CD1E	CD1e molecule [Source: VGNC Symbol; Acc: VGNC:27008]	−2.45	1.74E-04
CXCL12	C-X-C motif chemokine ligand 12 [Source: VGNC Symbol; Acc: VGNC:27848]	−2.44	6.06E-12
LY6G6C	Lymphocyte antigen 6 family member G6C [Source: VGNC Symbol; Acc: VGNC:31090]	−2.43	8.71E-09
KCNQ4	Potassium voltage-gated channel subfamily Q member 4 [Source: VGNC Symbol; Acc: VGNC:30489]	−2.40	4.37E-08
SLC6A15	Solute carrier family 6 member 15 [Source: VGNC Symbol; Acc: VGNC:34918]	−2.39	1.71E-02
BOLA-DQB	Major histocompatibility complex, class II, DQ beta [Source: NCBI gene; Acc: 282495]	−2.38	7.68E-03
CYGB	Cytoglobin [Source: VGNC Symbol; Acc: VGNC:50268]	−2.36	7.37E-08
ANK1	Ankyrin 1 [Source: NCBI gene; Acc: 353108]	−2.35	5.22E-03
RTN4RL1	Reticulon 4 receptor like 1 [Source: VGNC Symbol; Acc: VGNC:34207]	−2.34	4.80E-08
ENPP1	Ectonucleotide pyrophosphatase/phosphodiesterase 1 [Source: VGNC Symbol; Acc: VGNC:28504]	−2.33	3.33E-08
CHCHD6	Coiled-coil-helix-coiled-coil-helix domain containing 6 [Source: VGNC Symbol; Acc: VGNC:27274]	−2.33	3.33E-08
HRH4	Histamine receptor H4 [Source: VGNC Symbol; Acc: VGNC:29956]	−2.33	8.85E-07

a functional genomics approach to investigate changes in the whole-blood transcriptome, making two different comparisons; the first examined the difference in gene expression between all the BRD and NB animals, while the second explored the larger variation observed among the BRD animals.

As anticipated, we found that gene expression profiles in whole blood varied between animals diagnosed with BRD and those not exhibiting clinical signs of BRD. Analysis of the differential gene expression between phenotypically healthy cattle (NB) and those with BRD showed that, as with the tissues at infection sites, the major pathways activated in cattle with BRD were also associated with the host immune response.

The BRD animals also had lower expression of genes involved in hemoglobin synthesis. For example, *HBA1*, *HBA2*, *HBB*, and *ALAS2* were all downregulated in the BRD animals. These genes are involved in erythropoiesis and are regulated by iron availability (Chiabrando et al., 2014). Iron homeostasis is involved in oxygen transport, cellular respiration, and metabolic processes (Ali et al., 2017). The regulation of iron concentration in blood also plays an important role in modulating bacterial infection and contributes to the progression of lung disease (Roehrig et al., 2006; Ali et al., 2017). During bacterial infection, neutrophils maintain iron homeostasis by releasing LCN2 and lactoferrin (LTF) to sequester free iron (Ali et al., 2017) and protect the lung from oxidative stress induced by iron and HBA and HBB molecules (Tubsuwan et al., 2011). Furthermore, LCN2 decreases iron availability to limit the growth of pathogenic bacteria (Xiao et al., 2017; Pokorska et al., 2019). *Pasteurella multocida* express outer membrane protein receptors for iron-binding proteins, and the expression of these proteins increases during conditions of iron restriction (Prado et al., 2005). Animals with BRD show decreased expression of genes for hemoglobin and iron-binding proteins and regulators and an increase in genes for iron maintenance proteins (i.e., *LCN2* and *LTF*) that are released from neutrophils as a response to infection. In both comparisons of gene expression (BRD vs. NB and within the BRD animals), *LCN2* expression was increased while in the BRD vs. NB comparison, expression of genes encoding iron-binding proteins was lowered.

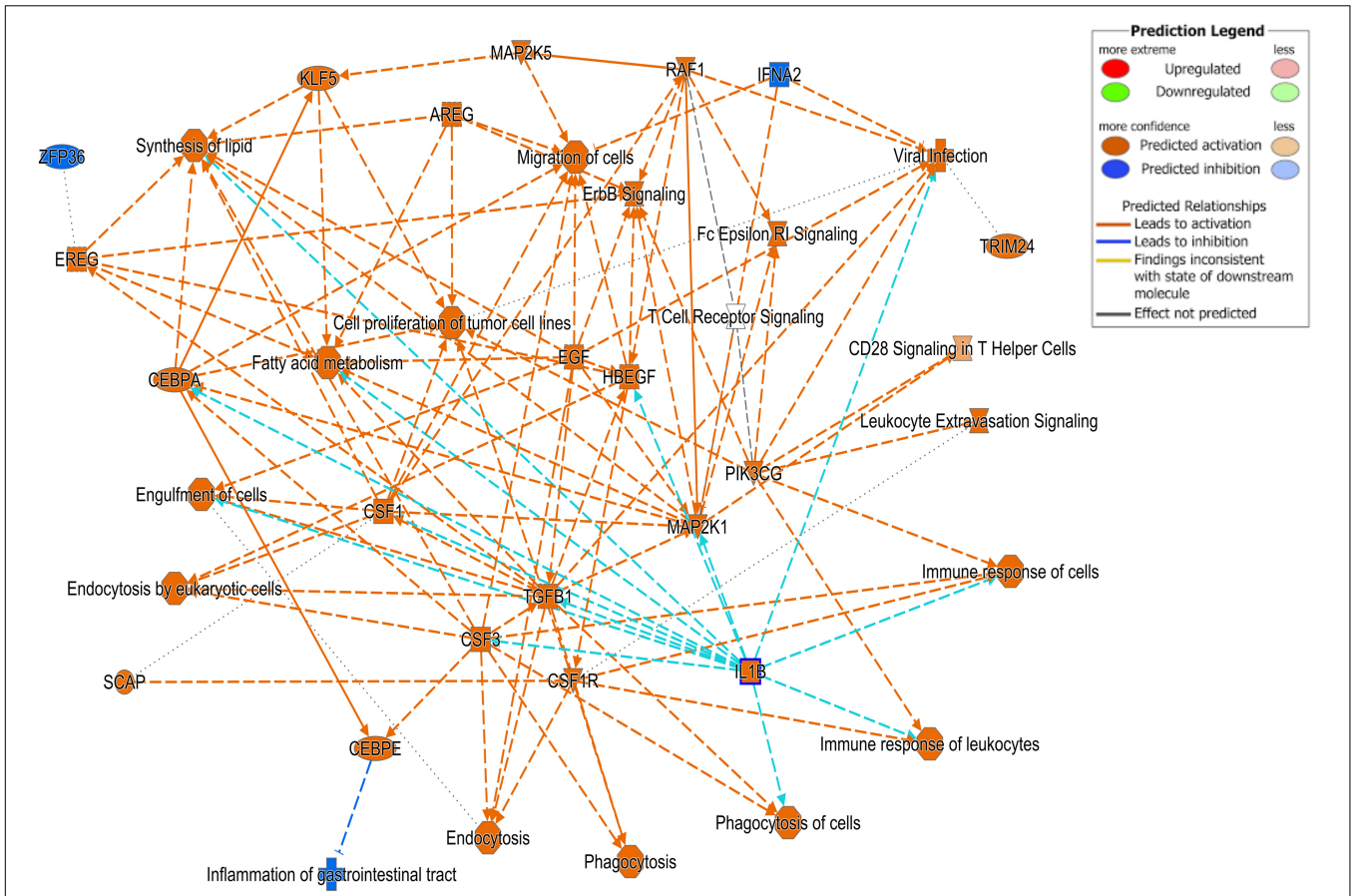

FIGURE 3 | Ingenuity Pathway Analysis (IPA). Cell signaling pathways involved in the viral response pathway identified as one of the top disease pathways according to z-score in the comparison between Cluster A animals and Clusters B and C.

Bovine respiratory disease is multifactorial (Taylor et al., 2010), and etiological diagnosis of BRD is difficult if not impossible to reach in a field setting (Pardon and Buczinski, 2020). Major BRD pathogens such as *Mannheimia haemolytica*, *P. multocida*, *Haemophilus somnus*, or *Mycoplasma bovis* can be isolated from both healthy and sick animals (Angen et al., 2009; Timsit et al., 2017, 2018). Furthermore, multiple BRD pathogens (i.e., viruses and bacteria) are often detected at the same time in the same animal (Angen et al., 2009; Fulton et al., 2009), and it is impossible to determine which ones are causing lung lesions and associated clinical signs without performing a postmortem examination (Fulton and Confer, 2012). This explains why identification of the individual microbial and viral species was not performed in this study.

Although identification of the individual microbial and viral species was not performed in this study, we may be able to infer what agents were present by comparing the gene expression results with those from specific challenge studies. For example, Tizioto et al. (2015) performed single pathogen challenges with the common pathogens in the BRD complex and examined gene expression in bronchial lymph nodes of these animals (Tizioto et al., 2015). The patterns of enriched genes in the blood transcriptome in this study share similar gene characteristics with previous investigations. For example, *S100A8*, *S100A9*, and *matrix metallopeptidase 9* were highly expressed in all of the specific challenges independent of pathogen (Rai et al., 2015; Tizioto et al., 2015). An increase in expression of *S100A8* and *S100A9* is also associated with toll-like receptor 4 (TLR4) binding (Wang et al., 2016). TLR4 forms complexes that lead to recruitment of members of IL1 receptor signaling to sites of infection (Bhattacharyya et al., 2013). Interestingly we also found upregulation of *IL1R2* and *IL1RAP* in the blood of the BRD animals. Expression of *IL1* and *IL1RAP* become elevated in the host when intracellular pathogens are present (Peters et al., 2013), and both viral and bacterial pathogens can often increase the expression of this cytokine to promote a cytotoxic T cell-mediated response. We also found increased expression of *SERPINB4*, which encodes a protein located in the skin, mucous membranes, and respiratory system to prevent pathogens from crossing epithelial barriers (Geiger et al., 2015).

A second comparison analyzed the differences within the BRD samples and compared the differences between the identified clusters. Expression of several genes encoding antimicrobial peptides was increased in Cluster A compared with Clusters B and C. These included the genes such as *LTF*, and several encoding cathelicidins (*CATH2*, *CATH3*, *CATH5*, and

TABLE 6 | Ingenuity Pathway Analysis (IPA) list of genes predicted to affect viral infection in Cluster A compared with B and C.

ID	Genes in dataset	Prediction	Expr log ratio	Findings
ENSBTAG00000024852	CAMP	Affected	8.561	Affects (1)
ENSBTAG00000001292	LTF	Affected	4.952	Affects (6)
ENSBTAG00000002635	PGLYRP1	Affected	4.617	Affects (1)
ENSBTAG00000016991	**EFNB2**©	**Increased**	**4.548**	**Increases** (4)
ENSBTAG00000017294	ORM1	Affected	4.39	Affects (1)
ENSBTAG00000004716	**RETN**	**Increased**	**3.478**	**Increases** (2)
ENSBTAG00000014149	**LCN2**	**Increased**	**3.092**	**Increases** (3)
ENSBTAG00000020676	MMP9	Affected	2.699	Affects (9)
ENSBTAG00000014046	BPI	Affected	2.617	Affects (1)
ENSBTAG00000020319	ALOX5	Affected	2.536	Affects (3)
ENSBTAG00000017866	**CD36**	**Increased**	**2.528**	**Increases** (7)
ENSBTAG00000006354	HP	Affected	2.511	Affects (1)
ENSBTAG00000005952	CEBPE	Affected	2.251	Affects (1)
ENSBTAG00000008059	CHRM3	Affected	2.106	Affects (3)
ENSBTAG00000048591	THBD	Affected	2.057	Affects (2)
ENSBTAG00000007169	**P2RX1**	**Increased**	**2.052**	**Increases** (2)
ENSBTAG00000039050	**P2RY2**	**Increased**	**2.051**	**Increases** (1)
ENSBTAG00000008951	ALPL	Affected	1.991	Affects (3)
ENSBTAG00000001034	IL18R1	Decreased	1.966	Decreases (2)
ENSBTAG00000012640	**S100A8**	**Increased**	**1.932**	**Increases** (4)
ENSBTAG00000021994	CACNA2D4	Affected	1.908	Affects (3)
ENSBTAG00000046152	MGAM	Affected	1.883	Affects (1)
ENSBTAG00000054057	NRG1	Affected	1.817	Affects (1)
ENSBTAG00000053072	**EFHC2**	**Increased**	**1.78**	**Increases** (1)
ENSBTAG00000014906	VCAN	Affected	1.764	Affects (1)
ENSBTAG00000040151	GCH1	Affected	1.723	Affects (1)
ENSBTAG00000038490	**CLEC4A**	**Increased**	**1.593**	**Increases** (22)
ENSBTAG00000012019	IRS2	Affected	1.544	Affects (1)
ENSBTAG00000020580	TCN1	Affected	1.538	Affects (1)
ENSBTAG00000046158	**CFB**	**Increased**	**1.519**	**Increases** (2)
ENSBTAG00000018517	**VLDLR**	**Increased**	**1.499**	**Increases** (1)
ENSBTAG00000006505	**S100A9**	**Increased**	**1.489**	**Increases** (6)
ENSBTAG00000019059	**ATG16L2**	**Increased**	**1.487**	**Increases** (2)
ENSBTAG00000012185	CLEC4E	Affected	1.474	Affects (1)
ENSBTAG00000038048	**MRC1**	**Increased**	**1.471**	**Increases** (1)
ENSBTAG00000016414	**VDR**	**Increased**	**1.468**	**Increases** (27)
ENSBTAG00000010763	**DUSP16**	**Increased**	**1.468**	**Increases** (2)
ENSBTAG00000014636	ZFHX3	Affected	1.428	Affects (1)
ENSBTAG00000006817	CBL	Decreased	1.417	Decreases (3)
ENSBTAG00000016206	MAOA	Affected	1.413	Affects (1)
ENSBTAG00000012052	**PADI4**	Increased	1.401	Increases (2)
ENSBTAG00000008592	FCGR1A	Decreased	1.382	Decreases (13)
ENSBTAG00000047338	**DCBLD1**	**Increased**	**1.327**	**Increases** (1)
ENSBTAG00000018255	ACTN1	Affected	1.318	Affects (1)
ENSBTAG00000047238	**ITGAM**	Increased	1.318	Increases (2)
ENSBTAG00000045565	NHSL2	Affected	1.316	Affects (1)
ENSBTAG00000013201	ALOX5AP	Affected	1.295	Affects (1)
ENSBTAG00000012638	**S100A12**	**Increased**	**1.264**	**Increases** (3)

Bolded rows identify genes predicted to have increased activity using the IPA analysis.

CATH6). LTF functions as an antimicrobial molecule but also has immunomodulatory qualities (Drago-Serrano et al., 2017), suggesting a potential therapeutic role for this protein. Cathelicidins are defined as host defense peptides that are highly expressed in bovine granulocytes and located at mucosal surfaces in the lungs, lymphoid tissues, and intestines of the

host (Baumann et al., 2017). Expression of four of the seven known bovine cathelicidin genes, *CATH2*, *3*, *5*, and *6*, was increased in the BRD animals. These peptides have been detected and isolated from sick animals and are generally not present in healthy tissues (Tomasinsig et al., 2002). Therefore, their identification as the top genes with the greatest fold-change increases in the BRD Cluster A suggests a strong host immune response in this group of affected animals. It has also been reported that *M. haemolytica* causes the induction of bovine beta-defensins, especially in animals with subacute and chronic infection (Fales-Williams et al., 2002), and we observed *enteric beta-defensin* as well as *beta-defensin 4A* among the top expressed genes in the BRD animals. It can be concluded that the expression of these defensin genes is indicative of chronic infection (Bhattacharyya et al., 2013) or simply the result of the host defense response stimulating helper T cell type 1 (TH1) and helper T cell type 2 (TH2) responses to help clear infection (Gurao et al., 2017).

The overall abundance of gamma delta T cells in ruminants is higher than in other species, and in non-ruminants, this cell subset has been associated with increasing production of TH2 cytokines (Plattner and Hostetter, 2011). Although this association has not been observed in ruminants, it has been reported that a CD163 relative, Workshop Cluster 1 (WC1), plays an important role in gamma delta T cell regulation in cattle (Herzig et al., 2010; Plattner and Hostetter, 2011), especially in young calves. This T cell subset also facilitates protective immunity following vaccinations (Davis et al., 1996; Guzman et al., 2012) and has been described to be involved in increased expression of major histocompatibility complex (MHC) class II on WC1+ cells through interaction with dendritic cells during *Mycobacterium bovis* infection (Price and Hope, 2009). When comparing Cluster A with Clusters B and C, expression of *WC1*, *WC1.1*, *WC1.3*, and *WC1-12* was significantly decreased in Cluster A. Animals in Cluster A showed lowered expression of *WC1* genes that directly promote antigen presentation and regulation of alpha beta T cells and CD4/CD8 antigens on WC1+ T cells (Ackermann et al., 2010). This suggests that the BRD animals in Cluster A were displaying lower antigen presentation and T cell regulation, suggesting that they may have been infected with a greater pathogen load that hinders the host immune response in comparison with that in the animals in Clusters B and C. Furthermore, as there was also an increase in the host antimicrobial response in Cluster A, these animals may also have had a unique pathogen subset leading to BRD than the animals in Clusters B and C.

Animals in Cluster A also exhibited a decrease in the expression of *GZMB*, which has many established roles in stimulating the cytotoxic T cell response and limiting viral replication in the host (Johnston et al., 2019). Granzyme B, in addition to leukotriene C4, IL4, and IL13, are involved in mediating allergic and asthmatic reactions in humans (Plattner and Hostetter, 2011). Basophil granulocytes are the major effector molecules in a TH2 immune response and are the source for leukotriene C4, IL4, and IL13. IL3 specifically leads to the synthesis of GZMB and contributes to the basophil granule population in the TH2 immune response (Tschopp et al., 2006), and it is one of the most potent cytokines with the longest duration of action (Tschopp et al., 2006). Therefore, the decreased expression of *GZMB* suggests that the animals in Cluster A had a lowered host immune response to infection than the animals in Clusters B and C.

CONCLUSION

In conclusion, the results suggest that the blood transcriptome provides a useful resource to investigate the biology of BRD in feedlot cattle. The whole-blood transcriptome may only give a general overview of the health status, e.g., severe infection from a systemic immune response compared with that from the response reported in tissues at the site of infection. However, results from the BRD subsets (Clusters A, B, and C) do show some similarities with gene expression results using tissue and fluids isolated directly from the sites of infection, as well as other studies that also used RNA sequencing to identify BRD in tissues and blood. Analysis of the pathogens present in the sampled animals may allow this commonality to be explored further. For example, it may be that specific pathways and genes expressed in whole blood are associated with individual pathogens, which could assist in directing targeted therapeutic treatments. Such transcriptome data may also provide information on potential therapeutic targets for BRD infection. Investigation of the WC1+ cell subset and cathelicidin antimicrobial peptides could be useful in this respect. Gene expression analysis of whole blood from BRD and NB cases provides new insights for understanding host response to infection and suggests that there is significant value in using blood for BRD studies. This approach is supported by recent results obtained by Scott et al. (2020) as well as Sun et al. (2020); however, in the future, we could increase the validity of our findings by screening more animals for the genes identified in this study using qPCR. Furthermore, genes upregulated in healthy animals may also be related to protective mechanisms that reduce an individual's susceptibility to BRD, and this warrants further investigation, as our findings put genes related to leukotriene biosynthesis and granzyme expression into this class of protective genes.

DATA AVAILABILITY STATEMENT

The RNAseq data are available at NCBI Gene Expression Omnibus (GEO) database under accession number GSE162156.

ETHICS STATEMENT

The animal study was reviewed and approved by University of Calgary Veterinary Sciences Animal Care Committee, AC15-0109. Written informed consent was obtained from the owners for the participation of their animals in this study.

AUTHOR CONTRIBUTIONS

GP, ET, and KO designed the project and obtained the funding. ET designed the field trial and collected the samples. JJ prepared and analyzed the sequencing data. LG provided advice on RNAseq analysis. GP, JJ, and ET interpreted the results and drafted the manuscript. All authors contributed to the writing and revisions of the manuscript and approved the final manuscript.

FUNDING

This publication is the result of research supported by the "Genomic Approaches to the Control of Bovine Respiratory Disease Complex (BRDC)" Grant, provided by Genome Alberta, Calgary, AB, Canada, through the Applied Livestock Genomics Program 2014, project code A222. This research is also part of the AMR–One Health Consortium, funded by the Major Innovation Fund Program of the Alberta Ministry of Economic Development, Trade and Tourism.

ACKNOWLEDGMENTS

JJ thanks Eoin O'Hara and Arun Kommadath for help with transcriptomic analyses. GP acknowledges the support of Alberta Innovates.

SUPPLEMENTARY MATERIAL

The Supplementary Material for this article can be found online at: https://www.frontiersin.org/articles/10.3389/fgene.2021.627623/full#supplementary-material

REFERENCES

Ackermann, M. R., Derscheid, R., and Roth, J. A. (2010). Innate immunology of bovine respiratory disease. *Vet. Clin. North Am. Food Anim. Pract.* 26, 215–228. doi: 10.1016/j.cvfa.2010.03.001

Aich, P., Babiuk, L. A., Potter, A. A., and Griebel, P. (2009). Biomarkers for prediction of bovine respiratory disease outcome. *Omi. A J. Integr. Biol.* 13, 199–209. doi: 10.1089/omi.2009.0012

Ali, M. K., Kim, R. Y., Karim, R., Mayall, J. R., Martin, K. L., Shahandeh, A., et al. (2017). Role of iron in the pathogenesis of respiratory disease. *Int. J. Biochem. Cell Biol.* 88, 181–195. doi: 10.1016/j.biocel.2017.05.003

Angen, O., Thomsen, J., Larsen, L. E., Larsen, J., Kokotovic, B., Heegaard, P. M. H., et al. (2009). Respiratory disease in calves: microbiological investigations on trans-tracheally aspirated bronchoalveolar fluid and acute phase protein response. *Vet. Microbiol.* 137, 165–171. doi: 10.1016/j.vetmic.2008.12.024

Babcock, A. H., Renter, D. G., White, B. J., Dubnicka, S. R., and Scott, H. M. (2010). Temporal distributions of respiratory disease events within cohorts of feedlot cattle and associations with cattle health and performance indices. *Prev. Vet. Med.* 97, 198–219. doi: 10.1016/J.PREVETMED.2010.09.003

Baumann, A., Kiener, M. S., Haigh, B., Perreten, V., and Summerfield, A. (2017). Differential ability of bovine antimicrobial cathelicidins to mediate nucleic acid sensing by epithelial cells. *Front. Immunol.* 8:59. doi: 10.3389/fimmu.2017.00059

Behura, S. K., Tizioto, P. C., Kim, J., Grupioni, N. V., Seabury, C. M., Schnabel, R. D., et al. (2017). Tissue tropism in host transcriptional response to members of the bovine respiratory disease complex. *Sci. Rep.* 7:17938. doi: 10.1038/s41598-017-18205-0

Bhattacharyya, S., Kelley, K., Melichian, D. S., Tamaki, Z., Fang, F., Su, Y., et al. (2013). Toll-like receptor 4 signaling augments transforming growth factor-β responses: a novel mechanism for maintaining and amplifying fibrosis in scleroderma. *Am. J. Pathol.* 182, 192–205. doi: 10.1016/j.ajpath.2012.09.007

Caswell, J. L. (2014). Failure of respiratory defenses in the pathogenesis of bacterial pneumonia of cattle. *Vet. Pathol.* 51, 393–409. doi: 10.1177/0300985813502821

CCAC (2009). *CCAC Guidelines on: The Care and Use of Farm Animals in Research, Teaching, and Testing*. Available online at: https://www.ccac.ca/Documents/Standards/Guidelines/Farm_Animals.pdf (accessed November 1, 2020).

Chen, J., Yang, C., Tizioto, P. C., Huang, H., Lee, M. O. K., Payne, H. R., et al. (2016). Expression of the bovine NK-Lysin gene family and activity against respiratory pathogens. *PLoS One* 11:e0158882. doi: 10.1371/journal.pone.0158882

Chiabrando, D., Mercurio, S., and Tolosano, E. (2014). Heme and erythropoieis: more than a structural role. *Haematologica* 99, 973–983. doi: 10.3324/haematol.2013.091991

Davis, W. C., Brown, W. C., Hamilton, M. J., Wyatt, C. R., Orden, J. A., Khalid, A. M., et al. (1996). Analysis of monoclonal antibodies specific for the γδ TcR. *Vet. Immunol. Immunopathol.* 52, 275–283. doi: 10.1016/0165-2427(96)05578-X

Dobin, A., Davis, C. A., Schlesinger, F., Drenkow, J., Zaleski, C., Jha, S., et al. (2013). STAR: ultrafast universal RNA-seq aligner. *Bioinformatics* 29, 15–21. doi: 10.1093/bioinformatics/bts635

Drago-Serrano, M. E., Campos-Rodríguez, R., Carrero, J. C., and de la Garza, M. (2017). Lactoferrin: balancing ups and downs of inflammation due to microbial infections. *Int. J. Mol. Sci.* 18:501. doi: 10.3390/ijms18030501

Fales-Williams, A. J., Gallup, J. M., Ramírez-Romero, R., Brogden, K. A., and Ackermann, M. R. (2002). Increased anionic peptide distribution and intensity during progression and resolution of bacterial pneumonia. *Clin. Diagn Lab. Immunol.* 9, 28L–32L. doi: 10.1128/CDLI.9.1.28-32.2002

Fulton, R. W., and Confer, A. W. (2012). Laboratory test descriptions for bovine respiratory disease diagnosis and their strengths and weaknesses: gold standards for diagnosis, do they exist? *Can. Vet. J.* 53, 754–761.

Fulton, R. W., Blood, K. S., Panciera, R. J., Payton, M. E., Ridpath, J. F., Confer, A. W., et al. (2009). Lung pathology and infectious agents in fatal feedlot pneumonias and relationship with mortality, disease onset, and treatments. *J. Vet. Diagn. Invest.* 21, 464–477. doi: 10.1177/104063870902100407

Geiger, M., Wahlmüller, F., and Furtmüller, M. (eds). (2015). *The Serpin Family: Proteins with Multiple Functions in Health and Disease*. Cham: Springer. doi: 10.1007/978-3-319-22711-5

Gershwin, L. J., Van Eenennaam, A. L., Anderson, M. L., McEligot, H. A., Shao, M. X., Toaff-Rosenstein, R., et al. (2015). Single pathogen challenge with agents of the bovine respiratory disease complex. *PLoS One* 10:e0142479. doi: 10.1371/journal.pone.0142479

Gurao, A., Kashyap, S. K., and Singh, R. (2017). β-defensins: an innate defense for bovine mastitis. *Vet. World* 10, 990–998. doi: 10.14202/vetworld.2017.990-998

Guzman, E., Price, S., Poulsom, H., and Hope, J. (2012). Bovine γδ T cells: cells with multiple functions and important roles in immunity. *Vet. Immunol. Immunopathol.* 148, 161–167. doi: 10.1016/J.VETIMM.2011.03.013

Herzig, C. T., Waters, R. W., Baldwin, C. L., and Telfer, J. C. (2010). Evolution of the CD163 family and its relationship to the bovine gamma delta T cell co-receptor WC1. *BMC Evol. Biol.* 10:181. doi: 10.1186/1471-2148-10-181

Johnston, D., Earley, B., McCabe, M. S., Lemon, K., Duffy, C., McMenamy, M., et al. (2019). Experimental challenge with bovine respiratory syncytial virus in dairy calves: bronchial lymph node transcriptome response. *Sci. Rep.* 9, 1–13. doi: 10.1038/s41598-019-51094-z

Kawayama, T., Kinoshita, T., Matsunaga, K., Kobayashi, A., Hayamizu, T., Johnson, M., et al. (2016). Responsiveness of blood and sputum inflammatory cells in Japanese COPD patients, non-COPD smoking controls, and non-COPD nonsmoking controls. *Int. J. Chron. Obstruct. Pulmon. Dis.* 11, 295–303. doi: 10.2147/COPD.S95686

Lindholm-Perry, A. K., Kuehn, L. A., McDaneld, T. G., Miles, J. R., Workman, A. M., Chitko-Mckown, C. G., et al. (2018). Complete blood count data and

leukocyte expression of cytokine genes and cytokine receptor genes associated with bovine respiratory disease in calves. *BMC Res. Notes* 11:786. doi: 10.1186/s13104-018-3900-x

Mulder, H. A., and Rashidi, H. (2017). Selection on resilience improves disease resistance and tolerance to infections1. *J. Anim. Sci.* 95, 3346–3358. doi: 10.2527/jas.2017.1479

Pardon, B., and Buczinski, S. (2020). Bovine respiratory disease diagnosis: what progress has been made in infectious diagnosis? *Vet. Clin. North Am. Food Anim. Pract.* 36, 425–444. doi: 10.1016/j.cvfa.2020.03.005

Peters, V. A., Joesting, J. J., and Freund, G. G. (2013). IL-1 receptor 2 (IL-1R2) and its role in immune regulation. *Brain Behav. Immun.* 32, 1–8. doi: 10.1016/j.bbi.2012.11.006

Plattner, B. L., and Hostetter, J. M. (2011). Comparative gamma delta T cell immunology: a focus on mycobacterial disease in cattle. *Vet. Med. Int.* 2011:214384.

Pokorska, J., Piestrzyńska-Kajtoch, A., Kułaj, D., Ochrem, A., and Radko, A. (2019). Polymorphism of bovine lipocalin-2 gene and its impact on milk production traits and mastitis in Holstein Friesian cattle. *Electron. J. Biotechnol.* 40, 17–21. doi: 10.1016/J.EJBT.2019.04.004

Prado, M. E., Dabo, S. M., and Confer, A. W. (2005). Immunogenicity of iron-regulated outer membrane proteins of *Pasteurella multocida* A:3 in cattle: molecular characterization of the immunodominant heme acquisition system receptor (HasR) protein. *Vet. Microbiol.* 105, 269–280. doi: 10.1016/j.vetmic.2004.11.009

Price, S. J., and Hope, J. C. (2009). Enhanced secretion of interferon-gamma by bovine gammadelta T cells induced by coculture with *Mycobacterium* bovis-infected dendritic cells: evidence for reciprocal activating signals. *Immunology* 126, 201–208. doi: 10.1111/j.1365-2567.2008.02889.x

Rai, A. N., Epperson, W. B., and Nanduri, B. (2015). Application of functional genomics for bovine respiratory disease diagnostics. *Bioinform. Biol. Insights* 9, 13–23. doi: 10.4137/BBi.s30525

Robinson, M. D., McCarthy, D. J., and Smyth, G. K. (2010). edgeR: a Bioconductor package for differential expression analysis of digital gene expression data. *Bioinformatics* 26, 139–140. doi: 10.1093/bioinformatics/btp616

Roehrig, S. C., Gunkel, N., Tran, H. Q., Selzer, P. M., Spehr, V., and Ullrich, H. J. (2006). The response of *Mannheimia haemolytica* to iron limitation: implications for the acquisition of iron in the bovine lung. *Vet. Microbiol.* 121, 316–329. doi: 10.1016/j.vetmic.2006.12.013

Scott, M. A., Woolums, A. R., Swiderski, C. E., Perkins, A. D., Nanduri, B., Smith, D. R., et al. (2020). Whole blood transcriptomic analysis of beef cattle at arrival identifies potential predictive molecules and mechanisms that indicate animals that naturally resist bovine respiratory disease. *PLoS One* 15:e0227507. doi: 10.1371/journal.pone.0227507

Sun, H.-Z., Srithayakumar, V., Jiminez, J., Jin, W., Hosseini, A., Raszek, M., et al. (2020). Longitudinal blood transcriptomic analysis to identify molecular regulatory patterns of bovine respiratory disease in beef cattle. *Genomics* 112, 3968–3977. doi: 10.1016/j.ygeno.2020.07.014

Taylor, J. D., Fulton, R. W., Lehenbauer, T. W., Step, D. L., and Confer, A. W. (2010). The epidemiology of BRD: what is the evidence for preventive measures? *Can. Vet. J.* 51, 1351. doi: 10.1128/CMR.16.1.79

Timsit, E., Assié, S., Quiniou, R., Seegers, H., and Bareille, N. (2011a). Early detection of bovine respiratory disease in young bulls using reticulo-rumen temperature boluses. *Vet. J.* 190, 136–142. doi: 10.1016/j.tvjl.2010.09.012

Timsit, E., Bareille, N., Seegers, H., Lehebel, A., and Assié, S. (2011b). Visually undetected fever episodes in newly received beef bulls at a fattening operation: occurrence, duration, and impact on performance. *J. Anim. Sci.* 89, 4272–4280. doi: 10.2527/jas.2011-3892

Timsit, E., Hallewell, J., Booker, C., Tison, N., Amat, S., and Alexander, T. W. (2017). Prevalence and antimicrobial susceptibility of *Mannheimia haemolytica*, *Pasteurella multocida*, and *Histophilus somni* isolated from the lower respiratory tract of healthy feedlot cattle and those diagnosed with bovine respiratory disease. *Vet. Microbiol.* 208, 118–125. doi: 10.1016/j.vetmic.2017.07.013

Timsit, E., Holman, D. B., Hallewell, J., and Alexander, T. W. (2016). The nasopharyngeal microbiota in feedlot cattle and its role in respiratory health. *Anim. Front.* 6, 44–50. doi: 10.2527/af.2016-0022

Timsit, E., Workentine, M., van der Meer, F., and Alexander, T. (2018). Distinct bacterial metacommunities inhabit the upper and lower respiratory tracts of healthy feedlot cattle and those diagnosed with bronchopneumonia. *Vet. Microbiol.* 221, 105–113. doi: 10.1016/j.vetmic.2018.06.007

Tizioto, P. C., Kim, J. W., Seabury, C. M., Schnabel, R. D., Gershwin, L. J., Van Eenennaam, A. L., et al. (2015). Immunological response to single pathogen challenge with agents of the bovine respiratory disease complex: an RNA-sequence analysis of the bronchial lymph node transcriptome. *PLoS One* 10:e0131459. doi: 10.1371/journal.pone.0131459

Tomasinsig, L., Scocchi, M., Di Loreto, C., Artico, D., and Zanetti, M. (2002). Inducible expression of an antimicrobial peptide of the innate immunity in polymorphonuclear leukocytes. *J. Leukoc. Biol.* 72, 1003–1010.

Tschopp, C. M., Spiegl, N., Didichenko, S., Lutmann, W., Julius, P., Virchow, J. C., et al. (2006). Granzyme B, a novel mediator of allergic inflammation: its induction and release in blood basophils and human asthma. *Blood* 108, 2290–2299. doi: 10.1182/blood-2006-03-010348

Tubsuwan, A., Munkongdee, T., Jearawiriyapaisarn, N., Boonchoy, C., Winichagoon, P., Fucharoen, S., et al. (2011). Molecular analysis of globin gene expression in different thalassaemia disorders: individual variation of βE pre-mRNA splicing determine disease severity. *Br. J. Haematol.* 154, 635–643. doi: 10.1111/j.1365-2141.2011.08770.x

USDA (2011). *USDA Feedlot 2011 "Part IV: Health and Health Management on U.S. Feedlots with a Capacity of 1,000 or More Head" USDA–APHIS–VS–CEAH–NAHMS. Fort Collins, CO #638.0913.* Available online at: https://www.aphis.usda.gov/aphis/ourfocus/animalhealth/monitoring-and-surveillance/nahms/nahms_feedlot_studies (accessed November 1, 2020).

Van Eenennaam, A., Neibergs, H., Seabury, C., Taylor, J., Wang, Z., Scraggs, E., et al. (2014). Results of the BRD CAP project: progress toward identifying genetic markers associated with BRD susceptibility. *Anim. Heal Res. Rev.* 15, 157–160. doi: 10.1017/S1466252314000231

Vinther, A. M. L., Heegaard, P. M. H., Skovgaard, K., Buhl, R., Andreassen, S. M., and Andersen, P. H. (2016). Characterization and differentiation of equine experimental local and early systemic inflammation by expression responses of inflammation-related genes in peripheral blood leukocytes. *BMC Vet. Res.* 12:83. doi: 10.1186/s12917-016-0706-8

Wang, Y., Zhang, Z., Zhang, L., Li, X., Lu, R., Xu, P., et al. (2016). S100A8 promotes migration and infiltration of inflammatory cells in acute anterior uveitis. *Sci. Rep.* 6:36140. doi: 10.1038/srep36140

Wolfger, B., Schwartzkopf-Genswein, K. S., Barkema, H. W., Pajor, E. A., Levy, M., and Orsel, K. (2015). Feeding behavior as an early predictor of bovine respiratory disease in North American feedlot systems. *J. Anim. Sci.* 93, 377–385. doi: 10.2527/jas.2013-8030

Xiao, X., Yeoh, B. S., and Vijay-Kumar, M. (2017). Lipocalin 2: an emerging player in iron homeostasis and inflammation. *Annu. Rev. Nutr.* 37, 103–130. doi: 10.1146/annurev-nutr-071816-064559

Conflict of Interest: The authors declare that the research was conducted in the absence of any commercial or financial relationships that could be construed as a potential conflict of interest.

frontiers in Microbiology

ORIGINAL RESEARCH
published: 17 March 2021
doi: 10.3389/fmicb.2021.643025

Specific Microbial Taxa and Functional Capacity Contribute to Chicken Abdominal Fat Deposition

Hai Xiang[1], Jiankang Gan[2], Daoshu Zeng[1], Jing Li[1], Hui Yu[1,2,3], Haiquan Zhao[1,3], Ying Yang[1], Shuwen Tan[1,3], Gen Li[1], Chaowei Luo[1], Zhuojun Xie[1], Guiping Zhao[1,4] and Hua Li[1,2,3]**

[1] Guangdong Provincial Key Laboratory of Animal Molecular Design and Precise Breeding, Foshan University, Foshan, China, [2] Guangdong Tinoo's Foods Group Co., Ltd., Qingyuan, China, [3] Xianxi Biotechnology Co. Ltd, Foshan, China, [4] Institute of Animal Sciences, Chinese Academy of Agricultural Sciences, Beijing, China

Genetically selected chickens with better growth and early maturation show an incidental increase in abdominal fat deposition (AFD). Accumulating evidence reveals a strong association between gut microbiota and adiposity. However, studies focusing on the role of gut microbiota in chicken obesity in conventional breeds are limited. Therefore, 400 random broilers with different levels of AFD were used to investigate the gut microbial taxa related to AFD by 16S rRNA gene sequencing of 76 representative samples, and to identify the specific microbial taxa contributing to fat-related metabolism using shotgun metagenomic analyses of eight high and low AFD chickens. The results demonstrated that the richness and diversity of the gut microbiota decrease as the accumulation of chicken abdominal fat increases. The decrease of Bacteroidetes and the increase of Firmicutes were correlated with the accumulation of chicken AFD. The Bacteroidetes phylum, including the genera *Bacteroides*, *Parabacteroides*, and the species, *B. salanitronis*, *B. fragilis*, and *P. distasonis*, were correlated to alleviate obesity by producing secondary metabolites. Several genera of Firmicutes phylum with circulating lipoprotein lipase activity were linked to the accumulation of chicken body fat. Moreover, the genera, *Olsenella* and *Slackia*, might positively contribute to fat and energy metabolism, whereas the genus, *Methanobrevibacter*, was possible to enhance energy capture, and associated to accumulate chicken AFD. These findings provide insights into the roles of the gut microbiota in complex traits and contribute to the development of effective therapies for the reduction of chicken fat accumulation.

Keywords: chickens, abdominal fat deposition, cecal microbiota, microbial composition, microbial functional, metabolism capacity

OPEN ACCESS

Edited by:
Xudong Sun, Heilongjiang Bayi Agricultural University, China

Reviewed by:
Young Min Kwon, University of Arkansas, United States
Marcello Abbondio, University of Sassari, Italy

****Correspondence:***
Guiping Zhao
zhaoguiping@caas.cn
Hua Li
okhuali@fosu.edu.cn

Specialty section:
This article was submitted to Systems Microbiology, a section of the journal Frontiers in Microbiology

Received: *17 December 2020*
Accepted: *24 February 2021*
Published: *17 March 2021*

Citation:
Xiang H, Gan J, Zeng D, Li J, Yu H, Zhao H, Yang Y, Tan S, Li G, Luo C, Xie Z, Zhao G and Li H (2021) Specific Microbial Taxa and Functional Capacity Contribute to Chicken Abdominal Fat Deposition. Front. Microbiol. 12:643025. doi: 10.3389/fmicb.2021.643025

INTRODUCTION

Genetically selected chickens with better growth and early maturation are accompanied by an incidental increase in abdominal fat accumulation (Abdalla et al., 2018). This results in a reduction in the quality of meat that can be considered unhealthy, as well as in an increase in feed cost (Jiang et al., 2017). To date, high-abdominal fat accumulation in commercial broilers hinders profitable farming. In recent years, the focus of research has been on genetic and nutritional regulation of

fatty acid synthesis and lipid deposition, and multiple genetic factors, including quantitative trait loci, candidate genes, mRNA, miRNA, and LncRNA, have been identified with the advances in omics technologies (Zhang et al., 2012, 2014; Demeure et al., 2013; Cui et al., 2018; Li H. et al., 2020; Zhang M. et al., 2020).

However, accumulating and emerging lines of evidence from humans (Backhed et al., 2004; Ley et al., 2005), mice (Ridaura et al., 2013), and livestock (Huang et al., 2020) have revealed a strong association between the gut microbiota and adiposity. For instance, the phylum Firmicutes is more abundant in obese than lean individuals, and vice versa, for Bacteroidetes (Ley et al., 2006). In contrast, after a weight loss program for obese individuals, the relative abundance of Bacteroidetes increased and was accompanied by a decrease in Firmicutes (Ley et al., 2006). Furthermore, by transferring gut microbiota from obese or lean mice to germ-free mice, it has been shown that a high Firmicutes to Bacteroidetes ratio increased body fat accumulation (Ley et al., 2005). For chickens, it has been revealed that the long-term divergent selection of chicken with abdominal fat deposition (AFD) not only altered the composition of gut microbiota, but also influenced its functions by enriching its relative abundance in certain microbial taxa (Ding et al., 2016; Hou et al., 2016). Moreover, the gut microbiota has been suggested to be largely independent of host genetics in regulating fat deposition in chickens (Wen et al., 2019). Furthermore, the duodenal and cecal microbiota have a greater contribution to fat deposition and could separately account for 24% and 21% of the variance in the abdominal fat mass after correcting for host genetic effects (Wen et al., 2019). Therefore, the gut microbiota is regarded as an important factor in modulating fat deposition in broiler chickens.

However, most available data are based on human or mammal models, which may not be completely suited in the case of chickens, because of its unique anatomy and physiology. Most currently published studies only describe the structure and function of the chicken gut microbiota (Ding et al., 2016), and the spatial and temporal changes upon specific stimulation resulting from feed additives (Shang et al., 2015), heat stress (Shi et al., 2019; Zaytsoff et al., 2020), and caged/free-range (Chen et al., 2019; Xiang et al., 2021). Meanwhile, the limited studies focusing on the possible contribution of gut microbiota in modulating chicken obesity have mainly examined this aspect using the divergently selected lean and fat broiler chicken lines (Ding et al., 2016; Hou et al., 2016), lacking in the ability to highlight the specific microbiota taxa associated with AFD in conventional chicken breeds.

In this study, the same random flock consisting of 400 broilers differentiated on AFD was used in the Tiannong Partridge Chickens commercial strain. AFD traits and fatty acid composition of all birds were determined in the flock. Based on their abdominal fat percentage (AFP), they were divided into high AFP (HH) and low AFP (LL) groups. Representative samples were then investigated using 16S rRNA gene sequencing to provide a global perspective on the gut microbial taxa related to AFD. Next, samples with extremely divergent AFP traits were subjected to shotgun metagenomic analysis to identify the specific gut microorganisms contributing to fat-related metabolism.

MATERIALS AND METHODS

Chicken and Sample Collection

A random commercial flock of Tiannong Partridge chickens, consisting of 5,000 hens of the same age, was raised free on a farm in Guangdong Tinoo's Foods Co. Ltd., and fed with a commercial standard diet during the age of 1 to 125 days. Then, on day 126, 400 random hens were collected and slaughtered using the mechanized slaughter line with moderate scalding water temperature. The same part of the pectoral muscle was collected from all hens and the cecum content was randomly collected from 140 chickens. All samples were rapidly frozen using dry ice and stored at −80°C for subsequent analyses.

Phenotypic Trait Measurements

The phenotypic traits of chickens, including body weight (BW), carcass weight (CW), eviscerated weight (EW), and abdominal fat weight (AFW), were measured on the spot, and the AFP was calculated later. A 2-g sample of each pectoral muscle tissue was homogenized and lipids were extracted following the Folch's lipids extraction procedure. The contents of intramuscular fat (IMF), triglycerides (TG), phospholipids (PL), and cholesterol (CHO) were measured using commercial kits (Nanjing Jiancheng Bioengineering Institute, Nanjing, China).

16S and Shotgun Metagenomic Sequencing

For 76 representative samples, total DNA was extracted from the cecal samples using the QIAamp Fast DNA Stool Mini Kit (QIAGEN, Hilden, Germany). The V3-V4 region of 16S rRNA gene was amplified with primer 341F/806R (341F: CCTACGGGNGGCWGCAG, 806R: GGACTACHVGGGTATCTAAT). The PCR reaction was conducted using Phusion® High-Fidelity PCR Master Mix (NEB, Beverly, MA, United States) with 30 cycles. PCR products were purified using the QIAquick Gel Extraction Kit (QIAGEN). Libraries were generated using the TruSeq® DNA PCR-Free Sample Preparation Kit (Illumina, San Diego, CA, United States) following the manufacturer's recommendations. Sequencing was conducted on the Illumina HiSeq2500 platform. For a subset of eight individuals, the same DNA extracts were subjected to shotgun metagenomic sequencing. Briefly, qualified genomic DNA was fragmented by sonication to a size of 350bp, and then end-repaired, A-tailed, and adaptor ligated using NEBNext® Ultra™ DNA Library Prep Kit for Illumina (NEB, United States) according to the preparation protocol. DNA fragments with length of 300–400 bp were enriched by PCR. Then libraries were paired-end sequenced on the Illumina HiSeq2500 platform.

16S rRNA Gene Data Processing

Paired-end reads were assembled using FLASH v1.2.11 (Magoc and Salzberg, 2011) with a minimum overlap of 10 bp and mismatch error rates of 2%. The QIIME2 pipeline was used for data quality control and analyses (Bolyen et al., 2019). All remaining high-quality reads were aligned and clustered into operational taxonomic units (OTUs) using an open reference

OTU picking protocol. Next, chimeras and singletons were filtered from the dataset, and OTUs with an average relative abundance of $<10^{-6}$ were removed from the analysis. The OTU abundance of each sample and taxonomic classification from phylum to species were then determined. Spearman's correlation was calculated using the psych package (v1.8.4) in R without further multiple testing. Microbes were analyzed at the kingdom, phylum, class, order, family, genus, and species levels.

Shotgun Metagenomic Data Processing

Shotgun metagenomic sequencing data were quality controlled by requiring a minimum of 4M paired-end reads per sample after Nextera library adaptor removal using Trimmomatic v0.39 (Bolger et al., 2014). Quality control methods were run using default parameters. Then, the clean data were assembled individually using MEGAHIT v1.1.2 (Li et al., 2015) stepping over a k-mer range of 21 to 99 to generate sample-derived assembly. Overall, *de novo* assembly statistics were evaluated as a combination of percent paired or singleton reads realigning to the assembly using BWA v0.7.17 (Li and Durbin, 2009). The unmapped reads of each sample were pooled for re-assembly using MEGAHIT v1.1.2 to generate a mixed assembly. Sample-derived assembly and mixed assembly were combined to obtain the final assembly for further analyses. After quality control, clean reads were used to generate taxonomic profiles with taxonomic classifier MetaOthello v1.0 using reads k-mer signatures of 31bp length (Liu et al., 2018). The open reading frame (ORF) was predicted based on the final assembly contigs (> 500 bp) using MetaGeneMark v3.38 with default parameters (Zhu et al., 2010). The predicted ORFs ≥ 300 bp in length from all samples were pooled and combined based on ≥ 95% identity and 90% read coverage using CD-HIT v4.6 (Li and Godzik, 2006) in order to reduce the number of redundant genes for the downstream assembly step. The reads were re-aligned to the predicted gene using BWA to count read numbers.

Abundance Calculation and Function Annotation

For 16S sequencing, the qualified OTU data were used to calculate α-diversity metrics using one-way analysis of variance (ANOVA) with the Duncan *post hoc* test using the vegan package v2.5.3. Bray-Curtis dissimilarity was employed as β-diversity measure and principal coordinate analysis (PCoA) plot was generated with the ape package. The different sites were statistically compared using analysis of similarity (ANOSIM) with 10,000 permutations. The *p*-values were adjusted by the false discovery rate (FDR) using the Benjamini-Hochberg method with the p.adjust function in R. To construct the sample classifier in each group, the random forest model was applied using the randomforest package v4.6.12 and pROC package v2.0.1 in R project.

The final gene catalog of shotgun metagenome analyses was obtained from non-redundant genes with a gene read count > 2. Clean reads were used to generate taxonomic profile using Kaiju v1.6.3 (Menzel et al., 2016). Bray-Curtis distance matrix based on gene, taxon and function abundance was calculated to evaluate the microbial community differences between samples (groups). The Welch's *t*-test, Wilcoxon rank test, Adonis (also called PERMANOVA), and the Anosim test were conducted using R project Vegan package. Differential analyses of genes and taxa were performed using metastats and LEfSe software v1.0 (Segata et al., 2011) based on the mean value of all annotated genes. To predict gene function, all unique ORFs were annotated using DIAMOND v0.9.24 (Buchfink et al., 2015) based on the KEGG (release 94.0), CAZy, and eggNOG 5.0 databases. And Welch's *t*-test and ANOVA were used to investigate the differences in gut functions including KEGG pathways, CAZy, and eggNOG activities.

To reveal the consistency of the results of the shotgun metagenomic and 16S rRNA gene sequencing, LEfSe software was also used to construct a microbiota classification phylogenetic tree based on the species with an average species abundance greater than 1%.

Co-occurrence Network Construction

The Co-occurrence network of all annotated genes, depicting the differentially enriched metagenomic microbial taxa and functional capacities with all phenotypes, was constructed according to their Pearson's correlation coefficient in all samples. Edges with Pearson's correlation coefficient > 0.8 or < -0.8 and $P < 0.05$ were used to construct the network. The resulting network was visualized with gephi-0.9.2 software.

Statistical Analyses

The mean ± standard deviation (SD) was calculated for all data. The data on host carcass phenotypes and fatty acid composition were examined for normality and homogeneity of variance. Normally distributed data were analyzed using ANOVA. Duncan *post hoc* test was used to analyze differences among groups when significance ($P < 0.05$) was detected using SPSS 23 (IBM, Armonk, NY, United States). For data that were not normally distributed, Kruskal-Wallis H and *post hoc* tests and Mann-Whitney tests were conducted in SPSS 23. All values with $P < 0.05$ were considered statistically significant.

RESULTS

Characterization of Host Phenotypes

All phenotypic characteristics, including carcass traits (BW, CW, and EW), AFW and AFP and pectoralis lipid composition (IMF, TG, CHO, and PL), fit the normal distribution in this study (**Figure 1A** and **Supplementary Figure 1**). Considerable variations were observed regarding both AFW and AFP in the Tiannong Partridge Chickens (**Supplementary Table 1**). Specifically, the average AFW of Tiannong Partridge Chickens was 43.59 g, and the top 10% of chickens had an average AFW about quadruple over the LL group (77.52 g vs. 19.15 g). Meanwhile, the average AFP was 4.23%, and the top 10% of chickens had an average AFP 3.5 times over the LL group (7.03% vs. 1.98%). The two AFD-related traits, namely, AFW and AFP, exhibited a high correlation ($r = 0.94$, $P = 0.000$) (**Figure 1A**). AFW was positively correlated with BW, CW, and EW ($r = 0.47-0.53$, $P < 0.01$), and the correlations between AFP

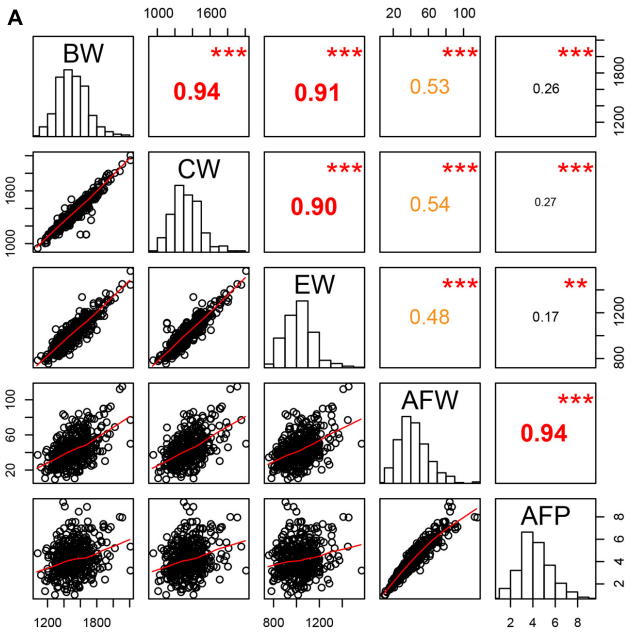

FIGURE 1 | Characterization of host phenotypes. **(A)** The statistic distribution of and correlations among each phenotype, while **(B)** shows the principal components of the carcass traits, the abdominal fat deposition, and the pectoralis lipid composition. BW, body weight; CW, carcass weight; EW, eviscerated weight; AFW, abdominal fat weight; AFP, abdominal fat percentage; IMF, intramuscular fat; TG, triglyceride; PL, phospholipid; CHO, cholesterol. The value in the upper triangular matrix represents the correlation coefficient; two * represents $P < 0.01$, and three * represents $P < 0.001$.

and these traits were much weaker but also significant ($r = 0.16$-0.26, $P < 0.05$) (**Figure 1A**). The pectoralis lipid composition had a weak association with AFD (**Supplementary Figure 1**). Furthermore, the variable principal component analyses on these phenotypes further suggested that AFD-related traits (AFW and AFP) were relatively independent of carcass traits and pectoralis lipid composition (**Figure 1B**).

Correlation Between Gut Microbial Composition and Abdominal Fat Deposition

To analyze the influence of intestinal flora on AFD, 76 chickens with different amounts of abdominal fat were selected for subsequent 16S rRNA gene studies. The 16S rRNA gene sequencing analysis produced a total of 7,745,067 quality-filtered effective tags from these samples, and 2,023 OTUs were then identified. The average Good's-Coverage index for each sample was 0.993 (0.991–0.994), implying sufficient sequencing depth (**Supplementary Figure 2**).

All sequenced samples were divided into two groups based on the AFP, namely, HH and LL chickens. The AFD, including AFW and AFP, were significantly divergent between LL and HH chickens (both $P = 0.000$), and the AFD in the HH group was about twice that in the LL group (**Supplementary Table 2**). The carcass traits, such as BW, CW, and EW, were significantly different between the HH and LL groups ($P < 0.05$), but there was only a 1.05-times change for HH to LL chickens (**Supplementary Table 2**). None of the pectoralis lipid contents were significantly different between the two groups (**Supplementary Table 2**).

The Spearman's correlation coefficient of gut microbiota diversity and AFP suggested that the richness and diversity of the gut microbiota decreased with an increase in AFD (**Figure 2A**). The difference in microbial flora structure between the LL and HH groups further confirmed the close relationship between the gut microbiome and AFD of Tiannong Partridge Chickens. The alpha diversity suggested that AFD had significant effects on the gut microbiome. Specifically, the Shannon and Simpson indices of the two groups were not significantly different (**Supplementary Figures 3A, 2B**), but the Chao1 (**Figure 2B**), sobs (**Supplementary Figure 2B**), and ACE (**Supplementary Figure 2C**) indices of the HH group were all lower than those of the LL group (all $P = 0.000$). Furthermore, beta diversity analyses revealed different gut microbial communities among chickens with different levels of AFD. Even though no distinct separation was observed between the leaner and fatter chickens using PCoA (**Figure 2C**), the Anosim and Adonis analyses (**Figures 2D,E**) demonstrated greater inter-group diversity than inner-group diversity between the LL and HH groups ($P = 0.001$), implying a different gut microbial composition between Tiannong Partridge Chickens with different levels of AFD.

Gut Microbes Associated With Abdominal Fat Deposition

A total of 1577 and 1515 OTUs were identified in the LL and HH groups, respectively, and 1375 of them were shared between the two groups. Subsequently, the OTUs were classified into 26 phyla, 64 classes, 97 orders, 164 families, and 332 genera.

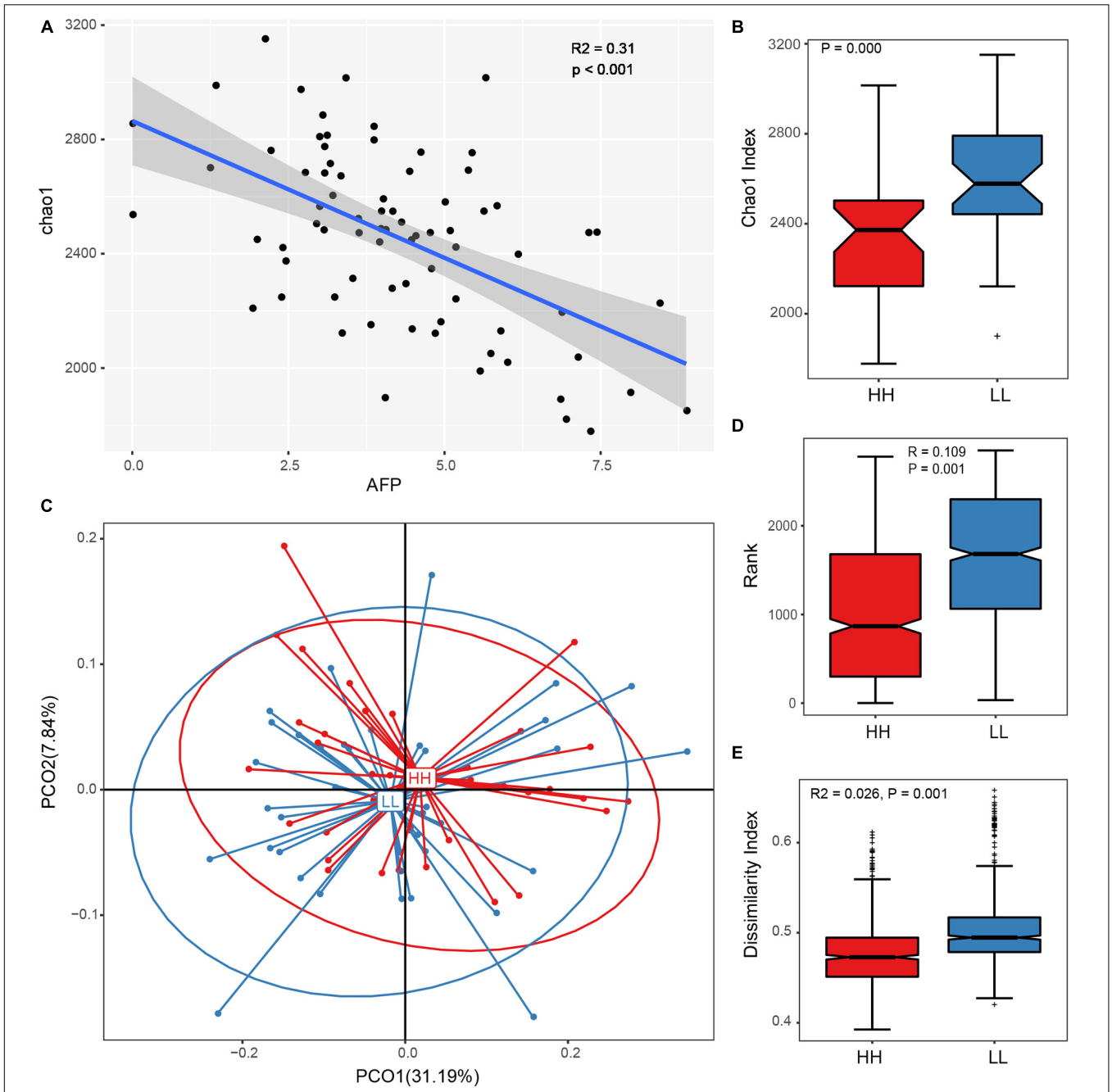

FIGURE 2 | Gut microbial diversity and community with different abdominal fat deposition. **(A)** The Spearman's correlation coefficient of the Chao1 index and the AFP of Tiannong Partridge Chickens, each dot represents on samples. **(B)** The comparison of Chao1 index between the high and low AFP chickens. **(C)** Represents the result of PCoA analysis based on OTUs of chickens with variant AF. **(D,E)** The results of Anosim and Adonis analyses. HH, high AFP chickens; LL, low AFP chickens.

To identify the microbes associated with the AFD in Tiannong Partridge chickens, the relative abundance of microbes was compared between LL and HH chickens. At phylum level, Bacteroidetes and Firmicutes dominated the gut microbial communities in both LL and HH chickens (**Supplementary Figure 4A**). However, there was no significant difference in the Bacteroidetes/Firmicutes ratio between the two groups (**Figure 3A**). Although some of the top 10 most abundant phyla had relatively great variation between the HH and LL groups (**Supplementary Figure 4B**), only Actinobacteria was more abundant in the HH chickens than in the LL chickens ($P < 0.05$) (**Figure 3B**). The relative abundances and the comparison of the top 10 abundant genera between the HH and LL groups were shown in **Supplementary Figures 4C,D**. Furthermore, the multi-test analysis revealed a total of 13 differentially enriched genera between the two groups (**Figure 3C**). Consistent with

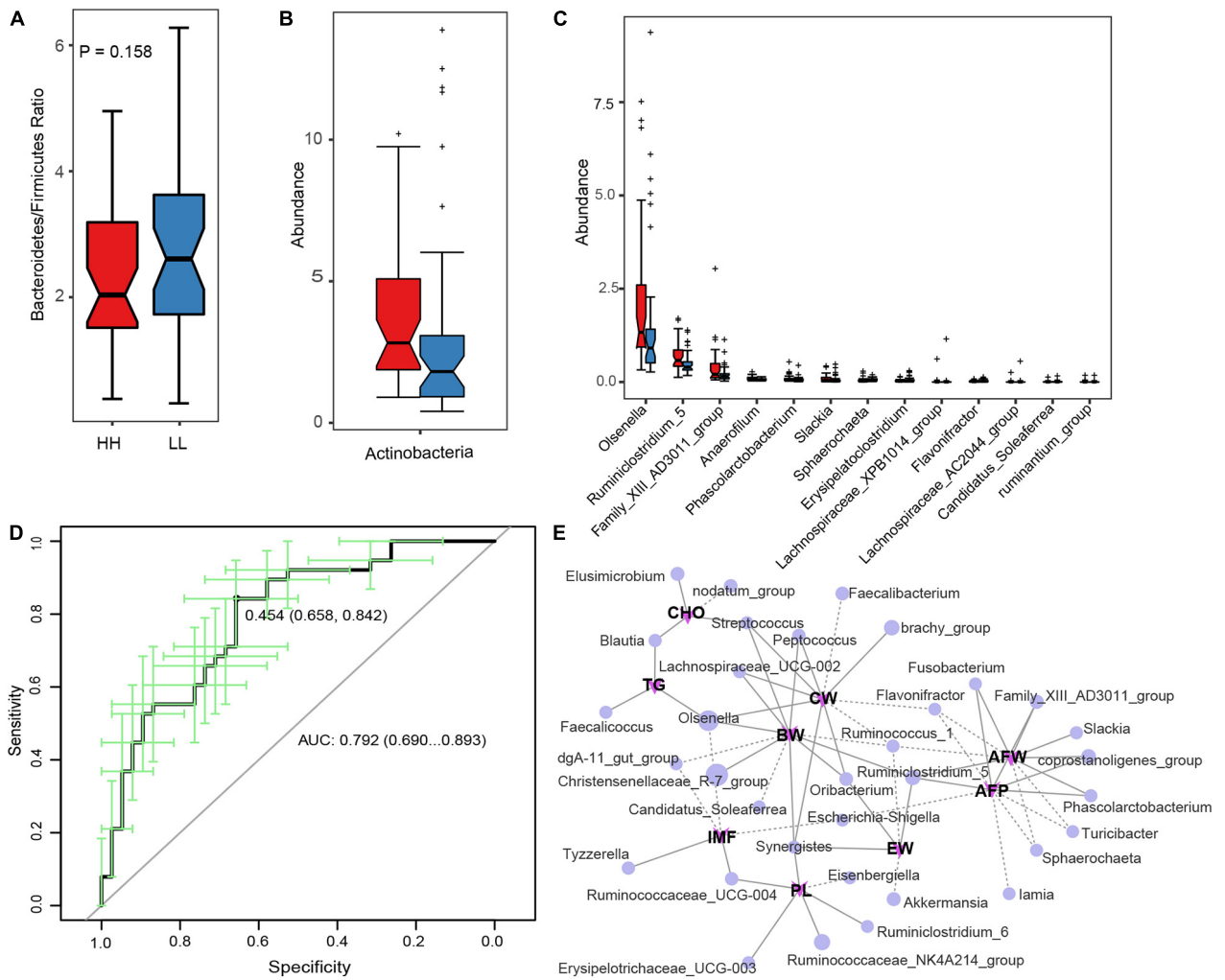

FIGURE 3 | Correlation between gut microbes and abdominal fat deposition. **(A)** The Bacteroidetes/Firmicutes ratio between the HH and LL chickens. **(B,C)** The differentially enriched microbial phylum and genera, respectively. **(D)** Represents the AUC of genus microbiota based on the AFP classification. **(E)** The Spearman's correlation network between genus microbiota and host phenotypes, the full line represents significant positive correlation ($P < 0.05$) while the dotted line represents significant negative correlation ($P < 0.05$). HH, high AFP chickens; LL, low AFP chickens. BW, body weight; CW, carcass weight; EW, eviscerated weight; AFW, abdominal fat weight; AFP, abdominal fat percentage; IMF, intramuscular fat; TG, triglyceride; PL, phospholipid; CHO, cholesterol.

the results of the phylum comparison, the genera, *Olsenella* and *Slackia,* belonging to the phylum Actinobacteria were more enriched in HH chickens. The genus, *Sphaerochaeta*, belonging to phylum *Spirochaetae*, was the most significantly enriched in the LL chickens. The remaining ten differentially enriched genera were all classified as phylum Firmicutes, of which genera *Anaerofilum*, *Ruminiclostridium 5*, *Family XIII AD3011* group, and *Phascolarctobacterium* were more abundant in the HH group, while *Lachnospiraceae XPB1014* group, *Lachnospiraceae AC2044* group, *Flavonifractor*, *Candidatus Soleaferrea*, *Erysipelatoclostridium*, and *ruminantium* group were more abundant in the LL group.

Furthermore, a random forest classifier based on the microbial genus was constructed to evaluate the diagnostic value of the AFP-associated microbiome. As a result, 14 genera, containing all 13 differentially enriched genera, were complied with an area under the receiver operating curve (AUC) of 79.2% (**Figure 3D**), suggesting that the gut microbiota genera were distinguished between the HH and LL chickens. Among them, the ten most indicative genera were *Sphaerochaeta*, *Anaerofilum*, *Erysipelatoclostridium*, *Family XIII AD3011* group, *Ruminiclostridium 5*, *Flavonifractor*, *Slackia*, *Candidatus Soleaferrea*, *Olsenella*, and *Phascolarctobacterium* (**Supplementary Figure 5**). **Figure 3E** also illustrated the multiple positive actions of the genera *Ruminiclostridium* 5 and the negative actions of the genera *Flavonifractor* on chicken body growth and AFD. Meanwhile, the genera *Family XIII AD3011* group, *Ruminiclostridium 5*, *Slackia*, *Fusobacterium*, and *Phascolarctobacterium* might positively contribute to the AFD of Tiannong Partridge chickens. Network analysis revealed that the genus *Olsenella* was negatively associated with chicken pectoralis TG content

and positively associated with BW and CW. The genera *Candidatus Soleaferrea* was also negatively associated with chicken BW. However, it also illustrated the multiple positive actions of the genera *Ruminiclostridium 5* and the negative actions of the genera *Flavonifractor* on chicken body growth and AFD. Additionally, the direct correlation analysis between the 13 differentially enriched genera and the host phenotype was completely consistent with the above results (**Supplementary Figure 6**).

Shotgun Metagenomic Species Associated With Extreme Abdominal Fat Deposition Traits

To delve into the specific gut species associated with abdominal fat deposition, shotgun metagenomic sequencing analysis was performed on a subset of eight samples of LL and HH. These samples represent 4.58- and 3.47-times diversity between LL and HH for AFW and AFP, respectively (**Supplementary Table 3**). A total of 30,099,632-46,034,303 clean reads were generated for each sample. In total, 2,729,686 genes were annotated for these samples. Subsequently, 39 phyla, 132 classes, 332 orders, 787 families, 1,772 genera, and 5,542 species were obtained and compared between the LL and HH chickens. The co-occurrence microbiota classification phylogenetic tree suggested good consistency of the shotgun metagenomic and 16S rRNA gene sequencing results (**Supplementary Figure 7**).

The greater inter-group diversity than the inner-group diversity ($P < 0.05$) of the shotgun metagenomic microbiome demonstrated distinct shotgun metagenomic species composition between chickens with extreme AFD traits (**Supplementary Figure 8**). LEfSe analysis of the taxonomic profiling based on the clean reads was first performed to identify the different shotgun metagenomic species between the high and low AFP chickens. The results clearly showed that the phylum Bacteroidetes, genus *Bacteroides*, *Parabacteroides*, and *Olsenella*, species *Bacteroides salanitronis* (*B. salanitronis*), *Bacteroides fragilis* (*B. fragilis*), and *Parabacteroides distasonis* (*P. distasonis*) were differentially enriched in the LL versus HH groups (**Figure 4A**). Specifically, the percentage of Bacteroidetes was higher in the lean (19.61%) than in the fat chickens (16.18%). The subordinate genera *Bacteroides* and *Parabacteroides* were more enriched in the lean (12.10% and 0.80%) than in the fat chickens (9.29% and 0.65%, respectively). Accordingly, *B. salanitronis* and *B. fragilis* as well as *P. distasonis*, were also more abundant in the lean (4.11%, 3.63%, and 0.80%) than in the fat chickens (2.79%, 2.98%, and 0.65%), respectively. Conversely, the percentage of genus *Olsenella* was higher in the fat (0.15%) than in the lean line (0.06%).

In addition, taxonomic differences at genus and species levels were identified based on the results of gene annotation between the HH and LL groups. As a result, phylum Bacteroidetes was notably more enriched in the LL group, while phylum Euryarchaeota was more enriched in the HH group. Nine genera were found to be significantly different between the HH and LL chickens, and all of them were more abundant in the HH group (**Figure 4B**). In order of significance, the different enriched genera included *Ruminococcus*, *Methanobrevibacter*, *Blautia*, *Clostridia noname*, *Anaerotruncus*, *Butyrivibrio*, *Ruminococcaceae noname*, *Faecalibacterium*, and *Lachnospiraceae noname*. In addition, a total of eight differentially enriched species were identified between the HH and LL groups (**Figure 4C**). Among them, *B. fragilis* and *B. sp. An279* were more abundant in the LL chickens, whereas the remaining six species, *Firmicutes bacterium CAG:110*, *Methanobrevibacter woesei* (*M. woesei*), *Olsenella mediterranea* (*O. mediterranea*), *Clostridia bacterium* (*C. bacterium*), *Ruminococcaceae bacterium* (*R. bacterium*), and *uncultured Clostridium sp.* were more abundant in the HH chickens.

Alterations of Microbial Function Associating to Abdominal Fat Deposition

To illustrate the functional alterations within the gut microbiome between high and low AFP chickens, the shotgun metagenomic genes were annotated to KO modules and KEGG pathways. Most genes in both LL and HH groups were annotated to carbohydrate metabolism, followed by amino acid metabolism (**Supplementary Figure 9**). In terms of KEGG pathways, Anosim and Adonis analyses demonstrated greater inter-group than inner-group diversity between the LL and HH groups ($P = 0.03$). NMDS analysis suggested distinct microbial functions associated with different AFDs of Tiannong Partridge Chickens (**Supplementary Figure 10**). In detail, 19 pathways were annotated by the differentially expressed KO modules between the LL and HH groups, and all these pathways belonged to the functional classification of metabolism (**Table 1**). Among them, seven pathways were upregulated in the HH chickens, including "metabolic pathways," "degradation of aromatic compounds," "sphingolipid metabolism," "galactose metabolism," "methane metabolism," "oxidative phosphorylation," and "phenylalanine, tyrosine, and tryptophan biosynthesis." Among them, six pathways belonged to the functional classes of "global and overview maps," "lipid metabolism," "carbohydrate metabolism," and "energy metabolism." Six pathways, including "photosynthesis," "glycine, serine, and threonine metabolism," "cyanoamino acid metabolism," "riboflavin metabolism," "monobactam biosynthesis," and "dioxin degradation" were downregulated in the HH chickens. These pathways are associated with the metabolism of amino acids, cofactors, secondary metabolites, and xenobiotics. In addition, six pathways, mainly associated with the metabolism of glycan, amino acids, cofactors, and vitamins, were annotated by both overexpressed and downregulated genes, including "lipopolysaccharide biosynthesis," "other glycan degradation," "phosphonate and phosphinate metabolism," "biotin metabolism," "folate biosynthesis," and "ubiquinone and other terpenoid-quinone biosynthesis."

Furthermore, the shotgun metagenomic genes were annotated to the eggNOG and CAZy databases. The Anosim and Adonis analyses suggested different microbial functions in both eggNOG ($P = 0.04$) and CAZy ($P = 0.03$) for the gut microbiota in LL and HH chickens, which were further evidenced by the

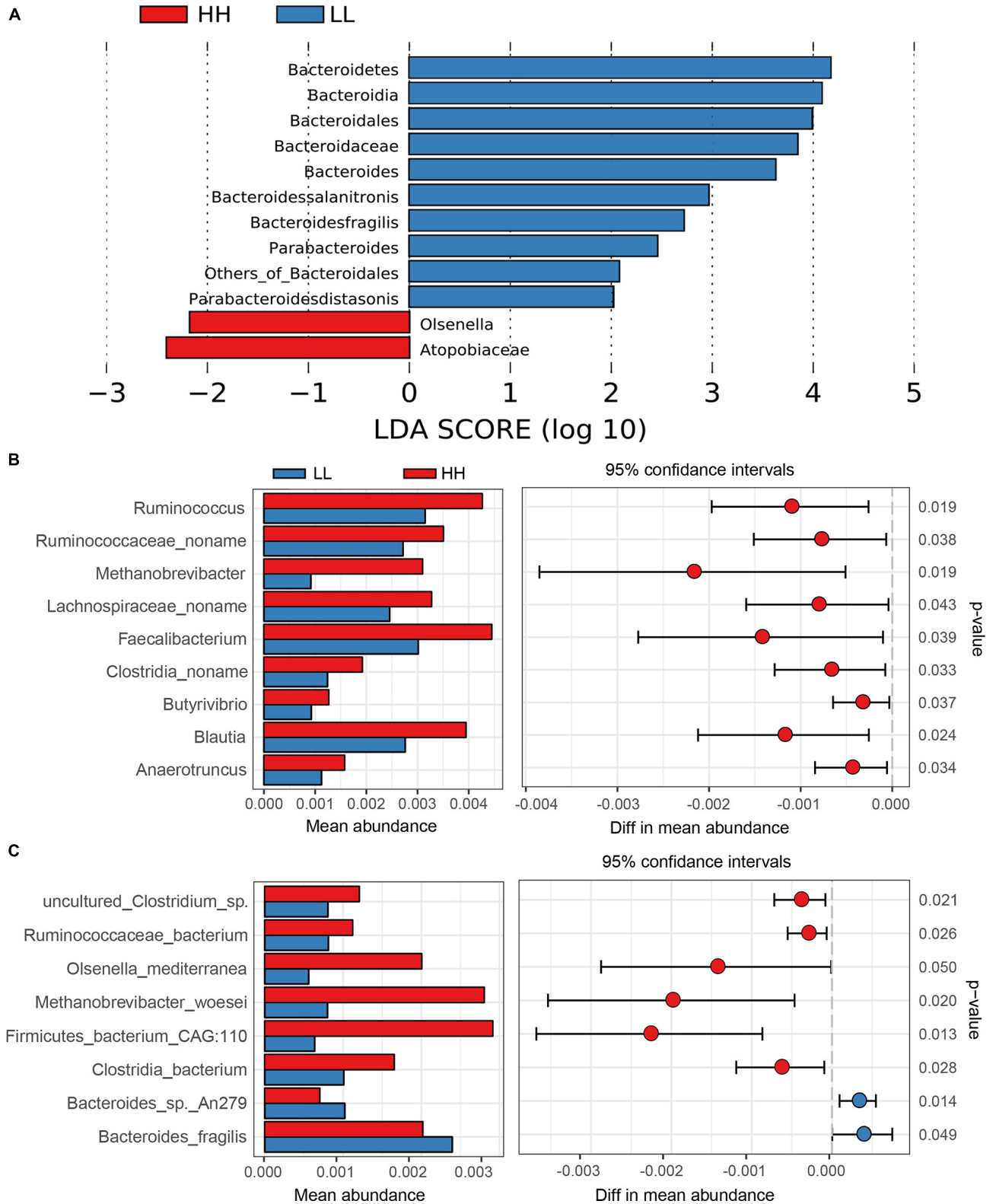

FIGURE 4 | The taxonomic differences between high and low AFP chickens. **(A)** Differentially enriched gut microorganism identified by the LEfSe analysis of the taxonomic profiling based on the clean reads. **(B)** The differentially enriched gut microorganism genus based on gene annotation. **(C)** The differentially enriched gut microorganism species based on gene annotation. HH, high AFP chickens; LL, low AFP chickens.

TABLE 1 | The regulation of microbial function in the high AFP chickens comparing to the low AFP chickens.

Pathway ID	KEGG pathway class	Pathway	Down expression genes	Up expression genes
ko01100	Global and overview maps	Metabolic pathways	–	307
ko01220	Global and overview maps	Degradation of aromatic compounds	–	5
ko00600	Lipid metabolism	Sphingolipid metabolism	–	10
ko00052	Carbohydrate metabolism	Galactose metabolism	–	23
ko00680	Energy metabolism	Methane metabolism	–	24
ko00190	Energy metabolism	Oxidative phosphorylation	–	20
ko00400	Amino acid metabolism	Phenylalanine, tyrosine and tryptophan biosynthesis	–	18
ko00195	Energy metabolism	Photosynthesis	1	–
ko00260	Amino acid metabolism	Glycine, serine and threonine metabolism	12	–
ko00460	Metabolism of other amino acids	Cyanoamino acid metabolism	6	–
ko00740	Metabolism of cofactors and vitamins	Riboflavin metabolism	4	–
ko00261	Biosynthesis of other secondary metabolites	Monobactam biosynthesis	5	–
ko00621	Xenobiotics biodegradation and metabolism	Dioxin degradation	1	–
ko00540	Glycan biosynthesis and metabolism	Lipopolysaccharide biosynthesis	6	8
ko00511	Glycan biosynthesis and metabolism	Other glycan degradation	8	19
ko00440	Metabolism of other amino acids	Phosphonate and phosphinate metabolism	3	4
ko00780	Metabolism of cofactors and vitamins	Biotin metabolism	6	10
ko00790	Metabolism of cofactors and vitamins	Folate biosynthesis	7	11
ko00130	Metabolism of cofactors and vitamins	Ubiquinone and other terpenoid-quinone biosynthesis	4	5

NMDS analyses (**Supplementary Figures 11**, **12**). Specifically, 200 orthologous groups (OG) were enriched, and 19 of them were differentially expressed between the HH and LL chickens (**Supplementary Table 4**). Among them, only three OGs, representing cell wall/membrane/envelope biogenesis and transcription, were high in HH chickens. The remaining OGs were more highly expressed in the LL chickens, suggesting more active microbial functions of carbohydrate transport and metabolism, energy production and conversion, and inorganic ion transport and metabolism in the LL chickens. However, 326 CAZy enzymes belonging to 6 CAZy activities were enriched. Most shotgun metagenomic genes of Tiannong Partridge Chickens were enriched in glycoside hydrolases (GH), glycosyltransferases (GT), and carbohydrate-binding modules (CBM) (**Supplementary Figure 13**). The HH and LL chickens had 25 different CAZy enzymes (**Supplementary Table 5**), of which 9 enzymes had high expression in HH group, while 16 enzymes were highly expressed in the LL groups. Four carbohydrate-binding modules (CBM), including family 50 (CBM50), 13 (CBM13), 34 (CBM34), and 37 (CBM37), were all high in the HH chickens. Glycoside hydrolase family 42 (GH42) and 49 (GH49), as well as glycosyltransferase family 39 (GT39), 66 (GT66), and 7 (GT7), were also highly expressed in the HH chickens. Meanwhile, the two polysaccharide lyases (PL0 and PL33) and the two carbohydrate esterases (CE2 and CE6) showed high expression in the LL chickens. In addition, a total of nine glycoside hydrolases (GH10, GH109, GH11, GH146, GH16, GH29, GH30, GH35, and GH67) and three glycosyltransferases (GT11, GT3, and GT30) were also highly expressed in the LL chickens.

Co-occurrence Network of Microbial Taxa and Function Capacities With Phenotypic Traits

To understand the contribution of the gut microbiota in chicken fat accumulation, a co-occurrence network representing microbial interactions of differentiated microbial taxa function capacities with phenotypic traits was constructed (**Figure 5** and **Supplementary Table 6**). Traits of AFW and AFP and carcass traits (BW, CW, and EW) had strong correlation with gut microbial community (Pearson's correlation coefficient > 0.8 or < -0.8, and $P < 0.05$) while the pectoralis lipid composition related traits (IMF, TG, CHO, and PL) were weakly correlated to the gut microbiome. Nine microbial taxa including three genera (*Methanobrevibacter*, *Ruminococcus*, and *Blautia*) and six species (*M. woesei*, *O. mediterranea*, *B. fragilis*, *B. sp. An279*, *Firmicutes bacterium CAG:110*, and *uncultured Clostridium sp.*) based on differentially expressed genes between the lean and fat chickens were enriched to several lipid and carbohydrate metabolism pathways. The most enriched pathways included "metabolism pathways," "methane metabolism," "lipopolysaccharide biosynthesis," "other glycan degradatin," "phenylalanine, tyrosine and tryptophan biosynthesis," "oxidative phosphorylation," "Glycine, serine and threonine metabolism," and "galactose metabolism". Notably, genera *Methanobrevibacter* and its subordinate *M. woesei* and *O. mediterranea* were shown participating to pathways including "metabolism pathways," "methane metabolism," and "glycan degradatin" and were strongly correlated to all AFD and carcass traits. *Firmicutes bacterium CAG:110* had close relationship with both AFW and AFP. *B. fragilis* and *B. sp. An279* only had close

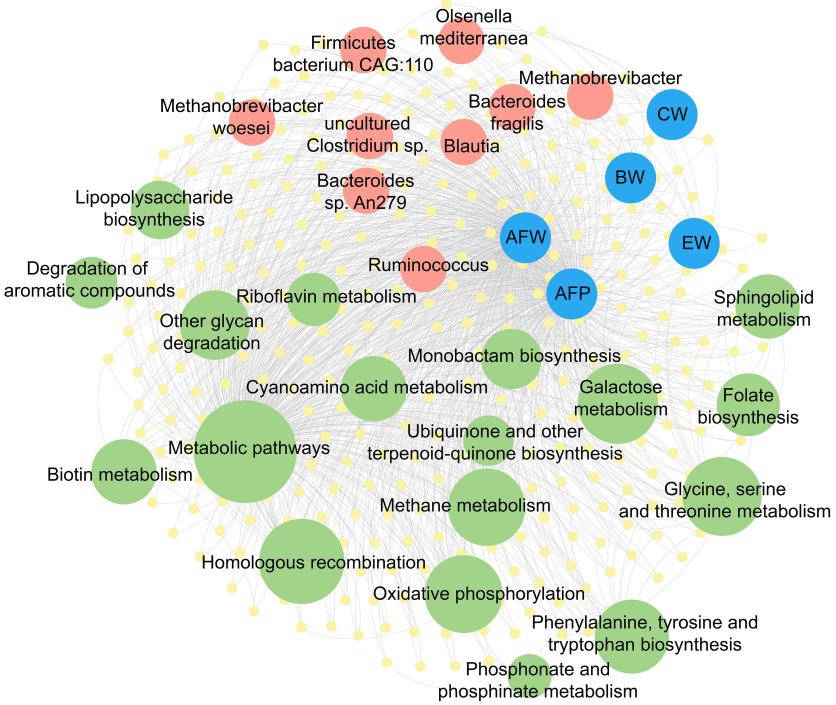

FIGURE 5 | Co-occurrence network of microbial taxa and function capacities with chicken phenotypic traits. The taxa (Red circles) and pathways (green circles) were annotated based on the (yellow circles). The yellow circles represent the differentially expressed genes, red circles represent the differentially enriched taxa, green circles in different size represent the enriched pathways with different degrees of enrichment, while blue circles represent the related chicken phenotypic traits. The gray lines represent edges with Pearson's correlation coefficient > 0.8 or < -0.8 and $P < 0.05$. BW, body weight; CW, carcass weight; EW, eviscerated weight; AFW, abdominal fat weight; AFP, abdominal fat percentage.

relationship with AFW but not AFP, while *Blautia* had strong correlation just with chicken carcass traits.

DISCUSSION

As the commercial line of the Chinese local chicken breed Qingyuan Partridge Chickens and Guangxi Partridge Chickens, Tiannong Partridge chickens completely retains the high quality of meat and flavor and has been selected for automatic sexing, early maturity, and better growth performance. By determining the AFD, carcass traits, and pectoralis lipid compositions of a random flock, this study revealed the differences in AFD among Tiannong Partridge Chickens. Like those in previous reports (Jiang et al., 2017; Abdalla et al., 2018), our results show that chickens genetically selected for earlier maturation and faster growth are characterized by increased AFD. The great variation and normal distribution of AFW and AFP in Tiannong Partridge Chickens suggest that this population is representative for the studying the contribution of gut microbes to AFD in the chicken industry. Meanwhile, the inconsistency between AFD and carcass traits also indicates that it is possible to manipulate the deposition of chicken abdominal fat while maintaining carcass traits (Jiang et al., 2017).

With the global investigation on gut microbial abundance related to AFD, our dataset shows that the richness and diversity of gut microbiota decrease along with an increase in chicken AFD, and that the gut microbial community is greatly affected by different levels of AFD. These results are in line with those of previous studies in humans (Li R. et al., 2020), mice (Ellekilde et al., 2014; Kong et al., 2019), and pigs (Qi et al., 2019). In this study, the comparison of the abundance of microbial taxa reveals that several microbes could be markers of the various levels of AFD. Although the Bacteroidetes/Firmicutes ratio in the HH and LL chickens is not significantly different based on the 16S analysis, a reduction in the abundance of Bacteroidetes and a proportional increase in Firmicutes are observed in HH chickens. Shotgun metagenomic analysis of the extremely high and low AFP chickens also shows less Bacteroidetes abundance in the fatter chickens. As two of the most abundant and ubiquitous chicken gut microbiota taxa, Firmicutes and Bacteroidetes have been widely reported to have varying numbers of relative abundances in fat and lean mice, and obesity has been correlated with a shift in the abundance of both Bacteroidetes and Firmicutes (Ley et al., 2005, 2006). Moreover, previous studies have shown that a high-fat diet changes the relative composition of the gut microbiota by increasing Firmicutes and decreasing Bacteroidetes at the phylum levels in both humans and mice (Serino et al., 2012; David et al., 2014; Zheng et al., 2017).

Different levels of selection-acquired obesity not only alters the composition of the gut microbiota, but also influences their

functional performance by enriching their relative abundance in microbial taxa. One mechanism through which the gut microbiota contribute to fat deposition is by providing microbial metabolic pathways that are not encoded by the host genome, and thus, regulating the host nutritional metabolism, including nutrient integration and energy capture (Hou et al., 2016; Schmidt et al., 2018).

Our results show that the Bacteroidetes phylum is closely associated with chicken AFD and its subordinate genera *Bacteroides* and *Parabacteroides* are more enriched in the lean chickens. Accordingly, the species *B. salanitronis*, *B. fragilis*, and *P. distasonis*, are less abundant in fat chickens. A previous study has revealed that Bacteroidetes are involved in many metabolic activities, including fermentation of carbohydrates, utilization of nitrogenous substances, and biotransformation of bile acids and steroids (Lan et al., 2006). In this study, the microbiota of LL chickens had high CAZy enzyme activities in carbohydrate esterase, polysaccharide lyase, and glycoside hydrolase for glucans and galactans as well as glycosyltransferase for nucleotide monophosphosugar. Furthermore, orthologous groups related to carbohydrate and inorganic ion transport and metabolism, as well as high energy production and conversion, show high abundance in the LL chicken gut microbiome. Moreover, pathways associated with the metabolism of amino acids, cofactors, secondary metabolites, and xenobiotics are found to be more enriched in LL chickens. These functional alternations are closely related to the Bacteroidetes phylum, which is further supported by correlation analyses of host phenotypes to different gut microorganisms. As it has been reported (Gronow et al., 2011), *B. salanitronis* contributes to the breakdown of food, produces nutrients and energy needed by the chicken, and can ferment glucose, sucrose, arabinose, cellobiose, lactose, xylose, and raffinose. However, it does not utilize trehalose, glycerol, mannitol, sorbitol, or melezitose (Gronow et al., 2011). On the other hand, the presence of phosphoenolpyruvate-oxaloacetate catalytic enzymes gene in *B. fragilis* genome may indicate the potential for efficient propionate synthesis (Xu et al., 2020). In the long-term evolutionary process, *B. fragilis* colonizes the host intestine, participates in the fermentation of glucose, fructose, galactose, lactose, sucrose, dextrin, etc., and plays an important role, especially in obesity, diabetes, and immunodeficiency diseases (Zhao et al., 2019; Donaldson et al., 2020). Meanwhile, *P. distasonis* has also been reported modulating host metabolism and alleviating obesity and metabolic dysfunctions via the production of succinate and secondary bile acids (Wang et al., 2019).

On the other hand, the subordinate genera of phylum Firmicutes, *Phascolarctobacterium*, *Family XIII AD3011* group, and *Ruminiclostridium 5*, are found to be more abundant in the high AFP chickens using 16S analyses. Moreover, eight of the nine differentially enriched genera between the extremely high and low AFP chickens, including *Anaerotruncus*, *Blautia*, *Butyrivibrio*, *Clostridia noname*, *Faecalibacterium*, *Lachnospiraceae noname*, *Ruminococcaceae noname*, and *Ruminococcus*, belong to the phylum Firmicutes and all are more abundant in the HH chickens. *Phascolarctobacterium* has been suggested associating with host metabolic state and mood by producing short-chain fatty acids (SCFA) such as acetate and propionate (Wu et al., 2017). Meanwhile, taxa of two predominantly butyrate-producing genus, *Faecalibacterium* and *Ruminococcus*, are also reported significantly more prevalent in obese individuals than in non-obese individuals (Maniar et al., 2019). As shown in the cecum and colon of rats (Shi et al., 2020), the increase in the *Family XIII AD3011* group may be involved in the production of skatole and indole. Moreover, the families *Lachnospiraceae*, *Clostridia,* and *Ruminococcaceae*, and genera *Ruminiclostridium*, *Blautia,* and *Butyrivibrio,* have been suggested as high fat diet-dependent gut taxa and are likely associated with lipid metabolism (Lin et al., 2016; Zietak et al., 2016; Kong et al., 2019; Hou et al., 2020). Specifically, the butyrate producing *Lachnospiraceae* and *Ruminococcaceae* are suggested to reduce lipopolysaccharide biosynthesis in mice (Kang et al., 2017). Therefore, it is reasonable for the both up- and down-regulation of lipopolysaccharide biosynthesis in the HH chickens, by considering the more abundant of *Lachnospiraceae noname* and less abundant of *Lachnospiraceae XPB1014* group and *Lachnospiraceae AC2044* group in the high AFP chickens. And according to the C_2–C_{18} fatty acid tests, *Clostridium perfringens* has the highest activity toward lauric acid (Kang et al., 2017). Owing to the widespread existence of these taxa, the microbiota in the HH chickens have more activities of carbohydrate-binding modules and high functional expression of lipids, carbohydrates, and energy metabolism. This is in line with the results that the increase in circulating lipoprotein lipase activity caused by gut microbiota results, in turn, in a significant increase in body fat deposition in the host.

Moreover, a high abundance of phylum Actinobacteria and its subordinate genera, *Olsenella* and *Slackia,* are observed in the HH chickens. A high abundance of *Olsenella* and *Slackia* has been observed in mice fed a high-fat diet (Gohir et al., 2019; Nagpal et al., 2019), suggesting their strong correlation with fat and energy metabolism. *Olsenella* has been suggested to positively correlate to methane metabolism and contribute to the metabolic pathways of glycolysis/gluconeogenesis, carbon fixation in photosynthetic organisms, pentose phosphate pathway, and ascorbate and aldarate metabolism (Zhang Y. et al., 2020). This may provide a potential mechanism for the positive correlation between the abundance of genus *Olsenella* to chicken BW, CW, and TG. In addition, phylum Euryarchaeota and its subordinate genus *Methanobrevibacter* and species *M. woesei* were also more abundant in the high AFP chickens. *Methanobrevibacter* is a common and important methanogenic taxon primarily inhabiting the cecum of chickens. Chickens with fewer *Methanobrevibacter* have significantly lower abdominal fat content than those with a higher abundance of *Methanobrevibacter* (35.51 vs. 55.59 g, respectively) (Wen et al., 2019). Apart from bacteria, the dominant gut species, *Methanobrevibacter smithii*, has been found extensively colonizing the small bowel as well as colon, and affects host calorie harvest and adiposity through the digestion of dietary polysaccharides (Hansen et al., 2011; Mathur et al., 2013). This subsequently improves the efficiency of microbial fermentation and enhances host energy capture. In addition, *Methanobrevibacter* has been

suggested to improve acetate and butyrate production and eliminate hydrogen and formate, which are vital carbon sources for colon epithelial cells (Samuel et al., 2007; Hansen et al., 2011). The increase in lipoprotein lipase activity in the villi of epithelia caused by gut microbiota leads to increased triglyceride uptake and peripheral fat storage. In this study, the methanogenic taxa, genus *Methanobrevibacter* and species *M. woesei*, were found to participate in the regulation of gut metabolism including methane metabolism, photosynthesis-antenna proteins, and various types of N-glycan biosynthesis. Our results also suggest a limited association of *Methanobrevibacter* abundance with other gut microbiota or any carcass traits, further supporting the feasibility of reducing fat deposition by inhibiting the caeca-associated genus, *Methanobrevibacter,* without affecting the proportion of carcass meat (Wen et al., 2019).

By revealing the strong correlations between the identified bacterial groups and the phenotypes related to chicken abdominal fat deposition, the present study demonstrates that gut microbiota is an important factor involving AFD in conventional chicken breeds. Moreover, some of the observed differential taxa and potential genes/metabolic pathways are suggested as possible biomarkers associated with chicken AFD. However, we acknowledge that the current dataset lacks evidence supporting the cause-effect relationship of specific taxon to AFD, since it does not provide what microbes are doing or the metabolites that they produce. Study using chickens involving administration of the candidate microbes are needed to further validate the contribution of these microbiota to chicken abdominal fat deposition. Furthermore, studies on the real expression of the suggested genes and metabolic pathways are expected to investigate the mechanistic and functional connection with AFD.

CONCLUSION

In conclusion, alterations in the gut microbiome and its association with metabolism capacity have preliminarily elucidated the contribution of gut microbiota to chicken abdominal fat deposition. The richness and diversity of the gut microbiota decrease as the accumulation of chicken abdominal fat increases. The decrease of Bacteroidetes and the increase of Firmicutes are correlated with the accumulation of chicken abdominal fat deposition. The Bacteroidetes phylum, including *Bacteroides*, *Parabacteroides*, and the species, *B. salanitronis*, *B. fragilis*, and *P. distasonis*, were correlated to alleviate obesity by producing secondary metabolites. Several genera of Firmicutes phylum with circulating lipoprotein lipase activity were linked to the accumulation of chicken body fat. Moreover, the genera, *Olsenella* and *Slackia,* might positively contribute to fat and energy metabolism, whereas the genus, *Methanobrevibacter,* was possible to enhance energy capture, and associated to accumulate chicken abdominal fat deposition. These findings provide insights into the roles of the gut microbiota in complex traits and contribute to the development of effective therapies for the reduction of chicken fat accumulation.

DATA AVAILABILITY STATEMENT

The raw data of 16S rRNA gene presented in the study are deposited in NCBI repository, accession number SRR13782987-SRR13783062, while the raw data of shotgun metagenomic sequencing are deposited in NCBI under accession number SRR13783083-SRR13783090.

ETHICS STATEMENT

The animal study was reviewed and approved by Laboratory Animal Welfare and Animal Experimental Ethical Inspection board of Foshan University. Written informed consent was obtained from the owners for the participation of their animals in this study.

AUTHOR CONTRIBUTIONS

HL, GZ, and HX designed this project. HX, JG, DZ, JL, HZ, YY, ST, GL, CL, and ZX performed the experiments and analyzed the data. HX, GZ, and HL interpreted the data and drafted the manuscript. All authors contributed critically to the drafts and gave final approval for the publication.

FUNDING

This work was funded by the Guangdong Provincial Key Laboratory of Animal Molecular Design and Precise Breeding (2019B030301010), the Guangdong Basic and Applied Basic Research Foundation (2019A1515110453), Foundation for Key Laboratory (2019KSYS011), and Creative Team (2019KCXTD006) in Guangdong Higher Education Institutes. The funding bodies contributed nothing to the study design, data analyses, data interpretation, or manuscript preparation.

ACKNOWLEDGMENTS

We express sincere thanks to Hengyong Li and Cong Liu (Guangdong Tinoo's Foods Group Co., Ltd.), Ying Li, Yuyu Hong, and Jun Xiao (Foshan University) and Dr. Huanxian Cui (Institute of Animal Sciences, Chinese Academy of Agricultural Sciences) for their great help with the experiment and in-depth discussion.

SUPPLEMENTARY MATERIAL

The Supplementary Material for this article can be found online at: https://www.frontiersin.org/articles/10.3389/fmicb.2021.643025/full#supplementary-material

Supplementary Figure 1 | The statistic distribution of the abdominal fat deposition and the pectoralis lipid composition and their correlations. BW, body weight; CW, carcass weight; EW, eviscerated weight; AFW, abdominal fat weight; AFP, abdominal fat percentage; IMF, intramuscular fat; TG, triglyceride;

PL, phospholipid; CHO, cholesterol. The value in the upper triangular matrix represents the correlation coefficient; one * represents $P < 0.05$, two * represents $P < 0.01$ and three * represents $P < 0.001$.

Supplementary Figure 2 | Good's-Coverage index for all samples.

Supplementary Figure 3 | Alpha diversity comparison between HH and LL. **(A)** Shannon index. **(B)** Simpson index. **(C)** Sobs index. **(D)** ACE index. HH, high AFP chickens; LL, low AFP chickens.

Supplementary Figure 4 | The top 10 abundant phyla and genera between HH and LL groups. **(A,B)** The microbial composition and comparison of the top 10 abundant phyla, respectively. **(C,D)** show the microbial composition and comparison of the top 10 abundant genera, respectively.

Supplementary Figure 5 | Random forest analyses on the of LL and HH chickens.

Supplementary Figure 6 | Correlation analyses between the differentially enriched genera and the host phenotype. BW, body weight; CW, carcass weight; EW, eviscerated weight; AFW, abdominal fat weight; AFP, abdominal fat percentage; IMF, intramuscular fat; TG, triglyceride; PL, phospholipid; CHO, cholesterol. The background color represents the correlation coefficient; one * represents $P < 0.05$ and two * represents $P < 0.01$.

Supplementary Figure 7 | The consistency of the results of the shotgun metagenomic and 16S rRNA gene sequencing. The small dots represent species, and the evolutionary branch tree represents the Kingdom, Phylum, Class, Order, Family, Genus and Species from the inside to the outside accordingly. The microorganisms with blue background were identified by both shotgun metagenomic sequencing and 16S rRNA gene sequencing, the microorganisms with green background were identified only by shotgun metagenomic sequencing, while the microorganisms with red background were identified only by 16S rRNA gene sequencing. The dot size indicates the average abundance of the microorganisms in all samples.

Supplementary Figure 8 | The Anosim and Adonis comparison on Phylum composition between chickens with extreme abdominal fat deposition traits. HH, high AFP chickens; LL, low AFP chickens.

Supplementary Figure 9 | Number of genes annotated to KEGG pathways for all samples.

Supplementary Figure 10 | NMDS analysis based on KEGG pathways. HH, high AFP chickens; LL, low AFP chickens.

Supplementary Figure 11 | NMDS analysis for eggNOG.C annotation. HH, high AFP chickens; LL, low AFP chickens.

Supplementary Figure 12 | NMDS analysis based on CAZy activities. HH, high AFP chickens; LL, low AFP chickens.

Supplementary Figure 13 | Number of genes annotated to each CAZy activities for all samples.

REFERENCES

Abdalla, B. A., Chen, J., Nie, Q., and Zhang, X. (2018). Genomic insights into the multiple factors controlling abdominal fat deposition in a chicken model. *Front. Genet.* 9:262. doi: 10.3389/fgene.2018.00262

Backhed, F., Ding, H., Wang, T., Hooper, L. V., Koh, G. Y., Nagy, A., et al. (2004). The gut microbiota as an environmental factor that regulates fat storage. *Proc. Natl. Acad. Sci. U.S.A.* 101, 15718–15723. doi: 10.1073/pnas.0407076101

Bolger, A. M., Lohse, M., and Usadel, B. (2014). Trimmomatic: a flexible trimmer for Illumina sequence data. *Bioinformatics* 30, 2114–2120. doi: 10.1093/bioinformatics/btu170

Bolyen, E., Rideout, J. R., Dillon, M. R., Bokulich, N., Abnet, C. C., Al-Ghalith, G. A., et al. (2019). Reproducible, interactive, scalable and extensible microbiome data science using QIIME 2. *Nat. Biotechnol.* 37, 852–857. doi: 10.1038/s41587-019-0209-9

Buchfink, B., Xie, C., and Huson, D. H. (2015). Fast and sensitive protein alignment using DIAMOND. *Nat. Methods* 12, 59–60. doi: 10.1038/nmeth.3176

Chen, S., Xiang, H., Zhang, H., Zhu, X., Wang, D., Wang, J., et al. (2019). Rearing system causes changes of behavior, microbiome, and gene expression of chickens. *Poult. Sci.* 98, 3365–3376. doi: 10.3382/ps/pez140

Cui, X., Cui, H., Liu, L., Zhao, G., Liu, R., Li, Q., et al. (2018). Decreased testosterone levels after caponization leads to abdominal fat deposition in chickens. *BMC Genom.* 19:344. doi: 10.1186/s12864-018-4737-3

David, L. A., Maurice, C. F., Carmody, R. N., Gootenberg, D. B., Button, J. E., Wolfe, B. E., et al. (2014). Diet rapidly and reproducibly alters the human gut microbiome. *Nature* 505, 559–563. doi: 10.1038/nature12820

Demeure, O., Duclos, M. J., Bacciu, N., Le Mignon, G., Filangi, O., Pitel, F., et al. (2013). Genome-wide interval mapping using SNPs identifies new QTL for growth, body composition and several physiological variables in an F-2 intercross between fat and lean chicken lines. *Genet. Sel. Evol.* 45:36. doi: 10.1186/1297-9686-45-36

Ding, J., Zhao, L., Wang, L., Zhao, W., Zhai, Z., Leng, L., et al. (2016). Divergent selection-induced obesity alters the composition and functional pathways of chicken gut microbiota. *Genet. Sel. Evol.* 48:93. doi: 10.1186/s12711-016-0270-5

Donaldson, G. P., Chou, W. C., Manson, A. L., Rogov, P., Abeel, T., Bochicchio, J., et al. (2020). Spatially distinct physiology of *Bacteroides fragilis* within the proximal colon of gnotobiotic mice. *Nat. Microbiol.* 5, 746–756. doi: 10.1038/s41564-020-0683-3

Ellekilde, M., Selfjord, E., Larsen, C. S., Jakesevic, M., Rune, I., Tranberg, B., et al. (2014). Transfer of gut microbiota from lean and obese mice to antibiotic-treated mice. *Sci. Rep.* 4:5922. doi: 10.1038/srep05922

Gohir, W., Kennedy, K. M., Wallace, J. G., Saoi, M., Bellissimo, C. J., Britz-McKibbin, P., et al. (2019). High-fat diet intake modulates maternal intestinal adaptations to pregnancy and results in placental hypoxia, as well as altered fetal gut barrier proteins and immune markers. *J. Physiol. Lond.* 597, 3029–3051. doi: 10.1113/Jp277353

Gronow, S., Held, B., Lucas, S., Lapidus, A., Del Rio, T. G., Nolan, M., et al. (2011). Complete genome sequence of *Bacteroides salanitronis* type strain (BL78(T)). *Stand. Genomic Sci.* 4, 191–199. doi: 10.4056/sigs.1704212

Hansen, E. E., Lozupone, C. A., Rey, F. E., Wu, M., Guruge, J. L., Narra, A., et al. (2011). Pan-genome of the dominant human gut-associated archaeon, *Methanobrevibacter smithii*, studied in twins. *Proc. Natl. Acad. Sci. U.S.A.* 108(Suppl. 1), 4599–4606. doi: 10.1073/pnas.1000071108

Hou, D., Zhao, Q., Yousaf, L., Xue, Y., and Shen, Q. (2020). Whole mung bean (*Vigna radiata* L.) supplementation prevents high-fat diet-induced obesity and disorders in a lipid profile and modulates gut microbiota in mice. *Eur. J. Nutr.* 59, 3617–3634. doi: 10.1007/s00394-020-02196-2

Hou, Q., Kwok, L. Y., Zheng, Y., Wang, L., Guo, Z., Zhang, J., et al. (2016). Differential fecal microbiota are retained in broiler chicken lines divergently selected for fatness traits. *Sci. Rep.* 6:37376. doi: 10.1038/srep37376

Huang, S. M., Wu, Z. H., Li, T. T., Liu, C., Han, D. D., Tao, S. Y., et al. (2020). Perturbation of the lipid metabolism and intestinal inflammation in growing pigs with low birth weight is associated with the alterations of gut microbiota. *Sci. Total Environ.* 719:137382. doi: 10.1016/j.scitotenv.2020.137382

Jiang, M., Fan, W. L., Xing, S. Y., Wang, J., Li, P., Liu, R. R., et al. (2017). Effects of balanced selection for intramuscular fat and abdominal fat percentage and estimates of genetic parameters. *Poult. Sci.* 96, 282–287. doi: 10.3382/ps/pew334

Kang, C., Wang, B., Kaliannan, K., Wang, X., Lang, H., Hui, S., et al. (2017). Gut microbiota mediates the protective effects of dietary capsaicin against chronic low-grade inflammation and associated obesity induced by high-fat diet. *mBio* 8:e00470-17. doi: 10.1128/mBio.00470-17

Kong, C., Gao, R., Yan, X., Huang, L., and Qin, H. (2019). Probiotics improve gut microbiota dysbiosis in obese mice fed a high-fat or high-sucrose diet. *Nutrition* 60, 175–184. doi: 10.1016/j.nut.2018.10.002

Lan, P. T. N., Sakamoto, M., Sakata, S., and Benno, Y. (2006). *Bacteroides barnesiae* sp nov., *Bacteroides salanitronis* sp nov and *Bacteroides gallinarum* sp nov., isolated from chicken caecum. *Int. J. Syst. Evol. Microbiol.* 56, 2853–2859. doi: 10.1099/ijs.0.64517-0

Ley, R. E., Backhed, F., Turnbaugh, P., Lozupone, C. A., Knight, R. D., and Gordon, J. I. (2005). Obesity alters gut microbial ecology. *Proc. Natl. Acad. Sci. U.S.A.* 102, 11070–11075. doi: 10.1073/pnas.0504978102

Ley, R. E., Turnbaugh, P. J., Klein, S., and Gordon, J. I. (2006). Microbial ecology: human gut microbes associated with obesity. *Nature* 444, 1022–1023. doi: 10.1038/4441022a

Li, D., Liu, C. M., Luo, R., Sadakane, K., and Lam, T. W. (2015). MEGAHIT: an ultra-fast single-node solution for large and complex metagenomics assembly

via succinct de Bruijn graph. *Bioinformatics* 31, 1674–1676. doi: 10.1093/bioinformatics/btv033

Li, H., and Durbin, R. (2009). Fast and accurate short read alignment with Burrows-Wheeler transform. *Bioinformatics* 25, 1754–1760. doi: 10.1093/bioinformatics/btp324

Li, H., Li, Y., Yang, L., Zhang, D., Liu, Z., Wang, Y., et al. (2020). Identification of a novel lipid metabolism-associated hepatic gene family induced by estrogen via eralpha in chicken (Gallus gallus). *Front. Genet.* 11:271. doi: 10.3389/fgene.2020.00271

Li, R., Huang, X., Liang, X., Su, M., Lai, K. P., and Chen, J. (2020). Integrated omics analysis reveals the alteration of gut microbe-metabolites in obese adults. *Brief. Bioinform*. 4:bbaa165. doi: 10.1093/bib/bbaa165

Li, W., and Godzik, A. (2006). Cd-hit: a fast program for clustering and comparing large sets of protein or nucleotide sequences. *Bioinformatics* 22, 1658–1659. doi: 10.1093/bioinformatics/btl158

Lin, H., An, Y., Hao, F., Wang, Y., and Tang, H. (2016). Correlations of fecal metabonomic and microbiomic changes induced by high-fat diet in the pre-obesity state. *Sci. Rep*. 6:21618. doi: 10.1038/srep21618

Liu, X. N., Yu, Y., Liu, J. P., Elliott, C. F., Qian, C., and Liu, J. Z. (2018). A novel data structure to support ultra-fast taxonomic classification of metagenomic sequences with k-mer signatures. *Bioinformatics* 34, 171–178. doi: 10.1093/bioinformatics/btx432

Magoc, T., and Salzberg, S. L. (2011). FLASH: fast length adjustment of short reads to improve genome assemblies. *Bioinformatics* 27, 2957–2963. doi: 10.1093/bioinformatics/btr507

Maniar, K., Singh, V., Kumar, D., Moideen, A., Bhattacharyya, R., and Banerjee, D. (2019). "Metformin: a candidate drug to control the epidemic of diabetes and obesity by way of gut microbiome modification," in *Microbiome and Metabolome in Diagnosis, Therapy, and other Strategic Applications*, eds J. Faintuch and S. Faintuch (Cambridge, MA: Academic Press), 401–408.

Mathur, R., Kim, G., Morales, W., Sung, J., Rooks, E., Pokkunuri, V., et al. (2013). Intestinal *Methanobrevibacter smithii* but not total bacteria is related to diet-induced weight gain in rats. *Obesity* 21, 748–754. doi: 10.1002/oby.20277

Menzel, P., Ng, K. L., and Krogh, A. (2016). Fast and sensitive taxonomic classification for metagenomics with Kaiju. *Nat. Commun.* 7:11257. doi: 10.1038/ncomms11257

Nagpal, R., Neth, B. J., Wang, S., Craft, S., and Yadav, H. (2019). Modified Mediterranean-ketogenic diet modulates gut microbiome and short-chain fatty acids in association with Alzheimer's disease markers in subjects with mild cognitive impairment. *EBioMedicine* 47, 529–542. doi: 10.1016/j.ebiom.2019.08.032

Qi, K. K., Men, X. M., Wu, J., and Xu, Z. W. (2019). Rearing pattern alters porcine myofiber type, fat deposition, associated microbial communities and functional capacity. *BMC Microbiol.* 19:181. doi: 10.1186/s12866-019-1556-x

Ridaura, V. K., Faith, J. J., Rey, F. E., Cheng, J. Y., Duncan, A. E., Kau, A. L., et al. (2013). Gut microbiota from twins discordant for obesity modulate metabolism in mice. *Science* 341:1241214. doi: 10.1126/science.1241214

Samuel, B. S., Hansen, E. E., Manchester, J. K., Coutinho, P. M., Henrissat, B., Fulton, R., et al. (2007). Genomic and metabolic adaptations of *Methanobrevibacter smithii* to the human gut. *Proc. Natl. Acad. Sci. U.S.A.* 104, 10643–10648. doi: 10.1073/pnas.0704189104

Schmidt, T. S. B., Raes, J., and Bork, P. (2018). The human gut microbiome: from association to modulation. *Cell* 172, 1198–1215. doi: 10.1016/j.cell.2018.02.044

Segata, N., Izard, J., Waldron, L., Gevers, D., Miropolsky, L., Garrett, W. S., et al. (2011). Metagenomic biomarker discovery and explanation. *Genome Biol.* 12:R60. doi: 10.1186/gb-2011-12-6-r60

Serino, M., Luche, E., Gres, S., Baylac, A., Bergé, M., Cenac, C., et al. (2012). Metabolic adaptation to a high-fat diet is associated with a change in the gut microbiota. *Gut* 61, 543–553. doi: 10.1136/gutjnl-2011-301012

Shang, H. M., Song, H., Shen, S. J., Yao, X., Wu, B., Wang, L. N., et al. (2015). Effects of dietary polysaccharides from the submerged fermentation concentrate of Hericium caput-medusae (Bull.:Fr.) Pers. on fat deposition in broilers. *J. Sci. Food Agric.* 95, 267–274. doi: 10.1002/jsfa.6711

Shi, D., Bai, L., Qu, Q., Zhou, S., Yang, M., Guo, S., et al. (2019). Impact of gut microbiota structure in heat-stressed broilers. *Poult. Sci.* 98, 2405–2413. doi: 10.3382/ps/pez026

Shi, J., Zhao, D., Song, S., Zhang, M., Zamaratskaia, G., Xu, X., et al. (2020). High-meat-protein high-fat diet induced dysbiosis of gut microbiota and tryptophan metabolism in wistar rats. *J. Agric. Food Chem.* 68, 6333–6346. doi: 10.1021/acs.jafc.0c00245

Wang, K., Liao, M., Zhou, N., Bao, L., Ma, K., Zheng, Z., et al. (2019). *Parabacteroides distasonis* Alleviates Obesity and Metabolic Dysfunctions via Production of Succinate and Secondary Bile Acids. *Cell Rep.* 26, 222–235.e5. doi: 10.1016/j.celrep.2018.12.028

Wen, C., Yan, W., Sun, C., Ji, C., Zhou, Q., Zhang, D., et al. (2019). The gut microbiota is largely independent of host genetics in regulating fat deposition in chickens. *ISME J.* 13, 1422–1436. doi: 10.1038/s41396-019-0367-2

Wu, F. F., Guo, X. F., Zhang, J. C., Zhang, M., Ou, Z. H., and Peng, Y. Z. (2017). Phascolarctobacterium faecium abundant colonization in human gastrointestinal tract. *Exp. Ther. Med.* 14, 3122–3126. doi: 10.3892/etm.2017.4878

Xiang, H., Chen, S., Zhang, H., Zhu, X., Wang, D., Liu, H., et al. (2021). Removal of roosters alters the domestic phenotype and microbial and genetic profile of hens. *Sci. China Life Sci.* 64. doi: 10.1007/s11427-020-1770-1

Xu, Y., Zhu, Y., Li, X., and Sun, B. (2020). Dynamic balancing of intestinal short-chain fatty acids: the crucial role of bacterial metabolism. *Trends Food Sci. Technol.* 100, 118–130. doi: 10.1016/j.tifs.2020.02.026

Zaytsoff, S. J. M., Uwiera, R. R. E., and Inglis, G. D. (2020). Physiological stress mediated by corticosterone administration alters intestinal bacterial communities and increases the relative abundance of clostridium perfringens in the small intestine of chickens. *Microorganisms* 8:1518. doi: 10.3390/microorganisms8101518

Zhang, H., Du, Z. Q., Dong, J. Q., Wang, H. X., Shi, H. Y., Wang, N., et al. (2014). Detection of genome-wide copy number variations in two chicken lines divergently selected for abdominal fat content. *BMC Genomics* 15:517. doi: 10.1186/1471-2164-15-517

Zhang, H., Wang, S. Z., Wang, Z. P., Da, Y., Wang, N., Hu, X. X., et al. (2012). A genome-wide scan of selective sweeps in two broiler chicken lines divergently selected for abdominal fat content. *BMC Genomics* 13:704. doi: 10.1186/1471-2164-13-704

Zhang, M., Liu, L., Chen, D., Zhang, X., Zhou, C., Gan, Q., et al. (2020). Functional microRNA screening for dietary vitamin E regulation of abdominal fat deposition in broilers. *Br. Poult. Sci.* 61, 344–349. doi: 10.1080/00071668.2020.1736265

Zhang, Y., Liu, Y., Li, J., Xing, T., Jiang, Y., Zhang, L., et al. (2020). Dietary resistant starch modifies the composition and function of caecal microbiota of broilers. *J. Sci. Food Agric.* 100, 1274–1284. doi: 10.1002/jsfa.10139

Zhao, S. J., Lieberman, T. D., Poyet, M., Kauffman, K. M., Gibbons, S. M., Groussin, M., et al. (2019). Adaptive evolution within gut microbiomes of healthy people. *Cell Host Microbe* 25, 656–667. doi: 10.1016/j.chom.2019.03.007

Zheng, X., Huang, F., Zhao, A., Lei, S., Zhang, Y., Xie, G., et al. (2017). Bile acid is a significant host factor shaping the gut microbiome of diet-induced obese mice. *BMC Biol.* 15:120. doi: 10.1186/s12915-017-0462-7

Zhu, W. H., Lomsadze, A., and Borodovsky, M. (2010). Ab initio gene identification in metagenomic sequences. *Nucleic Acids Res.* 38:e132. doi: 10.1093/nar/gkq275

Zietak, M., Kovatcheva-Datchary, P., Markiewicz, L. H., Stahlman, M., Kozak, L. P., and Backhed, F. (2016). Altered microbiota contributes to reduced diet-induced obesity upon cold exposure. *Cell Metab.* 23, 1216–1223. doi: 10.1016/j.cmet.2016.05.001

Conflict of Interest: JG, HY, and HL were employed by the company Guangdong Tinoo's Foods Group Co., Ltd.

The remaining authors declare that the research was conducted in the absence of any commercial or financial relationships that could be construed as a potential conflict of interest.

frontiers in Microbiology

ORIGINAL RESEARCH
published: 19 March 2021
doi: 10.3389/fmicb.2021.633276

Yeast Culture Improves Egg Quality and Reproductive Performance of Aged Breeder Layers by Regulating Gut Microbes

Yuchen Liu[1†], Xue Cheng[1†], Wenrui Zhen[2], Dan Zeng[3], Lujiang Qu[1], Zhong Wang[2] and Zhonghua Ning[1*]*

[1] National Engineering Laboratory for Animal Breeding and Key Laboratory of Animal Genetics, Breeding and Reproduction, Ministry of Agriculture and Rural Affairs, College of Animal Science and Technology, China Agricultural University, Beijing, China, [2] State Key Laboratory of Animal Nutrition, College of Animal Science and Technology, China Agricultural University, Beijing, China, [3] Huayu Agricultural Science and Technology Co., Ltd., Handan, China

OPEN ACCESS

Edited by:
Jing Wang,
Institute of Animal Husbandry and Veterinary Medicine, Beijing Academy of Agriculture and Forestry Sciences, China

Reviewed by:
Mariusz Korczyński,
Wrocław University of Environmental and Life Sciences, Poland
Ahmed Ali Saleh,
Kafrelsheikh University, Egypt
Jing Wang,
Feed Research Institute (CAAS), China

***Correspondence:**
Zhong Wang
wangzh@cau.edu.cn
Zhonghua Ning
ningzhh@cau.edu.cn

[†] These authors have contributed equally to this work

Specialty section:
This article was submitted to Systems Microbiology, a section of the journal Frontiers in Microbiology

Received: *25 November 2020*
Accepted: *15 February 2021*
Published: *19 March 2021*

Citation:
Liu Y, Cheng X, Zhen W, Zeng D, Qu L, Wang Z and Ning Z (2021) Yeast Culture Improves Egg Quality and Reproductive Performance of Aged Breeder Layers by Regulating Gut Microbes. Front. Microbiol. 12:633276. doi: 10.3389/fmicb.2021.633276

This study aimed to investigate the effects of dietary yeast culture (YC) supplementation on egg production, egg quality, reproductive performance, immune functions, antioxidant capacity, and intestinal microbial structure of aged hens. A total of 224 Hy-Line Brown layers (54 weeks old) were randomly assigned to two dietary treatments. The control group was fed a basal diet and the YC group was supplemented with YC at 2.0 g/kg of their diet. Each group had seven replicates with 16 hens each. The study was conducted over a period of 8 weeks. Results indicated that YC addition had no significant effect on laying performance. However, it significantly improved egg quality and hatching rate, enhanced ileum crude fat digestibility, increased the serum parameters of lysozyme (LZM) and total antioxidation capacity (T-AOC) ($P < 0.05$), and reduced serum aspartate aminotransferase (AST) levels ($P < 0.05$). Using 16S rRNA analysis, we found that addition of YC significantly altered ileum microbial composition. Linear discriminant analysis of effect size (LEfSe) showed significant enrichment of *Bacilli* and *Lactobacilli* in the YC group. PICRUSt analysis of the ileal microbiota found that glutathione metabolism, ubiquinone, and other terpenoid-quinone biosynthesis and lipopolysaccharide biosynthesis protein pathways were highly enriched in the YC group compared with the basal diet group. In summary, the addition of YC can improve egg quality, immune functions, antioxidant capacity, reproduction efficiency, and digestive absorption by increasing the abundance of *Lactobacilli* and *Bacilli*. Furthermore, it also improves the biosynthesis of lipopolysaccharide proteins, glutathione metabolism, and the synthesis of ubiquinone and other terpenoid-quinone metabolic pathways.

Keywords: yeast culture, aged layer, performance, egg quality, microbiome, reproduction

INTRODUCTION

With an increase in large-scale layers, especially under conditions of high-density rearing, aged layers are susceptible to various stress factors that can lead to several problems such as imbalance in intestinal microbiota, reduction in antioxidant capacity (Liu et al., 2018), increase in immune inflammatory responses (Attia et al., 2020), and a decline in performance (Bar et al., 1999), egg quality (Bar et al., 1999), and reproductive efficiency (Liu et al., 2018). These changes lead to economic losses to the poultry industry. Although antibiotics are often used to control

and treat pathogenic bacterial infections, such as those caused by pathogenic *Escherichia coli, Clostridium perfringens*, and *Salmonella* in aged hens, their use has been gradually banned during the laying period in many countries due to egg safety, antibiotic resistance, and environmental pollution issues (Wang et al., 2015). Thus, it is important and interesting to maintain gut health, enhance antioxidant activity, and delay senescence of aged hens through nutritional strategies, thus improving their laying performance and egg quality, and extending their lifespan.

Yeast culture (YC) is a type of microecological product produced under specific conditions of yeast fermentation. It contains yeast and various metabolites. YC is rich in proteins, small peptides, oligosaccharides, vitamins, minerals, enzymes and a variety of unknown growth factors which can provide abundant nutrition for gut microbes, stimulate the proliferation of beneficial bacteria and inhibit the growth of harmful bacteria (Liu et al., 2019). Several experiments have suggested that YC has a positive effect on layers and broilers. For example, Zhang J.C. et al. (2020) reported that YC addition at 3.0 g/kg of feed improves the performance of aged layers by upregulating intestinal digestive enzyme activity and intestinal health-related gene expression. Another study in broilers showed that dietary YC supplementation at 0.1 g/kg increases daily weight gain and reduces *Campylobacter* in the cecum (Froebel et al., 2019). In addition, yeast bioactive substances can alleviate the negative effects of *Eimeria* infection on the growth of poultry, improving the structure of the jejunum mucosa and increasing the content of IgA in the egg yolk (Lu et al., 2019). The addition of YC at 2.5 g/kg activates macrophages, thereby increasing lysozyme content in the serum of laying hens, thus contributing to their resistance of pathogenic bacteria and enhancing their immunity (Gao et al., 2008). Further, studies have also reported that this immunity induced by YC is passed on to offspring and reduces symptoms of coccidiosis infection (Lu et al., 2019; Sun and Kim, 2019). In addition, some previous studies have shown that YC administration positively affects poultry laying performance and intestinal health (Zhang J.C. et al., 2020). We suspect that this is because of improvements within the intestinal microbiota community, which then increase the proportion of beneficial microorganisms and inhibit the reproduction of harmful microorganisms. However, at present, there is insufficient research on the influence of YC supplementation on the productive and reproductive performance of aged layers, and it is unclear whether YC affects these parameters by regulating the layers' intestinal microbiome. Therefore, this study aimed to explore whether YC supplementation can improve laying performance, egg quality, and reproductive performance of breeder-aged layers by improving the intestinal microbial flora structure.

MATERIALS AND METHODS

Birds, Diets, and Management

The present experiment was conducted according to the principles of the Animal Care and Use Committee of China Agricultural University. A total of 224 Hy-Line Brown laying hens (54 weeks old) were randomly assigned to two dietary treatments: a basal diet (control group, DC) and a basal diet supplemented with 2.0 g/kg of YC (Tianxiangyuan Biotechnology, Co., Ltd.), with seven replicates of 16 hens each (four birds per cage). The YC contained the following: crude protein, 53.71%; polypeptide, 12.53%; polypeptide/crude protein, 23.33%; amino acid, 1.06%; phosphorus, 7.1 mg/g; organic acid, 8.79%; pH, 4.43; and water, 46.12%. The study was conducted for an experimental period of 9 weeks (commenced from 55 weeks old), including 1 week for adaptation (54 weeks old) and 8 weeks for the experiments. The study was performed in HuaYu Poultry Breeding Co., Ltd (Handan, Hebei). All bird management was consistent with the recommendations of the Hy-Line Brown laying hen management guide. The basal diets (**Table 1**) comprised maize and soybean, and conformed to the Nutrients Requirements of Laying Hens of China (NY/T33-2004).

Performance Parameters

Egg numbers and weights were collected daily. Hens were weighed individually at the beginning and end of the experiment. The average egg yield, egg weight, broken egg ratio, abnormal egg (including double yolk egg, sand-shell egg, soft-shell egg, and those with obvious malformed-shell eggs) ratio during the intervals of 55–59 and 59–63 weeks were measured. Feed consumption was recorded, and the feed conversion ratio (FCR, feed/egg, g/g) was calculated every 28 days (FCR = feed intake per replicate/total weight of eggs laid per replicate). Mortality was documented every day as it appeared.

TABLE 1 | Ingredients and nutrient composition of basal diet.

Ingredients	Percent	Nutrient level[c]	Percent
Corn (CP 8.3%)	64.0	ME (MJ/kg)	16.01
Soybean meal (CP 44.0%)	19.8	CP (%)	16.04
Soybean oil	0.7	CF (%)	3.24
Wheat bran	3.0	Methionine (%)	0.24
Limestone	9.5	Lysine (%)	0.70
Calcium hydrogen phosphate	1.00	Calcium (%)	3.49
Sodium chloride	0.30	Total P (%)	0.32
DL-Methionine (98%)	0.10		
L-Lysine HCL (78%)	0.07		
Vitamin premix[a]	0.03		
Mineral premix[b]	0.20		
Choline chloride (50%)	0.15		
Phytase	0.02		
NSP enzyme	0.02		
Total	100.0		

[a]*Supplied per kilogram of diet: vitamin A, 13,500 IU; vitamin D3, 4,500 IU; vitamin E, 75 IU; vitamin K3, 3.6 mg; vitamin B1, 3.0 mg; vitamin B2, 9.24 mg; vitamin B6, 6.0 mg; nicotinic acid, 66 mg; pantothenic acid, 16.8 mg; biotin, 0.54 mg; folic acid, 2.10 mg; vitamin B12, 0.03 mg; vitamin C, 135 mg; choline, 675 mg; ethoxyquinoline, 15 mg.*

[b]*Mineral premix provided per kilogram of complete diet: iron, 80 mg; copper, 10 mg; manganese, 100 mg; zinc, 100 mg; iodine, 0.35 mg; selenium, 0.30 mg.*

[c]*ME, CP, and CF were measured values, and the other nutrients were calculated values.*

Egg Quality Parameters

At the end of the study, 70 eggs were randomly collected per group (10 eggs per replicate) to determine egg quality indices. Egg index and eggshell color were measured using an egg-shaped index tester and an eggshell color tester (Konicaminolta CM-2600d), respectively. The color indices L*, a*, and b* represent lightness, redness, and yellowness, respectively. Eggshell breaking strength was measured using a quasi-static compression device (Robotmation, Japan). Eggshell thickness was measured at three locations, the lower end, middle end, and upper end, by using a micrometer screw gauge. Albumen height, Haugh units, and yolk color were measured using an automatic egg quality analysis instrument (Robotmation EMT-5200, Japan).

Blood Biochemical Parameters

Blood samples from the wing vein were collected from one hen per replicate at the end of the experiment. Serum was collected and stored at −20°C until analysis. The kits for analyzing Immunoglobulin G (IgG), Immunoglobulin A (IgA), Lysozyme (LZM), Malondialdehyde (MDA), Glutathione (GSH), Glutathione Peroxidase (GSH-PX), total antioxidation capacity (T-AOC), alanine aminotransferase (ALT), and aspartate aminotransferase (AST) were purchased from Nanjing Jiancheng Bioengineering Institute (Nanjing, China). The standard hemagglutination antigens H5N6, H5N8, and Newcastle disease (ND) (Qingdao Yebio Bioengineering Co., Ltd., China) were used to detect serum antibody titers using the hemagglutination-inhibition assay.

Ileal Nutrient Digestibility

From days 52 to 56 of the experiment, 0.5% titanium dioxide, an indigestible marker, was mixed into the feed of each group. At the end of the study, eight hens were slaughtered by cervical dislocation, and their ileum samples were collected in a circular aluminum box. These were immediately held on dry ice and quickly transferred to a −80°C refrigerator for storage until analysis. In the same group, ileum contents of every two hens were mixed, dried by baking at 105°C for 24 h, removed, and then placed in a desiccator for 4 h until the weight was constant. The contents were then ground (0.5 mm screen) for later use. The samples were used for analyzing crude protein, crude fat, and gross energy according to the standard procedures of the Association of Official Analytical Chemists (2006).

Reproductive Performance

All the hens were inseminated for two consecutive days, on the 51st and 52nd day, of the formal experiment. The semen was mixed and came from the same group of cocks to ensure that the semen quality would not affect fertilization and incubation. Breeding eggs were then collected on the 55th day. The total number of eggs produced on that day and the number of qualified breeding eggs were recorded. The breeding eggs were uniformly transferred to a commercial hatchery for incubation. On the 18th day of incubation, the eggs were illuminated, and the number of fertilized eggs in each group was recorded. The same repeating group of fertilized eggs were then placed in a string bag with a recording card. On the 21st day of incubation, the total number of nestlings and healthy nestlings were recorded. Finally, the rates of hatched eggs and fertilized eggs, the hatching rate, and the healthy bird rate were calculated.

Intestinal Microbiome

Six birds were randomly selected per treatment at the end of the experiment. The ileal microbial genomic DNA was extracted using the QIAamp 96 PowerFecal QIAcube HT kit (5) (Cat. No. 51531) according to the manufacturer's protocols. Quality and quantity of DNA were verified using NanoDrop and agarose gel electrophoresis. The extracted DNA was diluted to a standard concentration of 1 ng/μL and stored at −20°C until further processing. The universal bacterial V3–V4 region of the 16S rRNA genes was amplified using polymerase chain reaction (PCR) bar-coded primers 343 F (5′-TACGGRAGGCAGCAG-3′) and 798 R (5′-AGGGTATCTAATCCT-3′). PCR was performed at 95°C for 2 min, followed by 30 cycles of 95°C for 30 s, annealing at 55°C for 30 s and at 72°C for 30 s, and a final extension at 72°C for 5 min. PCR products were detected using 1% agarose gel electrophoresis. They were further purified using the AxyPrep DNA Gel Extraction Kit (Axygen Biosciences, Union City, CA, United States) and quantified using QuantiFluor^{TM} ONE dsDNA System (Promega, United States) according to the manufacturers' protocols. The purified amplicons were pooled in equimolar concentrations and loaded on an Illumina MiSeq platform (Oebiotech, Shanghai, China). Sequencing was performed using a paired-end (2 × 300) configuration. All operations followed standard protocols. The raw data were uploaded to the National Center for Biotechnology Information's Sequence Read Archive database (SRA accession: PRJNA675783).

Bioinformatics Analyses

Bacterial data were subjected to bioinformatics analyses. Raw sequencing data, which were in the FASTQ format, were demultiplexed and quality-filtered using QIIME software (version 1.8.0) (Caporaso et al., 2010). First, trimmomatic software (Bolger et al., 2014) was used to pre-process the paired-end sequences and detect and remove ambiguous bases. Second, FLASH software (Reyon et al., 2012) was used to assemble paired-end reads. Reads with Q20 values greater than 75% were retained, and chimaeras in reads were removed. Removed primer sequences were subjected to the Vsearch software and clustered with clean reads (Edgar et al., 2011). A sequence similarity of 97% was used to classify and generate operational taxonomic units (OTUs). All representative sequences were annotated and blasted against the Silva database (version 123) with the RDP classifier (confidence threshold of 70%) (Wang et al., 2007). Alpha and beta diversity were calculated using QIIME 1.8 scripts. The Venn diagram and species accumulation curves were implemented using the R Vennerable and vegan packages, respectively.

Linear discriminant analysis of effect size (LEfSe) and indicator analysis were used to identify iconic representative species. LEfSe analysis[1] was performed to identify taxonomic compositions that were significantly altered by YC treatment.

[1] http://huttenhower.sph.harvard.edu/galaxy/

A linear discriminant analysis value higher than 4.0 and alpha value for the factorial Kruskal–Wallis test with P value below 0.05 were selected for plotting and analysis. Then, we performed indicator species analysis, and the R indval package was used to detect potential signature OTUs.

Phylogenetic Investigation of Communities by Reconstruction of Unobserved States (PICRUSt 1.0.0) was used to predict metagenome functions of each sample based on its 16S rRNA marker gene sequences (Langille et al., 2013). We selected a closed reference OTU and used the sampled reads against the Greengenes 16S rRNA Gene Database (13.5). PICRUSt software was used to normalize the resulting OTU table and make metagenomic inferences with the Kyoto Encyclopaedia of Genes and Genomes (KEGG) Orthologs databases. STAMP software (Parks et al., 2014) was used to visualize significant differences in KEGG functional pathways at level 2 or 3 by Welch's t-test using the Benjamini–Hochberg false discovery rate method. All PICRUSt analyses were performed online: https://huttenhower.sph.harvard.edu/galaxy/root.

Microbial network analysis was used to explore the relationships among bacteria. The R psych package was used to calculate the correlation coefficient and P value. Values of $P > 0.05$ and $r < 0.6$ were treated with 0. Then, the Gephi 0.9.2 software was used to visualize the network correlation diagram for microbes.

Statistics Analysis

All the apparent data were analyzed using the statistical software SPSS 24.0 (SPSS Inc., Chicago, IL, United States). Normalized data were analyzed with a normal distribution test and homogeneity test of variance. Student's t-test was used for the indices that passed the test; otherwise, the Wilcoxon non-parametric test was used. The measurement of the relative abundance (%) of bacteria within the microbiome at phylum and genus levels was performed using the non-parametric Kruskal–Wallis test to validate the significant difference. The results were expressed as the mean and standard error. Differences at $P < 0.05$ were considered significant, whereas P values between 0.05 and 0.1 were interpreted as trends.

RESULTS

Laying Performance and Egg Quality

The laying performance analysis data of hens are shown in **Table 2**. No significant difference was observed in egg yield, egg weight, FCR, and body weight among the groups ($P > 0.05$). However, the damaged egg ratio at 55–59 weeks of age showed a significant reduction trend ($P = 0.059$). The egg quality index analysis data are shown in **Table 3**. During the 8-week experimentation period, the addition of YC significantly improved egg quality, thus increasing shell strength, yolk color, egg albumen, height, and the Haugh unit.

Blood Biochemical Parameters

The blood biochemical parameters data are shown in **Table 4**. The serum parameters of lysozyme and T-AOC significantly increased, while AST levels significantly decreased in the YC group. However, serum antibody responses were not significantly influenced by YC addition.

Reproductive Performance

The reproductive performance analysis data are shown in **Table 5**. Results showed that YC supplementation significantly increased the hatching rate, showing an evident trend, thus augmenting the rate of fertilization ($P = 0.075$) and number of healthy chicks ($P = 0.064$). However, YC did not affect the rate of qualified eggs.

TABLE 2 | Effect of supplemental yeast culture (YC) on performance of laying hens.

Items	Egg production, %	Egg weight, g	Damaged egg, %	Abnormal egg, %	FCR, g feed/g egg	Feed intake, g/day/hen	Body weight, kg
Values at 55–59 weeks of age							Initial
DC	74.1	62.2	4.9	2.8	2.3	107.2	2.1
YC	78.3	62.2	3.5	3.4	2.3	109.4	2.1
SEM	1.58	0.32	0.39	0.46	0.44	0.99	0.02
P-value	0.2	1	0.06	0.55	0.36	0.29	0.74
Values at 59–63 weeks of age							–
DC	76.5	62.6	4.4	5.3	2.4	115.3	–
YC	74.8	62.4	4.8	5.8	2.5	114.5	–
SEM	2	0.23	0.6	0.74	0.06	1.22	–
P-value	0.68	0.76	0.73	0.74	0.7	0.75	–
Values at 55–63 weeks of age							Final
DC	75.3	62.4	4.6	4.1	2.4	111.2	2.2
YC	76.6	62.3	4.1	4.5	2.4	111.8	2.1
SEM	1.56	0.26	0.42	0.57	0.04	0.98	0.03
P-value	0.69	0.87	0.56	0.68	0.77	0.75	0.74

FCR, feed conversion ratio.

TABLE 3 | Effect of supplemental YC on the egg quality of laying hens.

Item	DC	YC	SEM	*P*-value
Egg index	1.3	1.3	0.00	0.80
L	59.2	59.5	0.38	0.67
A	18.7	18.5	0.17	0.46
B	30.1^a	29.5^b	0.14	0.02
Shell strength, kg/cm^2	4.0^b	4.3^a	0.07	0.02
Egg weight, g	61.1	61.6	0.38	0.57
Yolk color	7.7^b	8.1^a	0.09	0.01
Egg albumen height, mm	5.8^b	6.1^a	0.07	0.02
Haugh unit	74.6^b	77.0^a	0.53	0.02
Eggshell thickness, mm	0.4	0.4	0.00	0.26

^{a,b}*Different superscripts within a row means significantly different (P < 0.05).*

TABLE 4 | Effect of supplemental YC on the serum parameters of laying hens.

Item[1]	DC	YC	SEM	*P*-value
Blood biochemical parameters				
IgG, g/L	4.4	4.5	0.15	0.93
IgA, g/L	2.2	2.2	0.04	0.65
LZM, μg/mL	4.4^b	5.0^a	0.14	0.03
MDA, nmol/mL	5.6	5.5	0.13	0.92
GSH, mg/L	3.2	3.1	0.04	0.46
GSH-PX, active unit	619.7	594.9	10.23	0.26
T-AOC, U/mL	6.2^b	6.8^a	0.15	0.05
ALT, U/L	0.9	0.7	0.15	0.66
AST, U/L	196.3	176.4	5.93	0.09
Antibody titers				
H5-6, log_2	7.5	6.7	0.26	0.11
H5-8, log_2	8.8	8.5	0.19	0.40
ND, log_2	11.5	12.0	0.22	0.27
H9, log_2	11.5	11.8	0.19	0.40

^{a,b}*Different superscripts within a row means significantly different (P < 0.05).*
^{1}*IgG, Immunoglobulin G; IgA, Immunoglobulin A; LZM, Lysozyme; MDA, Malondialdehyde; GSH, Glutathione; GSH-PX, Glutathione Peroxidase; T-AOC, Total Antioxidant Capacity; ALT, Alanine Aminotransferase; AST, Aspartate Aminotransferase; ND, Newcastle disease.*

TABLE 5 | Effect of supplemental YC on hatching rate of laying hens.

Item	Qualified egg rate, %	Fertilization rate,%	Hatching rate, %	Healthy chick rate, %
DC	88.6	87.9	87.0^b	86.8
YC	88.8	93.2	94.9^a	98.8
SEM	1.71	1.49	1.96	3.29
P-value	0.97	0.08	0.04	0.06

^{a,b}*Different superscripts within a column means significantly different (P < 0.05).*

Ileum Nutrient Digestibility

The ileum nutrient digestibility analysis data are shown in **Table 6**. Although YC supplementation significantly improved the digestibility of ileum crude fat, the effect on digestibility of crude protein and energy was of little significance.

TABLE 6 | Effect of supplemental YC on the nutrient digestibility of laying hens.

Item	Crude protein, %	Energy, %	Crude fat, %
DC	77.3	76.7	64.0^b
YC	79.8	77.3	81.3^a
SEM	1.28	1.36	4.62
P-value	0.40	0.84	0.05

^{a,b}*Different superscripts within a column means significantly different (P < 0.05).*

Intestinal Bacterial Richness, Diversity, and Similarity

A total of 321,038 clean tags and 300,949 valid tags were obtained through sequencing. Through these, an average of 27,359 high-quality sequences were harvested for each ileal sample. Both the Good's coverage rarefaction curve and the species accumulation curve indicated that the sequencing depth and sample quantity were sufficient to fully reflect the ileum microbial community composition (**Figures 1A,B**).

The DC and the YC groups harvested 468 and 454 OTUs, respectively. Out of these, 248 were present in both groups (**Figure 1D**). Alpha diversity was evaluated using the Chao1 diversity index, through observed species richness, the Simpson's diversity index, and the Shannon diversity index (**Figure 1C**). Results indicated that the Shannon (P = 0.023) and Simpson's diversity indices (P = 0.001) of the YC group were significantly higher than those for the DC group, indicating that the former group's intestinal flora is more evenly distributed.

Beta diversity, which was based on weighted UniFrac distances, was calculated using principal coordinate analysis through both 2D and 3D plots (**Figure 2**). The DC and YC groups were well separated, with 63.35, 15.49, and 11.11% variation explained by principal components PC1, PC2, and PC3, respectively (ANOSIM = 0.041). Results showed that microorganism composition in the ileum of hens was significantly altered by YC supplementation.

Ileal Microbial Community Structure

The ileal microbial community structure is shown in **Figures 3A,B**. **Figure 3A** indicates the relative abundance of microbial composition at the phylum level. Accounting for more than 98% of the bacterial community, Firmicutes, Proteobacteria, and Bacteroidetes were the predominant phyla in the DC and YC groups. However, in the DC group only, the relative abundance of Firmicutes decreased from 90.79 to 77.54% (P = 0.144), while that of Proteobacteria increased from 5.94% to 17.19% (P = 0.201). The relative abundance of other bacterial phyla did not change significantly.

Figures 3B,C and **Table 7** show the relative abundance of the ileal microbial composition at the genus level. Results revealed that *Lactobacilli*, *Romboutsia*, *Tyzzerella_3*, and *Turicibacter* were the predominant genera, followed by *Enterococcus*, *Gallibacterium*, *Helicobacter,* and *Escherichia_Shigella*. Among them, the relative abundance of *Lactobacilli* increased from 14.38 to 49.83% (P = 0.032), while that of *Romboutsia* decreased from 58.68 to 19.54% (P = 0.028) when YC was added.

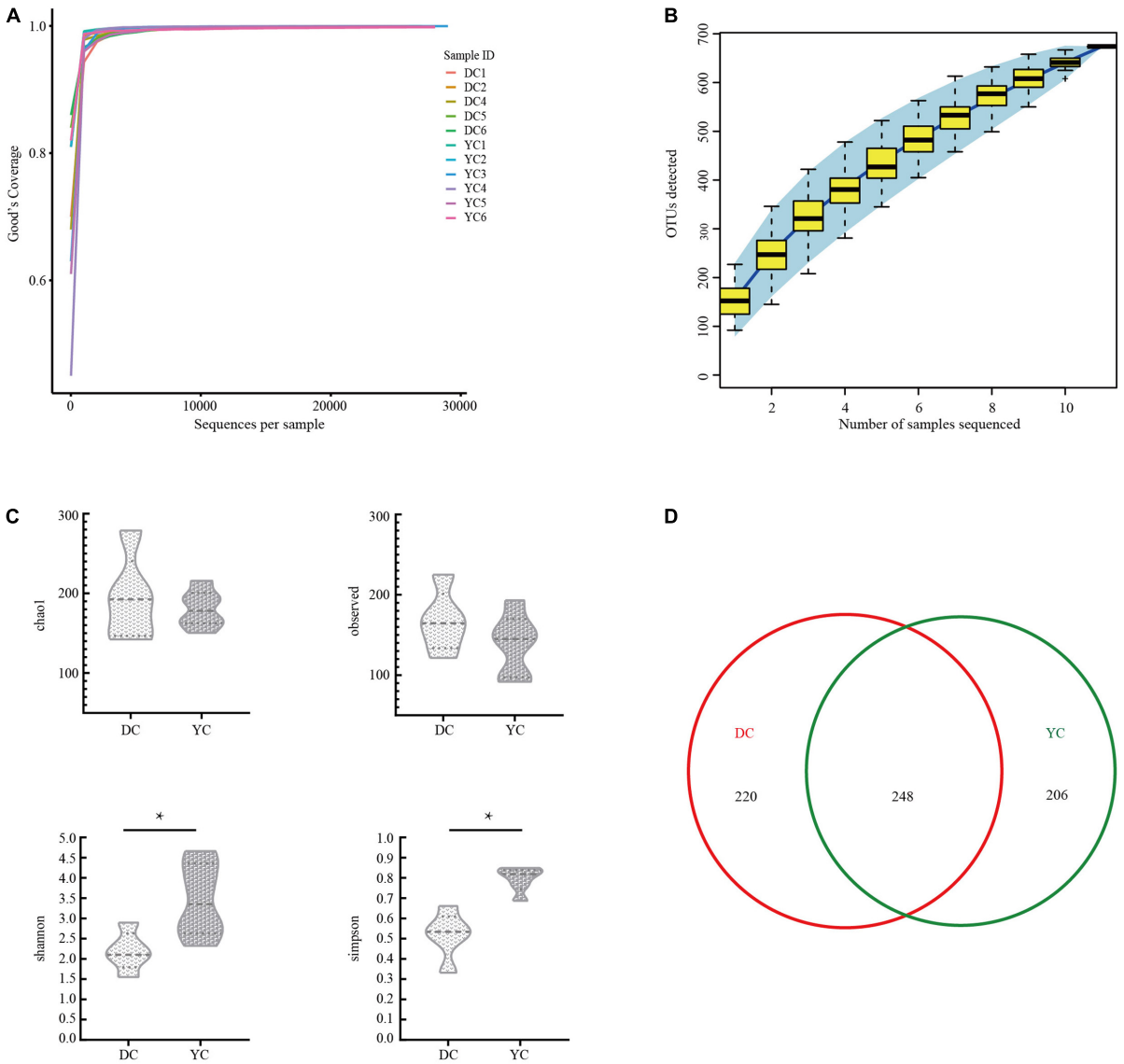

FIGURE 1 | The overall description of gut microorganism in basal diet control group (DC) and yeast culture (YC) group. **(A)** The alpha diversity rarefaction curve of 16S rRNA gene sequence to estimate the rationality of sequencing depth (at 97% similarity). *X*-axis was the sequencing sampling depth, and the *Y*-axis was the corresponding Good's Coverage index. Different sample curves were represented by different colors. **(B)** Species accumulation curve is used to estimate the rationality of sequencing sample quantity. The *X*-axis is the number of sequencing samples, and the *Y*-axis is the number of operational taxonomic unit (OTU) detected. **(C)** Alpha-diversity evaluation of ileum flora richness and evenness. **(D)** Venn diagram is used to represent the amount of OUTs that is unique or common to each group.

LEfSe analysis was conducted to determine differential bacterial form. In the YC group, Bacilli, *Lactobacilli*, and Gammaproteobacteria were significantly enriched; in the DC group, Peptostreptococcaceae, Clostridia, and *Romboutsia* were significantly enriched (**Figures 4A,B**).

To extend and confirm the LEfSe results, indicator analysis was performed at the OTU level (**Figure 4C**). Results showed that *Lactobacilli* (OTU_47, OTU_4) were the indicator species in the YC group while *Romboutsia* (OTU_13), *Roseburia* (OTT_578), *Faecalibacterium* (OTT_43), and *Prevotellaceae_UCG_001* (OTU_208) were the indicator species in the DC group.

Ileal Microbial Network

A microbial interaction network was used to analyze the reciprocity relationships among bacterial communities. **Figure 5** describe the interaction networks of the YC and DC groups, respectively. In the DC group, the bacterial network comprised 33 nodes and 72 edges, with an average node connectivity degree of 4.364. In the YC group, the bacterial network comprised 71 nodes and 376 edges, with an average node connectivity degree of 10.592. The network complexity of the YC group was higher than that of the DC group, indicating that the microbiota of the YC group was more closely related to each other. In the

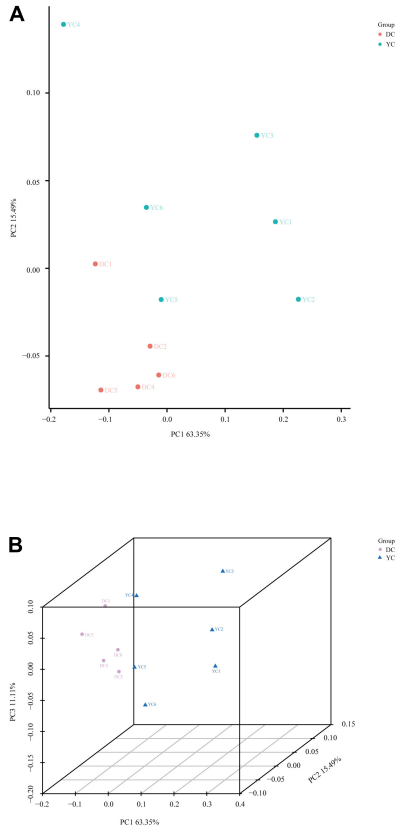

FIGURE 2 | Principal coordinate analysis of ileal microbial community. **(A)** (PCoA)-2D. **(B)** (PCoA)-3D.

YC group, *Neisseria* and *Odoribacter* showed the highest node connectivity degree (degree = 22), followed by *Alloprevotella*, *Rhizobium*, *Methylophilus*, *Prevotellaceae_NK3B31_group*, and *Bacteroides* (degree = 21). However, predominant bacteria such as *Lactobacilli* (degree = 9) and *Romboutsia* (degree = 2) had very low node connectivity degree. In the DC group, *Alloprevotella*, *Roseburia*, and *Bacteroides* had the highest node connectivity degree (degree = 11), followed by *Prevotellaceae_UCG_001*, *Rikenellaceae_RC9_gut_group,* and *Lachnospiraceae_NK4A136_group* (degree = 9). Similar to the YC group, predominant bacteria such as *Romboutsia* (degree = 1) and *Lactobacilli* (degree = 1) showed relatively low node connectivity degree in the DC group.

In the YC and DC groups, *Lactobacilli* and *Romboutsia* showed the highest proportions, respectively. The positive correlation was more than the negative correlation. Moreover, in the network interaction structure, the bacterial groups with the highest and lowest relative abundance in the intestinal tract had a lower degree of correlation with other bacteria.

Predicted Functions of Ileal Bacterial Communities

PICRUSt analysis was used to predict metagenome functions associated with bacterial communities based on 16S rRNA sequencing data. Results showed significant differences between groups at KEGG levels 2 and 3 (**Figure 6**). At KEGG level 2, the glycan biosynthesis and metabolism pathways were significantly enriched by YC supplementation, while the transcription pathway was significantly downregulated. At KEGG level 3, seven pathways were enriched through YC supplementation, including the phosphatidylinositol signaling system, glutathione metabolism, ubiquinone and other terpenoid-quinone biosynthesis, chaperones, and folding catalysts, lipopolysaccharide biosynthesis proteins, and cell motility and secretion. Pathways such as ABC transporters, transporters, and sporulation were overrepresented in the DC group.

DISCUSSION

Yeast culture did not significantly affect the laying performance of layers, a result that was not in agreement with some previous studies. Zhang J.C. et al. (2020) reported that adding 3.0 g/kg YC to the feed of 67-week-old hens can improve their egg-laying rate and the total egg weight, and reduce the feed/egg ratio. Lu et al. (2019) found that the addition of YC alleviated laying performance loss and intestinal damage caused by *Eimeria* in broiler breeders. The variable results of the present study could be attributed to the good health of the hens used in this experiment. Additionally, some reports have indicated that differences may be due to the changes in the treatment of YC, especially factors such as administration time and period, diet, and environment (Gadde et al., 2017).

In this study, YC was found to significantly increase eggshell strength, egg albumen height and Haugh unit. However, it significantly reduced the b* value of egg shell color. In line with our findings, several previous studies have demonstrated that adding yeast or yeast extract can significantly improve egg weight, albumen height, Haugh unit, eggshell strength, and nutrient content (Zhong et al., 2016; Özsoy et al., 2018; Gaboardi et al., 2019); however, other studies have shown that dietary YC supplementation has no significant effect on eggshell strength, egg weight, albumen height, Haugh unit, and yolk color (Yalçin et al., 2008; Zhang J.C. et al., 2020). The positive effect of YC on egg quality may be associated with the presence of bioactive substances such as enzymes, vitamins, amino acids, polypeptides, and oligosaccharides in it (Jensen et al., 2008). Moreover, the presence of many carotenoids in YC, which promote pigment deposition in the egg yolk, may also be a factor in its effectiveness (Kot et al., 2019). As our results indicate improvements in egg quality, the increased hatching rate, the improved fertilization rate, and the healthy chick rate can also be associated with the egg quality and the increased eggshell strength and density, which prevent pathogenic microorganisms from entering the eggs. Moreover, YC also contains a large amount of trace elements, such as selenium and zinc that improve embryonic and early postnatal development of the aged layer (Hostetler et al., 2003; Sun et al., 2012). A previous study has shown that adding yeast bioactives significantly improves the level of IgA in the egg yolk (Lu et al., 2019), resulting in enhanced chick immunity and improved reproductive performance of the aged layers.

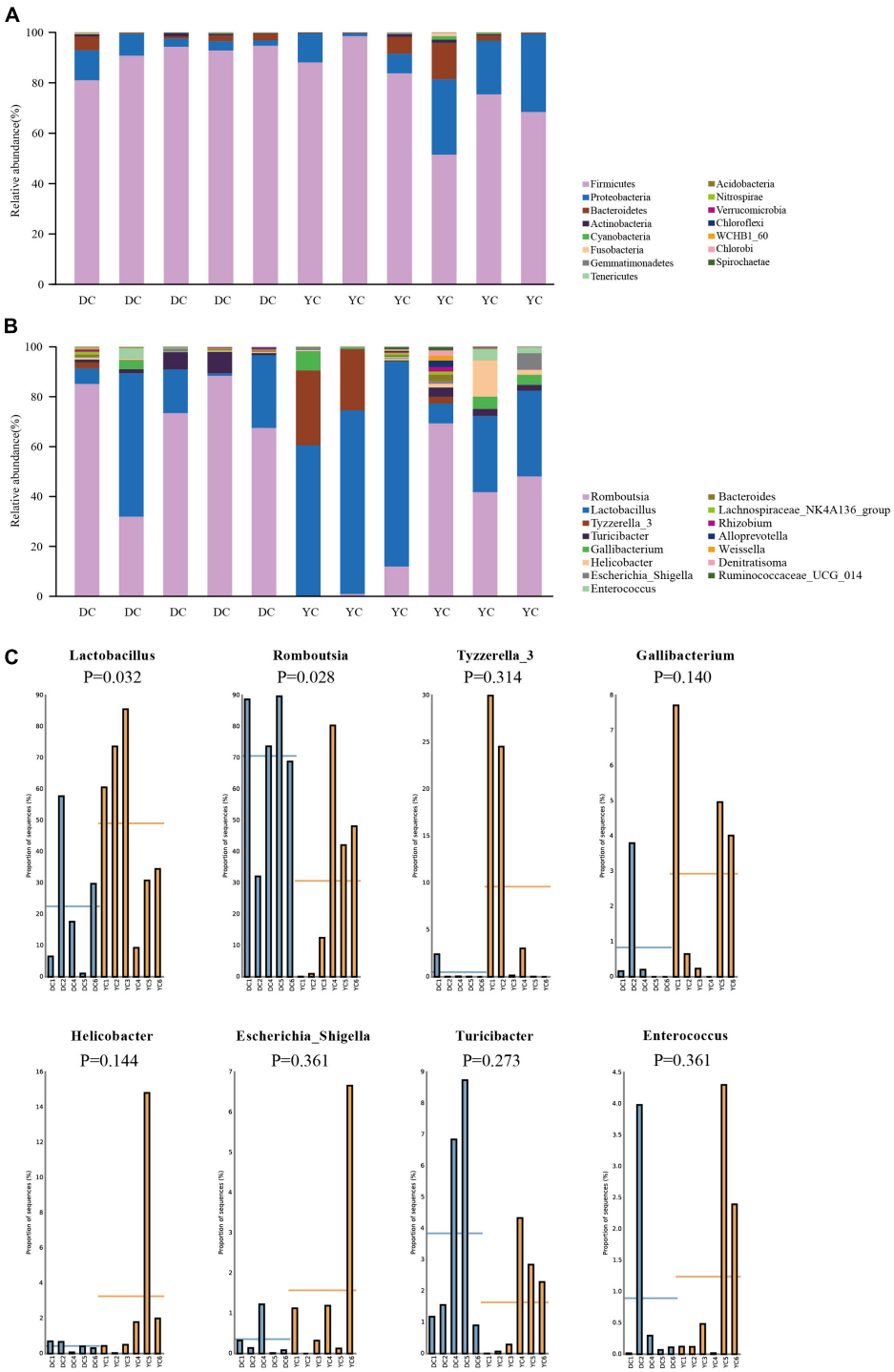

FIGURE 3 | The microbial community structure in DC and YC groups. **(A)** Stacked bar chart of ileum microbial structure at phylum level. Top15 bacterial are shown in the graph. **(B)** Stacked bar chart of ileum microbial structure at genus level. Top15 bacterial are shown in the graph. **(C)** Relative abundance of microbial which was greater than 1% between DC and YC groups.

Hens in the late laying stage are considered to be affected by oxidative stress and ovarian aging; furthermore, an increase in lipid and protein oxidation substantially influences the normal physiology of layers (Liu et al., 2018). To counter such oxidation, T-AOC is an important integrative index that reflects antioxidant capacity (Zhang S. et al., 2020). Our results indicated that YC supplementation significantly increased lysozyme and T-AOC in serum and reduced serum AST. Similarly, a previous study

TABLE 7 | Effect of supplemental YC on the Ileum bacteria of laying hens at genus level (%).

Classification levels of bacteria		Diet[1]		SEM[2]	*P*-value
Phylum	**Genus**	**DC**	**YC**		
Firmicutes	*Lactobacillus*	14.4^{b}	49.8^{a}	4.79	0.03
Firmicutes	*Romboutsia*	58.7^{a}	19.5^{b}	8.88	0.03
Firmicutes	*Tyzzerella_3*	0.4	9.1	3.23	0.31
Firmicutes	*Turicibacter*	3.3	1.1	0.80	0.27
Firmicutes	*Enterococcus*	0.4	1.0	0.34	0.36
Proteobacteria	*Gallibacterium*	0.4	2.6	0.73	0.14
Proteobacteria	*Helicobacter*	0.3	2.6	1.09	0.14
Proteobacteria	*Escherichia_Shigella*	0.3	1.2	0.45	0.36
Bacteroidetes	*Uncultured_bacterium*	0.7	1.4	0.51	0.86
–	Other	16.1	11.1	5.48	0.86

[1] *The relative abundance of Genus less than 1% are not listed. Values are means, n = 6.*
[2] *SEM, standard error of the mean.*
[a,b] *Different superscripts within a row means significantly different (P < 0.05).*

showed that supplemented yeast hydrolysates tended to increase serum T-AOC (Fu et al., 2019). Thus, improvements in serum T-AOC and lysozyme activity indicated that YC administration can improve antioxidant capacity and enhance innate immunity (Min et al., 2015) of layers. AST normally exists in liver cells, and plasma AST and alanine aminotransferase contents are the most sensitive indicators of liver injury in poultry (Lumeij, 1997; Yousefi et al., 2005). Under normal circumstances, the upper limit of AST content in poultry plasma is 230 IU/L (Jones, 1999). In our study, AST content in both groups was within the normal range; however, it showed a trend of significant decrease after YC addition, which is a positive signal for liver function.

Feed digestibility and absorption gradually decreased as the age of layer hens increased (Duan et al., 2015). Thus, improving feed digestibility and availability through nutritional strategies is important to maintain constant egg production, egg quality, and health in aged hens. The results of this study showed that YC supplementation significantly improved the digestibility of crude fat, but its effect on the digestibility of energy or crude protein was of little significance. The digestion, absorption, and utilization of fat largely depend on trypsin digestive enzymes and emulsifiers (Aloulou et al., 2015). Additionally, studies have shown that the addition of YC can significantly increase the activity of duodenal enzymes in aged layers. Moreover, YC is known to contain enzymes and organic acids. Thus, our results suggest that increased fat digestion and absorption is possibly related to stimulating endogenous enzyme secretion or enzymes contained in YC (Dawood et al., 2020;

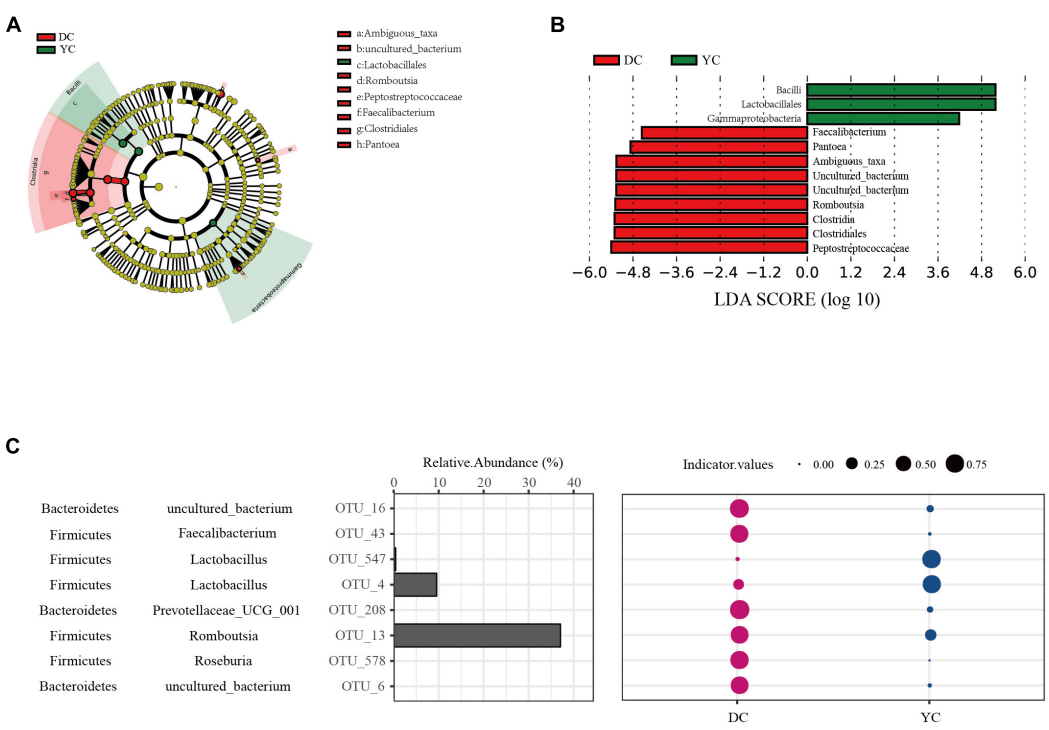

FIGURE 4 | Ileal marker microbial in DC and YC groups. **(A,B).** Linear discriminant analysis coupled with effect size (LEfSe) is used to explore differences between treatment groups. **(A)** Cladogram plot of LEfSe analysis. **(B)** Histogram of LDA value distribution between DC and YC groups. **(C)** Indicator analysis is used to search for Indicator OTUs. The first column is phylum level annotation information, the second column is genus level annotation information, the third column represents the corresponding OTU, the fourth column represents the relative abundance of each OTU, and the bubble diagram represents the indicator values. Only significant ($P < 0.05$) OTUs are shown.

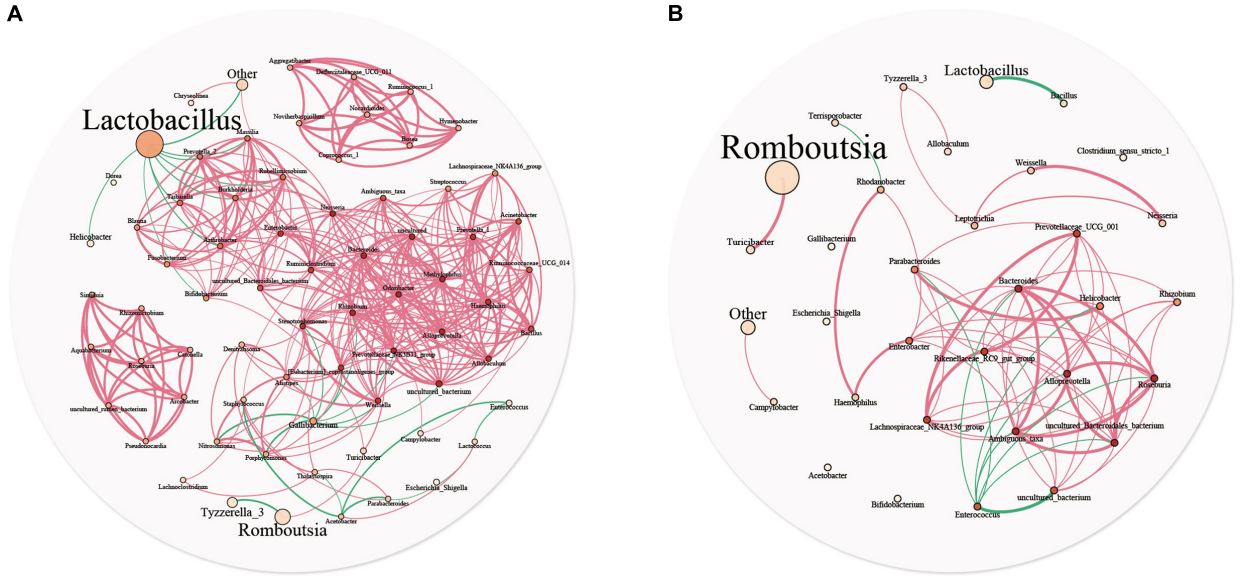

FIGURE 5 | Microbial community network analysis is used to explore the relationship between the two groups. Each genus is represented by different nodes, the size of which represents the relative abundance of the genus, and the color of the nodes represents the degree. The thickness of the edges represents the correlation coefficient, the thicker, the greater of correlation. The red line represents positive correlation, and the cyan line represents negative correlation.

Zhang J.C. et al., 2020). Intestinal microorganisms can produce bioactive substances and substantially influence health, nutrition, and immunity (Hooper et al., 2002; Ley et al., 2008; Xu M. et al., 2020). Our study showed that adding YC could alter the ileum microbial community structure in aged layers. The results of this study showed that Firmicutes, *Bacteroides*, and Proteobacteria were the dominant microbial species in the ileum, which was confirmed by other studies (Wang et al., 2018; Spring et al., 2020). After YC supplementation, the relative abundance of Firmicutes decreased (from 90.76 to 77.64%) while that of Proteobacteria (from 5.92 to 17.08%) and Bacteroidetes (from 2.31 to 3.94%) increased. The proportion of Firmicutes/*Bacteroides* (F/B) also increased (from 100.12 to 332.29). Studies have shown that the F/B ratio is related to inflammatory bowel disease (Frank et al., 2007), obesity (Turnbaugh et al., 2008), and type 2 diabetes mellitus (Remely et al., 2014). In this study, the decrease in Firmicutes and the increased F/B values indicated that YC might have a regulating effect on lipid metabolism and gut health and also reduce fat deposition in aged layers.

All the results of this study indicated that *Lactobacilli* were the dominant genus in the ileum, accompanied by a significant decrease in *Romboutsia* in the YC group. A study by Li et al. (2018) found that in day-old sika deer, *Halomonas* (48.9%), *Lactobacilli* (21.4%), and *Escherichia Shigella* (19.2%) were the dominant genera in the jejunum and ileum; with increasing age, the abundance of *Lactobacilli* began to reduce gradually from 21.4 to 6.0%. *Romboutsia* appeared and gradually became the dominant species with a relative abundance of 22.9%. Since our results suggest higher abundance of *Lactobacilli* in the intestinal tract after YC supplementation, it may be a good indicator of aged layers as *Lactobacilli* are involved in metabolic activity, such as decomposing proteins and sugars in food, synthesizing vitamins and promoting the fermentation and degradation of fat (Wu et al., 2015). Moreover, carbohydrates can be converted by *Lactobacilli* into lactic acid for further use by other bacteria (Wu et al., 2018). *Lactobacilli* have been shown to be negatively correlated with lipid metabolism. They accelerate the synthesis of lipid peroxidation metabolites and are positively related to intestinal health (Chen et al., 2020). Some experiments related to the addition of *Lactobacilli* also revealed that they have the potential to improve the performance, digestion, and feed utilization efficiency of broilers and laying hens (Saleh et al., 2017, 2020). *Romboutsia* can metabolize carbohydrates, synthesize amino acids and vitamins, and are sensitive to bile acids (Gerritsen et al., 2017). Some studies suggest that *Romboutsia* may be linked to obesity (Hu et al., 2019) and liver injury (Yu et al., 2020). Furthermore, a large number of studies have directly or indirectly proved that *Romboutsia* and *Lactobacilli* show opposing trends in relative abundance (Chen et al., 2019; Lee et al., 2019; Qiao et al., 2019; Xu S. et al., 2020). Based on these results, we can speculate that these two bacteria have especially strong competitive exclusion effects. The increased abundance of *Lactobacilli* following a decrease in *Romboutsia* may be due to polysaccharides in YC being used by *Lactobacilli* to produce a large number of short-chain fatty acids and lactic acid, which reduce intestinal pH. Another reason may be the increased shedding of *Romboutsia* due to the occupied effect of *Lactobacilli* (Baldwin et al., 2018; Qiao et al., 2018; Bunte et al., 2020).

Gut microbes can convert indigestible glycans into short-chain fatty acids such as butyrate, propionate, and acetate

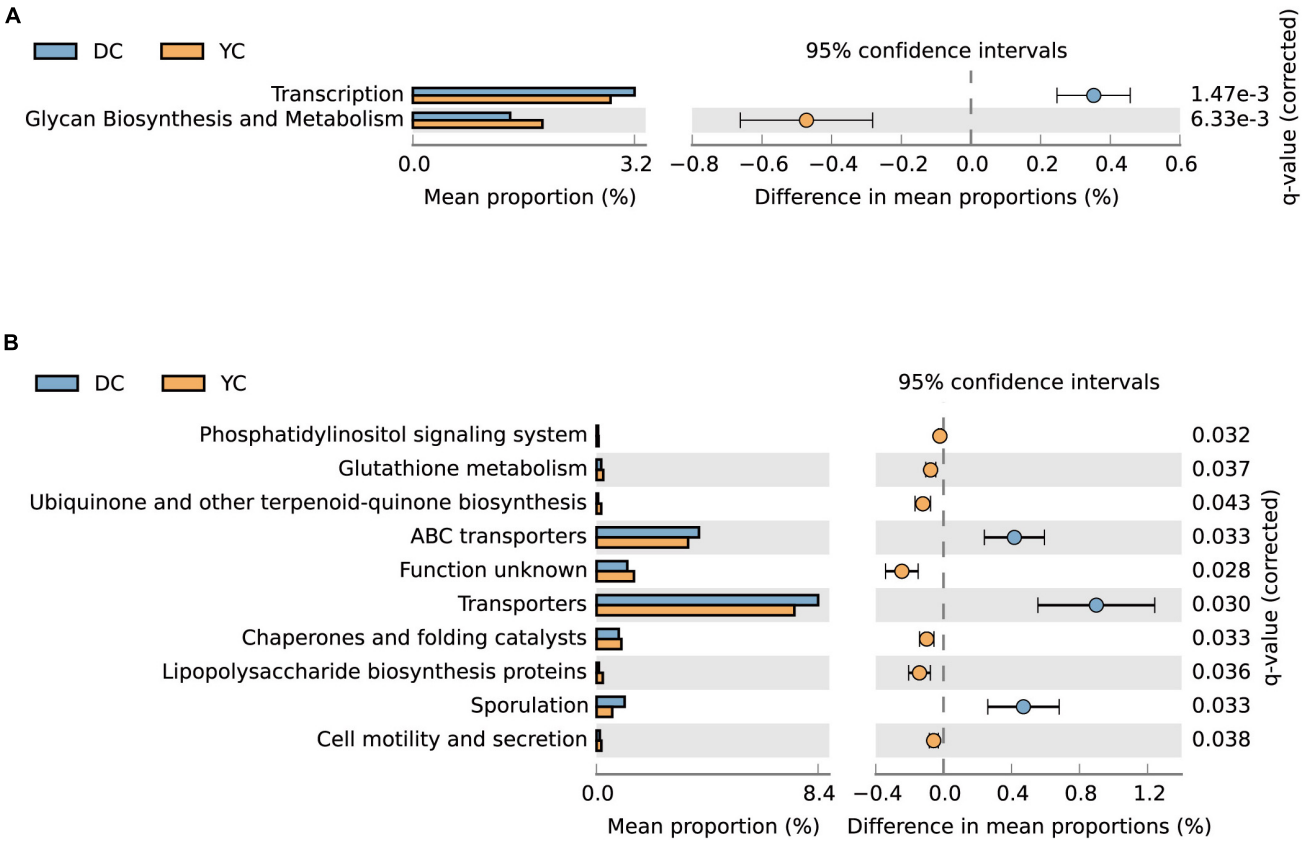

FIGURE 6 | The microorganism function prediction in DC and YC groups. The second level **(A)** and third level **(B)** of Kyoto Encyclopaedia of Genes and Genomes (KEGG) pathway are shown in the extended error bar. The corrected *p*-value is listed at the right. Blue and yellow represent DC and YC, respectively.

as nutrients for hindgut intestinal epithelial cells (Koropatkin et al., 2012; Sun et al., 2016). YC contains a large amount of glucan and mannooligosaccharides, which can induce the upregulation of glycan biosynthesis and metabolism pathways in microorganisms. Glutathione metabolism is generally considered to be related to the promotion of cell redox balance. It has antioxidant and detoxifying effects and provides a protective response (Xu et al., 2015). Glutathione-S-transferase and glutathione peroxidase are two important enzymes involved in glutathione metabolism (Schneider et al., 2016). In this study, we found that serum T-AOC content in the YC group increased significantly, which may be associated with improvement in intestinal microbial glutathione metabolic function. Ubiquinone and other terpenoid-quinone usually refer to hydrocarbon or terpenoid derivatives, and their oligomers, such as coenzyme Q10, squalene, farnesol, vitamin A, E, and K, are necessary for life activities. The upregulation of ubiquinone and other terpenoid-quinone biosynthesis pathways in YC-treated hens may be related to improvement in laying performance. Lipopolysaccharides, also known as endotoxins, are not only the main component of the outer membrane of Gram-negative bacteria but are also the main cause of inflammation and part of the natural immune response of animals. The upregulation of the lipopolysaccharide biosynthesis protein pathway after YC supplementation may be associated with an increase in lysozyme activity in the serum. Furthermore, we found that the sporulation pathway was significantly downregulated by YC. Spores are formed by bacteria in a near-dormant state. They can store the bacteria's hereditary material in an unsuitable and harmful environment (Huang and Hull, 2017; Bressuire-Isoard et al., 2018). Metabolism in the spore state is 10 million times slower than that in normally growing bacteria. YC supplementation may contribute toward improving the original harsh ecological environment within which microorganisms live, along with increasing the vitality of bacterial communities and strengthening network relationships. ABC transporters use the energy generated through ATP binding and hydrolysis to transport various substrates on the cell membrane. They have transport and excretion roles in prokaryotes and eukaryotes, and can remove toxins and drugs from cells. Research has shown that the ABC transporter system plays a very important role in the adaptation of *Escherichia coli* to unsuitable environments (Moussatova et al., 2008; Cario, 2017). Hence, the upregulation of the ABC transporter pathway in the DC group in our study could be due to the poor ecological environment, which need to excrete a large amount of toxic substrates.

Interestingly, we found that YC supplementation substantially improved the relationships among bacteria in the ileum. An increase in *Lactobacilli* abundance in the YC group led to more complex interactions among the bacteria. Such a complex network has been suggested to increase resistance against pathogen invasions because the pathogens would have to adapt to the external environment and compete for the original ecological niche with the existing bacteria (Wei et al., 2015; Mendes et al., 2018). As the DC group had very low bacterial connectivity, and based on its function prediction, we speculated that many bacteria may be in the resting state, and the loss of one niche will substantially influence the whole microbial community. On the contrary, the YC group had very high bacterial connectivity; even when it suffered from a pathogen invasion or was missing one niche, the neighboring niches supplemented any gaps. Moreover, connectivity among bacteria limits the nutrient supply for any invasive microorganisms, causing their extinction. Therefore, a complex network of microbes shows stronger resistance to external influences.

In addition, we found that within networks of intestinal microbial relationships, bacteria that were in high abundance showed a lower degree of correlation. Furthermore, the number of positive correlation was significantly more than negative correlation in the whole network relationship. Interestingly, common probiotics such as *Lactobacilli*, *Enterococcus*, and *Acetobacter* were mostly found to be negatively correlated with other bacteria, which may be because they produce bacteriocin to inhibit the growth and reproduction of other bacteria (Corr et al., 2009). *Lactobacilli* enhance the degree of correlation between bacteria and improve the consistency of bacterial flora. An increase in *Lactobacilli* abundance after YC administration was accompanied by a more complex correlation between bacterial communities. *Lactobacilli* could thus improve the intestinal microenvironment of layers and inhibit the growth of some pathogenic bacteria. Therefore, YC supplementation can result in good health of layers.

CONCLUSION

In conclusion, this study suggested that adding 2.0 g/kg YC to the diet of breeder-aged layers can improve their egg quality and reproductive efficiency. It may also be beneficial for their antioxidant capacity and systemic immunity. Moreover, it can improve the structure of aged layers' intestinal microbial flora by increasing the abundance of *Lactobacilli* and the consistency of bacterial flora, resulting in improved feed digestion, absorption, and gut health.

DATA AVAILABILITY STATEMENT

The datasets presented in this study can be found in online repositories. The names of the repository/repositories and accession number(s) can be found below: https://www.ncbi.nlm.nih.gov/, PRJNA675783.

ETHICS STATEMENT

The animal study was reviewed and approved by principle of the Animal care and Use Committee of China Agricultural University.

AUTHOR CONTRIBUTIONS

YL and XC performed the study, contributed to most of the experiments, and wrote the manuscript. WZ and DZ provided calculation and operation support. ZW, ZN, and LQ designed the study, evaluated the test details, and revised the manuscript. All authors contributed to this study and approved to submit the final manuscript.

FUNDING

This study was supported by the China Agriculture Research System (CARS-40). Funders had no participation in the study design, analysis, or writing of this article.

ACKNOWLEDGMENTS

We would like to thank Editage (www.editage.cn) for English language editing.

REFERENCES

Aloulou, A., Schué, M., Puccinelli, D., Milano, S., Delchambre, C., Leblond, Y., et al. (2015). Yarrowia lipolytica lipase 2 is stable and highly active in test meals and increases fat absorption in an animal model of pancreatic exocrine insufficiency. *Gastroenterology* 149, 1910.e5–1919.e5. doi: 10.1053/j.gastro.2015.08.047

Attia, Y. A., Al-Harthi, M. A., and El-Maaty, H. M. A. (2020). Calcium and cholecalciferol levels in late-phase laying hens: effects on productive traits, egg quality, blood biochemistry, and immune responses. *Front. Vet. Sci.* 7:389. doi: 10.3389/fvets.2020.00389

Baldwin, S., Hughes, R. J., Van, T. T. H., Moore, R. J., and Stanley, D. (2018). At-hatch administration of probiotic to chickens can introduce beneficial changes in gut microbiota. *PLoS One* 13:e0194825. doi: 10.1371/journal.pone.0194825

Bar, A., Vax, E., and Striem, S. (1999). Relationships among age, eggshell thickness and vitamin D metabolism and its expression in the laying hen. *Comp. Bioch. Physiol. Part AMol, Integr. Physiol.* 123, 147–154. doi: 10.1016/S1095-6433(99)00039-2

Bolger, A. M., Lohse, M., and Usadel, B. (2014). Trimmomatic: a flexible trimmer for Illumina sequence data. *Bioinformatics* 30, 2114–2120. doi: 10.1093/bioinformatics/btu170

Bressuire-Isoard, C., Broussolle, V., and Carlin, F. (2018). Sporulation environment influences spore properties in Bacillus: evidence and insights on underlying molecular and physiological mechanisms. *FEMS Microbiol. Rev.* 42, 614–626. doi: 10.1093/femsre/fuy021

Bunte, S., Grone, R., Keller, B., Keller, C., Galvez, E., Strowig, T., et al. (2020). Intestinal microbiota of fattening pigs offered non-fermented and fermented liquid feed with and without the supplementation of non-fermented coarse cereals. *Microorganisms* 8:638. doi: 10.3390/microorganisms8050638

Caporaso, J. G., Kuczynski, J., Stombaugh, J., Bittinger, K., Bushman, F. D., Costello, E. K., et al. (2010). QIIME allows analysis of high-throughput

community sequencing data. *Nat. Methods* 7, 335–336. doi: 10.1038/nmeth.f.303

Cario, E. (2017). P-glycoprotein multidrug transporter in inflammatory bowel diseases: more questions than answers. *World J. Gastroenterol.* 23, 1513–1520. doi: 10.3748/wjg.v23.i9.1513

Chen, Y., Wang, J., Yu, L., Xu, T., and Zhu, N. (2020). Microbiota and metabolome responses in the cecum and serum of broiler chickens fed with plant essential oils or virginiamycin. *Sci. Rep.* 10, 1–14. doi: 10.1038/s41598-020-60135-x

Chen, Z., Zhou, D., Han, S., Zhou, S., and Jia, G. (2019). Hepatotoxicity and the role of the gut-liver axis in rats after oral administration of titanium dioxide nanoparticles. *Particle Fibre Toxicol.* 16, 1–17. doi: 10.1186/s12989-019-0332-2

Corr, S. C., Hill, C., and Gahan, C. G. (2009). Understanding the mechanisms by which probiotics inhibit gastrointestinal pathogens. *Adv. Food Nutr. Res.* 56, 1–15. doi: 10.1016/S1043-4526(08)00601-3

Dawood, M. A., Magouz, F. I., Essa, M., and Mansour, M. (2020). Impact of yeast fermented poultry by-product meal on growth, digestive enzyme activities, intestinal morphometry and immune response traits of common carp (Cyprinus carpio). *Ann. An. Sci.* 1, 939–959. doi: 10.2478/aoas-2020-0021

Duan, X., Li, F., Mou, S., Feng, J., Liu, P., and Xu, L. (2015). Effects of dietary L-arginine on laying performance and anti-oxidant capacity of broiler breeder hens, eggs, and offspring during the late laying period. *Poult. Sci.* 94, 2938–2943. doi: 10.3382/ps/pev283

Edgar, R. C., Haas, B. J., Clemente, J. C., Quince, C., and Knight, R. (2011). UCHIME improves sensitivity and speed of chimera detection. *Bioinformatics* 27, 2194–2200. doi: 10.1093/bioinformatics/btr381

Frank, D. N., Amand, A. L. S., Feldman, R. A., Boedeker, E. C., Harpaz, N., and Pace, N. R. (2007). Molecular-phylogenetic characterization of microbial community imbalances in human inflammatory bowel diseases. *Proc. Natl. Acad. Sci. U.S.A.* 104, 13780–13785. doi: 10.1073/pnas.0706625104

Froebel, L., Jalukar, S., Lavergne, T., Lee, J., and Duong, T. (2019). Administration of dietary prebiotics improves growth performance and reduces pathogen colonization in broiler chickens. *Poult. Sci.* 98, 6668–6676. doi: 10.3382/ps/pez537

Fu, R., Chen, D., Tian, G., Zheng, P., Mao, X., Yu, J., et al. (2019). Effect of dietary supplementation of Bacillus coagulans or yeast hydrolysates on growth performance, antioxidant activity, cytokines and intestinal microflora of growing-finishing pigs. *Anim/ Nutr.* 5, 366–372. doi: 10.1016/j.aninu.2019.06.003

Gaboardi, G. C., Alves, D., de los Santos, D. G., Xavier, E., Nunes, A. P., Finger, P., et al. (2019). Influence of Pichia pastoris X-33 produced in industrial residues on productive performance, egg quality, immunity, and intestinal morphometry in quails. *Sci. Rep.* 9, 1–14. doi: 10.1038/s41598-019-51908-0

Gadde, U., Kim, W., Oh, S., and Lillehoj, H. S. (2017). Alternatives to antibiotics for maximizing growth performance and feed efficiency in poultry: a review. *Anim. Health Res. Rev.* 18, 26–45. doi: 10.1017/S1466252316000207

Gao, J., Zhang, H., Yu, S., Wu, S., Yoon, I., Quigley, J., et al. (2008). Effects of yeast culture in broiler diets on performance and immunomodulatory functions. *Poult. Sci.* 87, 1377–1384. doi: 10.3382/ps.2007-00418

Gerritsen, J., Hornung, B., Renckens, B., van Hijum, S. A., dos Santos, V. A. M., Rijkers, G. T., et al. (2017). Genomic and functional analysis of Romboutsia ilealis CRIBT reveals adaptation to the small intestine. *PeerJ* 5:e3698. doi: 10.7717/peerj.3698

Hooper, L. V., Midtvedt, T., and Gordon, J. I. (2002). How host-microbial interactions shape the nutrient environment of the mammalian intestine. *Annu. Rev. Nutr.* 22, 283–307. doi: 10.1146/annurev.nutr.22.011602.092259

Hostetler, C. E., Kincaid, R. L., and Mirando, M. A. (2003). The role of essential trace elements in embryonic and fetal development in livestock. *Vet. J.* 166, 125–139. doi: 10.1016/S1090-0233(02)00310-6

Hu, S., Xu, Y., Gao, X., Li, S., Jiang, W., Liu, Y., et al. (2019). Long-chain bases from sea cucumber alleviate obesity by modulating gut microbiota. *Mar. Drugs* 17:455. doi: 10.3390/md17080455

Huang, M., and Hull, C. M. (2017). Sporulation: how to survive on planet Earth (and beyond). *Curr. Genet.* 63, 831–838. doi: 10.1007/s00294-017-0694-7

Jensen, G., Patterson, K., and Yoon, I. (2008). Yeast culture has anti-inflammatory effects and specifically activates NK cells. *Comp. Immunol. Microbiol. Infect. Dis.* 31, 487–500. doi: 10.1016/j.cimid.2007.08.005

Jones, M. P. (1999). Avian clinical pathology. *Vet. Clinics N. Am.* 2, 663–687. doi: 10.1016/S1094-9194(17)30115-9

Koropatkin, N. M., Cameron, E. A., and Martens, E. C. (2012). How glycan metabolism shapes the human gut microbiota. *Nat. Rev. Microbiol.* 10, 323–335. doi: 10.1038/nrmicro2746

Kot, A. M., Błażejak, S., Kieliszek, M., Gientka, I., and Bryś, J. (2019). Simultaneous production of lipids and carotenoids by the red yeast Rhodotorula from waste glycerol fraction and potato wastewater. *Appl. Biochem. Biotechnol.* 189, 589–607. doi: 10.1007/s12010-019-03023-z

Langille, M. G., Zaneveld, J., Caporaso, J. G., McDonald, D., Knights, D., Reyes, J. A., et al. (2013). Predictive functional profiling of microbial communities using 16S rRNA marker gene sequences. *Nat. Biotechnol.* 31, 814–821. doi: 10.1038/nbt.2676

Lee, S. M., Kim, N., Nam, R. H., Park, J. H., Choi, S. I., Park, Y.-T., et al. (2019). Gut microbiota and butyrate level changes associated with the long-term administration of proton pump inhibitors to old rats. *Sci. Rep.* 9, 1–11. doi: 10.1038/s41598-019-43112-x

Ley, R. E., Hamady, M., Lozupone, C., Turnbaugh, P. J., Ramey, R. R., Bircher, J. S., et al. (2008). Evolution of mammals and their gut microbes. *Science* 320, 1647–1651. doi: 10.1126/science.1155725

Li, Z., Wang, X., Zhang, T., Si, H., Nan, W., Xu, C., et al. (2018). The development of microbiota and metabolome in small intestine of sika deer (Cervus nippon) from birth to weaning. *Front. Microbiol.* 9:4. doi: 10.3389/fmicb.2018.00004

Liu, X., Lin, X., Mi, Y., Li, J., and Zhang, C. (2018). Grape seed proanthocyanidin extract prevents ovarian aging by inhibiting oxidative stress in the hens. *Oxid. Med. Cell. Longev.* 2018:9390810. doi: 10.1155/2018/9390810

Liu, Y.-Z., Chen, X., Zhao, W., Lang, M., Zhang, X.-F., Wang, T., et al. (2019). Effects of yeast culture supplementation and the ratio of non-structural carbohydrate to fat on rumen fermentation parameters and bacterial-community composition in sheep. *Anim. Feed Sci. Technol/* 249, 62–75. doi: 10.1016/j.anifeedsci.2019.02.003

Lu, Z., Thanabalan, A., Leung, H., Akbari Moghaddam Kakhki, R., Patterson, R., and Kiarie, E. (2019). The effects of feeding yeast bioactives to broiler breeders and/or their offspring on growth performance, gut development, and immune function in broiler chickens challenged with Eimeria. *Poult. Sci.* 98, 6411–6421. doi: 10.3382/ps/pez479

Lumeij, J. (1997). "Avian clinical biochemistry," in *Clinical Biochemistry of Domestic Animals*, eds J. J. Kaneko and C. E. Cornelius (Amsterdam: Elsevier), 857–883.

Mendes, L. W., Mendes, R., Raaijmakers, J. M., and Tsai, S. M. (2018). Breeding for soil-borne pathogen resistance impacts active rhizosphere microbiome of common bean. *ISME J.* 12, 3038–3042. doi: 10.1038/s41396-018-0234-6

Min, Y., Li, L., Liu, S., Zhang, J., Gao, Y., and Liu, F. (2015). Effects of dietary distillers dried grains with solubles (DDGS) on growth performance, oxidative stress, and immune function in broiler chickens. *J. Appl. Poult. Res.* 24, 23–29. doi: 10.3382/japr/pfv002

Moussatova, A., Kandt, C., O'Mara, M. L., and Tieleman, D. P. (2008). ATP-binding cassette transporters in *Escherichia coli*. *Biochim. Biophys. Acta Biomembr.* 1778, 1757–1771. doi: 10.1016/j.bbamem.2008.06.009

Özsoy, B., Karadağoğlu, Ö, Yakan, A., Önk, K., Çelik, E., and Şahin, T. (2018). The role of yeast culture (*Saccharomyces cerevisiae*) on performance, egg yolk fatty acid composition, and fecal microflora of laying hens. *Revista Brasileira de Zootecnia* 47:e20170159. doi: 10.1590/rbz4720170159

Parks, D. H., Tyson, G. W., Hugenholtz, P., and Beiko, R. G. (2014). STAMP: statistical analysis of taxonomic and functional profiles. *Bioinformatics* 30, 3123–3124. doi: 10.1093/bioinformatics/btu494

Qiao, H., Shi, H., Zhang, L., Song, Y., Zhang, X., and Bian, C. (2019). Effect of Lactobacillus plantarum supplementation on production performance and fecal microbial composition in laying hens. *Open Life Sci.* 14, 69–79. doi: 10.1515/biol-2019-0009

Qiao, H., Zhang, L., Shi, H., Song, Y., and Bian, C. (2018). *Astragalus* affects fecal microbial composition of young hens as determined by 16S rRNA sequencing. *AMB Express* 8:70. doi: 10.1186/s13568-018-0600-9

Remely, M., Aumueller, E., Jahn, D., Hippe, B., Brath, H., and Haslberger, A. (2014). Microbiota and epigenetic regulation of inflammatory mediators in type 2 diabetes and obesity. *Beneficial Microbes* 5, 33–43. doi: 10.3920/BM2013.006

Reyon, D., Tsai, S. Q., Khayter, C., Foden, J. A., Sander, J. D., and Joung, J. K. (2012). FLASH assembly of TALENs for high-throughput genome editing. *Nat. Biotechnol.* 30, 460–465.

Saleh, A., Amber, K., and Mohammed, A. (2020). Dietary supplementation with avilamycin and *Lactobacillus acidophilus* effects growth performance and the

expression of growth-related genes in broilers. *Anim. Prod. Sci.* 60, 1704–1710. doi: 10.1071/AN19030

Saleh, A. A., Gálik, B., Arpášová, H., Capcarová, M., Kalafová, A., Šimko, M., et al. (2017). Synergistic effect of feeding *Aspergillus* awamori and lactic acid bacteria on performance, egg traits, egg yolk cholesterol and fatty acid profile in laying hens. *Ital. J. Anim. Sci.* 16, 132–139. doi: 10.1080/1828051X.2016.1269300

Schneider, S. A., Scharffetter, C., Wagner, A. E., Boesch, C., Bruchhaus, I., Rimbach, G., et al. (2016). Social stress increases the susceptibility to infection in the ant *Harpegnathos saltator*. *Sci. Rep.* 6, 1–7. doi: 10.1038/srep25800

Spring, S., Premathilake, H., DeSilva, U., Shili, C., Carter, S., and Pezeshki, A. (2020). Low protein-High carbohydrate diets alter energy balance, gut microbiota composition and blood metabolomics profile in young pigs. *Sci. Rep.* 10, 1–15. doi: 10.1038/s41598-020-60150-y

Sun, H.-Y., and Kim, I.-H. (2019). Dietary supplementation of mixed yeast culture derived from *Saccharomyces cerevisiae* and *Kluyveromyces maxianus*: effects on growth performance, nutrient digestibility, meat quality, blood parameters, and gut health in broilers. *J. Poult. Sci.* 56, 140–147. doi: 10.2141/jpsa.0180052

Sun, Q., Guo, Y., Ma, S., Yuan, J., An, S., and Li, J. (2012). Dietary mineral sources altered lipid and antioxidant profiles in broiler breeders and posthatch growth of their offsprings. *Biol. Trace Element Res.* 145, 318–324. doi: 10.1007/s12011-011-9196-5

Sun, Y., Su, Y., and Zhu, W. (2016). Microbiome-metabolome responses in the cecum and colon of pig to a high resistant starch diet. *Front. Microbiol.* 7:779. doi: 10.3389/fmicb.2016.00779

Turnbaugh, P. J., Bäckhed, F., Fulton, L., and Gordon, J. I. (2008). Diet-induced obesity is linked to marked but reversible alterations in the mouse distal gut microbiome. *Cell Host Microbe* 3, 213–223. doi: 10.1016/j.chom.2008.02.015

Wang, Q., Garrity, G. M., Tiedje, J. M., and Cole, J. R. (2007). Naive Bayesian classifier for rapid assignment of rRNA sequences into the new bacterial taxonomy. *Appl. Environ. Microbiol.* 73, 5261–5267. doi: 10.1128/AEM.00062-07

Wang, S., Chen, L., He, M., Shen, J., Li, G., Tao, Z., et al. (2018). Different rearing conditions alter gut microbiota composition and host physiology in Shaoxing ducks. *Sci. Rep.* 8, 1–13. doi: 10.1038/s41598-018-25760-7

Wang, X., Ryu, D., Houtkooper, R. H., and Auwerx, J. (2015). Antibiotic use and abuse: a threat to mitochondria and chloroplasts with impact on research, health, and environment. *Bioessays* 37, 1045–1053. doi: 10.1002/bies.201500071

Wei, Z., Yang, T., Friman, V.-P., Xu, Y., Shen, Q., and Jousset, A. (2015). Trophic network architecture of root-associated bacterial communities determines pathogen invasion and plant health. *Nat. Commun.* 6, 1–9. doi: 10.1038/ncomms9413

Wu, C., Yang, Z., Song, C., Liang, C., Li, H., Chen, W., et al. (2018). Effects of dietary yeast nucleotides supplementation on intestinal barrier function, intestinal microbiota, and humoral immunity in specific pathogen-free chickens. *Poult. Sci.* 97, 3837–3846. doi: 10.3382/ps/pey268

Wu, C.-C., Weng, W.-L., Lai, W.-L., Tsai, H.-P., Liu, W.-H., Lee, M.-H., et al. (2015). Effect of Lactobacillus plantarum strain K21 on high-fat diet-fed obese mice. *Evid. Based Comp. Altern. Med.* 2015:391767. doi: 10.1155/2015/391767

Xu, B., Chen, M., Yao, M., Ji, X., Mao, Z., Tang, W., et al. (2015). Metabolomics reveals metabolic changes in male reproductive cells exposed to thirdhand smoke. *Sci, Rep.* 5:15512. doi: 10.1038/srep15512

Xu, M., Wang, C., Krolick, K. N., Shi, H., and Zhu, J. (2020). Difference in post-stress recovery of the gut microbiome and its altered metabolism after chronic adolescent stress in rats. *Sci. Rep.* 10, 1–10. doi: 10.1038/s41598-020-60862-1

Xu, S., Shi, J., Dong, Y., Li, Z., Wu, X., Lin, Y., et al. (2020). Fecal bacteria and metabolite responses to dietary lysozyme in a sow model from late gestation until lactation. *Sci. Rep.* 10, 1–13. doi: 10.1038/s41598-020-60131-1

Yalçin, S., Özsoy, B., Erol, H., and Yalçin, S. (2008). Yeast culture supplementation to laying hen diets containing soybean meal or sunflower seed meal and its effect on performance, egg quality traits, and blood chemistry. *J. Appl. Poult. Res.* 17, 229–236. doi: 10.3382/japr.2007-00064

Yousefi, M., Shivazad, M., and Sohrabi-Haghdoost, I. (2005). Effect of dietary factors on induction of fatty liver-hemorrhagic syndrome and its diagnosis methods with use of serum and liver parameters in laying hens. *Int. J. Poult. Sci.* 4, 568–572. doi: 10.3923/ijps.2005.568.572

Yu, L., Wang, L., Yi, H., and Wu, X. (2020). Beneficial effects of LRP6-CRISPR on prevention of alcohol-related liver injury surpassed fecal microbiota transplant in a rat model. *Gut Microbes* 11, 1015–1029. doi: 10.1080/19490976.2020.1736457

Zhang, J.-C., Chen, P., Zhang, C., Khalil, M. M., Zhang, N.-Y., Qi, D.-S., et al. (2020). Yeast culture promotes the production of aged laying hens by improving intestinal digestive enzyme activities and the intestinal health status. *Poult. Sci.* 99, 2026–2032. doi: 10.1016/j.psj.2019.11.017

Zhang, S., Wu, Z., Heng, J., Song, H., Tian, M., Chen, F., et al. (2020). Combined yeast culture and organic selenium supplementation during late gestation and lactation improve preweaning piglet performance by enhancing the antioxidant capacity and milk content in nutrient-restricted sows. *Anim. Nutr.* 6, 160–167. doi: 10.1016/j.aninu.2020.01.004

Zhong, S., Liu, H., Zhang, H., Han, T., Jia, H., and Xie, Y. (2016). Effects of Kluyveromyces marxianus isolated from tibetan mushrooms on the plasma lipids, egg cholesterol level, egg quality and intestinal health of laying hens. *Braz. J. Poult. Sci.* 18, 261–268. doi: 10.1590/1806-9061-2015-0070

Conflict of Interest: DZ was employed by company Huayu Agricultural Science and Technology Co., Ltd.

The remaining authors declare that the research was conducted in the absence of any commercial or financial relationships that could be construed as a potential conflict of interest.

frontiers in Veterinary Science

DATA REPORT
published: 05 May 2021
doi: 10.3389/fvets.2021.662536

Metabolite Profile of Sheep Serum With High or Low Average Daily Gain

Tao Feng[1,2,3]*, *Hongxiang Ding*[1,2,3], *Jing Wang*[4], *Wei Xu*[5], *Yan Liu*[1,2]* and *Ákos Kenéz*[5]

[1] Institute of Animal Husbandry and Veterinary Medicine (IAHVM), Beijing Academy of Agriculture and Forestry Sciences (BAAFS), Beijing, China, [2] Joint Laboratory of Animal Science Between IAHVM of BAAFS and Division of Agricultural Science and Natural Resource of Oklahoma State University, Beijing, China, [3] College of Animal Science and Technology, Henan University of Science and Technology, Luoyang, China, [4] College of Animal Science and Technology, Hebei North University, Zhangjiakou, China, [5] Department of Infectious Diseases and Public Health, City University of Hong Kong, Hong Kong, China

Keywords: metabolomics, sheep, average daily gain, metabolic pathway, serum

INTRODUCTION

Sheep industry is a major branch of animal husbandry throughout the north and central parts of China mainly for mutton and wool production (1, 2). Body weight gain during the fattening period is an important determinant for carcass weight. Sheep average daily gain (ADG) refers to the average weight gain of sheep during a certain period and is an important economic growth trait that improves production efficiency and economic benefits. Specifically, ADG has been reported to have a positive correlation coefficient ($r = 0.53$) with final body weight in growing lambs (3). The ADG of lamb or sheep is affected by genetic basis, nutrition level, growth stage, and management system (4–6). In sheep feedlots, lambs with the same genetic basis, same age, same management system, and very similar initial body weight often develop a large standard deviation in ADG, accounting for unwanted differences in final body weights (7, 8). To our knowledge, few studies reported the underlying metabolic mechanism of such an inter-individual difference.

Selecting those lambs expected to have high ADG, at the earliest as possible in their longevity, or at least before the fattening period, could obviously increase the profitability of sheep feedlots (9, 10). Recently, several serum components (hormones, metabolites, hematological, and biochemical parameters) have been identified as biomarkers to evaluate the residual feed intake of sheep (11, 12), an indicator of feed conversion efficiency. Metabolomics can qualitatively and quantitatively analyze hundreds of metabolites in diverse samples, which can be extensively used to study physiological and pathophysiological process such as starving and intrauterine growth restriction in sheep (13, 14). Blood is considered as an ideal sample in sheep metabolomics research and is potentially used to reflect the metabolic status on a whole body level (15). As we have known, alterations in the blood metabolome profiles of sheep during the fattening period, particularly in fattening sheep with the same genetic basis, same age, same management system, but high or low ADG, are still unclear. Therefore, the aims of the present study were (i) to reveal the metabolic characteristics of lambs with high or low ADG under the same management system and (ii) to investigate the potential metabolic pathways related to the growth performance of sheep.

METHODS

Experiments were performed at the Experimental Station of Beijing Academy of Agriculture and Forestry Sciences in the Yangyuan county, Zhangjiakou city, Heibei province, northeast of China. A total of 200 crossbreed male lambs (*Ovis aries*) of Dorper rams and Mongolia ewes after weaning (45 days of age) were housed in eight sheltered outdoor paddocks and fed total mixed ration (TMR). Clean water and mineralized salt licks were available *ad libitum*. From 75 days of age, 50 lambs with similar body weight were selected and reared in individual pens indoors (0.7 × 1.0 m) until 120 days

OPEN ACCESS

Edited by:
Haidong Yao,
Karolinska Institutet (KI), Sweden

Reviewed by:
Shengguo Zhao,
Chinese Academy of Agricultural Sciences, China
Fugui Fang,
Anhui Agricultural University, China

***Correspondence:**
Yan Liu
liuyanxms@163.com
Tao Feng
fengtao_gs@163.com

Specialty section:
This article was submitted to Livestock Genomics, a section of the journal Frontiers in Veterinary Science

Received: *01 February 2021*
Accepted: *02 March 2021*
Published: *05 May 2021*

Citation:
Feng T, Ding H, Wang J, Xu W, Liu Y and Kenéz Á (2021) Metabolite Profile of Sheep Serum With High or Low Average Daily Gain. Front. Vet. Sci. 8:662536. doi: 10.3389/fvets.2021.662536

of age. Briefly, the lambs were acclimatized, lasting 15 days before formal assessment. At 90 days, 40 lambs with similar body weight were selected to do ADG research lasting 30 days. Lamb TMR was compounded based on the recommendations of sheep feeding standard in China (NY/T816-2004) and contained digestible energy of 11.83 $MJ{\cdot}kg^{-1}$, metabolic energy of 9.73 $MJ{\cdot}kg^{-1}$, 14.61% crude protein, 0.39% calcium, and 0.25% phosphorus. Body weight of lambs was accurately measured in the morning before feeding, and at 75, 90, and 120 days of age, using calibrated electronic scales. ADG was calculated based on body weight. Differences in ADG between the high ADG and low ADG lamb group were analyzed using a *t*-test. A $P < 0.05$ indicated statistical significance.

At 120 days of age, after weighting, blood samples were drawn from the jugular vein of the top seven lambs with the greatest ADG and the bottom seven lambs with the lowest ADG using needles and vacutainers covered with anti-coagulant (BD Vacutainer, USA) for a minimum of 6 ml. The blood was placed at room temperature for 4 h and then centrifuged at 2,000 g for 30 min at 4°C. Serum separation was carefully proceeded. The serum was aliquoted and rapidly frozen by dry ice. Frozen serum samples were stored at −80°C until metabolomics analyses.

Using 100 μl of serum, metabolites were extracted using methanol. Extracts were sonicated, and after centrifugation, the supernatant was gently added to sample vials for LC-MS/MS analysis. A pooled quality control sample (QC) was performed for system conditioning and quality control. Chromatographic separation of the metabolites was operated on a Thermo UHPLC system equipped with an ACQUITY UPLC HSS T3 (100 mm × 2.1 mm i.d., 1.8 μm; Waters, Milford, USA).

Following LC-MS/MS analyses, the raw data were inputted into the Progenesis QI 2.3 (Non-linear Dynamics, Waters, USA) for peak picking and alignment. Mass spectra of these metabolic characteristics were discerned through the accurate mass, MS/MS fragments spectra, and isotope ratio difference, by scanning in public available biochemical databases such as the Human Metabolome Database (HMDB) (http://www.hmdb.ca/) and the Metlin database (https://metlin.scripps.edu/). A multivariate statistical analysis was conducted using "ropls" (Version 1.6.2, http://bioconductor.org/packages/release/bioc/html/ropls.html) R package from Bioconductor on Majorbio Cloud Platform (https://cloud.majorbio.com). Principal component analysis (PCA) was applied to check outliers and present trends. Partial least squares discriminate analysis (PLS-DA) was used to

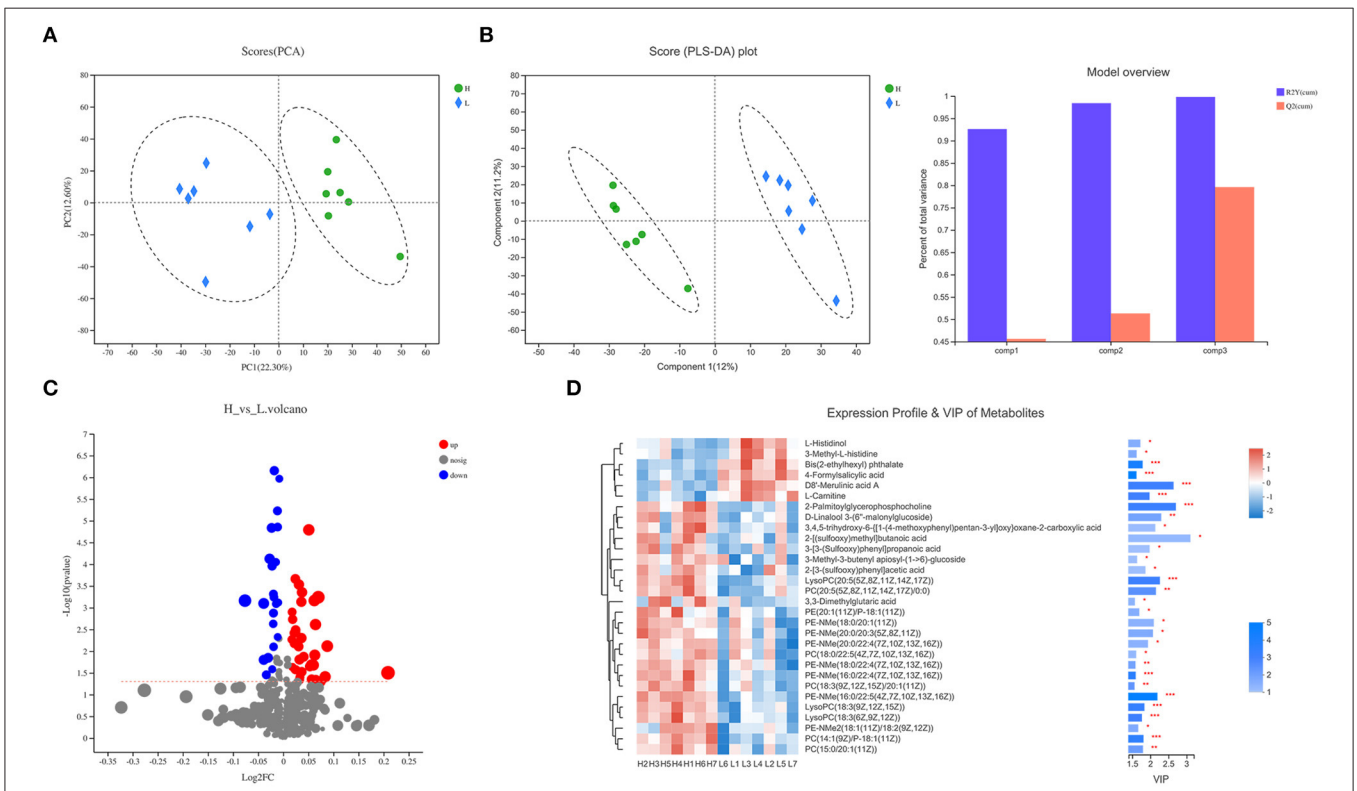

FIGURE 1 | Serum metabolite profile of lambs with different average daily gain (ADG). **(A)** PCA score plot for serum metabolites of high ADG lambs (H) and low ADG lambs (L). **(B)** PLS-DA score plot for serum metabolites of high ADG lambs (H) and low ADG lambs (L), and model overview showing high R2Y and Q2. **(C)** Enhanced Volcano plots of OPLS-DA showing fold changes (log_2FC) and the negative logarithm (base 10) of the *P*-values of 57 differential serum metabolites in high ADG lambs compared with low ADG lambs. **(D)** Expression profile, VIP score, and *P*-value of the top 30 differential serum metabolites in high ADG lambs compared with low ADG lambs.

identify the general metabolic changes in serum of sheep between high and low ADG. Variable importance in the projection (VIP) was computed by an orthogonal partial least squares discriminate analysis (OPLS-DA) model. Differential metabolites among ESI groups were summarized and annotated into their biochemical pathways through metabolic enrichment and pathway analysis based on database matching (KEGG, http://www.genome.jp/kegg/). Furthermore, Volcano plot was used to compare the size of the fold change to statistical significance.

RESULTS

At the beginning of the lamb fattening trial, when lambs were 90 days of age, the mean (SD in parentheses) body weight of seven original lambs corresponding to the high ADG was 26.7 (0.9) kg, while the mean body weight of seven original lambs corresponding to the low ADG was 26.8 (0.8) kg. At the end of the lamb trial, the body weight of the seven lambs with the highest weight gain was 35.67 (0.8) kg and the body weight of the seven lambs with the lower weight gain was 32.56 (1.0) kg. The ADG of high weight gain lambs was 298.1 (15.9) g·day^{-1}, which differed ($P < 0.01$) from the ADG of low weight gain lambs 191.9 (23.6) g·day^{-1}, while the average ADG of all lambs tested was 239.5 (34.8) g·day^{-1} ($n = 40$).

Variation of ADG depends on sheep breeds and ages. Previous studies showed that crossbreed of specialized mutton breeds and local sheep breeds had greater ADG than local sheep. For local sheep breeds under a barn feeding fattening system, 6-month Altay and Hu lambs presented ADG from 100 to 200 g·day^{-1} (16), while ADG of 3-month Ningxia Tan sheep lambs was between 90 and 130 g·day^{-1} (17) and ADG of Small Tail Han sheep lambs was between 140 and 180 g·day^{-1} (18). Furthermore, the ADG of crossbreed lambs of Dorper and Small Tailed Han sheep was between 265 and 322 g·day^{-1} in pens (19). In our study, crossbreed lambs of Dorper rams and Mongolia ewes at 4-month age exhibited excellent growth performance with an average ADG of 240 g·day^{-1}. Crossbreed lambs are recommended to produce lamb meat in the north part of China.

In the LC-MS spectra of lamb serum with high or low ADG, 10,231 metabolites were initially found. After quality control and discernment, 462 compounds were reliably detected. The PCA score plot presented that the first and second principal components (PCs) clarified 22.3 and 12.6% of the variation, respectively (**Figure 1A**). As expected, the separated plot representing high and low ADG can be observed in the PCA plot. Next, PLS-DA was executed to exhibit the variations between the high and low ADG lambs. As shown in **Figure 1B**, the PLS-DA analysis demonstrated that the serum metabolites of the low ADG lambs distinctly differed from those of the high ADG lambs. Correspondingly, the values of R2Y and Q2 were 0.998 and 0.796, respectively (**Figure 1**), indicating good interpretability and predictability by this PLS-DA model. A value of Q2 = 1 indicates a perfect discrimination of metabolites profiles between groups.

In comparison, a total 57 differential serum metabolites were found according to the Volcano plot ($P < 0.05$, VIP > 1.0, and $\log_2$FC > 1 or < 1.0), of which 35 metabolites showed up-regulation and 22 showed down-regulation (**Figure 1C** and **Supplementary Table 1**). A total of 50 differential serum metabolites were annotated in six superclasses according to the HMDB database, of which 36 belonged to lipids and lipid-like molecules, 5 belonged to organic nitrogen compounds, 4 belonged to organic acids and derivatives, 2 belonged to benzenoids, 2 belonged to organic oxygen compounds, and 1 belonged to organoheterocyclic compounds. Expression profile and VIP of the top 30 metabolites based on the OPLS-DA model are shown in **Figure 1D**. Regarding the KEGG pathway, the four pathways including at least two differential serum metabolites annotated were metabolic pathways [L-Histidinol, Myristic acid, D-Sedoheptulose 7-phosphate, L-Arginine, and PC(14:1(9Z)/20:2(11Z,14Z))], biosynthesis of amino acids (L-Histidinol, D-Sedoheptulose 7-phosphate, and L-Arginine), glycerophospholipid metabolism [PC(14:1(9Z)/20:2(11Z,14Z)), LysoPC(20:5(5Z,8Z,11Z,14Z,17Z)), and LysoPC(18:3(6Z,9Z,12Z))], and histidine metabolism (L-Histidinol and 3-Methyl-L-histidine), respectively. Based on our results, the serum metabolome prolife of lambs was affected by high or low ADG.

As shown in **Figure 1D** and **Supplementary Table 1**, most of the lipids and lipid-like molecules were accumulated in serum samples of high ADG lambs compared with low ADG ones, including LysoPC(20:5(5Z,8Z,11Z,14Z,17Z)) and PC(14:1(9Z)/20:2 (11Z,14Z)), which are metabolites involved in glycerophospholipid metabolism. In detail, LysoPC(20:5(5Z,8Z,11Z,14Z,17Z)) and PC(14:1(9Z)/20:2(11Z,14Z)) had a high concentration in serum of high ADG lambs [$\log_2$(FC) = 1.04 and 1.02]. Lysophospholipids (LPL) mainly include lysophosphatidylcholine (LPC), lysophosphatidic acid (LPA), lysophosphatidylethanolamine (LPE), and lysophosphatidylinositol (LPI), which are derivatives of phospholipid with absence of a fatty acid chain by hydrolysis (20). LPL could be a potent feed additive to improve production and feed efficiency according to studies in non-ruminant animals (21, 22), as well as in ruminants (23, 24). Recently, research showed that LPL supplementation could increase ADG in lambs, potentially through altering feed digestion (25), and intermediating bacterial phospholipid turnover as one of the cellular growth factor or potent lipid mediator in bacteria (26). Moreover, LPC could alter enterocyte monolayer permeability via protein kinase C (27).

Amino acids in tissue and in serum seemed to change under various physiological status, such as starvation, fasting, grazing, and stress in sheep (14) and dairy cows (28). During starvation in sheep, circulating amino acids had a general trend to increase mainly because muscle proteins were mobilized to improve gluconeogenesis in the livers by enhancing amino acids supply (14). Three metabolites (L-Arginine, L-Histidinol, and D-Sedoheptulose 7-phosphate) were identified to increase in circulation of low ADG lambs (**Supplementary Table 1**). Arginine is a conditionally essential amino acid in livestock

and has a potential role on regulating energy partitioning between fat and lean deposition (29). Intriguingly, in lower body weight suckling lambs affected by intrauterine growth restriction, arginine supplementation increased ADG and decreased feed conversion rate (30). In the growing period in Dorper and Damara sheep, seasonal weight loss resulting from dietary restriction resulted in an increased arginine level in liver, but a decreased level in Australia Merino, while histidine level increased in all three sheep studied during dietary restriction (14). Plasma arginine was reported to increase in feed-restricted dairy cows, too (28). Collectively, these results showed that circulating amino acid concentrations changed to satisfy requirements of growth needs and normal metabolism in sheep.

Histidine can be a substrate for gluconeogenesis and protein synthesis; however, it can also affect the active site of enzymes (31). L-Histidinol and 3-Methyl-L-histidine (annotated in histidine metabolism pathway) were down-regulated in lambs with high ADG (**Figure 1D** and **Supplementary Table 1**), indicating that histidine metabolism had a trend of less activity, potentially to support faster growth and development in lambs in an intensive fattening system. Moreover, histidine metabolism seems to be up-regulated under nutritional restriction. It was reported that plasma L-histidine level decreased in barn confinement sheep compared with free grazing sheep due to high body weight gain (32).

Collectively, the purpose of this report was to reveal serum metabolome profiles of fattening lambs in a barn feeding fattening system, with particular attention to unique metabolites in lambs with high or low ADG. Our findings showed that differential metabolites affected by ADG belonged to lipids and lipid-like molecules, organic nitrogen compounds, organic acids and derivatives, benzenoids, organic oxygen compounds, and organoheterocyclic compounds. The identified metabolites have an effect on regulating metabolic pathways, biosynthesis of amino acids, glycerophospholipid metabolism, and histidine metabolism. These results indicate that selected serum metabolites could have potential application to estimate sheep with different ADG. Further larger-size studies with more various cohorts of sheep are desired to validate our finding.

DATA AVAILABILITY STATEMENT

The original contributions presented in the study are included in the article/**Supplementary Material**, further inquiries can be directed to the corresponding author/s.

ETHICS STATEMENT

The animal study was reviewed and approved by Beijing Academy of Agriculture and Forestry Sciences.

AUTHOR CONTRIBUTIONS

TF and YL conceived the study. JW and TF obtained funding. HD performed animal trials and data collection. WX and TF performed data interpretation. TF and HD wrote the manuscript. WX and ÁK performed manuscript revision. All authors read and approved the final manuscript content.

FUNDING

This work was supported by the Science Foundation of Institute of Animal Husbandry and Veterinary Medicine, Beijing Academy of Agriculture and Forestry Sciences (XMSSYJJ202101), the Achievement Transformation Project of Beijing Academy of Agriculture and Forestry Sciences (2018017 and 2020607), and the Key Research and Development Plan Program of Hebei Province (20326629D).

ACKNOWLEDGMENTS

We thank all staff of the Experimental Station of Beijing Academy of Agriculture and Forestry Sciences (located in the Yangyuan county, Zhangjiakou city, Heibei province) for their assistance during the sample collection.

SUPPLEMENTARY MATERIAL

The Supplementary Material for this article can be found online at: https://www.frontiersin.org/articles/10.3389/fvets.2021.662536/full#supplementary-material

REFERENCES

1. Li Q, Lu Z, Jin M, Fei X, Quan K, Liu Y, et al. verification and analysis of sheep tail type-associated gene polymorphisms. *Animals.* (2020) 10:89. doi: 10.3390/ani10010089
2. Quan K, Li J, Han H, Wei H, Zhao J, Si HA, et al. Review of Huang-Huai sheep, a new multiparous mutton sheep breed first identified in China. *Trop Anim Health Prod.* (2020) 53:35. doi: 10.1007/s11250-020-02453-w
3. Zhang X, Wang W, Mo F, La Y, Li C, Li F. Association of residual feed intake with growth and slaughtering performance, blood metabolism, and body composition in growing lambs. *Sci Rep.* (2017) 7:12681. doi: 10.1038/s41598-017-13042-7
4. Arthy V, Venkataramanan R, Sivaselvam SN, Sreekumar C, Balasubramanyam D. Genetic evaluation of growth in farmers' flocks of Madras Red sheep under long-term selection in a group breeding scheme. *Trop Anim Health Prod.* (2018) 50:1463–71. doi: 10.1007/s11250-018-1581-z
5. Santos A, Giraldez FJ, Mateo J, Frutos J, Andrés S. Programming Merino lambs by early feed restriction reduces growth rates and increases fat accretion during the fattening period with no effect on meat quality traits. *Meat Sci.* (2018) 135:20–6. doi: 10.1016/j.meatsci.2017.08.007
6. Atti N, Mahouachi M. The effects of diet, slaughter weight and docking on growth, carcass composition and meat quality of fat-tailed Barbarine lambs. A review. *Trop Anim Health Prod.* (2011) 43:1371–8. doi: 10.1007/s11250-011-9865-6
7. Beltrão ES, de Azevedo Silva AM, Filho JMP, de Moura JFP, de Oliveira JPF, Oliveira RL, et al. Effect of different blend levels of spineless cactus and Mombasa hay as roughage on intake, digestibility, ingestive behavior, and performance of lambs. *Trop Anim Health Prod.* (2021) 53:140. doi: 10.1007/s11250-021-02585-7

8. Chen X, Mi H, Cui K, Zhou R, Tian S, Zhang L. Effects of diets containing finger millet straw and corn straw on growth performance, plasma metabolites, immune capacity, and carcass traits in fattening lambs. *Animals.* (2020) 10:1285. doi: 10.3390/ani10081285
9. Muir SK, Linden N, Knight M, Behrendt R, Kearney G. Sheep residual feed intake and feeding behaviour: are 'nibblers' or 'binge eaters' more efficient. *Anim Prod Sci.* (2018) 58:1459–64. doi: 10.1071/AN17770
10. Jackson T, Heard J, Malcolm B. System changes to a lamb farm in south-west victoria: some pre-experimental modelling. *AFBM J.* (2014) 11:1–18. doi: 10.22004/ag.econ.198725
11. Goldansaz SA, Markus S, Berjanskii M, Rout M, Guo AC, Wang Z, et al. Candidate serum metabolite biomarkers of residual feed intake and carcass merit in sheep. *J Anim Sci.* (2020) 98:skaa298. doi: 10.1093/jas/skaa298
12. Rincon-Delgado RM, Gutierrez H, Perez-Vszq ED, Muro-Reyes A, Diaz-Garci LH, Banuelos-VR, et al. Relationship of residual feed intake on specific hematological and biochemical parameters in Rambouillet sheep. *Agri J.* (2011) 6:87–91. doi: 10.3923/aj.2011.87.91
13. Chang EI, Wesolowski SR, Gilje EA, Baker PR, Reisz JA, D'Alessandro A, et al. Skeletal muscle amino acid uptake is lower and alanine production is greater in late gestation intrauterine growth-restricted fetal sheep hindlimb. *Am J Physiol Regul Integr Comp Physiol.* (2019) 317:R615–29. doi: 10.1152/ajpregu.00115.2019
14. Ribeiro DM, Madeira MS, Kilminster T, Scanlon T, Oldham C, Greeff J, et al. Amino acid profiles of muscle and liver tissues of Australian Merino, Damara and Dorper lambs under restricted feeding. *J Anim Physiol Anim Nutr.* (2019) 103:1295–302. doi: 10.1111/jpn.13148
15. Psychogios N, Hau DD, Peng J, Guo AC, Mandal R, Bouatra S, et al. The human serum metabolome. *PLoS ONE.* (2011) 6:e16957. doi: 10.1371/journal.pone.0016957
16. Zhou J, Ji K, Liu H, Zhang Y, Degen AA, Jiao D, et al. Effect of air temperature on growth performance, apparent digestibilities, rumen fermentation and serum metabolites in Altay and Hu lambs. *J Anim Physiol Anim Nutr.* (2020) 104:1023–33. doi: 10.1111/jpn.13318
17. Jiang B, Wang T, Zhou Y, Li F. Effects of enzyme + bacteria treatment on growth performance, rumen bacterial diversity, KEGG pathways, and the CAZy spectrum of Tan sheep. *Bioengineered.* (2020) 11:1221–32. doi: 10.1080/21655979.2020.1837459
18. Du H, Erdene K, Chen S, Qi S, Bao Z, Zhao Y, et al. Correlation of the rumen fluid microbiome and the average daily gain with a dietary supplementation of Allium mongolicum Regel extracts in sheep. *J Anim Sci.* (2019) 97:2831–43. doi: 10.1093/jas/skz139
19. Jia P, Cui K, Ma T, Wan F, Wang W, Yang D, et al. Influence of dietary supplementation with *Bacillus licheniformis* and *Saccharomyces cerevisiae* as alternatives to monensin on growth performance, antioxidant, immunity, ruminal fermentation and microbial diversity of fattening lambs. *Sci Rep.* (2018) 8:16712. doi: 10.1038/s41598-018-35081-4
20. Mnasri T, Hérault J, Gauvry L, Loiseau C, Poisson L, Ergan F, et al. Lipase-catalyzed production of lysophospholipids. *OCL.* (2017) 24:D405. doi: 10.1051/ocl/2017011
21. Polycarpo GV, Burbarelli MF, CarÃo AC, Merseguel CE, Dadalt JC, Maganha SR, et al. Effects of lipid sources, lysophospholipids and organic acids in maize-based broiler diets on nutrient balance, liver concentration of fat-soluble vitamins, jejunal microbiota and performance. *Br Poult Sci.* (2016) 57:788–98. doi: 10.1080/00071668.2016.1219019
22. Wang QQ, Long SF, Hu JX, Li M, Pan L, Piao XS. Effects of dietary lysophospholipid complex supplementation on lactation performance, and nutrient digestibility in lactating sows. *Anim Feed Sci Technol.* (2019) 251:56–63. doi: 10.1016/j.anifeedsci.2018.12.009
23. Lee C, Morris DL, Copelin JE, Hettick JM, Kwon IH. Effects of lysophospholipids on short-term production, nitrogen utilization, and rumen fermentation and bacterial population in lactating dairy cows. *J Dairy Sci.* (2019) 102:3110–20. doi: 10.3168/jds.2018-15777
24. He Y, Zhong R, Cheng L, You P, Li Y, Sun X. Effects of the supplementation of lysophospholipids through pelleted total mixed rations on blood biochemical parameters and milk production and composition of mid-lactation dairy cows. *Animals.* (2020) 10:E215. doi: 10.3390/ani10020215
25. Huo Q, Li B, Cheng L, Wu T, You P, Shen S, et al. Dietary supplementation of lysophospholipids affects feed digestion in lambs. *Animals.* (2019) 9:E805. doi: 10.3390/ani9100805
26. Zheng L, Lin Y, Lu S, Zhang J, Bogdanov M. Biogenesis, transport and remodeling of lysophospholipids in Gram-negative bacteria. *Biochim Biophys Acta Mol Cell Biol Lipids.* (2017) 1862:1404–13. doi: 10.1016/j.bbalip.2016.11.015
27. Sawai T, Lampman R, Hua Y, Segura B, Drongowski RA, Coran AG, et al. Lysophosphatidylcholine alters enterocyte monolayer permeability via a protein kinase C/Ca^{2+} mechanism. *Pediatr Surg Int.* (2002) 187:591–4. doi: 10.1007/s00383-002-0860-x
28. Laeger T, Görs S, Metges CC, Kuhla B. Effect of feed restriction on metabolites in cerebrospinal fluid and plasma of dairy cows. *J Dairy Sci.* (2012) 95:1198–208. doi: 10.3168/jds.2011-4506
29. Wu G, Bazer FW, Dai Z, Li D, Wang J, Wu Z. Amino acid nutrition in animals: protein synthesis and beyond. *Annu Rev Anim Biosci.* (2014) 2:387–417. doi: 10.1146/annurev-animal-022513-114113
30. Zhang H, Peng A, Guo S, Wang M, Loor JJ, Wang H. Dietary N-carbamylglutamate and l-arginine supplementation improves intestinal energy status in intrauterine-growth-retarded suckling lambs. *Food Funct.* (2019) 10:1903–14. doi: 10.1039/c8fo01618f
31. Brosnan ME, Brosnan JT. Histidine metabolism and function. *J Nutr.* (2020) 150(Suppl. 1):2570–5S. doi: 10.1093/jn/nxaa079
32. Wang B, Luo Y, Su R, Yao D, Hou Y, Liu C, et al. Impact of feeding regimens on the composition of gut microbiota and metabolite profiles of plasma and feces from Mongolian sheep. *J Microbiol.* (2020) 58:472–82. doi: 10.1007/s12275-020-9501-0

Conflict of Interest: The authors declare that the research was conducted in the absence of any commercial or financial relationships that could be construed as a potential conflict of interest.

frontiers in Microbiology

ORIGINAL RESEARCH
published: 12 May 2021
doi: 10.3389/fmicb.2021.675480

Alterations of Serum Metabolites and Fecal Microbiota Involved in Ewe Follicular Cyst

Tao Feng[1,2,3], Hongxiang Ding[1,2,3], Jing Wang[4], Wei Xu[5], Yan Liu[1,2]* and Ákos Kenéz[5]*

[1] Institute of Animal Husbandry and Veterinary Medicine (IAHVM), Beijing Academy of Agriculture and Forestry Sciences (BAAFS), Beijing, China, [2] Joint Laboratory of Animal Science Between IAHVM of BAAFS and Division of Agricultural Science and Natural Resource, Oklahoma State University, Beijing, China, [3] College of Animal Science and Technology, Henan University of Science and Technology, Luoyang, China, [4] College of Animal Science and Technology, Hebei North University, Zhangjiakou, China, [5] Department of Infectious Diseases and Public Health, City University of Hong Kong, Hong Kong, China

While the interactions of the gut microbiome and blood metabolome have been widely studied in polycystic ovary disease in women, follicular cysts of ewes have been scarcely investigated using these methods. In this study, the fecal microbiome and serum metabolome were used to compare between ewes diagnosed with ovarian cystic follicles and ewes with normal follicles, to investigate alterations of the fecal bacterial community composition and metabolic parameters in relation to follicular cystogenesis. Ewes from the same feeding and management system were diagnosed with a follicular cyst (n = 6) or confirmed to have normal follicles (n = 6) by using a B-mode ultrasound scanner. Blood serum and fresh fecal samples of all ewes were collected and analyzed. The α-diversity of fecal microbiome did not differ significantly between follicular cyst ewes and normal follicle ewes. Three genera (*Bacteroides*, *Anaerosporobacter*, and *Angelakisella*) were identified and their balance differentiated between follicular cyst and normal follicle ewes. Alterations of several serum metabolite concentrations, belonging to lipids and lipid-like molecules, organic acids and derivatives, organic oxygen compounds, benzenoids, phenylpropanoids and polyketides, and organoheterocyclic compounds, were associated with the presence of a follicular cyst. Correlation analysis between fecal bacterial communities and serum metabolites indicated a positive correlation between *Anaerosporobacter* and several fatty acids, and a negative correlation between *Bacteroides* and L-proline. These observations provide new insights for the complex interactions of the gut microbiota and the host serum lipid profiles, and support gut microbiota as a potential strategy to treat and prevent follicular cysts in sheep.

Keywords: sheep, follicular cysts, microbial diversity, metabolome, host-microbiota interactions

OPEN ACCESS

Edited by:
Xudong Sun,
Heilongjiang Bayi Agricultural University, China

Reviewed by:
Youji Ma,
Gansu Agricultural University, China
Hailing Luo,
China Agricultural University, China

****Correspondence:***
Tao Feng
fengtao_gs@163.com
Yan Liu
liuyanxms@163.com

Specialty section:
This article was submitted to Systems Microbiology, a section of the journal Frontiers in Microbiology

Received: *03 March 2021*
Accepted: *16 April 2021*
Published: *12 May 2021*

Citation:
Feng T, Ding H, Wang J, Xu W, Liu Y and Kenéz Á (2021) Alterations of Serum Metabolites and Fecal Microbiota Involved in Ewe Follicular Cyst. Front. Microbiol. 12:675480. doi: 10.3389/fmicb.2021.675480

INTRODUCTION

Cystic ovarian follicle is one of the ovarian dysfunctions in humans and livestock, resulting mainly from several alterations in follicle development and ovulatory mechanisms, causing female infertility (Mutinati et al., 2013; Ortega et al., 2016). It is generally recognized that functional alterations of the hypothalamus-pituitary-gonadal axis caused by imbalance of ovarian endocrine

homeostasis is the main cause of follicular cysts (Christman et al., 2000; Medan et al., 2004; Mutinati et al., 2013). Absence or abnormal release of hypothalamic gonadotropin-releasing hormone (GnRH) or lack of luteinizing hormone (LH) surge were considered as one of the endocrine reasons to induce a follicular cyst, identified as a target for symptomatic therapies to treat infertility (Medan et al., 2004; Abdalla et al., 2020). In humans, ovarian diseases with a phenotype of follicular cysts are collectively referred to as polycystic ovary syndrome (PCOS). For the past few years, the relationship between the gut microbiota and metabolic status attracted significant attention to reveal the etiology and pathological mechanisms of PCOS, based on intestinal bacterial communities influencing energy absorption, short chain fatty acid production, and lipopolysaccharide release (Liu et al., 2017; Zhao et al., 2020). Previous studies also showed that bacterial diversity of gut microbial communities had an effect on PCOS depending on host metabolic parameters (Lüll et al., 2020). Additionally, altered fecal microbiome and metabolome and their associations with diseases, such as kidney disease and chronic obstructive pulmonary disease, were reported in humans (Chen et al., 2019; Bowerman et al., 2020). Further associations were revealed between cysteine levels on pregnancy outcome in sows and myostatin phenotype affecting lean meat proportion in pigs (Ding et al., 2019; Pei et al., 2021).

Ovarian cyst is one of the reasons of infertility in sheep and goat (Medan et al., 2004; Palmieri et al., 2011). The incidence of follicular cysts in sheep was reported highly variable, ranging from 0.2 to 6% (Smith et al., 1999; Palmieri et al., 2011). According to the previous studies, the reason of ewes' follicular cysts includes inhibition of preovulatory LH surge by adrenocorticotrophic hormone (ATCH) (Palmieri et al., 2011), lower concentration of plasma progesterone (Medan et al., 2004), overweight (Christman et al., 2000), and *Toxoplasma gondii* infection (Moraes et al., 2010). As far as we know, there were few studies about the relationship between the gut microbiota or blood metabolome and follicular cysts in ewes, and about the associations of the gut microbiota and the blood metabolome in relation to cystogenesis in sheep. Thus, the aims of the present study were: (1) to characterize the alterations of fecal microbial communities, (2) to identify patterns of serum metabolome profiles, and (3) to reveal the associations of gut microbiota and metabolome in follicular cysts ewes compared with normal follicle ewes. The objective of this research was to provide potential targets of gut microbiota or metabolic pathways for therapeutic and preventive interventions of follicular cyst in sheep.

MATERIALS AND METHODS

Experimental Station

Experiments were performed at the Experimental Station of Beijing Academy of Agriculture and Forestry Sciences in Yangyuan County, Zhangjiakou City, Hebei Province, Northeast of China. All the experiments were carried out according to the International Guiding Principles for Biomedical Research Involving Animals, and the respective permit was granted by Beijing Academy of Agriculture and Forestry Sciences (SYXQ-2012-0034).

Ewes and Reproduction Management

A total of 320 crossbreed ewes (*Ovis aries*) of Merino rams and Small Tailed Han ewes aged 2–4 years were housed in a four sheltered outdoor paddocks and were fed a total mixed ration (TMR) of 2,000 g per head per day after weaning. The TMR composition was based on the recommendations of sheep feeding standards in China (NY/T816-2004). Clean water and mineralized salt licks were available *ad libitum*. From 1 May to 31 May, eight rams were put into each ewe paddock to mate ewes naturally. On 5 July, conception was identified by pregnancy diagnosis using a B-mode ultrasound scanner (Honda HS-1600V, Honda Electronics, Tokyo, Japan).

Ultrasonography

Besides pregnancy diagnosis, the B-mode scanner was used to diagnose ovarian follicular cyst by transrectal ultrasonography collaborated with a 7.5 MHz transducer as mentioned by Steckler et al. (2008) and Palmieri et al. (2011). Based on the follicular diameter and the presence or absence of a fetal sac, ewes were divided into three groups: pregnant, follicular cyst, and non-pregnant with normal follicles. Ewes were diagnosed with follicular cyst when the follicle diameter was greater than 10 mm (Medan et al., 2004; Palmieri et al., 2011). Ewes diagnosed with ovarian follicular cyst were re-evaluated after 8 days, and animals were enrolled for sample collection if the follicular cyst was confirmed to still be greater than 10 mm.

Fecal Sample Collection and Microbiota Analysis

Fresh fecal samples were individually collected from six ewes with a follicular cyst diameter greater than 10 mm, after the second ultrasonography. Fresh fecal samples of six non-pregnant ewes with normal follicles from the same herd were collected at the same time. The samples were quickly frozen in liquid nitrogen and submitted to the laboratory. Genomic DNA of the 12 samples were extracted using an E.Z.N.A. Stool DNA Isolation Kit (Omega Bio-tek, Norcross, GA, United States) following the recommended instructions and confirmed with 1.2% agarose gel, of which the DNA yield and purity were measurement of absorbance using NanoDrop 2000 UV-vis spectrophotometer (Thermo Fisher Scientific, Wilmington, United States). A pair of barcode-modified universal primer 338F and 806R (forward: 5′-ACTCCTACGGGAGGCAGCA-3′; reverse: 5′-GGACTACHVGGGTWTCTAAT-3′) was used to amplify the V3 + V4 hypervariable fragments from the bacterial 16S rDNA (Wang et al., 2018). The PCR products were purified using an AxyPrep DNA Gel Extraction Kit (Axygen Biosciences, Union City, CA, United States), following the manufacturer's instructions. The DNA fragment amplicons were sequenced on an Illumina MiSeq PE300 platform/NovaSeq PE250 platform (Illumina, San Diego, United States) according to the standard procedures of Majorbio Bio-Pharm Technology Co. Ltd.

(Shanghai, China). The raw reads were approved by the NCBI Sequence Read Archive (SRA) database with accession number SRP308293.

The raw sequencing reads of 16S rRNA gene were demultiplexed, quality-filtered by fastp version 0.20.0 (Chen et al., 2018) and merged by FLASH version 1.2.7 (Magoč and Salzberg, 2011). Optimized, high-quality sequences were clustered using UPARSE version 7.1 into operational taxonomic units (OTUs) at 97% sequence identity, and chimeric sequences were discerned and filtered out. The taxonomy of each OTU representative sequence was analyzed by Ribosomal Database Project (RDP) naive Bayesian classifier against the 16S rRNA database (Release 138)[1] (Wang et al., 2018). Alpha diversity (Shannon and Simpson estimators for diversity evaluation, Chao and ACE estimators for abundance evaluation) was analyzed by Mothur v. 1.31.2. Principle coordinates analysis (PCoA) was used to visualize differences in fecal community composition reflecting its beta diversity. The linear discriminant analysis effect size (LEfSe) algorithm was performed to identify the taxa differences responsible for different groups. The biomarkers of LEfSe analysis conducted in the microbiota study had an effect-size threshold of two. PICRUSt2 was used to identify metabolic activities of the gut microbiota (Zhang et al., 2021). Predicted metabolic profile for Kyoto Encyclopedia of Genes and Genomes (KEGG) Orthologs (KO) were mapped on database matching[2].

Blood Sample Collection and Metabolomics Analysis

Blood was collected from the same ewes enrolled for fecal microbiome analysis ($n = 6$ with follicle cyst, $n = 6$ with normal follicles) via jugular venipuncture into 10-mL vacuum tubes. Blood samples were undisturbed and kept at room temperature for 4 h and then centrifuged at 2,000 *g* for 30 min at 4°C to isolate the sera, which were subsequently stored at −80°C until further analysis.

Using 100 μL serum, metabolites were extracted using methanol. Extracts were sonicated, and after centrifugation, the supernatants were gently added to sample vials for LC-MS/MS analysis. A pooled quality control sample (QC) was used for system conditioning and quality control. Chromatographic separation of the metabolites was operated on a Thermo UHPLC system equipped with an ACQUITY UPLC HSS T3 (100 mm × 2.1 mm i.d., 1.8 μm; Waters, Milford, United States). Following LC-MS/MS analyses, the raw data were inputted into the Progenesis QI 2.3 (Non-linear Dynamics, Waters, United States) for peak picking and alignment. Mass spectra of these metabolic characteristics were discerned through the accurate mass, MS/MS fragments spectra, and isotope ratio difference, by scanning in publicly available biochemical databases such as the Human metabolome database (HMDB)[3] and Metlin database[4]. A multivariate statistical analysis was conducted using "ropls" (Version1.6.2)[5] R package from Bioconductor on Majorbio Cloud Platform[6]. Principle component analysis (PCA) was applied to check outliers and present trends. Partial least squares-discriminant analysis (PLS-DA) was used to identify the general metabolic changes in serum of sheep with or without follicular cyst. Variable importance in the projection (VIP) was computed by an orthogonal partial least squares discriminant analysis (OPLS-DA) model. Differential metabolites between groups were identified ($P < 0.05$, VIP-value > 1), and annotated into their biochemical pathways through metabolic enrichment and pathway analysis based on database matching (KEGG) (see text footnote 2). Further, Volcano plot was used to compare the size of the fold change to statistical significance. Regarding VIP value of metabolites, * means significant difference between ewes with follicular cyst and normal follicle ($P < 0.05$), ** means significant difference ($P < 0.01$), and *** means significant difference ($P < 0.001$).

Correlation Between Serum Metabolites and Fecal Microbial Taxa

The cooperativity of two-dimensional shapes produced from superimposition of PCA from microbiome and metabolome was conducted by Procrustes analysis (PA). Mainly, the correlation between relative abundance of fecal microbiota at genus levels and differential metabolites was analyzed by R package ggplot2 (McHardy et al., 2013; Mazhar et al., 2021). $P < 0.05$ were considered to have significant difference. Representation of the *P*-value is as follows: * $P < 0.05$, ** $P < 0.01$, and *** $P < 0.001$.

RESULTS

Cysts Diagnosis

In the present study, transrectal ultrasonography by a B-mode scanner identified ovarian follicular cysts clearly and effectively in sheep. Ewes diagnosed with a follicular cyst demonstrated a sharp image of anechoic (round and black) structure with an antrum greater than 10 mm in diameter (**Figure 1A**), while sheep with normal follicles showed a smaller antrum (**Figure 1B**). The average diameter of the follicles in cyst and normal sheep were 11.6 ± 0.5 mm and 3.6 ± 0.3 mm, respectively.

Fecal 16S rRNA Sequencing

A total of 545,894 reads were sequenced in the amplified 16S rRNA genes, after quality checks in 12 samples. As for follicular cyst ewes, the mean (SD in parentheses) reads was 46,627 (2,407), while 44,355 (4,980) reads were obtained in normal follicle ewes. Among the high-quality sequences, the minimum length was 248 bp and the maximum length was 511 bp. The read length for all samples was 413 bp on average, in which more than 99.9% of reads exceeded 400 bp. Reads were clustered into 2,000 OTUs using a 97% similarity threshold. OTUs ranged from 346 to 778 per sample were obtained. Based on sequencing results and rarefaction analysis, the depth of sequence obtained was adequate

[1]http://www.arb-silva.de

[2]http://www.genome.jp/kegg/

[3]http://www.hmdb.ca/

[4]https://metlin.scripps.edu/

[5]http://bioconductor.org/packages/release/bioc/html/ropls.html

[6]https://cloud.majorbio.com

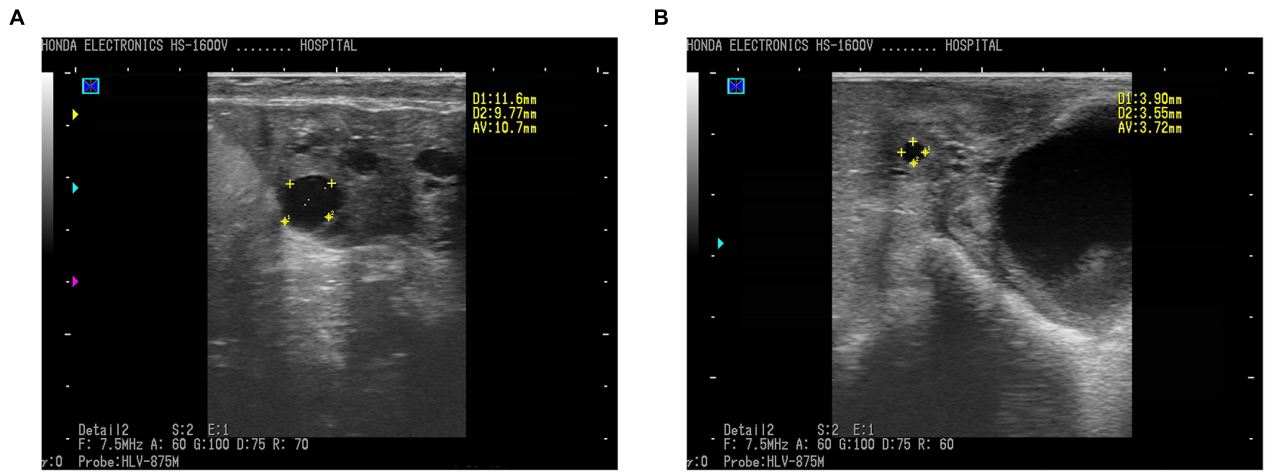

FIGURE 1 | Ultrasound photos of ovaries of ewes imaged using a 7.5 MHz transducer and B-mode scanner. **(A)** Follicular cyst with 10.70 mm in diameter in sheep. **(B)** Normal follicle with 3.72 mm in diameter. Scale bars represent 10 mm. Follicles (round black structures) marked with yellow crosses showed anechoic structure.

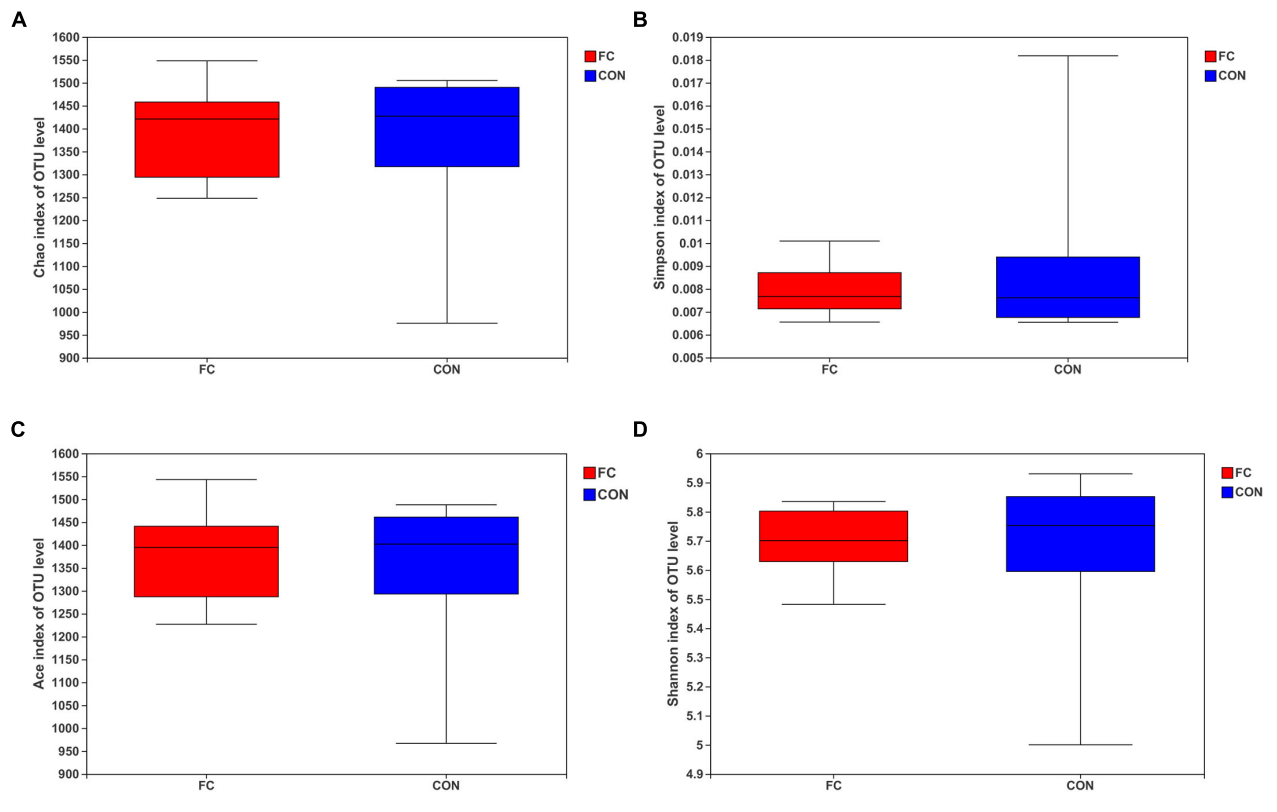

FIGURE 2 | Alpha diversity for the fecal microbiota in follicular cyst and normal follicle ewes. **(A)** Chao index; **(B)** Simpson index; **(C)** ACE index; **(D)** Shannon index.

to reflect species richness, indicating that the sequencing system (Illumina Miseq) we used identified most of the fecal bacterial diversity in the present study.

Alpha Diversity of Fecal Microbiota

The Chao, Simpson, ACE, and Shannon estimators were used to evaluate fecal microbiome taxon abundance and diversity (**Figure 2**). No significant difference was found in the fecal microbiome diversity comparing the follicular cyst ewes with the normal follicle ewes by student's *t*-test (all $P > 0.05$). Meanwhile, the Good's coverage estimator was more than 99% for fecal samples of follicular cyst ewes and normal follicle ewes, indicating that the dominant bacterial phenotypes were included in our study.

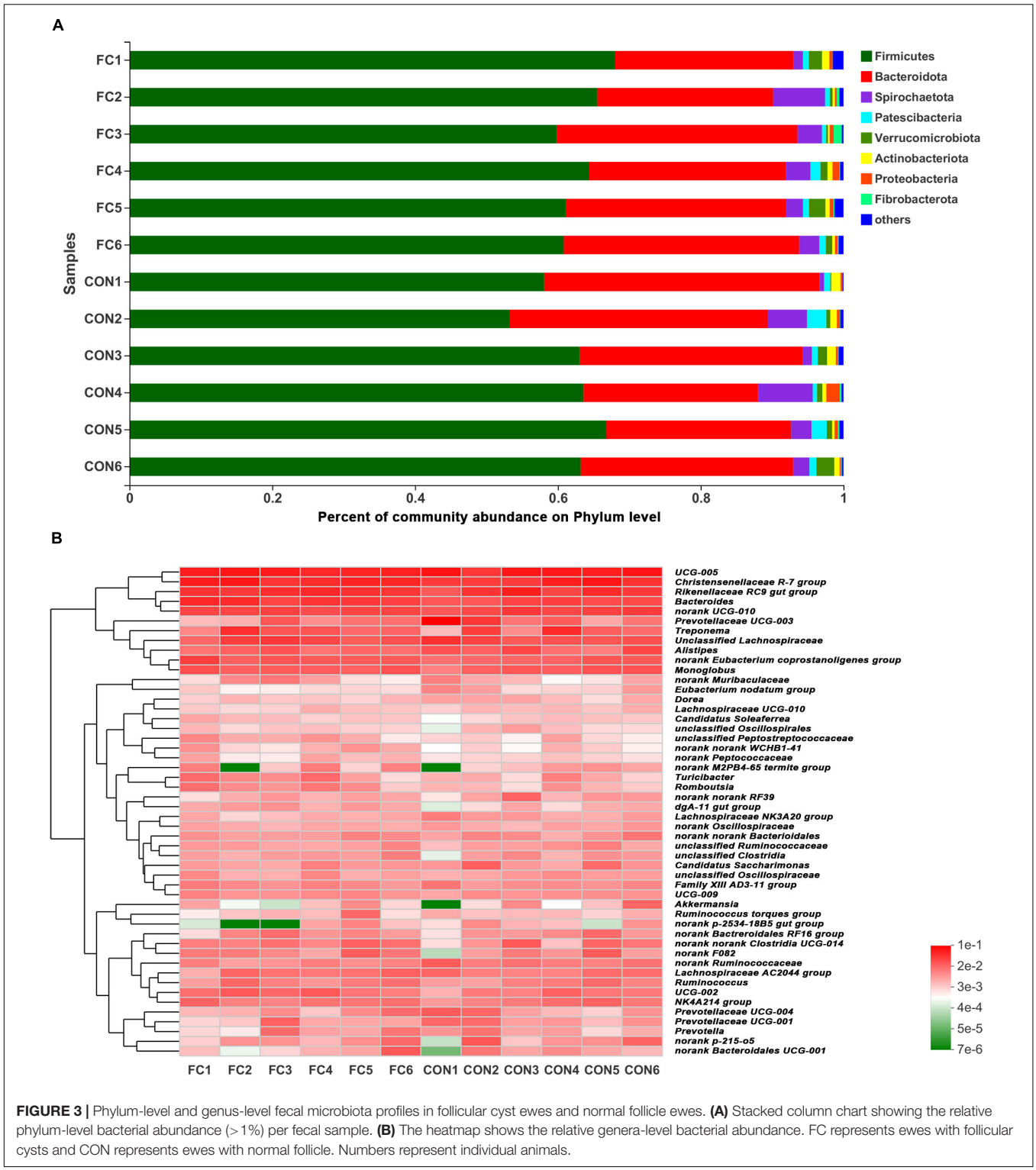

FIGURE 3 | Phylum-level and genus-level fecal microbiota profiles in follicular cyst ewes and normal follicle ewes. **(A)** Stacked column chart showing the relative phylum-level bacterial abundance (>1%) per fecal sample. **(B)** The heatmap shows the relative genera-level bacterial abundance. FC represents ewes with follicular cysts and CON represents ewes with normal follicle. Numbers represent individual animals.

Fecal Microbiota Composition

A total of 2,000 OTUs were identified in fecal samples of follicular cyst ewes and normal follicle ewes, in which 1,645 OTUs were co-existent, 195 OTUs were follicular cyst ewes only, and 160 OTUs were normal follicle ewes only.

At phylum level, Firmicutes and Bacteroidetes (Firmicutes > Bacteroidetes) were the two dominant taxa in both groups and accounted for 92.41% for follicular cyst ewes and 92.35% for normal follicle ewes of total phylum, on average. Other three phyla were present at lower frequencies,

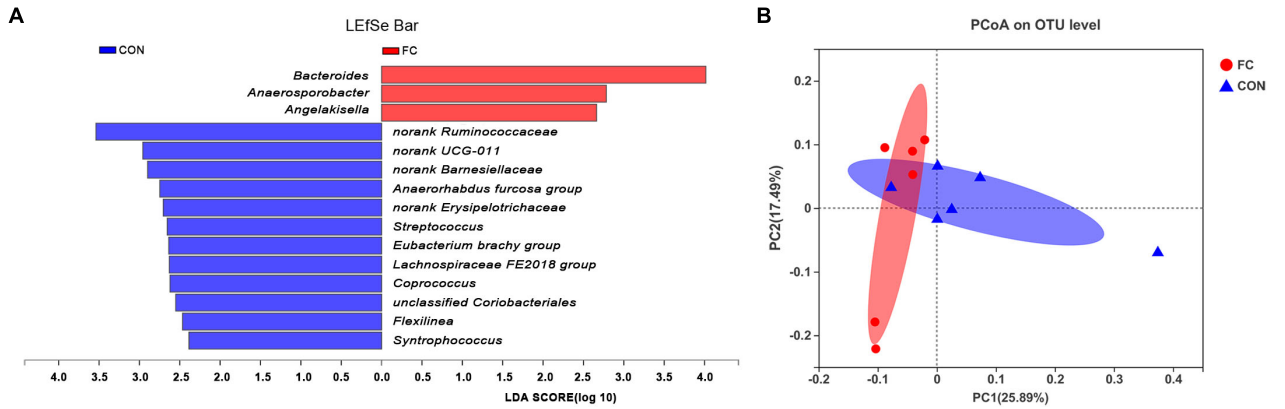

FIGURE 4 | Differences between bacterial taxa in follicular cyst ewes and normal follicle ewes. **(A)** The linear discriminant analysis (LDA) effect size (LEfSe) algorithm displayed significant differences between follicular cyst ewes and normal follicle ewes at genus level. **(B)** The principal coordinate analysis (PCoA) plots of the fecal microbiota based on the unweighted UniFrac showed the extent of variation in fecal microbial community between follicular cyst ewes and normal follicle ewes at OUT level. FC represents ewes with follicular cysts and CON represents ewes with normal follicle. Red bars represent OTU that are more abundant in follicular cyst ewes' fecal samples than in normal follicle controls.

including Spirochaetota, Patescibateria, and Verrucomicrobiota. In fecal samples of follicular cyst ewes, these three taxa (Spirochaetota > Verrucomicrobiota > Patescibateria) accounted for 5.42% on average, while in normal follicle ewes they (Spirochaetota > Patescibateria > Verrucomicrobiota) accounted for 5.70% on average (**Figure 3A**).

At genus level, a hierarchically clustered heatmap of the fecal microbiota composition of ewes was shown in **Figure 3B**. *UCG-005* (10.37%), *Christensenellaceae_R-7_group* (7.48%), *Rikenellaceae_RC9_gut_group* (6.20%), *Prevotellaceae_UCG-003* (5.18%), and *Bacteroides* (4.05) were the top five dominant genera in follicular cyst ewes on average, while *UCG-005* (9.64%), *Christensenellaceae_R-7_group* (8.81%), *Rikenellaceae_RC9_gut_group* (6.78%), *Bacteroides* (6.26%), and *Treponema* (3.30%) were the top five dominant genera in normal follicle ewes on average.

LEfSe analysis manifested significant differences between follicular cyst ewes and normal follicle ewes from phylum to genus level according to relative OTU abundance (**Supplementary Figure 1**). Ewes with follicular cyst had enriched Bacteroidaceae at family level, *Bacteroides*, *Anaerosporobacter*, and *Angelakisella* at genus level. However, ewes with normal follicle were abundant with 1 at phylum level, 1 at class level, 3 at order level, 5 at family level, and 12 at genus level (**Figure 4A** and **Supplementary Figure 1**).

Principle coordinates analysis (PCoA) indicated differences of fecal bacterial communities between ewes with follicular cyst and normal follicle (**Figure 4B**).

A total of 204 functional pathways were predicted with PICRUSt2 by comparing against KEGG orthologs. KEGG pathways including ABC transporters, purine metabolism and aminoacyl-tRNA biosynthesis were higher in follicular cyst ewes than normal follicle ewes, which showed a good response to KEGG pathways enrichment in metabolomics.

Serum Metabolite Profile

In the serum LC-MS spectra of ewes with follicular cyst or with normal follicle, 10,598 metabolites were initially found. After quality control and discernment, 948 compounds were reliably detected. The PCA score plot presented that the first and second principal components (PCs) covered 25.50% and 18.20% of the variation, respectively (**Figure 5A**). Scores representing follicular cyst and normal follicle samples were separated in the PCA plot. PLS-DA was performed to analyze the serum metabolome profile variations between the follicular cyst and normal follicle ewes. As shown in **Figure 5B**, the PLS-DA analysis demonstrated that the serum metabolites of the follicular cyst ewes distinctly differed from those of the normal follicle ewes. Correspondingly, the values of R2Y and Q2 were 0.998 and 0.878, respectively (**Figure 5C**), indicating good interpretability and predictability by this PLS-DA model. A value of Q2 = 1 indicates a perfect discrimination of metabolite profiles between groups.

Difference in Serum Metabolite

In comparison, a total of 44 differential serum metabolites were found according to the Volcano plot, of which 16 metabolites showed up-regulation and 28 showed down-regulation in ewes with follicle cyst (**Figure 6A** and **Supplementary Table 1**). A total of 40 differential serum metabolites were annotated in 7 superclasses according to HMDB database, of which 20 belonged to lipids and lipid-like molecules, 7 belonged to organic acids and derivatives, 4 belonged to organic oxygen compounds, 3 belonged to benzenoids, 3 belonged to phenylpropanoids and polyketides, 2 belonged to nucleosides, nucleotides, and analogs, and 1 belonged to organoheterocyclic compounds. Expression profile and VIP of top 30 metabolites based on the OPLS-DA model was shown in **Figure 6B**.

Regarding KEGG pathway, the four pathways including at least two differential serum metabolites annotated were aminoacyl-tRNA biosynthesis (L-proline and L-histidine),

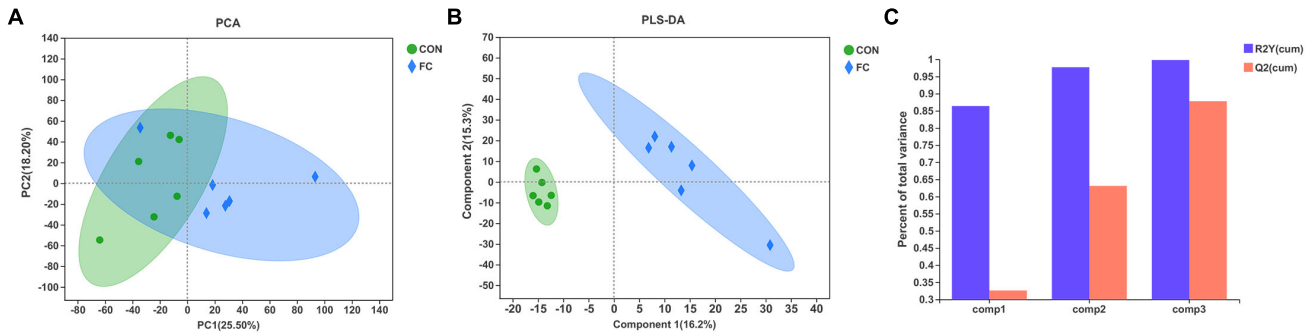

FIGURE 5 | Difference of serum metabolite profiles of ewes with follicular cyst or normal follicle. **(A)** PCA score plot for serum metabolites of ewes with follicular cyst or normal follicle. **(B)** PLS-DA score plot for serum metabolites of ewes with follicular cyst or normal follicle. **(C)** The model overview showing high R2Y and Q2 in PLS-DA. The values of R2Y and Q2 were 0.998 and 0.878, respectively. FC represents ewes with follicular cysts and CON represents ewes with normal follicle.

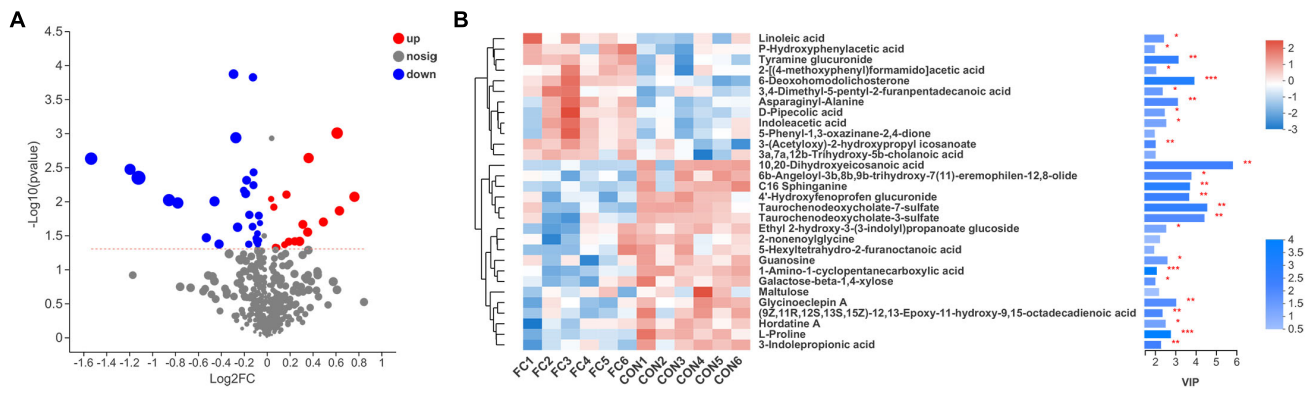

FIGURE 6 | Serum metabolite profiles of ewes with follicular cyst or normal follicle. **(A)** Enhanced Volcano plots of OPLS-DA showing fold changes (log_2FC) and the negative logarithm (base 10) of the *P*-values of 44 differential serum metabolites in follicular cyst ewes compared with normal follicle ewes. **(B)** Expression profile, VIP score, and *P*-value of the top 30 differential serum metabolites in follicular cyst ewes compared with normal follicle ewes. *Significant difference in serum metabolome between ewes with follicular cyst and normal follicle ($P < 0.05$), **significant difference ($P < 0.01$), and ***significant difference ($P < 0.001$).

protein digestion and absorption (L-proline and L-histidine), purine metabolism (Diadenosine tetraphosphate and Guanosine), and ABC transporters (L-proline and L-histidine), respectively. Based on our results, the serum metabolome profiles of ewes were affected by the presence or absence of follicular cyst.

Correlation Between Serum Metabolites and Fecal Microbial Taxa

In order to identify if there was any inter-omic syntropy, a two-dimensional principal component distribution plot (30.43% in PC1 and 17.68% in PC2) was generated with square (microbe) or dot (metabolome) (**Figure 7A**). Procrustes analysis showed a strong cooperativity of fecal microbiome profiles and serum metabolome (**Figure 7A**: Monte Carlo $P < 0.01$). To further investigate the relationship between metabolites and microbes, a correlation matrix was conducted based on the Pearson's correlation coefficient (**Figure 7B**). A total of 11 genera of microorganisms and 29 metabolites were included in the heatmap matrix. The results demonstrated several significant metabolite–microbe relationships, such as L-proline had a strong positive correlation ($P < 0.05$) with *Anaerorhabdus* but had a strong negative correlation ($P < 0.01$) with *Bacteroides*.

DISCUSSION

Alteration of Fecal Microbiota in Ewes With Follicular Cyst or Normal Follicle

Polycystic ovary syndrome (PCOS) is a common ovarian disease in women with a prevalence of 8–13% (Zhao et al., 2020). Multiple studies have confirmed the close relationship between the gut microbiota and PCOS (Mammadova et al., 2020; Zhao et al., 2020). Follicular cysts were also discovered in sheep (Christman et al., 2000; Palmieri et al., 2011) and goat (Medan et al., 2004; Maia et al., 2018). To our knowledge, there has been no scientific report on the correlation between gut microbiota and follicular cyst in sheep. Several studies were reviewed that PCOS patients had a decreased α-diversity and different β-diversity composition in gut microbiota compared with healthy controls (Guo et al., 2021). In the

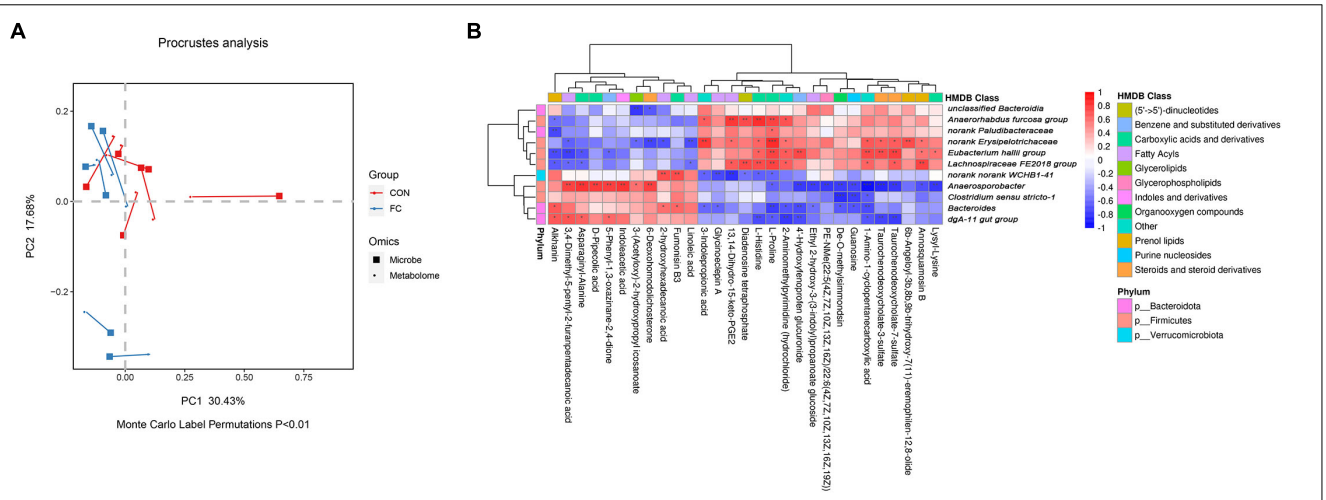

FIGURE 7 | Correlation between serum metabolites and fecal microbial taxa in ewes. **(A)** Procrustes analysis of fecal microbiome and serum metabolome in ewes with follicular cyst and normal follicle. Fecal and serum samples are showed as squares and dots, respectively. Fecal and serum samples from the same individual are connected by red (control ewes) and blue (follicular cyst ewes) lines. **(B)** Correlation analysis between fecal microbiome and serum metabolome in the ewes with follicular cyst and normal follicle. Red represents a positive correlation, while blue represents a negative correlation. *Significant correlation between fecal microbiome and serum metabolome ($P < 0.05$), **significant correlation ($P < 0.01$), and ***significant correlation ($P < 0.001$).

present study, no significant change was identified for α-diversity index of OTU level in fecal microbiota of follicular cyst ewes compared with normal follicle ewes. As for β-diversity composition in fecal microbial community, ewes with a follicular cyst were enriched at family level (Bacteroidaceae) and at genus level (*Bacteroides*, *Anaerosporobacter*, and *Angelakisella*). Bacteroidaceae was reported with a lower percent of relative abundance in gastrointestinal microbiota of PCOS girls (Jobira et al., 2020), while the family Bacteroidaceae had a higher level either in gut microbial community of women phenotyped as PCOS with insulin resistance or PCOS alone (Zeng et al., 2019). At genus level, bacterial taxa including *Coprococcus*, *Bacteroides*, *Prevotella*, *Lactobacillus*, *Parabacteroides*, *Escherichia/Shigella*, and *Faecalibacterium prausnitzii* were reviewed to be clearly altered in the gut microbiota of PCOS patients (Guo et al., 2021), of which *Bacteroides* was the most significant alteration in fecal microbiota of follicular cyst ewes in our study. Up to date, there has been no report on the relationship between fecal *Anaerosporobacter* genus or *Angelakisella* genus and follicular cysts. It was speculated that *Anaerosporobacter* may cause vascular damage and worsen renal function in murine models (Li et al., 2020), and the alteration in abundance of *Anaerosporobacter* in gut microbiome composition may cause coronary artery diseases (Toya et al., 2020). *Angelakisella*, a new bacterial species isolated from human ileum (Mailhe et al., 2017), was identified to regulate short chain fatty acids production in gut microbiota (Qiu et al., 2021). Alterations of *Anaerosporobacter* genus and *Angelakisella* genus in gut microbiota are firstly reported to have potential effects on follicular cyst in sheep, however, the precise mechanism of the two bacterial taxa in cyst development and cyst maintenance warrants further studies.

Alterations of Serum Metabolites in Ewes With Follicular Cyst or Normal Follicle

The serum metabolome profile of ewes with follicular cyst or normal follicle were found to be different using LC-MS/MS metabolomics analysis in our study. Alterations of serum compounds belonging to lipids and lipid-like molecules, organic acids and derivatives, organic oxygen compounds, benzenoids, phenylpropanoids and polyketides, and organoheterocyclic compounds were highlighted between follicular cyst and normal follicle ewes. Furthermore, according to the OPLS-DA model and VIP values, several metabolites are suggested as potential biomarkers or key metabolites to indicate the metabolic basis of follicular cysts development and maintenance in sheep.

PCOS was considered to be associated with turbulence of lipid metabolism in females (RoyChoudhury et al., 2016). As shown in **Figure 6B** and **Supplementary Table 1**, compounds annotated to lipids and lipid-like molecules were the most dominantly altered metabolites in follicular cyst ewes, according to HMDB database classification in our study. Linoleic acid (C18:2, n-6) is a common fatty acid in plasma and in granulosa cells in sheep, which is an essential fatty acid for arachidonic acid (C20:4, n-6) and eicosanoids synthesis (Mattos et al., 2000; Wonnacott et al., 2010). Linoleic acid inhibited oocyte maturation in cattle both *in vivo* and *in vitro* (Homa and Brown, 1992; Marei et al., 2010). However, in sheep, linoleic acid had an inhibitory effect on embryo development *in vitro* (Amini et al., 2016).

3,4-dimethyl-5-pentyl-2-furannonanoic acid, furan fatty acids with pentyl side chain, was produced from linoleic acid (Batna et al., 1993), and had a capacity to confront the intracellular negative effects consequences resulting from oxidative stress (Teixeira et al., 2013). The effect of 3,4-dimethyl-5-pentyl-2-furannonanoic acid on follicular cyst in sheep is still unknown and requires further studies.

Amino acids and their metabolic intermediates are of huge influence on anabolism and metabolic pathways. A disequilibrium of normal amino acid levels could trigger pathophysiological changes causing of infertility (Wu, 2009). In PCOS patients, serum levels of two amino acids, including proline and histidine, were reported to be down-regulated, compared with healthy controls (Atiomo and Daykin, 2012; Unni et al., 2015; RoyChoudhury et al., 2016). Proline and histidine were demonstrated to have negative association with inflammation and oxidative stress (Niu et al., 2012). Low levels of proline and histidine in PCOS patients might be a result of an increased utilization of proline and histidine to counteract oxidative stress during follicular cysts (Unni et al., 2015). Therefore, strategies to increase the levels of proline and histidine are anticipated to counteract the disorders caused by inflammation and oxidative stress during follicular development.

Indoleacetic acid, an organoheterocyclic compounds, is a major degradation product of L-tryptophan (an essential amino acids for ruminant animals), found in ruminal bacteria, as well as in blood and in several tissues in sheep and goats (Mohammed et al., 2003; Andrade et al., 2005). In ovarian tissues, indoleacetic acid was suspected to bind to growth factors (Ferreira et al., 2001), consequently improving the enzyme activity of the peroxidases during lipid peroxidation (Candeias et al., 1995). An *in vitro* study showed that lower concentration of indoleacetic acid improved follicle development, while higher doses demonstrated cytotoxicity in the absence of follicle-stimulating hormone (FSH) (Costa et al., 2010). In the present study, high abundance of indoleacetic acid likely had a negative effect on normal follicle development.

Correlation Between Fecal Bacterial Communities and Serum Metabolites in Ewes

Potential mechanisms of follicular cyst development may include circulating lipid and amino acid levels, affected by gut microbial composition. Little is known about the relationship between *Anaerosporobacter* and fatty acid absorption and metabolism. In the present study, positive correlations were identified between *Anaerosporobacter* and six serum compounds including 6-deoxohomodolichosterone, 3-(acetyloxy)-2-hydroxypropyl icosanoate, 3,4-dimethyl-5-pentyl-2-furanpentadecanoic acid, indoleacetic acid, asparaginyl-alanine, and D-pipecolic acid. Negative correlations were found between *Bacteroides* and L-proline and 3-indolepropionic acid. Changed abundance of *Anaerosporobacter* in fecal bacterial community and fatty acid composition in blood had been proved to associate with artery function (Toya et al., 2020; Samson et al., 2021). Coccidiosis, a disease due to *Eimeria* infection, was characterized by an increased abundance of *Bacteroides* and a decreased serum concentration of histidine and proline in mice (Huang et al., 2018). Alterations of gut microbiota and serum metabolome and their correlations could better explain the formation and maintenance of follicle cysts in ewes. Nevertheless, the causes of sheep follicular cyst were found by statistical analysis of omics data and from a relatively small number of samples. Further studies with evaluation the effects of microbiology or/and metabolites identified in the present study on ewe follicular cyst, and with larger size samples, are desired to validate our findings.

CONCLUSION

To conclude, we found correlations between the gut microbiome composition and various circulating metabolites in relation to follicle cyst development in ewes, suggesting complex interactions between gut microbiota, serum metabolome, and ovarian follicle dysfunction. Ewes' follicular cyst development may be affected by three pathways: (1) a high intestinal abundance of *Bacteroides*, *Anaerosporobacter* and *Angelakisella*; (2) accumulation of organic acids and derivatives (such as D-pipecolic acid, asparaginyl-alanine, fumonisin B3) and lipids and lipid-like molecules (linoleic acid, 2-hydroxyhexadecanoic acid, 3,4-dimethyl-5-pentyl-2-furanpentadecanoic acid) in serum; and (3) a respective interactions of fecal microbiota and serum metabolites. A bacteria-metabolite multilayer can enhance our comprehension of the metabolite pathways significantly associated to the microbial communities of follicular cysts in sheep. Based on the present multi-omics study, further studies are needed to verify the results.

DATA AVAILABILITY STATEMENT

The datasets presented in this study can be found in online repositories. The names of the repository/repositories and accession number(s) can be found below: https://www.ncbi.nlm.nih.gov/sra/?term=SRP308293.

ETHICS STATEMENT

The animal study was reviewed and approved by the Beijing Academy of Agriculture and Forestry Sciences.

AUTHOR CONTRIBUTIONS

TF and YL conceived the study. JW and TF obtained the funding. HD performed the animal trials and the data collection. WX and TF performed the data interpretation. TF and HD wrote the manuscript. WX and ÁK performed the manuscript revision. All authors read and approved the final manuscript content.

FUNDING

This work support by the Science Fundation of Institute of Animal Husbandry and Veterinary Medicine, Beijing Academy of Agriculture and Forestry Sciences (XMSSYJJ202101), the Achievement Transformation Project of Beijing Academy of Agriculture and Forestry Sciences (2020607), the Key Research

and Development Plan Program of Hebei Province (20326629D), and the Innovative Capacity Improvement Program of Hebei Province (20536601D).

ACKNOWLEDGMENTS

We thank all staff of the Experimental Station of Beijing Academy of Agriculture and Forestry Sciences (located in Yangyuan County, Zhangjiakou City, Hebei Province) for their assistance during the sample collection.

SUPPLEMENTARY MATERIAL

The Supplementary Material for this article can be found online at: https://www.frontiersin.org/articles/10.3389/fmicb.2021.675480/full#supplementary-material

Supplementary Figure 1 | The linear discriminant analysis (LDA) effect size (LEfSe) algorithm of significant differences between fecal bacterial taxa in follicular cyst ewes and normal follicle ewes from family to genus level.

Supplementary Table 1 | List of identified metabolites differentially accumulated in serum samples from follicular cyst ewes compared with control ewes.

REFERENCES

Abdalla, H., de Mestre, A. M., and Salem, S. E. (2020). Efficacy of ovulation synchronization with timed artificial insemination in treatment of follicular cysts in dairy cows. *Theriogenology* 154, 171–180. doi: 10.1016/j.theriogenology.2020.05.029

Amini, E., Asadpour, R., Roshangar, L., and Jafari-Joozani, R. (2016). Effect of linoleic acid supplementation on *in vitro* maturation, embryo development and apoptotic related gene expression in ovine. *Int. J. Reprod. Biomed.* 144, 255–262. doi: 10.29252/ijrm.14.4.255

Andrade, E. R., Marcondes Seneda, M., Alfieri, A. A., de Oliveira, J. A., Frederico Rodrigues Loureiro Bracarense, A. P., Figueiredo, J. R., et al. (2005). Interactions of indole acetic acid with EGF and FSH in the culture of ovine preantral follicles. *Theriogenology* 64, 1104–1113. doi: 10.1016/j.theriogenology.2005.03.001

Atiomo, W., and Daykin, C. A. (2012). Metabolomic biomarkers in women with polycystic ovary syndrome: a pilot study. *Mol. Hum. Reprod.* 18, 546–553. doi: 10.1093/molehr/gas029

Batna, A., Scheinkönig, J., and Spiteller, G. (1993). The occurrence of furan fatty acids in *Isochrysis sp.* and *Phaeodactylum tricornutum*. *Biochim. Biophys. Acta* 1166, 171–176. doi: 10.1016/0005-2760(93)90093-o

Bowerman, K. L., Rehman, S. F., Vaughan, A., Lachner, N., Budden, K. F., Kim, R. Y., et al. (2020). Disease-associated gut microbiome and metabolome changes in patients with chronic obstructive pulmonary disease. *Nat. Commun.* 11:5886. doi: 10.1038/s41467-020-19701-0

Candeias, L. P., Folkes, L. K., Porssa, M., Partick, J., and Wardman, P. (1995). Enhancement of lipid peroxidation by indole-3-acetic acid and derivates: substituent effects. *Free Rad. Res.* 23, 403–418. doi: 10.3109/10715769509065262

Chen, S., Zhou, Y., Chen, Y., and Gu, J. (2018). fastp: an ultra-fast all-in-one FASTQ preprocessor. *Bioinformatics* 34, i884–i890. doi: 10.1093/bioinformatics/bty560

Chen, Y., Chen, D., Chen, L., Liu, J., Vaziri, N. D., Guo, Y., et al. (2019). Microbiome-metabolome reveals the contribution of gut-kidney axis on kidney disease. *J. Transl. Med.* 17:5. doi: 10.1186/s12967-018-1756-4

Christman, S. A., Bailey, M. T., Head, W. A., and Wheaton, J. E. (2000). Induction of ovarian cystic follicles in sheep. *Domest. Anim. Endocrinol.* 19, 133–146. doi: 10.1016/s0739-7240(00)00077-1

Costa, S. H., Santos, R. R., Rondina, D., Andrade, E. R., Ohashi, O. M., Rodrigues, A. P., et al. (2010). Effects of IAA in combination with FSH on *in vitro* culture of ovine preantral follicles. *Zygote* 18, 89–92. doi: 10.1017/S0967199409990104

Ding, S., Fang, J., Liu, G., Veeramuthu, D., Naif Abdullah, A. D., and Yin, Y. (2019). The impact of different levels of cysteine on the plasma metabolomics and intestinal microflora of sows from late pregnancy to lactation. *Food Funct.* 10, 691–702. doi: 10.1039/c8fo01838

Ferreira, M. A., Brasil, A. F., Silva, J. R., Andrade, E. R., Rodrigues, A. P., and Figueiredo, J. R. (2001). Effects of storage time and temperature on atresia of goat ovarian preantral follicles held in M199 with or without indole-3-acetic acid supplementation. *Theriogenology* 55, 1607–1617. doi: 10.1016/s0093-691x(01)00506-4

Guo, J., Shao, J., Yang, Y., Niu, X., Liao, J., Zhao, Q., et al. (2021). Gut microbiota in patients with polycystic ovary syndrome: a systematic review. *Reprod. Sci.* doi: 10.1007/s43032-020-00430-0 [Epub online ahead of print],

Homa, S. T., and Brown, C. A. (1992). Changes in linoleic acid during follicular development and inhibition of spontaneous breakdown of germinal vesicles in cumulus-free bovine oocytes. *J. Reprod. Fertil.* 94, 153–160. doi: 10.1530/jrf.0.0940153

Huang, G., Zhang, S., Zhou, C., Tang, X., Li, C., Wang, C., et al. (2018). Influence of *Eimeria falciformis* infection on gut microbiota and metabolic pathways in mice. *Infect. Immun.* 86, e00073–18. doi: 10.1128/IAI.00073-18

Jobira, B., Frank, D. N., Pyle, L., Silveira, L. J., Kelsey, M. M., and Garcia-Reyes, Y. (2020). Obese adolescents with PCOS have altered biodiversity and relative abundance in gastrointestinal microbiota. *J. Clin. Endocrinol. Metab.* 105, e2134–e2144. doi: 10.1210/clinem/dgz263

Li, Y., Su, X., Gao, Y., Lv, C., Gao, Z., Liu, Y., et al. (2020). The potential role of the gut microbiota in modulating renal function in experimental diabetic nephropathy murine models established in same environment. *Biochim. Biophys. Acta. Mol. Basis. Dis.* 1866:165764. doi: 10.1016/j.bbadis.2020.165764

Liu, R., Zhang, C., Shi, Y., Zhang, F., Li, L., Wang, X., et al. (2017). Dysbiosis of gut microbiota associated with clinical parameters in polycystic ovary syndrome. *Front. Microbiol.* 8:324. doi: 10.3389/fmicb.2017.00324

Lüll, K., Arffman, R. K., Sola-Leyva, A., Molina, N. M., Aasmets, O., Herzig, K. H., et al. (2020). The gut microbiome in polycystic ovary syndrome and its association with metabolic traits. *J. Clin. Endocrinol. Metab.* 106, 858–871. doi: 10.1210/clinem/dgaa848

Magoč, T., and Salzberg, S. L. (2011). FLASH: fast length adjustment of short reads to improve genome assemblies. *Bioinformatics* 27, 2957–2963. doi: 10.1093/bioinformatics/btr507

Maia, A. L. R. S., Brandão, F. Z., Souza-Fabjan, J. M. G., Veiga, M. O., Balaro, M. F. A., Facó, O., et al. (2018). Transrectal ultrasound evaluation in tropical dairy goats: an indispensable tool for the diagnosis of reproductive disorders. *Trop. Anim. Health Prod.* 50, 787–792. doi: 10.1007/s11250-017-1496-0

Mailhe, M., Ricaboni, D., Vitton, V., Cadoret, F., Fournier, P. E., and Raoult, D. (2017). 'Angelakisella massiliensis' gen. nov., sp. nov., a new bacterial species isolated from human ileum. *New Microbes New Infect.* 16, 51–53. doi: 10.1016/j.nmni.2017.01.003

Mammadova, G., Ozkul, C., Yilmaz Isikhan, S., Acikgoz, A., and Yildiz, B. O. (2020). Characterization of gut microbiota in polycystic ovary syndrome: findings from a lean population. *Eur. J. Clin. Invest.* 51:e13417. doi: 10.1111/eci.13417

Marei, W. F., Wathes, D. C., and Fouladi-Nashta, A. A. (2010). Impact of linoleic acid on bovine oocyte maturation and embryo development. *Reproduction* 139, 979–988. doi: 10.1530/REP-09-0503

Mattos, R., Staples, C. R., and Thatcher, W. W. (2000). Effects of dietary fatty acids on reproduction in ruminants. *Rev. Reprod.* 5, 38–45. doi: 10.1530/ror.0.0050038

Mazhar, S. H., Li, X., Rashid, A., Su, J., Xu, J., Brejnrod, A. D., et al. (2021). Co-selection of antibiotic resistance genes, and mobile genetic elements in the presence of heavy metals in poultry farm environments. *Sci. Total. Environ.* 755:142702. doi: 10.1016/j.scitotenv.2020.142702

McHardy, I. H., Goudarzi, M., Tong, M., Ruegger, P. M., Schwager, E., Weger, J. R., et al. (2013). Integrative analysis of the microbiome and metabolome of the human intestinal mucosal surface reveals exquisite inter-relationships. *Microbiome* 1:17. doi: 10.1186/2049-2618-1-17

Medan, M. S., Watanabe, G., Sasaki, K., and Taya, K. (2004). Transrectal ultrasonic diagnosis of ovarian follicular cysts in goats and treatment with GnRH. *Domest. Anim. Endocrinol.* 27, 115–124. doi: 10.1016/j.domaniend.2004.03.006

Mohammed, N., Onodera, R., and Or-Rashid, M. M. (2003). Degradation of tryptophan and related indolic compounds by ruminal bacteria, protozoa and their mixture *in vitro*. *Amino Acids* 24, 73–80. doi: 10.1007/s00726-002-0330-8

Moraes, E. P., Freitas, A. C., Gomes-Filho, M. A., Guerra, M. M., Silva, M. A., Pereira, M. F., et al. (2010). Characterization of reproductive disorders in ewes given an intrauterine dose of Toxoplasma gondii tachyzoites during the intrauterine insemination. *Anim. Reprod. Sci.* 122, 36–41. doi: 10.1016/j.anireprosci.2010.07.001

Mutinati, M., Rizzo, A., and Sciorsci, R. L. (2013). Cystic ovarian follicles and thyroid activity in the dairy cow. *Anim. Reprod. Sci.* 138, 150–154. doi: 10.1016/j.anireprosci.2013.02.024

Niu, Y. C., Feng, R. N., Hou, Y., Li, K., Kang, Z., Wang, J., et al. (2012). Histidine and arginine are associated with inflammation and oxidative stress in obese women. *Br. J. Nutr.* 108, 57–61. doi: 10.1017/S0007114511005289

Ortega, H. H., Díaz, P. U., Salvetti, N. R., Hein, G. J., Marelli, B. E., Rodríguez, F. M., et al. (2016). Follicular cysts: a single sign and different diseases. a view from comparative medicine. *Curr. Pharm. Des.* 2236, 5634–5645. doi: 10.2174/1381612822666160804100941

Palmieri, C., Schiavi, E., and Della Salda, L. (2011). Congenital and acquired pathology of ovary and tubular genital organs in ewes: a review. *Theriogenology* 75, 393–410. doi: 10.1016/j.theriogenology.2010.09.020

Pei, Y., Chen, C., Mu, Y., Yang, Y., Feng, Z., Li, B., et al. (2021). Integrated microbiome and metabolome analysis reveals a positive change in the intestinal environment of Myostatin edited Large White pigs. *Front. Microbiol.* 12:628685. doi: 10.3389/fmicb.2021.628685

Qiu, X., Macchietto, M. G., Liu, X., Lu, Y., Ma, Y., and Guo, H. (2021). Identification of gut microbiota and microbial metabolites regulated by an antimicrobial peptide lipocalin 2 in high fat diet-induced obesity. *Int. J. Obes.* 45, 143–154. doi: 10.1038/s41366-020-00712-2

RoyChoudhury, S., Mishra, B. P., Khan, T., Chattopadhayay, R., Lodh, I., Datta Ray, C., et al. (2016). Serum metabolomics of Indian women with polycystic ovary syndrome using H NMR coupled with a pattern recognition approach. *Mol. Biosyst.* 12, 3407–3416. doi: 10.1039/c6mb00420b

Samson, F. P., Fabunmi, T. E., Patrick, A. T., Jee, D., Gutsaeva, D. R., and Jahng, W. J. (2021). Fatty acid composition and stoichiometry determine the angiogenesis microenvironment. *ACS Omega* 6, 5953–5961. doi: 10.1021/acsomega.1c00196

Smith, K. C., Parkinson, T. J., and Long, S. E. (1999). Abattoir survey of acquired reproductive abnormalities in ewes. *Vet. Rec.* 144, 491–496. doi: 10.1136/vr.144.18.491

Steckler, T. L., Lee, J. S., Ye, W., Inskeep, E. K., and Padmanabhan, V. (2008). Developmental programming: exogenous gonadotropin treatment rescues ovulatory function but does not completely normalize ovarian function in sheep treated prenatally with testosterone. *Biol. Reprod.* 79, 686–695. doi: 10.1095/biolreprod.108.068643

Teixeira, A., Cox, R. C., and Egmond, M. R. (2013). Furan fatty acids efficiently rescue brain cells from cell death induced by oxidative stress. *Food Funct.* 4, 1209–1215. doi: 10.1039/c3fo60094g

Toya, T., Corban, M. T., Marrietta, E., Horwath, I. E., Lerman, L. O., Murray, J. A., et al. (2020). Coronary artery disease is associated with an altered gut microbiome composition. *PLoS One* 15:e0227147. doi: 10.1371/journal.pone.0227147

Unni, S. N., Lakshman, L. R., Vaidyanathan, K., Subhakumari, K. N., and Menon, N. L. (2015). Alterations in the levels of plasma amino acids in polycystic ovary syndrome–A pilot study. *Indian J. Med. Res.* 142, 549–554. doi: 10.4103/0971-5916.171281

Wang, J., Ji, H., Wang, S., Liu, H., Zhang, W., Zhang, D., et al. (2018). *Lactobacillus plantarum* probiotic promotes intestinal barrier function by strengthening the epithelium and modulating gut microbiota. *Front. Microbiol.* 9:1953. doi: 10.3389/fmicb.2018.01953

Wonnacott, K. E., Kwong, W. Y., Hughes, J., Salter, A. M., Lea, R. G., Garnsworthy, P. C., et al. (2010). Dietary omega-3 and -6 polyunsaturated fatty acids affect the composition and development of sheep granulosa cells, oocytes and embryos. *Reproduction* 139, 57–69. doi: 10.1530/REP-09-0219

Wu, G. (2009). Amino acids: metabolism, functions, and nutrition. *Amino Acids* 37, 1–17. doi: 10.1007/s00726-009-0269-0

Zeng, B., Lai, Z., Sun, L., Zhang, Z., Yang, J., Li, Z., et al. (2019). Structural and functional profiles of the gut microbial community in polycystic ovary syndrome with insulin resistance (IR-PCOS): a pilot study. *Res. Microbiol.* 170, 43–52. doi: 10.1016/j.resmic.2018.09.002

Zhang, C. Y., Peng, X. X., Shao, H. Q., Li, X. Y., Wu, Y., and Tan, Z. J. (2021). Gut microbiota comparison between intestinal contents and mucosa in mice with repeated stress-related diarrhea provides novel insight. *Front. Microbiol.* 12:626691. doi: 10.3389/fmicb.2021.626691

Zhao, X., Jiang, Y., Xi, H., Chen, L., and Feng, X. (2020). Exploration of the relationship between gut microbiota and polycystic ovary syndrome (PCOS): a review. *Geburtshilfe Frauenheilkd.* 80, 161–171. doi: 10.1055/a-1081-2036

Conflict of Interest: The authors declare that the research was conducted in the absence of any commercial or financial relationships that could be construed as a potential conflict of interest.

frontiers in Microbiology

ORIGINAL RESEARCH
published: 18 May 2021
doi: 10.3389/fmicb.2021.623739

Probiotics *Bacillus licheniformis* Improves Intestinal Health of Subclinical Necrotic Enteritis-Challenged Broilers

*Liugang Kan†, Fangshen Guo†, Yan Liu, Van Hieu Pham, Yuming Guo and Zhong Wang**

State Key Laboratory of Animal Nutrition, College of Animal Science and Technology, China Agricultural University, Beijing, China

OPEN ACCESS

Edited by:
Jing Wang, Institute of Animal Husbandry and Veterinary Medicine, Beijing Academy of Agriculture and Forestry Sciences, China

Reviewed by:
Nikola Puvaèa, University Business Academy in Novi Sad, Serbia
Rifat Ullah Khan, University of Agriculture, Faisalabad, Pakistan
Jesica Blajman, CONICET Santa Fe, Argentina
Tagang Aluwong, Ahmadu Bello University, Nigeria
Jianping Wang, Sichuan Agricultural University, China

***Correspondence:**
Zhong Wang
wangzh@cau.edu.cn

† These authors have contributed equally to this work

Specialty section:
This article was submitted to Systems Microbiology, a section of the journal Frontiers in Microbiology

Received: *30 October 2020*
Accepted: *25 March 2021*
Published: *18 May 2021*

Citation:
Kan L, Guo F, Liu Y, Pham VH, Guo Y and Wang Z (2021) Probiotics Bacillus licheniformis Improves Intestinal Health of Subclinical Necrotic Enteritis-Challenged Broilers. Front. Microbiol. 12:623739. doi: 10.3389/fmicb.2021.623739

Necrotic enteritis infection poses a serious threat to poultry production, and there is an urgent need for searching effective antibiotic alternatives to control it with the global ban on in-feed antibiotics. This study was conducted to investigate the effects of dietary *Bacillus licheniformis* replacing enramycin on the growth performance and intestinal health of subclinical necrotic enteritis (SNE)-challenged broilers. In total, 504 1-day-old Arbor Acres male chickens were selected and subsequently assigned into three treatments, including PC (basal diet + SNE challenge), PA (basal diet extra 10 mg/kg enramycin + SNE challenge), and PG (basal diet extra 3.20×10^9 and 1.60×10^9 CFU *B. licheniformis* per kg diet during 1–21 days and 22–42 days, respectively + SNE challenge). Results showed that *B. licheniformis* significantly decreased the intestinal lesion scores and down-regulated the *Claudin-3* mRNA levels in jejunum of SNE-infected broilers on day 25, but increased the *mucin-2* gene expression in broilers on day 42. In addition, *B. licheniformis* significantly up-regulated the mRNA levels of *TRIF* and *NF-κB* of SNE-challenged broilers compared with the control group on day 25 and *TLR-4*, *TRIF* compared with the control and the antibiotic group on day 42. The mRNA expression of growth factors (*GLP-2* and *TGF-β2*) and HSPs (*HSP60*, *HSP70*, and *HSP90*) were up-regulated in *B. licheniformis* supplementary group on days 25 and 42 compared with group PC. LEfSe analysis showed that the relative abundance of *Lachnospiraceae_UCG_010* was enriched in the PG group; nevertheless, *Clostridiales_vadinBB60* and *Rnminococcaceae_NK4A214* were in PA. PICRUSt analysis found that the metabolism of cofactors and vitamins, amino acid metabolism, and carbohydrate metabolism pathways were enriched, whereas energy metabolism, membrane transport, cell motility, and lipid metabolism were suppressed in *B. licheniformis*-supplemented groups as compared with the PC control. In conclusion, dietary supplementation of *B. licheniformis* alleviated the intestinal damage caused by SNE challenge that coincided with modulating intestinal microflora structure and barrier function as well as regulating intestinal mucosal immune responses.

Keywords: subclinical necrotic enteritis, *Bacillus licheniformis*, intestinal health, immune response, microflora, broiler chicken

INTRODUCTION

Necrotic enteritis (NE) is an intestinal bacterial disease in poultry caused by *Clostridium perfringens* infection and annually costs up to six billion US dollars in production globally (Wade and Keyburn, 2015). *C. perfringens* is a spore-forming, strictly anaerobic Gram-positive bacterium which could produce up to 17 kinds of toxins (Parish, 1961). According to the secreted toxins, *C. perfringens* can be divided into five types: types A, B, C, D, and E. NE was caused by *C. perfringens* type A and/or C infection (Engström et al., 2003; Prescott et al., 2016). NE is typically divided into clinical NE and subclinical NE. Clinical NE usually exhibits mass death with a mortality rate up to 50% and causes intestinal ulcer erosion, bloody feces, and so on (Lee et al., 2011; Alnassan et al., 2014). However, SNE leads to mild intestinal damage in the flock, resulting in inappetence, malabsorption, poor digestion, and further impaired growth performance with a mortality generally less than 5% (Timbermont et al., 2011). Therefore, chronic intestinal mucosal damage in SNE-infected broilers causes more serious economic losses than clinical NE infections due to the difficulty in detection. Previous studies have demonstrated that NE infection is usually accompanied by intestinal lesions in broilers, disorders in intestinal microflora (Latorre et al., 2018), intestinal inflammation (Collier et al., 2008; Park et al., 2008), and damages of intestinal tight junction and mucus barrier in broilers (Golder et al., 2011; Forder et al., 2012; Guo et al., 2014). Therefore, modulation on intestinal health may be a great strategy to control NE infection in broiler.

In the post-antibiotic era, apart from plant extracts (Abudabos et al., 2017; Yin et al., 2017), organic acids (Song et al., 2017), polysaccharides (Tian et al., 2016), and vaccines (Mishra and Smyth, 2017), probiotics had been demonstrated to be an effective measure to promote animal growth (Khan and Naz, 2013; Mingmongkolchai and Panbangred, 2018). Evidences indicated that probiotics were one of the effective methods to prevent SNE infection in poultry for its protection on intestinal health (Venessa et al., 2016; Wang Y. et al., 2017). *Bacillus licheniformis* is a Gram-positive bacterium and characterized by high temperature and stress resistance. Previous studies had found that *B. licheniformis* could produce a variety of biologically active substances, such as digestive enzymes, lysozyme, bacteriocin, and antibacterial peptides, which promote animal performance by improving feed digestibility, stimulating the development of immune system, enhancing intestinal mucosal barrier function, inhibiting the colonization of pathogenic bacteria, promoting the proliferation of potentially beneficial microorganisms, and maintaining the balance of intestinal microflora (Rozs et al., 2001; Kim et al., 2004; Zhou et al., 2016). For example, Wang Y. et al. (2017) reported that *B. licheniformis* up-regulated the gene expression of tight junction proteins (TJP) and *mucin-2* in laying hens, thus maintaining the intestinal mechanical barrier and reducing intestinal permeability. Other research noted that probiotics *Bacillus* spp. strengthened host intestinal mucosal immunity through increasing the mRNA expression levels of TLRs, associated downstream adaptor proteins, and *NF-κB* in broiler chickens (Rajput et al., 2017), up-regulating the mRNA levels of cytokines and sIgA (Baikui et al., 2016). In addition, diets supplemented with *B. licheniformis* could also modulate the composition and structure of intestinal microbiota in broiler chickens challenged with NE (Lin et al., 2017; Xu et al., 2018). Some researchers have confirmed that probiotics *Bacillus* spp. as feed additives had achieved promising results in preventing and controlling NE infection in poultry (Jayaraman et al., 2013; Zhou et al., 2016; Wu et al., 2018). However, probiotic strains differ regarding their properties and clinical effects that they elicit; these differences are even observed when the strains belong to the same bacterial species. Therefore, the aim of this study was to explore whether *B. licheniformis* could alleviate the SNE infection similar to enramycin and reveal its action mechanism by determining intestinal barrier function, the immune responses as well as intestinal microflora.

MATERIALS AND METHODS

Experimental Animals, Diets, and Treatments

A total of 504 1-day-old male Arbor Acres chicks with an average weight at 43.9 g (SD 0.87) were purchased from Beijing Arbor Acres Poultry Breeding Company (Beijing, China). On arrival, chicks were weighed and randomly assigned to three groups. Each group contained 12 replicates with 14 birds per replicate. Each replicate was reared in a separate isolator ($240 \times 60 \times 60$ cm^3). The treatment groups were as follows: (1) positive control group (PC, basal diet + SNE infection); (2) antibiotic group (PA, basal diet extra 10 mg/kg enramycin + SNE infection); (3) *B. licheniformis*-treated group (PG, basal diet extra 3.20×10^9 CFU *B. licheniformis* per kg diet [days 1–21], 1.60×10^9 CFU *B. licheniformis* per kg diet [days 21–42] + SNE infection). *B. licheniformis* used in this study was provided by Chr. Hansen Co., Ltd. (Denmark) at a density of 3.20×10^9 CFU/g. Antibiotic-free and coccidiostat-free corn–soybean meal basal diets were formulated according to National Research Council (1994) requirements for starter (days 1 to 21) and grower (days 22 to 42) periods. The composition and nutrient levels of the basal diet are presented in **Table 1**. The experimental diet was formulated by mixing the basal diet with *B. licheniformis* to reach 3.20×10^9 and 1.60×10^9 CFU/kg of diet in the starter and grower periods, respectively. To ensure the homogeneity of the additives, approximately 5 kg of the basal diet mixed with the additive was thoroughly mixed using a plastic bucket. Starter diets were pelleted and crumbled, whereas grower diets were just pelleted. All birds were reared in a farm and fed *ad libitum* and allowed to access water freely throughout the entire experimental period. Room temperature was maintained at 33°C during first 5 days and then gradually decreased by 2°C weekly until a final room temperature of 24°C was reached. Artificial light was provided in a 23 h light/1 h dark program. In addition, all birds were immunized with Newcastle disease virus vaccine plus infectious bronchitis virus vaccine via drinking water on day 21.

Experimental Induction of SNE

Avian *C. perfringens* type A strain CVCC2030 (China Veterinary Culture Collection Center, Beijing, China) was used for infection in this study. *C. perfringens* was anaerobically cultured in thioglycolate broth for 24 h at 37°C, then aseptically transferred into a cooked meat medium (CM605; Beijing Land Bridge Technology Co., Ltd.) supplemented with dried meat particles (CM607; Beijing Land Bridge Technology Co., Ltd.) and iron powders (Shanghai Kefeng Industry & Commerce Co., Ltd.) and incubated anaerobically for 18 h at 37°C. Establishment of SNE model in broilers referenced Wu et al. (2018) with little modifications. Briefly, each bird in this study was orally gavaged with 12,000 *Eimeria maxima* oocysts (College of Veterinary Medicine, China Agricultural University, Beijing, China) at 12 days of age, and subsequently with 1 ml of *C. perfringens* (1×10^9 CFU/ml) once a day during days 17 to 23 to establish the SNE model.

Growth Performance

On days 21 and 42, the body weight (BW) and feed intake of each replicate were recorded. Then the average gain (AG), feed intake (FI), and feed conversion ratio (FCR) were calculated for days 1–21, 22–42, and 1–42, respectively. Death of birds in each replicate was recorded daily and was used for determining the mortality.

TABLE 1 | Composition and nutrient levels of the basal diets.

Items	Weeks 0–3	Weeks 4–6
Ingredient, %		
Corn (CP 7.8%)	37.15	55.33
Wheat middlings	0	5.00
Wheat	20.00	0
Soybean meal (CP 46.8%)	34.00	31.00
Soybean oil	4.80	5.00
Limestone	0.90	0.70
Dicalcium phosphate	2.00	2.00
DL-Methionine, 98%	0.23	0.19
L-Lysine sulfate, 78%	0.15	0.10
Sodium chloride	0.30	0.30
Ethoxyquinoline, 33%	0.05	0.05
Choline chloride, 50%	0.24	0.15
Vitamin premix[a]	0.03	0.03
Mineral premix[b]	0.15	0.15
Total	100	100
Nutrient levels		
Metabolizable energy, Mcal/kg	3.03	3.10
Crude protein, %	21.77	19.80
Calcium, %	1.06	0.95
Non-phytate, %	0.45	0.42
Lysine, %	1.23	1.10
Methionine, %	0.52	0.46
Met + Cys, %	0.83	0.74

[a] *Vitamin premix provided per kilogram of complete diet: vitamin A 12,500 IU; vitamin D_3 2500 IU; vitamin E 30 IU; vitamin K_3 2.65 mg; vitamin B_{12} 0.025 mg; biotin 0.0325 mg; folic acid 1.25 mg; nicotinic acid 50 mg; pantothenic acid 12 mg; riboflavin 6 mg; thiamine mononitrate 2 mg.*

[b] *Mineral premix provided per kilogram of complete diet: iron 80 mg; copper 8 mg; manganese 100 mg; zinc 75 mg; iodine 0.35 mg; selenium 0.15 mg.*

Intestinal Lesion Score and Sample Collection

On days 25 and 42, one bird per replicate was randomly selected, weighed, and euthanized by jugular exsanguination. The middle segments of jejunum (approximately 1 cm) were cut off carefully and gently rinsed with ice-cold sterile saline to remove internal digesta. Subsequently, the jejunum segments were fixed in 4% paraformaldehyde immediately for further morphology analysis. Another jejunum sample was collected and washed, then frozen in liquid nitrogen immediately and stored at −80°C for the subsequent gene expression analysis. Liver and cecal digesta samples were put into sterile tubes, snap-frozen in liquid nitrogen, and transferred to −80°C. Liver samples were used to determine microbial translocation, while cecal samples were used to determine bacterial populations, short-chain fatty acid (SCFA) contents, and DNA extraction. The duodenum, jejunum, and ileum of each bird were cut longitudinally and scored 0 (none) to 4 (severe) for NE gut lesions by three independent observers blindly as previously described by Gholamiandehkordi et al. (2007) with some modifications.

The scoring criteria are as follows: 0 = no obvious lesions; 1 = thin and friable intestine with hemorrhagic spots (1–5 foci); 2 = small gas production and focal necrosis or ulceration (hemorrhagic spots 6–15); 3 = gas-filled intestine and patches of necrosis 1 to 2 cm long; 4 = diffuse necrosis with great amounts of gas in the intestine.

Bacterial Population of Cecal Digesta and Liver Bacterial Translocation

Quantification of bacterial population in cecal digesta (or liver) was done with techniques as previously described (Wu et al., 2018). Briefly, approximately 1 g of each sample was diluted with 9 ml ice-cold sterile buffered peptone water (CM201; Land Bridge Technology Ltd.) and homogenized. The homogenized suspension of each sample was serially diluted up to 10^{-7}, then 100 μl of each dilution was plated on selective ager plates for bacterial quantification. Each sample was plated in duplicate. Commercial media were used for cultivation of *C. perfringens* (tryptose–sulfite–cycloserine agar, TSC, CM 138; Beijing Land Bridge Technology Co., Ltd.), coliform bacteria (Eosin–Methylene Blue Agar, EMB, CM105; Beijing Land Bridge Technology Co., Ltd.) and lactic acid bacteria (de Man, Rogosa, and Sharpe agar, MRS, CM 188; Land Bridge Technology Co., Ltd.). *C. perfringens* and lactic acid bacteria were incubated anaerobically for 48 h at 37°C, while coliform bacteria were incubated aerobically for 24 h at 37°C. The number of colony-forming units was expressed as a logarithmic transformation per gram of cecal digesta (or liver).

Intestinal Morphology Observation and Analysis

Fixed jejunum tissues were embedded in paraffin, then sliced into 5-μm thickness, deparaffinized in xylene, rehydrated, and mounted on glass slides. Periodic acid–Schiff (PAS) stain was used to stain the sections for determining the number of goblet cells, whereas H&E stain was used for villous morphology measurement. Five intact villi in every slide were chosen for measurement of goblet cells, villus height (VH), and crypt depth (CD) with Image-pro plus 6.0 (Media Cybernetics, Inc., Rockville, MD, United States) at ×40 magnification. The means of villus height and crypt depth were calculated and subsequently were used to obtain the VH/CD.

Gene Expression in Jejunum

Extraction of total RNA in jejunum was performed using Trizol reagent (Invitrogen Life Technologies, Carlsbad, CA, United States) according to the manufacturer's instructions. The concentration and purity of total RNA were determined by using a NanoDrop-2000 spectrophotometer (Thermo Fisher Scientific, Waltham, MA, United States). Then, complementary DNA (cDNA) was synthesized by using Primer Script RT Reagent kit (Takara Bio Inc.) according to the manufacturer's instructions. Using the synthesized cDNA as a template, quantitative real-time PCR (qRT-PCR) was performed in Applied Biosystems' 7500 Fast Real-Time PCR System with SYBR Premix Ex Taq kit (Takara Bio Inc.) in accordance with the manufacturer's guidelines. Thermocycling protocol was as follows: 95°C for 30 s, followed by 40 cycles of 95°C for 5 s and 60°C for 34 s for denaturation and annealing/extension, respectively. The purity and specificity of PCR products were determined by melt curve analysis. All data were analyzed using the $2^{-\Delta\Delta Ct}$ method, and glyceraldehyde 3-phosphate dehydrogenase (*GAPDH*) and β-*actin* were used to normalize the relative mRNA levels (Livak and Schmittgen, 2001). All samples ($n = 6$) from each group on days 25 and 42 were done in triplicate. Target genes include TJP genes (*Occludin*, *Claudin-1*, *Claudin-3*, Zonula occludens-1[*ZO-1*], *mucin-2*), TLR signal pathway-related genes (*TLR-4*, *TLR-2*, *TRIF*, *MyD88*, *NF-κB*, *IL-1β*, *IL-10*, *IL-17*, *IFN-γ*, *TNF-α*), heat shock protein genes (*HSP60*, *HSP70*, *HSP90*), and growth factor genes (*IGF-2*, *GLP-2*, *TGF-β2*). Primers of target genes used in this study are presented in **Supplementary Tables 1, 2**.

SCFA Concentration in Cecal Content

A total of 0.5–1.0 g cecal digesta from day 42 sample was weighed and put into a 10-ml polypropylene tube with 8 ml deionized water, then an ultrasonic bath was performed for 30 min, the suspension subsequently was centrifuged at 8000 rpm for 10 min. The supernatant was collected and diluted 10-fold, and then filtered with a 0.22-μm filtrator. Next, 25 μl of filtered solution was subjected to high-performance ion chromatography system (ICS-3000; Dionex, United States) for conductivity detection analysis. Organic acids were separated on an AS11 analytical column (250 × 4 mm^2) and an AG11 guard column under the following gradient conditions (the gradient was based on potassium hydroxide): 0–5 min, 0.8–1.5 mM; 5–10 min, 1.5–2.5 mM; and 10–15 min, 2.5 mM; the flow rate was 1.0 ml/min. The results of SCFAs were expressed as milligrams per kilogram of digesta.

Microbial DNA Extraction, 16S rRNA Gene Amplification, Sequencing, and Bioinformatics Analysis

Bacterial DNA extraction of day 25 cecal digesta was performed by using PowerSoil DNA Isolation Kit (ANBIOSCI Tech Ltd., United States) according to the manufacturer's instructions. Integrity of DNA was appraised by agarose gel electrophoresis, then the qualified DNA was used as template for the V3–V4 region of bacterial 16S rRNA gene amplification with barcoded primer pair 338F: 5′-ACTCCTACGGGAGGCAGCA-3′ and 806R: 5′-GGACTACHVGGGTWTCTAAT-3′. The KAPA HiFi Hotstart ReadyMix PCR kit (Kapa Biosystems, United States) was used in the PCR amplification and the procedures were as follows: 98°C for 2 min (1 cycle), 98°C for 30 s/50°C for 30 s/72°C for 1 min (25 cycles), and finally 72°C lasts for 5 min. The amplification products were determined by 2% agarose gel and purified with AxyPrep DNA Gel Extraction Kit (Axygen Biosciences, Union City, CA, United States). Amplicon libraries were sequenced on Illumina HiSeq 2500 platform (Illumina, San Diego, CA, United States) at Biomarker Technologies Co., Ltd. (Beijing, China). The sequencing data were merged using FLASH (version 1.2.11) to get raw tags. Raw tags were then subjected to filtration (Trimmomatic, version 0.33) and chimera sequences removed (UCHIME, version 8.1) to obtain effective tags. UCLUST (Edgar, 2010) was used to cluster effective tags into operational taxonomic units (OTUs) at a similarity level of 97% with QIIME software (version 1.8.0) (Caporaso et al., 2010). Afterward, basing on the Silva taxonomic database, OTUs were annotated. Venn diagram, rarefaction curve, and bacteria relative abundance were created with R software (version 2.15.3). Alpha diversity, including ACE, Chao1, Simpson, and Shannon index, were investigated by Mothur (version 1.30), and the significance of these items was determined using a Mann–Whitney *U* test. β Diversity was calculated from binary_jaccard distance (PERMANOVA/ANOSIM analysis) in QIIME software. A two-sided Student's *t*-test was used to determine the significance of the differences between groups. Line discriminant analysis (LDA) effect size (LEfSe[1]) (Segata et al., 2011) tool was used to determine statistically different biomarkers between groups (LDA value: 2) based on the taxonomic files obtained from the QIIME analysis. The raw sequences used in our study had been uploaded at the Sequence Read Archive of the National Center for Biotechnology Information, with the study accession number PRJNA574872. The functions of the cecum metagenomes were predicted using PICRUSt (Phylogenetic investigation of communities by reconstruction of unobserved states) analysis based on high-quality sequences (Langille et al., 2013).

[1]http://huttenhower.sph.harvard.edu/lefse/

Statistical Analysis

All results were displayed as means ± SEM. Statistical significance of growth performance, intestinal lesion scores, bacterial population, intestinal morphology, gene expression, and SCFA content were determined by one-way ANOVA, followed by Duncan's multiple comparison test (SPSS, version 20.0, Chicago, IL, United States). Kruskal–Wallis test was employed to analyze the difference in bacterial relative abundance. Significant difference was declared when $P < 0.05$.

RESULTS

Growth Performance

We measured four indexes concerning broiler chickens' productivity as shown in **Table 2**. There was no significant difference in BW, AG, FI, and FCR between groups, while numerically higher BW, AG, and lower FCR were observed in PA and PG groups when compared with PC group at days 21–42 and days 1–42, and the value of those indexes of PA and PG group were close to each other. There was no significant difference in mortality among groups.

Small Intestine Lesion Scores and Jejunum Morphology

As shown in **Table 3**, lesion scores of duodenum and small intestine in PG group were significantly lower than those in PC and PA group and jejunum lesion score in PG group was lower than PA group on 2 days post-infection (DPI) ($P < 0.05$). Similarly, there was a tendency that lesion scores of ileum in PG were lower than in PC and PA groups ($0.05 < P < 0.1$). In addition, lesion scores of duodenum, jejunum, and small intestine in PA group were comparable with PC group. At 42 days of age (19 DPI), no significant difference was detected of intestinal lesion scores in the three experiment groups. We also investigated the jejunum morphology of broilers at 2 DPI (**Table 4**). It was found that the number of goblet cells were significantly decreased in PA group compared with PC and PG group ($P < 0.05$). However, the jejunum villus height (VH), crypt depth (CD), and VH/CD values were not changed significantly among groups.

TABLE 2 | Effects of *B. licheniformis* and enramycin on growth performance of broilers challenged with SNE.

Items	PC	PA	PG	SEM	*P* values
Days 1–21					
BW (g/bird)	641	652	640	5.7	0.623
AG (g/bird)	598	609	597	5.7	0.624
FI (g/bird)	856	866	853	6.4	0.694
FCR	1.43	1.42	1.43	0.005	0.631
Mortality (%)	0.00	1.19	0.60	0.439	0.555
Days 21–42					
BW (g/bird)	2346	2394	2395	11.1	0.103
AG (g/bird)	1705	1734	1753	10.8	0.178
FI (g/bird)	2996	2991	3036	14.4	0.384
FCR	1.76	1.73	1.73	0.008	0.221
Mortality (%)	1.19	1.19	0.60	0.418	0.807
Days 1–42					
BW (g/bird)	2346	2394	2395	11.1	0.103
AG (g/bird)	2303	2351	2352	11.1	0.103
FI (g/bird)	3852	3865	3892	16.8	0.614
FCR	1.67	1.64	1.65	0.006	0.101
Mortality (%)	1.19	2.38	1.19	0.577	0.636

Data are presented as means ± SEM (n = 12; cage was used as experimental unit). PC, basal diet + SNE; PA, basal diet extra antibiotics + SNE; PG, basal diet extra B. licheniformis + SNE.
BW, body weight; AG, average gain; FI, feed intake; FCR, feed conversion rate (FI/AG).

TABLE 3 | Effects of *B. licheniformis* and enramycin on intestinal lesion scores of broilers challenged with SNE.

Items	PC	PA	PG	SEM	*P* values
Day 25					
Duodenum	1.13^{a}	1.08^{a}	0.38^{b}	0.081	0.000
Jejunum	0.75^{ab}	1.04^{a}	0.67^{b}	0.060	0.022
Ileum	0.29	0.38	0.08	0.061	0.097
Small intestine	2.17^{a}	2.50^{a}	1.13^{b}	0.927	0.000
Day 42					
Duodenum	0.58	0.42	0.50	0.049	0.378
Jejunum	0.29	0.29	0.25	0.051	0.856
Ileum	0.04	0.00	0.13	0.027	0.147
Small intestine	0.92	0.71	0.88	0.080	0.541

Data are presented as means ± SEM (n = 12; cage was used as experimental unit). PC, basal diet + SNE; PA, basal diet extra antibiotics + SNE; PG, basal diet extra B. licheniformis + SNE. Means within a row lacking a common superscript differ significantly (P < 0.05).

TABLE 4 | Effects of *B. licheniformis* and enramycin on jejunal morphology of 25-day-old broilers challenged with SNE.

Items	PC	PA	PG	SEM	*P* values
Goblet cells	194.8^{a}	149.5^{b}	204.6^{a}	8.196	0.005
VH (μm)	706.8	692.3	738.1	30.014	0.828
CD (μm)	180.5	191.8	196.4	6.964	0.953
VH/CD	4.12	3.65	3.68	0.159	0.459

Data are presented as means ± SEM (n = 6; cage was used as experimental unit). PC, basal diet + SNE; PA, basal diet extra antibiotics + SNE; PG, basal diet extra B. licheniformis + SNE. Means within a row lacking a common superscript differ significantly (P < 0.05).
Goblet cells, the number of goblet cells on a villus; VH, villus height; CD, crypt depth.

Cecal Bacterial Population and Liver *Clostridium perfringens* Translocation

Table 5 shows the results of cecal bacterial population and liver *C. perfringens* translocation. At 25 days of age (2 DPI), SNE-infected birds fed diets supplemented with enramycin exhibited significantly reduced population of *C. perfringens* in cecum and liver in contrast to that in PC and PG groups ($P < 0.05$). However, probiotic supplementation failed to decrease the population of *C. perfringens* in both cecum and

TABLE 5 | Effects of *B. licheniformis* and enramycin the amounts of bacteria (lg CFU/g[1]) in cecal digesta of broilers challenged with SNE.

	Items	PC	PA	PG	SEM	*P* values
Day 25						
Cecal digesta	*Clostridium perfringens*	4.62[a]	1.75[b]	4.11[a]	0.423	0.004
	Escherichia coli	6.67	7.51	6.52	0.229	0.166
	Lactobacillus	10.15	9.83	9.48	0.222	0.495
Liver	*Clostridium perfringens*	1.56[a]	0.17[b]	1.46[a]	0.233	0.011
Day 42						
Cecal digesta	*Clostridium perfringens*	1.24	1.53	0.90	0.270	0.657
	Escherichia coli	6.75[b]	7.73[a]	6.83[b]	0.154	0.007
	Lactobacillus	8.69	8.16	8.26	0.178	0.469
Liver	*Clostridium perfringens*	0.38	0.17	0.27	0.127	0.804

Data are presented as means ± SEM (n = 6; cage was used as experimental unit). PC, basal diet + SNE; PA, basal diet extra antibiotics + SNE; PG, basal diet extra B. licheniformis + SNE. Means within a row lacking a common superscript differ significantly (P < 0.05).
[1]lg CFU/g, log 10 colony-forming units per gram of cecal digesta.

TABLE 6 | Effects of *B. licheniformis* and enramycin on tight junction protein and *mucin-2* gene expression in jejunum of broilers challenged with SNE.

Items	PC	PA	PG	SEM	*P* values
Day 25					
Occludin	1.03	0.82	0.83	0.048	0.128
Claudin-1	1.08	1.05	0.87	0.081	0.555
Claudin-3	1.01[a]	0.87[b]	0.72[b]	0.045	0.026
ZO-1	1.02	1.18	0.93	0.059	0.239
Mucin-2	1.01	0.94	1.01	0.036	0.677
Day 42					
Occludin	1.02	1.13	1.12	0.049	0.629
Claudin-1	1.03	1.04	0.90	0.051	0.505
Claudin-3	1.01[b]	1.48[a]	1.10[b]	0.073	0.008
ZO-1	1.01	1.22	1.23	0.044	0.064
Mucin-2	1.04[c]	1.79[b]	2.80[a]	0.202	0.000

Data are presented as means ± SEM (n = 6; cage was used as experimental unit). PC, basal diet + SNE; PA, basal diet extra antibiotics + SNE; PG, basal diet extra B. licheniformis + SNE. Means within a row lacking a common superscript differ significantly (P < 0.05).
ZO, zonula occludens.

TABLE 7 | Effects of *B. licheniformis* and enramycin on TLR signal pathway-related gene expression in jejunum of broilers challenged with SNE.

Items	PC	PA	PG	SEM	*P* values
Day 25					
TLR-4	1.02	1.35	1.29	0.077	0.174
TLR-2	1.02	1.21	1.18	0.077	0.592
TRIF	1.00[b]	1.24[a]	1.33[a]	0.045	0.002
MyD88	1.07	1.17	0.88	0.067	0.227
NF-κB	1.01[b]	1.52[a]	1.42[a]	0.080	0.012
IL-1β	1.11	1.85	1.66	0.218	0.378
IL-10	1.07	1.19	0.90	0.094	0.475
IL-17	1.10[b]	2.72[a]	1.40[b]	0.262	0.021
IFN-γ	1.05	1.12	1.05	0.089	0.932
TNF-α	1.02	1.37	1.35	0.074	0.084
Day 42					
TLR-4	1.02[b]	1.04[b]	1.52[a]	0.075	0.002
TLR-2	1.05	0.84	1.10	0.068	0.299
TRIF	1.02[b]	0.76[c]	1.30[a]	0.061	0.000
MyD88	1.01	1.09	0.98	0.045	0.590
NF-κB	1.04[b]	1.16[b]	1.48[a]	0.072	0.024
IL-1β	1.03[ab]	0.61[b]	1.17[a]	0.097	0.039
IL-10	1.07	0.74	1.04	0.092	0.276
IL-17	0.98[a]	0.45[b]	0.99[a]	0.097	0.016
IFN-γ	1.03	0.85	0.96	0.055	0.445
TNF-α	1.04	1.13	1.35	0.066	0.151

Data are presented as means ± SEM (n = 6; cage was used as experimental unit). PC, basal diet + SNE; PA, basal diet extra antibiotics + SNE; PG, basal diet extra B. licheniformis + SNE. Means within a row lacking a common superscript differ significantly (P < 0.05).

liver. Furthermore, no significant differences were observed in *Escherichia coli* and *Lactobacilli* population in cecum between PC, PA, and PG groups. At 42 days of age, the cecal *Escherichia coli* population in the PA group was significantly higher than that in the PC and PG groups ($P < 0.05$). Similarly, the difference between PG and PC group was not statistically significant.

Jejunal Tight Junction Protein Gene and Mucin Gene Expression

As depicted in **Table 6**, the expression of *Claudin-3* in the jejunum of SNE-infected chickens fed with *B. licheniformis* was lower than that in the PC group at day 25 ($P < 0.05$), but no significant difference was seen between PG and PA group. Only a downtrend of *Claudin-3* levels was detected in PA group when compared with PC group. At 42 days of age, *Claudin-3* mRNA levels in PA group were significantly up-regulated when compared with the PC and PG groups ($P < 0.05$). Besides, a tendency was detected that the *ZO-1* expression of PA and PG group was higher than PC group ($0.05 < P < 0.1$). Similar with the results of the number of goblet cells on villus, *mucin-2* expression levels in the PA and PG groups were significantly increased when compared with the PC group at day 42 ($P < 0.05$). Moreover, the gene expression of *mucin-2* in the PG group was much higher than that in the antibiotic supplemented group ($P < 0.05$).

Jejunal Toll-Like Receptors Signaling Pathway and Immune-Related Cytokine Gene Expression

Table 7 presents the results of jejunal TLRs signaling pathway and immune-related cytokine gene expression in broilers. On day 25, dietary antibiotics and *B. licheniformis* significantly up-regulated the mRNA levels of *TRIF* and *NF-κB* in jejunum of SNE-infected broiler chickens compared with the PC group ($P < 0.05$). Moreover, the mRNA expression level of *IL-17* gene was significantly up-regulated in the PA group than that

TABLE 8 | Effects of *B. licheniformis* and enramycin on recovery protein gene expression in jejunum of broilers challenged with SNE.

Items	PC	PA	PG	SEM	*P* values
Day 25					
HSP60	1.04^{b}	1.24^{b}	2.53^{a}	0.183	0.000
HSP70	1.03	1.17	1.19	0.046	0.309
HSP90	1.01^{c}	1.83^{b}	2.51^{a}	0.177	0.000
IGF-2	1.04^{b}	1.65^{a}	1.05^{b}	0.102	0.010
GLP-2	1.04^{b}	1.81^{a}	2.22^{a}	0.175	0.010
TGF-β2	1.02^{b}	1.65^{a}	1.37^{ab}	0.097	0.018
Day 42					
HSP60	1.03^{b}	1.13^{b}	1.58^{a}	0.075	0.001
HSP70	1.01^{b}	0.95^{b}	1.37^{a}	0.055	0.000
HSP90	1.02^{b}	0.65^{c}	1.37	0.083	0.000
IGF-2	1.04	1.13	1.47	0.093	0.141
GLP-2	1.09^{b}	1.34^{b}	1.83^{a}	0.108	0.011
TGF-β2	1.02^{b}	1.24^{b}	1.65^{a}	0.081	0.001

Data are presented as means ± SEM (n = 6; cage was used as experimental unit). PC, basal diet + SNE; PA, basal diet extra antibiotics + SNE; PG, basal diet extra B. licheniformis + SNE. Means within a row lacking a common superscript differ significantly (P < 0.05).
HSP, heat shock protein; IGF, insulin-like growth factors; GLP, glucagon-like peptide.

TABLE 9 | Effects of *B. licheniformis* and enramycin on concentration of short-chain fatty acids in cecal content of 42-day-old broilers (mg/kg).

Items	PC	PA	PG	SEM	*P* values
Lactic acid	297.2	216.6	390.1	69.34	0.619
Formic acid	215.7^{b}	276.1^{a}	273.9^{a}	12.74	0.027
Acetic acid	3958.7	3886.8	3737.9	138.68	0.822
Propionic acid	2467.9	1843.1	2091.2	135.81	0.170
Butyric acid	1584.2	1284.4	1415.1	97.46	0.480
Isobutyric acid	61.5	52.9	69.3	6.780	0.655
Valeric acid	121.7	101.7	125.1	6.547	0.305
Isovaleric acid	66.0	92.7	73.2	9.328	0.508

Data are presented as means ± SEM (n = 6; cage was used as experimental unit). PC, basal diet + SNE; PA, basal diet extra antibiotics + SNE; PG, basal diet extra B. licheniformis + SNE. Means within a row lacking a common superscript differ significantly (P < 0.05).

TABLE 10 | Effects of *B. licheniformis* and enramycin on alpha diversity of cecal microbiota of 25-day-old broilers challenged with SNE.

Items	PC	PA	PG	SEM	*P* values
ACE	417.1	365.8	393.1	15.123	0.407
Chao1	423.6	384.7	397.5	19.036	0.280
Simpson	0.115	0.126	0.101	0.019	0.870
Shannon	3.46	3.21	3.40	0.167	0.746

Data are presented as means ± SEM (n = 6; cage was used as experimental unit). PC, basal diet + SNE; PA, basal diet extra antibiotics + SNE; PG, basal diet extra B. licheniformis + SNE. Means within a row lacking a common superscript differ significantly (P < 0.05).

in the PC and PG groups ($P < 0.05$). On day 42, jejunal mRNA expression levels of *TLR-4*, *TRIF*, and *NF-κB* were significantly increased in the PG group when compared with the PC and PA groups ($P < 0.05$). Interestingly, birds fed diet supplemented with antibiotics had significantly lower *IL-17* and *TRIF* mRNA levels in contrast to the PC group ($P < 0.05$). In addition, supplementation of *B. licheniformis* also significantly up-regulated *IL-1*β mRNA levels compared with the PA group ($P < 0.05$).

Gene Expression of Jejunal Heat Shock Proteins and Growth Factors

On day 25, when compared with the PC group, addition of antibiotics in feed significantly up-regulated the relative gene expressions of *HSP90*, *IGF-2*, *GLP-2*, and *TGF-β2* in the jejunum of SNE-infected broilers ($P < 0.05$, **Table 8**). Meanwhile, higher mRNA levels of *HSP60*, *HSP90*, and *GLP-2* were also detected in the PG group when compared with the PC group ($P < 0.05$). On day 42, dietary antibiotics had significantly lower mRNA levels of *HSP90* than that in PC group ($P < 0.05$), whereas birds fed diets supplemented with *B. licheniformis* exhibited significantly higher gene expression of *HSP60*, *HSP70*, *HSP90*, *GLP-2*, and *TGF-β2* when compared with the PC and PA groups ($P < 0.05$).

Short-Chain Fatty Acids in Cecal Content

On day 42, we investigated the SCFA concentrations in cecal content of SNE-infected broilers (**Table 9**). Significant changes were only observed in the formic acid concentration between groups. The concentration of formic acid in the PA and PG groups were significantly increased compared with the PC group ($P < 0.05$), but no significant differences were detected between PA and PG groups ($P > 0.05$).

Cecal Microbiome

A total of 1,440,717 pairs of reads were generated after 16S rRNA sequencing of 18 cecal digesta samples. Then, we obtained 1,191,203 effective Tags after splicing, filtering, and removal of chimeras, and an average of 66,178 effective Tags were obtained from each sample. Based on 97% sequence similarity, Tags were clustered into 510 OTUs, of which 475 OTUs were shared by three groups, and only 2, 4, and 1 OTUs were exclusive in PC, PA, and PG groups, respectively (**Supplementary Figure 1**). Furthermore, the alpha diversity analysis of cecal microbiota showed that no significant difference in ACE, Chao1, Simpson, and Shannon index between groups ($P > 0.05$ and **Table 10**).

The representative sequences of OTUs were annotated with Silva database. Then we analyzed the bacterial composition in phylum and genus level of samples. The most abundant (top 6) phyla of bacteria are presented in **Supplementary Figure 2A**. At the phylum level, the cecal microbiota was dominated by *Firmicutes*, *Bacteroidetes*, *Proteobacteria*, and *Tenericutes*, together accounting for over 99.7% of the total sequences. However, no significant differences were detected in those phyla between groups ($P > 0.05$, **Table 11**). The top 10 abundant bacteria in genus level were *Faecalibacterium*, *Lactobacillus*, *Barnesiella*, *[Ruminococcus]_torques_group*,

TABLE 11 | Effects of *B. licheniformis* and enramycin on relative abundances of phyla in cecal microbiota of 25-day-old broilers challenged with SNE (%).

Items	PC	PA	PG	SEM	*P* values
Firmicutes	72.68	72.41	86.55	3.751	0.203
Bacteroidetes	23.27	20.71	10.47	3.938	0.519
Proteobacteria	2.20	4.61	1.01	1.012	0.325
Tenericutes	1.68	1.84	1.70	0.388	0.805
Actinobacteria	0.12	0.44	0.26	0.094	0.805

Data are presented as means ± SEM (n = 6; cage was used as experimental unit). PC, basal diet + SNE; PA, basal diet extra antibiotics + SNE; PG, basal diet extra B. licheniformis + SNE.

TABLE 12 | Effects of *B. licheniformis* and enramycin on relative abundances of genus in cecal microbiota of 25-day-old broilers challenged with SNE (%).

Items	PC	PA	PG	SEM	*P* values
Faecalibacterium	11.29	10.89	17.44	2.955	0.366
Lactobacillus	6.38	15.43	5.75	4.093	0.414
Barnesiella	12.68	9.45	0.17	3.304	0.116
[Ruminococcus]_torques_group	5.67	5.34	8.33	1.024	0.587
Alistipes	5.21	3.58	8.60	1.462	0.399
Ruminococcaceae_UCG-014	5.57	4.27	6.67	0.817	0.484
uncultured_bacterium_f_Lachnospiraceae	3.95	4.60	5.13	0.762	0.738
uncultured_bacterium_f_Ruminococcaceae	5.58	4.10	3.71	0.601	0.444
Bacteroides	4.26	7.06	0.01	1.364	0.244
Megamonas	0.00	2.47	8.37	1.954	0.419

Data are presented as means ± SEM (n = 6; cage was used as experimental unit). PC, basal diet + SNE; PA, basal diet extra antibiotics + SNE; PG, basal diet extra B. licheniformis + SNE. Means within a row lacking a common superscript differ significantly (P < 0.05).

Alistipes, *Ruminococcaceae_UCG-014*, *uncultured_bacterium_f_Lachnospiraceae*, *uncultured_bacterium_f_Rumi-noccoccaceae*, *Bacteroides*, and *Megamonas*. The relative abundance of Others and Unclassified bacterium were 36.0% (**Supplementary Figure 2B**). Similarly, no significant differences were detected in abundance of those genera between groups ($P > 0.05$, **Table 12**). Then binary_jaccard algorithm for PERMANOVA/ANOSIM analysis (Beta diversity box plot, **Figure 1**) was used to evaluate differences in cecal bacterial community structure between different groups. As shown in **Figure 1**, β diversity of the PC group was significantly different from the PA and PG groups; nevertheless, no significant differences were detected in β diversity between the PA and PG groups.

LEfSe analysis was used to determine the statistically different biomarkers between groups. As presented in **Figure 2**, when compared with the PC group, *Peptostreptococcaceae*, *Intestinibacter*, and *Eisenbergiella* were less abundant in the PA group (**Figure 2A**); nevertheless, *Lachnospiraceae_UCG_010* were enriched in the PG group when compared with group PC (**Figure 2B**). Furthermore, *Clostridiales_vadinBB60_group*, *g_uncultured_bacterium_f_Clostridiales_vadinBB60_group*, *Family_XIII_AD3011_group*, and *Ruminococcaceae_NK4A214_group* were more abundant in the PG group in contrast to the PA group (**Figure 2C**).

Predicting the Function of Intestinal Bacteria

PICRUSt analysis showed a significant functional gene difference between group PC and PA or PG (**Figure 3**). We found that six pathways were enriched in group PC and eight pathways were in group PA and PG altogether. Besides, 10 pathways were enriched in group PA and 12 pathways in group PA uniquely explaining the fact that the functional profiles representing the microbial communities in group PA and PG were relatively similar and different. Notably, metabolic pathways were mostly common among the significantly differentially represented pathways, which indicated the different metabolic status between groups. Comparing with the group PA, energy metabolism, amino metabolism, and cell motility were enriched in the PC group ($P < 0.01$, **Figure 3A**), whereas carbohydrate metabolism, nucleotide metabolism, xenobiotics biodegradation and metabolism, and membrane transport were significantly enriched in PA group ($P < 0.001$). Compared with the group PG, translation, membrane transport, signal transduction, and cell motility were enriched in the PC group ($P < 0.001$, **Figure 3B**), and metabolism of cofactors and vitamins, biosynthesis of other secondary metabolites, amino acid metabolism, folding sorting and degradation, endocrine system, excretory system, immune system, nervous system, transport, and catabolism were enhanced in group PG ($P < 0.001$).

DISCUSSION

Necrotic enteritis caused by *C. perfringens* infection destroys the gut integrity of chickens and seriously damages the intestinal function of poultry, leading to a decline in the growth performance (Abudabos et al., 2017). Related studies had shown that probiotics play a positive role on animal health and prevention of NE diseases. Zhou et al. (2016) reported that the body weight decreased significantly after broilers were infected with NE, while FCR increased. However, the improved growth performance was observed when broilers were pre-treated with *B. licheniformis* H2. Whelan et al. (2018) also demonstrated that *Bacillus subtilis* DSM32315 alleviated the adverse impact on growth performance of broiler chickens caused by NE infection. Interestingly, Lin et al. (2017) found that diets supplemented with *B. licheniformis* H2 which was used in Zhou et al. (2016) research had no significant improvement on body weight, feed intake, and FCR of *C. perfringens* challenged broilers. In accordance with Lin's study, our results showed that pre-treatment with *B. licheniformis* had no improvement on growth performance of SNE-infected broilers. *B. licheniformis* was believed to prevent NE in broilers, but the mechanism of action of *B. licheniformis* as a probiotic for the control and prevention of NE is not totally clear. In addition, the function of *B. licheniformis* may differ from different strains and dietary concentrations (Knap et al., 2010). Thus, the optimum application rate of *B. licheniformis* used in studies may need further identified. Furthermore, differences in housing environment, broiler breed, administration route of probiotic *B. licheniformis* as well as the way to establish NE model may influence the outcome of *B. licheniformis* addition

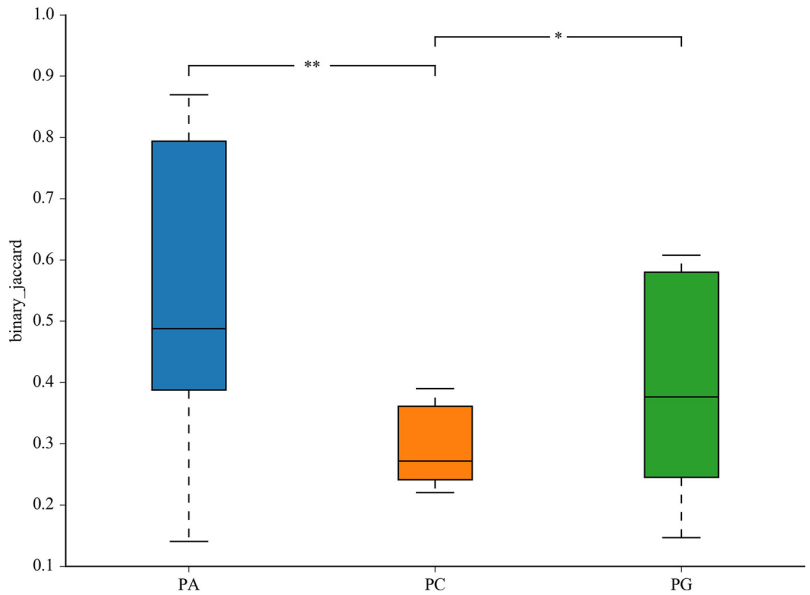

FIGURE 1 | Differential cecum microbiota community (β diversity) between groups in 25-day-old broilers. PC, basal diet + SNE; PA, basal diet extra antibiotics + SNE; PG, basal diet extra *B. licheniformis* + SNE. Values are means with their standard errors. $^{*}P < 0.05$, $^{**}P < 0.01$.

(Ramlucken et al., 2020). However, an improved body weight and FCR of 21–42 days and 1–42 days were seen in the PG and PA group although statistical difference was not reached, indicating that *B. licheniformis* and enramycin may protect broilers from SNE infection and alleviated growth performance loss caused by SNE to a certain degree. Studies had reported that probiotics *Bacillus* spp. increased the activity of digestive enzymes such as amylase and protease, and secreted some unknown growth-promoting factors which were helpful for intestinal development, feed degradation, and animal growth (Wang and Gu, 2010; Zhou et al., 2010). This may be one of the potential mechanisms by which probiotics *Bacillus* spp. improved the growth performance of SNE-infected broilers (Bai et al., 2016).

Intestinal lesion scores, intestinal microbiota balance, bacterial translocation, and intestinal morphology were important indicators for evaluating intestinal integrity and barrier function of broilers. The results of intestinal lesion scores in this study showed that the addition of *B. licheniformis* significantly reduced the duodenal and total intestinal lesion scores of SNE-infected broilers, which proved that the addition of *B. licheniformis* to diets effectively alleviated intestine damage caused by SNE infection in broilers. Consistent with our results, Wu et al. (2018) reported that *B. coagulans* significantly reduced intestinal lesion scores of broilers. The results from Jayaraman et al. (2013) also showed that the addition of *B. subtilis* PB6 significantly decreased the incidence and severity of intestinal lesions in *C. perfringens*-challenged broilers. In addition, in line with previous studies (Jayaraman et al., 2013; Wang H. et al., 2017; Wu et al., 2018), our results showed that SNE infection led to increased proliferation of cecal *C. perfringens* and higher *C. perfringens* invasion in the liver, indicating the imbalance of intestinal microflora and barrier damage of intestinal in broilers. After the supplementation of enramycin, lower *C. perfringens* load in the cecal contents and liver were observed compared with SNE-challenged birds, which proved that enramycin can effectively inhibit the growth of *C. perfringens*, thereby preventing pathogens or endotoxins from entering the systemic circulation. At 42 days of age, cecal *E. coli* numbers of broiler chickens in the antibiotics (enramycin) supplement group were significantly higher than that in the other groups. This may mainly be due to the growth inhibiting effect of enramycin on Gram-positive bacteria, especially to the harmful *Clostridium* in the intestinal tract, thus leading to the mass proliferation of Gram-negative bacteria such as *E. coli* (Sanjay et al., 2018). The intestinal mucus layer is the first defense barrier dialogued with microorganisms. The mucins secreted by goblet cells are important components of the mucus layer, providing a series of potential recognition sites for intestinal common microorganisms. At the same time, research noted that *C. perfringens* could not synthesize a variety of amino acids (Shimizu et al., 2002) so that the intestinal mucins served as an amino acid source of *C. perfringens* (Collier et al., 2008). In the present study, the addition of enramycin reduced the goblet cells in the jejunum, which may result in a decline in intestinal mucin secretion and a decreased availability of amino acids for *C. perfringens*, thereby inhibiting the growth and proliferation and translocation of *C. perfringens*. The morphological structure and integrity of intestine were associated with growth performance. Consistent with the growth performance that there was only numerically improvement between groups rather than differing significantly, the addition of *B. licheniformis* or enramycin had no significant improvement in the VH, CD, and VH/CD ratios in the jejunum of SNE-infected broilers. Inversely, Jayaraman et al. (2013) reported

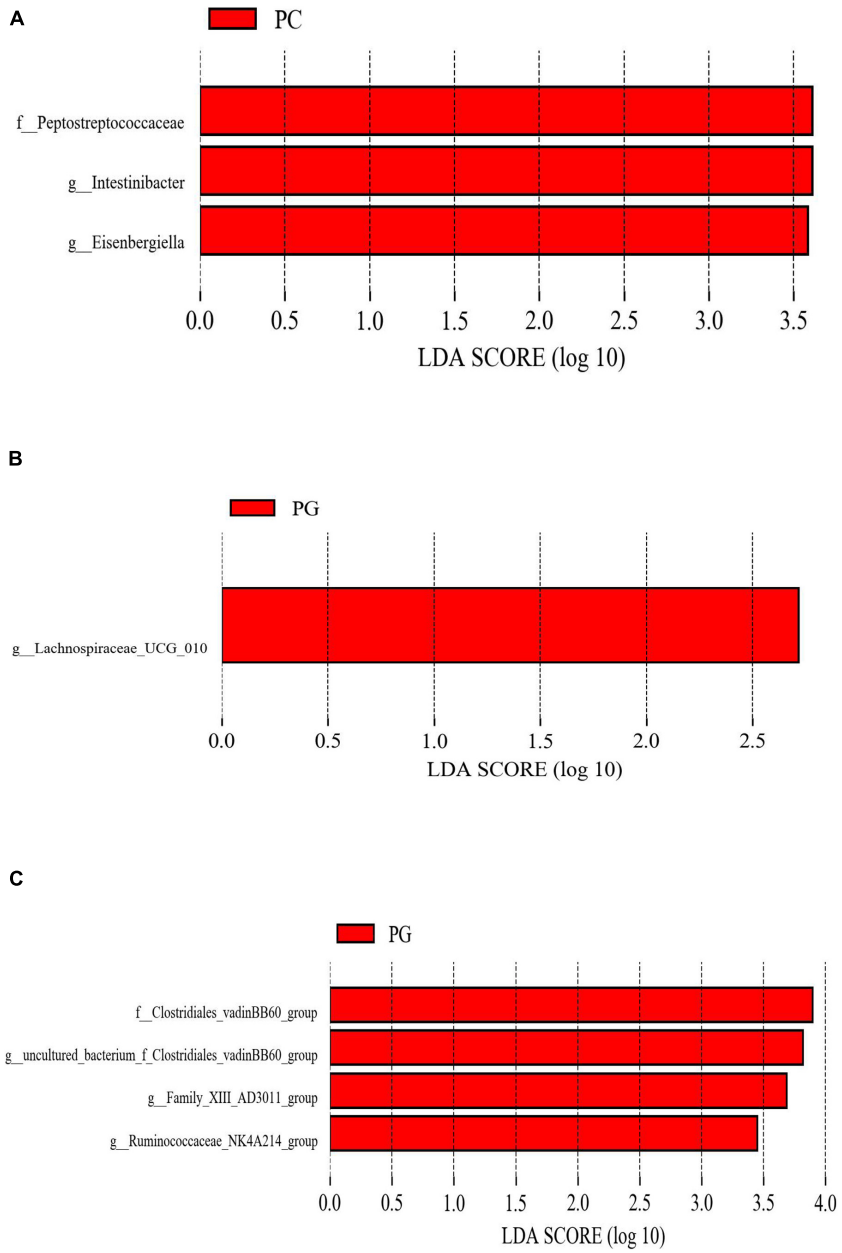

FIGURE 2 | The different phylotypes differed between groups using LEfSe analysis. These figures show the bacteria of which the LDA Score is greater than the set value (the default setting is 2.0) between groups PC and PA. **(A)** Groups PC and PG. **(B)** Groups PG and PA. **(C)** The length of the histogram represents the size of the difference species (i.e., LDA Score), and the different colors represent the different groups. PC, basal diet + SNE; PA, basal diet extra antibiotics + SNE; PG, basal diet extra *B. licheniformis* + SNE.

that diets added with *B. subtilis* PB6 significantly increased the intestinal VH and VH/CD ratio of NE-infected broilers, protected the intact villi structure of intestine, and reduced the FCR. As we know that the biofunction of probiotics varies from strain to strain, even the probiotic strains from the same species may work differently (Wang H. et al., 2017). Therefore, the contradictory results may partially be due to the different probiotic strains used in different studies. The aforementioned results also demonstrated that *B. licheniformis* and enramycin could mitigate intestinal injury of SNE-infected broilers in different aspects.

To determine the underlying mechanism responsible for this result, we further investigated the gene expression of tight junction proteins, *mucin-2* and TLR signaling pathway related factors, and the alterations in cecal microbiota. The intestinal tight junction (TJ) complex composed of occludins, claudins, ZOs, and other TJ proteins that control the intestinal paracellular permeability facilitates the exchange of water, ions, and other

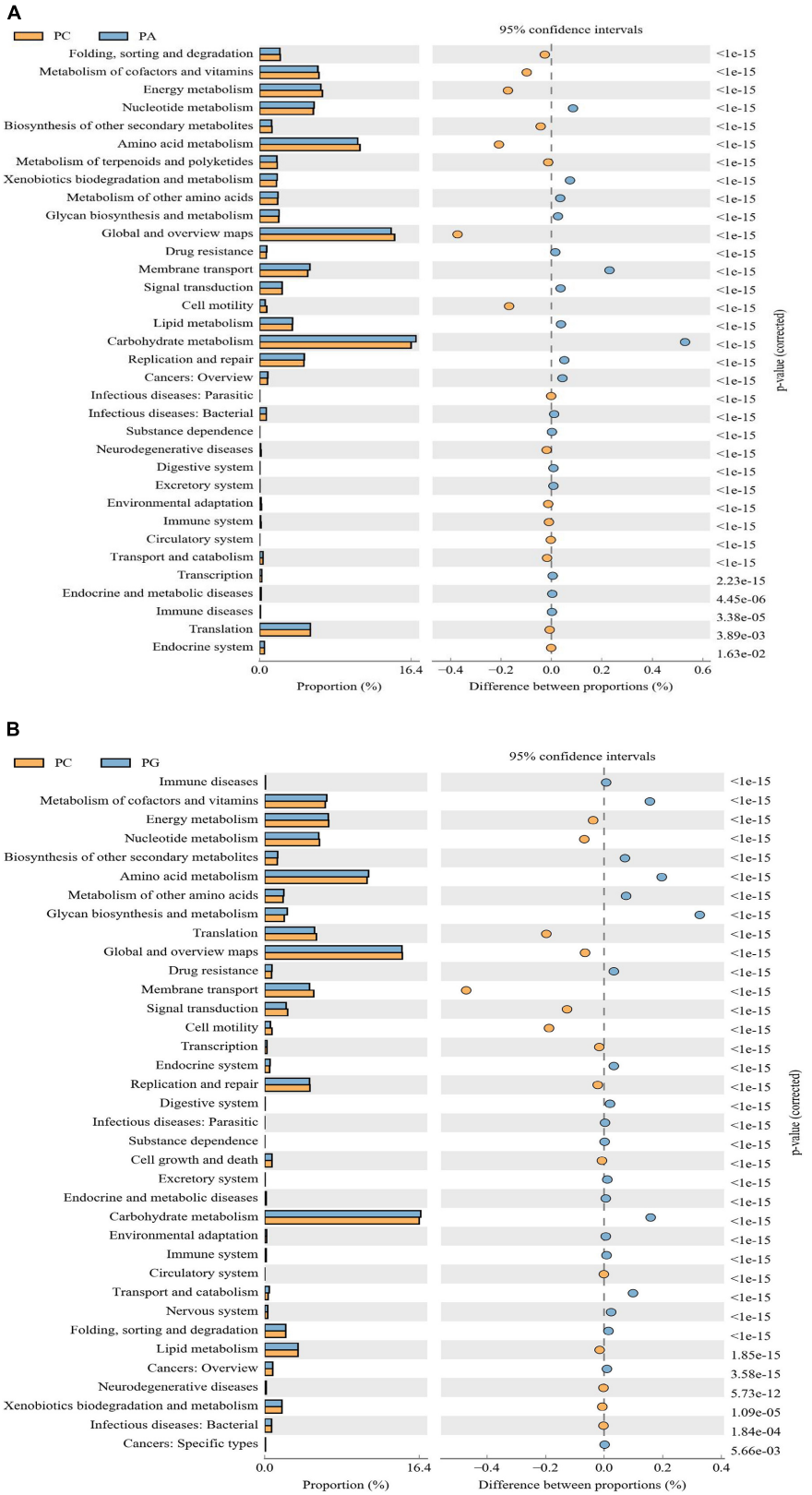

FIGURE 3 | The microbial pathways grouped into level-2 functional categories using PICRUSt. PC between groups PC and PA **(A)**, and groups PC and PG **(B)**. PC, basal diet + SNE; PA, basal diet extra antibiotics + SNE; PG, basal diet extra *B. licheniformis* + SNE.

nutrients with external environment, and also plays an important role in resisting the invasion of intestinal pathogens and toxins (Awad et al., 2017). Many pathogens indirectly impair the TJ structures of the intestinal tract by activating the signaling cascades of the host cells (Wageha et al., 2017), while the *C. perfringens* enterotoxin directly uses the TJ proteins *Claudin-3* and *Claudin-4* as cellular receptors to attach, leading to TJ degradation and increased paracellular permeability (Fujita et al., 2000; Veshnyakova et al., 2010). In the present study, results showed that addition of *B. licheniformis* significantly down-regulated the expression of *Claudin-3* mRNA in the jejunum of SNE-infected broilers on day 25 and a decreasing trend was also observed in the enramycin group, indicating that *B. licheniformis* and enramycin can reduce the intestinal *C. perfringens* adhesion by down-regulating *Claudin-3* mRNA levels, thereby protecting the intestinal mechanical barrier and paracellular permeability. Mucin-2 is one of the mucins which participates in the formation of mucous layer and protects intestinal mucosal barrier integrity (Michael McGuckin et al., 2011). On day 42, *C. perfringens* loads in the cecal contents of SNE-infected broilers was decreased, and broilers in each group were in the late stage of SNE infection or in the normal health status as can be seen from the results of intestinal lesion scores. At this time point, the gene expressions of *Claudin-3* and *mucin-2* were significantly up-regulated in the enramycin supplemented group, and the mRNA levels of *mucin-2* were also increased in the *B. licheniformis* supplemented group, indicating that *B. licheniformis* and enramycin may convey a protection on the intestinal TJs and mucus layers of broilers (Aliakbarpour et al., 2012; Rajput et al., 2013). In addition, the results also showed that the addition of *B. licheniformis* or enramycin significantly increased the content of cecal formic acid in 42-day-old broilers. Formic acid, a kind of SCFA, is produced by intestinal bacteria fermenting undigested starch or fiber polysaccharides that are unused to the host. SCFAs have important physiological significance to the host (Meimandipour et al., 2010; Rinttila and Apajalahti, 2013), of which formic acid could improve the intestinal morphology of broilers (Garcia et al., 2007) and inhibit the growth of pathogens (Bourassa et al., 2018). The results of the present study showed that *B. licheniformis* or enramycin can maintain the intestinal health by increasing the content of cecal formic acid in SNE-infected broilers.

When intestinal pathogens invade the host, they can be recognized by pattern recognition receptors. For example, TLRs can identify various pathogen-related molecular patterns and transmit the signals downstream through their linker proteins such as *TRIF* and *MyD88* to activate *NF-κB*, which can be transferred into the nucleus and thus induce the expression of target genes to regulate the immune and inflammation response, cell proliferation, and regeneration (Wertz and Dixit, 2010; Huebener and Schwabe, 2013). In line with other studies (Jung et al., 2015; Rajput et al., 2017), we found that at the peak period of *C. perfringens* infection (2 DPI), adding *B. licheniformis* or enramycin to the diet significantly increased the jejunal mRNA expression of *TRIF* and *NF-κB* in broilers, which indicates the activation of TLR-NF-κB signaling pathway, although the mRNA levels of *TLR-4* and *TLR-2* were not changed. The TLR-NF-κB signaling pathway is included in the innate immune response. Its activation causes a series of signal transductions, which leads to the activation and cellular responses of immune-related cells, and subsequently induces the secretion of cytokines, growth factors (*TGF-β*, *IGF-2*, *GLP-2*), type I IFNs, and chemokines (Kawai and Akira, 2007). Cytokines are effector molecules that transmit information between immune cells and determine the nature of the immune response at the infection site. For example, *IL-17* secreted by Th17 cells is an inflammatory cytokine that stimulates the production of granulocytes, promotes the production of antimicrobial peptides by epithelial cells, and enhances innate immunity (Eyerich et al., 2017). Consistent with previous studies (Fasina and Lillehoj, 2018), in this experiment, the addition of enramycin significantly up-regulated the mRNA levels of *IL-17*, indicating that the innate immune function of the broiler intestines was enhanced and effectively resisted the *C. perfringens* infection. However, unlike previous results (Rajput et al., 2013, 2017; Wang Y. et al., 2017), our results found that *B. licheniformis* did not significantly affect the gene expression of cytokines, such as *IL-1β*, *IL-10*, *IL-17*, and *TNF-α* after activation of TLR-NF-κB signaling pathway. This may be due to the different physiological functions of different probiotic strains (Kang and Sin-Hyeog, 2015). Although there were no significant changes detected on the expression of cytokines, adding *B. licheniformis* significantly up-regulated the expression of growth factors (*GLP-2*, *TGF-β2*), *HSP60*, *HSP70*, and *HSP90*, which was consistent with previous studies (Selvam et al., 2009; Okamoto et al., 2012; Rajput et al., 2017; Tang et al., 2019). Growth factors can promote the cell differentiation, mucosal development, and repair of damaged tissues (Bulut et al., 2008; Massagué, 2012; Camati et al., 2017), while HSPs are anti-stress proteins with molecular chaperone activity that protects cells and tissues from temperature stress or protein denaturation caused by infection, enhancing the resistance to environmental stress (Lindquist and Craig, 1988; Malago et al., 2001). In this experiment, *B. licheniformis* activated the TLR-NF-κB signaling pathway in jejunum of SNE-infected broilers, and afterward up-regulating the expression of jejunal growth factors and HSPs, enhancing the ability of tissue repairing and anti-stress of host, but did not affect the gene expression of pro-inflammatory cytokines. Similarly, adding enramycin also activated the TLR-NF-κB signaling pathway in jejunum of 25-day-old SNE-infected broilers, and also increased the gene expression of growth factors (*IGF-2*, *GLP-2*, *TGF-β2*) and *HSP90*. Furthermore, the gene expression of the proinflammatory cytokine *IL-17* was also up-regulated in broilers. Therefore, *B. licheniformis* had an effect of enhancing immunity in contrast to the enramycin. However, the results on day 42 showed that enramycin down-regulated the TLR-NF-κB signaling pathway, the gene expression of pro-inflammatory cytokines and HSPs in jejunum of healthy broilers, indicating that enramycin decreased the level of immunity and anti-stress of broilers and thus transferred more energy and nutrients to animals for growing. Based on the aforementioned results, we suggested that the impact of *B. licheniformis* on broiler challenged with SNE was focused on the repair and anti-stress of intestine which was different from enramycin's pro-inflammatory effects although they all activated the TLR-NF-κB signaling pathway.

Intestinal microbiota affects animal gut development, immune maturation, intestinal barrier, and host susceptibility to pathogens (Sekirov et al., 2010). Therefore, it is important to investigate infection, pre-treatment of *B. licheniformis*, or enramycin on intestinal microflora in broilers infected with SNE. Results showed that there was no significant difference in cecal microbiota α-diversity between groups. In accordance with our study, researchers found that α-diversity of gut microbiota was not affected by NE infection (Lin et al., 2017; Latorre et al., 2018), antibiotics supplementation (Sanjay et al., 2018), or probiotics *Bacillus* spp. (Qin et al., 2018) supplementation in broilers. We speculated that *C. perfringens* infection (Lin et al., 2017), and pre-treatment with antibiotics (Costa et al., 2017; Sanjay et al., 2018) or probiotics *Bacillus* spp. (Ahmed et al., 2014; Prieto et al., 2014) regulated the proliferation of minor microorganisms in the intestine of broilers thus the α-diversity in each group tended to be consistent. In terms of cecal bacterial community structure (β diversity), *B. licheniformis* adding group was similar to the enramycin group, but significantly different from the PC group, indicating that SNE infection caused a disturbance in cecal microflora in broilers, while adding *B. licheniformis* or enramycin modulated the bacterial community structure. Consistent with our results, Lin et al. (2017) and Xu et al. (2018) demonstrated that NE infection destroyed the community structure of intestinal microbes in broiler chickens and deviated it from normal state, whereas adding probiotics *Bacillus* spp. alleviated the disorder of intestinal microflora and restored it into homeostasis.

LEfSe analysis showed that the addition of enramycin reduced the relative abundance of *Peptostreptococcaceae*, *Intestinibacter*, and *Eisenbergiella* in SNE-infected broilers. It was reported that *Peptostreptococcaceae* were commensal bacteria in the intestine whose proportion in healthy animals was higher than that of diseased animals (Ma et al., 2011; Leng et al., 2016). However, other studies had also reported the presence of opportunistic pathogens in *Peptostreptococcaceae* may cause host disease (Ma et al., 2011). D'Andreano et al. (2017) compared the jejunal microflora of healthy and hemorrhagic enteritis turkeys, finding that *Peptostreptococcaceae* were only detected in the jejunum of hemorrhagic enteritis turkeys, which suggested that certain bacteria in *Peptostreptococcaceae* may also act as harmful bacteria and destroy the intestinal health of the host. For example, *Intestinibacter*, a genus of *Peptostreptococcaceae*, was significantly higher in the feces of patients with inflammatory diseases (such as Crohn's disease) than that in healthy individuals (Forbes et al., 2018), which further confirmed our hypothesis. In addition, some studies suggested that the genus *Eisenbergiella* contains potential pathogenic bacteria (Bernard et al., 2017). Bao et al. (2018) reported that the abundance of *Eisenbergiella* was significantly increased in the feces of *Echinococcus granulosus*-infected rats, and speculated that *Eisenbergiella* might be associated with the host's Th2 immune response. Therefore, in the present study, the enhanced intestinal barrier function and decreased *C. perfringens* liver translocation of broilers in enramycin group may partially relate to the decreased abundance of *Peptostreptococcaceae*, *Intestinibacter*, and *Eisenbergiella*. Compared with the PC group, we noted that the addition of *B. licheniformis* increased the abundance of *Lachnospiraceae_UCG_010* in the cecum of SNE-infected broilers. Researchers reported that the abundance of *Lachnospiraceae_UCG_010* was significantly reduced in feces of patients with irritable bowel syndrome, while it was increased in healthy individuals (Zhuang et al., 2018), suggesting that *Lachnospiraceae_UCG_010* may be beneficial intestinal bacteria and positively correlate with intestinal health. In this experiment, the increased abundance of *Lachnospiraceae_UCG_010* in the *B. licheniformis* supplement group was consistent with an increase in intestinal barrier function and a decline in intestinal lesion scores. In line with our results, many studies reported that probiotics *Bacillus* spp. modified the intestinal microflora of NE-infected broilers (Langille et al., 2013; Lin et al., 2017; Xu et al., 2018). Moreover, *Clostridiales_vadinBB60_group* and one of its genera were enriched in the *B. licheniformis* group when compared with the enramycin group. *Clostridiales_vadinBB60_group* contains a variety of bacteria producing butyric acid. Studies had reported that the increased abundance of *Clostridiales_vadinBB60_group* was accompanied by the enhanced serum antioxidant capacity in mice (Shimizu et al., 2002). In addition, Zhang et al. (2018) noted that the presence of *Clostridiales_vadinBB60_group* was detected in the feces of diabetic rats after treated with liraglutide. It was speculated that *Clostridiales_vadinBB60_group* may also be beneficial bacteria in intestinal tract, which was good for host health. *Ruminococcaceae_NK4A214_group* may also be a potentially beneficial bacterium. Studies had demonstrated that the abundance of *Ruminococcaceae_NK4A214_group* was reduced in obese rats and gout patients (Shao et al., 2017; Zhao et al., 2017). In contrast, *Family_XIII_AD3011_group* is considered to be a potential pathogen, and many studies reported that the abundance of *Family_XIII_AD3011_group* is positively associated with the diabetes (Zhang et al., 2018). Our results showed that the addition of *B. licheniformis* increased the abundance of *Clostridiales_vadinBB60_group*, *g_uncultured_bacterium_f_Clostridiales_vadinBB60_group*, *Family_XIII_AD3011_group*, and *Ruminococcaceae_NK4A214_group* were enriched in *B. licheniformis* supplemented group compared with the enramycin group, indicating that the recovery effect of *B. licheniformis* on cecal microbiome disorders of SNE-infected broilers is better than enramycin.

The observed shifts in the intestinal microbiota may regulate gut physiological function, host health, and growth. The PICRUSt aims to predict the unobserved characters from phylogenetic information regarding the organisms in the community. Vitamins are organic compounds which could be produced by bacteria notably vitamin K and B groups, regulating the construction and supporting normal physiological function of host (Rowland et al., 2018). An important role it serves is being cofactors for enzymes. Results presented the metabolism of cofactors and vitamins pathway was enriched in group PG, indicating a positive regulative effect of *B. licheniformis* on the activity of enzymatic metabolism (Rozs et al., 2001). However, it was lower in group PA which may result from the antibiotic effect of enramycin. Membrane transport, a vital pathway for the survival of bacteria in the gut ecosystem (Lyons et al., 2017), was increased in group PA, which may point out an

attempt to compensate for the antibiotic effect of enramycin. Regarding energy metabolism pathway, it was enriched in group PC comparing with group PG and PA, showing an energy metabolites disorder in SNE infection broilers (Chan et al., 2020). Cell motility is the determinant step of pathogen bacteria in early local invasion (Lin et al., 2017). The abundance of cell motility was enriched in PC group as compared with the PA and PG group, indicating the anti-infective effect of *B. licheniformis* and enramycin. In addition, it was found that carbohydrate metabolism pathways were enriched in group PA and PG, according with increased concentration of formic acid in cecum content. As reported, carbohydrate could be metabolized by microflora into SCFAs which were known to boost intestinal health by its trophic and anti-inflammatory effects (Kles and Chang, 2006; Lamas et al., 2018). Qing et al. (2018) noted that SNE infection could affect the hepatic lipid metabolism of chickens and probiotic pretreatment may provide a prophylaxis strategy against SNE infection through regulating lipid metabolism (Zhou et al., 2016; Lin et al., 2017). Agreed with those reports, we found that *B. licheniformis* supplement down-regulated the abundance of lipid metabolism pathway; however, enramycin up-regulated it, showing the different regulative effect of *B. licheniformis* and enramycin on cecum microbial function in the SNE-challenged broilers. Amino acid metabolite polyamines such as putrescine, spermidine, and spermine are harmful to hosts (Stevanato et al., 2012; Bonaiuto et al., 2015). Nevertheless, it was revealed that polyamines support gut physiology by strengthening barrier function, promoting gut maturation, increasing anti-oxidant capacity, and regulating immune function (Lagishetty and Naik, 2008; Bekebrede et al., 2020). As shown that amino acid metabolism pathway was enriched in group PG, this may confirm the hypothesis that *B. licheniformis* could adjust immune function through activating TLR-NF-κB signaling pathway. Therefore, the effect of *B. licheniformis* or enramycin on SNE-challenged broilers needs to be further investigated. Thus, dietary supplementation with antibiotic enramycin and probiotic *B. licheniformis* affected important predicted functions of the intestinal microbiota of the NE-challenged birds.

CONCLUSION

Dietary supplementation with *B. licheniformis* or enramycin mitigated the negative effects of SNE infection in broilers and alleviated intestinal damage, suggesting *B. licheniformis* could be used as an antibiotic alternative. *B. licheniformis* protected the intestinal health of SNE-infected broilers mainly mediated by increasing the number of beneficial bacteria *Lachnospiraceae_UCG_010* and formate acid content in the cecum, modulating TLR-NF-κB signaling pathway, and up-regulating jejunal *mucin-2*, growth factor (*GLP-2* and *TGF-β2*), and HSP (*HSP60*, *HSP70*, and *HSP90*) mRNA levels. However, the addition of enramycin maintained the intestinal barrier function mediated by reducing intestinal and liver *C. perfringens* load, increasing the cecal formate acid concentration, affecting the TLR-NF-κB signaling pathway, and up-regulating intestinal tight junction protein *Claudin-3*, *mucin-2*, pro-inflammatory cytokines together with growth factors and HSPs. This study showed that there are similarities and differences on the mechanism of *B. licheniformis* and enramycin in relieving intestinal damage of SNE-infected broilers. More studies are needed to confirm these results in the future.

DATA AVAILABILITY STATEMENT

The original contributions presented in the study are publicly available. This data can be found here: https://www.ncbi.nlm.nih.gov/, PRJNA728387.

ETHICS STATEMENT

The animal study was reviewed and approved by China Agricultural University Animal Care and Use Committee (statement no. CAU20170601-2).

AUTHOR CONTRIBUTIONS

ZW designed the research. LK, YL, and VP performed the experiments and analyzed the data. FG wrote the manuscript. ZW and YG participated in the revision of the manuscript. All authors contributed to data interpretation and approved the final version of the article.

FUNDING

The authors declare that this study received funding from Chr. Hansen Co., Ltd. (Denmark). The funder was not involved in the study design, collection, analysis, interpretation of data, the writing of this article or the decision to submit it for publication.

SUPPLEMENTARY MATERIAL

The Supplementary Material for this article can be found online at: https://www.frontiersin.org/articles/10.3389/fmicb.2021.623739/full#supplementary-material

REFERENCES

Abudabos, A. M., Alyemni, A. H., Dafalla, Y. M., and Khan, R. U. (2017). The effect of phytogenics on growth traits, blood biochemical and intestinal histology in broiler chickens exposed to *Clostridium perfringens* challenge. *J. Appl. Anim. Res.* 46, 691–695. doi: 10.1080/09712119.2017.1383258

Ahmed, S. T., Islam, M. M., Mun, H. S., Sim, H. J., Kim, Y. J., and Yang, C. J. (2014). Effects of Bacillus amyloliquefaciens as a probiotic strain on growth

performance, cecal microflora, and fecal noxious gas emissions of broiler chickens. *Poult. Sci.* 93, 1963–1971. doi: 10.3382/ps.2013-03718

Aliakbarpour, H. R., Chamani, M., Rahimi, G., Sadeghi, A. A., and Qujeq, D. (2012). The *Bacillus subtilis* and lactic acid bacteria probiotics influences intestinal mucin gene expression, histomorphology and growth performance in broilers. *Asian Australas. J. Anim. Sci.* 25, 1285–1293. doi: 10.5713/ajas.2012.12110

Alnassan, A. A., Kotsch, M., Shehata, A. A., Kruger, M., Daugschies, A., and Bangoura, B. (2014). Necrotic enteritis in chickens: development of a straightforward disease model system. *Vet. Rec.* 174, 455–457. doi: 10.1136/vr.102066

Awad, W. A., Hess, C., and Hess, M. (2017). Enteric pathogens and their toxin-induced disruption of the intestinal barrier through alteration of tight junctions in chickens. *Toxins* 9:60. doi: 10.3390/toxins9020060

Bai, K., Huang, Q., Zhang, J., He, J., Zhang, L., and Wang, T. (2016). Supplemental effects of probiotic *Bacillus subtilis* fmbJ on growth performance, antioxidant capacity, and meat quality of broiler chickens. *Poult. Sci.* 96, 74–82. doi: 10.3382/ps/pew246

Baikui, W., Jiangtao, Y., Guoshun, B., Yulong, M., Guoqiao, Y., and Weifen, L. (2016). Effects of *Bacillus subtilis* B10 on immune function, antioxidant indices and serum biochemical parameters of broilers. *Feed Ind.* 37, 47–51. doi: 10.13302/j.cnki.fi.2016.17.011

Bao, J., Zheng, H., Wang, Y., Zheng, X., He, L., Qi, W., et al. (2018). *Echinococcus granulosus* infection results in an increase in *Eisenbergiella* and *Parabacteroides* genera in the gut of mice. *Front. Microbiol.* 9:2890. doi: 10.3389/fmicb.2018.02890

Bekebrede, A., Keijer, J., Gerrits, W., and Boer, V. (2020). The molecular and physiological effects of protein-derived polyamines in the intestine. *Nutrients* 12:197. doi: 10.3390/nu12010197

Bernard, K., Burdz, T., Wiebe, D., Balcewich, B. M., Zimmerman, T., Lagacé-Wiens, P., et al. (2017). Characterization of isolates of Eisenbergiella tayi, a strictly anaerobic Gram-stain variable bacillus recovered from human clinical materials in Canada. *Anaerobe* 44, 128–132. doi: 10.1016/j.anaerobe.2017.03.005

Bonaiuto, E., Grancara, S., Martinis, P., Stringaro, A., and Paolo, M. L. D. (2015). A novel enzyme with spermine oxidase properties in bovine liver mitochondria: identification and kinetic characterization. *Free Radic. Biol. Med.* 81, 88–99. doi: 10.1016/j.freeradbiomed.2015.01.001

Bourassa, D. V., Wilson, K. M., Ritz, C. R., Kiepper, B. K., and Buhr, R. J. (2018). Evaluation of the addition of organic acids in the feed and/or water for broilers and the subsequent recovery of *Salmonella typhimurium* from litter and ceca. *Poult. Sci.* 97, 64–73. doi: 10.3382/ps/pex289

Bulut, K., Pennartz, C., Felderbauer, P., Meier, J. J., Banasch, M., Bulut, D., et al. (2008). Glucagon like peptide-2 induces intestinal restitution through VEGF release from subepithelial myofibroblasts. *Eur. J. Pharmacol.* 578, 279–285. doi: 10.1016/j.ejphar.2007.08.044

Camati, P. R., Giovanini, A. F., de Miranda Peixoto, H. E., Schuanka, C. M., Giacomel, M. C., de Araújo, M. R., et al. (2017). Immunoexpression of IGF1, IGF2, and osteopontin in craniofacial bone repair associated with autogenous grafting in rat models treated with alendronate sodium. *Clin. Oral Investig.* 21, 1895–1903. doi: 10.1007/s00784-016-1975-0

Caporaso, J. G., Kuczynski, J., Stombaugh, J., Bittinger, K., Bushman, F. D., Costello, E. K., et al. (2010). QIIME allows analysis of high-throughput community sequencing data. *Nat. Methods* 7, 335–336. doi: 10.1038/nmeth.f.303

Chan, S. Y., Probert, F., Radford-Smith, D. E., Hebert, J. C., Claridge, T. D. W., Anthony, D. C., et al. (2020). Post-inflammatory behavioural despair in male mice is associated with reduced cortical glutamate-glutamine ratios, and circulating lipid and energy metabolites. *Sci. Rep.* 10:16857. doi: 10.1038/s41598-020-74008-w

Collier, C. T., Hofacre, C. L., Payne, A. M., Anderson, D. B., Kaiser, P., Mackie, R. I., et al. (2008). Coccidia-induced mucogenesis promotes the onset of necrotic enteritis by supporting *Clostridium perfringens* growth. *Vet. Immunol. Immunopathol.* 122, 104–115. doi: 10.1016/j.vetimm.2007.10.014

Costa, M. C., Bessegatto, J. A., Alfieri, A. A., Weese, J. S., and Oba, A. (2017). Different antibiotic growth promoters induce specific changes in the cecal microbiota membership of broiler chicken. *PLoS One* 12:e0171642. doi: 10.1371/journal.pone.0171642

D'Andreano, S., Sànchez Bonastre, A., Francino, O., Cuscó Martí, A., Lecchi, C., Grilli, G., et al. (2017). Gastrointestinal microbial population of turkey (*Meleagris gallopavo*) affected by hemorrhagic enteritis virus. *Poult. Sci.* 96, 3550–3558. doi: 10.3382/ps/pex139

Edgar, R. C. (2010). Search and clustering orders of magnitude faster than BLAST. *Bioinformatics* 26, 2460–2461. doi: 10.1093/bioinformatics/btq461

Engström, B. E., Fermér, C., Lindberg, A., Saarinen, E., Båverud, V., and Gunnarsson, A. (2003). Molecular typing of isolates of *Clostridium perfringens* from healthy and diseased poultry. *Vet. Microbiol.* 94, 225–235. doi: 10.1016/S0378-1135(03)00106-8

Eyerich, K., Dimartino, V., and Cavani, A. (2017). IL-17 and IL-22 in immunity: driving protection and pathology. *Eur. J. Immunol.* 47, 607–614. doi: 10.1002/eji.201646723

Fasina, Y. O., and Lillehoj, H. S. (2018). Characterization of intestinal immune response to *Clostridium perfringens* infection in broiler chickens. *Poult. Sci*. 98, 188–198. doi: 10.3382/ps/pey390

Forbes, J. D., Chen, C. Y., Knox, N. C., Marrie, R. A., El-Gabalawy, H., De Kievit, T., et al. (2018). A comparative study of the gut microbiota in immune-mediated inflammatory diseases - Does a common dysbiosis exist? *Microbiome* 6:221. doi: 10.1186/s40168-018-0603-4

Forder, R., Nattrass, G. S., Geier, M. S., Hughes, R. J., and Hynd, P. I. (2012). Quantitative analyses of genes associated with mucin synthesis of broiler chickens with induced necrotic enteritis. *Poult. Sci.* 91, 1335–1341. doi: 10.3382/ps.2011-02062

Fujita, K., Katahira, J., Horiguchi, Y., Sonoda, N., Furuse, M., and Tsukita, S. (2000). *Clostridium perfringens* enterotoxin binds to the second extracellular loop of claudin-3, a tight junction integral membrane protein. *FEBS Lett.* 476, 258–261. doi: 10.1016/S0014-5793(00)01744-0

Garcia, V., Catala-Gregori, P., Hernandez, F., Megias, M. D., and Madrid, J. (2007). Effect of formic acid and plant extracts on growth, nutrient digestibility, intestine mucosa morphology, and meat yield of broilers. *J. Appl. Poultry Res.* 16, 555–562. doi: 10.3382/japr.2006-00116

Gholamiandehkordi, A. R., Timbermont, L., Lanckriet, A., Van Den Broeck, W., Pedersen, K., Dewulf, J., et al. (2007). Quantification of gut lesions in a subclinical necrotic enteritis model. *Avian Pathol.* 36, 375–382. doi: 10.1080/03079450701589118

Golder, H. M., Geier, M. S., Forder, R. E. A., Hynd, P. I., and Hughes, R. J. (2011). Effects of necrotic enteritis challenge on intestinal micro-architecture and mucin profile. *Br. Poult. Sci.* 52, 500–506. doi: 10.1080/00071668.2011.587183

Guo, S., Liu, D., Zhao, X., Li, C., and Guo, Y. (2014). Xylanase supplementation of a wheat-based diet improved nutrient digestion and mRNA expression of intestinal nutrient transporters in broiler chickens infected with *Clostridium perfringens*. *Poult. Sci.* 93, 94–103. doi: 10.3382/ps.2013-03188

Huebener, P., and Schwabe, R. F. (2013). Regulation of wound healing and organ fibrosis by toll-like receptors. *Biochim. Biophys. Acta* 1832, 1005–1017. doi: 10.1016/j.bbadis.2012.11.017

Jayaraman, S., Thangavel, G., Kurian, H., Mani, R., Mukkalil, R., and Chirakkal, H. (2013). *Bacillus subtilis* PB6 improves intestinal health of broiler chickens challenged with *Clostridium perfringens*-induced necrotic enteritis. *Poult. Sci.* 92, 370–374. doi: 10.3382/ps.2012-02528

Jung, J. U., Shin, J. U., Rhee, Y. K., Cho, C. O., and Lee, K. A. (2015). In vitro and *in vivo* immunostimulatory activity of an exopolysaccharide-enriched fraction from *Bacillus subtilis*. *J. Appl. Microbiol.* 118, 739–752. doi: 10.1111/jam.12742

Kang, H. J., and Sin-Hyeog, I. M. (2015). Probiotics as an immune modulator. *J. Nutr. Sci. Vitaminol.* 61, S103–S105. doi: 10.3177/jnsv.61.S103

Kawai, T., and Akira, S. (2007). Signaling to NF-κB by Toll-like receptors. *Trends Mol. Med.* 13, 460–469. doi: 10.1016/j.molmed.2007.09.002

Khan, R. U., and Naz, S. (2013). Application of probiotics in poultry production. *Worlds Poult. Sci. J.* 69, 621–632. doi: 10.1017/S0043933913000627

Kim, Y., Cho, J. Y., Kuk, J. H., Moon, J. H., Cho, J. I., Kim, Y. C., et al. (2004). Identification and antimicrobial activity of phenylacetic acid produced by *Bacillus licheniformis* isolated from fermented soybean, Chungkook-Jang. *Curr. Microbiol.* 48, 312–317. doi: 10.1007/s00284-003-4193-3

Kles, K. A., and Chang, E. B. (2006). Short-chain fatty acids impact on intestinal adaptation, inflammation, carcinoma, and failure. *Gastroenterology* 130, S100–S105. doi: 10.1053/j.gastro.2005.11.048

Knap, I., Lund, B., Kehlet, A. B., Hofacre, C., and Mathis, G. (2010). *Bacillus licheniformis* prevents necrotic enteritis in broiler Chickens. *Avian Dis.* 54, 931–935. doi: 10.1637/9106-101509-ResNote.1

Lagishetty, C. V., and Naik, S. R. (2008). Polyamines: potential anti-inflammatory agents and their possible mechanism of action. *Indian J. Pharmacol.* 40, 121–125. doi: 10.4103/0253-7613.42305

Lamas, B., Natividad, J. M., and Sokol, H. (2018). Aryl hydrocarbon receptor and intestinal immunity. *Mucosal Immunol.* 11, 1024–1038. doi: 10.1038/s41385-018-0019-2

Langille, M. G. I., Zaneveld, J., Caporaso, J. G., McDonald, D., Knights, D., Reyes, J. A., et al. (2013). Predictive functional profiling of microbial communities using 16S rRNA marker gene sequences. *Nat. Biotechnol.* 31, 814–821. doi: 10.1038/nbt.2676

Latorre, J. D., Bishnu, A., Park, S. H., Teague, K. D., Graham, L. E., Mahaffey, B. D., et al. (2018). Evaluation of the epithelial barrier function and Ileal microbiome in an established necrotic enteritis challenge model in broiler Chickens. *Front. Vet. Sci.* 5:199. doi: 10.3389/fvets.2018.00199

Lee, K. W., Lillehoj, H. S., Jeong, W., Jeoung, H. Y., and An, D. J. (2011). Avian necrotic enteritis: experimental models, host immunity, pathogenesis, risk factors, and vaccine development. *Poult. Sci.* 90, 1381–1390. doi: 10.3382/ps.2010-01319

Leng, Y., Yi, M., Fan, J., Bai, Y., Ge, Q., and Yao, G. (2016). Effects of acute intra-abdominal hypertension on multiple intestinal barrier functions in rats. *Sci. Rep.* 6:22814. doi: 10.1038/srep22814

Lin, Y., Xu, S., Zeng, D., Ni, X., Zhou, M., Zeng, Y., et al. (2017). Disruption in the cecal microbiota of chickens challenged with *Clostridium perfringens* and other factors was alleviated by *Bacillus licheniformis* supplementation. *PLoS One* 12:e0182426. doi: 10.1371/journal.pone.0182426

Lindquist, S., and Craig, E. A. (1988). The heat-shock proteins. *Annu. Rev. Genet.* 22, 631–677. doi: 10.1146/annurev.ge.22.120188.003215

Livak, K. J., and Schmittgen, T. D. (2001). Analysis of relative gene expression data using real-time quantitative PCR and the 2(-Delta Delta C(T)) Method. *Methods* 25, 402–408. doi: 10.1006/meth.2001

Lyons, P. P., Turnbull, J. F., Dawson, K. A., and Crumlish, M. (2017). Phylogenetic and functional characterization of the distal intestinal microbiome of rainbow trout *Oncorhynchus mykiss* from both farm and aquarium settings. *J. Appl. Microbiol.* 12, 347–363. doi: 10.1111/jam.13347

Ma, C., Wu, X., Nawaz, M., Li, J., Yu, P., Moore, J. E., et al. (2011). Molecular characterization of fecal microbiota in patients with viral Diarrhea. *Curr. Microbiol.* 63, 259–266. doi: 10.1007/s00284-011-9972-7

Malago, J. J., Koninkx, J. F. J. G., and Dijk, J. E. V. (2001). BioOne Online Journals - The heat shock response and cytoprotection of the intestinal epithelium. *Cell Stress Chaperon* 10, 4–6. doi: 10.1379/CSC-91.1

Massagué, J. (2012). TGFβ signalling in context. *Nat. Rev. Mol. Cell Biol.* 13, 616–630. doi: 10.1016/j.ejphar.2007.08.044

Meimandipour, A., Shuhaimi, M., Soleimani, A. F., Azhar, K., Hair-Bejo, M., Kabeir, B. M., et al. (2010). Selected microbial groups and short-chain fatty acids profile in a simulated chicken cecum supplemented with two strains of *Lactobacillus*. *Poult. Sci.* 89, 470–476. doi: 10.3382/ps.2009-00495

Michael McGuckin, M. A., Lindén, S. K., Sutton, P., and Florin, T. H. (2011). Mucin dynamics and enteric pathogens. *Nat. Rev. Microbiol.* 9, 265–278. doi: 10.1038/nrmicro2538

Mingmongkolchai, S., and Panbangred, W. (2018). Bacillus probiotics: an alternative to antibiotics for livestock production. *J. Appl. Microbiol.* 124, 1334–1346. doi: 10.1111/jam.13690

Mishra, N., and Smyth, J. A. (2017). Oral vaccination of broiler chickens against necrotic enteritis using a non-virulent NetB positive strain of *Clostridium perfringens* type A. *Vaccine* 32, 6858–6865. doi: 10.1016/j.vaccine.2017.10.030

National Research Council (1994). *Nutrient Requirements of Poultry* 9th Edn, Washington, DC: National Academies Press.

Okamoto, K., Fujiya, M., and Nata, T. (2012). W1835 competence and sporulation factor derived from *Bacillus Subtilis* improves epithelial cell injury in intestinal inflammation via immunomodulation and cytoprotection. *Int. J. Colorectal Dis.* 27, 1039–1046. doi: 10.1016/S0016-5085(10)63455-5

Parish, W. E. (1961). Necrotic enteritis in the fowl (*Gallus gallus domesticus*). I. Histopathology of the disease and isolation of a strain of *Clostridium welchii*. *J. Comp. Pathol.* 71, 377–393. doi: 10.1016/S0368-1742(61)80043-X

Park, S. S., Lillehoj, H. S., Allen, P. C., Park, D. W., Fitzcoy, S., Bautista, D. A., et al. (2008). Immunopathology and cytokine responses in broiler chickens coinfected with Eimeria maxima and *Clostridium perfringens* with the use of an animal model of necrotic enteritis. *Avian Dis.* 52, 14–22. doi: 10.1637/7997-041707-Reg

Prescott, J. F., Smyth, J. A., Shojadoost, B., and Vince, A. (2016). Experimental reproduction of necrotic enteritis in chickens: a review. *Avian Pathol.* 45, 317–322. doi: 10.1080/03079457.2016.1141345

Prieto, M. L., O'Sullivan, L., Tan, S. P., McLoughlin, P., Hughes, H., Gutierrez, M., et al. (2014). *In vitro* assessment of marine bacillus for use as livestock probiotics. *Mar. Drugs* 12, 2422–2445. doi: 10.3390/md12052422

Qin, C., Gong, L., Zhang, X., Wang, Y., Wang, Y., Wang, B., et al. (2018). Effect of *Saccharomyces boulardii* and *Bacillus subtilis* B10 on gut microbiota modulation in broilers. *Anim. Nutr.* 4, 358–366.

Qing, X., Zeng, D., Wang, H., Ni, X., and Jing, B. (2018). Analysis of hepatic transcriptome demonstrates altered lipid metabolism following *Lactobacillus johnsonii* BS15 prevention in chickens with subclinical necrotic enteritis. *Lipids Health Dis.* 17:93. doi: 10.1186/s12944-018-0741-5

Rajput, I. R., Li, L. Y., Xin, X., Wu, B. B., Juan, Z. L., Cui, Z. W., et al. (2013). Effect of *Saccharomyces boulardii* and *Bacillus subtilis* B10 on intestinal ultrastructure modulation and mucosal immunity development mechanism in broiler chickens. *Poult. Sci.* 92, 956–965. doi: 10.3382/ps.2012-02845

Rajput, I. R., Ying, H., Yajing, S., Arain, M. A., and Wenhua, L. (2017). Correction: *Saccharomyces boulardii* and *Bacillus Subtilis* B10 modulate TLRs and cytokines expression patterns in jejunum and ileum of broilers. *PLoS One* 12:e0173917. doi: 10.1371/journal.pone.0173917

Ramlucken, U., Lalloo, R., Roets, Y., Moonsamy, G., and Thantsha, M. S. (2020). Advantages of bacillus based probiotics in poultry production. *Livest. Sci.* 241:104215. doi: 10.1016/j.livsci.2020.104215

Rinttila, T., and Apajalahti, J. (2013). Intestinal microbiota and metabolites—Implications for broiler chicken health and performance. *J. Appl. Poult. Res.* 22, 647–658. doi: 10.3382/japr.2013-00742

Rowland, I., Gibson, G., Heinken, A., Scott, K., Swann, J., Thiele, I., et al. (2018). Gut microbiota functions: metabolism of nutrients and other food components. *Eur. J. Nutr.* 57, 1–24. doi: 10.1007/s00394-017-1445-8

Rozs, M., Manczinger, L., Cs, V., and Kevei, F. (2001). Secretion of a trypsin-like thiol protease by a new keratinolytic strain of *Bacillus licheniformis*. *FEMS Microbiol. Lett.* 205, 221–224. doi: 10.1016/S0378-1097(01)00462-1

Sanjay, K., Chongxiao, C., Nagaraju, I., Orosco, W. G., Manpreet, S., Kyun, K. W., et al. (2018). Effect of antibiotic withdrawal in feed on chicken gut microbial dynamics, immunity, growth performance and prevalence of foodborne pathogens. *PLoS One* 13:e0192450. doi: 10.1371/journal.pone.0192450

Segata, N., Izard, J., Waldron, L., Gevers, D., Miropolsky, L., Garrett, W. S., et al. (2011). Metagenomic biomarker discovery and explanation. *Genome Biol.* 12:R60. doi: 10.1186/gb-2011-12-6-r60

Sekirov, I., Russell, S. L., Antunes, L. C. M., and Finlay, B. B. (2010). Gut microbiota in health and disease. *Physiol. Rev.* 71, 242–246. doi: 10.1152/physrev.00045.2009

Selvam, R., Maheswari, P., Kavitha, P., Ravichandran, M., Sas, B., and Ramchand, C. N. (2009). Effect of *Bacillus subtilis* PB6, a natural probiotic on colon mucosal inflammation and plasma cytokines levels in inflammatory bowel disease. *Indian J. Biochem. Biophys.* 46, 79–85. doi: 10.1007/s00249-008-0372-2

Shao, T., Li, S., Li, H., Xie, Z., He, Z., and Wen, C. (2017). Combined signature of the fecal microbiome and metabolome in patients with gout. *Front. Microbiol.* 8:268. doi: 10.3389/fmicb.2017.00268

Shimizu, T., Ohtani, K., Hirakawa, H., Ohshima, K., Yamashita, A., Shiba, T., et al. (2002). Complete genome sequence of *Clostridium perfringens*, an anaerobic flesh-eater. *Proc. Natl. Acad. Sci. U.S.A.* 99, 996–1001. doi: 10.1073/pnas.022493799

Song, B., Li, H., Wu, Y., Zhen, W., and Guo, Y. (2017). Effect of microencapsulated sodium butyrate dietary supplementation on growth performance and intestinal barrier function of broiler chickens infected with necrotic enteritis. *Anim. Feed Sci. Technol.* 232, 6–15. doi: 10.1016/j.anifeedsci.2017.07.009

Stevanato, R., Cardillo, S., Braga, M., Iuliis, A. D., Battaglia, V., Toninello, A., et al. (2012). Preliminary kinetic characterization of a copper amine oxidase from rat liver mitochondria matrix. *Amino Acids* 42, 2531–2531. doi: 10.1007/s00726-012-1227-9

Tang, W., Qian, Y., Yu, B., Zhang, T., Gao, J., He, J., et al. (2019). Effects of *Bacillus subtilis* DSM32315 supplementation and dietary crude protein level on performance, gut barrier function and microbiota profile in weaned piglets. *J. Anim. Sci.* 97, 2125–2138. doi: 10.1093/jas/skz090

Tian, X., Shao, Y., Guo, Y., and Wang, Z. (2016). Effects of dietary yeast beta-glucans supplementation on growth performance, gut morphology, intestinal *Clostridium perfringens* population and immune response of broiler chickens challenged with necrotic enteritis. *Anim. Feed Sci. Technol.* 215, 144–155. doi: 10.1016/j.anifeedsci.2016.03.009

Timbermont, L., Haesebrouck, F., Ducatelle, R., and Van Immerseel, F. (2011). Necrotic enteritis in broilers: an updated review on the pathogenesis. *Avian Pathol.* 40, 341–347. doi: 10.1080/03079457.590967

Venessa, E., Wang, J., Alexander, V. P., Freddy, H., Marie, J., Gwen, F., et al. (2016). The probiotic *Butyricicoccus pullicaecorum* reduces feed conversion and protects from potentially harmful intestinal microorganisms and necrotic enteritis in broilers. *Front. Microbiol.* 7:1416. doi: 10.3389/fmicb.2016.01416

Veshnyakova, A., Protze, J., Rossa, J., Blasig, I. E., Krause, G., and Piontek, J. (2010). On the interaction of *Clostridium perfringens* Enterotoxin with Claudins. *Toxins* 2, 1336–1356. doi: 10.3390/toxins2061336

Wade, B., and Keyburn, A. (2015). The true cost of necrotic enteritis. *World Poult. Sci. J.* 31, 16–17.

Wageha, A., Claudia, H., and Michael, H. (2017). Enteric pathogens and their toxin-induced disruption of the intestinal barrier through alteration of tight junctions in chickens. *Toxins* 9:60.

Wang, H., Ni, X., Xiaodan, Q., Lei, L., Jing, L., Abdul, K., et al. (2017). Probiotic enhanced intestinal immunity in broilers against subclinical necrotic enteritis. *Front. Microbiol.* 8:1592. doi: 10.3389/fimmu.2017.01592

Wang, Y., Du, W., Lei, K., Wang, B., Wang, Y., Zhou, Y., et al. (2017). Effects of dietary *Bacillus licheniformis* on gut physical barrier, immunity, and reproductive hormones of laying hens. *Probiotics Antimicrob Proteins* 9, 292–299. doi: 10.1007/s12602-017-9252-3

Wang, Y., and Gu, Q. (2010). Effect of probiotic on growth performance and digestive enzyme activity of Arbor Acres broilers. *Res. Vet. Sci.* 89, 163–167. doi: 10.1016/j.rvsc.2010.03.009

Wertz, I. E., and Dixit, V. M. (2010). Signaling to NF-κB: regulation by ubiquitination. *Cold Spring Harb. Perspect. Biol.* 2:a003350. doi: 10.1101/cshperspect.a003350

Whelan, R. A., Doranalli, K., Rinttilä, T., Vienola, K., Jurgens, G., and Apajalahti, J. (2018). The impact of *Bacillus subtilis* DSM 32315 on the pathology, performance, and intestinal microbiome of broiler chickens in a necrotic enteritis challenge. *Poult. Sci.* 98, 3450–3463. doi: 10.3382/ps/pey500

Wu, Y., Shao, Y., Song, B., Zhen, W., Wang, Z., Guo, Y., et al. (2018). Effects of *Bacillus coagulans* supplementation on the growth performance and gut health of broiler chickens with *Clostridium perfringens*-induced necrotic enteritis. *J. Anim. Sci. Biotechnol.* 9:9. doi: 10.1186/s40104-017-0220-2

Xu, S., Lin, Y., Zeng, D., Zhou, M., Zeng, Y., Wang, H., et al. (2018). *Bacillus licheniformis* normalize the ileum microbiota of chickens infected with necrotic enteritis. *Sci. Rep.* 8:1744. doi: 10.1038/s41598-018-20059-z

Yin, D., Du, E., Yuan, J., Gao, J., Wang, Y. L., Aggrey, S. E., et al. (2017). Supplemental thymol and carvacrol increases ileum *Lactobacillus* population and reduces effect of necrotic enteritis caused by *Clostridium perfringes* in chickens. *Sci. Rep.* 7:7334. doi: 10.1038/s41598-017-07420-4

Zhang, Q., Xiao, X., Zheng, J., Li, M., Yu, M., Ping, F., et al. (2018). Featured article: structure moderation of gut microbiota in liraglutide-treated diabetic male rats. *Exp. Biol. Med.* 243, 34–44. doi: 10.1177/1535370217743765

Zhao, L., Zhang, Q., Ma, W., Tian, F., Shen, H., and Zhou, M. (2017). A Combination of quercetin and resveratrol reduces obesity in high-fat diet-fed rats by modulation of gut microbiota. *Food Funct.* 8, 4644–4656. doi: 10.1039/C7FO01383C

Zhou, M., Zeng, D., Ni, X., Tu, T., Yin, Z., Pan, K., et al. (2016). Effects of *Bacillus licheniformis* on the growth performance and expression of lipid metabolism-related genes in broiler chickens challenged with *Clostridium perfringens*-induced necrotic enteritis. *Lipids Health Dis.* 15:48. doi: 10.1186/s12944-016-0219-2

Zhou, X., Wang, Y., Gu, Q., and Li, W. (2010). Effect of dietary probiotic, *Bacillus coagulans*, on growth performance, chemical composition, and meat quality of Guangxi Yellow chicken. *Poult. Sci.* 89, 588–593. doi: 10.3382/ps.2009-00319

Zhuang, X., Tian, Z., Li, L., Zeng, Z., Chen, M., and Xiong, L. (2018). Fecal microbiota alterations associated with diarrhea-predominant irritable bowel syndrome. *Front. Microbiol.* 9:1600. doi: 10.3389/fmicb.2018.01600

Conflict of Interest: The authors declare that the research was conducted in the absence of any commercial or financial relationships that could be construed as a potential conflict of interest.

frontiers in Microbiology

ORIGINAL RESEARCH
published: 01 June 2021
doi: 10.3389/fmicb.2021.665776

Assessing the Response of Ruminal Bacterial and Fungal Microbiota to Whole-Rumen Contents Exchange in Dairy Cows

*Madison S. Cox[1,2], Courtney L. Deblois[1,2] and Garret Suen[1]**

[1] Department of Bacteriology, University of Wisconsin-Madison, Madison, WI, United States, [2] Microbiology Doctoral Training Program, University of Wisconsin-Madison, Madison, WI, United States

A major goal for the dairy industry is to improve overall milk production efficiency (MPE). With the advent of next-generation sequencing and advanced methods for characterizing microbial communities, efforts are underway to improve MPE by manipulating the rumen microbiome. Our previous work demonstrated that a near-total exchange of whole rumen contents between pairs of lactating Holstein dairy cows of disparate MPE resulted in a reversal of MPE status for ∼10 days: historically high-efficiency cows decreased in MPE, and historically low-efficiency cows increased in MPE. Importantly, this switch in MPE status was concomitant with a reversal in the ruminal bacterial microbiota, with the newly exchanged bacterial communities reverting to their pre-exchange state. However, this work did not include an in-depth analysis of the microbial community response or an interrogation of specific taxa correlating to production metrics. Here, we sought to better understand the response of rumen communities to this exchange protocol, including consideration of the rumen fungi. Rumen samples were collected from 8 days prior to, and 56 days following the exchange and were subjected to 16S rRNA and ITS amplicon sequencing to assess bacterial and fungal community composition, respectively. Our results show that the ruminal fungal community did not differ significantly between hosts of disparate efficiency prior to the exchange, and no change in community structure was observed over the time course. Correlation of microbial taxa to production metrics identified one fungal operational taxonomic unit (OTU) in the genus *Neocallimastix* that correlated positively to MPE, and several bacterial OTUs classified to the genus *Prevotella*. Within the *Prevotella*, *Prevotella_1* was found to be more abundant in high-efficiency cows whereas *Prevotella_7* was more abundant in low-efficiency cows. Overall, our results suggest that the rumen bacterial community is a primary microbial driver of host efficiency, that the ruminal fungi may not have as significant a role in MPE as previously thought, and that more work is needed to better understand the functional roles of specific ruminal microbial community members in modulating MPE.

Keywords: ruminal contents exchange, ruminal microbiota, milk production efficiency, dairy cattle, rumen

OPEN ACCESS

Edited by:
Xudong Sun, Heilongjiang Bayi Agricultural University, China

Reviewed by:
Ilma Tapio, Natural Resources Institute Finland (Luke), Finland
Shengguo Zhao, Institute of Animal Sciences, Chinese Academy of Agricultural Sciences, China

****Correspondence:***
Garret Suen
gsuen@wisc.edu

Specialty section:
This article was submitted to Systems Microbiology, a section of the journal Frontiers in Microbiology

Received: *08 February 2021*
Accepted: *06 May 2021*
Published: *01 June 2021*

Citation:
Cox MS, Deblois CL and Suen G (2021) Assessing the Response of Ruminal Bacterial and Fungal Microbiota to Whole-Rumen Contents Exchange in Dairy Cows. Front. Microbiol. 12:665776. doi: 10.3389/fmicb.2021.665776

INTRODUCTION

Tremendous gains have been made in dairy cattle efficiency and productivity through efforts in breeding and management over the last several decades (Miglior et al., 2017). However, breeding for high production has resulted in consequent decreases in animal health and longevity (Knaus, 2009). This has led to an interest in breeding-independent strategies for improving milk production efficiency (MPE) to ensure a sustainable and economically viable future for the dairy industry. One promising avenue for improving MPE is through modulation of the rumen microbial community. The rumen microbiota is essential for the degradation of feed components into volatile fatty acids (VFAs), which have various fates once absorbed by the host. Inter-animal variability in rumen microbial metabolism can therefore result in differences in both milk volume and components by altering the pool of precursors available to the host. Importantly, the rumen microbial community has been repeatedly implicated in milk efficiency variability and production metrics in dairy cattle (Jami et al., 2014; Jewell et al., 2015; Shabat et al., 2016; Wallace et al., 2019).

The rumen contains a diverse, multi-domain microbial consortium of archaea, bacteria, fungi, and ciliate protozoa. Bacteria are the most abundant and diverse members of this community, with 10^{10}–10^{11} cells/gram (Choudhury et al., 2015), and are the most thoroughly studied group in the rumen ecosystem. Fungi, which are much less abundant in the rumen at 10^{3}–10^{5} cells/gram, are remarkably efficient fiber degraders that play an important role in the initial colonization and physical disruption of feed particles (Russell and Hespell, 1981; Akin and Borneman, 1990; Gordon and Phillips, 1998). Protozoa are known to have a role in VFA production, but in concert with archaea, are thought to have a greater importance in methane production, leading to a net energy loss.

The majority of studies that seek to implicate members of the rumen microbiome in host efficiency have focused primarily on the bacteria. However, due to the functional importance of the fungal community in digestion, recent consideration has been paid to the role of the ruminal fungi in overall fermentation (Puniya et al., 2015). For example, removal of anaerobic fungal populations in sheep has been demonstrated to negatively impact feed digestibility *in vivo* (Gao et al., 2013). Additionally, supplementation with rumen-derived fungal isolates increased feed digestibility and weight gain in buffalo calves (Tripathi et al., 2007). However, no studies to date have specifically linked native rumen fungal communities to performance metrics in dairy cattle.

Our previous study sought to provide evidence that near complete replacement of the rumen microbiota alone is sufficient to alter MPE (Weimer et al., 2017). In that study, an exchange of rumen contents was performed between three pairs of lactating Holstein cows with disparate MPE. For 7–10 days following the exchange, 5 of the 6 cows saw a reversal in MPE status from the pre-exchange baseline. This change in efficiency status was accompanied by a concurrent change in bacterial community structure. Within 10 days, MPE status and bacterial community structure returned to the expected baseline for the 5 affected hosts. This suggested a strong link between bacterial community composition and MPE, but also underscored the strong host-specificity of the adult rumen bacterial community, which apparently was able to re-establish even after extreme perturbation. We note that our previous study only included a cursory analysis of the ruminal bacterial community and did not consider other microbial community members such as the ruminal fungi.

Here, we expand on our previous findings by providing a more comprehensive analysis of the recovery of the rumen microbial community following near complete whole rumen contents exchange, including a focus on the ruminal fungal community. Given the demonstrated importance of the rumen fungal community in fiber degradation, we expect that high- and low-efficiency hosts would have distinct fungal communities prior to the exchange, and that the response of the rumen fungal community to the exchange protocol would mirror that of the bacterial community. Additionally, we sought to identify specific microbial community features, within both the bacteria and the fungi, that could be implicated in the observed differences in MPE.

MATERIALS AND METHODS

Animal Trial and Sample Collection

The animal trial, DNA extraction, and bacterial community sequencing were performed as previously published in Weimer et al. (2017) under protocol A01427, as approved by the College of Agricultural and Life Sciences' Animal Care and Use Committee, University of Wisconsin–Madison. Briefly, three pairs of healthy, lactating, ruminally cannulated 3rd-lactation Holstein dairy cows were selected on the basis of disparate dry matter intake (DMI) with similar energy corrected milk (ECM) over their first two lactation cycles, designated as either high or low milk production efficiency within each pair (HE and LE, respectively). An exchange of whole rumen contents was performed between the HE and LE member of each pair (∼95% of rumen contents removed), and ECM and DMI were recorded from 8 days prior to and 56 days following the exchange. Gross feed efficiency (GFE) was calculated as ECM/DMI. Solid- and liquid-phase rumen contents were collected at 18 timepoints relative to the exchange for characterization of microbial communities (sampling days relative to the exchange: −8, −7, −5, −4, −1, day 0 pre-exchange, day 0 post-exchange, 1, 2, 3, 7, 10, 14, 21, 28, 35, 42, 56).

Amplicon Sequencing

Bacterial communities were characterized by sequencing of the variable 4 (V4) region of the 16S rRNA gene using a one-step protocol with barcoded primers (Kozich et al., 2013) and as previously described (Weimer et al., 2017). Fungal community sequencing was performed using custom barcoded primers designed according to the protocol outlined in Kozich et al. (2013). Barcodes were added to universal ITS4 primers (Taylor et al., 2016)

(ITS4-Fun (5′-AATGATACGGCGACCACCGAGATCTACAC-TATGGTAATT-AA-AGCCTCCGCTTATTGATATGCTTAART-3′). Full sequences of barcoded primers can be found in **Supplementary Data Sheet 1**. A total of 50 ng of template DNA, 5 pmol of each primer, and 12.5 μL of 2X HotStart Ready Mix (KAPA Biosystems, Wilmington, MA, United States) and water to a total reaction volume of 25 μL were used for each PCR reaction. PCR conditions were: 3 min at 95°C for initial denaturation, 35 cycles of 30 s at 95°C, 30 s at 58°C, 30 s at 72°C, then 5 min at 72°C for final extension. Samples were run on a 1% low-melt agarose gel, and amplified DNA was extracted from the gel using the ZR-96 Zymoclean Gel DNA Recovery Kit (Zymo Research, Irvine, CA, United States). Extracts were equimolarly pooled and combined with the PhiX control library (Illumina, Inc., San Diego, CA, United States) at a 9:1 ratio. The combined library was loaded onto the Illumina MiSeq (Illumina, Inc., San Diego, CA, United States) for paired-end sequencing using the 2 × 300 bp v3 sequencing kit. Bacterial sequences from this project are deposited in the National Center for Biotechnology Information (NCBI) Short Read Archive (SRA) under the BioProject number PRJNA329260. Fungal sequences are deposited under BioProject number PRJNA695353.

Sequence Cleanup

For both bacterial and fungal amplicons, sequences were demultiplexed by sample-specific indices on the Illumina MiSeq. Further processing and quality controls were performed in the program mothur v1.42.1 according to the most recent versions of our lab's standard analysis pipelines (**Supplementary Data Sheet 2**), as adapted from the Schloss lab protocol (Kozich et al., 2013). Paired-end sequences were combined to form contigs and poor-quality contigs were removed from analysis. Bacterial sequences were aligned to the SILVA 16S rRNA gene reference alignment database v132 (Pruesse et al., 2007), and contigs that did not align to the V4 region were eliminated. Preclustering was performed (bacteria: diff = 2, fungi: diff = 4) to account for sequencing error, and fungal sequences were subjected to an internal Needleman alignment during this process (Needleman and Wunsch, 1970). Chimeric sequences were identified and removed using the UCHIME algorithm in mothur (Edgar et al., 2011). Sequences that could not be classified at the Kingdom level were eliminated. Singleton sequences were removed from the dataset prior to operational taxonomic unit (OTU) clustering.

Sequence and Statistical Analysis

Clustering of OTUs at a sequence similarity of 97% was performed for both amplicons using the OptiClust algorithm in mothur (Westcott and Schloss, 2017). Bacterial sequences were classified using the SILVA 16S rRNA gene reference database v132 and fungal sequences were categorized using the UNITE v6.0 database (Nilsson et al., 2019), with a bootstrap cutoff of 80. Good's coverage was calculated in mothur (Good, 1953). Normalization was applied in mothur (bacteria: 10,000 sequences/sample, fungi: 2,450 sequences/sample). Shannon's Diversity (Shannon, 1948), Chao's Richness (Chao, 1984), and post-normalization Good's coverage were calculated in mothur. Representative sequences for each OTU were generated using the get.oturep command in mothur. The NCBI's online nucleotide BLAST server was used to identify cultured isolates with high sequence similarity to representative sequences of select OTUs (Madden, 2002).

Statistical analysis was performed in R v3.6.3 (R Core Team, 2020) using RStudio v1.2.5033 (R Studio Team, 2020). Differences in alpha diversity statistics by time period and initial host efficiency status were assessed by two-way ANOVA, with Tukey's HSD used as a *post hoc* test in the case of significance ($p < 0.05$). Non-significant interaction terms were removed from model formulae to better characterize main effects.

Beta diversity was calculated as Bray-Curtis dissimilarity (Bray and Curtis, 1957) and visualized with non-metric multidimensional scaling (NMDS) with square root transformed data in the R package vegan, v2.5-6 (Okansen et al., 2016). Differences in community structure between groups of samples were assessed by permutational multivariate ANOVA (vegan:adonis2, by = "margin"). Samples were assessed within sample type (solid or liquid fraction of the rumen contents) and amplicon (bacterial or fungal), with permutations stratified within individual to control for multiple sampling. Samples were assessed by initial efficiency status and categorical time within the sample period, as previously described (Weimer et al., 2017) (Pre = day -8 to day 0 pre-exchange, Post1 = day 0 post-exchange to day 7, Post2 = day 10 to day 56). These time periods were selected by Weimer et al. (2017) to capture the change in MPE status, which persisted for ∼7 days post-exchange, and the return to baseline MPE at 10–56 days post-exchange. Non-significant interaction terms were removed from model formulae to better characterize main effects. Pairwise comparisons between groups of samples were also calculated using the adonis function, with *P*-values FDR-corrected for multiple comparisons.

To streamline visualization of correlation networks, OTUs with <0.1% overall abundance were removed from the analysis (bacterial abundance cutoff: 2,146; fungal abundance cutoff: 522). Matrices of Pearson's correlation coefficients were generated for within sample type, initial efficiency, and time period (Pre, Post1, Post2) using the rcorr function in the Hmisc package for R (Harrell Jr., 2020). Correlations that were weak (<0.70) or not highly significant ($\alpha < 0.001$) were removed, and correlation matrices were used to generate correlation networks using igraph (Csardi and Nepusz, 2006). The degree-centrality of networks was calculated by domain using igraph. Differences in degree over time within initial efficiency status and domain were assessed using Kruskal-Wallis tests. Pairwise Wilcoxon tests were performed with FDR-correction applied to resultant *P*-values. Beanplots were generated using beanplot:beanplot in R (Kampstra, 2008). The 10 OTUs with the greatest degree centrality were selected from each of the pre-exchange networks (HE liquids, HE solids, LE liquids, and LE solids) and were subjected to Kruskal-Wallis testing to assess change over time, within sample type and host efficiency. *Post hoc* testing was performed as pairwise Wilcoxon rank sum tests with FDR correction applied to *P*-values. These OTUs were also correlated to production variables (ECM and GFE). Spearman's ρ statistic was calculated between normalized OTU abundance and the

phenotypic variable across all animals and time points, separated by sample type (liquids and solids). FDR correction was applied to *P*-values.

Individual species which differed between the categorical time periods were identified using the similarity percentages (SIMPER) function in vegan (vegan:simper) within amplicon, sample type, and initial efficiency status (Okansen et al., 2016). OTUs that explained >1% of the difference between time points were subjected to Kruskal-Wallis tests, with FDR-correction applied to resultant *P*-values.

Operational taxonomic units that were identified in the SIMPER analysis were correlated to phenotypic variables (ECM, GFE, molar fraction acetate, molar fraction propionate, molar fraction butyrate), as previously determined in Weimer et al. (2017). Spearman's ρ statistic was calculated between OTU abundance and the variable of interest across all cows and time points, separated by amplicon (bacterial and fungal) and sample type. FDR-corrected *P*-values were calculated for each of these correlations using the cor.test function from the R package stats (R Core Team, 2020).

Linear discriminant analysis effect size (LEfSe) was performed on abundance-filtered, relative-abundance-transformed OTU matrices for Pre-exchange samples, within sample type and domain (Segata et al., 2011). The Huttenhower lab's Galaxy instance was used with default parameters (Kruskal-Wallis $P < 0.05$, Pairwise Wilcoxon $P < 0.05$, logarithmic LDA score > 2.0)[1] to obtain a list of candidate OTUs which were diagnostic of initial efficiency. Implicated OTUs were regressed against ECM and GFE, and *P*-values were FDR-corrected.

RESULTS

Sequencing

Solid and liquid rumen samples were taken from three pairs of healthy lactating Holstein dairy cows at 18 timepoints over 64 days. These 216 samples were subjected to bacterial and fungal amplicon sequencing. Two samples were not subjected to fungal community sequencing because of insufficient DNA yields (RSL61d42 and RSL97d42). Bacterial sequencing generated 7,996,986 high-quality sequences with an average of 37,023 ± 2491 SE sequences per sample and a range of 10,049–328,315 sequences per sample. Fungal sequencing yielded 2,168,129 high-quality sequences an average of 10,131 ± 276 SE sequences per sample and a range of 2450–23,811 sequences per sample. Pre-normalization Good's coverage was >97% for all bacterial samples, and >99% for all fungal samples, indicating that the sequencing depth was adequate to accurately characterize the communities of interest. Post-normalization there were a total of 2,147,014 bacterial and 523,784 fungal sequences used in analysis. Post-normalization Good's coverage was >93% for all bacterial samples and >98% for all fungal samples. Sequencing results are summarized in **Supplementary Data Sheet 3**. Normalized OTU tables and taxonomic classification of OTUs can be found in **Supplementary Data Sheet 4**.

[1]http://huttenhower.sph.harvard.edu/galaxy

Alpha Diversity

Alpha diversity analysis was performed for each amplicon and sample type separately (**Supplementary Figure 1**). In the liquid phase, changes in Shannon's diversity for the bacterial community over the time course were not dependent on efficiency status ($F_{2,102} = 1.679$, $P = 0.192$). Ignoring efficiency status, there was no change in bacterial Shannon's index by time period ($F_{2,104} = 0.346$, $P = 0.708$). Rumen liquids derived from HE animals had lower bacterial Shannon's diversity than those derived from LE liquids ($F_{2,104} = 18.353$, $P < 0.001$). For the rumen solids, there was no significant interaction between efficiency status and time period for Shannon's diversity of bacterial communities ($F_{2,102} = 2.258$, $P = 0.110$), and no significant difference between timepoints, irrespective of initial efficiency status ($F_{2,104} = 0.359$, $P = 0.699$). Similar to the liquid-derived samples, rumen solids derived from initially HE animals were less bacterially diverse than those derived from LE animals ($F_{2,104} = 10.038$, $P = 0.002$).

The impact of study period on Chao's richness in liquid phase samples did not differ by initial efficiency status ($F_{2,102} = 0.566$, $P = 0.569$). Without consideration of efficiency, there was no change in bacterial species richness over time in the liquid samples ($F_{2,104} = 1.023$, $P = 0.363$). Overall, bacterial species richness in liquid samples did not differ by efficiency status ($F_{2,104} = 1.228$, $P = 0.270$). In solid-derived rumen samples, time period and efficiency status were not independent in their effect on Chao's richness of bacterial communities ($F_{2,102} = 3.883$, $P = 0.024$). In these samples, HE cows had lower Chao's richness than LE cows in the Post2 period ($P = 0.037$), and LE cows differed from Pre to Post2 ($P = 0.025$). All other pairwise comparisons were not significant ($P > 0.05$).

In the liquid phase, changes in fungal community Shannon's diversity over time was independent of efficiency status ($F_{2,100} = 2.069$, $P = 0.132$). There was no change in liquid fungal community richness over time ($F_{2,102} = 1.562$, $P = 0.215$) or by efficiency status ($F_{2,102} = 0.111$, $P = 0.739$). In solid-phase samples, there was no significant interaction between study period and efficiency status ($F_{2,102} = 0.111$, $P = 0.895$). There was overall no change in richness by time period ($F_{2,104} = 0.713$, $P = 0.493$) or efficiency status ($F_{2,104} = 0.410$, $P = 0.523$).

The impact of time on fungal community richness liquid-phase samples was independent of efficiency status ($F_{2,100} = 0.651$, $P = 0.524$). There was no impact of study period on fungal community species richness in liquids ($F_{2,102} = 1.423$, $P = 0.246$), nor was there an impact of initial efficiency status on richness ($F_{2,102} = 0.535$, $P = 0.466$). Solid-phase fungal community richness likewise did not show an interaction between time period and efficiency status ($F_{2,102} = 2.406$, $P = 0.095$). There was no impact on fungal species richness in rumen solids-derived samples by either time period ($F_{2,104} = 0.611$, $P = 0.545$) or efficiency status ($F_{2,104} = 0.304$, $P = 0.583$).

Beta Diversity

Beta diversity analysis was performed for each amplicon and sample type separately. For ease of interpretation, pairs of animals

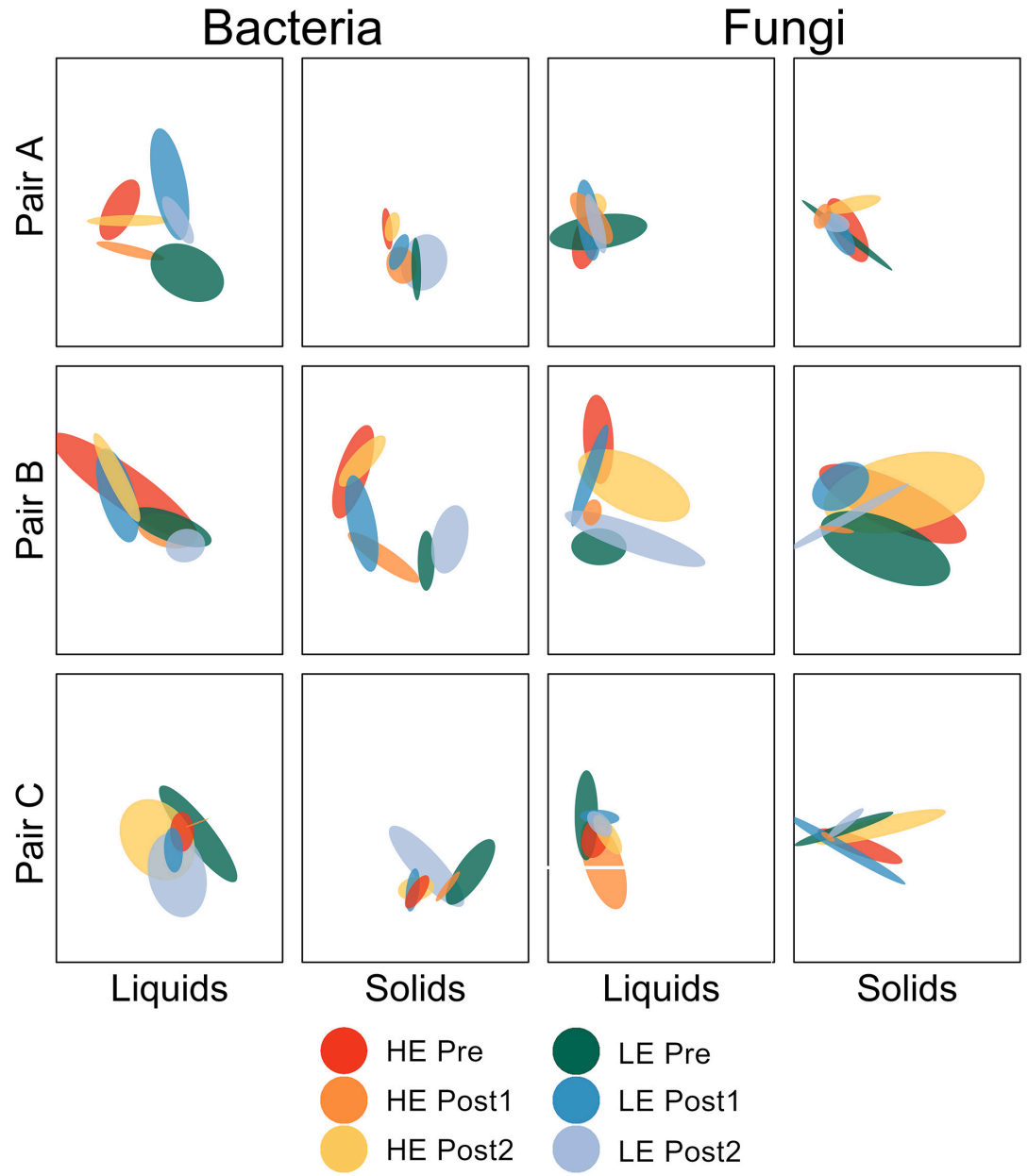

FIGURE 1 | Non-metric multidimensional scaling plot depicting Bray-Curtis dissimilarity of bacterial and fungal communities by pair of host animals. Standard error ellipses are color coded by initial MPE of host and time within study.

were plotted separately (**Figure 1**). Between-sample diversity was calculated as Bray-Curtis dissimilarity and visualized with standard error ellipses to better illustrate the behavior of groups of points within a given host animal across the time series.

For the bacterial communities in the liquid phase (all three pairs of animals considered together), the change in community structure over time differed by efficiency status (P = 0.007). HE Pre was distinct from HE Post1 (P = 0.016), but not from HE Post2 (P = 1.000). LE Pre was not distinct from LE Post1 (P = 0.183) or LE Post2 (P = 0.708), but LE Post1 was distinct from LE Post2 (P = 0.016). All other pairwise comparisons were non-significant ($P > 0.05$). For the ruminal solids, the change in bacterial community structure over time was also dependent on efficiency status ($P < 0.001$). HE Pre was distinct from HE Post1 ($P < 0.001$), but only marginally distinct from HE Post2 ($P = 0.090$). HE Post1 was distinct from HE Post2 ($P < 0.001$). LE Pre was distinct from LE Post1 ($P < 0.001$), but not from LE Post2 ($P = 0.178$). LE Post1 was distinct from LE Post2 ($P = 0.015$). No other pairwise comparisons were significant ($P > 0.05$).

Fungal community structure change over time was dependent on efficiency status in rumen liquids ($P = 0.012$). HE Pre was not distinct from HE Post1 (P = 0.109) or HE Post2 (P = 0.510).

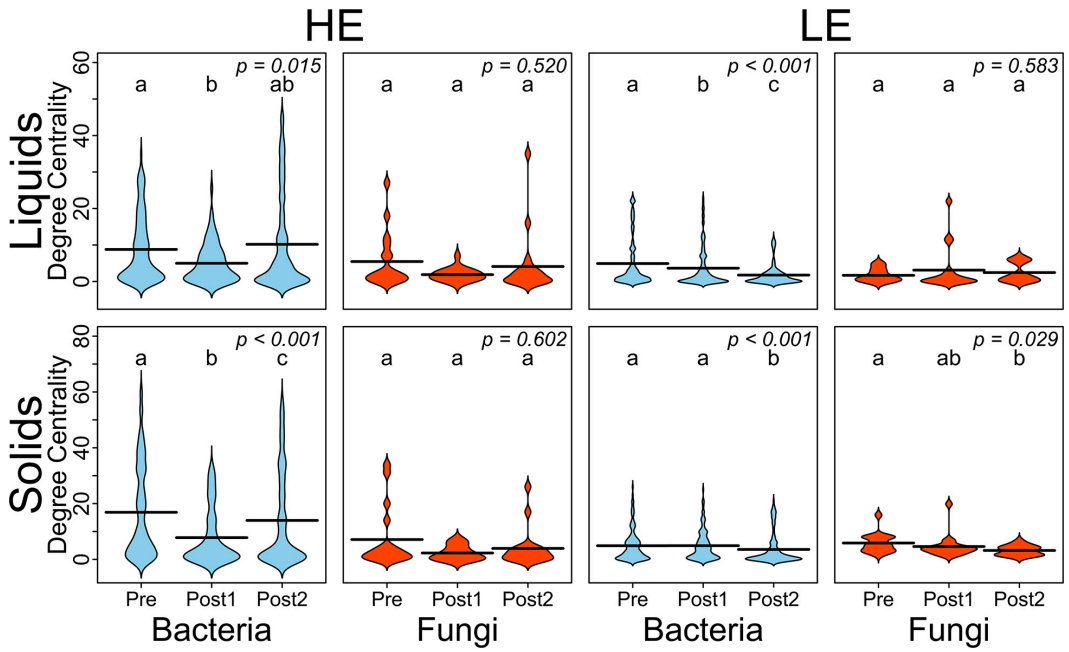

FIGURE 2 | Beanplots expressing average degree-centrality of nodes by domain and over time for HE and LE-derived rumen liquids and solids. Shared letters indicate no difference in degree between timepoints ($P > 0.05$).

HE Post1 was marginally distinct from HE Post2 ($P = 0.054$). LE Pre was marginally distinct from LE Post1 ($P = 0.054$), but not distinct from LE Post2 ($P = 0.225$). LE Post1 was distinct from LE Post2 ($P = 0.044$). All other pairwise comparisons were non-significant ($P > 0.05$). For the rumen solids, the impact of time period on fungal community structure differed by efficiency ($P = 0.006$). HE Pre was distinct from HE Post1 ($P = 0.048$), but not from HE Post2 ($P = 338$). HE Post1 was distinct from HE Post2 ($P = 0.048$). LE Pre was distinct from LE Post1 ($P = 0.041$), but not from LE Post2 ($P = 0.114$). LE Post1 was distinct from LE Post2 ($P = 0.041$). All other pairwise comparisons were non-significant ($P > 0.05$).

Network Analysis

To better understand the interactions of the ruminal bacterial and fungal communities, as it relates to MPE, we conducted a correlation network analysis. Correlation networks were generated by time period (Pre, Post1, and Post2), separately for liquid and solids samples and for initial host efficiency (**Supplementary Figure 2**). Degree-centrality, which is the number of edges connected to a node in a network, was averaged within sample type, time point, host efficiency, and domain for each of the networks as summarized in **Figure 2**. In HE samples for both solid and liquid phases, the average degree-centrality of bacterial nodes in the network decreased from Pre to Post1, then recovered in Post2. This pattern was not upheld in LE samples, where the average bacterial node centrality either decreased and failed to recover (LE liquids) or did not decrease appreciably until Post2 (LE solids). The average degree-centrality of fungal nodes in these networks was largely unaffected by the exchange, except in the case of LE solids where there was a decrease from Pre to Post2.

The 10 nodes with the highest degree centrality scores were extracted from each of the four pre-exchange networks (HE Liquids, HE solids, LE Liquids, and LE Solids) and their variation over time was assessed (**Table 1**). Notably, many of the OTUs which increased significantly in Post1 in HE samples were classified to the genus *Prevotella_1* (B_OTU 4, B_OTU 5, B_OTU 6, B_OTU 10, B_OTU 24, B_OTU 54, B_OTU 70, and B_OTU 144). All of these OTUs also decreased in LE samples in this period, with the exception of B_OTU 6 and B_OTU 70, which did not change in these samples over the time course. Conversely, B_OTU 52, which classified to the genus *Prevotella_7*, increased in LE samples in Post1 and decreased in HE samples. One fungal genus was identified as a highly influential node in all four of the pre-exchange networks: F_OTU 3, which classified to the genus *Piromyces*. The abundance of this OTU increased in HE solids in the Post1 period but was unaffected in HE liquids and LE samples. The degree-implicated OTUs were also correlated to ECM and GFE, but no significant correlations resulted from this analysis (**Supplementary Table 1**).

Individual Taxa

We then sought to identify individual taxa within the bacterial and fungal communities that contributed to the observed phenotypic reversal of MPE by conducting a SIMPER analysis on two sets of contrasting time periods: Pre vs. Post1 and Post1 vs. Post2. This analysis was designed to identify taxa that were transferred into the new host from the donor, and that were present during the reversal of efficiency status, as previously

TABLE 1 | Kruskal-Wallis tests of influential OTUs in Pre-exchange networks.

Block	OTU	Taxonomy	IN	Pre mean ± SE	Post1 mean ± SE	Post2 mean ± SE	$\chi^2_{df=2}$	*P*-value
HE Liquids	B_OTU 5	Prevotellaceae;*Prevotella_1*	both	208.3 ± 33.0^{a}	374.3 ± 36.5	235.2 ± 34.2^{a}	9.669	0.020
	B_OTU 20	Lachnospiraceae;*Oribacterium*	both	72.0 ± 16.8^{a,b}	19.0 ± 6.5^{a}	92.2 ± 21.3^{b}	9.540	0.020
	B_OTU 52	Prevotellaceae;*Prevotella_7*	both	115.7 ± 30.7^{a,b}	44.3 ± 15.8^{a}	132.9 ± 24.4^{b}	5.870	0.078
	B_OTU 1	Succinivibrionaceae;*Succinivibrionaceae_UCG-001*	HE	1904.6 ± 301.4^{ab}	1181.3 ± 362.6^{a}	2153.0 ± 291.9^{b}	6.314	0.067
	F_OTU 3	Neocallimastigaceae;*Piromyces*	HE	195.6 ± 27.0^{a}	377.8 ± 36.8^{a}	232.6 ± 25.4^{a}	12.297	0.008
	B_OTU 4	Prevotellaceae;*Prevotella_1*	HE	122.1 ± 39.8^{a}	200.1 ± 59.1	137.8 ± 50.2^{a}	4.565	0.129
	B_OTU 7	Succinivibrionaceae;*Succinivibrionaceae_UCG-002*	HE	21.7 ± 7.3^{a}	85.7 ± 16.8^{a}	28.3 ± 8.7^{a}	14.933	0.005
	B_OTU 24	Prevotellaceae;*Prevotella_1*	HE	22.6 ± 3.4^{a}	48.5 ± 6.2	24.3 ± 4.3^{a}	12.779	0.008
	B_OTU 54	Prevotellaceae;*Prevotella_1*	HE	8.1 ± 1.3^{a}	9.7 ± 1.7	5.8 ± 0.9^{a}	3.685	0.188
	B_OTU 65	Lachnospiraceae;Lachnospiraceae_XPB1014_group	HE	16.2 ± 4.1^{a}	37.8 ± 4.0^{a}	14.2 ± 3.6^{a}	14.632	0.005
	B_OTU 70	Prevotellaceae;*Prevotella_1*	HE	3.8 ± 0.9^{a}	6.7 ± 1.2	2.6 ± 0.7^{a}	9.002	0.023
	B_OTU 131	Lachnospiraceae;Lachnospiraceae_XPB1014_group	HE	380.4 ± 73.6^{a,b}	364.9 ± 43.8^{a}	357.5 ± 70.2^{b}	0.044	0.978
	B_OTU 6	Prevotellaceae;*Prevotella_1*	LE	153.0 ± 22.9^{a}	268.1 ± 24.6	166.0 ± 20.2^{a}	10.526	0.016
	B_OTU 27	Prevotellaceae;*Prevotella_7*	LE	220.6 ± 52.0^{a}	129.3 ± 49.6^{a}	220.5 ± 44.2^{a}	1.483	0.503
	B_OTU 49	Veillonellaceae;Veillonellaceae_unclassified	LE	25.5 ± 5.5^{a,b}	16.5 ± 5.7^{a}	38.7 ± 6.6^{b}	6.352	0.067
	B_OTU 81	Prevotellaceae;*Prevotella_1*	LE	23.4 ± 5.9^{a}	9.0 ± 2.0^{a}	21.8 ± 4.5^{a}	5.299	0.096
	B_OTU 134	Lachnospiraceae_unclassified	LE	61.8 ± 26.7^{a}	10.0 ± 4.7^{a}	25.7 ± 10.1^{a}	2.358	0.344
	B_OTU 168	Lachnospiraceae_unclassified	LE	9.9 ± 3.0^{a,b}	5.1 ± 2.3^{a}	13.5 ± 2.7^{b}	6.455	0.067
	B_OTU 171	Prevotellaceae;Prevotellaceae_unclassified	LE	25.8 ± 5.3^{a}	5.7 ± 2.3	27.0 ± 6.1^{a}	14.313	0.005
HE Solids	B_OTU 24	Prevotellaceae;*Prevotella_1*	both	24.5 ± 7.7^{a}	70.3 ± 14.2	27.7 ± 8.1^{a}	11.713	0.020
	B_OTU 70	Prevotellaceae;*Prevotella_1*	both	10.4 ± 2.6^{a}	19.4 ± 2.4	9.4 ± 1.7^{a}	9.303	0.029
	B_OTU 131	Lachnospiraceae;Lachnospiraceae_XPB1014_group	both	7.6 ± 1.9^{a}	16.8 ± 2.8	7.3 ± 1.5^{a}	9.654	0.029
	B_OTU 17	Prevotellaceae;*Prevotella_1*	HE	72.2 ± 7.2^{a}	77.6 ± 4.4^{a}	73.6 ± 3.6^{a}	0.894	0.639
	B_OTU 20	Lachnospiraceae;*Oribacterium*	HE	175.9 ± 35.0^{a,b}	101.0 ± 39.9^{a}	186.5 ± 29.2^{b}	7.190	0.056
	B_OTU 35	Prevotellaceae;*Prevotella_7*	HE	103.6 ± 22.6^{a}	38.7 ± 19.0^{a}	75.4 ± 14.1^{a}	4.590	0.121
	B_OTU 42	Ruminococcaceae_NK4A214_group	HE	41.7 ± 4.5^{a}	54.2 ± 5.3^{a}	42.0 ± 3.3^{a}	5.606	0.083
	B_OTU 52	Prevotellaceae;*Prevotella_7*	HE	32.9 ± 7.5^{a}	11.5 ± 4.3^{a}	24.5 ± 4.1^{a}	6.086	0.077
	B_OTU 83	Prevotellaceae;*Prevotella_1*	HE	14.3 ± 1.7^{a}	9.2 ± 1.5^{a}	9.3 ± 1.2^{a}	5.469	0.083
	B_OTU 144	Prevotellaceae;*Prevotella_1*	HE	2.2 ± 0.5^{a}	4.5 ± 0.7^{b}	2.8 ± 0.5^{a,b}	7.159	0.056
	F_OTU 3	Neocallimastigaceae;*Piromyces*	LE	107.2 ± 8.5^{a}	150.4 ± 11.3	106.2 ± 5.9^{a}	11.374	0.020
	B_OTU 10	Prevotellaceae;*Prevotella_1*	LE	60.0 ± 10.7^{a}	53.3 ± 16.4	61.1 ± 7.3^{a}	2.173	0.357
	B_OTU 49	Veillonellaceae;Veillonellaceae_unclassified	LE	25.3 ± 2.9^{a}	35.5 ± 3.9^{a}	25.1 ± 1.7^{a}	5.945	0.077
	B_OTU 65	Lachnospiraceae_XPB1014_group	LE	8.6 ± 0.8^{a}	5.4 ± 0.9^{a}	7.3 ± 0.8^{a}	5.981	0.077
	B_OTU 97	Bacteroidia_unclassified;Bacteroidia_unclassified	LE	10.4 ± 1.5^{a}	24.8 ± 4.2^{a}	12.3 ± 1.0^{a}	13.470	0.020
	B_OTU 109	Lachnospiraceae;probable_genus_10	LE	24.4 ± 3.9^{a}	24.7 ± 3.6	31.2 ± 2.7^{a}	2.833	0.273
	B_OTU 1	Succinivibrionaceae;*Succinivibrionaceae_UCG-001*	HE	690.4 ± 205.6^{a}	1106.7 ± 259.7^{a}	422.1 ± 147.2^{a}	6.464	0.068
	F_OTU 3	Neocallimastigaceae;*Piromyces*	HE	521.9 ± 58.9^{a}	325.1 ± 82.2^{a}	447.2 ± 68.9^{a}	3.129	0.234
	B_OTU 4	Prevotellaceae;*Prevotella_1*	HE	359.6 ± 27.3^{a}	261.3 ± 28.7	426.9 ± 36.7^{a}	11.256	0.008
	B_OTU 7	Succinivibrionaceae;*Succinivibrionaceae_UCG-002*	HE	224.9 ± 30.1^{a}	221.1 ± 79.5^{a}	288.2 ± 64.4^{a}	1.630	0.443

(Continued)

TABLE 1 | Continued

Block	OTU	Taxonomy	IN	Pre mean ± SE	Post1 mean ± SE	Post2 mean ± SE	$\chi^2_{df=2}$	*P*-value
	B_OTU 24	Prevotellaceae;*Prevotella_1*	HE	72.6 ± 10.5^{a}	31.7 ± 8.6	73.8 ± 8.5^{a}	11.143	0.008
	B_OTU 54	Prevotellaceae;*Prevotella_1*	HE	53.4 ± 6.0^{a}	31.7 ± 5.4	47.9 ± 3.2^{a}	6.743	0.065
	B_OTU 65	Lachnospiraceae;Lachnospiraceae_XPB1014_group	HE	8.7 ± 1.2^{a}	7.4 ± 1.3^{a}	10.6 ± 1.1^{a}	4.052	0.157
	B_OTU 70	Prevotellaceae;*Prevotella_1*	HE	29.8 ± 4.2^{a}	20.8 ± 4.2^{a}	30.6 ± 3.8^{a}	2.115	0.367
	B_OTU 131	Lachnospiraceae;Lachnospiraceae_XPB1014_group	HE	7.2 ± 1.6^{a,b}	3.9 ± 1.1^{a}	8.0 ± 1.2^{b}	5.656	0.080
	B_OTU 6	Prevotellaceae;*Prevotella_1*	LE	272.9 ± 21.4^{a}	212.2 ± 25.7^{a}	282.6 ± 18.9^{a}	4.643	0.124
	B_OTU 27	Prevotellaceae;*Prevotella_7*	LE	37.5 ± 23.1^{a}	103.1 ± 36.4^{a}	33.0 ± 27.2	13.348	0.005
	B_OTU 49	Veillonellaceae;Veillonellaceae_unclassified	LE	9.9 ± 3.8^{a}	20.0 ± 6.2^{a}	7.0 ± 2.4^{a}	5.854	0.080
	B_OTU 81	Prevotellaceae;*Prevotella_1*	LE	9.6 ± 3.4^{a}	26.3 ± 5.6	10.1 ± 1.6^{a}	12.639	0.005
	B_OTU 134	Lachnospiraceae_unclassified	LE	14.3 ± 10.0^{a}	38.6 ± 21.7^{a}	0.0 ± 0.0^{a}	5.782	0.080
	B_OTU 168	Lachnospiraceae_unclassified	LE	2.0 ± 1.2^{a}	6.5 ± 2.4	0.9 ± 0.5^{a}	15.963	0.002
	B_OTU 171	Prevotellaceae;Prevotellaceae_unclassified	LE	5.1 ± 2.5^{a}	30.2 ± 8.2	6.4 ± 1.8^{a}	17.392	0.002
LESolids	B_OTU 24	Prevotellaceae;*Prevotella_1*	both	84.2 ± 9.4^{a}	26.7 ± 7.3	66.6 ± 9.4^{a}	15.590	0.002
	B_OTU 70	Prevotellaceae;*Prevotella_1*	both	22.7 ± 1.9^{a}	10.3 ± 2.0	19.2 ± 2.2^{a}	13.784	0.003
	B_OTU 131	Lachnospiraceae;Lachnospiraceae_XPB1014_group	both	26.3 ± 2.4^{a}	18.6 ± 3.1^{a}	24.5 ± 2.7^{a}	4.449	0.150
	B_OTU 17	Prevotellaceae;*Prevotella_1*	HE	90.8 ± 5.4a	87.8 ± 4.1^{a}	90.3 ± 6.2^{a}	0.058	0.972
	B_OTU 20	Lachnospiraceae;*Oribacterium*	HE	9.8 ± 3.4^{a}	110.4 ± 30.2	36.8 ± 24.2^{a}	21.334	<0.001
	B_OTU 35	Prevotellaceae;*Prevotella_7*	HE	0.8 ± 0.3^{a}	42.1 ± 12.9	13.7 ± 10.3^{a}	11.099	0.010
	B_OTU 42	Ruminococcaceae_NK4A214_group	HE	62.1 ± 2.4^{a}	41.4 ± 4.3	59.0 ± 3.4^{a}	14.230	0.003
	B_OTU 52	Prevotellaceae;*Prevotella_7*	HE	1.2 ± 0.5^{a}	15.9 ± 6.1	4.4 ± 2.6^{a}	10.034	0.013
	B_OTU 83	Prevotellaceae;*Prevotella_1*	HE	6.6 ± 0.7^{a}	9.9 ± 1.9^{a}	6.4 ± 0.8^{a}	2.083	0.424
	B_OTU 144	Prevotellaceae;*Prevotella_1*	HE	5.5 ± 0.6^{a}	2.5 ± 0.5	5.3 ± 0.9^{a}	15.398	0.002
	F_OTU 3	Neocallimastigaceae;*Piromyces*	LE	123.3 ± 23.8^{a}	105.3 ± 26.6^{a}	133.1 ± 23.2^{a}	0.462	0.840
	B_OTU 10	Prevotellaceae;*Prevotella_1*	LE	170.4 ± 11.2^{a}	128.7 ± 6.8^{b}	146.9 ± 7.3^{a,b}	9.451	0.015
	B_OTU 49	Veillonellaceae;Veillonellaceae_unclassified	LE	16.6 ± 4.7^{a}	39.1 ± 8.0	15.0 ± 5.1^{a}	10.450	0.012
	B_OTU 65	Lachnospiraceae_XPB1014_group	LE	47.1 ± 4.1^{a}	41.9 ± 3.7^{a}	43.4 ± 3.0^{a}	0.820	0.747
	B_OTU 97	Bacteroidia_unclassified;Bacteroidia_unclassified	LE	5.3 ± 0.9^{a}	7.3 ± 0.8^{a}	5.0 ± 0.6^{a}	4.444	0.150
	B_OTU 109	Lachnospiraceae;probable_genus_10	LE	31.4 ± 3.8^{a}	18.7 ± 2.3	34.6 ± 3.9^{a}	9.538	0.015
	B_OTU 110	Lachnospiraceae;Lachnospiraceae_unclassified	LE	13.3 ± 2.6^{a}	18.5 ± 2.9^{a}	14.9 ± 2.9^{a}	2.329	0.401
	B_OTU 171	Prevotellaceae;Prevotellaceae_unclassified	LE	0.8 ± 0.2^{a}	7.5 ± 1.2	2.9 ± 1.2^{a}	25.028	<0.001

The nodes with the 10 greatest values for degree centrality were selected. The implicating network is listed under "IN." Tests were performed within blocks of sample type and efficiency status. Post hoc testing was performed as Wilcoxon rank sum tests with FDR correction applied to P-values. Means sharing letters are not significantly different (α = 0.05). All samples normalized to prior to analysis (bacteria: 10,000 sequences/sample, fungi: 2,450 sequences/sample).

TABLE 2 | Kruskal-Wallis tests of SIMPER-implicated taxa.

Amplicon	Testing Block	Implicating contrast(s)	OTU	Classification	Pre Mean ± SE	Post1 Mean ± SE	Post2 Mean ± SE	$\chi^2_{df=2}$	*P*-value
Bacteria	HE Liquids	Pre/Post1	B_OTU 19	Prevotellaceae; *Prevotella_1*	55.6 ± 8.2^{a}	139.7 ± 15.1	75.2 ± 10.4^{a}	16.349	<0.001
		Pre/Post1, Post1/Post2	B_OTU 3	Prevotellaceae; *Prevotella_1*	322.3 ± 27.3^{a}	414.3 ± 29.4	320.2 ± 20.5^{a}	6.953	0.031
			B_OTU 4	Prevotellaceae; *Prevotella_1*	195.6 ± 27.0^{a}	377.8 ± 36.8	232.6 ± 25.4^{a}	12.297	0.002
			B_OTU 5	Prevotellaceae; *Prevotella_1*	208.3 ± 33.0^{a}	374.3 ± 36.5	235.2 ± 34.2^{a}	9.669	0.007
			B_OTU 6	Prevotellaceae; *Prevotella_1*	153.0 ± 22.9^{a}	268.1 ± 24.6	166.0 ± 20.2^{a}	10.526	0.005
		Post1/Post2	B_OTU 1	Succinivibrionaceae; *Succinivibrionaceae UCG-001*	1904.6 ± 301.4^{a,b}	1181.3 ± 362.6^{a}	2153.0 ± 291.9^{b}	6.314	0.043
			B_OTU 2	Prevotellaceae; *Prevotella_1*	653.5 ± 77.8^{a}	759.8 ± 53.9^{a}	593.2 ± 59.9^{a}	5.012	0.082
			B_OTU 29	Prevotellaceae; *Prevotella_7*	145.7 ± 33.6^{a}	119.6 ± 55.8^{a}	251.1 ± 46.7^{a}	7.214	0.027
			B_OTU 52	Prevotellaceae; *Prevotella_7*	115.7 ± 30.7^{a,b}	44.3 ± 15.8^{a}	132.9 ± 24.4^{b}	5.870	0.053
	HE Solids	Pre/Post1, Post1/Post2	B_OTU 18	Lachnospiraceae; *Butyrivibrio_2*	61.4 ± 8.6^{a}	124.0 ± 19.7	62.5 ± 6.6^{a}	10.512	0.005
		Post1/Post2	B_OTU 7	Succinivibrionaceae; *Succinivibrionaceae UCG-002*	56.3 ± 19.2^{a}	151.5 ± 35.0	62.2 ± 21.9^{a}	7.181	0.028
			B_OTU 20	Lachnospiraceae; *Oribacterium*	175.9 ± 35.0^{a,b}	101.0 ± 39.9^{a}	186.5 ± 29.2^{b}	7.190	0.027
	LE Liquids	Post1/Post2	B_OTU 1	Succinivibrionaceae; *Succinivibrionaceae UCG-001*	690.4 ± 205.6^{a,b}	1106.7 ± 259.7^{a}	422.1 ± 147.2^{b}	6.464	0.039
			B_OTU 3	Prevotellaceae; *Prevotella_1*	423.9 ± 26.3^{a,b}	367.7 ± 23.5^{a}	462.8 ± 27.6^{b}	6.930	0.031
			B_OTU 4	Prevotellaceae; *Prevotella_1*	359.6 ± 27.3^{a}	261.3 ± 28.7	426.9 ± 36.7^{a}	11.256	0.004
			B_OTU 5	Prevotellaceae; *Prevotella_1*	398.8 ± 33.1^{a}	278.2 ± 35.1	462.3 ± 31.8^{a}	12.875	0.002
			B_OTU 27	Prevotellaceae; *Prevotella_7*	37.5 ± 23.1^{a}	103.1 ± 36.4^{a}	33.0 ± 27.2	13.348	0.001
			B_OTU 29	Prevotellaceae; *Prevotella_7*	38.1 ± 23.8^{a}	112.0 ± 44.5	47.0 ± 35.3^{a}	12.078	0.002
			B_OTU 52	Prevotellaceae; *Prevotella_7*	33.9 ± 21.4^{a}	74.8 ± 26.6	20.2 ± 15.4^{a}	14.165	<0.001
	LE Solids	Pre/Post1	B_OTU 5	Prevotellaceae; *Prevotella_1*	153.8 ± 20.7	79.4 ± 13.4^{a}	100.7 ± 14.6^{a}	9.063	0.011
		Pre/Post1, Post1/Post2	B_OTU 20	Lachnospiraceae; *Oribacterium*	9.8 ± 3.4^{a}	110.4 ± 30.2	36.8 ± 24.2^{a}	21.334	<0.001
Fungi	HE Liquids	Pre/Post1	F_OTU 5	Neocallimastigaceae; *Neocallimastix*	141.2 ± 22.5^{a}	61.5 ± 8.3^{b}	117.0 ± 23.0^{a,b}	9.305	0.010
		Pre/Post1, Post1/Post2	F_OTU 7	Saccharomycetales Incertae sedis; *Wickerhamomyces anomalus*	149.1 ± 29.7^{a}	45.0 ± 19.3	170.0 ± 48.4^{a}	14.854	<0.001
		Post1/Post2	F_OTU 2	Neocallimastigaceae; unclassified	277.9 ± 46.2^{a}	513.8 ± 74.2	239.4 ± 38.9^{a}	9.678	0.008
			F_OTU 9	Neocallimastigaceae; *Piromyces*	44.6 ± 13.2^{a,b}	44.3 ± 7.5^{a}	20.1 ± 3.8^{b}	6.436	0.040
	HE Solids	Pre/Post1	F_OTU 5	Neocallimastigaceae; *Neocallimastix*	209.9 ± 28.4	75.3 ± 7.9^{a}	111.3 ± 17.3^{a}	20.020	<0.001
			F_OTU 6	Neocallimastigaceae; *Neocallimastix*	88.1 ± 14.3^{a}	145.5 ± 8.1^{b}	121.0 ± 13.8^{a,b}	7.192	0.027
			F_OTU 10	Saccharomycetales Incertae sedis; *Debaryomyces prosopidis*	64.2 ± 36.7^{a}	5.1 ± 3.3	15.6 ± 5.1^{a}	9.556	0.008
		Pre/Post1, Post1/Post2	F_OTU 2	Neocallimastigaceae; unclassified	310.5 ± 62.8^{a}	518.9 ± 52.4	242.6 ± 60.8^{a}	10.504	0.005
			F_OTU 3	Neocallimastigaceae; *Piromyces*	67.5 ± 23.0^{a}	92.3 ± 13.8	41.1 ± 13.1^{a}	9.950	0.007
			F_OTU 7	Saccharomycetales Incertae sedis; *Wickerhamomyces anomalus*	141.1 ± 68.6^{a}	7.6 ± 1.9	238.4 ± 84.9^{a}	18.930	<0.001
		Post1/Post2	F_OTU 4	Neocallimastigaceae; *Piromyces*	182.6 ± 28.7^{a,b}	186.9 ± 14.9^{a}	110.4 ± 22.7^{b}	7.749	0.021
			F_OTU 11	Trichocomaceae; *Penicillium roqueforti*	2.9 ± 1.6^{a}	0.3 ± 0.2^{a}	173.0 ± 81.7	32.528	<0.001

(Continued)

TABLE 2 | Continued

Amplicon	Testing Block	Implicating contrast(s)	OTU	Classification	Pre Mean ± SE	Post1 Mean ± SE	Post2 Mean ± SE	$\chi^2_{df=2}$	*P*-value
	LE Liquids	Pre/Post1, Post1/Post2	F_OTU 5	Neocallimastigaceae; *Neocallimastix*	62.4 ± 23.5^a	158.2 ± 21.0^b	71.3 ± 8.4^c	19.725	<0.001
		Post1/Post2	F_OTU 4	Neocallimastigaceae; *Piromyces*	323.0 ± 31.6^a	387.4 ± 68.3^a	147.2 ± 16.9	19.223	<0.001
			F_OTU 7	Saccharomycetales Incertae sedis; *Wickerhamomyces anomalus*	54.8 ± 11.4^a	24.2 ± 5.4	105.2 ± 26.3^a	9.436	0.009
			F_OTU 11	Trichocomaceae; *Penicillium roqueforti*	1.3 ± 0.7^a	0.1 ± 0.1^a	44.0 ± 15.6	31.621	<0.001
	LE Solids	Pre/Post1	F_OTU 5	Neocallimastigaceae; *Neocallimastix*	64.3 ± 8.7^a	199.7 ± 26.8^b	120.6 ± 11.7^c	22.600	<0.001
		Pre/Post1, Post1/Post2	F_OTU 7	Saccharomycetales Incertae sedis; *Wickerhamomyces anomalus*	37.6 ± 12.7^a	8.7 ± 3.8	32.4 ± 13.6^a	11.572	0.003
		Post1/Post2	F_OTU 4	Neocallimastigaceae; *Piromyces*	252.2 ± 36.4^{a,b}	298.1 ± 46.2^a	168.6 ± 18.3^b	7.687	0.021
			F_OTU 11	Trichocomaceae; *Penicillium roqueforti*	1.0 ± 0.3^a	0.1 ± 0.1^b	112.0 ± 96.4^c	26.006	<0.001

Tests performed within amplicon, sample type, and efficiency status. Post hoc testing was performed as Wilcoxon rank sum tests with FDR correction applied to P-values. Means sharing letters are not significantly different (α = 0.05). All samples normalized to prior to analysis (bacteria: 10,000 sequences/sample, fungi: 2,450 sequences/sample).

described (Weimer et al., 2017). SIMPER-identified taxa that explained at least 1% of the variation in between any two time periods within efficiency status, rumen phase, and amplicon type were subjected to Kruskal-Wallis tests as summarized in **Table 2**.

Similar to the OTUs implicated in the above network analysis, many of the bacterial OTUs in the liquid phase derived from HE cows that increased significantly in Post1, relative to Pre and Post2, were classified to the genus *Prevotella_1* (B_OTU 3, B_OTU 4,B_OTU 5, B_OTU 6, and B_OTU 19). In addition, many OTUs that tended to decrease in Post1 were classified to *Prevotella_7* (B_OTU 29 and B_OTU 52). The opposite pattern was observed in LE liquid samples: OTUs classifying to *Prevotella_1* tended to decrease in Post1 relative to Pre and Post2 (B_OTU 3, B_OTU 4, and B_OTU 5), and those classifying to *Prevotella_7* tended to increase (B_OTU 29 and B_OTU 52). In solid-derived samples from HE animals, an OTU classifying to the genus *Oribacterium* (B_OTU 20) was more abundant in Post2 than Post1, though neither differed from Pre. This OTU showed a marked increase in Post1 in LE solids, then returned to baseline abundance in Post2. An OTU classified to Succinivibrionaceae *UCG_002* (B_OTU 7) and another classified to *Butyrivibrio_2* (B_OTU 18) were more abundant in HE solid samples in Post1 relative to Pre and Post2.

The summed abundance of all OTUs classified to genera *Prevotella_1* and *Prevotella_7* was assessed over the time course in rumen liquids (**Figure 3**). Pre-exchange, *Prevotella_1* was more abundant in LE cows, while *Prevotella_7* was more abundant in HE cows ($P < 0.05$). *Prevotella_1* increased in HE cows in the Post1 period, then returned to pre-exchange abundance. Conversely, *Prevotella_7* increased in LE cows in the Post1 period before returning to pre-exchange abundance in Post2.

In liquid phase samples from HE cows, a fungal OTU classified to the genus *Neocallimastix* decreased from the Pre to Post1 period (**Table 1**, F_OTU 5), and increased significantly and remained greater than pre-exchange abundance in Post2. The inverse was seen in LE liquids: F_OTU 5 increased from Pre to Post1 and was at an intermediate abundance in Post2. In both HE and LE animals for both solid and liquid rumen fractions, an OTU classified to *Wickerhamomyces anomalus* decreased sharply in Post1 relative to Pre and Post2 (F_OTU 7). Our fungal sequencing was also able to detect the presence of a known silage spoilage organism, *Penicillium roqueforti* (F_OTU 11), in HE solids and in LE liquids and solids. It was present at very low abundance in Pre and Post1, then increased sharply in Post2.

Phenotypic Correlations

We then performed a correlation analysis of our SIMPER-implicated OTUs with a number of phenotypic variables. Two production-associated variables (ECM and GFE) and the molar fractions of the three most abundant ruminal VFAs (acetate, propionate, and butyrate) were considered. The results of this correlation analysis are summarized in **Figure 4**.

Bacterial OTUs correlated to production metrics tended to be weak and non-significant, except for a trend toward a negative relationship between B_OTU 3 (*Prevotella_1*) and both ECM and GFE, and also between B_OTU 2 (*Prevotella_1*) and B_OTU 4 (*Prevotella_1*) with GFE in rumen liquids

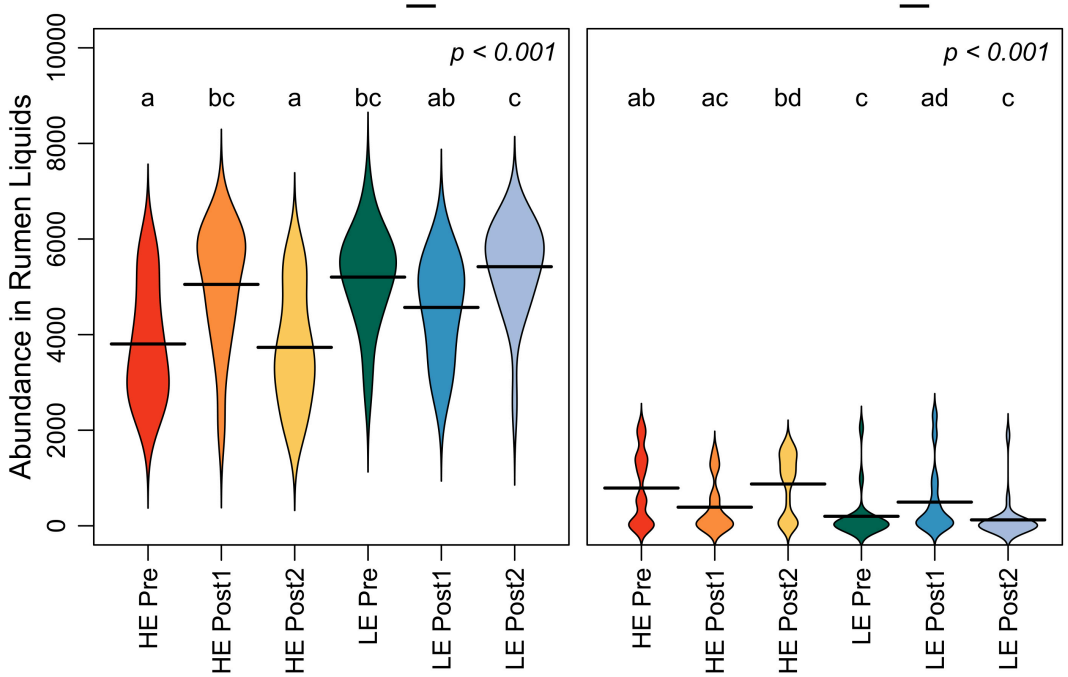

FIGURE 3 | Beanplots expressing abundance of normalized bacterial reads classifying to genera *Prevotella_1* and *Prevotella_7* in liquid-derived rumen samples by time within the study and initial host efficiency. Shared letters indicate no difference in read abundance ($p > 0.05$).

($P < 0.001$). Significant and relatively stronger correlations were observed between bacterial OTUs and the relative abundance of specific VFAs. Several bacterial OTUs had highly significant positive correlations to the molar fraction of acetate in rumen liquids (B_OTU 2: *Prevotella_1*, B_OTU 3: *Prevotella_1*, B_OTU 4: *Prevotella_1*, B_OTU 5: *Prevotella_1*, B_OTU 6: *Prevotella_1*, and B_OTU 19: *Prevotella_1*), and several had significant negative correlations to acetate (B_OTU 1: *Succinivibrionaceae UCG-001*, B_OTU 27: *Prevotella_7*, B_OTU 29: *Prevotella_7*, and B_OTU 52: *Prevotella_7*). Similarly, a number of bacterial OTUs were significantly positively (B_OTU 3: *Prevotella_1*, B_OTU 4: *Prevotella_1*, B_OTU 5: *Prevotella_1*, B_OTU 6: *Prevotella_1*, and B_OTU 19: *Prevotella_1*) and negatively (B_OTU 1: *Succinivibrionaceae UCG-001*, B_OTU 27: *Prevotella_7*, B_OTU 29: *Prevotella_7*, and B_OTU 52: *Prevotella_7*) correlated to butyrate abundance in rumen liquids. Propionate tended to have the strongest correlation coefficients in rumen liquids, and followed the exact inverse pattern of acetate in terms of direction of correlation to OTUs the interrogated (positive: B_OTU 1: *Succinivibrionaceae UCG-001*, B_OTU 27: *Prevotella_7*, B_OTU 29: *Prevotella_7*, B_OTU 52: *Prevotella_7*; negative: B_OTU 2: *Prevotella_1*, B_OTU 3: *Prevotella_1*, B_OTU 4: *Prevotella_1*, B_OTU 5: *Prevotella_1*, B_OTU 6: *Prevotella_1*, and B_OTU 19: *Prevotella_1*). No significant correlation was seen between ECM or GFE and the SIMPER-implicated OTUs in rumen solids ($P > 0.05$). Acetate was significantly positively correlated with B_OTU 5 (*Prevotella_1*), B_OTU 7 (*Prevotella_1*), B_OTU 18 (*Butyrivibrio_2*), and negatively correlated with B_OTU 20 (*Oribacterium*) in rumen solids. Butyrate had a positive relationship with B_OTU 7 (*Succinivibrionaceae UCG-002*) and B_OTU 18 (*Butyrivibrio_2*) and a negative relationship with B_OTU 20 (*Oribacterium*). Conversely, propionate was negatively correlated with B_OTU 5 (*Prevotella_1*), B_OTU 7 (*Succinivibrionaceae UCG-002*), and B_OTU 18 (*Butyrivibrio_2*) and strongly positively correlated with B_OTU 20 (*Oribacterium*).

Overall, correlations between the production metrics and the abundance of SIMPER-implicated fungal OTUs were weaker. In rumen liquids, F_OTU 9 (*Piromyces*) was weakly but significantly negatively correlated with GFE. Acetate was positively correlated to F_OTU 2 (unclassified Neocallimastigaceae) and F_OTU 4 (*Piromyces*), and negatively correlated to F_OTU 7 (*Wickerhamomyces anomalus*) in rumen liquids. Negative correlation was observed between butyrate abundance and F_OTU 4 (*Piromyces*) and F_OTU 5 (*Neocallimastix*) in rumen liquids. F_OTU 5 (*Neocallimastix*) was positively correlated to propionate abundance in rumen solids, and F_OTU 2 (unclassified Neocallimastigaceae) and F_OTU 9 (*Piromyces*) were negatively correlated. In rumen solids, F_OTU 6 (*Neocallimastix*) showed a strong positive correlation with ECM, and was the strongest correlation seen between any SIMPER-implicated OTU (bacterial or fungal) and a production metric. F_OTU 6 (*Neocallimastix*) was also positively correlated with GFE in these samples. No other fungal OTUs showed significant correlations with production metrics in rumen solids. In solid samples, acetate

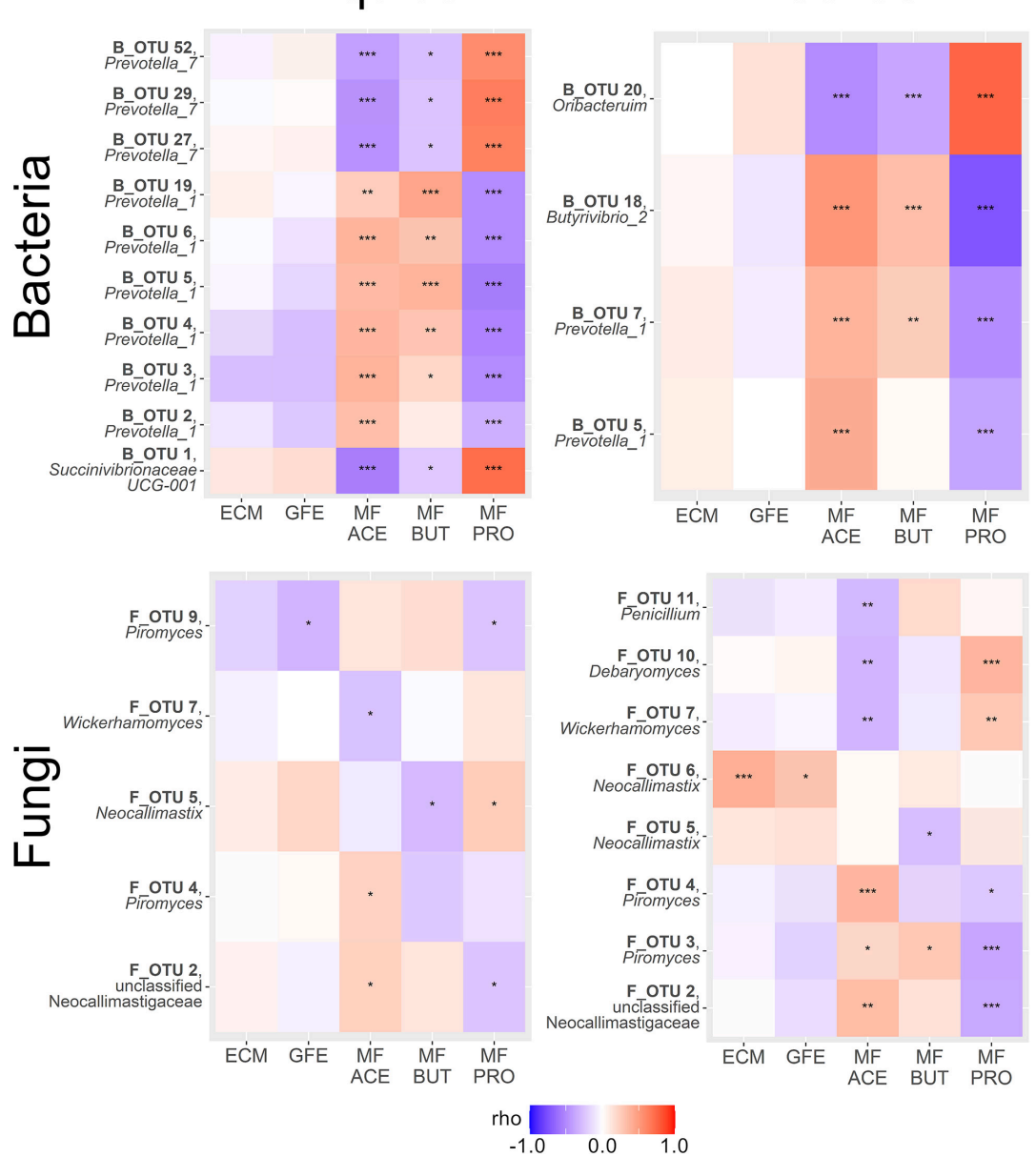

FIGURE 4 | Heatmaps summarizing correlations between SIMPER-implicated OTUs and phenotypic variables of interest within amplicon and sample type. Variables are energy corrected milk (ECM), gross feed efficiency (GFE), and molar fraction acetate (MF ACE), propionate (MF PRO) and butyrate (MF BUT). Genera displayed beneath OTU names. Color scale reflects strength and direction of correlation (Spearman's ρ statistic), and asterisks within the heatmap indicate statistical significance (*$P < 0.05$, **$P < 0.01$, ***$P < 0.001$).

was positively correlated with F_OTU 4 (*Piromyces*), F_OTU 5 (*Neocallimastix*), and F_OTU 6 (*Neocallimastix*) and negatively correlated with F_OTU 7 (*Wickerhamomyces anomalus*), F_OTU 10 (*Debaryomyces prosopidis*), and F_OTU 11 (*Penicillium roqueforti*). Butyrate had a positive correlation with F_OTU 3 (*Piromyces*), and no other significant correlations. F_OTU 2 (unclassified Neocallimastigaceae), F_OTU 3 (*Piromyces*), and F_OTU 4 (*Piromyces*) were negatively correlated with propionate abundance in rumen solids, and F_OTU 7 (*Wickerhamomyces anomalus*) and F_OTU 10 (*Debaryomyces prosopidis*) were negatively correlated.

Linear Discriminant Analysis

Linear discriminant analysis effect size implicated several OTUs as diagnostic of HE or LE rumen solids and liquids in the Pre-exchange samples. Implicated OTUs and their effect size are shown in **Supplementary Figures 3–6**. Within sample type and domain, all LEfSe-implicated OTUs were individually

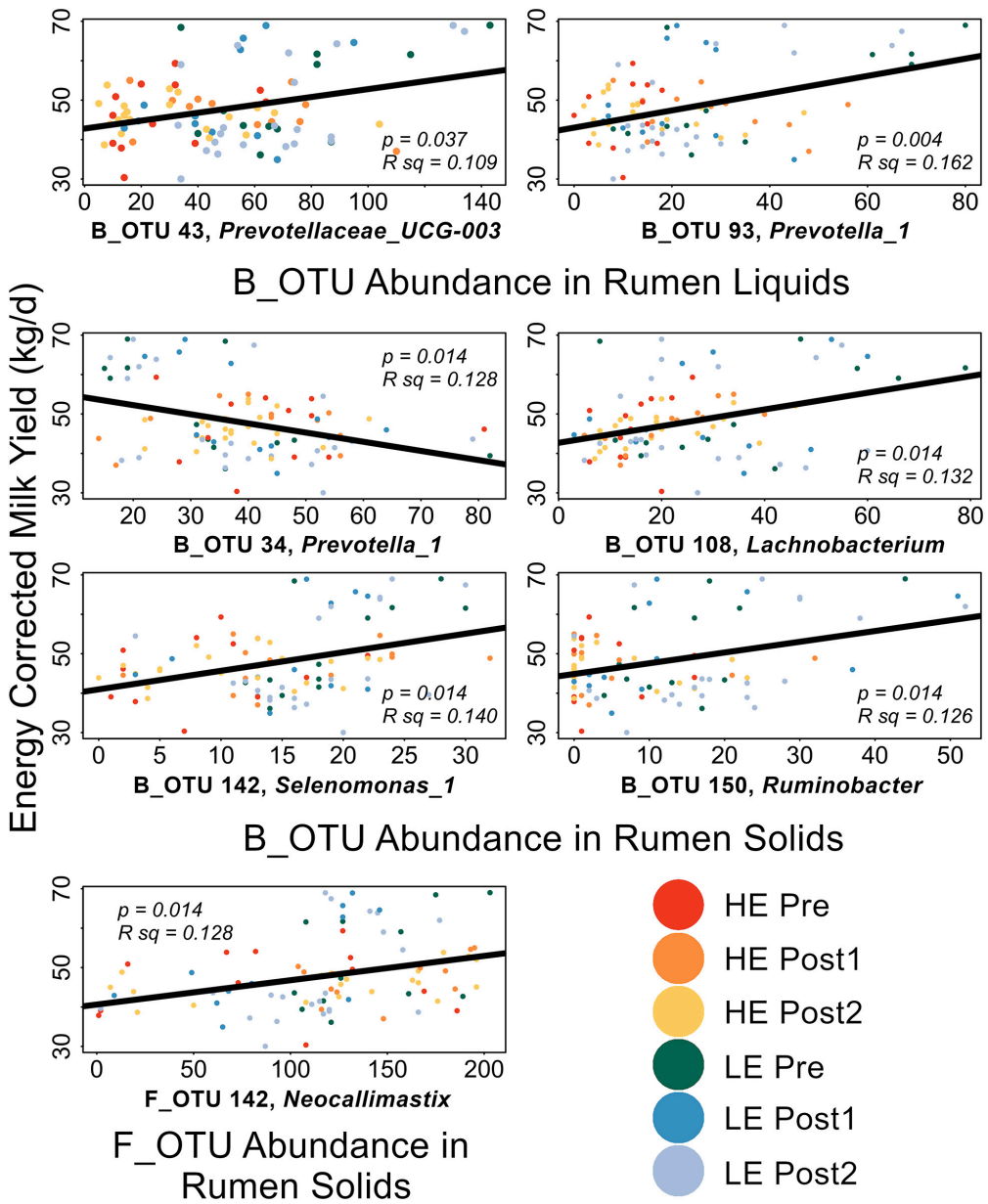

FIGURE 5 | Scatterplots of LEfSe-implicated OTUs with significant correlations to production metrics. FDR-corrected *p*-values and the R^2 values for the linear mode (black) are expressed on each plot. Points are color coded by initial efficiency of host and time within trial. Genus-level classification of the OTUs are as follows: B_OTU 43: *Prevotellaceae_UCG-003*; B_OTU 93: *Prevotella_1*; B_OTU 34: *Prevotella_1*; B_OTU 108: *Lachnobacterium*; B_OTU 150: *Ruminobacter*; B_OTU 142: *Selenomonas_1*; F_OTU 6: *Neocallimastix*.

correlated to ECM and GFE (Liquids: 51 B_OTUs, 4 F_OTUs; Solids: 93 B_OTUs, 5 F_OTUs, **Supplementary Table 2**). Significant correlations are shown in **Figure 5**. GFE did not show significant correlations with any of the LEfSe-implicated OTUs. In rumen liquids, B_OTU 43 (*Prevotella_UCG3*) and B_OTU 93 (*Prevotella_1*) were significantly positively correlated with ECM. In rumen solids, B_OTU 108 (*Lachnobacterium*), B_OTU 150 (*Ruminobacter*), B_OTU 142 (*Selenomonas_1*), and F_OTU 6 (*Neocallimastix*) were positively correlated with ECM; B_OTU 34 (*Prevotella_1*) was significantly negatively correlated with ECM.

DISCUSSION

Manipulation of the rumen microbial community is a promising approach for improving MPE (Jami et al., 2014; Bickhart and Weimer, 2017; Weimer et al., 2017). Our previous work demonstrated the ability to alter MPE though wholesale exchange of ruminal contents, but also underscored the resistance of the mature rumen microbiota to long-term perturbation (Weimer et al., 2017). The mechanism behind the re-establishment of the native microbiota following the exchange is not known, but it

is likely a confluence of several factors, which may include re-seeding of the lumen by the epimural community; differences in physical factors such as rumen retention, meal frequency, and fluid intake; bioactive compounds in saliva; and host modulation of ruminal VFA profiles. The goal of this work was to more thoroughly investigate rumen microbial community recovery with an emphasis on the ruminal fungal community, and to identify specific microbial taxa that may have contributed to the observed shift in host efficiency.

Weimer et al. (2017) established that ruminal bacterial diversity, richness, and community structure tended to shift from the pre-exchange baseline to reflect the donor community in the Post1 period, then returned to a more similar pre-exchange community in Post2. Here, we reprocessed the original bacterial sequence data using updated analysis methodologies and found that the conclusions drawn from alpha and beta diversity analysis, in response to the exchange, are upheld in this study.

The rumen fungal community, although functionally important in fiber degradation, did not differ pre-exchange between HE and LE hosts by either alpha or beta diversity metrics in our analysis. This contradicts our initial hypothesis and was unexpected given the known importance of anaerobic fungi in improving the digestibility of lignocellulosic feed in the rumen (Russell and Hespell, 1981; Tripathi et al., 2007; Sehgal et al., 2008; Gao et al., 2013; Puniya et al., 2015). Given this lack of contrast pre-exchange, it is perhaps not unexpected that changes over the time course were not observed. As such, while the ruminal bacterial community, as a whole, has been demonstrated to correlate to efficiency metrics in dairy cattle (Jewell et al., 2015; Shabat et al., 2016), the contributions of the ruminal fungal community to efficiency phenotypes appears to be through the action of individual influential taxa, rather than through more complex community-scale function. This community-scale similarity between hosts of differing efficiency status may indicate that ruminal fungi play a narrower role *in vivo* than previously thought. This supports the widely held assumption that the primary function of the anaerobic fungi is physical disruption of fibrous tissues in the earliest stages of feed particle colonization. In later colonization, slow-growing fungi are thought to be outcompeted by fiber-adherent bacteria, which would likely have a greater impact on the pool of metabolites available to the host, and therefore have a greater impact on efficiency metrics.

Our analysis of network connectivity quantified by degree-centrality revealed that bacterial communities were more disturbed by the exchange than fungal communities. The degree-centrality of a node in a correlation network is calculated as the number of edges connecting to the node. In our analysis, this represents the number of strong positive correlations a given OTU has to other bacterial and fungal OTUs. In HE samples, both liquid- and solid-associated bacterial communities saw a decrease in average degree-centrality in Post1 relative to Pre, and a recovery in Post2 (though only partially in the case of HE solids). In contrast, LE bacterial communities had less average degree connectivity at the outset and did not recover after the exchange. Generally, it appears that HE communities are more resilient and are more able than the LE communities to recover complex network interactions following a major disturbance. This indicates that the HE microbial community may display greater elasticity and resilience in the face of perturbation, which may underlie the relatively lower bacterial community diversity which has been reported in HE cows (Shabat et al., 2016; Weimer et al., 2017).

This finding points to the potential for establishing exogenous microbial communities in historically LE cows: if LE communities have inherently lower resilience, then it may be possible to introduce long-term, high-resilience HE communities. We note that the exchange protocol used in this study was insufficient to achieve a new stable state in LE cows despite this disparity, and further work should focus on identifying and overcoming barriers to exogenous community introduction. This may include a greater understanding of the influence of both host immunity and genetics on ruminal microbial community maintenance, a consideration of the metabolic capacities of the ruminal microbiota in HE and LE cows, and methodological changes that may aid exogenous community establishment (i.e., rinsing the rumen prior to introducing the new community or intervening early in life prior to the establishment of the adult ruminal microbial community). Additionally, fungal communities tended to have lower degree connectivity than bacterial communities, irrespective of host efficiency status or study phase, which suggests that fungi do not exert a strong influence on efficiency at the community-level. This reinforces the theory that fungi are not major contributors to the pool of metabolites that serve as milk precursors (Russell and Hespell, 1981).

Many of the bacterial OTUs that were found to change over the time course in either LE or HE cows were classified to the genus *Prevotella*. This observation agrees with Jewell et al. (2015) who showed that some members of this genus are strongly correlated (either positively or negatively) to feed efficiency. Recent updates to the SILVA taxonomic classification database allowed for a more thorough taxonomic division of the *Prevotella* based on sequence identity. *Prevotella_1*, which was more abundant in LE cows in the Pre period and was transferred to HE cows in the Post1 period, contains the type species *Prevotella melaninogenica* and the rumen-derived isolate *P. ruminicola* (Henderson et al., 2019). In the Global Rumen Census dataset (Henderson et al., 2019), which was used to resolve these taxa, *Prevotella_1* accounted for approximately 18% of all reads and was present in 100% of the samples. *Prevotella_7* was much less abundant, with an average of 1% of reads and a prevalence of ∼68%. BLAST analysis of the representative sequences of the two SIMPER-implicated OTUs classifying to *Prevotella_7* revealed that they do not have high sequence similarity (>97%) with any cultured isolates of *Prevotella.* The *Prevotella_1* are better characterized, and three of these OTUs have >97% sequence identity with isolates of *P. ruminicola* (B_OTU 2, B_OTU 3, and B_OTU 5), but the rest have below species-level sequence identity with cultured isolates. Because these genus designations were created based on sequence identity, rather than genomic or phenotypic analysis, very little is known about the variation in metabolism that may impact precursors available to the host. *Prevotella* are generally thought to be major producers of propionate and can utilize a

diverse range of substrates (Krause et al., 2003), which is reflected in the strong positive correlations between OTUs classified to *Prevotella_7* and the molar fraction of propionate in the rumen fluid in this study. However, our data also shows a negative relationship between OTUs classified to *Prevotella_1* and the molar fraction of propionate, indicating that more research is needed to determine the specific role of members of this genus in the rumen community. The high prevalence of *Prevotella_1* as a member of highly influential nodes in our network analysis implies that this group may play a role in maintenance and recovery of microbial community structures in the rumen.

F_OTU 3 is a member of the genus *Piromyces* and was found to be highly central to pre-exchange networks regardless of efficiency status or sample type. This OTU accounted for 10% of total fungal reads overall (range: 0–42%). This genus, like others in the Neocallimastigomycota, is known to host a large suite of cellulolytic and hemicellulolytic species (Gruninger et al., 2014). However, the large amount of functional redundancy among the rumen anaerobic fungi makes it difficult to determine how this specific OTU might be exerting influence over the larger microbial community network (Gruninger et al., 2018).

The only fungal OTU with a relatively strong, significant positive correlation to any production metric was F_OTU 6, which is classified to the genus *Neocallimastix* in the phylum Neocallimastigomycota and accounted for 4% of fungal reads (range: 0–8.3%). Members of this phylum are obligate anaerobic fungi that are common in the gastrointestinal tracts of herbivores (Akin et al., 1988; Akin and Borneman, 1990; Lee et al., 2000). Cultured representatives of the *Neocallimastix* ferment sugars to lactate, ethanol, formate, and hydrogen (Lowe et al., 1987). In the rumen, they are among a number of anaerobic fungi whose fermentation of cellulose and hemicellulose are crucial to exposing plant surface area to allow bacterial adherence to plant fiber (Akin and Borneman, 1990). In one study, a culture of *Neocallimastix* fed to buffalo calves led to an increase in feed efficiency, which was attributed to improved fermentation of feed (Sehgal et al., 2008). These fungi are difficult to isolate in the lab, which confounds detailed study of metabolism and microbe-microbe interactions. The representative sequence for F_OTU 6 has high sequence identity with *Neocallimastix lanati*, a recent sheep fecal isolate (99.4% identity, JGI MycoCosm BLAST)[2]. This isolate is a promising candidate for probiotic development due to its ability to grow quickly on defined media. Future work assessing the use of *N. lanati* as a probiotic for increasing milk production and feed efficiency should consider the community-level factors that may help this species to establish and be maintained in the rumen.

It is important to note that the fungal primers used in this study were general primers, as opposed to primers specific to rumen anaerobic fungi in the phylum Neocallimastigomycota. As such, our community analysis included organisms which originate in the diet and do not have a known role in feed degradation in the rumen, such as *Penicillium roqueforti* and *Wickerhamomyces anomalus*. In doing so, this work captures the impact of the exchange protocol on the whole fungal community, including but not limited to those members of the community known to be fibrolytic. However, the inclusion of feed-derived fungal taxa in the analysis may have limited our ability to detect differences in functionally important taxa. Future work could include fungal community sequencing with Neocallimastigomycota-specific primers to determine if focusing on this subset of the community might reveal some interesting contrasts.

In this study, we demonstrate that changes in MPE that result from near-total whole rumen contents exchange in dairy cows is driven primarily by the ruminal bacterial community. Surprisingly, we found that the ruminal fungal community did not differ significantly between hosts of disparate historic MPE, indicating that they were not markedly impacted by the exchange protocol. This supports the hypothesis that the primary role of rumen fungi is in physical disruption of feed particles rather than large and impactful contributions to the pool of metabolites that impact downstream production. Two important exceptions are a specific OTU of *Neocallimastix*, which appears to have a positive impact on MPE and whose recent isolation will allow closer study of its unique role in rumen function, and one OTU of *Piromyces* that appears to exert an outsized influence on microbial community networks in the rumen. Future work in whole-rumen probiotics to improve MPE should focus primarily on the bacterial community with particular attention to the bacterial genera *Prevotella_1* and *Prevotella_7* and the fungal genera *Neocallimastix and Piromyces*.

DATA AVAILABILITY STATEMENT

The datasets presented in this study can be found in online repositories. The names of the repository/repositories and accession number(s) can be found below: https://www.ncbi.nlm.nih.gov/bioproject/PRJNA329260/, PRJNA329260 and https://www.ncbi.nlm.nih.gov/bioproject/PRJNA695353/, PRJNA695353.

ETHICS STATEMENT

The animal study was reviewed and approved by the College of Agricultural and Life Sciences Animal Care and Use Committee, University of Wisconsin-Madison.

AUTHOR CONTRIBUTIONS

GS conceived and designed the experiments. MC, CD, and GS performed the experiments. MC analyzed the data and wrote the original draft. MC and GS acquired the funding supporting this study. All authors reviewed and approved the final manuscript.

FUNDING

This work was supported by United States Department of Agriculture (USDA) National Institute of Food and Agriculture

[2]https://mycocosm.jgi.doe.gov/Neolan1/Neolan1.home.html

(NIFA) HATCH Grant WIS02007 and a USDA Agriculture and Food Research Initiative (AFRI) Competitive Grant 2015-67015-23246 to GS. MC was supported by a USDA AFRI Education and Literacy Initiative Predoctoral Fellowship 2018-67011-27997 and the Jack & Marion Goetz Wisconsin Distinguished Graduate Fellowship.

ACKNOWLEDGMENTS

We would like to thank Dr. Michael Millican for providing us with the custom fungal primers used in this study and all members of the Suen laboratory for their support, insightful discussions, and careful reading of the manuscript. Finally, we also thank Dr. Paul Weimer for his work in executing the animal trial and for his valuable feedback during the preparation of this manuscript.

SUPPLEMENTARY MATERIAL

The Supplementary Material for this article can be found online at: https://www.frontiersin.org/articles/10.3389/fmicb.2021.665776/full#supplementary-material

REFERENCES

Akin, D. E., and Borneman, W. S. (1990). Role of rumen fungi in fiber degradation. *J. Dairy Sci.* 73, 3023–3032. doi: 10.3168/jds.S0022-0302(90)78989-8

Akin, D. E., Borneman, W. S., and Windham, W. R. (1988). Rumen fungi: morphological types from Georgia cattle and the attack on forage cell walls. *BioSystems* 21, 385–391. doi: 10.1016/0303-2647(88)90037-8

Bickhart, D. M., and Weimer, P. J. (2017). Host–rumen microbe interactions may be leveraged to improve the productivity of dairy cows. *J. Dairy Sci.* 2017:133328. doi: 10.3168/JDS.2017-13328

Bray, R. J., and Curtis, J. T. (1957). An ordination of the upland forest communities of Southern Wisconsin. *Ecol. Monogr.* 27, 325–349.

Chao, A. (1984). Nonparametric estimation of the number of classes in a population. *Scand. J. Stat.* 11, 265–270.

Choudhury, P. K., Salem, A. Z. M., Jena, R., Kumar, S., Singh, R., and Puniya, A. K. (2015). Rumen microbiology: An overview. *Rumen Microbiol.* 2015, 1–379. doi: 10.1007/978-81-322-2401-3_1

Csardi, G., and Nepusz, T. (2006). *The igraph software package for complex network research. InterJournal, Complex Systems* 1695. Available online at: https://igraph.org (accessed February 7, 2021).

Edgar, R. C., Haas, B. J., Clemente, J. C., Quince, C., and Knight, R. (2011). UCHIME improves sensitivity and speed of chimera detection. *Bioinformatics* 27, 2194–2200. doi: 10.1093/bioinformatics/btr381

Gao, A., Wang, H., Yang, J., and Shi, C. (2013). The effects of elimination of fungi on microbial population and fiber degradation in sheep rumen. *Appl. Mechan. Material.* 2013, 224–231. doi: 10.4028/www.scientific.net/AMM.295-298.224

Good, I. J. (1953). The population frequencies of species and the estimation of population parameters. *Biometrika* 40, 237–264. doi: 10.1093/biomet/40.3-4.237

Gordon, G. L. R., and Phillips, M. W. (1998). The role of anaerobic gut fungi in ruminants. *Nutr. Res. Rev.* 11, 133–168. doi: 10.1079/NRR19980009

Gruninger, R. J., Nguyen, T. T. M., Reid, I. D., Yanke, J. L., Wang, P., Abbott, D. W., et al. (2018). Application of transcriptomics to compare the carbohydrate active enzymes that are expressed by diverse genera of anaerobic fungi to degrade plant cell wall Carbohydrates. *Front. Microbiol.* 9:1581. doi: 10.3389/fmicb.2018.01581

Gruninger, R. J., Puniya, A. K., Callaghan, T. M., Edwards, J. E., Youssef, N., Dagar, S. S., et al. (2014). Anaerobic fungi (phylum Neocallimastigomycota): Advances in understanding their taxonomy, life cycle, ecology, role and biotechnological potential. *FEMS Microbiol. Ecol.* 90, 1–17. doi: 10.1111/1574-6941.12383

Harrell, F. E. Jr.. (2020). *Hmisc: Harrell Miscellaneous. R package version 4.4-1.* Available online at: https://cran.r-project.org/package=Hmisc (accessed February 7, 2021).

Henderson, G., Yilmaz, P., Kumar, S., Forster, R. J., Kelly, W. J., Leahy, S. C., et al. (2019). Improved taxonomic assignment of rumen bacterial 16S rRNA sequences using a revised SILVA taxonomic framework. *PeerJ.* 2019:6496. doi: 10.7717/peerj.6496

Jami, E., White, B. A., Mizrahi, I., Turnbaugh, P., Gordon, J., Arumugam, M., et al. (2014). Potential role of the bovine rumen microbiome in modulating milk composition and feed efficiency. *PLoS One* 9:e85423. doi: 10.1371/journal.pone.0085423

Jewell, K. A., McCormick, C. A., Odt, C. L., Weimer, P. J., and Suen, G. (2015). Ruminal bacterial community composition in dairy cows is dynamic over the course of two lactations and correlates with feed efficiency. *Appl. Environ. Microbiol.* 81, AEM.720–AEM.715. doi: 10.1128/AEM.00720-15

Kampstra, P. (2008). Beanplot: A boxplot alternative for visual comparison of distributions. *J. Stat. Soft.* 28, 1–9.

Knaus, W. (2009). Dairy cows trapped between performance demands and adaptability †. *J. Sci. Food Agric.* 89, 1107–1114. doi: 10.1002/jsfa.3575

Kozich, J. J., Westcott, S. L., Baxter, N. T., Highlander, S. K., and Schloss, P. D. (2013). Development of a dual-index sequencing strategy and curation pipeline for analyzing amplicon sequence data on the MiSeq Illumina sequencing platform. *Appl. Environ. Microbiol.* 79, 5112–5120. doi: 10.1128/AEM.01043-13

Krause, D. O., Denman, S. E., Mackie, R. I., Morrison, M., Rae, A. L., Attwood, G. T., et al. (2003). Opportunities to improve fiber degradation in the rumen: microbiology, ecology, and genomics. *FEMS Microbiol. Rev.* 27, 663–693. doi: 10.1016/S0168-6445(03)00072-X

Lee, S. S., Ha, J. K., and Cheng, K.-J. (2000). Influence of an anaerobic fungal culture administration on in vivo ruminal fermentation and nutrient digestion. *Anim. Feed Sci. Technol.* 88, 201–217. doi: 10.1016/S0377-8401(00)00216-9

Lowe, S. E., Theodorou, M. K., and Trinci, A. P. J. (1987). Growth and fermentation of an anaerobic rumen fungus on various carbon sources and effect of temperature on development. *Appl. Environ. Microbiol.* 53, 1210–1215. doi: 10.1128/aem.53.6.1210-1215.1987

Madden, T. (2002). "The BLAST Sequence Analysis Tool," in *The NCBI Handbook [Internet]*, eds J. McEntyre and J. Ostell (Bethesda, MD: National Center for Biotechnology Information (US)).

Miglior, F., Fleming, A., Malchiodi, F., Brito, L. F., Martin, P., and Baes, C. F. (2017). A 100-Year Review: Identification and genetic selection of economically important traits in dairy cattle. *J. Dairy Sci.* 100, 10251–10271. doi: 10.3168/jds.2017-12968

Needleman, S. B., and Wunsch, C. D. (1970). A general method applicable to the search for similarities in the amino acid sequence of two proteins. *J. Mol. Biol.* 48, 443–453. doi: 10.1016/0022-2836(70)90057-4

Nilsson, R. H., Larsson, K. H., Taylor, A. F. S., Bengtsson-Palme, J., Jeppesen, T. S., Schigel, D., et al. (2019). The UNITE database for molecular identification of fungi: Handling dark taxa and parallel taxonomic classifications. *Nucleic Acids Res.* 47, D259–D264. doi: 10.1093/nar/gky1022

Okansen, J., Blanchet, F. G., Kindt, R., Legendre, P., Minchin, P. R., O'Hara, R. B., et al. (2016). *vegan: Community Ecology Package*. Available online at: http://cran.r-project.org/package=vegan (accessed February 7, 2021).

Pruesse, E., Quast, C., Knittel, K., Fuchs, B. M., Ludwig, W., Peplies, J., et al. (2007). SILVA: a comprehensive online resource for quality checked and aligned ribosomal RNA sequence data compatible with ARB. *Nucleic Acids Res.* 35, 7188–7196. doi: 10.1093/nar/gkm864

Puniya, A. K., Salem, A. Z. M., Kumar, S., Dagar, S. S., Griffith, G. W., Puniya, M., et al. (2015). Role of live microbial feed supplements with reference to anaerobic fungi in ruminant productivity: A review. *J. Integr. Agric.* 14, 550–560. doi: 10.1016/S2095-3119(14)60837-6

Russell, J. B., and Hespell, R. B. (1981). Microbial Rumen Fermentation. *J. Dairy Sci.* 64, 1153–1169. doi: 10.3168/jds.S0022-0302(81)82694-X

Segata, N., Izard, J., Waldron, L., Gevers, D., Miropolsky, L., Garrett, W. S., et al. (2011). Metagenomic biomarker discovery and explanation. *Genome Biol.* 2011, 12. doi: 10.1186/gb-2011-12-6-r60

Sehgal, J. P., Jit, D., Puniya, A. K., and Singh, K. (2008). Influence of anaerobic fungal administration on growth, rumen fermentation and nutrient digestion in female buffalo calves. *J. Anim. Feed Sci.* 17, 510–518. doi: 10.22358/jafs/66678/2008

Shabat, S. K. B., Sasson, G., Doron-Faigenboim, A., Durman, T., Yaacoby, S., Berg Miller, M. E., et al. (2016). Specific microbiome-dependent mechanisms underlie the energy harvest efficiency of ruminants. *ISME J.* 2016, 1–15. doi: 10.1038/ismej.2016.62

Shannon, C. E. (1948). A mathematical theory of communication. *Bell Syst. Tech. J.* 27, 379–423.

Taylor, D. L., Walters, W. A., Lennon, N. J., Bochicchio, J., Krohn, A., Caporaso, J. G., et al. (2016). Accurate estimation of fungal diversity and abundance through improved lineage-specific primers optimized for Illumina amplicon sequencing. *Appl. Environ. Microbiol.* 82, 7217–7226. doi: 10.1128/AEM.02576-16

R Core Team (2020). *R: A Language and Environment for Statistical Computing*. Vienna: R Core team.

R Studio Team (2020). *RStudio: Integrated Development for R*. Boston, MA: R Studio Team.

Tripathi, V. K., Sehgal, J. P., Puniya, A. K., and Singh, K. (2007). Effect of administration of anaerobic fungi isolated from cattle and wild blue bull (*Boselaphus tragocamelus*) on growth rate and fibre utilization in buffalo calves. *Arch. Anim. Nutr.* 61, 416–423. doi: 10.1080/17450390701556759

Wallace, R. J., Sasson, G., Garnsworthy, P. C., Tapio, I., Gregson, E., Bani, P., et al. (2019). A heritable subset of the core rumen microbiome dictates dairy cow productivity and emissions. *Sci. Adv.* 5, 8391–8394. doi: 10.1126/sciadv.aav8391

Weimer, P. J., Cox, M. S., Vieira, de Paula, T., Lin, M., Hall, M. B., et al. (2017). Transient changes in milk production efficiency and bacterial community composition resulting from near-total exchange of ruminal contents between high- and low-efficiency Holstein cows. *J. Dairy Sci.* 100, 7165–7182. doi: 10.3168/jds.2017-12746

Westcott, S. L., and Schloss, P. D. (2017). OptiClust, an improved method for assigning amplicon-based sequence data to operational taxonomic units. *mSphere* 2:17. doi: :10.1128/mspheredirect.00073-17

Conflict of Interest: The authors declare that the research was conducted in the absence of any commercial or financial relationships that could be construed as a potential conflict of interest.

frontiers in Veterinary Science

ORIGINAL RESEARCH
published: 10 August 2021
doi: 10.3389/fvets.2021.677897

Transcriptome Analysis Identifies Strategies Targeting Immune Response-Related Pathways to Control Enterotoxigenic *Escherichia coli* Infection in Porcine Intestinal Epithelial Cells

Qiong Wu[1,2], *Defeng Cui*[1,2], *Xinyu Chao*[1], *Peng Chen*[1], *Jiaxuan Liu*[1], *Yiding Wang*[1], *Tongjian Su*[1], *Meng Li*[1], *Ruyu Xu*[1], *Yaohong Zhu*[3]* and *Yonghong Zhang*[1,2]*

[1] *Department of Animal Medicine, College of Animal Science and Technology, Beijing University of Agriculture, Beijing, China,*
[2] *Beijing Key Laboratory of Traditional Chinese Veterinary Medicine, Beijing University of Agriculture, Beijing, China,*
[3] *Department of Clinical Veterinary Medicine, College of Veterinary Medicine, China Agricultural University, Beijing, China*

OPEN ACCESS

Edited by:
Xudong Sun,
Heilongjiang Bayi Agricultural University, China

Reviewed by:
Xiangbing Mao,
Sichuan Agricultural University, China
Wentao Lyu,
Zhejiang Academy of Agricultural Sciences, China
Haoyu Liu,
Uppsala University, Sweden

***Correspondence:**
Yaohong Zhu
zhu_yaohong@hotmail.com
Yonghong Zhang
yhh2266@126.com

Specialty section:
This article was submitted to Livestock Genomics, a section of the journal Frontiers in Veterinary Science

Received: *17 May 2021*
Accepted: *05 July 2021*
Published: *10 August 2021*

Citation:
Wu Q, Cui D-F, Chao X-Y, Chen P, Liu J-X, Wang Y-D, Su T-J, Li M, Xu R-Y, Zhu Y-H and Zhang Y-H (2021) Transcriptome Analysis Identifies Strategies Targeting Immune Response-Related Pathways to Control Enterotoxigenic Escherichia coli Infection in Porcine Intestinal Epithelial Cells. Front. Vet. Sci. 8:677897. doi: 10.3389/fvets.2021.677897

Enterotoxigenic *Escherichia coli* (ETEC) is an important cause of post-weaning diarrhea (PWD) worldwide, resulting in huge economic losses to the swine industry worldwide. In this study, to understand the pathogenesis, the transcriptomic analysis was performed to explore the biological processes (BP) in porcine intestinal epithelial J2 cells infected with an emerging ETEC strain isolated from weaned pigs with diarrhea. Under the criteria of |fold change| (FC) ≥ 2 and $P < 0.05$ with false discovery rate < 0.05, a total of 131 referenced and 19 novel differentially expressed genes (DEGs) were identified after ETEC infection, including 96 upregulated DEGs and 54 downregulated DEGs. The Gene Ontology (GO) analysis of DEGs showed that ETEC evoked BP specifically involved in response to lipopolysaccharide (LPS) and negative regulation of intracellular signal transduction. The Kyoto Encyclopedia of Genes and Genomes (KEGG) pathway analysis revealed that immune response-related pathways were mainly enriched in J2 cells after ETEC infection, in which tumor necrosis factor (TNF), interleukin 17, and mitogen-activated protein kinase (MAPK) signaling pathways possessed the highest rich factor, followed by nucleotide-binding and oligomerization domain-like receptor (NLRs), C-type lectin receptor (CLR), cytokine–cytokine receptor interaction, and Toll-like receptor (TLR), and nuclear factor kappa-B (NF-κB) signaling pathways. Furthermore, 30 of 131 referenced DEGs, especially the nuclear transcription factor AP-1 and NF-κB, participate in the immune response to infection through an integral signal cascade and can be target molecules for prevention and control of enteric ETEC infection by probiotic *Lactobacillus reuteri*. Our data provide a comprehensive insight into the immune response of porcine intestinal epithelial cells (IECs) to ETEC infection and advance the identification of targets for prevention and control of ETEC-related PWD.

Keywords: transcriptome (RNA-seq), intestinal epithelia cell, immune response, *Escherichia coli*, porcine, enrichment analysis

INTRODUCTION

Enterotoxigenic *Escherichia coli* (ETEC) is one of the most common causes of diarrhea in animals and humans. Enterotoxigenic *Escherichia coli* is responsible for an estimated 75 million diarrheal episodes and approximately 50,000 deaths in children younger than 5 years annually (1). The breakout of ETEC infection in farm animals often attracts a lot of attention due to the possibility of spreading to humans through animal productions. In neonatal and weaned pigs, diarrhea associated with ETEC results in huge economic losses in the pig industry because of high morbidity, mortality, and growth retardation (2, 3). Enterotoxigenic *Escherichia coli*-expressing F4 fimbriae are the most prevalent strains in pigs (4) and include three fimbrial variants of F4ab, F4ac, and F4ad (5). F4ab and F4ac variants are typically associated with diarrhea in pigs (6). The incidence of ETEC infection has become a more frequent reason for severe diarrhea in global swine production. Across Europe, ETEC is detected in 60% of post-weaning diarrhea (PWD)-affected farms (7). Enterotoxigenic *Escherichia coli* is also responsible for the spread of antibiotic resistance in the environment (8). Thus, clarifying the pathogenesis of ETEC is essential for identifying effective prevention strategies for ETEC-related pig diarrhea.

Intestinal epithelial cells (IECs) are in the front line of host defense against pathogens and possess as the crucial mediators of barrier function. Enterotoxigenic *Escherichia coli* interacts with IECs and secretes heat-labile (LT) or heat-stable enterotoxin (ST) enterotoxins, leading to acute intestinal inflammation and diarrhea (9). Besides, IECs are also indispensable for activating innate immune responses and subsequently for inducing adaptive immunity (10). Lipopolysaccharide (LPS) is generally the most potent immunostimulant from Gram-negative bacteria. In general, the innate immune response of IECs is initiated by bind of the pathogen-associated molecular pattern to specialized pattern recognition receptors, including membrane-bound Toll-like receptors (TLRs) and cytoplasmic nucleotide-binding and oligomerization domain-like receptors (NLRs) (11). The detection of pathogen-associated molecular patterns by pattern recognition receptors activates nuclear factor kappa-B (NF-κB) and mitogen-activated protein kinase (MAPK) signaling pathways and triggers transcriptional expression of various pro-inflammatory chemokines, cytokines, and antimicrobial peptides for recruitment and activation of inflammatory cells, thereby inducing host immune responses (12, 13). However, the immune response-related pathogenesis of ETEC, especially the ETEC clinical isolates, is still unclear.

Transcriptome analysis is a useful approach to reveal the comprehensive expression profile of genes involving the host response to pathogen infection. The transcriptomic response of porcine IECs to ETEC reference strains was previously reported. Comparative transcriptomic analysis observed strong differential responses of porcine IECs to F4ab, F4ac, or F18ac ETEC and confirmed that the apical membrane of the IECs represents a first barrier against enteric pathogen infection (9, 14). Enterotoxigenic *Escherichia coli* K88 (serotype O149:K91:K88ac) challenge induces differential expression of genes encoding intestinal ion transporters and water channel aquaporins in young piglets, probably by regulation of the cyclic adenosine monophosphate–protein kinase A signaling pathway (15). The differential genes confirmed by transcriptome analysis can be a potential target for preventing pathogen infection. For example, a soluble and highly fermentable dietary fiber with carbohydrases improves growth performance in pigs infected with F18 ETEC, in part due to a reduction in inflammatory intermediates (16). Dietary supplementation with live yeast limits the early activation of the gene sets related to the impairment of the jejunal mucosa, thus counteracting the detrimental effect of F4 ETEC infection in susceptible pigs (17).

This study aimed to explore the transcriptional change profile of porcine intestinal epithelial J2 cells after infection with a pig diarrhea-related ETEC isolate and determine the potential target for prevention and control for ETEC infection.

MATERIALS AND METHODS

Bacterial Strains

Enterotoxigenic *Escherichia coli* BUA2008 was isolated from the intestinal contents of weaned pigs with diarrhea in our laboratory and used in this study. The ETEC BUA2008 harbors the genes encoding virulence factor *E. coli*-secreted protein A, STa, STb, and LTa.

Lactobacillus reuteri BP325 was originally isolated from the gastrointestinal tract of a healthy weaning piglet in our laboratory. The strain was identified through standard morphological, biochemical, and physiological tests and by 16s rRNA gene sequence analysis. *Lactobacillus reuteri* BP325 could inhibit the growth of ETEC BUA2008 and be tolerant to acid and bile salt *in vitro*. *Lactobacillus reuteri* BP325 was grown in De Man, Rogosa, and Sharpe broth (Oxoid, Hampshire, United Kingdom) for 24 h at 37°C under microaerophilic conditions. After overnight incubation, bacteria were inoculated 1:100 in fresh De Man, Rogosa, and Sharpe broth and grown for approximately 8 h until reaching the mid-log phase.

Intestinal Epithelial Cell Line J2 Cell Culture Condition and Treatment

The porcine intestinal epithelial cell line (IPEC)-J2 cells were cultured in Dulbecco's modified Eagle medium/F12 medium (Invitrogen, Carlsbad, CA, USA) supplemented with 10% heat-inactivated fetal calf serum, 100 μg/ml of streptomycin, and 100 U/ml of penicillin at 37°C in an atmosphere of 5% carbon dioxide and 95% air at 95% relative humidity. Cells (1×10^5 cells/well) were seeded onto a six-well collagen-coated polytetrafluoroethylene transwell filter, and confluent cell monolayers were treated under two different conditions: (i) medium alone (CN); (ii) ETEC infection alone [3×10^6 colony-forming unit (CFU)] at a multiplicity of infection of 30:1 (EC). At 2 h after ETEC infection, the IPEC-J2 cells were washed three times with phosphate-buffered saline (PBS), and then, total RNA was extracted using TRIzol (Invitrogen) according to the manufacturer's instructions for subsequent library construction and sequencing.

For validating whether the genes related to differential inflammatory pathways obtained from RNA-seq were the targets in controlling ETEC infection, confluent J2 cell monolayers were treated under four different conditions: (i) medium alone; (ii) ETEC infection alone (3×10^6 CFU); (iii) incubation with BP325 (3×10^7 CFU) only for 2 h; or (iv) preincubation with BP325 (3×10^7 CFU) for 2 h before exposure to ETEC infection. At 2 h after preincubation with BP325, the IPEC-J2 cells were washed three times with PBS and immediately infected with ETEC (3×10^6 CFU) for 2 h. After infection, the IPEC-J2 cells were washed three times with PBS, and then, total RNA was harvested using TRIzol for quantitative real-time polymerase chain reaction (qRT-PCR) analysis, and the supernatant samples were collected for enzyme-linked immunosorbent assay (ELISA) analysis.

Library Construction and Sequencing

The RNA integrity was tested by 1% agarose gel electrophoresis, and RNA quality and quantity were evaluated using NanoDrop 2000. The RNA integrity number was further assessed with Agilent 2100 using an RNA 6000 Nano kit (Agilent Technologies, Santa Clara, CA, USA). Samples with qualified purity (RNA integrity number $\geq$9, OD260/280 $\geq$1.9, and OD260/230 $\geq$1.5) were used for subsequent sequencing library preparation. Poly-(A)-containing messenger RNA (mRNA) was enriched using oligo (dT) beads and were broken into short fragments using mentation buffer. The first-strand complementary DNA was synthesized with reverse transcriptase and random hexamer primers using mRNA as templates. Then, the second-strand complementary DNA was synthesized using the buffer, DNA polymerase I, deoxynucleoside triphosphates, and RNase H, followed by end-repair and adapter ligation. Finally, PCR amplification was carried out to obtain the final libraries. The constructed library was quantified and pooled in the flow cell. After cBot clustering using a cBotCluster Generation System, the library preparations were sequenced using Illumina high-throughput sequencing platform Novaseq 6000, and paired-end reads of 150-bp length were generated.

Genome Alignment and Gene Annotation

The raw reads were quality filtered using Trimmomatic software. The clean reads were obtained after discarding reads containing adapter sequences, low-quality reads with Q10 <30, reads with undetermined base information >10%, and reads that were shorter than 50 bp after the adapter was removed and truncated. The clean reads were aligned to the reference genome Sscrofa11 of the pig (http://asia.ensembl.org/Sus_scrofa/Info/Index) using TopHat v2.1.1 (http://ccb.jhu.edu/software/tophat/index.shtml). The mapped reads were assembled into transcripts using StringTie v1.3.3b (http://ccb.jhu.edu/software/stringtie/). The genes were annotated by BLAST based on Gene Ontology (GO), Cluster of Orthologous Groups of proteins (COG), and Kyoto Encyclopedia of Genes and Genomes (KEGG) databases.

Analysis of Gene Expression Levels and Identification of Differentially Expressed Genes

The expression of genes was calculated and normalized to fragments per kilobases per million reads (FPKMs) using RSEM v1.3.1 (http://deweylab.biostat.wisc.edu/rsem/). Differentially expressed genes (DEGs) between CN and EC groups were identified using DESeq2 v1.24.0 (http://bioconductor.org/packages/stats/bioc/DESeq2/). The *P*-value was adjusted using Benjamini and Hochberg's approach (BH) for controlling the false discovery rate. Genes with an adjusted $P < 0.05$ and fold change (FC) ≥ 2 or ≤ -2 were assigned as DEGs. A heatmap of DEGs was constructed using the heatmap.2 implemented in the R package gplots (https://cran.r-project.org/web/packages/gplots).

Gene Ontology and Kyoto Encyclopedia of Genes and Genomes Enrichment Analysis of Differentially Expressed Genes

Gene Ontology enrichment analysis was carried out to specify the potential roles of DEGs based on Fisher's exact test using Goatools v0.6.5 (https://github.com/tanghaibao/GOatools). The *P*-value was adjusted by BH, and GO terms with adjusted $P < 0.05$ were considered significantly enriched. Furthermore, KEGG enrichment analysis was carried out to assess significantly enriched metabolic or signal transduction pathways using KOBAS v2.1.1 (http://kobas.cbi.pku.edu.cn/download.php).

Venn, Correlation Analysis of Expression, and Protein–Protein Interaction Analysis

A Venn diagram was generated using the Venndiagram R package (https://cran.r-project.org/web/packages/Venndiagram) to obtain EC-unique genes and an overview of the DEGs among different annotation levels. Correlation analysis of gene expression was performed, and differential correlation was calculated using Fisher's transformation of Spearman rank correlation to determine the significance of a change in correlation between two conditions. The statistic *P*-value was corrected by the BH method. Correlations with an absolute Spearman's correlation >0.8 and adjusted $P < 0.05$ were transformed into links between two DEGs, and correlation networks were displayed with Cytoscape v2.8.2. Protein–protein interaction (PPI) analysis of DEGs was carried out based on the Search Tool for the Retrieval of Interacting Genes/Proteins database v11.0 (http://string-db.org/), and the minimum Search Tool for the Retrieval of Interacting Genes/Proteins score was set at 1,000. The interaction with a combined score >0.4 was considered to be significant. The protein network was visualized using Cytoscape v2.8.2.

Quantitative Real-Time Polymerase Chain Reaction

Quantitative real-time polymerase chain reaction was performed using a QuantStudio 3 RT-PCR system (ThermoFisher Scientific, Waltham, MA, USA). Primer sequences are listed in **Supplementary Table 1**. Complementary DNA was synthesized

and amplified with SYBR Premix DimerEraser (TakaRa Biotechnology Inc., Shiga, Japan). Each sample was assayed in duplicate. Relative quantification of mRNA expression was performed by normalizing the cycle threshold values of the target genes to the cycle threshold values of the housekeeping gene encoding. The $2^{-\Delta\Delta CT}$ method relative to the reference gene encoding glyceraldehyde-3-phosphate dehydrogenase was used to analyze the FC of target genes between CN and EC groups.

Enzyme-Linked Immunosorbent Assay

The concentrations of interleukin (IL)-1β and IL-6 were determined using commercially available porcine-specific ELISA kits (IL-1β: #PLB00B, IL-6: #P6000B; R&D Systems, Minneapolis, MN, USA) according to the manufacturer's instructions.

Data Accession Number

The raw transcriptome data have been deposited in the US National Center for Biotechnology Information Sequence Read Archive database under accession no. SRR13291685–SRR13291693.

Statistical Analysis

Statistical analysis was performed using the IBM SPSS Statistics 21 (SPSS Inc., Chicago, IL, USA) software package. Natural logarithm transformation was performed before analysis for ELISA data of IL-1β and IL-6 to achieve a normal distribution. Differences between means were compared using one-way analysis of variance, followed by Tukey's honestly significant difference *post-hoc* test. A P-value of <0.05 was considered statistically significant. Data were visualized using GraphPad Prism 5 software (Graphpad Software Inc., San Diego, CA, USA). All experiments were performed three times.

RESULTS

Quality Control and Transcriptome Assembly

A total of 348.2 million raw reads (approximately 52.6 Gbps) were yielded across six samples. After removing low-quality reads, ambiguous and adaptor reads, retaining 344 million high-quality clean reads (approximately 51.2 Gbps, 50.6–61.7 million reads for each sample) were used for subsequent assembly and analysis. The average of Q20 and Q30 of clean reads across all samples was above 98.3 and 94.9%, respectively, indicating that the obtained clean reads were of high quality. Compared with the pig reference genome Sscrofa11, 93.5 and 93.2% of total reads for CN and EC groups were uniquely mapped on the *sus scrofa* genome, respectively, and the GC content for CN and EC groups was more than 51.2% (**Supplementary Table 2**).

The clean reads of genes were normalized to FPKM values to precisely evaluate the gene expression levels. The saturation curve of sequencing showed that the FPKM values of approximately 42% of genes in CN and EC groups were below 3.5, and only a few of 7% genes were highly expressed with FPKM values higher than 60. Most of the genes with medium or above expression levels (i.e., the genes with FPKM value of 3.5–60) were nearly saturated at 51% of the sequencing reads (ordinate value tended to 1), indicating that the overall quality of saturation was high, and the sequencing quantity could cover most of the expressed genes (**Supplementary Table 3** and **Supplementary Figure 1**). A Spearman's correlation matrix analysis of the FPKM distribution among biological replicates for all six samples showed that the correlation indices of the mapped genes in different groups were different, but the differences within the groups were small, indicating a high consistency of measurements within each group and high reproducibility of the sequencing data (**Figure 1A**). Principal component analysis was carried out to evaluate the clustering nature of these samples. Principal components 1 and 2 explained 32.4 and 23.3% of the distributions of the different groups, respectively (**Figure 1B**). The samples of each group were clustered together, and data showed good correlation and repeatability.

Analysis of Gene Expression and Functional Annotation

A total of 27,001 genes were found from all samples, including 25,880 (95.8%) referenced genes and 1,121 (4.2%) unannotated novel genes. Of 25,880 referenced genes, a total of 23,375 genes could be annotated using GO (20,488), KEGG (16,308), COG (22,389), NR (23,133), Swiss-Prot (22,155), and Pfam (20,554) databases (**Figure 2A**). The COG database contains orthologous proteins and is used to classify and predict their possible function. The referenced genes were assigned into 22 orthologous COG clusters (**Figure 2B**). Some genes may be assigned into several clusters in COG categories, whereas some were assigned to the same cluster but with different protein orthologous similarities. A total of 10,628 genes were assigned to "unknown function" (class S). The majority of genes were distributed in "intracellular trafficking, secretion, and vesicular transport" (class U; 3,861 genes), followed by "post-translational modification, protein turnover, chaperones" (class O; 2,149 genes), and "transcription" (class K; 1,252 genes).

Gene Ontology analysis revealed that a total of 20,481 genes were mapped to 64 GO terms, with 17,454 genes assigned to biological process (BP), 18,2023 genes assigned to cellular component (CC), and 17,580 genes assigned to molecular function (MF). In the BP ontology, cellular processes (15,647 genes) and single-organism processes (13,216 genes) were the most enriched GO terms. In the CC ontology, the most enriched terms were cell (15,592 genes), and cell part (15,476 genes) was the most enriched GO term. In the MF ontology, binding (12,651 genes) and catalytic activities (5,743 genes) were the most enriched GO terms (**Figure 2C**).

Kyoto Encyclopedia of Genes and Genomes pathway analysis helps to better understand the biological functions of genes. A total of 3,209 genes were annotated and classified into six

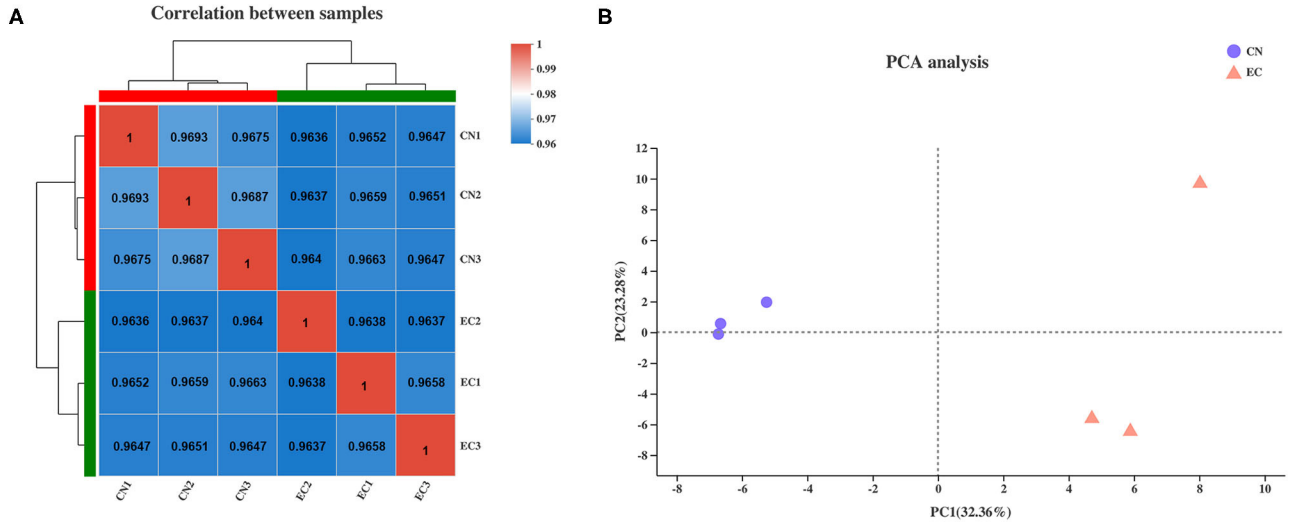

FIGURE 1 | Correlation analysis and principal component analysis of samples. **(A)** Heatmap of hierarchical clustering for six samples using Spearman method. Bold values represented R^2 for replicates of each sample. **(B)** Principal component analysis plot of samples. Each point represented one sample. Percentages were contribution ratios.

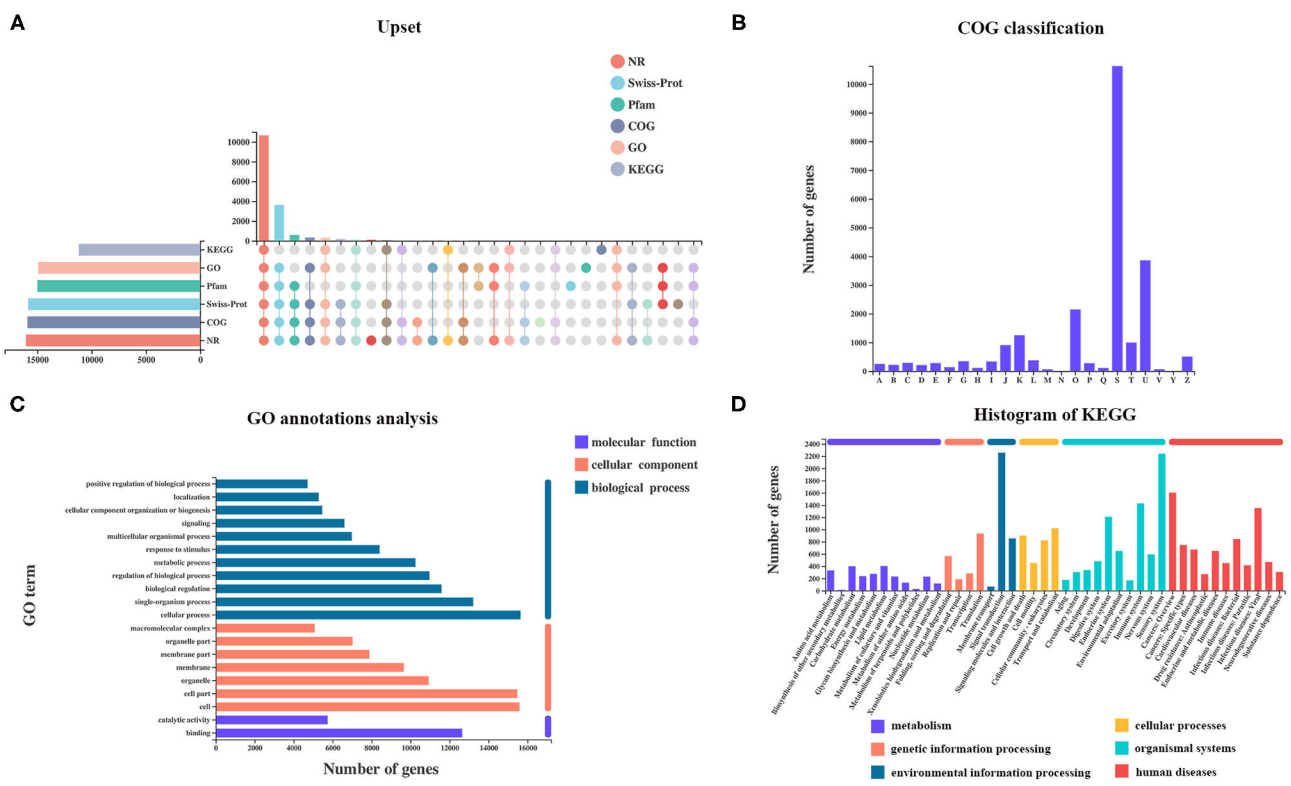

FIGURE 2 | Analysis of referenced gene expression and functional annotation. **(A)** Number of genes annotated using KEGG, GO, Pfam, Swiss-Prot, COG, and NR datasets. **(B)** COG, **(C)** GO, and **(D)** KEGG classifications of referenced genes were summarized.

first KEGG categories (metabolism, environmental information processing, cellular processes, genetic information processing, human diseases, and organismal system) and 335 second KEGG categories. Signal transduction (2,257 genes) was the most abundant KEGG pathway, followed by the sensory system (2,240 genes) (**Figure 2D**).

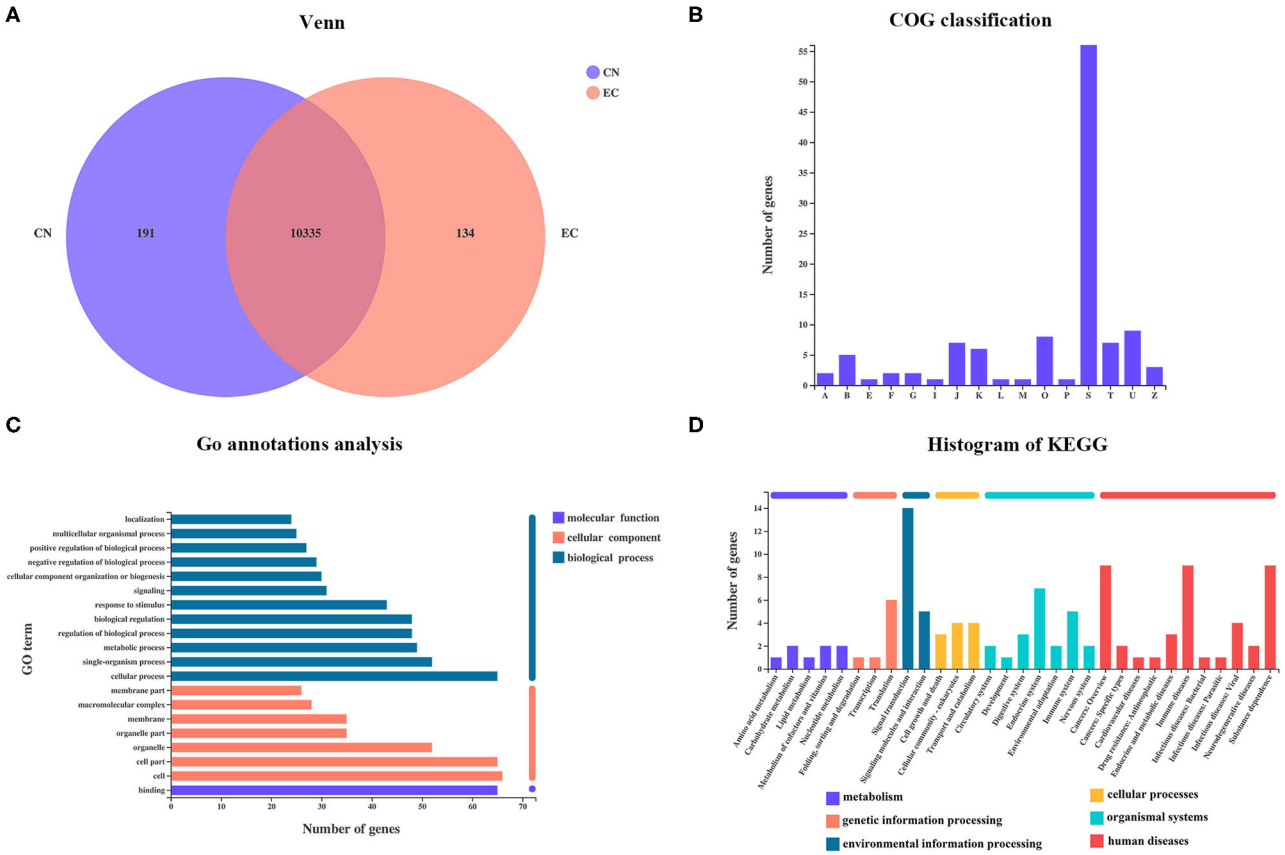

FIGURE 3 | Identification of EC-unique genes and functional analysis. **(A)** Venn diagram of shared referenced genes between CN and EC groups. **(B)** COG, **(C)** GO, and **(D)** KEGG classifications of 134 EC-unique genes were summarized.

A total of 12,227 novel transcripts were found in the 61,408 transcripts identified, including 389 transcripts with exonic overlap with reference on the opposite strand, 506 with transfer falling entirely within a reference intron, 9,450 with potentially novel isoform: at least one splice junction was shared with a reference transcript, 1,265 unknown and intergenic transcripts, and 350 with generic exonic overlap with a reference transcript (**Supplementary Figure 2**).

A total of 1,106 novel genes (accounting for 98.7% of all novel genes) and 11,670 novel transcripts (accounting for 95.4% of all novel transcripts) were successfully annotated after BLAST, with 242 and 8,280 in the GO database, 63 and 6,932 in the KEGG database, 289 and 9,906 in COG database, 757 and 10,909 in the NR database, 187 and 9,782 in the Swiss-Prot database, and 122 and 8,907 in the Pfam database, respectively (**Supplementary Figure 3A**, **Supplementary Table 4**). The COG analysis showed that 307 novel genes were assigned into nine COG functional categories (**Supplementary Figure 3B**), including "chromatin structure and dynamics" (class B; 21 genes), "post-translational modification, protein turnover, chaperones" (class O; 11 genes), "intracellular trafficking, secretion, and vesicular transport" (class U; 7 genes), "translation, ribosomal structure, and biogenesis" (class J; 6 genes), "energy production and conversion" (class C; 4 genes), "transcription" (class K; 3 genes), "signal transduction mechanisms" (class T; 3 genes), and "cytoskeleton" (class Z; 2 genes). Importantly, 814 genes not assigned to any COG class, as well as 250 genes of unknown function (class S), were enriched in the novel genes. According to the GO analysis, the novel genes were divided into multiple functional groups (**Supplementary Figure 3C**), in which MF, BP, and CC were the most enriched terms. Catalytic activity (131 genes) and binding (96 genes) in MF, membrane (108 genes) and membrane part (104 genes) in a CC, and cellular process (87 genes) and metabolic process (76 genes) in the BP were the most enriched ontology terms. A total of 40 novel genes were classified into 112 KEGG pathways, mainly functioning in the phagosome, Ras signaling pathway, cyclic adenosine monophosphate signaling pathway, calcium signaling pathway, endocytosis, and tuberculosis (**Supplementary Figure 3D**).

Identification of EC-Unique Genes and Functional Analysis

From the Venn diagram, 134 referenced genes were uniquely present in the EC group (**Figure 3A**). A total of 55 EC-unique genes could be annotated to 15 COG functional

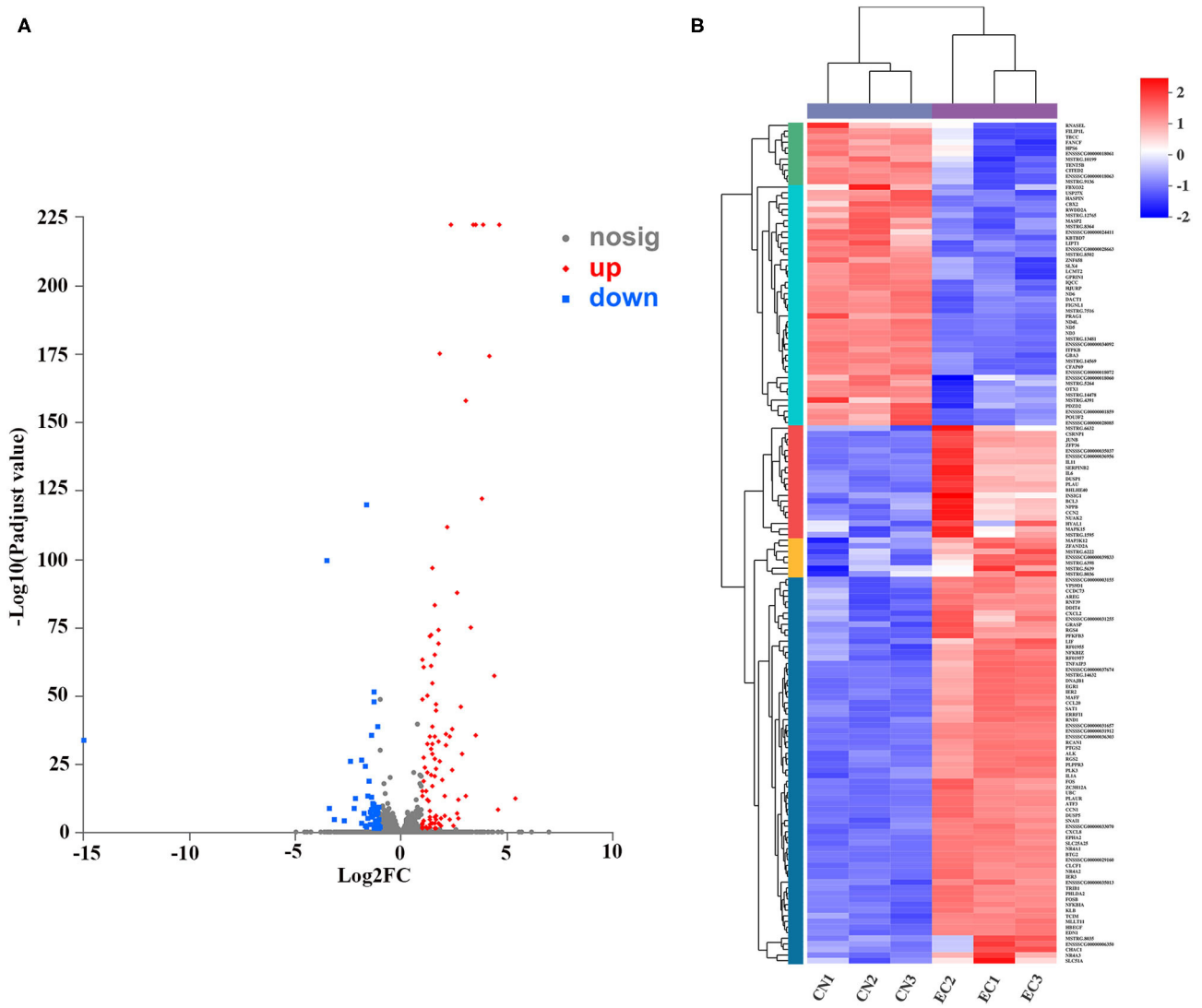

FIGURE 4 | Identification and expression of DEGs. **(A)** Volcano plot of DEGs between CN and EC groups. X-axis represented fold change of expression of DEGs, and Y-axis represented statistical significance of fold change. Each point represented a DEG. Red dots represented significantly upregulated DEGs; blue dots represented significantly downregulated genes; gray dots represented insignificantly DEGs. **(B)** Cluster heatmap of DEGs. Rows and columns represented genes and samples. Legend represented Log_2FC of gene abundance. Red and blue indicated high and low expression of DEGs, respectively.

categories, including "intracellular trafficking, secretion, and vesicular transport" (class U; 9 genes), "post-translational modification, protein turnover, chaperones" (class O; 8 genes), "translation, ribosomal structure, and biogenesis" (Class J; 7 genes), "signal transduction mechanisms" (class T; 7 genes), "transcription" (class K; 6 genes), and so on (**Figure 3B**). According to the GO analysis, 96 of 134 EC-unique genes were assigned to 45 GO terms and were specific to the cellular process, cell, cell parts, and binding (**Figure 3C**). A total of 47 EC-unique genes were assigned to 86 second KEGG categories, mainly functioning in signal transduction, immune diseases, substance dependence, immune system, and translation (**Figure 3D**).

Analysis of Differentially Expressed Genes

A rigorous comparison at adjusted $P < 0.05$ and $\log_2FC \geq 1$ for upregulated genes or $\log_2FC \leq -1$ for downregulated genes using the DESeq method were carried out to identify the DEGs. The list of DEGs, along with their FCs and annotations, were presented in **Supplementary Table 5**. A total of 150 DEGs (131 referenced genes and 19 novel genes) between CN and EC groups were found, including 96 upregulated DEGs and 54 downregulated DEGs (**Figure 4A**). The hierarchical cluster heatmap showed that expression profiles of DEGs after ETEC infection were distinctly different (**Figure 4B**). The top 10 upregulated genes were *CCL20*, *NR4A1*, *NR4A3*, *FOSB*, *NR4A2*, *EGR1*, *FOS*, *RCAN1*, *DDIT4*, and *CXCL2*. The top 10

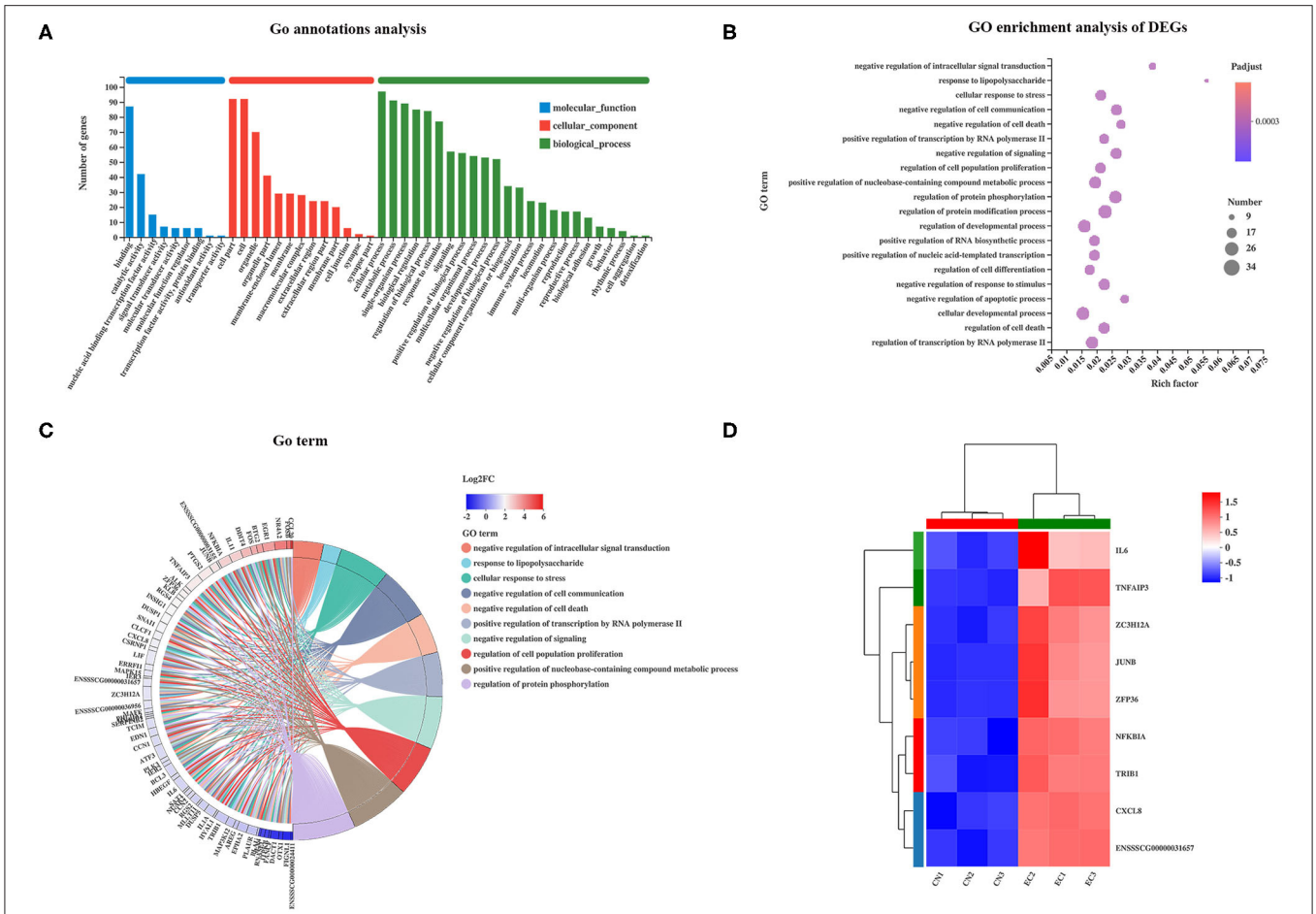

FIGURE 5 | GO enrichment analysis of DEGs. **(A)** GO functional annotation of DEGs. **(B)** GO enrichment analysis of DEGs. Enriched bubble chart showing enrichment of GO functions. X-axis represented enrichment ratio, and Y-axis represented top 20 GO terms. Number: Bubble size represented number of genes annotated to a KEGG Pathway. Padjust: color indicated enriched adjusted *p*-value. **(C)** GOChord plot of top 10 ranked GO terms. Chords indicated a detailed relationship between expression levels of DEGs (left semicircle perimeter) and their enriched GO terms (right semicircle perimeter). Genes are linked to their annotated terms *via* colored ribbons. **(D)** Heatmap of DEGs enriched in GO term "the response to LPS" showing the expression profile.

downregulated genes were *GBA3*, *POU3F2*, *CFAP69*, *MASP2*, *ND5*, *USP27X*, *FIGNL1*, *CBX2*, *KBTBD7*, and *LCMT2*.

Gene Ontology Function Analysis of Differentially Expressed Genes

Gene Ontology analysis was performed to characterize the functional terms of gene expression changes exposure to ETEC infection. Among the 131 referenced DEGs mentioned earlier, 113 were divided into three principal GO terms of level 2 (**Figure 5A**): MF (101 genes, 9 GO terms of level 2), CC (101 genes, 13 GO terms of level 2), and BP (101 genes, 24 GO terms of level 2). The DEGs assigned to the cellular process (97 genes) occupied the maximum proportion, followed by that assigned to cell (92 genes), cell part (92 genes), and metabolic process (91 genes). The GO enrichment analysis was performed at the level of adjusted $P < 0.05$. The top 20 ranked GO terms of DEGs are shown in **Figure 5B**. The response to LPS and negative regulation of intracellular signal transduction terms classified into BP class occupied the strongest enrichment degrees. The nine DEGs encoding NF-κB inhibitor alpha, tribbles pseudokinase 1, tumor necrosis factor (TNF) alpha-induced protein 3, C-X-C motif chemokine ligand 8, AP-1 transcription factor subunit JunD proto-oncogene and JunB proto-oncogene, ZFP36 ring finger protein, zinc finger CCCH-type containing 12A, and IL-6 were directly related to response to LPS and were unregulated in the EC group (**Figures 5C,D**). The regulation of protein modification process term (34 genes) contained the most abundant DEGs, followed by cellular developmental process (32 genes), and regulation of developmental process (31 genes).

Kyoto Encyclopedia of Genes and Genomes Pathway Analysis of Differentially Expressed Genes

Of 131 referenced DEGs, 55 upregulated and 15 downregulated DEGs were annotated to 152 second KEGG categories. The KEGG pathways enriched in the upregulated DEGs were mainly

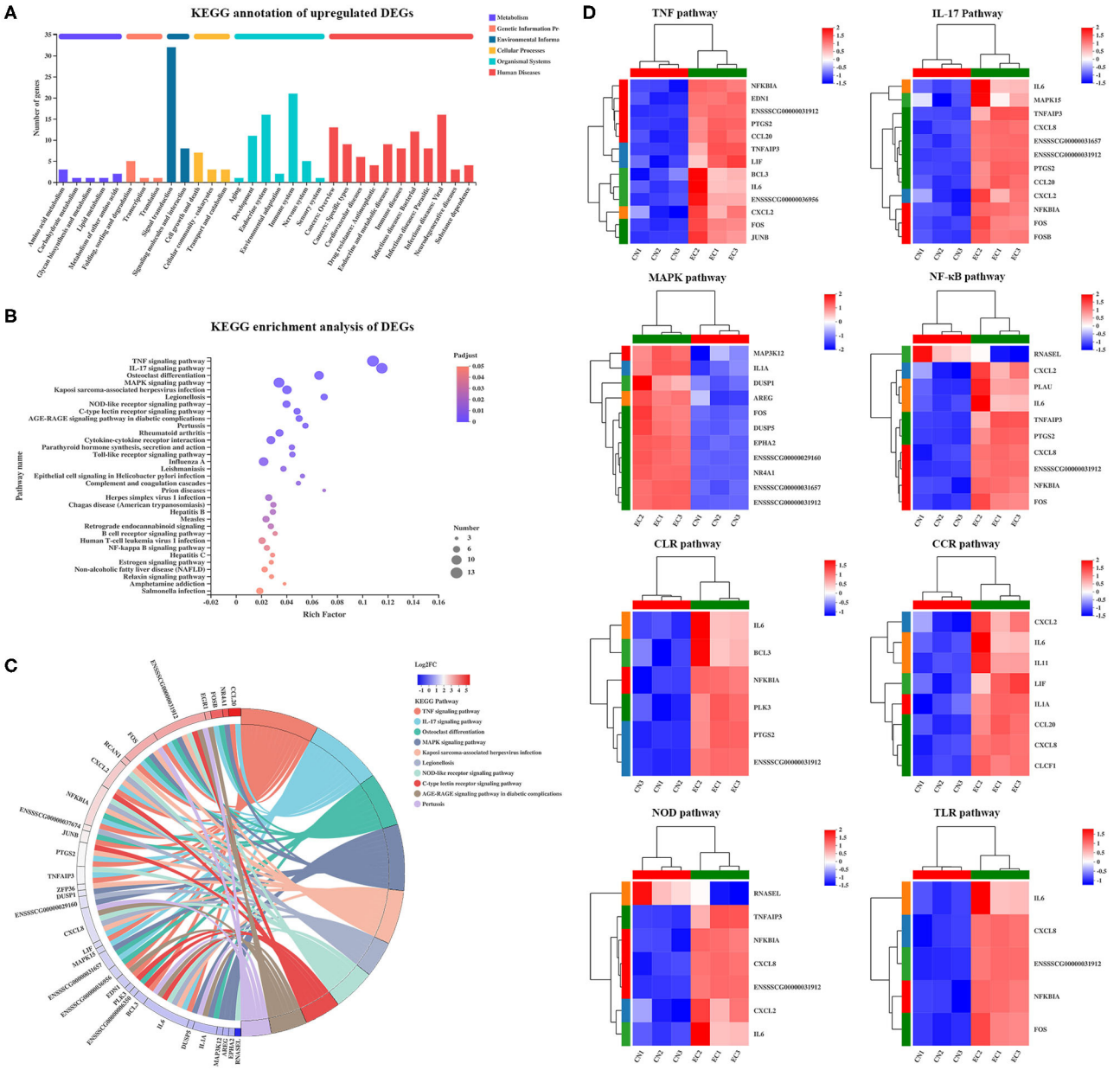

FIGURE 6 | KEGG enrichment analysis of DEGs. **(A)** KEGG pathway annotation of DEGs. **(B)** KEGG enrichment analysis of DEGs. Enriched bubble chart showing enrichment of KEGG pathways. X-axis represented enrichment ratio, and Y-axis represented top 20 KEGG pathways. Number: Bubble size represented number of genes annotated to a KEGG Pathway. Padjust: color indicated enriched adjusted *p*-value. **(C)** KEGGChord plot of top 10 ranked KEGG pathways. Chords indicated a detailed relationship between expression levels of DEGs (left semicircle perimeter) and their enriched KEGG pathways (right semicircle perimeter). Genes are linked to their annotated terms *via* colored ribbons. **(D)** Heatmap of DEGs enriched in immune response-related KEGG pathways showing expression profile in CN and EC groups.

specific to signal transduction (32 genes) and immune system (21 genes), and the KEGG pathways enriched in the downregulated DEGs were mainly specific to environmental adaptation (four genes) and energy metabolism (four genes) (**Figure 6A**). Kyoto Encyclopedia of Genes and Genomes Pathway enrichment analysis was performed to identify differential genes-related signal transduction and biochemical metabolic pathways. As a result, a total of 33 KEGG pathways were significantly enriched and were mainly involved in the immune response. Among these pathways, the TNF (adjusted *P*-value of $2.52E^{-11}$), IL-17 (adjusted *P*-value of $5.29E^{-11}$), and MAPK (adjusted *P*-value of $9.06E^{-5}$) signaling pathways possessed the highest rich factor (**Figure 6B**). Besides, some immune response-associated KEGG pathways were also enriched, including

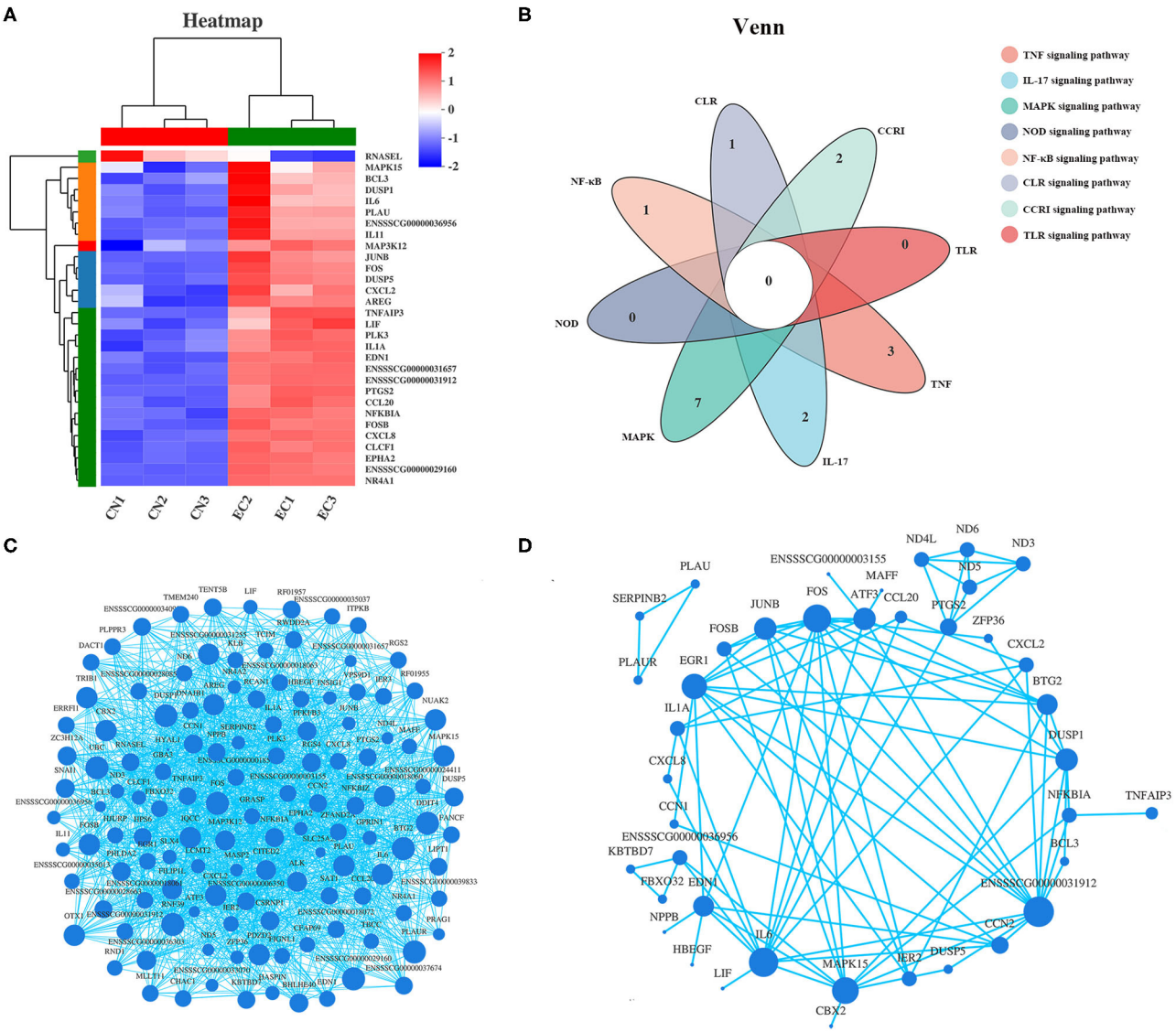

FIGURE 7 | Expression pattern of "core DEGs." **(A)** Heatmap of "core DEGs" showing expression profile in CN and EC groups. **(B)** Venn diagram of "core DEGs" enriched in immune response-related pathways. **(C)** Correlation analysis and **(D)** protein–protein interaction of gene expression of 131 referenced DEGs providing a rationale for functional significance of "core DEGs." Size of each node corresponded to number of connections (degree).

NLR (adjusted *P*-value of $6.61E^{-5}$), C-type lectin receptor (CLR) (adjusted *P*-value of $2.56E^{-5}$), cytokine–cytokine receptor interaction (adjusted *P*-value of $2.52E^{-11}$), TLR (adjusted *P*-value of $4.63E^{-4}$), and NF-κB (adjusted *P*-value of $6.4E^{-3}$) signaling pathways. Furthermore, the DEGs mapped to the immune response-associated KEGG pathways mentioned earlier and their expression patterns were identified (**Figure 6C**). Of the 131 DEGs, a total of 30 DEGs were involved in the immune response-associated KEGG pathways discussed earlier (**Figure 6D**), including TNF (13 genes), IL-17 (12 genes), MAPK (11 genes), NLR (7 genes), CLR (8 genes), cytokine–cytokine receptor interaction (8 genes), TLR (5 genes), and NF-κB (5 genes) signaling pathways. These 30 "core DEGs" determined the IPEC-J2 cell immune response to ETEC infection.

Correlation Analysis of Expression of "Core Differentially Expressed Genes" and Protein–Protein Interaction

Among the 30 "core DEGs," only the *RNAsel* gene encoding ribonuclease L was downregulated, and the other 29 genes were upregulated after ETEC infection (**Figure 7A** and **Supplementary Table 6**). According to the Venn diagram (**Figure 7B**), some "core DEGs" were directly related to several inflammatory signaling pathways, whereas some were assigned

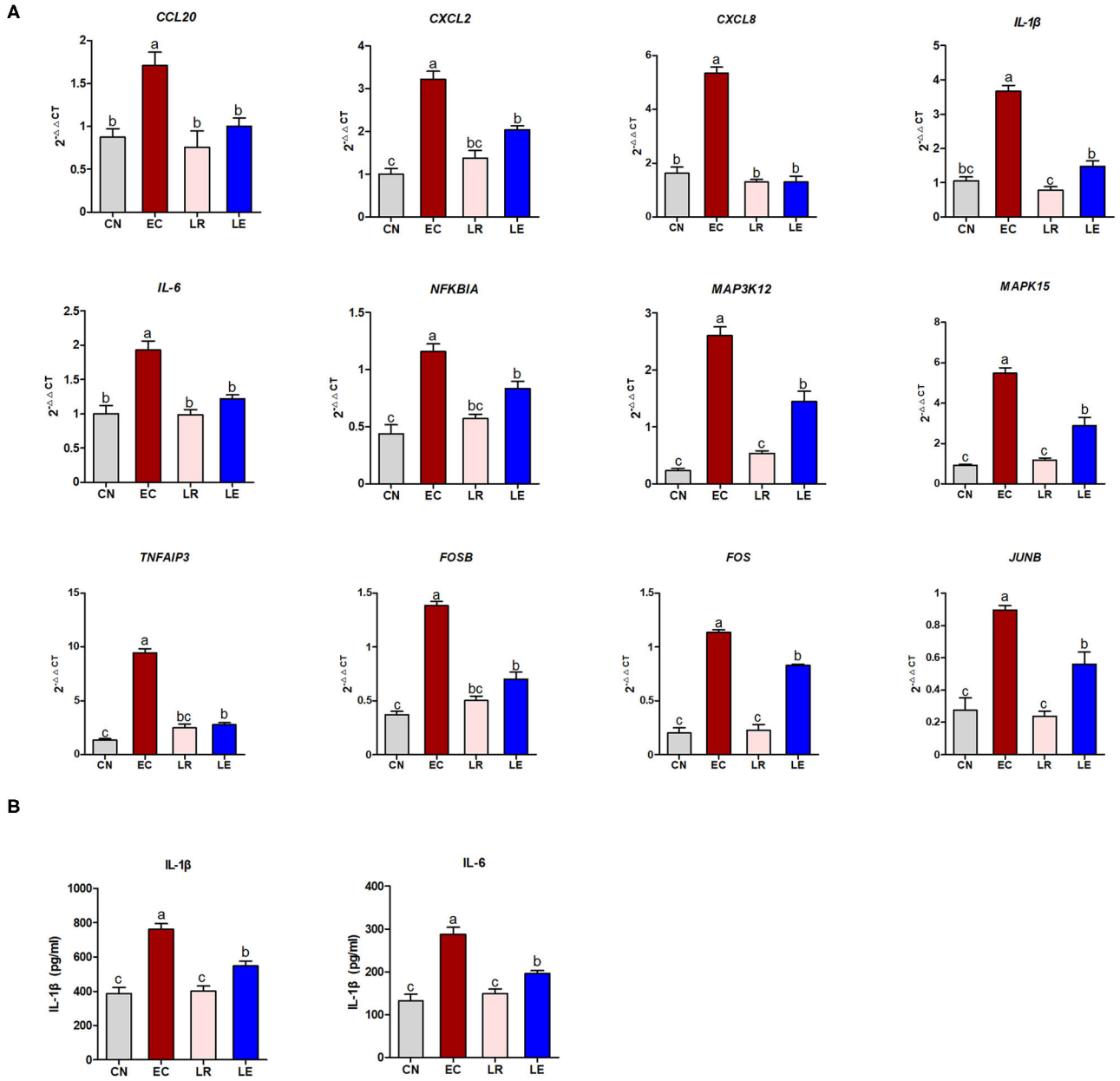

FIGURE 8 | qRT-PCR and ELISA validation of selected DEGs. **(A)** qRT-PCR was performed to validate immune response-related 12 selected DEGs. **(B)** ELISA was performed to measure concentration of IL-1β and IL-6.

to the specific signaling pathways. For example, two genes (*FOS* and ENSSSCG00000031912) participated in ETEC-induced activation of TNF, IL-17, and MAPK signaling pathways. Five genes (*NFKBIA*, *FOS*, *CXCL8*, *IL-6*, and ENSSSCG00000031912) were involved in the TLR and NF-κB signaling pathways. No gene was related to all inflammatory signaling pathways. Correlation analysis of gene expression in the 131 DEGs provided a rationale for the functional significance of "core DEGs" (**Figure 7C**). Some genes in the "core DEGs," such as *MAPK15*, *IL-6*, *CXCL2*, *NFKBIA*, *FOS*, and *TNFAIP3*, had the strongest correlation with other genes, indicating that the "core DEGs" had a coordinating function in the J2 cell response to ETEC infection. Protein products of DEGs among CN and EC groups identified multiple interactions with medium to high confidence (scores ranging from 0.4 to 1). The main protein interaction cluster derived from the 131 DEGs contained 40 nodes, each representing one protein and connected by 89 edges (**Figure 7D**). The *IL-6*, *FOS*, *MAPK15*, *JUNB*, *EDN1*, *DUSP1*, and the gene with unknown function (gene id: ENSSSCG00000031912) had the highest scores for betweenness

centrality, indicating they were most important for connections with other proteins.

Quantitative Real-Time Polymerase Chain Reaction and Enzyme-Linked Immunosorbent Assay Validation of "Core Differentially Expressed Genes"

According to the KEGG enrichment analysis, correlation analysis of gene expression, and PPI results, 12 "core DEGs" (*CCL20*, *CXCL2*, *CXCL8*, *IL-1β*, *IL-6*, *NFKBIA*, *MAP3K12*, *MAPK15*, *TNFAIP3*, *FOSB*, *FOS*, and *JUNB*) involving the inflammatory signaling pathways were chosen for qRT-PCR to validate the RNA-seq results. The results showed that the differential expression patterns of the 12 "core DEGs" were in accord with those detected by RNA-seq analysis (**Figure 8A**), indicating that the RNA-seq data could reliably reflect the alteration of gene expression. The operational errors in experimental treatments may result in differences in FC expression.

To further validate whether these "core DEGs" were the targets in controlling ETEC infection, the J2 cells were pre-incubated with probiotic *L. reuteri* BP325, followed by ETEC infection. **Figure 8A** shows that pretreatment with probiotic *L. reuteri* BP325 significantly attenuated the ETEC-induced increased mRNA expression in the 12 "core DEGs." Furthermore, pretreatment with probiotic *L. reuteri* BP325 significantly suppressed the elevated IL-1β and IL-6 levels in the supernatant of J2 cells caused by ETEC (**Figure 8B**).

DISCUSSION

Enterotoxigenic *Escherichia coli*'s are the most prevalent intestinal pathogen strains causing PWD in pigs (18). Understanding the pathogenic mechanism of ETEC is the primary task of prevention and control of PWD. The criteria set of *P*-value and FC significantly affects the number of DEGs and results of functional and pathway enrichment analysis. A previous study showed that 2,443 DEGs were found in J2 cells infected F4ab ETEC with under the criteria of $|FC| > 1.5$ and $P < 0.05$ with FDR < 0.252, whereas only 1,188 DEGs were found under the criteria of $|FC| > 2$ and $P < 0.05$ (9). This study was attempted to identify the main response pathways induced by ETEC as prevention targets in the future, and thus a rigorous comparison at $|FC| \geq 2$ and $P < 0.05$ with FDR < 0.05 was carried out. A total of 96 upregulated and 54 downregulated DEGs mainly functioned in response to LPS and negative regulation of intracellular signal transduction terms. Pathway enrichment analysis revealed that the DEGs were mostly enriched in TNF, IL-17, and MAPK signaling pathways, followed by immune response-associated NLR, CLR, cytokine–cytokine receptor interaction, TLR, and NF-κB signaling pathways. Of 131 referenced DEGs, 30 DEGs were involved in the immune response-related pathways discussed earlier, namely "core DEGs," and could represent the target molecules for the prevention and control of enteric ETEC infection. Correlation analysis of gene expression and PPI showed that IL-6 was located in the center of the protein interaction network, with the most connections with other proteins. Furthermore, the RNA-seq data were validated using qRT-PCR and ELISA methods. Finally, we verified the potential of the DEGs as targets of prevention and control for ETEC infection through pretreating J2 cells with a probiotic *L. reuteri* strain isolated from a healthy swine gut.

By comparing the gene expression level in CN and EC groups to produce a Venn diagram, we found 134 referenced genes uniquely present in the EC group. These EC-unique genes mainly functioned in cellular processes, such as nucleosome assembly, DNA packaging complex, or protein–DNA complex. Nucleosomes serve as the repeating units of cellular chromatin and play an important role in innate immune responses (19). Physiologically, nucleosome assembly is typically associated with DNA replication. It was reported that adenovirus-encoding protein VII interacts with cellular chromatin and binds nucleosomes, leading to sequestration of the high-mobility group protein B family members and abrogation of immune responses (20). These EC-unique gene functions may represent an immune evasion strategy of pathogens in which nucleosome binding is exploited to control the immune response.

Gene Ontology enrichment analysis of 131 referenced DEGs revealed the regulation of protein modification process term (34 genes) contained the most abundant DEGs, whereas the response to LPS and negative regulation of intracellular signal transduction terms classified into BP class occupied the strongest enrichment degrees. Comparable studies have shown that ETEC induced typical immune-related signaling pathways in porcine IECs, but the extent of the inflammatory response is different due to the difference in ETEC strain, infection time, infection concentration, and cell lines. The cell junction organization and extracellular matrix organization terms are enriched in the DEGs of ETEC strain 11501-infected IPEC-1 cells (21).

By KEGG analysis, 33 KEGG pathways enriched were mainly involved in the immune response. Toll-like receptor, NF-κB, and TNF signaling pathways were significantly enriched in the EC group. Toll-like receptor signaling pathway is crucial for the regulation and activation of numerous pro-inflammatory molecules. *Escherichia coli* LPS binding to TLR4 promotes activation of downstream TRIF-dependent and MyD88-dependent pathways, which in turn induces production of a cascade of activated molecules, such as NF-κB, AP-1, and inflammatory cytokines (22). Consistent with the present study, enriched TLR and NF-κB signaling pathways are also found in porcine IECs infected with various ETEC strains (9, 21). NF-κB contains a family of transcription factors, which functions in regulating various biological responses, including proliferation, cell apoptosis, and invasiveness. Phosphorylated IκB (an inhibitor of p65) activates p65 and induces the activation of NF-κB. In our study, *UBC* encoding ubiquitin C and *TNFAIP3* encoding TNF alpha-induced protein 3 were significantly regulated after ETEC infection. Ubiquitin is a highly conserved protein, functioning as a tag in the selective proteolysis of 26S proteasome to abnormal proteins. UBC serves as an intermediary molecule in the activation of NF-κB signaling by TNF (23). UBS could modify many cytosolic proteins recruited by TNF/TNF-R1 and then regulates the activity of the NF-κB

pathway. These data indicate that ETEC may modulate the TLR and NF-κB pathways *via* TNF-UBC pathways.

C-type lectin receptor constitutes a large superfamily of proteins that act as pattern-recognition receptors for pathogen-derived carbohydrates (24). C-type lectin receptor pathway is enriched in the IPEC-1 cells infected with ETEC strain 11501 (21). Mitogen-activated protein kinase is a downstream cascade pathway of many growth-factor receptors (25), which is activated by a broad array of extracellular stimuli. Mitogen-activated protein kinase pathway regulates and participates in various BPs, such as immune response to pathogen infection and focal adhesion (26) that also controlling cell communication (27). In this study, *MAP3K12* and *MAPK15* genes were related to the enriched MAPK pathway. *MAP3K12* and *MAPK15* genes are associated with p38 and ERK MAPK signaling pathways, respectively. MAP3K21 is a negative regulator of TLR4 signaling (28). MAP3K21 is strongly correlated with F4ac ETEC-related diarrhea in pigs (14). Activation of p38 MAPK induces phosphorylation of c-Jun and promotes its transactivation activity; in turn, c-Jun combines to target gene promoters as heterodimers, AP-1, with c-Fos (29). ERK MAPK pathway mediates the production of pro-inflammatory cytokine IL-8, IL-1β, and TNF-α *via* TLR2/TLR4 (30).

IL-17 is a pro-inflammatory cytokine family and exerts unique functions to bridge the innate and adaptive immune systems (31). In the context of infectious diseases, IL-17 initiates innate repair responses and host defense against bacterial infections at the mucosa, but, intriguingly, upregulated production of IL-17 can also exacerbate the severity of some inflammation (32). Interest in the efficacy and safety of novel therapeutic strategies based around IL-17 dramatically increases (33). IL-17 family consists of six members: IL-17A, IL-17B, IL-17C, IL-17D, IL-17E (also called IL-25), and IL-17F (34). It is well known that IL-17A and IL-17F from T helper17 cells induce pro-inflammatory chemokines, cytokines, and antimicrobial peptides, such as calprotectin, β-defensin, and cathelicidins (35). IL-17B and IL-17F participate in the immune response to protect pigs against $F4^+$ ETEC infection and could aid in the design of future ETEC vaccines (36). IL-17C and its receptor IL-17RE are preferentially expressed in IECs and can be directly induced by bacteria (37). IL-17C can also trigger the production of inflammatory mediators, tight junctions, chemokines, and antimicrobial peptides, protecting host defense against microbial infection (38). LPS activation of TLR4 or flagellin activation of TLR5 can induce IL-17C production in small IECs (39, 40). Recently, Luo et al. reported that TLR5-mediated IL-17C expression in IECs enhances pig epithelial defense against $F4^+$ ETEC infection by inducing the expression of antimicrobial peptides and tight junctions (41). In this study, *NFKBIA*, *AP-1* (*FOS* and *FOSB*), pro-inflammatory cytokine *IL-6*, chemokine *CXCL2*, *CXCL8*, and *CCL20* were directly related to the IL-17 pathway. In the peripheral blood leukocytes, the recombinant IL-17C could activate the NF-κB signaling and strongly promote the expression of chemokines (CXCL8, CXCL12, and CXCL13), pro-inflammatory factors (TNF-α, IL-1β, IL-6, and IFN-γ), and antibacterial peptide hepcidin (42). RNA-seq showed that the IL-17 pathway is enriched in the chicken lungs co-infected with *Mycoplasma gallisepticum* and ETEC, and IL-17 and some inflammasome-related genes (CXCL1, CXCL2, CXCL8, NF-κB, and AP-1) are significantly upregulated (43). Our data illustrate the importance of the IL-17 pathway in the pathogenesis of ETEC.

Furthermore, of the 131 DEGs, a total of 30 DEGs were involved in the immune response-associated KEGG pathways discussed earlier. These 30 "core DEGs" determined the IPEC-J2 cell immune response to ETEC infection. Correlation analysis of gene expression results showed that some genes in the "core DEGs," such as *MAPK15*, *IL-6*, *CXCL2*, *NFKBIA*, *FOS*, and *TNFAIP3*, had the strongest correlation with other genes, indicating that the "core DEGs" had a coordinating function in the J2 cell response to ETEC infection. *IL-6* was identified as a differential node protein exerting the highest degree in the PPI network, which was likely to act as a key regulator in ETEC-mediated immune response in J2 cells. Besides, *FOS*, *MAPK15*, *JUNB*, *EDN1*, *DUSP1*, and the gene with unknown function (gene id: ENSSSCG00000031912) belonging to the 30 "core DEGs" had the highest scores for betweenness centrality, indicating they were most important for connections with other proteins. The FOS gene family consists of four members: FOS, FOSB, FOSL1, and FOSL2. These genes could encode leucine zipper proteins that can dimerize with proteins of the JUN family, thereby forming the transcription factor complex AP-1. Genes for AP-1 are immediate-early genes that regulate a wide range of physiological responses such as cell death, inflammation, and proliferation. In this study, FOS, FOSB, and JUNB genes were significantly upregulated and directly related to multiple enriched pathways, such as TLR, NF-κB, IL-17, MAPK, and TNF pathways, as shown by Venn analysis. Further qRT-PCR analysis validated the RNA-seq data. Our findings indicate that immune response-related signaling pathways mediated by nuclear transcription factor AP-1 and NF-κB determine the fate of ETEC-infected J2 cells and may also be the targets for further prevention and control.

The main strategies for preventing and controlling intestinal infection involve the overuse and misuse of antibiotics, which leads to the development of antibiotic resistance to commensal and opportunistic bacteria in both animals and humans. With China's ban on the addition of non-therapeutic antibiotics to animal feeds since January 1, 2020, the development of alternatives to conventional antibiotics is urgent. Probiotics are defined as "live microorganisms, which when administered in adequate amounts confer a health benefit to the host;" therefore, they represent a promising alternative to antibiotics for controlling enteric infections. Probiotic *Lactobacillus* is a major component of the gut microbiota and can protect the host against enteric pathogens through modulation of both local and systemic host immune responses (44, 45). In this study, we explored the regulatory effect of *L. reuteri* on the targeted genes and immune-related pathways obtained by RNA-seq. qRT-PCR resulted showed that ETEC infection significantly increased the expression of *CCL20*, *CXCL2*, *CXCL8*, *AP-1*, *IL-1*, *IL-6*, *IL-11*, *NFKBIA*, *MAP3K12*, *MAPK15*, *PTGS2*, and *TNFAIP3*, which pretreatment with *L. reuteri* inhibited these increases. *Lactobacillus reuteri* also attenuated the production of IL-6 induced by ETEC in the supernatant of J2 cells. The previous

study using microarray analysis reported that *L. jensenii* TL2937 exerts anti-inflammatory immunobiotics for the prevention of inflammatory intestinal disorders in pigs by inhibiting the ETEC-induced high expression of chemokines (*CCL8*, *CXCL5*, *CXCL9*, *CXCL10*, and *CXCL11*) (46). *Lactobacillus rhamnosus* ATCC 7469 protects IECs from ETEC-induced damage, partly through the anti-inflammatory response involving synergism between TLR2 and nucleotide-binding and oligomerization domain 1 (47). Our previous study also showed that *L. rhamnosus* GR-1 ameliorates *E. coli*-induced inflammation and cell damage *via* attenuation of NLR NLRP3 and NLRC4 inflammasome activation (48, 49). Swine-derived probiotic *Lactobacillus plantarum* modulates porcine intestinal endogenous host defense peptide synthesis through TLR2/MAPK/AP-1 signaling pathway (50). Our data suggest that immune response-related signaling pathways obtained by RNA-seq represent the targets for preventing and controlling enteric ETEC infection in pigs.

In conclusion, ETEC infection elicits a strong immune response of porcine IECs, which is a result of the cooperation of multiple signaling pathways, including TNF, IL-17, MAPK, NF-κB, NLR, CLR, TLR, and cytokine–cytokine receptor interaction signaling pathways. Some key node genes, especially the nuclear transcription factor AP-1 and NF-κB, participate in the immune response to ETEC infection through an integral signal cascade and can be target molecules for prevention and control of enteric infection by probiotics.

DATA AVAILABILITY STATEMENT

The raw transcriptome data have been deposited in the US National Center for Biotechnology Information Sequence Read Archive database under accession no. SRR13291685–SRR13291693.

ETHICS STATEMENT

The animal study was reviewed and approved by the Animal Care and Use Committee of Beijing University of Agriculture.

AUTHOR CONTRIBUTIONS

QW, D-FC, Y-HZhu, and Y-HZhang: conceived and designed the experiments and prepared the manuscript. J-XL, X-YC, PC, Y-DW, T-JS, ML, and R-YX: performed the RNA extraction, qRT-PCR, and ELISA. QW, D-FC, Y-HZhu, and Y-HZhang: performed the analysis of data. All authors contributed to the article and approved the submitted version.

FUNDING

This work was supported financially by the General Projects of Beijing Municipal Education Commission Science and Technology Plan (project no. KM202010020009), Undergraduate Scientific Research Project of Cross-Training Program of High-Level Talents in Beijing Universities (project no. PXM2020_014207_000009), Beijing Innovation Consortium of Swine Research System (project no. BAIC02), Research Project for Youth Teachers of Beijing University of Agriculture (project no. SXQN201904), and National Natural Science Foundation of China (project no. 31873034).

SUPPLEMENTARY MATERIAL

The Supplementary Material for this article can be found online at: https://www.frontiersin.org/articles/10.3389/fvets.2021.677897/full#supplementary-material

Supplementary Figure 1 | Saturation curve of sequencing of each sample. Each color line represented the saturation curve of gene expression at different expression levels in the sample.

Supplementary Figure 2 | Classification of new transcripts. New transcripts were classified according to the overlapping relationship between spliced transcripts and known transcripts. The percentage of new transcripts was shown.

Supplementary Figure 3 | Analysis of novel gene expression and functional annotation. **(A)** The number of genes annotated using KEGG, GO, Pfam, Swiss-Prot, COG, and NR datasets. **(B)** COG, **(C)** GO, and **(D)** KEGG classifications of novel genes were summarized.

Supplementary Table 1 | Sequences of oligonucleotide primers used for real-time PCR, length of the respective PCR product, and gene accession number.

Supplementary Table 2 | Statistics of filtered transcriptome data.

Supplementary Table 3 | Statistics of comparing with reference genome.

Supplementary Table 4 | Statistical table of functional annotation of genes and transcripts.

Supplementary Table 5 | Annotation of DEGs between CON and LPS groups.

Supplementary Table 6 | Expression of 30 "core DEGs" involved in inflammatory signaling pathways.

REFERENCES

1. Khalil IA, Troeger C, Blacker BF, Rao PC, Brown A, Atherly DE, et al. Morbidity and mortality due to shigella and enterotoxigenic *Escherichia coli* diarrhoea: the global burden of disease study 1990–2016. *Lancet Infect Dis.* (2018) 18:1229–40. doi: 10.1016/S1473-3099(18)30475-4
2. Devriendt B, Verdonck F, Summerfield A, Goddeeris BM, Cox E. Targeting of *Escherichia coli* F4 fimbriae to Fcgamma receptors enhances the maturation of porcine dendritic cells. *Vet Immunol Immunopathol.* (2010) 135:188–98. doi: 10.1016/j.vetimm.2009.11.013
3. Wang W, Liu Y, Tang H, Yu Y, Zhang Q. ITGB5 plays a key role in *Escherichia coli* F4ac-induced diarrhea in piglets. *Front Immunol.* (2019) 10:2834. doi: 10.3389/fimmu.2019.02834
4. Garcia V, Gambino M, Pedersen K, Haugegaard S, Olsen JE, Herrero-Fresno A. F4- and F18-positive enterotoxigenic *Escherichia coli* isolates from diarrhea of postweaning pigs: genomic characterization. *Appl Environ Microbiol.* (2020) 86:e01913–20. doi: 10.1128/AEM.01913-20
5. Li Y, Qiu X, Li H, Zhang Q. Adhesive patterns of *Escherichia coli* F4 in piglets of three breeds. *J Genet Genomics.* (2007) 34:591–9. doi: 10.1016/S1673-8527(07)60067-8
6. Nguyen UV, Coddens A, Melkebeek V, Devriendt B, Goetstouwers T, Poucke MV, et al. High susceptibility prevalence for F4(+) and F18(+) *Escherichia coli* in Flemish pigs. *Vet Microbiol.* (2017) 202:52–7. doi: 10.1016/j.vetmic.2016.01.014
7. Luppi A, Gibellini M, Gin T, Vangroenweghe F, Vandenbroucke V, Bauerfeind R, et al. Prevalence of virulence factors in enterotoxigenic *Escherichia coli*

isolated from pigs with post-weaning diarrhoea in Europe. *Porcine Health Manag.* (2016) 2:20. doi: 10.1186/s40813-016-0039-9
8. Wang M, Zeng Z, Jiang F, Zheng Y, Shen H, Macedo N, et al. Role of enterotoxigenic *Escherichia coli* prophage in spreading antibiotic resistance in a porcine-derived environment. *Environ Microbiol.* (2020) 22:4974–84. doi: 10.1111/1462-2920.15084
9. Zhou C, Liu Z, Jiang J, Yu Y, Zhang Q. Differential gene expression profiling of porcine epithelial cells infected with three enterotoxigenic *Escherichia coli* strains. *BMC Genomics.* (2012) 13:330. doi: 10.1186/1471-2164-13-330
10. Peterson LW, Artis D. Intestinal epithelial cells: regulators of barrier function and immune homeostasis. *Nat Rev Immunol.* (2014) 14:141–53. doi: 10.1038/nri3608
11. Hu MM, Shu HB. Cytoplasmic mechanisms of recognition and defense of microbial nucleic acids. *Annu Rev Cell Dev Biol.* (2018) 34:357–79. doi: 10.1146/annurev-cellbio-100617-062903
12. Afonina IS, Zhong Z, Karin M, Beyaert R. Limiting inflammation-the negative regulation of NF-kappaB and the NLRP3 inflammasome. *Nat Immunol.* (2017) 18:861–9. doi: 10.1038/ni.3772
13. Zhou M, Xu W, Wang J, Yan J, Shi Y, Zhang C, et al. Boosting mTOR-dependent autophagy via upstream TLR4-MyD88-MAPK signalling and downstream NF-kappaB pathway quenches intestinal inflammation and oxidative stress injury *EBio Med.* (2018) 35:345–60. doi: 10.1016/j.ebiom.2018.08.035
14. Wang W, Zhou C, Tang H, Yu Y, Zhang Q. Combined analysis of DNA methylome and transcriptome reveal novel candidate genes related to porcine *Escherichia coli* F4ab/ac-induced diarrhea. *Front Cell Infect Microbiol.* (2020) 10:250. doi: 10.3389/fcimb.2020.00250
15. Zhu C, Ye JL, Yang J, Yang KM, Chen Z, Liang R, et al. Differential expression of intestinal ion transporters and water channel aquaporins in young piglets challenged with enterotoxigenic *Escherichia coli* K88. *J Anim Sci.* (2017) 95:5240–52. doi: 10.2527/jas2017.1806
16. Li Q, Burrough ER, Gabler NK, Loving CL, Sahin O, Gould SA, et al. A soluble and highly fermentable dietary fiber with carbohydrases improved gut barrier integrity markers and growth performance in F18 ETEC challenged pigs. *J Anim Sci.* (2019) 97:2139–53. doi: 10.1093/jas/skz093
17. Trevisi P, Latorre R, Priori D, Luise D, Archetti I, Mazzoni M, et al. Effect of feed supplementation with live yeast on the intestinal transcriptome profile of weaning pigs orally challenged with *Escherichia coli* F4. *Animal.* (2017) 11:33–44. doi: 10.1017/S1751731116001178
18. Fairbrother JM, Nadeau E, Gyles CL. *E scherichia coli* in postweaning diarrhea in pigs: an update on bacterial types, pathogenesis, and prevention strategies. *Anim Health Res Rev.* (2005) 6:17–39. doi: 10.1079/AHR2005105
19. Smale ST, Tarakhovsky A, Natoli G. Chromatin contributions to the regulation of innate immunity. *Annu Rev Immunol.* (2014) 32:489–511. doi: 10.1146/annurev-immunol-031210-101303
20. Avgousti DC, Herrmann C, Kulej K, Pancholi NJ, Sekulic N, Petrescu J, et al. A core viral protein binds host nucleosomes to sequester immune danger signals. *Nature.* (2016) 535:173–7. doi: 10.1038/nature18317
21. Tkacikova L, Mochnacova E, Tyagi P, Kissova Z, Bhide M. Comprehensive mapping of the cell response to *E. coli* infection in porcine intestinal epithelial cells pretreated with exopolysaccharide derived from *Lactobacillus reuteri. Vet Res.* (2020) 51:49. doi: 10.1186/s13567-020-00773-1
22. Zughaier SM, Zimmer SM, Datta A, Carlson RW, Stephens DS. Differential induction of the toll-like receptor 4-MyD88-dependent and -independent signaling pathways by endotoxins. *Infect Immun.* (2005) 73:2940–50. doi: 10.1128/IAI.73.5.2940-2950.2005
23. Verhelst K, Verstrepen L, Carpentier I, Beyaert R. Linear ubiquitination in NF-kappaB signaling and inflammation: What we do understand and what we do not. *Biochem Pharmacol.* (2011) 82:1057–65. doi: 10.1016/j.bcp.2011.07.066
24. Mayer S, Raulf MK, Lepenies B. C-type lectins: their network and roles in pathogen recognition and immunity. *Histochem Cell Biol.* (2017) 147:223–37. doi: 10.1007/s00418-016-1523-7
25. Fang JY, Richardson BC. The MAPK signalling pathways and colorectal cancer. *Lancet Oncol.* (2005) 6:322–7. doi: 10.1016/S1470-2045(05)70168-6
26. Sompallae R, Stavropoulou V, Houde M, Masucci MG. The MAPK signaling cascade is a central hub in the regulation of cell cycle, apoptosis and cytoskeleton remodeling by tripeptidyl-peptidase II. *Gene Regul Syst Bio.* (2008) 2:253–265. doi: 10.4137/GRSB.S882
27. Zhou L, Chen J, Li Z, Li X, Hu X, Huang Y, et al. Integrated profiling of microRNAs and mRNAs: microRNAs located on Xq273 associate with clear cell renal cell carcinoma. *PLoS ONE.* (2010) 5:e15224. doi: 10.1371/journal.pone.0015224
28. Seit-Nebi A, Cheng W, Xu H, Han J. MLK4 has negative effect on TLR4 signaling. *Cell Mol Immunol.* (2012) 9:27–33. doi: 10.1038/cmi.2011.15
29. Jin YJ Ji Y, Jang YP, Choung SY. *Acer tataricum* subsp. *ginnala* inhibits skin photoaging via regulating MAPK/AP-1, NF-kappaB, and TGFbeta/Smad signaling in UVB-irradiated human dermal fibroblasts. *Molecules.* (2021) 26:662. doi: 10.3390/molecules26030662
30. Sun Z, Li Y, Chen H, Xie L, Xiao J, Luan X, et al. *Chlamydia trachomatis* glycogen synthase promotes MAPK-mediated proinflammatory cytokine production via TLR2/TLR4 in THP-1 cells. *Life Sci.* (2021) 271:119181. doi: 10.1016/j.lfs.2021.119181
31. Chamoun MN, Blumenthal A, Sullivan MJ, Schembri MA, Ulett GC. Bacterial pathogenesis and interleukin-17: interconnecting mechanisms of immune regulation, host genetics, and microbial virulence that influence severity of infection. *Crit Rev Microbiol.* (2018) 44:465–86. doi: 10.1080/1040841X.2018.1426556
32. Gaffen SL, Jain R, Garg AV, Cua DJ. The IL-23-IL-17 immune axis: from mechanisms to therapeutic testing. *Nat Rev Immunol.* (2014) 14:585–600. doi: 10.1038/nri3707
33. Puig L. Brodalumab: the first anti-IL-17 receptor agent for psoriasis. *Drug Today.* (2017) 53:283–97. doi: 10.1358/dot.2017.53.5.2613690
34. Song X, He X, Li X, Qian Y. The roles and functional mechanisms of interleukin-17 family cytokines in mucosal immunity. *Cell Mol Immunol.* (2016) 13:418–31. doi: 10.1038/cmi.2015.105
35. Das S, Khader S. Yin and yang of interleukin-17 in host immunity to infection. *F1000Res.* (2017) 6:741. doi: 10.12688/f1000research.10862.1
36. Luo Y, Van Nguyen U. de la Fe Rodriguez PY, Devriendt B, Cox E. F4+ ETEC infection and oral immunization with F4 fimbriae elicits an IL-17-dominated immune response. *Vet Res.* (2015) 46:121. doi: 10.1186/s13567-015-0264-2
37. Song X, Gao H, Lin Y, Yao Y, Zhu S, Wang J, et al. Alterations in the microbiota drive interleukin-17C production from intestinal epithelial cells to promote tumorigenesis. *Immunity.* (2014) 40:140–52. doi: 10.1016/j.immuni.2013.11.018
38. Huang J, Meng S, Hong S, Lin X, Jin W, Dong C. IL-17C is required for lethal inflammation during systemic fungal infection. *Cell Mol Immunol.* (2016) 13:474–83. doi: 10.1038/cmi.2015.56
39. Song X, Zhu S, Shi P, Liu Y, Shi Y, Levin SD, et al. IL-17RE is the functional receptor for IL-17C and mediates mucosal immunity to infection with intestinal pathogens. *Nat Immunol.* (2011) 12:1151–8. doi: 10.1038/ni.2155
40. Im E, Jung J, Rhee SH. Toll-like receptor 5 engagement induces interleukin-17C expression in intestinal epithelial cells. *J Interferon Cytokine Res.* (2012) 32:583–91. doi: 10.1089/jir.2012.0053
41. Luo Y, Xu J, Zhang C, Jiang C, Ma Y, He H, et al. Toll-like receptor 5-mediated IL-17C expression in intestinal epithelial cells enhances epithelial host defense against F4+ ETEC infection. *Vet Res.* (2019) 50:48. doi: 10.1186/s13567-019-0665-8
42. Ding Y, Ao J, Chen X. Comparative study of interleukin-17C (IL-17C) and IL-17D in large yellow croaker *Larimichthys crocea* reveals their similar but differential functional activity. *Dev Comp Immunol.* (2017) 76:34–44. doi: 10.1016/j.dci.2017.05.014
43. Wu Z, Ding L, Bao J, Liu Y, Zhang Q, Wang J, et al. Co-infection of *Mycoplasma gallisepticum* and *Escherichia coli* triggers inflammatory injury involving the IL-17 signaling pathway, *Front Microbiol.* (2019) 10:2615. doi: 10.3389/fmicb.2019.02615
44. Zhang W, Zhu YH, Yang GY, Liu X, Xia B, Hu X, et al. *Lactobacillus rhamnosus* GG affects microbiota and suppresses autophagy in the intestines of pigs challenged with *Salmonella Infantis. Front Microbiol.* (2017) 8:2705. doi: 10.3389/fmicb.2017.02705
45. Zhang W, Wu Q, Zhu Y, Yang G, Yu J, Wang J, et al. Probiotic *Lactobacillus rhamnosus* GG induces alterations in ileal microbiota with associated $CD3^{-}CD19^{-}T\text{-}bet^{+}IFN\text{-}\gamma^{+/-}$ cell subset homeostasis in pigs challenged with *Salmonella enterica* serovar 4,[5],12:i: *Front Microbiol.* (2019) 10:977. doi: 10.3389/fmicb.2019.00977

46. Kobayashi H, Albarracin L, Sato N, Kanmani P, Kober AK, Ikeda-Ohtsubo W, et al. Modulation of porcine intestinal epitheliocytes immunetranscriptome response by *Lactobacillus jensenii* TL2937. *Benef Microbes*. (2016) 7:769–782. doi: 10.3920/BM2016.0095
47. Zhang W, Zhu YH, Yang JC, Yang GY, Zhou D, Wang JF, et al. selected *Lactobacillus rhamnosus* strain promotes EGFR-independent Akt activation in an enterotoxigenic *Escherichia coli* K88-infected IPEC-J2 cell model. *PLoS ONE*. (2015) 10:e0125717. doi: 10.1371/journal.pone.0125717
48. Wu Q, Liu MC, Yang J, Wang JF, Zhu YH. *Lactobacillus rhamnosus* GR-1 ameliorates *Escherichia coli*-induced inflammation and cell damage via attenuation of ASC-independent NLRP3 inflammasome activation. *Appl Environ Microbiol*. (2016) 82:1173–82. doi: 10.1128/AEM.03044-15
49. Wu Q, Zhu YH, Xu J, Liu X, Duan C, Wang MJ, et al. *Lactobacillus rhamnosus* GR-1 ameliorates *Escherichia coli*-induced activation of NLRP3 and NLRC4 inflammasomes with differential requirement for ASC. *Front Microbiol*. (2018) 9:1661. doi: 10.3389/fmicb.2018.01661
50. Wang J, Zhang W, Wang S, Liu H, Zhang D, Wang Y, et al. Swine-derived probiotic *Lactobacillus plantarum* modulates porcine intestinal endogenous host defense peptide synthesis through TLR2/MAPK/AP-1 signaling pathway. *Front Immunol*. (2019) 10:2691. doi: 10.3389/fimmu.2019.02691

Conflict of Interest: The authors declare that the research was conducted in the absence of any commercial or financial relationships that could be construed as a potential conflict of interest.

Publisher's Note: All claims expressed in this article are solely those of the authors and do not necessarily represent those of their affiliated organizations, or those of the publisher, the editors and the reviewers. Any product that may be evaluated in this article, or claim that may be made by its manufacturer, is not guaranteed or endorsed by the publisher.

frontiers in Microbiology

ORIGINAL RESEARCH
published: 19 August 2021
doi: 10.3389/fmicb.2021.690091

Gut and Vagina Microbiota Associated With Estrus Return of Weaning Sows and Its Correlation With the Changes in Serum Metabolites

Jia Zhang†, Min Liu†, Shanlin Ke, Xiaochang Huang, Shaoming Fang, Maozhang He, Hao Fu, Congying Chen and Lusheng Huang**

State Key Laboratory of Pig Genetic Improvement and Production Technology, Jiangxi Agricultural University, Nanchang, China

More and more studies have indicated that gut microbiota takes part in the biosynthesis and metabolism of sex hormones. Inversely, sex hormones influence the composition of gut microbiota. However, whether microbiota in the gut and vagina is associated with estrus return of weaning sows is largely unknown. Here, using 16S rRNA gene sequencing in 158 fecal and 50 vaginal samples, we reported the shifts in the gut and vaginal microbiota between normal return and non-return sows. In fecal samples, *Lactobacillus* and S24-7 were enriched in normal return sows, while *Streptococcus luteciae*, Lachnospiraceae, *Clostridium*, and *Mogibacterium* had higher abundance in non-return sows. In vaginal swabs, the operational taxonomic units (OTUs) annotated to Clostridiales, Ruminoccaceae, and *Oscillospira* were enriched in normal return sows, while those OTUs annotated to *Campylobacter*, *Anaerococcus*, *Parvimonas*, *Finegoldia*, and *Dorea* had higher abundances in non-return sows. Co-abundance group (CAG) analysis repeated the identification of the bacterial taxa associated with the estrus return of weaning sows. The predicted functional capacities in both gut and vaginal microbiome were changed between normal return and non-return sows. Serum metabolome profiles were determined by non-targeted metabolome analysis in seven normal return and six non-return sows. The metabolite features having higher abundance in normal return sows were enriched in the pathways Steroid hormone biosynthesis, Starch and sucrose metabolism, Galactose metabolism, and Vitamin B6 metabolism, while the metabolite features belonging to organic acids and derivatives, indoles and derivatives, sulfoxides, and lignans and neolignans had significantly higher abundance in non-return sows. Correlation analysis found that the changes in gut microbiota were associated with the shifts of serum metabolites and suggested that certain bacteria might affect estrus return of weaning sow through serum metabolites. These findings may provide new insights for understanding the role of the gut and vaginal microbiota in sow return to estrus after weaning.

Keywords: return to estrus, fecal microbiota, vaginal microbiota, sow, 16S rRNA gene sequencing, serum metabolome

OPEN ACCESS

Edited by:
Jing Wang,
Institute of Animal Husbandry and Veterinary Medicine, Beijing Academy of Agriculture and Forestry Sciences, China

Reviewed by:
Xin Wu,
Chinese Academy of Sciences (CAS), China
Xihong Zhou,
Institute of Subtropical Agriculture, Chinese Academy of Sciences, China
Jiangchao Zhao,
University of Arkansas, United States

****Correspondence:***
Congying Chen
chcy75@hotmail.com
Lusheng Huang
lushenghuang@hotmail.com

† These authors have contributed equally to this work

Specialty section:
This article was submitted to Systems Microbiology, a section of the journal Frontiers in Microbiology

Received: *02 April 2021*
Accepted: *28 July 2021*
Published: *19 August 2021*

Citation:
Zhang J, Liu M, Ke S, Huang X, Fang S, He M, Fu H, Chen C and Huang L (2021) Gut and Vagina Microbiota Associated With Estrus Return of Weaning Sows and Its Correlation With the Changes in Serum Metabolites. Front. Microbiol. 12:690091. doi: 10.3389/fmicb.2021.690091

INTRODUCTION

In the past decades, the reproductive performance of the pig has been improved dramatically. Weaned pigs per sow per year (PSY) in Denmark increased from 23.5 in 2000 to 33.6 in 2018 (Board, 2020). Among the reproduction traits of sows, delayed return to estrus or even non-return after weaning has been becoming one of the main problems influencing pig production. In the modern pig industry, more than 85% of sows will return to estrus within 7 days after weaning (Poleze et al., 2006; Leite et al., 2011). The interval from weaning to heat is a key indicator representing sow ability of return to reproduction after weaning and also a decisive factor affecting non-production days (NPDs) and therefore reducing PSY. The failed estrus return brings a big economic loss to the swine industry. The interval from weaning to estrus is affected by numerous factors, including nutrition, genetics, environment, management, weight loss, boar exposure, health, and mycotoxins (Levis and Hogg, 1989; Poleze et al., 2006). The heritability estimated for the interval from weaning to estrus in sows is low (0.07, 0.02, and 0.07 for the first three parities) (Leite et al., 2011), suggesting that genetics is not the major factor influencing the estrus return of weaning sows.

In recent years, more and more studies have reported the important roles of gut microbiota in pig production performances, e.g., growth, health, and even reproduction (Suo et al., 2012; Hermann-Bank et al., 2015; Ramayo-Caldas et al., 2016; Yang et al., 2018; Wang et al., 2019). Sow estrus is initiated by follicular development and the synthesis and release of sex hormones, especially estrogens. Studies have revealed that the gut microbial community plays an important role in estrogen metabolism. The use of antibiotics and the change of gut microbial community will affect host steroid hormone level in older adults (Adlercreutz et al., 1984). The decrease in the diversity of gut microbiota will impair the estrogen level (Baker et al., 2017). In humans, the systemic estrogens and estrogen metabolites are significantly affected by the composition of gut microbiota (Flores et al., 2012). In contrast, the changes of sex hormones affect the gut microbiota community in female mice (Acharya et al., 2019). Estrogen can mediate the changes of the gut microbiome in mice, which causes sex differences in obesity and metabolic syndrome (Kaliannan et al., 2018). Higher abundance of *Lactobacillus* was found in the fecal microbiota of the mice fed diet containing estrogenic isoflavones (Menon et al., 2013). To our knowledge, whether the interval from weaning to estrus is associated with the gut microbiome is largely unknown at present.

The microbiota in vagina may also relate to the reproductive performance of sows. The structure and composition of the vaginal and cervix microbiota will undergo a dramatic change in response to the pregnant condition of sows (Shuo, 2016). Miller et al. (2017) found that the bacterial composition in baboon vagina was changed profoundly under the different reproductive conditions and during ovarian cycle phases. Meanwhile, the vaginal microbiota has an important influence on human reproduction physiology including menstrual cycle (Henderson and Nibali, 2016). However, whether the vaginal microbiota is associated with the return of weaned sows is also unknown.

Therefore, in this study, we profiled the composition of gut and vaginal microbiota in more than 150 sows to analyze the relationship of the gut and vagina microbiota with sow non-return after weaning. Furthermore, we determined and compared serum metabolite profiles between normal estrus return and non-return sows to identify metabolite biomarkers associated with the failed estrus return. By integrating microbiota and metabolite data, we suggested that the changes in gut microbiota were associated with the shifts of serum metabolites and may further influence the interval from weaning to estrus.

MATERIALS AND METHODS

Experimental Animals and Sample Collection

A total of 158 Landrace × Yorkshire F1 sows were used in this study. Most of experimental sows were at the parity 2 (58 sows), 3 (40), 4 (26), and 5 (25). The other nine sows were at the parity 6–7. All experimental sows were housed in pens with concrete slatted floor, natural light, and power ventilation, and provided corn–soybean formula diets. Sows were fed two times per day. Water was *ad libitum* available from nipple drinkers. Fecal samples were manually collected from each animal's anus and dispensed in 2-ml tubes on the date of weaning. At the same time, a total of 50 vaginal samples were also collected from these 158 sows at the posterior region of the vagina by the sterile swabs. All samples were immediately frozen in liquid nitrogen, and stored at −80°C until use. The experimental sows had been observed estrus twice per day (8:00 a.m. and 4:00 p.m.) since their offspring were weaned at the age of 28 days. According to the interval from weaning to return to estrus, the 158 sows were classified into two groups: normal return group (144 feces samples and 39 vagina samples), sows in this group returned to estrus within 7 days after weaning; and non-return group (14 feces and 11 vaginal samples), sows in this group did not return to estrus in more than 14 days after weaning. All sows were healthy and did not receive probiotic or antibiotic therapy within 2 months of sample collection. A total of 13 blood samples were collected from the sows described above, including seven samples from normal return group, and six samples from non-return group. Serum was isolated from these 13 blood samples by centrifuging at 1500 × *g* (rcf) for 15 min and stored at −80°C until use.

Ethics Statement

All procedures involving experimental animals satisfied the requirement of the guidelines for the care and use of experimental animals established by the Ministry of Agriculture and Rural Affairs of China. This study was approved by the Animal Care and Use Committee (ACUC) at Jiangxi Agricultural University (No. JXAU2011-006).

Microbial DNA Extraction and 16S rRNA Gene Sequencing

Microbial DNA was extracted from feces and vaginal swab samples with the QIAamp DNA Stool Mini Kit (Qiagen,

Germany) following the manufacturer's manuals (McOrist et al., 2002). The concentration and integrity of DNA samples were measured by a Nanodrop-1000 (Thermo Fisher Scientific, United States) and 0.8% agarose gel electrophoresis. The barcode fusion primer 515F (5′-GTGCCAGCMGCCGCGGTAA-3′) and 806R (5′-GGACTACHVGGGTWTCTAAT-3′) were used to amplify the V4 hypervariable region of the 16S rRNA gene. After purification, the PCR products were used to construct the libraries and sequenced by the paired-end method on an Illumina MiSeq platform (Illumina, United States).

Sequencing Data Analysis

Raw data of 16S rRNA gene sequencing were cleaned by filtering low-quality reads and removing the primers and barcode sequences (Fadrosh et al., 2014). Tags were assembled from high-quality paired-end clean reads by FLASH (v.1.2.11) (Magoč and Salzberg, 2011). To avoid statistical bias caused by uneven sequencing depth, the sequencing data were rarefied to 24,913 tags for each fecal sample and 27,070 tags for each vaginal sample (the lowest number of tags per sample). Operational taxonomic units (OTUs) were clustered at the cutoff of 97% sequence identity using the USEARCH (v7.0.1090) (Majaneva et al., 2015). The taxonomic assignments of OTUs were performed using the RDP classifier program (v2.2) (Wang et al., 2007). The α-diversity including observed OTUs and Chao index was analyzed by Mothur (v.1.39.5) (Schloss et al., 2009). The β-diversity was analyzed by QIIME (v.1.9.1) (Caporaso et al., 2010). A normalized OTU abundance table was used for principal coordinate analysis (PCoA) based on weighted and unweighted UniFrac distances *via* Vegan package in R (Dixon, 2003). The effect of parity on gut and vagina microbial composition of sows was also evaluated by PCoA based on weighted UniFrac distances. The PICRUSt software (v.1.0.0) was used to predict the functional capacities of the gut microbiome (KEGG Orthology) from 16S rRNA gene sequencing data against the Greengenes database (Langille et al., 2013).

Comparisons of the α- and β-diversity of the gut microbiota between normal return and non-return sows were performed using the Wilcoxon rank-sum test and PREMANOVA. Permutation was set at 10,000 times. The significance threshold was set at p-value < 0.05. Linear discriminant analysis effect size (LEfSe) analysis was used to identify OTUs, genus, and KEGG pathways showing differential abundances between normal return and non-return sows with the standard parameters ($p < 0.05$ and $|\text{LDA}|$ score > 2.0) (Segata et al., 2011).

Construction of Co-abundance Groups (CAGs) of the Gut Microbiota

Microbes that likely work together to contribute to the same ecological function could be identified by clustering co-abundance groups (CAGs) based on their co-variation of abundance (Wu et al., 2021). We constructed CAGs of the gut microbiota in experimental sows. A total of 517 OTUs that existed in at least 20% of the tested samples were used for the construction of CAGs. The correlations among 517 OTUs were calculated by the SparCC algorithm *via* the SpiecEasi package in R (Kurtz et al., 2015). Only those OTUs with SparCC correlation scores greater than 0.2 were clustered into CAGs. The correlation values were converted to a correlation distance (1–correlation value), and the OTUs were clustered using the Ward clustering algorithm *via* WGCNA package in R (Langfelder and Horvath, 2008). Similar clusters were subsequently merged if the correlation between the CAG's eigenvectors exceeded 0.8. The CAG network was visualized in Cytoscape (v.3.7.2) (Shannon et al., 2003).

Determination of Serum Untargeted Metabolomic Profiling and Data Analysis

Serum untargeted metabolomic analysis was performed by UPLC-QTOF-MS (ultra-performance liquid chromatography method with quadrupole time-of-flight mass spectrometry). In brief, all serum samples were thawed at 4°C and precipitated using precool methanol (Merck Corporation, Germany) at 1:3 of serum:methanol at room temperature. The mixtures were vortexed for 1 min, and then incubated at −20°C for 20 min. After centrifuged at 15,000 × g (rcf) for 15 min at 4°C, the supernatants were transferred into clean EP tubes and dried using a vacuum evaporator. The samples were resolved in 150 μl of water:methanol (85%:15% v/v) and stored at 4°C until measurement. A standard quality control (QC) sample was prepared by mixing and blending equal volume of each of 13 tested serum samples.

The samples were run on a 100 mm × 2.1 mm Bridged ethyl hybrid (BEH) C18 UPLC column (Waters Corporation, United States) that was packed with 1.7-μm particles by using a gradient elution of water +0.1% formic acid and acetonitrile as mobile phases. The capillary voltage was set at 3.0 kV for positive electrospray ion mode (ES+) and 2.5 kV for negative electrospray ion mode (ES−). The source and desolvation temperature were set at 120 and 350°C, respectively. Leucine enkephalin was used as the lock mass (m/z 556.2771 in ES+, and 554.2615 in ES−) at a concentration of 100 ng/ml and a flow rate of 5 μl/min for all analyses. The serum samples were eluted at a flow rate of 0.3 ml/min and a column temperature of 40°C on ES+ model for 22 min and ES− model for 18 min.

Mass spectrometry analysis was performed in both ES+ and ES− models with Waters QTOF Premier (Waters Corporation, United States). The mass range was set at 50–1200 m/z in a scan time of 0.3 s and an interscan delay of 0.02 s. System control and data collection were performed by MassLynx software (Waters Corporation, United States). The Progenesis QI software (v2.0) (Non-linear Dynamics, United Kingdom) was used for non-targeted signal detection, signal integration and feature alignment (Rusilowicz, 2016). MetaScope embedded in the Progenesis QI was used to annotate metabolites not only based on neutral mass, isotope distribution and retention time, but also based on the collisional cross-sectional area and MS/MS fragmentation data in the HMDB database. Each retained peak was then normalized to the QC sample using MetNormalize (Shen et al., 2016). The relative RSD value of the metabolites in the QC samples was set at a threshold of 30% to standardize the reproducibility of the metabolomic datasets.

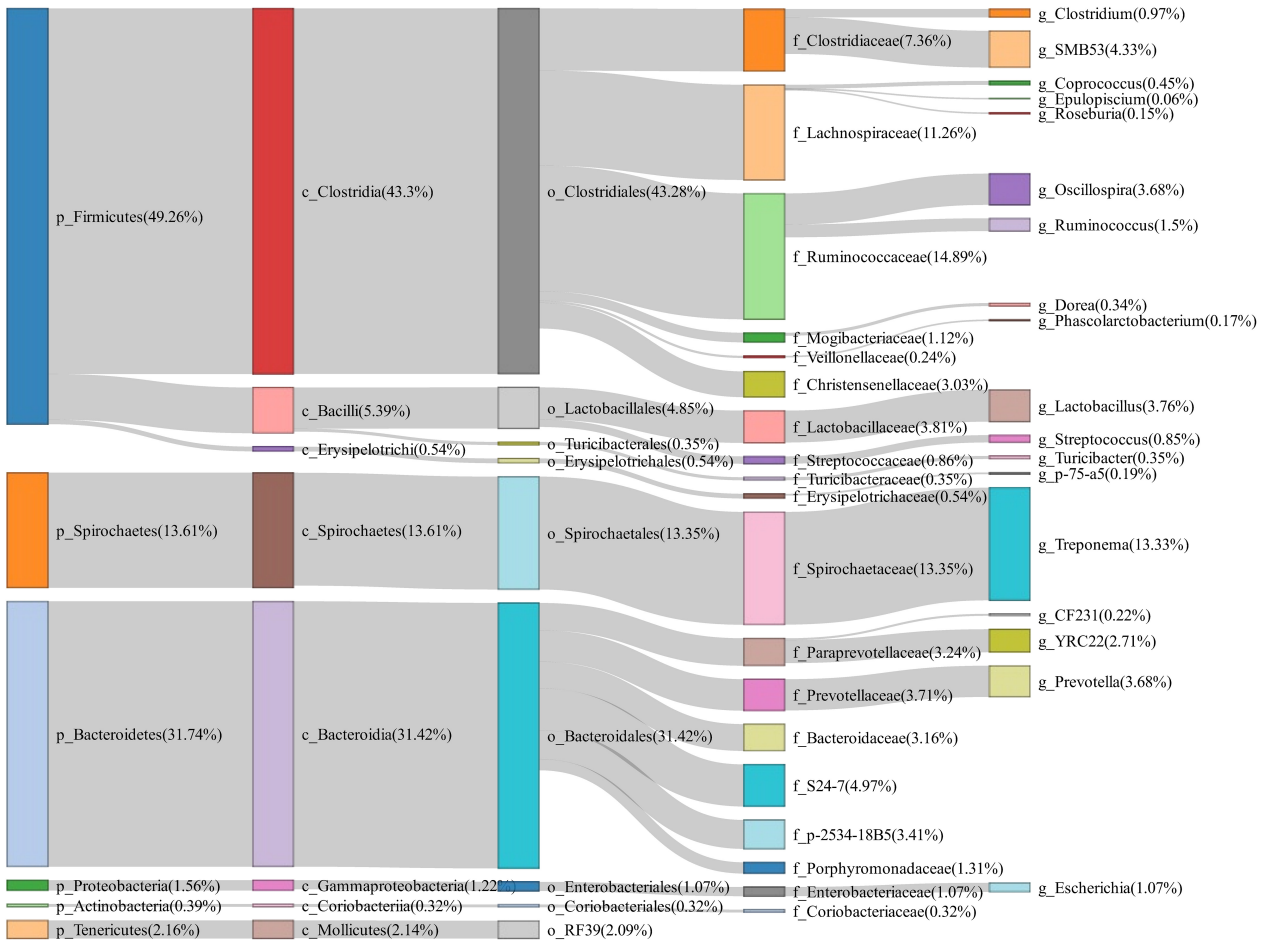

FIGURE 1 | Sankey diagram showing the bacterial composition of feces samples from experimental sows. The colored columns from left to right represent the proportions of bacterial taxa from phylum to genus levels.

Considering the limited number of metabolites (only 278 serum metabolites from pigs) in the Livestock Metabolome Database (LMDB), molecular mass data (m/z) was compared to the HMDB database (Wishart et al., 2018) to annotate the serum metabolites. If the difference between the observed mass and the theoretical mass is less than 10 ppm, the metabolite was labeled as the mass. Partial Least Squares Discriminant Analysis (PLS-DA) was performed to evaluate the differentiation of the untargeted metabolome between two groups of sows by online MetaboAnalyst (V4.0). Metabolites selected as differential candidates for further statistical analysis were identified based on variable importance in the projection (VIP) at the threshold of 1 from the PLS-DA model, which was validated at the significance threshold of $p < 0.05$, by the non-parametric univariate method (Mann–Whitney–Wilcoxon test).

Clustering of Serum Metabolite Modules

Topological networks were constructed for serum metabolites using WGCNA in R package (Langfelder and Horvath, 2008) at a soft threshold of 9 and 5 for positive ion mode and negative ion, according to the scale-free topology criterion ($R^2 = 0.9$). At the threshold of deepSplit of 4 and minimum cluster size of 5, metabolite modules were isolated from the topological network with the dynamic hybrid tree-cutting algorithm (Langfelder et al., 2008). The first principal component of each module was chosen as the representative measurement of its metabolic profile. Modules were subsequently merged if the correlation between the first principal components of the serum metabolite clusters exceeded 0.8. Wilcoxon rank-sum tests were performed to identify the differential metabolic modules between normal return and non-return sows at a significant threshold of p-value ≤ 0.05. Further pathway enrichment analysis was performed for the metabolites in differentially metabolic modules using the "untargeted metabolomic pathway analysis" function section in online MetaboAnalyst (v4.0) (Chong et al., 2019).

Spearman Correlation Analysis Between Gut Microbiome and Serum Metabolome

A total of 13 sows (7 normal return sows and 6 non-return sows) with both serum metabolome and gut microbiome data were used to evaluate the correlation between the changes of

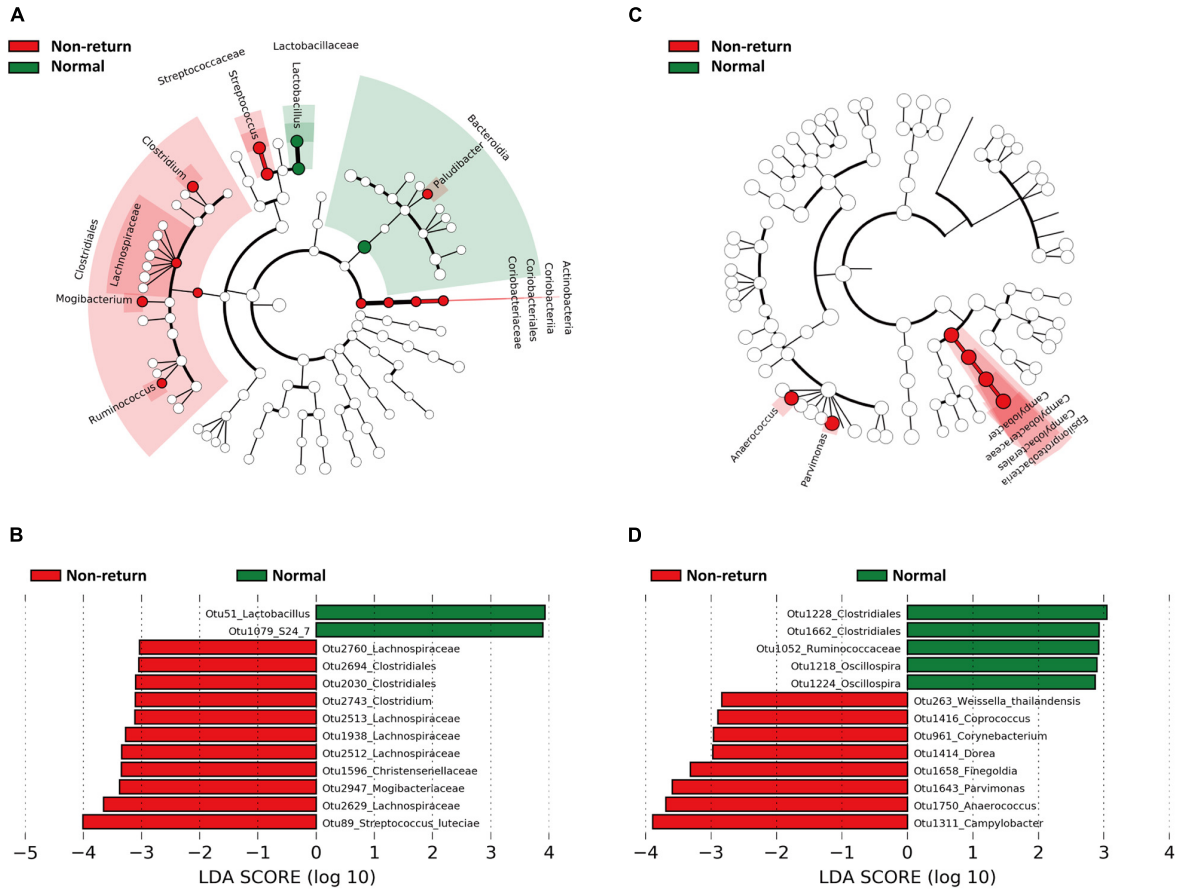

FIGURE 2 | Bacterial taxa and OTUs showing different abundances between normal return and non-return sows identified by Linear discriminant analysis effect size (LEfSe) analysis. The cycles from inside to outside represent kingdom, phylum, class, order, family, and genus. **(A)** Bacterial taxa showing different abundances between normal return and non-return sows in fecal samples (| LDA| score > 2, $p < 0.05$). **(B)** Differential OTUs in fecal samples (| LDA| score > 3, $p < 0.05$). **(C)** Differential bacterial taxa in vaginal samples (| LDA| score > 2, $p < 0.05$). **(D)** Differential OTUs in vaginal samples (| LDA| score > 2, $p < 0.05$).

the gut microbiome and the shifts of serum metabolome. The CAGs and metabolite modules showing differential abundances between two groups were identified by the Wilcoxon rank-sum test. Spearman correlations between CAGs and serum metabolite modules or between differential OTUs and metabolites were calculated using R software (v.3.6.1). The Benjamini–Hochberg method was used to control the false discovery rate (FDR). The visualization of the correlations was plotted using the ggplot2 package in R software (v.3.6.1).

RESULTS

Comparison of Gut Microbial Composition Between Normal Return and Non-return Sows

To evaluate the changes of fecal microbiota composition between normal return and non-return sows, a total of 158 fecal samples were collected and 16S rRNA gene sequencing was performed. The rarefaction curve suggested an adequate amount of sequencing data for the microbial diversity analysis (**Supplementary Figure 1**). Based on 97% similarity of the sequence identity, a total of 3,036 OTUs were obtained in fecal samples. At the phylum level, Firmicutes (49.26%), Bacteroidetes (31.74%), and Spirochaetes (13.61%) were most abundant in fecal samples. At the genus level, the relative abundances of *Treponema* (13.33%), *SMB53* (4.33%), *Lactobacillus* (3.76%), *Oscillospira* (3.68%), and *Prevotella* (3.68%) were listed in the top five (**Figure 1**).

We then compared the gut microbiota composition between normal return and non-return sows. Compared to normal return sows, the sows showing non-return of heat cycle after weaning had the higher observed species and Chao index, but this difference did not achieve a significant level ($p > 0.05$) (**Supplementary Figure 2A**). PCoA based on Weighted UniFrac distance showed a significant difference in the β-diversity of gut microbiota between normal return and non-return sows ($p = 0.013$), but not for the PCoA based on Unweighted UniFrac distances ($p = 0.247$) (**Supplementary Figure 2B**).

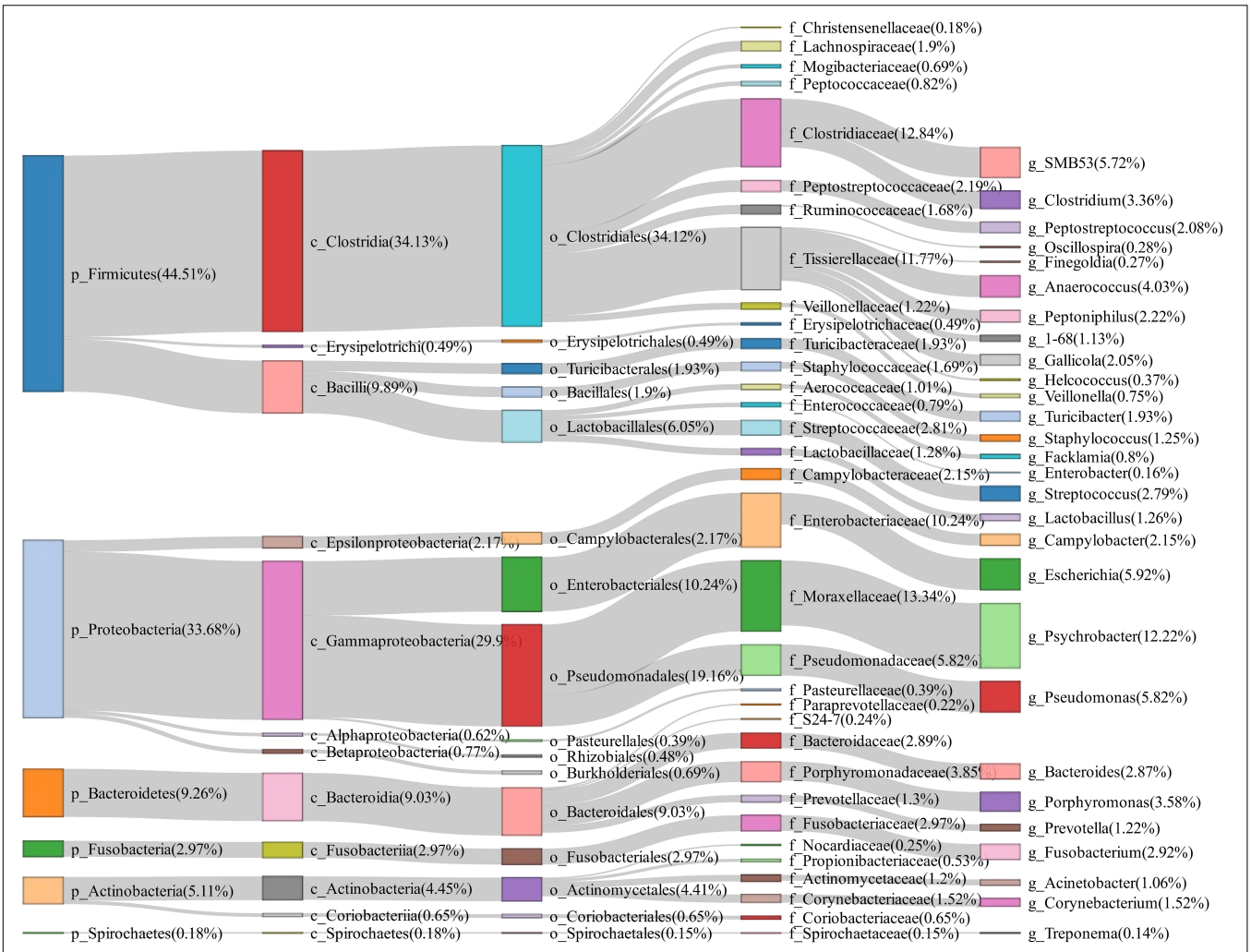

FIGURE 3 | Sankey diagram showing the bacterial composition of vagina swab samples from experimental sows. The colored columns from left to right represent the proportions of bacterial taxa from phylum to genus levels.

Linear discriminant analysis effect size was used to identify gut bacterial taxa showing different abundances between normal return and non-return sows. At the taxonomy level, we identified that Bacteroidia, Lactobacillaceae, and *Lactobacillus* were enriched in sows showing normal return, while Actinobacteria, Clostridiales, Lachnospiraceae, Streptococcaceae, *Streptococcus*, *Clostridium*, *Mogibacterium*, *Ruminococcus*, and *Paludibacter* had higher abundances in non-return sows (**Figure 2A**). At the OTU level, we identified a total of 55 OTUs showing different abundances between normal return and non-return sows at the significance thresholds of $p < 0.05$ and LDA > 2, including 13 OTUs with LDA > 3 (**Supplementary Table 1**). Among these 13 OTUs, two OTUs were annotated to *Lactobacillus* and S24-7 (Bacteroidetes), respectively, and enriched in normal return sows, and the other 11 OTUs were annotated to Mogibacteriaceae, Lachnospiraceae, Christensenellaceae, *Clostridium*, and *Streptococcus luteciae*, and enriched in non-return sows (**Figure 2B**).

The Composition of Vagina Microbiota and Identification of Bacterial Taxa Associated With Non-return of Estrus in Weaned Sows

A total of 50 vaginal swab samples were collected and 16S rRNA gene sequencing was performed. We obtained a total of 2,170 OTUs in these samples. Firmicutes (44.51%), Proteobacteria (33.68%), and Bacteroidetes (9.26%) had the highest abundance in the vagina of tested sows, and *Psychrobacter* (12.22%), *Escherichia* (5.92%), *Pseudomonas* (5.82%), *SMB53* (5.72%), and *Anaerococcus* (4.03%) were the most abundant bacterial genera (**Figure 3**).

We did not observe a significant difference of the α-diversity of vaginal microbial composition between normal return and non-return sows ($p > 0.05$) (**Supplementary Figure 3A**). PCoA based on both Weighted UniFrac distance and Unweighted UniFrac distances showed a significant difference in the β-diversity of

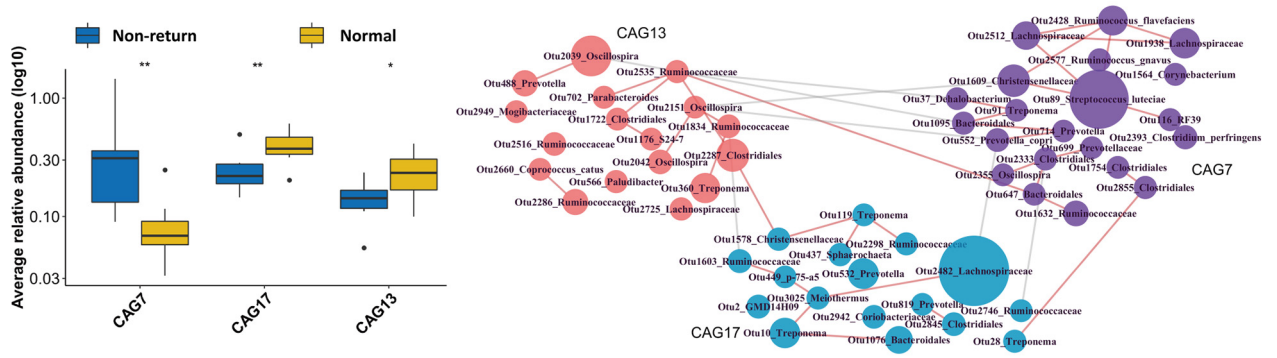

FIGURE 4 | Identification of differential Co-abundance group (CAGs) between normal return and non-return sows. **(A)** Three CAGs showing different enrichments between normal return and non-return sows. Wilcoxon rank-sum test was used to test the different enrichments, $^{*}p \leq 0.1$, $^{**}p \leq 0.05$. **(B)** The horizontal network diagram of three CAGs showing different abundances between normal return and non-return sows. The diagram shows that the OTUs were enriched between normal return and non-return sows. The name of each OTU node was annotated based on the RDP classifier and the size of the nodes represent the abundance of OTU. The thickness of the connections between nodes indicates the weight of the correlation coefficient between OTUs. Lines were drawn only when its correlation coefficient is greater than 0.2. The red lines represent a positive correlation and the gray lines represent a negative correlation. The colors of the nodes represent different types of CAG.

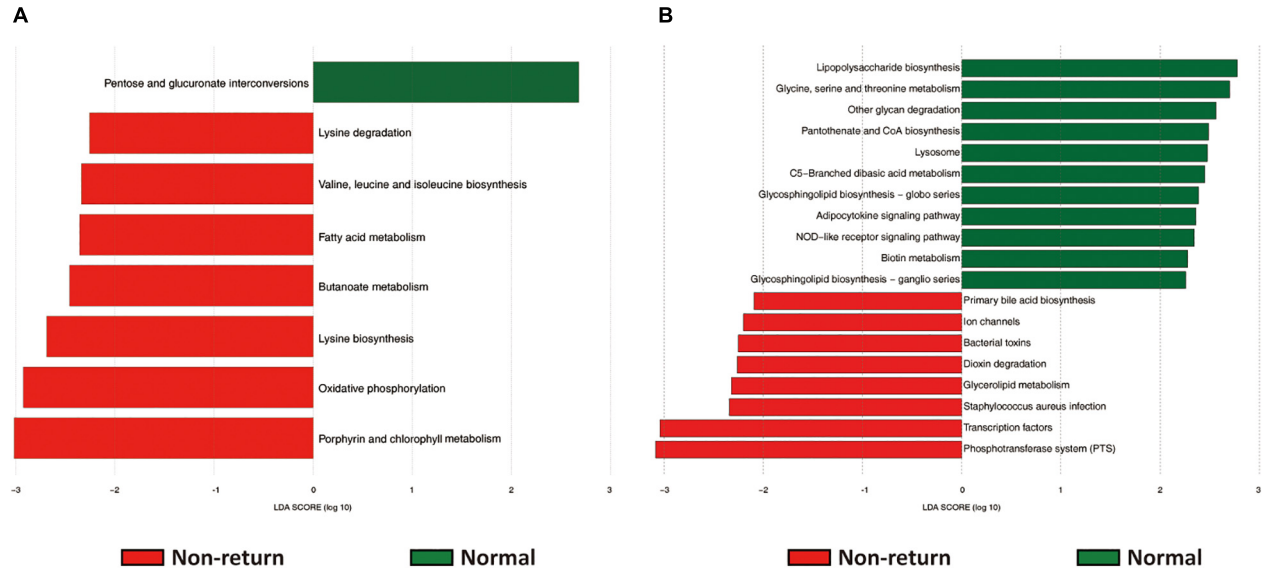

FIGURE 5 | The predicted function capacities of the gut and vaginal microbiome showing different abundances between normal return and non-return sows. Linear discriminant analysis effect size (LEfSe) analysis was used to identify differential KEGG pathways (level 3). **(A)** Differential KEGG pathways identified in fecal samples (| LDA| score > 2, $p < 0.05$). **(B)** Differential KEGG pathways identified in vaginal samples (| LDA| score > 2, $p < 0.05$).

vaginal microbiota between two groups of sows ($p = 0.02$ and 0.03) (**Supplementary Figure 3B**).

The bacterial taxa showing different abundances in vaginal samples between normal return and non-return sows were identified by LEfSe. Epsilonproteobacteria (including campypylobacterales, campylobacteraceae, and *Campylobacter*), *Anaerococcus*, and *Parvimonas* had higher abundances in non-return sows (**Figure 2C**). At the OTU level, a total of 13 OTUs showed different abundances between normal return and non-return sows ($p < 0.05$ and LDA > 2). Among them, five OTUs annotated to Clostridiales, Ruminoccaceae, and *Oscillospira* were enriched in normal return sows, while those OTUs annotated to *Campylobacter*, *Anaerococcus*, *Parvimonas*, *Finegoldia*, and *Dorea* had higher abundances in non-return sows (**Figure 2D**).

Some bacterial taxa showing different abundances between normal return and non-return sows were identified in both feces and vagina samples. For example, *Oscillospira* and Ruminococcaceae were enriched in normal return sows, while *Coprococcus*, Lachnospiraceae, and *Dorea*

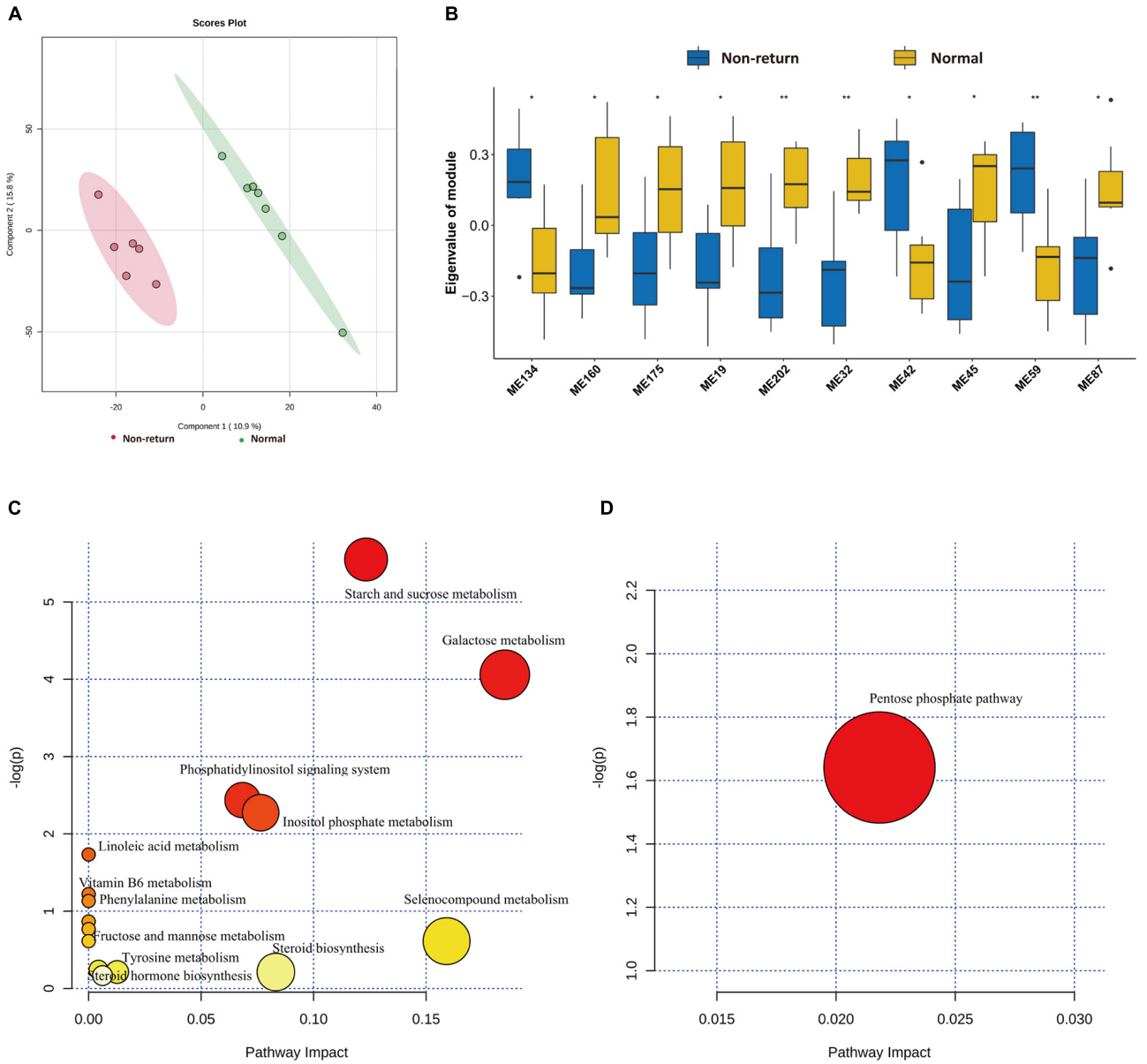

FIGURE 6 | Identification of differential metabolic profiles between normal return and non-return Sows. **(A)** PLS-DA diagram of serum metabolic profiles shows significant differences of serum metabolites profiles between normal return and non-return sows. **(B)** Box plots indicate 10 co-abundance clusters of serum metabolites between normal return and non-return sows. *t*-test was used for difference analysis, * $p < 0.05$, ** $p < 0.01$. **(C)** The KEGG pathway enriched by serum metabolite features having higher abundance in serum of normal sows. **(D)** The KEGG pathways enriched by serum metabolite features having higher abundance in serum of non-return sows. The *x*-axis and the size of dots indicate the KEGG pathway impact of differential serum metabolite features, and the *y*-axis shows the $-\log_{10}$ of significant *p*-value in metabolite enrichment analysis. The size and color of dots represent the value of the KEGG pathway impact.

were enriched in non-return sows (**Supplementary Table 1** and **Figure 2D**).

CAGs of OTUs Associated With the Return of Estrus in Weaned Sows

As a complex microecological system, gut microbes interact with each other and form functional groups. A co-abundance network of OTUs was constructed in 13 samples from the sows, which also had serum metabolomic data (to further analyze the correlation between CAGs and metabolite modules). The 517 OTUs present in at least 20% of the samples were co-clustered based on the SparCC correlation coefficient. A total of 30 CAGs were obtained (**Supplementary Table 2**). Among them, CAG7 and CAG17 showed significantly different enrichments between normal return and non-return sows (**Figure 4A**, $p = 0.01$ and 0.05, respectively), and CAG13 showed the tendency of association with normal return of estrus (**Figure 4A**, $p = 0.1$). CAG13,

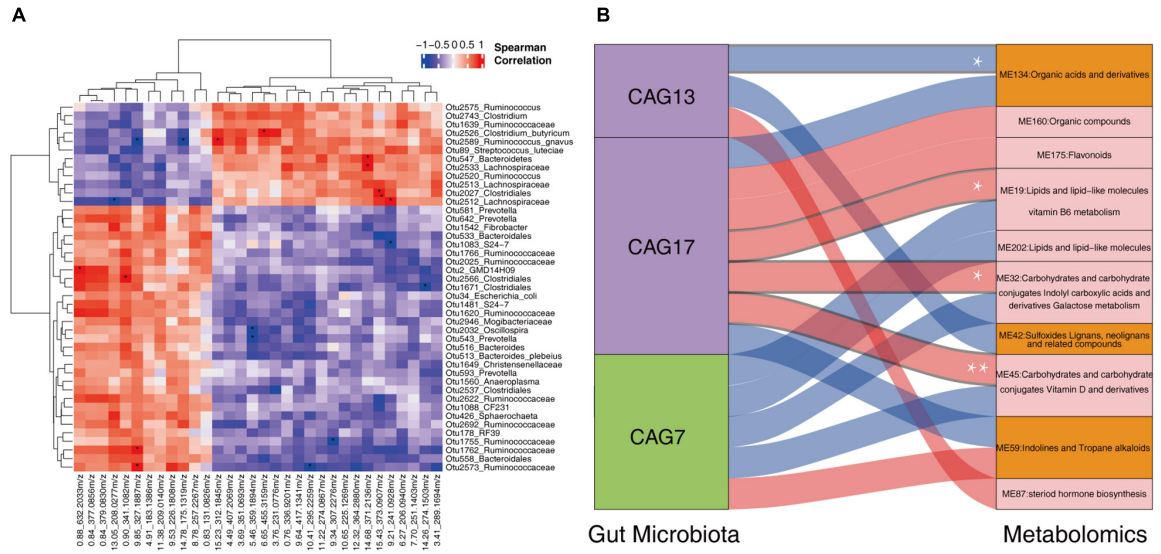

FIGURE 7 | The correlations between fecal microbiota and host serum metabolite profile. **(A)** The heatmap of the correlations between differential fecal microbiota and serum metabolites. Spearman correlation coefficients were calculated. Red represents positive correlation and blue represents negative correlation. The star in the grid indicates the significant threshold *FDR < 0.05. **(B)** Spearman correlation analysis between the CAGs and the metabolite modules. The connections with a coefficient greater than 0.4 were plotted. The thickness of the connections between CAGs and metabolic modules represents the weight of the correlation coefficient. Red connections represent positive correlation, and blue connections represent negative correlation. In the column of CAGs, the green box represents the CAGs that were significantly enriched in non-return sows, and the purple boxes represent the CAGs that were significantly enriched in normal return sows. In the metabolome column, the orange boxes represent metabolic modules that were significantly enriched in non-return sows, and the pink boxes represent metabolic modules significantly enriched in normal return sows. *FDR < 0.05, **FDR < 0.01.

which included the OTUs that were annotated to *Oscillospira*, Ruminococcaceae, Clostridiales, and *Parabacteroides*, and the CAG 17, which was composed of the OTUs that were annotated to Lachnospiraceae, *Treponema*, and Bacteroidales, were significantly enriched in normal return sows. Conversely, CAG7, which was composed of 21 OTUs, including OTU 89 (*S. luteciae*), OTU 2428 (*Ruminococcus flavefaciens*), OTU 2577 (*Ruminococcus gnavus*), OTU 2512 (*Lachnospiraceae*), OTU 1928 (*Lachnospiraceae*), OTU 552 (*Prevotella copri*), and OTU 2393 (*Clostridium perfringens*), was significantly enriched in non-return sows (**Figure 4B**). Particularly, OTU 89 (*S. luteciae*) was the hub OTU in the CAG7 and also identified to enrich in non-return sows at the OTU level (**Supplementary Figure 4**).

The Changes of Potential Functional Capacity of Fecal Microbiome and Vaginal Microbiome Between Normal Return and Non-return Sows

The potential functional capacities of both fecal and vaginal microbiome were predicted by PICRUSt based on 16S rRNA gene sequencing data. We investigated the shifts of potential functional capacities of gut and vaginal microbiome between normal return and non-return sows. At level 3 of KEGG pathways, we identified a total of eight pathways in the fecal microbiome showing differential abundances between two groups of sows. Among them, seven pathways had higher relative abundances in non-return sows, namely, Lysine biosynthesis; Fatty acid metabolism; Valine, leucine, and isoleucine biosynthesis; Lysine degradation; Oxidative phosphorylation; Butanoate metabolism; and Porphyrin and chlorophyll metabolism (LDA score > 2), while only one pathway (Pentose and glucuronate interconversions) was significantly enriched in normal return sows (**Figure 5A**). In the vaginal microbiome, 19 KEGG pathways had different enrichments between two groups of sows, namely, 11 pathways significantly enriched in normal return sows, such as Pantothenate and CoA biosynthesis, Metabolism of cofactors and vitamins; Glycine, serine, and threonine metabolism; NOD-like receptor signaling pathway; and Other glycan degradation, and 8 pathways enriched in non-return sows, including Bacterial toxins, *Staphylococcus aureus* infection, Glycerolipid metabolism, and Dioxin degradation (**Figure 5B** and **Supplementary Table 3**).

Comparison of Serum Metabolome Profiles Between Normal Return and Non-return Sows

To evaluate the shifts of serum metabolites between normal return and non-return sows, non-targeted metabolomics analysis was performed in 13 serum samples described above (method). After quality control, a total of 3,813 metabolite features were obtained for subsequent analysis, including 2,402 metabolite features from positive ion mode and 1,411 features from negative ion mode. Significant shifts of serum metabolites were observed between normal return and non-return sows (**Figure 6A**). We identified a total of 32 metabolites showing different abundances between normal return and non-return sows. These metabolite

features were annotated according to the HMDB database. The metabolite features enriched in normal return sows were mainly annotated to carbohydrates and carbohydrate conjugates, fatty alcohol esters, zearalenones, and hydropyridines, while those metabolite features enriched in non-return sows were annotated to diterpenoids, fatty acids and conjugates, hydroxycinnamic acids and derivatives, fatty alcohols, tropane alkaloids, indoles, and derivatives (**Supplementary Table 4**).

Considering the complex relationships among serum metabolites, 3,813 metabolite features in all 13 samples were clustered into 273 co-abundance modules using WGCNA, including 208 modules in positive ion mode and 65 modules in negative ion mode. Among these modules, 10 modules showed differential enrichments between normal return and non-return sows (**Figure 6B**). Seven metabolite modules containing 57 metabolite features were significantly enriched in normal return sows. These 57 metabolite features were annotated to organic compounds, flavonoids, lipids and lipid-like molecules, carbohydrates and carbohydrate conjugates, indolyl carboxylic acids and derivatives, and vitamin D and derivatives (**Supplementary Table 5**), and were enriched in the pathways Steroid hormone biosynthesis, Starch and sucrose metabolism, Galactose metabolism, and Vitamin B6 metabolism (**Figure 6C**). Three metabolite modules containing 23 metabolite features had significantly higher abundance in non-return sows. These 23 metabolite features belonged to tropane alkaloids, indoles and derivatives, sulfoxides, lignans, and neolignans (**Supplementary Table 5**), and were significantly enriched in Pentose phosphate pathway (**Figure 6D**).

The Correlation Between the Changes in Gut Microbiota and the Shifts of Serum Metabolites

We further evaluated the correlation between the shifts of fecal microbiota and the changes of host serum metabolites in 13 sows described above. LEfSe analysis identified 43 OTUs showing differential abundance between normal return and non-return sows (**Supplementary Figure 4**, $|\text{LDA}| > 2$, $p < 0.05$). Most of these differential OTUs (27/43) were also identified in the whole dataset (158 samples), such as those OTUs annotated to Bacteroidales, S24-7, Ruminococcaceae, *Oscillospira*, Christensenellaceae, Sphaerochaeta, *Ruminococcus*, Clostridiales, Ruminococcaceae, Lachnospiraceae, *Clostridium butyricum*, *Clostridium*, and *S. luteciae*. We then analyzed the correlations between 43 differential OTUs and 32 differential serum metabolites described above. At the significance threshold of FDR < 0.05, we identified 20 significant correlations. OTU 2526 (*C. butyricum*), OTU 2589 (*R. gnavus*), OTU 2027 (Clostridiales), OTU 2512 (Lachnospiraceae), OTU 547 (Bacteroidetes) and OTU 2533 (Lachnospiraceae), all of which had higher abundances in the gut microbiota of non-return sows, were positively correlated with (3 beta, 17 alpha, 23S)-17,23-Epoxy-3,28,29-trihydroxy-27-norlanost-8-en-24-one (6.65_455.3159 m/z), Alosetron (15.23_312.1845 m/z), 3-Feruloyl-1,5-quinolactone (15.43_373.0907 m/z), Erythrose (9.21_241.0928 m/z), and Ecgonine (14.68_371.2136 m/z), respectively (FDR < 0.05). These five metabolites also had higher abundances in non-return sows (**Supplementary Table 4**). The OTU 2 (GMD14H09), OTU 2566 (Clostridiales), OTU 1762 (Ruminococcaceae), and OTU 2573 (Ruminococcaceae), which showed enrichments in normal return sows, showed positive correlations with the metabolites enriched in normal return sows [3′-Sialyllactose (0.88_632.2033 m/z), Lactulose (0.90_341.1082 m/z), and Metixene (9.85_327.1887 m/z), respectively]. We also observed the significant correlations between those differential OTUs and serum metabolites, which showed different directions of enrichment between normal return and non-return sows. For example, OTU 2589 (*Ruminococcus gnavus*) was negatively correlated with Metixene (9.85_3.27.1887 m/z) and 2,4,6-Triethyl-1,3,5-trioxane (14.78_17 5.1319 m/z) (**Figure 7A**).

We then evaluated the correlations between three differential CAGs (CAG7, CAG13, and CAG17) and 10 differential metabolite modules (ME32, ME19, ME42, ME134, ME160, ME175, ME202, ME45, ME59, and ME87). Those correlations with coefficient (r^2) > 0.4 were selected. CAG17 was positively correlated with ME45 (mainly including Carbohydrates and carbohydrate conjugates, and Vitamin D and derivatives), ME32 (Carbohydrates and carbohydrate conjugates, and Indolyl carboxylic acids and derivatives), and ME19 (Lipids and lipid-like molecules, related to Vitamin B6 metabolism), and CAG13 was negatively correlated with ME134 (Organic acids and derivatives) (FDR < 0.05, **Figure 7B**). However, no significant correlation was identified between CAG7 and metabolite modules. It implies that the changes in the fecal microbiota might lead to the shift of serum metabolites and was further associated with non-return in weaned sows.

DISCUSSION

The interval from weaning to heat return has a significant effect on sows PSY. It affects the economic benefit of the pig industry. In this study, we explored the relationship between fecal and vaginal microbiota and the heat return of weaned sows. The serum metabolome was also measured to identify metabolites associated with non-return of estrus in weaned sows. We found that the changes in gut microbiota contributed to the shifts of serum metabolites and may further affect sow estrus return after weaning. To our knowledge, we firstly investigated the effect of gut and vaginal microbiota composition with sow estrus return of weaned sows by integrating serum metabolome analyses.

Consistent with the previous reports (Xiao et al., 2017; Dong-Jie et al., 2018), Firmicutes, Bacteroidetes, and Spirochaetes are the most abundant phyla in the fecal microbiota of sows. However, different from that in the gut, Firmicutes, Proteobacteria, and Bacteroidetes were the dominant phyla in vaginal bacterial communities, and this result was consistent with Kwawukume's observation (Kwawukume, 2017). Recent studies have demonstrated that the prevalence and relative abundance of the genus *Lactobacillus*, which is the most abundant genus in women's vagina and helps host against pathogens and infection (Ventolini, 2015), varied in the vagina across different mammalian species (Miller et al., 2016). In this study,

Lactobacillus only accounts for an average of 1.31% of relative abundance in all tested vaginal samples. A previous study indicated that Lactobacillaceae had high abundances in the vaginal of Göttingen minipigs and showed no significant changes during heat cycle (Lorenzen et al., 2015).

Different parities may affect the gut microbial composition of sows (Gaukroger et al., 2021). However, in this study, we did not observe the significant difference of the microbial compositions of the gut and vagina among parities (**Supplementary Figure 5**). This should be due to the fact that most experimental sows were at the parity 2 to 5 (94.3%). Their ages were not significantly different. Similar to the result reported previously (Xu et al., 2020), non-return sows had higher observed species ($p = 0.08$) and Chao index ($p < 0.05$) of fecal microbiota than normal return sows. This may be due to the fact that sex hormones in normal return sows reduced the diversity of gut microbiota. We identified gut and vaginal microbes associated with the return to estrus of weaned sows. *Lactobacillus*, S27-4, and Bacteroidia were enriched in the gut of normal return sows. *Lactobacillus* was associated with low body mass index (BMI) or normal weight (Choi et al., 2019; Zhu et al., 2019). It has also been reported that both feed-induced obese Ossabaw miniature pigs and genetically obese Iberian pigs exhibit poor reproductive performance (Gonzalez-Añover et al., 2011; Newell-Fugate et al., 2014). Severely obese women show a higher probability of hormonal disorders, menstrual disorders, anovulatory cycles, and ovulation abnormalities than normal-weight women (Hartz et al., 1979). Mouse model experiments show that obesity is negatively correlated with estrus performance and leads to infertility (Bermejo-Alvarez et al., 2012). S24-7 is a family belonging to Bacteroidetes, which widely exists in the intestinal tract of animals. It is now named Muribaculaceae (Lagkouvardos et al., 2019). The abundance of S24-7 in the gut of sows is increased during pregnancy and decreased during weaning (Ji et al., 2019). The S24-7 has the capacity to degrade complex carbohydrates (Lagkouvardos et al., 2019), and members of *Bacteroides* have plant polysaccharide degrading enzymes, which can participate in polysaccharide degradation (Zou et al., 2019). CAG13 and CAG17 were enriched in normal return sows. These two CAGs were composed of OTUs belonging to the bacteria mainly related to anti-inflammatory and polysaccharide metabolism, including Ruminococcaceae, Lachnospiraceae, and *Oscillospira* (Scott et al., 2014; Konikoff and Gophna, 2016; Esquivel-Elizondo et al., 2017). Ruminococcaceae and Lachnospiraceae have been reported to produce butyrate, which plays the roles in anti-inflammatory response (Liu et al., 2019). *Oscillospira* can use the host glycogen to produce energy (Kohl et al., 2014), and the abundance of *Oscillospira* was significantly reduced in patients with inflammation (Gophna et al., 2017). Studies have shown that Ruminococcaceae, Lachnospiraceae, *Oscillospira*, and *Treponema* can ferment dietary fiber (Niu et al., 2015; Upadhyaya et al., 2016; Yu-Jiao et al., 2016). Conversely, *Streptococcus luteciae* (Liang et al., 2014), *Ruminococcus gnavus* (Hall et al., 2017), *Prevotella copri* (Pedersen et al., 2016), and *Clostridium perfringens* (Cree et al., 2016), which were annotated to the OTUs in the CAG7 have been reported to associate pro-inflammatory.

We showed that serum metabolites had a significant shift between normal return and non-return sows. This result was consistent with a previous report (Xu et al., 2020). Carbohydrates and their conjugates, and lipids and lipid-like molecules were enriched in normal return sows, Carbohydrates and lipids can compensate for the energy loss and meet the nutritional requirements during sow lactation. Generally, most sows will encounter energy loss and weight loss during lactation. After weaning, sows need to replenish energy and nutrition for estrus again. The metabolites showing different abundances between normal return and non-return sows were enriched to the pathways of galactose metabolism, starch and sucrose metabolism, and vitamin B6 metabolism. This result suggested that the differential metabolites may provide sows with the energy and vitamin requirements for estrus. The supplement of vitamin B6 can significantly increase the production of luteinizing hormone (LH) in sows during estrus (Dalto et al., 2015). Unexpectedly, the metabolites of Metixene (9.85_3.27.1887 m/z) and Astemizole (15.88_459.2560 m/z) were enriched in normal return sows. Both Metixene and Astemizole can be used to relieve or treat Parkinson's disease (Moller et al., 2005; Styczynska-Soczka et al., 2017). Some studies speculated that Parkinson's disease may be related to estrogen secretion (Shulman, 2002). Women with higher lifetime estrogen levels have a lower risk of Parkinson's disease (Gatto et al., 2014). However, the relationship between these metabolites and the sow heat return needs to be further confirmed.

The module composed of vitamin D and its derivatives was enriched in normal return sows, and positively correlated with the CAG17, which was also enriched in normal return sows. Several studies have shown that vitamin D, especially 1α, 25-(OH)2-vitamin D3, has a great influence on the reproductive performance of sows (Lauridsen et al., 2010). 1α, 25-(OH)2-vitamin D3 can regulate the calcium and phosphorus metabolism, and enhance calcium and phosphorus absorption, which benefits sows by quickly restoring body condition after weaning and shortening the interval from weaning to estrus (Jie et al., 2018). The metabolites having the higher abundances in normal return sows were also enriched in the pathway of Steriod hormone biosynthesis. As we have known, many steroid hormones, including sex hormones, play a very important role in the reproductive physiology of pigs. Steroid hormones regulate the endocrine balance through the hypothalamic–pituitary–gonadal axis (HPGA) (Hengevoss et al., 2015), thereby affecting the sow's sexual cycle and estrus. The metabolites enriched in the serum of non-return sows have been reported to inhibit estrus expressions, such as tropane alkaloids, indole and its derivatives, sulfoxides, lignans, and neolignans. Atropine belongs to tropane alkaloids that can inhibit the effect of oxytocin in goats during estrus (Fodor and Dharanipragada, 1994). Indoles have anti-gonadotropin effects (Reiter and Vaughan, 1977). All these metabolites were correlated with heat return-associated gut microbiota. We speculate that the gut microbiota can participate in the physiological processes of estrus in sows through another manner by regulating the metabolites related to the steriod hormone biosynthesis or influencing

the effect of sex hormone. However, the causality and the underlying mechanisms have not been elucidated. Further studies are needed to investigate the mechanism of the key microbiota and metabolites identified in this study affecting estrus return of sows after weaning.

In summary, this study innovatively investigated the effect of sow gut and vaginal microbiota on non-return of sows after weaning and found several microbes that may affect the return of sow estrus. The metabolites and metabolic modules show different abundances between normal return and non-return sows and may be used as markers associated with the return of sow estrus after weaning. The correlation analysis between the gut microbiota and serum metabolites indicated that the changes of gut microbiome should be related to the shifts of serum metabolites between normal return and non-return sows. These results provide new insights into the understanding of the effect of gut and vaginal microbiota on sow estrus return after weaning and suggest that gut and vaginal microbiota may be treated as a target regulating sow estrus. Unfortunately, only 13 serum samples were collected and the metabolomics analysis was performed. In a future study, we will collect more serum samples for metabolomics analysis to further confirm the relationship of fecal microbiota and serum metabolites and elucidate the possible mechanism of the gut and vagina microbes affecting sow estrus return by integrating the multi-omics data.

DATA AVAILABILITY STATEMENT

The datasets generated from this study were submitted to China National GeneBank Database (CNGBdb) with accession code: CNP0001739.

ETHICS STATEMENT

The animal study was reviewed and approved by the Ministry of Agriculture and Rural Affairs of China. This study was approved by the Animal Care and Use Committee (ACUC) at Jiangxi Agricultural University (No. JXAU2011-006).

AUTHOR CONTRIBUTIONS

LH designed this study and revised the manuscript. CC designed the experiments and wrote and revised the manuscript. JZ analyzed the data and wrote the manuscript. ML analyzed the data and revised the manuscript. SK, XH, SF, MH, and HF performed the experiments. All authors read and approved the final manuscript.

FUNDING

This work was supported by the National Natural Science Foundation of China (31772579 and 31760654).

SUPPLEMENTARY MATERIAL

The Supplementary Material for this article can be found online at: https://www.frontiersin.org/articles/10.3389/fmicb.2021.690091/full#supplementary-material

Supplementary Figure 1 | The rarefaction curve of 16S rRNA gene sequencing data. **(A)** Fecal samples. **(B)** Vaginal samples.

Supplementary Figure 2 | Comparison of α-diversity and β-diversity of gut microbiota between normal return and non-return Sows. **(A)** Comparison of the α-diversity (observed species and Chao index) in the fecal samples between normal return and non-return sows. Wilcoxon rank-sum test was used for comparison analysis. **(B)** PCoA of gut microbiota based on Weighted UniFrac distance and Unweighted UniFrac distance between the normal return and non-return sows. PERMANOVA was used for significant test. The number of permutations was set at 10000 times. $p < 0.05$ means achievement of significant level, R^2 value suggested the degree of interpretation of the differences in the sample by the grouping factors.

Supplementary Figure 3 | Comparative analysis of the α-diversity and β-diversity of microbiota between normal return and non-return sows in vaginal swab samples. **(A)** Comparison of the α-diversity (observed species and Chao index) in the vaginal samples between normal return and non-return sows. **(B)** PCoA of vaginal microbiota based on Weighted UniFrac distance and Unweighted UniFrac distance between the normal return and non-return sows.

Supplementary Figure 4 | The OTUs showing different abundances between normal return and return and non-return sows in 13 feces samples from sows that had serum metabolome data. LEfSe analysis was used to identify the differential OTUs between the two groups (| LDA| score > 2, $p < 0.05$).

Supplementary Figure 5 | Comparison of the microbial compositions of feces and vaginal swab samples among seven parities by PCoA based on weighted UniFrac distance. **(A)** Feces samples; **(B)** vaginal swab samples. The results showed that the effect of parity on the microbial compositions of feces and vaginal swab samples was not significant. The effect size (R^2) was estimated via envfit (vegan) based on weighted UniFrac distance.

Supplementary Table 1 | The OTUs showing differential abundances between normal return and non-return sows in 158 fecal samples.

Supplementary Table 2 | The OTUs are clustered into co-abundance groups (CAGs) by the SparCC Algorithm.

Supplementary Table 3 | Differential KEGG pathways of fecal and vaginal microbiome between normal return and non-return sows.

Supplementary Table 4 | Differential serum metabolites between normal return and non-return sows.

Supplementary Table 5 | Differential metabolite modules of serum compounds via WGCNA method between normal return and non-return sows.

REFERENCES

Acharya, K. D., Gao, X., Bless, E. P., Chen, J., and Tetel, M. J. (2019). Estradiol and high fat diet associate with changes in gut microbiota in female ob/ob mice. *Sci. Rep.* 9:20192.

Adlercreutz, H., Pulkkinen, M. O., Hämäläinen, E. K., and Korpela, J. T. (1984). Studies on the role of intestinal bacteria in metabolism of synthetic and natural steroid hormones. *J. Steroid Biochem.* 20, 217–229. doi: 10.1016/0022-4731(84)90208-5

Baker, J. M., Al-Nakkash, L., and Herbst-Kralovetz, M. M. (2017). Estrogen-gut microbiome axis: physiological and clinical implications. *Maturitas* 103, 45–53. doi: 10.1016/j.maturitas.2017.06.025

Bermejo-Alvarez, P., Rosenfeld, C. S., and Roberts, R. M. (2012). Effect of maternal obesity on estrous cyclicity, embryo development and blastocyst gene

expression in a mouse model. *Hum. Reprod.* 27, 3513–3522. doi: 10.1093/humrep/des327

Board. (2020). *2018 Pig Cost Of Production In Selected Countries*. England: Agriculture and Horticulture Development Board.

Caporaso, J. G., Kuczynski, J., Stombaugh, J., Bittinger, K., Bushman, F. D., and Costello, E. K. (2010). QIIME allows analysis of high-throughput community sequencing data. *Nat. Methods* 7, 335–356.

Choi, W. J., Dong, H. J., Jeong, H. U., Jung, H. H., Kim, Y. H., and Kim, T. H. (2019). Antiobesity Effects of Lactobacillus plantarum LMT1-48 Accompanied by Inhibition of *Enterobacter cloacae* in the Intestine of Diet-Induced Obese Mice. *J. Med. Food* 22, 560–566. doi: 10.1089/jmf.2018.4329

Chong, J., Wishart, D. S., and Xia, J. (2019). Using MetaboAnalyst 4.0 for Comprehensive and Integrative Metabolomics Data Analysis. *Curr. Protoc. Bioinformatics* 68:e86.

Cree, B. A., Spencer, C. M., Varrin-Doyer, M., Baranzini, S. E., and Zamvil, S. S. (2016). Gut microbiome analysis in neuromyelitis optica reveals overabundance of Clostridium perfringens. *Ann. Neurol.* 80, 443–447. doi: 10.1002/ana.24718

Dalto, D. B., Roy, M., Audet, I., Palin, M.-F., Guay, F., Lapointe, J., et al. (2015). Interaction between vitamin B6 and source of selenium on the response of the selenium-dependent glutathione peroxidase system to oxidative stress induced by oestrus in pubertal pig. *J. Trace Elem. Med. Biol.* 32, 21–29. doi: 10.1016/j.jtemb.2015.05.002

Dixon, P. (2003). VEGAN, a package of R functions for community ecology. *J. Veg. Sci.* 14, 927–930. doi: 10.1111/j.1654-1103.2003.tb02228.x

Dong-Jie, Z., Yue-Ling, Z., Wen-Tao, W., Liang, W., and Di, L. (2018). Character Analysis of Gut Microbiota in Min Pig. *Chin. J. Anim. Sci.* 54, 27–32.

Esquivel-Elizondo, S., Ilhan, Z. E., Garcia-Peña, E. I., and Krajmalnik-Brown, R. (2017). Insights into Butyrate Production in a Controlled Fermentation System via Gene Predictions. *mSystems* 2, e00051–17.

Fadrosh, D. W., Ma, B., Gajer, P., Sengamalay, N., Ott, S., Brotman, R. M., et al. (2014). An improved dual-indexing approach for multiplexed 16S rRNA gene sequencing on the Illumina MiSeq platform. *Microbiome* 2:6. doi: 10.1186/2049-2618-2-6

Flores, R., Shi, J., Fuhrman, B., Xu, X., Veenstra, T. D., Gail, M. H., et al. (2012). Fecal microbial determinants of fecal and systemic estrogens and estrogen metabolites: a cross-sectional study. *J. Transl. Med.* 10:253. doi: 10.1186/1479-5876-10-253

Fodor, G., and Dharanipragada, R. (1994). Tropane alkaloids. *Nat. Prod. Rep.* 11, 443–450.

Gatto, N. M., Deapen, D., Stoyanoff, S., Pinder, R., Narayan, S., Bordelon, Y., et al. (2014). Lifetime exposure to estrogens and Parkinson's disease in California teachers. *Park. Relat. Disord.* 20, 1149–1156. doi: 10.1016/j.parkreldis.2014.08.003

Gaukroger, C. H., Edwards, S. A., Walshaw, J., Nelson, A., Adams, I. P., Stewart, C. J., et al. (2021). Shifting sows: longitudinal changes in the periparturient faecal microbiota of primiparous and multiparous sows. *Animal* 15:100135. doi: 10.1016/j.animal.2020.100135

Gonzalez-Añover, P., Encinas, T., Torres-Rovira, L., Pallares, P., Muñoz-Frutos, J., Gomez-Izquierdo, E., et al. (2011). Ovulation rate, embryo mortality and intrauterine growth retardation in obese swine with gene polymorphisms for leptin and melanocortin receptors. *Theriogenology* 75, 34–41. doi: 10.1016/j.theriogenology.2010.07.009

Gophna, U., Konikoff, T., and Nielsen, H. B. (2017). Oscillospira and related bacteria - From metagenomic species to metabolic features. *Environ. Microbiol.* 19, 835–841. doi: 10.1111/1462-2920.13658

Hall, A. B., Yassour, M., Sauk, J., Garner, A., Jiang, X., Arthur, T., et al. (2017). A novel Ruminococcus gnavus clade enriched in inflammatory bowel disease patients. *Genome Med.* 9:103.

Hartz, A., Barboriak, P. N., Wong, A., Katayama, K. P., and Rimm, A. A. (1979). The association of obesity with infertility and related menstural abnormalities in women. *Int. J. obes.* 3, 57–73.

Henderson, B., and Nibali, L. (2016). *The Human Microbiota And Chronic Disease: Dysbiosis As A Cause Of Human Pathology*. Hoboken, New Jersey: Wiley Blackwell.

Hengevoss, J., Piechotta, M., Muller, D., Hanft, F., Parr, M. K., Schanzer, W., et al. (2015). Combined effects of androgen anabolic steroids and physical activity on the hypothalamic-pituitary-gonadal axis. *J. Steroid Biochem. Mol. Biol.* 150, 86–96. doi: 10.1016/j.jsbmb.2015.03.003

Hermann-Bank, M. L., Skovgaard, K., Stockmarr, A., Strube, M. L., Larsen, N., Kongsted, H., et al. (2015). Characterization of the bacterial gut microbiota of piglets suffering from new neonatal porcine diarrhoea. *BMC Vet. Res.* 11:139. doi: 10.1186/s12917-015-0419-4

Ji, Y. J., Li, H., Xie, P. F., Li, Z. H., Li, H. W., Yin, Y. L., et al. (2019). Stages of pregnancy and weaning influence the gut microbiota diversity and function in sows. *J. Appl. Microbiol.* 127, 867–879. doi: 10.1111/jam.14344

Jie, L., Pengyun, L., and Yongcheng, H. (2018). Analysis of the effect of 1α,25-(OH)2-vitamin D3 on sow performance. *Swine Ind. Sci.* 35, 96–98.

Kaliannan, K., Robertson, R. C., Murphy, K., Stanton, C., Kang, C., Wang, B., et al. (2018). Estrogen-mediated gut microbiome alterations influence sexual dimorphism in metabolic syndrome in mice. *Microbiome* 6:205.

Kohl, K. D., Amaya, J., Passement, C. A., Dearing, M. D., and Mccue, M. D. (2014). Unique and shared responses of the gut microbiota to prolonged fasting: a comparative study across five classes of vertebrate hosts. *FEMS Microbiol. Ecol.* 90, 883–894. doi: 10.1111/1574-6941.12442

Konikoff, T., and Gophna, U. (2016). Oscillospira: a Central, Enigmatic Component of the Human Gut Microbiota. *Trends Microbiol.* 24, 523–524. doi: 10.1016/j.tim.2016.02.015

Kurtz, Z. D., Muller, C. L., Miraldi, E. R., Littman, D. R., Blaser, M. J., and Bonneau, R. A. (2015). Sparse and compositionally robust inference of microbial ecological networks. *PLoS Comput. Biol.* 11:e1004226. doi: 10.1371/journal.pcbi.1004226

Kwawukume, A. (2017). *The gut and vaginal microbiome profiles of pregnant sows and their contribution to neonatal piglet gut microbiome development*. Ph.D. thesis. Winnipeg, Manitoba: University of Manitoba.

Lagkouvardos, I., Lesker, T. R., Hitch, T. C. A., Galvez, E. J. C., Smit, N., Neuhaus, K., et al. (2019). Sequence and cultivation study of Muribaculaceae reveals novel species, host preference, and functional potential of this yet undescribed family. *Microbiome* 7:28.

Langfelder, P., and Horvath, S. (2008). WGCNA: an R package for weighted correlation network analysis. *BMC Bioinformatics* 9:559. doi: 10.1186/1471-2105-9-559

Langfelder, P., Zhang, B., and Horvath, S. (2008). Defining clusters from a hierarchical cluster tree: the Dynamic Tree Cut package for R. *Bioinformatics* 24, 719–720. doi: 10.1093/bioinformatics/btm563

Langille, M. G., Zaneveld, J., Caporaso, J. G., Mcdonald, D., Knights, D., Reyes, J. A., et al. (2013). Predictive functional profiling of microbial communities using 16S rRNA marker gene sequences. *Nat. Biotechnol.* 31, 814–821. doi: 10.1038/nbt.2676

Lauridsen, C., Halekoh, U., Larsen, T., and Jensen, S. K. (2010). Reproductive performance and bone status markers of gilts and lactating sows supplemented with two different forms of vitamin D. *J. Anim. Sci.* 88, 202–213. doi: 10.2527/jas.2009-1976

Leite, C. D., Lui, J. F., Albuquerque, L. G., and Alves, D. N. (2011). Environmental and genetic factors affecting the weaning-estrus interval in sows. *Genet. Mol. Res.* 10, 2692–2701. doi: 10.4238/2011.november.4.2

Levis, D. G., and Hogg, A. (1989). *EC89-1908 Swine Reproductive Problems: Noninfectious Causes*. Lincoln, Nebraska, United States: University of Nebraska-Lincoln

Liang, X., Li, H., Tian, G., and Li, S. (2014). Dynamic microbe and molecule networks in a mouse model of colitis-associated colorectal cancer. *Sci. Rep.* 4:4985.

Liu, H., Chen, X., Hu, X., Niu, H., Tian, R., Wang, H., et al. (2019). Alterations in the gut microbiome and metabolism with coronary artery disease severity. *Microbiome* 7:68.

Lorenzen, E., Kudirkiene, E., Gutman, N., Grossi, A. B., Agerholm, J. S., Erneholm, K., et al. (2015). The vaginal microbiome is stable in prepubertal and sexually mature Ellegaard Gottingen Minipigs throughout an estrous cycle. *Vet. Res.* 46:125.

Magoč, T., and Salzberg, S. L. (2011). FLASH: fast length adjustment of short reads to improve genome assemblies. *Bioinformatics* 27, 2957–2963. doi: 10.1093/bioinformatics/btr507

Majaneva, M., Hyytiainen, K., Varvio, S. L., Nagai, S., and Blomster, J. (2015). Bioinformatic Amplicon Read Processing Strategies Strongly Affect Eukaryotic Diversity and the Taxonomic Composition of Communities. *PLoS One* 10:e0130035. doi: 10.1371/journal.pone.0130035

McOrist, A. L., Jackson, M., and Bird, A. R. (2002). A comparison of five methods for extraction of bacterial DNA from human faecal samples. *J. Microbiol. Methods* 50, 131–139. doi: 10.1016/s0167-7012(02)00018-0

Menon, R., Watson, S. E., Thomas, L. N., Allred, C. D., Dabney, A., Azcarate-Peril, M. A., et al. (2013). Diet Complexity and Estrogen Receptor β Status Affect the Composition of the Murine Intestinal Microbiota. *Appl. Environ. Microbiol.* 79, 5763–5773. doi: 10.1128/aem.01182-13

Miller, E. A., Beasley, D. E., Dunn, R. R., and Archie, E. A. (2016). Lactobacilli Dominance and Vaginal pH: why Is the Human Vaginal Microbiome Unique? *Front. Microbiol.* 7:1936. doi: 10.3389/fmicb.2016.01936

Miller, E. A., Livermore, J. A., Alberts, S. C., Tung, J., and Archie, E. A. (2017). Ovarian cycling and reproductive state shape the vaginal microbiota in wild baboons. *Microbiome* 5:8.

Moller, J. C., Korner, Y., Dodel, R. C., Meindorfner, C., Stiasny-Kolster, K., Spottke, A., et al. (2005). Pharmacotherapy of Parkinson's disease in Germany. *J. Neurol.* 252, 926–935.

Newell-Fugate, A. E., Taibl, J. N., Clark, S. G., Alloosh, M., Sturek, M., and Krisher, R. L. (2014). Effects of Diet-Induced Obesity on Metabolic Parameters and Reproductive Function in Female Ossabaw Minipigs. *Comp. Med.* 64, 44–49. doi: 10.7570/jomes20043

Niu, Q., Li, P., Hao, S., Zhang, Y., Kim, S. W., Li, H., et al. (2015). Dynamic distribution of the gut microbiota and the relationship with apparent crude fiber digestibility and growth stages in pigs. *Sci. Rep.* 5:9938.

Pedersen, H. K., Gudmundsdottir, V., Nielsen, H. B., Hyotylainen, T., Nielsen, T., Jensen, B. A., et al. (2016). Human gut microbes impact host serum metabolome and insulin sensitivity. *Nature* 535, 376–381. doi: 10.1038/nature18646

Poleze, E., Bernardi, M. L., Amaral Filha, W. S., Wentz, I., and Bortolozzo, F. P. (2006). Consequences of variation in weaning-to-estrus interval on reproductive performance of swine females. *Livest. Sci.* 103, 124–130. doi: 10.1016/j.livsci.2006.02.007

Ramayo-Caldas, Y., Mach, N., Lepage, P., Levenez, F., Denis, C., Lemonnier, G., et al. (2016). Phylogenetic network analysis applied to pig gut microbiota identifies an ecosystem structure linked with growth traits. *ISME J.* 10, 2973–2977. doi: 10.1038/ismej.2016.77

Reiter, R. J., and Vaughan, M. K. (1977). Pineal antigonadotrophic substances: polypeptides and indoles. *Life Sci.* 21, 159–171. doi: 10.1016/0024-3205(77)90298-3

Rusilowicz, M. J. (2016). *Computational Tools For The Processing And Analysis Of Time-Course Metabolomic Data*. York, United Kingdom: University of York.

Schloss, P. D., Westcott, S. L., Ryabin, T., Hall, J. R., Hartmann, M., Hollister, E. B., et al. (2009). Introducing mothur: open-source, platform-independent, community-supported software for describing and comparing microbial communities. *Appl. Environ. Microbiol.* 75, 7537–7541. doi: 10.1128/aem.01541-09

Scott, K. P., Martin, J. C., Duncan, S. H., and Flint, H. J. (2014). Prebiotic stimulation of human colonic butyrate-producing bacteria and bifidobacteria, in vitro. *FEMS Microbiol. Ecol.* 87, 30–40. doi: 10.1111/1574-6941.12186

Segata, N., Izard, J., Waldron, L., Gevers, D., Miropolsky, L., Garrett, W. S., et al. (2011). Metagenomic biomarker discovery and explanation. *Genome Biol.* 12:R60.

Shannon, P., Markiel, A., Ozier, O., Baliga, N. S., Wang, J. T., Ramage, D., et al. (2003). Cytoscape: a software environment for integrated models of biomolecular interaction networks. *Genome Res.* 13, 2498–2504. doi: 10.1101/gr.1239303

Shen, X., Gong, X., Cai, Y., Guo, Y., Tu, J., Li, H., et al. (2016). Normalization and integration of large-scale metabolomics data using support vector regression. *Metabolomics* 12:89.

Shulman, L. M. (2002). Is there a connection between estrogen and Parkinson's disease? *Park. Relat. Disord.* 8, 289–295. doi: 10.1016/s1353-8020(02)00014-7

Shuo, G. (2016). *Analysis of Hormone and Microflora in Genital Tract of High or Low Prolificacy Sows 12 Days Post Insemination*. Nanjing, China: Nanjing Agricultural University.

Styczynska-Soczka, K., Zechini, L., and Zografos, L. (2017). Validating the Predicted Effect of Astemizole and Ketoconazole Using a Drosophila Model of Parkinson's Disease. *Assay Drug Dev. Technol.* 15, 106–112. doi: 10.1089/adt.2017.776

Suo, C., Yin, Y., Wang, X., Lou, X., Song, D., Wang, X., et al. (2012). Effects of lactobacillus plantarumZJ316 on pig growth and pork quality. *BMC Vet. Res.* 8:89. doi: 10.1186/1746-6148-8-89

Upadhyaya, B., Mccormack, L., Fardin-Kia, A. R., Juenemann, R., Nichenametla, S., Clapper, J., et al. (2016). Impact of dietary resistant starch type 4 on human gut microbiota and immunometabolic functions. *Sci. Rep.* 6:28797.

Ventolini, G. (2015). Vaginal Lactobacillus: biofilm formation in vivo - clinical implications. *Int. J. Womens Health* 7, 243–247. doi: 10.2147/ijwh.s77956

Wang, H., Hu, C., Cheng, C., Cui, J., Ji, Y., Hao, X., et al. (2019). Unraveling the association of fecal microbiota and oxidative stress with stillbirth rate of sows. *Theriogenology* 136, 131–137. doi: 10.1016/j.theriogenology.2019.06.028

Wang, Q., Garrity, G. M., Tiedje, J. M., and Cole, J. R. (2007). Naive Bayesian classifier for rapid assignment of rRNA sequences into the new bacterial taxonomy. *Appl. Environ. Microbiol.* 73, 5261–5267. doi: 10.1128/aem.00062-07

Wishart, D. S., Feunang, Y. D., Marcu, A., Guo, A. C., Liang, K., Vázquez-Fresno, R., et al. (2018). HMDB 4.0: the human metabolome database for 2018. *Nucleic Acids Res.* 46, D608–D617.

Wu, G., Zhao, N., Zhang, C., Lam, Y. Y., and Zhao, L. (2021). Guild-based analysis for understanding gut microbiome in human health and diseases. *Genome Med.* 13:22. doi: 10.1186/s13073-021-00840-y

Xiao, Y., Li, K., Xiang, Y., Zhou, W., Gui, G., and Yang, H. (2017). The fecal microbiota composition of boar Duroc, Yorkshire, Landrace and Hampshire pigs. *Asian-Australas J. Anim. Sci.* 30, 1456–1463. doi: 10.5713/ajas.16.0746

Xu, K., Bai, M., Liu, H., Duan, Y., Zhou, X., Wu, X., et al. (2020). Gut microbiota and blood metabolomics in weaning multiparous sows: associations with oestrous. *J. Anim. Physiol. Anim. Nutr.* 104, 1155–1168. doi: 10.1111/jpn.13296

Yang, H., Yang, M., Fang, S., Huang, X., He, M., Ke, S., et al. (2018). Evaluating the profound effect of gut microbiome on host appetite in pigs. *BMC Microbiol.* 18:215. doi: 10.1186/s12866-018-1364-8

Yu-Jiao, J., Qian, Z., Mei-Mei, G., Wen, C., Yu-Long, Y., and Xiang-Feng, K. (2016). Effect of diets with high- or low-level nutrient on colonic microbial community structure and metabolites in Huanjiang mini-pigs. *Microbiol. China* 43, 1650–1659.

Zhu, K., Tan, F., Mu, J., Yi, R., Zhou, X., and Zhao, X. (2019). Anti-Obesity Effects of Lactobacillus fermentum CQPC05 Isolated from Sichuan Pickle in High-Fat Diet-Induced Obese Mice through PPAR-alpha Signaling Pathway. *Microorganisms* 7:194. doi: 10.3390/microorganisms7070194

Zou, Y., Xue, W., Luo, G., Deng, Z., Qin, P., Guo, R., et al. (2019). 1,520 reference genomes from cultivated human gut bacteria enable functional microbiome analyses. *Nat. Biotechnol.* 37, 179–185. doi: 10.1038/s41587-018-0008-8

Conflict of Interest: The authors declare that the research was conducted in the absence of any commercial or financial relationships that could be construed as a potential conflict of interest.

Publisher's Note: All claims expressed in this article are solely those of the authors and do not necessarily represent those of their affiliated organizations, or those of the publisher, the editors and the reviewers. Any product that may be evaluated in this article, or claim that may be made by its manufacturer, is not guaranteed or endorsed by the publisher.

frontiers in Microbiology

ORIGINAL RESEARCH
published: 10 September 2021
doi: 10.3389/fmicb.2021.709611

Breeding Strategy Shapes the Composition of Bacterial Communities in Female Nile Tilapia Reared in a Recirculating Aquaculture System

*Yousri Abdelhafiz[1], Jorge M. O. Fernandes[1], Simone Larger[2], Davide Albanese[2], Claudio Donati[2], Omid Jafari[1,3], Artem V. Nedoluzhko[1] and Viswanath Kiron[1]**

[1]Faculty of Biosciences and Aquaculture, Nord University, Bodø, Norway, [2]Unit of Computational Biology, Fondazione Edmund Mach, San Michele all'Adige, Italy, [3]International Sturgeon Research Institute, Iranian Fisheries Science Research Institute, Agricultural Research, Education and Extension Organization, Rasht, Iran

OPEN ACCESS

Edited by:
Haidong Yao, Karolinska Institutet (KI), Sweden

Reviewed by:
Hetron Mweemba Munang'andu, Norwegian University of Life Sciences, Norway
Hien Van Doan, Chiang Mai University, Thailand

***Correspondence:**
Viswanath Kiron
kiron.viswanath@nord.no

Specialty section:
This article was submitted to Systems Microbiology, a section of the journal Frontiers in Microbiology

Received: *14 May 2021*
Accepted: *13 August 2021*
Published: *10 September 2021*

Citation:
Abdelhafiz Y, Fernandes JMO, Larger S, Albanese D, Donati C, Jafari O, Nedoluzhko AV and Kiron V (2021) Breeding Strategy Shapes the Composition of Bacterial Communities in Female Nile Tilapia Reared in a Recirculating Aquaculture System. Front. Microbiol. 12:709611. doi: 10.3389/fmicb.2021.709611

In industrial animal production, breeding strategies are essential to produce offspring of better quality and vitality. It is also known that host microbiome has a bearing on its health. Here, we report for the first time the influence of crossbreeding strategy, inbreeding or outbreeding, on the buccal and intestinal bacterial communities in female Nile tilapia (*Oreochromis niloticus*). Crossbreeding was performed within a family and between different fish families to obtain the inbred and outbred study groups, respectively. The genetic relationship and structure analysis revealed significant genetic differentiation between the inbred and outbred groups. We also employed a 16S rRNA gene sequencing technique to understand the significant differences between the diversities of the bacterial communities of the inbred and outbred groups. The core microbiota composition in the mouth and the intestine was not affected by the crossbreeding strategy but their abundance varied between the two groups. Furthermore, opportunistic bacteria were abundant in the buccal cavity and intestine of the outbred group, whereas beneficial bacteria were abundant in the intestine of the inbred group. The present study indicates that crossbreeding can influence the abundance of beneficial bacteria, core microbiome and the inter-individual variation in the microbiome.

Keywords: breeding, Nile tilapia, microbiome, 16S amplicon, whole-genome sequencing, core microbiome

INTRODUCTION

Animals are bred for food, fibers, transport, protection, company as well as for other purposes such as scientific research (Flint and Woolliams, 2008). Domestication of different animals, mainly livestock species started several years ago and presently crossbreeding programs are essential tools to improve the productivity, efficiency, and sustainability of domesticated animals (Hill, 2014, 2016). Initially, livestock were selected based on desired phenotypic traits. Over the past 50 years, there has been a remarkable increase

in livestock production due to the improvement in breeding practices and better understanding of genetics. Genetics plays an important role in modern breeding programs, which combine basic breeding concepts and emerging technologies (Schultz et al., 2020).

Crossbreeding of farmed animals and agricultural plants is well-established compared to those of farmed aquatic animals (D'ambrosio et al., 2019; Gratacap et al., 2019). However, the production of fish based on crossbreeding programs is expected to increase as the farming of fish such as Nile tilapia (*Oreochromis niloticus*) and Atlantic salmon (*Salmo salar*) is expanding rapidly (Gjedrem et al., 2012; Gjedrem and Rye, 2018; Mehar et al., 2019). Several strategies such as selective breeding have been implemented to increase the production of fast-growing fish species and their disease resistance (Lind et al., 2012; Ina-Salwany et al., 2019). Nevertheless, outbreak of many diseases such as Tenacibaculosis (yellow mouth), Streptococcosis and Vibriosis has led to high mortality in fish farms and the industry has suffered huge economic losses (Jantrakajorn et al., 2014; Ina-Salwany et al., 2019; Wynne et al., 2020). The industry has hardly taken steps to selectively breed fishes in order to shape the microbiota as an indicator of health. It has been reported that selective breeding can produce fishes with microbiota that can be manipulated to improve disease resistance (Piazzon et al., 2020).

Currently, there are many genetically improved tilapia and GIFT (Genetically Improved Farmed Tilapia) is the most known breed. Although many studies have employed genetically improved tilapia (Bolivar and Newkirk, 2002; Romana-Eguia et al., 2005; Santos et al., 2013; Mehar et al., 2019), to our knowledge there are only a couple of reports about the microbiome composition in selectively bred fish (Kokou et al., 2018; Brown et al., 2019). In mouse, selective breeding is known to increase the inter-individual gut microbiota similarity (Pang et al., 2012); variation is less in the case of inbred animals compared to their outbred counterparts (Hufeldt et al., 2010). Researchers have also succeeded in producing outbred mice with stable gut microbiota (Hart et al., 2018). Furthermore, the association between the gut microbiome and breeding was studied in mouse models by analysing the effect of the gut microbiome on different breeds (Pang et al., 2012; Kreisinger et al., 2014; Ericsson et al., 2015; Oriá et al., 2018). This link was also explored in plants by examining the impact of the microorganisms on host phenotype (Wagner et al., 2020). Moreover, the microbial taxa that is widespread among the host population is vertically transmitted, and host factors provide them with the optimum ecosystem for colonization (Risely, 2020).

Selective breeding affects host genetic selection, which in turn shapes the gut microbiome (Kokou et al., 2018) that has an important role in, among others, maintaining the host health. The paucity of information regarding the mating strategy-caused changes in fish microbiome that can signal disease propensity led us to examine the differences in the bacteria associated with inbred and outbred Nile tilapia using next-generation sequencing technology.

MATERIALS AND METHODS

Fish Husbandry and Sample Collection

Fertilized eggs ($n = 180$) of Nile tilapia, were obtained from wild fish captured from the Nile river, Luxor, Egypt (location GPS: 25°39'56'' N, 32°37'07'' E). These eggs were disinfected with hydrogen peroxide for 10 min and placed in egg rockers (Cobalt Aquatics, Rock Hill, South Carolina, United States) installed in a 60 L tank with UV treated water, containing 5% NaCl. Around 85% of the eggs were hatched at 28°C within 4 days. The hatched larvae were placed in fish transport bags filled with UV treated and 100% oxygen saturated water. These larvae were shipped, within approximately 18 h, to the Research Station of Nord University, Bodø, Norway *via* air and their survival rate exceeded 95%. The transported larvae were reared at a maximum density of 27 fish/m^3 for 5 months in a freshwater recirculating system. The rearing conditions were: dissolved oxygen – 100%, water temperature –28°C, photoperiod – LD 13:11. The fish were fed Amber Neptun pellets (0.15–0.8 mm, Skretting, Stavanger, Norway) during the rearing period. These fish were designated as the F0 generation and were used for the breeding study.

We randomly chose males and females and produced the inbred and outbred groups. When the fish reached 3,570 degree·days, we anesthetized and PIT-tagged them for tracing the individual families.

Prior to sampling, fish were not fed for 48 h. They were sacrificed by immersion in an emulsion containing 12 ml of clove oil (Sigma Aldrich, St. Louis, Missouri, United States), 96% ethanol (1:10 v/v) and 10 L of water (Simões et al., 2011; Konstantinidis et al., 2020). Female fish were used for the study as they are maternal mouthbrooders. Twenty fish each from the inbred and outbred groups were used in this study, and three body sites (mouth, anterior and posterior intestine) of female Nile tilapia were targeted for examining the bacterial communities. Mucus samples from the buccal cavity were taken using swabs (Copan Italia, Brescia, Italy), which were transferred to cryotubes and immediately frozen in liquid nitrogen. Then, the same fish were aseptically dissected to collect the anterior and posterior intestine. The intestine samples were also transferred to cryotubes and snap-frozen in liquid nitrogen. The collected samples were stored at −80°C until further use.

DNA Extraction for Whole-Genome Sequencing

DNA was extracted from fast muscle using DNeasy Blood and Tissue Kit based on the guidelines provided by the manufacturer (Qiagen, Hilden, Germany). The Invitrogen Qubit 3.0 fluorometer (ThermoFisher Scientific, Waltham, Massachusetts, United States) was used to quantify the concentration of DNA in the samples. Quality (based on 260/280 and 260/230 absorbance ratios) and integrity (based on DIN values) of the extracted DNA samples were checked using Nanodrop 1000 Spectrophotometer (ThermoFisher Scientific) and TapeStation 2200 DNA screen (Agilent Technologies, Santa Clara, California, United States), respectively.

DNA Extraction for 16S Amplicon Analysis

All the procedures mentioned here were performed under sterile conditions. Before extracting the DNA, intestine samples were transferred to a sterile Petri dish and placed on a cool-pack on dry ice. The intestine was opened and transferred to a 5 ml tube containing 1.4 mm Zirconium oxide beads (Cayman Chemical, Ann Arbor, Michigan, United States) and 2 ml of InhibitEX buffer (Qiagen). Thereafter, DNA was extracted immediately using QIAamp DNA stool Mini Kit (Qiagen) according to the manufacturer's protocol. The final elution volume was 75 µl (ATE buffer). The same extraction method was employed for the mouth samples. The quality and quantity of the extracted DNA were checked with NanoDrop spectrophotometer ND-8000 (ThermoFisher Scientific).

Libraries Preparation and Sequencing

Whole-Genome Sequences

The Nextera DNA Flex library preparation kit with dual indices was used to prepare whole genome libraries based on the manufacturer's protocol (Illumina, San Diego, California, United States). After tagmentation of the extracted gDNA samples using Bead-linked transposomes at 55°C for 15 min, the sheared and tagmented gDNA was washed at 30°C for 15 min. Amplification of the tagmented gDNA was performed using a 5-cycle PCR programme wherein the index 1 (i7) and index 2 (i5) adapters were added for sequencing cluster formation. The PCR program was started with an incubation at 68°C for 3 min and a subsequent pre-denaturation at 98°C for 3 min. In the following step, 5 cycles of denaturation at 98°C for 45 s, annealing at 62°C for 30 s and extension at 68°C for 2 min were first performed, followed by a final extension at 68°C for 1 min. In the final step of the library preparation, the amplified libraries were purified through a double-sided bead (Bead-linked transposome; Illumina) purification procedure. The quality and normality of the libraries were assessed with the Agilent Tapestation instrument using High Sensitivity D1000 screen tape. After normalization based on the minimum observed molarity, the barcoded samples were pooled before the sequencing run. The 75 bp paired-end sequencing was done on a NextSeq 500 sequencer (Illumina) at the sequencing platform of Nord University.

Bacterial 16S Sequences

Under sterile conditions, 16S rRNA gene libraries were constructed from DNA extracts using the specific bacterial primers 341F (5'CCTACGGGNGGCWGCAG 3') and 805R (5'GACTACNVGGGTWTCTAATCC 3'; Klindworth et al., 2013) flanked by overhang Illumina adapters targeting the hypervariable V3–V4 region (~460 bp). PCR reactions were performed for each sample in 25 µl, using Q5® High-Fidelity 2X Master Mix (New England Biolabs, Ipswich, Massachusetts, United States) and 2.5 µl of DNA template (5 ng/µl). PCR conditions consisted of an initial denaturation step at 95°C for 10 min (1 cycle), 30 cycles at 95°C for 30 s, 57°C for 30 s, 72°C for 1 min, and a final extension step at 72°C for 7 min (1 cycle).

An agarose gel (1.5%) was employed to check the amplified products. The PCR products were purified using the CleanNGS system (CleanNA, Waddinxveen, Netherlands) following the manufacturer's instructions. The purified product was subjected to a second PCR (8 cycles, 16S Metagenomic Sequencing Library Preparation, Illumina); this step was done to add dual indices and Illumina sequencing adapters Nextera XT Index Primer (Illumina). CleanNGS (CleanNA) was used to purify the obtained amplicon libraries. The quality of the libraries was checked on a Tapestation 2200 platform (Agilent Technologies). Thereafter, the libraries were quantified using the Quant-IT PicoGreen dsDNA assay kit (ThermoFisher Scientific) by the Synergy2 microplate reader (Biotek, Winooski, Vermont, United States). Next, the pooled libraries were quantified using the KAPA Library quantification kit (Roche, Basel, Switzerland). The libraries were checked by realtime qPCR LightCycler 480 (Roche) and then sequenced on an Illumina® MiSeq (PE300) platform (MiSeq Control Software 2.5.0.5 and Real-Time Analysis software 1.18.54.0).

Sequence Analysis

Whole-Genome Sequences

In order to perform demultiplexing and obtain the fastq files, the Illumina Experiment Manager v1.18.1 along with bcl2fastq v2.20.0.422 was used. Thereafter, dual adapter indexes and Ns from the 3' end of the raw reads were trimmed and the quality of the cleaned fastq files was assessed employing Trime_galore v0.4.4 (Babraham Bioinformatics; http://www.bioinformatics.babraham.ac.uk/projects/trim_galore/). The clean reads were then aligned to the reference genome O_niloticus_UMD_NMBU, GCA_001858045.3 (Conte et al., 2017) using Bowtie2 v0.12.8 with the --very-sensitive option (Langmead and Salzberg, 2012). The bcftools pipeline was applied for variant calling (Li, 2011), and the generated SAM files were converted to the binary format and sorted based on coordinates using samtools v1.9. Also, the samtools markedup command was used to mark duplicate reads. Then variants were called using bcftools mpileup command (bcftools 1.9) with the minimum base and mapping quality of 20 (−q 20 −Q 20). Using bcftools filter command accompanied by the options --SnpGap 5 -i 'MQ > 20 and QUAL>20 and DP > 100 and DP < 450 and TYPE = "snp," only SNP variants were kept in the Variant Call Format (VCF). The missing genotypes were imputed using imp-states = 1,600 option in Beagle v5.0 (Browning and Browning, 2016). Thereafter, using vcftools, the non-biallelic SNP variants were omitted so that the generated VCF file had only the biallelic SNPs (Danecek et al., 2011). This VCF file was read by vcfR package (Knaus and Grünwald, 2017).

Bacterial 16S Amplicon Sequences

The generated reads were truncated at 270 bp using VSEARCH (Rognes et al., 2016), and then processed using MICCA pipeline (v1.7.2; Albanese et al., 2015). Sequences with a minimum overlap length of 60 bp and a maximum mismatch of 20 bp were merged. Next, the forward and reverse primers were trimmed off the merged reads and reads which did not contain

the primers were discarded. Thereafter, the sequences with an expected error rate (Edgar and Flyvbjerg, 2015) >0.75 were filtered out and shorter than 400 bp sequences were discarded. Filtered reads were denoised using the "*de novo* unoise" method implemented in MICCA, which utilise UNOISE3 algorithm (Edgar, 2016). The denoising method generates amplicon sequence variants (ASVs) which is based on correcting sequencing errors and determining true biological sequences at single-nucleotide resolution. The taxonomic assignment of the representative bacterial ASVs was performed using RDP classifier. The sequences were aligned using the NAST (Desantis et al., 2006) multiple sequence aligner, and a phylogenetic tree was prepared using the FastTree software available in the MICCA pipeline.

Statistical Analysis of Host Genetic Data

To quantify the genetic diversity of the inbred and outbred groups, we first determined the genetic diversity within members of the crossbred groups, and then the between groups genetic diversity. For this, we quantified the level of heterozygosity, using the population package of the Stacks 2.3b. Next, to assess the level of genetic differentiation based on allele frequencies between different groups, the F_{st} index was calculated using the StAMPP package (Pembleton et al., 2013). In order to quantify the genetic relationship between the inbred and outbred groups, Nei-based genetic distance between individuals was estimated using poppr (Kamvar et al., 2015) and adegenet (Jombart, 2008) packages and visualized using pheatmap package (Kolde and Kolde, 2015). Then the genetic relationship between the crossbred groups was assessed by PCoA (employing the abovementioned Nei-based genetic distance), also using the ape package (Paradis and Schliep, 2019). PERMANOVA (Permutational Multivariate Analysis of Variance) was performed to decipher the significance of genetic differences between the inbred and outbred groups. To further analyze the population structure of the inbred and outbred groups, admixture analysis was performed in adegenet for values of ancestries (K) from 1 to 10 with 10 repeats for each value of K, decided based on Bayesian Information Criteria. Four samples were removed due to the low quality of sequences.

Statistical Analysis of 16S Amplicon Data

Statistical analysis was conducted using R (version 3.6.3) software. The packages phyloseq (McMurdie and Holmes, 2013) and vegan (Oksanen et al., 2013) were employed to analyse the data. All plots were made using ggplot2 package (Wickham, 2011).

To understand the differences between the proportions of different bacteria in the inbred and outbred groups, we performed chi-square test and the associated *post hoc* analyses. A subset of the most dominant phyla was employed for this analysis. The similarities/differences in α-diversity were checked by Wilcoxon rank-sum test. Bacterial β-diversity was determined using unweighted and weighted UniFrac distances (Lozupone and Knight, 2005). Differences between the bacterial communities of the two groups were visualized by PCoA. After checking the dispersions within the data set of each group, statistically significant differences between the groups were assessed using PERMANOVA (Anderson, 2001; with 9,999 permutations), implemented in adonis function of the vegan R-package (Oksanen et al., 2013). DESeq2 (Love et al., 2014) package was employed to detect the differentially abundant ASVs in the non-rarefied data (McMurdie and Holmes, 2014). The core microbiota was analysed using the packages microbiome and microbiome utilities; at a detection level of 0.2% and prevalence level of 90%. The differences in the core bacterial community in the two crossbred groups were analysed by performing PERMANOVA on weighted and unweighted UniFrac distances. The abundances in the different ASVs which made up the core microbiome were analyzed using Spearman test (Zar, 2014) and correlation plot package (Wei and Simko, 2017).

RESULTS

Genetic Background-Associated Changes in the Microbiome of Nile Tilapia

A total of 11,578,530 SNPs were obtained after the initial SNP calling. Bcftools was employed to first calculate genotype likelihoods for each position and then filter out every position with actual sequence variant. Thus, 4,693,720 SNPs were filtered out and finally after biallelic filtration, 6,825,083 SNP variants with an average coverage of 1.74 per sample were used in the final VCF file.

The genetic diversity analysis based on nucleotide sequences revealed that the observed heterozygosity (Ho) values were slightly higher compared to the expected heterozygosity values (He; **Table 1**).

The fixation index (F_{st}) value within groups was 0.04 for both Inbred-S1 vs. Inbred-C6 and Outbred-S3 vs. Outbred-C9 comparisons. On the other hand, the F_{st} values between crossbred groups were in the range 0.06–0.08 (**Table 2**).

The Nei-based genetic distances between the inbred and outbred groups were employed to generate a heatmap to understand their genetic relationships; differences between the

TABLE 1 | Observed (Ho) and expected (He) heterozygosity of the crossbred female Nile tilapia.

	Ho	*He*
Outbred-S3	0.171	0.157
Inbred-S1	0.164	0.153
Inbred-C6	0.167	0.155
Outbred-C9	0.166	0.149

TABLE 2 | Genetic differentiation, based on *Fst* index, of the crossbred female Nile tilapia.

	Outbred-S3	**Inbred-S1**	**Inbred-C6**	**Outbred-C9**
Outbred-S3	-			
Inbred-S1	0.061	-		
Inbred-C6	0.077	0.041	-	
Outbred-C9	0.044	0.058	0.074	-

groups are seen in **Supplementary Figure 1**. Principal Coordinates Analysis (PCoA) based on the Nei-based genetic distance indicated that the first two components captured 17.7 and 7.8% of the variation in the data set (**Figure 1A**). Furthermore, a PERMANOVA test based on the same genetic distance showed that the inbred and outbred groups were significantly different ($p = 0.001$). The genetic sub-population clustering based on admixture analysis revealed that K = 2 was the optimal number to explain the genetic structure of the inbred and outbred groups (**Supplementary Figure 2**). The results also indicated that 4 inbred individuals are genetically similar to the outbred population.

To delineate the effect of genetic selection on gut microbiota composition, the inbred and outbred Nile tilapia were reared in a common garden and the environmental and nutritional factors that affect the microbiota were kept constant throughout the experimental period. The amplicon library of 16S rRNA gene, generated 12,034,190 high-quality reads with an average coverage of 54,016 reads per sample. Due to the variation in sample size, the reads were rarefied to 18,000 reads per sample (without replacement). Out of the 120 samples, six libraries with a number of reads below the cut off were discarded. After normalization we obtained 14,228 ASVs, distributed among 30 phyla and 695 genera.

First, we investigated the dominant communities in the two groups. In their order of dominance, the most dominant bacterial phyla in both the inbred and outbred fish groups were *Proteobacteria*, *Fusobacteria*, *Firmicutes*, *Bacteroidetes*, and *Actinobacteria* (**Figure 1B**). This order of dominance was reflected in the microbial composition at the genus level also. Most of the dominant genera in the two crossbred groups belonged to the phylum *Proteobacteria* (*Acinetobacter*,

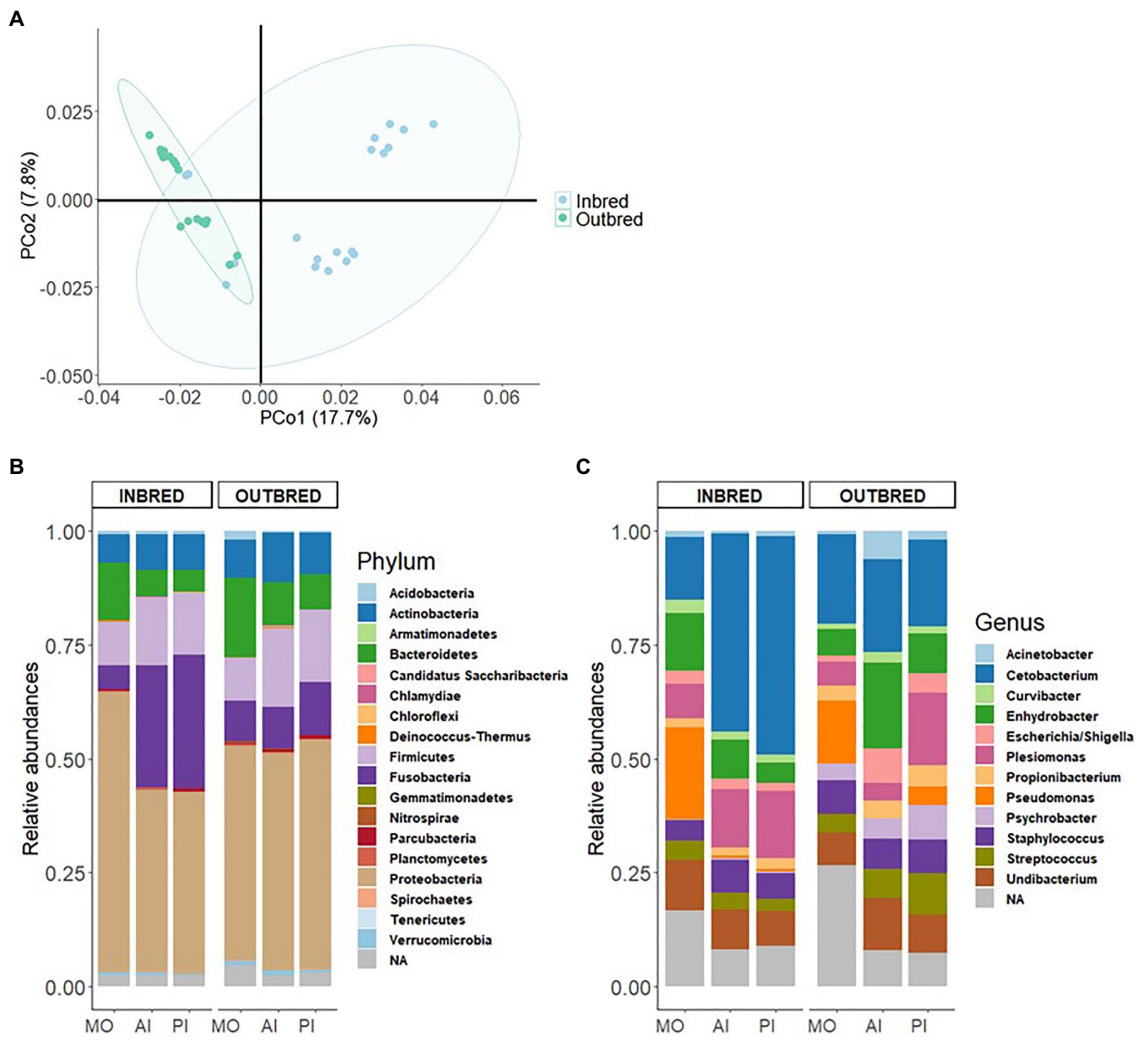

FIGURE 1 | Genetic differentiation and microbiome in the inbred and outbred groups of Nile tilapia. **(A)** Principal coordinates analysis (PCoA) plot based on 6,825,083 SNPs of the inbred and outbred groups. The ellipses were generated assuming that the data are from a multivariate normal distribution. **(B)** Phylum-level relative abundance of the microbial composition in the inbred and outbred groups. **(C)** Relative abundance of top 12 genera in the inbred and outbred groups.

Curvibacter, *Enhydrobacter*, *Escherichia/Shigella*, *Plesiomonas*, *Pseudomonas*, *Psychrobacter*, and *Undibacterium*). The most abundant genus was *Cetobacterium* which belongs to the phylum *Fusobacteria* (**Figure 1C**).

To understand the differences in proportions of the dominant communities in each study group, we performed chi-square test. The analyses revealed that the abundances of the most dominant phyla in both the inbred and outbred groups were significantly different (**Supplementary Table 1**).

To characterize the microbial diversity within the samples, we calculated three ecological indexes, namely the Chao1 estimator of the number of species, which is a measure of richness, the Shannon diversity which measures the evenness of the microbial populations and the Simpson diversity, which measures the importance of dominant species (Marcon and Hérault, 2015; Hsieh et al., 2016). Shannon diversity analysis showed that the microbial diversity in the mouth of the inbred group was lower compared to the outbred group (**Figure 2**, $p = 0.01$). The Simpson diversity analysis indicated that there were fewer dominant ASVs in the posterior intestine of the inbred group (**Figure 3**, $p = 0.04$). Although there were no significant differences in species richness of the communities associated with the two groups, in each body site (**Supplementary Table 2**), there was an increasing trend ($p = 0.08$; inbred higher richness) in the case of the anterior intestine (**Figure 4**). Furthermore, the diversity analysis of dominant bacteria (Simpson diversity) in the mouth and anterior intestine revealed a trend in differences ($p = 0.08$ and 0.06, respectively; **Figures 2, 4**).

Beta diversity analysis was performed to evaluate the overall dissimilarity between the two crossbred groups (**Figure 5**). The results of PERMANOVA on the unweighted UniFrac distances showed a significant difference between the bacterial composition in the posterior intestine of the inbred and outbred groups ($p = 0.003$). There was no significant difference between the communities in the mouth or the anterior intestine of the two groups ($p = 0.082$ and 0.311, respectively). In the mouth, there may exist a difference in composition between the two groups, based on the observed trend (**Table 3**).

Considering the weighted UniFrac distance, there was a significant difference in the community composition of the anterior intestine ($p = 0.001$). In addition, there was a significant difference in the community of posterior intestine ($p = 0.003$), but not in the case of mouth ($p = 0.37$; **Table 3**).

Differential Abundance of ASVs: Outbred Group vs. Inbred Group

The package DESeq2 was used to identify the ASVs with a significantly different abundance in the outbred group compared to the inbred group. In the mouth, the bacteria belonging to *Actinobacteria*, *Armatimonadetes*, *Firmicutes*, and *Proteobacteria* were differentially abundant. There were six genera that belonged to the phylum *Proteobacteria*. Bacteria belonging to two genera (*Psychrobacter* and *Polaromonas*) were 5-fold higher in the outbred group, while those of *Pseudomonas* and *Acinetobacter* were 20-fold higher in the same group. Furthermore, an ASV of the genus *Limnohabitans* was about 9-fold lower and *Comamonas* was 20-fold lower in the outbred group. *Lachnospiracea_incertae_sedis* were about 5-fold higher in the outbred group, whereas the genus *Bacillus* was 20-fold lower. These two genera belong to the phylum *Firmicutes*. Also, *Armatimonadetes_gp5* was 20-fold lower in the outbred group (**Supplementary Figure 3**). In the anterior intestine, the majority of the ASVs that were differentially abundant in the outbred group had fold changes between −5 and −15

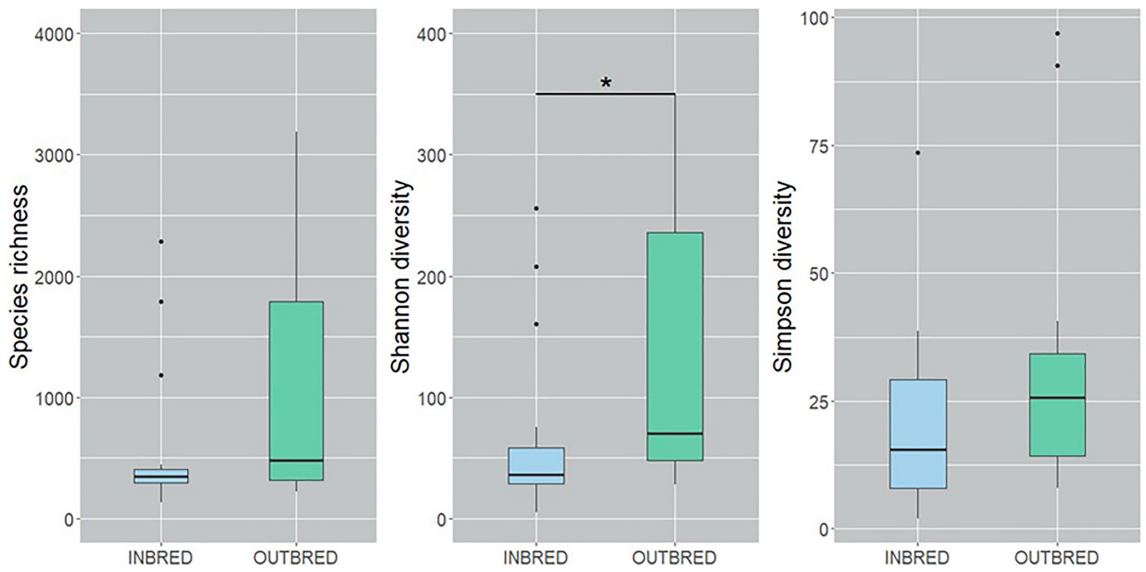

FIGURE 2 | Alpha diversity of the bacteria in the mouth of the inbred and outbred groups of Nile tilapia. Species richness of the groups is not significantly different. Shannon diversity is higher in the outbred group ($p = 0.007$, indicated with an asterisk). Simpson diversity indicated an increasing trend in the dominant ASVs of the outbred group ($p = 0.08$). The boxplots show minimum, lower quartile, median, upper quartile and maximum values.

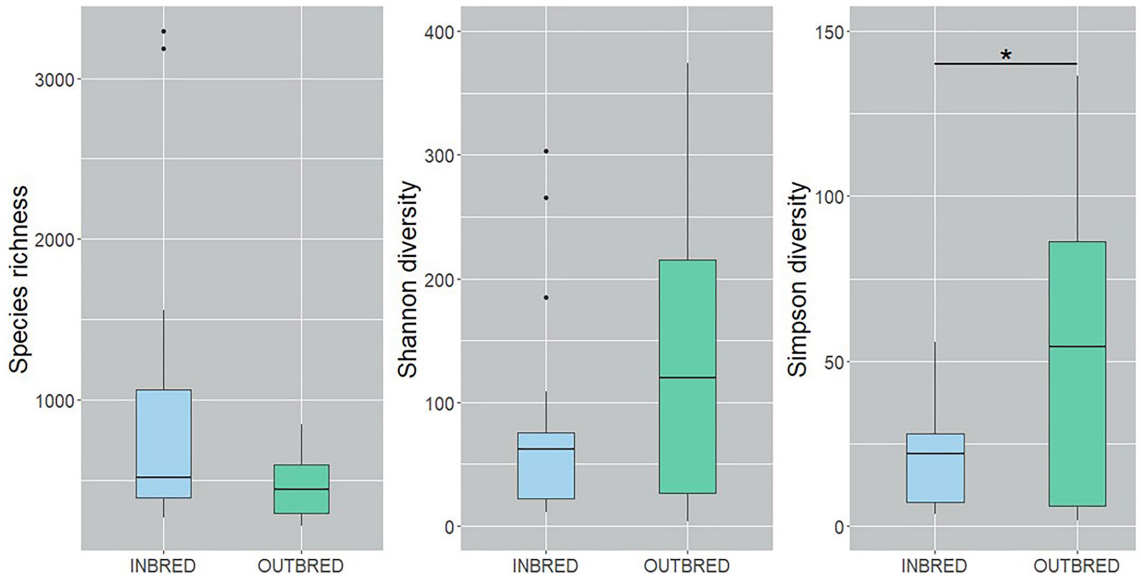

FIGURE 3 | Alpha diversity of the bacteria in the posterior intestine of the inbred and outbred groups of Nile tilapia. Simpson diversity analysis showed that the dominant ASVs are higher in the outbred groups ($p = 0.04$, indicated with an asterisk). The boxplots show minimum, lower quartile, median, upper quartile and maximum values.

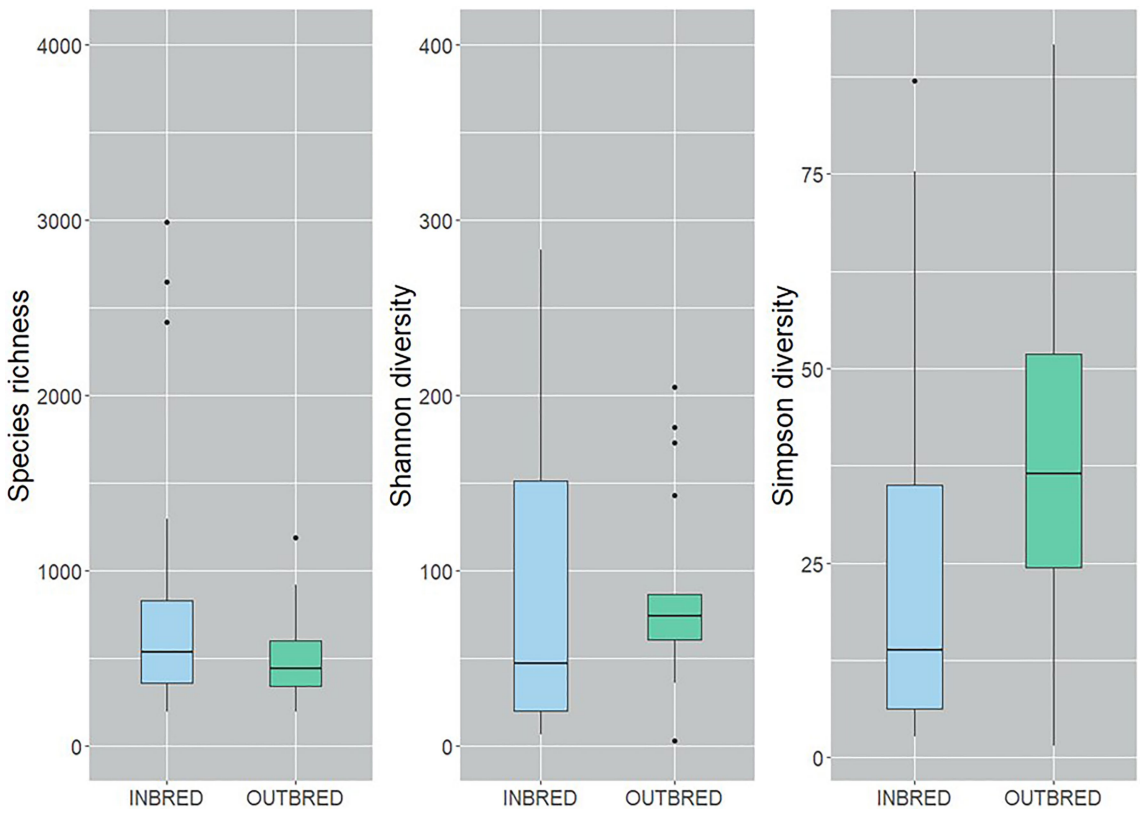

FIGURE 4 | Alpha diversity of the bacteria in the anterior intestine of the inbred and outbred groups of Nile tilapia. There is an increasing trend in the species richness of the inbred group ($p = 0.07$). Simpson diversity shows an increasing trend in the dominant ASVs of the outbred group ($p = 0.06$). The boxplots show minimum, lower quartile, median, upper quartile and maximum values.

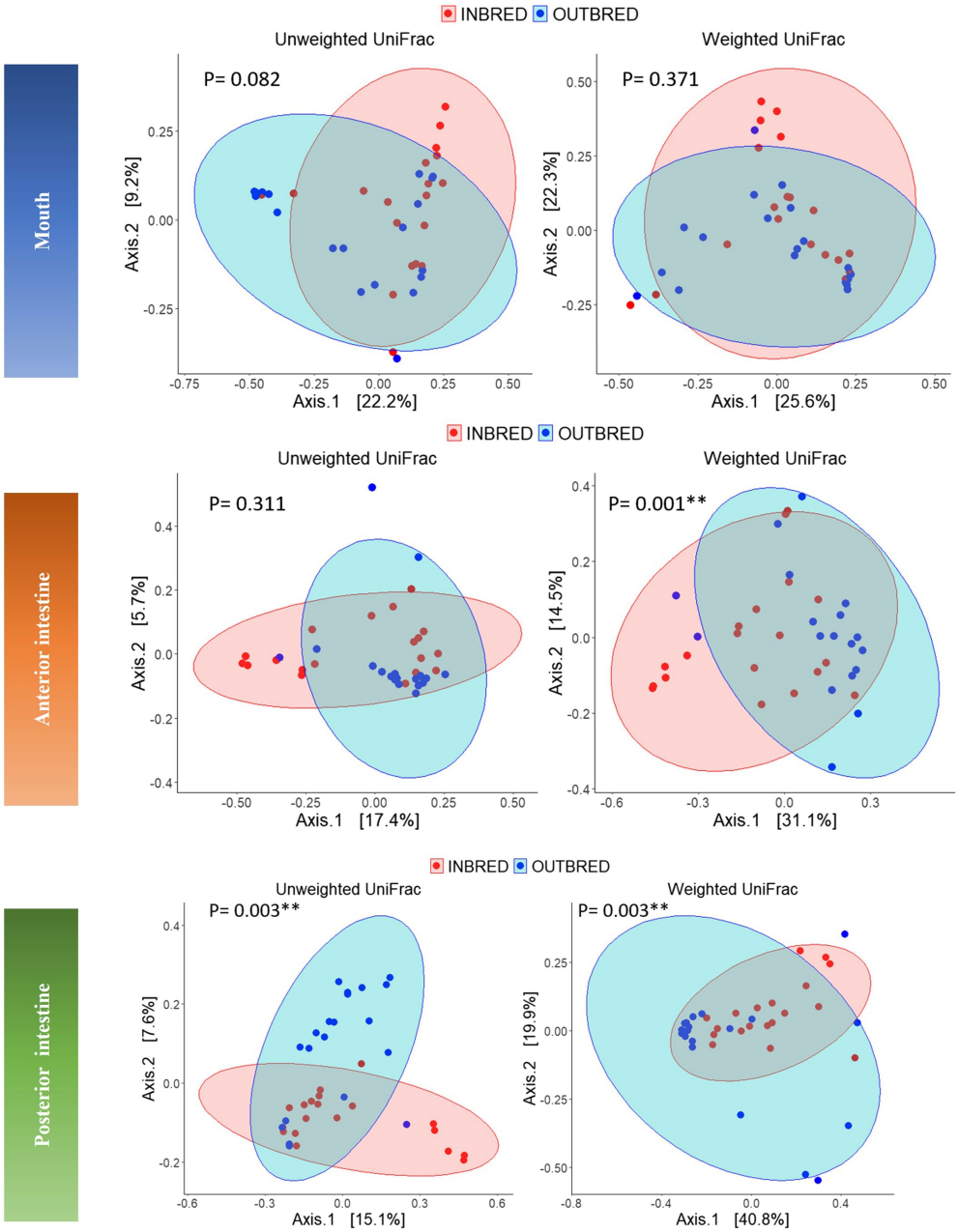

FIGURE 5 | Principal coordinates analyses (PCoA) using unweighted and weighted UniFrac distance matrices of the bacteria in the different body sites of the inbred and outbred groups of Nile tilapia. The ellipses were generated assuming that the data are from a multivariate normal distribution.

(**Supplementary Figures 4**, **5**) compared to the inbred group. However, the fold changes of the differentially abundant ASVs of *Bacteroidetes*, *Fusobacteria*, and *Proteobacteria* in the anterior intestine were between −5 and −10 (**Supplementary Figure 4** shows selected differentially abundant ASVs; **Supplementary Figure 5** shows all the differentially abundant ASVs). Similarly, in the posterior intestine, out of 31 ASVs that were differentially abundant, 30 ASVs had fold changes between −5 and −28 in the outbred group, while only one ASV that belongs to *Acinetobacter* was 20-fold higher in the outbred group (**Supplementary Figure 6**). Moreover, ASVs of *Pediococcus* and *Bifidobacterium* which belong to *Firmicutes* and *Actinobacteria*, respectively, were lower (log fold change; −5 and −8, respectively) in the posterior intestine of the outbred group (**Supplementary Figure 6**).

Core Microbiome and Variability in Taxa

In the mouth, 9 ASVs of the core microbiota belonged to the genera *Staphylococcus*, *Curvibacter*, *Undibacterium*, *Escherichia/Shigella*, *Enhydrobacter*, *Propionibacterium*, and

TABLE 3 | Results of the analysis of homogeneity of group dispersions and PERMANOVA using distance (unweighted and weighted UniFrac) matrices.

Comparison	Variable	Unweighted UniFrac distance			Weighted UniFrac distance		
		p-value dispersions	R^2	*p*-value adonis	*p*-value dispersions	R^2	*p*-value adonis
Outbred vs. Inbred	Mouth	0.86	0.08	0.08	0.62	0.029	0.37
	Anterior intestine	0.20	0.03	0.31	0.27	0.14	0.001**
	Posterior intestine	0.60	0.05	0.003**	0.05	0.10	0.003**

**Indicates $p < 0.05$.

Cetobacterium. However, two bacteria were classified only up to the order level – *Actinomycetales, Sphingobacteriales* (**Figure 6**). Taking all the 9 ASVs together, we observed a significant difference in the core microbiome in the inbred and outbred groups; only for unweighted UniFrac distance ($R^2 = 0.073$, $p = 0.043$; weighted UniFrac distance showed no significant difference; $R^2 = 0.024$, $p = 0.445$; **Table 4**). In the anterior and posterior intestine, the core ASVs were *Staphylococcus*, *Plesiomonas*, *Undibacterium*, *Enhydrobacter*, *Propionibacterium*, and *Cetobacterium* (**Figures 7A,B**). One extra genus was a member of the core microbiota in the anterior intestine (*Escherichia*/*Shigella*). One ASV in the anterior and posterior intestine was not classified up to the genus level, but was annotated as *Actinomycetales* (**Figures 7A,B**). The core microbiota in the anterior intestine of the inbred group was different from that of the outbred group; the weighted UniFrac distances-based assessment indicated the significant difference (PERMANOVA test; $R^2 = 0.155$, $p = 0.001$) between the two crossbred groups. As for the posterior intestine, we cannot specify that there is a significant difference between the crossbred groups (**Table 4**). The inter-individual variation in the abundance of the core microbiota in the intestine samples of the inbred group was less pronounced compared to the outbred groups (**Supplementary Figure 7**). On the other hand, the inter-individual variation in the abundances was more pronounced in the mouth of the inbred compared to the outbred group (**Supplementary Figure 8**).

DISCUSSION

The genetic structure of wild/domestic/experimental animals can be altered through breeding to retain desired phenotypic and genotypic traits across generations. It is known that selective breeding can preserve desired traits, which can affect the bacterial profile that is highly correlated to host health.

Gut microbiota in fish has been studied extensively in recent years considering mainly its importance in host health. In the present study, we used genetically distinct (based on SNP analysis) inbred and outbred Nile tilapia to investigate the impact of crossbreeding on the composition of the mouth and intestine bacteria.

Mouth and Intestine Bacterial Community Composition and Diversity in the Inbred and Outbred Groups

Although male Nile tilapia are widely farmed because of their higher growth rate, in the present study, we analyzed the microbial community in females, which are mouthbrooders. Hence, we believe that studying the microbial communities in its mouth will yield interesting results. In humans, microbiota is transferred from different body sites of mothers to infants (Ferretti et al., 2018). Moreover, microbial symbionts from discus (*Symphysodon aequifasciata*, another fish of the family Cichlidae) parents are vertically transferred to fry through feeding of a cutaneous mucus secretion (Sylvain and Derome, 2017). The most dominant phyla found in our samples were *Proteobacteria*, *Fusobacteria*, *Firmicutes*, *Bacteroidetes*, and *Actinobacteria* (**Supplementary Figure 9**). These are known to be the most represented phyla in model fishes such as zebrafish and threespine stickleback (Legrand et al., 2020). They are also dominant in farmed fishes like Nile tilapia even though many factors including diet (Ray et al., 2017; Souza et al., 2020), rearing systems (Giatsis et al., 2015; Yukgehnaish et al., 2020), and salinity (Zhang et al., 2016; Yukgehnaish et al., 2020) affect the abundance of these phyla in the gut. However, the role of crossbreeding in shaping microbial communities has not yet been reported in fish although it is studied in mice (Pang et al., 2012; Kreisinger et al., 2014), mammals (Alessandri et al., 2019), and plants (Wagner et al., 2020).

The dominant phyla were the same in both the inbred and outbred groups of Nile tilapia. *Proteobacteria* are facultative anaerobes, and they are the most abundant bacterial phylum in fish gut (Egerton et al., 2018). Furthermore, bacteria such as *Escherichia* and *Enhydrobacter* belonging to this phylum have the ability to make the gut environment conducive to strict anaerobes which colonize healthy gut (Shin et al., 2015). Although the aforementioned genera were present in the mouth and intestine of both the outbred and inbred fish, their abundances in the two groups were different. In addition, the genus *Curvibacter* which was present in both groups is known to have a critical role in colonization in freshwater invertebrates (Wein et al., 2018).

Alpha diversity analysis revealed that our crossbreeding strategy increased the microbial evenness in the mouth of the outbred group, in which we observed apparently higher species richness. The increasing trend in the dominant bacteria in the mouth and the anterior intestine of the outbred group along with the significant increase in the posterior intestine suggests that the dominant bacteria in the outbred groups are more diverse compared to the inbred group. On the other hand, the increasing trend in the species richness in the anterior intestine of the inbred group suggests that the bacterial

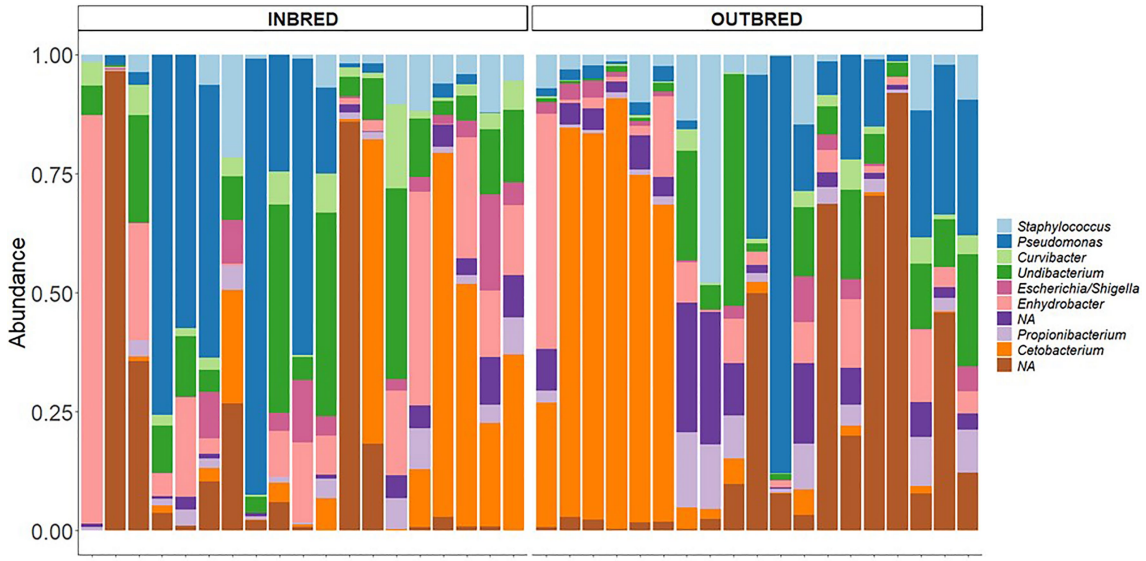

FIGURE 6 | Core microbiota in the mouth of the inbred and outbred groups of Nile tilapia. NAs: Not classified at the genus level, but at the order level, they are classified as *Actinomycetales*, *Sphingobacteriales*, in both groups.

TABLE 4 | Results of the analysis of homogeneity of group dispersions and PERMANOVA using distance (unweighted and weighted UniFrac) matrices of the core microbiota.

		Unweighted UniFrac distance			Weighted UniFrac distance		
Comparision	**Variable**	***p*-value dispersions**	***R*²**	***p*-value adonis**	***p*-value dispersions**	***R*²**	***p*-value adonis**
Outbred vs. Inbred	Mouth	0.834	0.0734	0.043*	0.742	0.0241	0.445
	Anterior intestine	0.08	0.0355	0.352	0.323	0.1553	0.0011**
	Posterior intestine	0.208	0.0181	0.541	0.003**	0.1238	0.0025**

*Indicates $p < 0.05$ and **indicates $p < 0.01$.

community is more diverse in this intestinal segment of the inbred group compared to the outbred group. The abovementioned findings are similar to the results of the PCoA analysis that used UniFrac distances. Microbial diversity is believed to have a positive correlation with host health (Deng et al., 2019). However, Reese and Dunn (2018) have stated that "understanding diversity in host-associated microbial communities will not be as simple as 'more diversity is better'." Hence, it is not ideal to correlate host health with the diversity in the outbred group. Studies in Nile tilapia have not reported a significant difference in the diversity of gut microbiota as a pathogenic effect (Suphoronski et al., 2019; Silva et al., 2020). On the other hand, while diet was shown to increase the species richness of bacteria in the gut, another environmental factor, salinity, was found to decrease the richness of bacteria in Nile tilapia (Zhang et al., 2016). The implication of the increasing trend in diversity in the anterior intestine of the inbred group should be clarified by conducting studies on the bacteria in this segment and their effect on nutritional physiology (Hallali et al., 2018). Thus, in addition to the aforementioned factors, we suggest that crossbreeding is a determinant of both the mouth and intestine bacterial diversity in female Nile tilapia.

Significant Differences Between the ASV Abundance of the Inbred and Outbred Groups

Fish gut harbors complex and diverse microbial communities, and the site is a reservoir of many opportunistic pathogens belonging to the genera *Acinetobacter*, *Aeromonas*, *Psychrobacter*, *Flavobacterium*, *Pseudomonas*, and *Pleisomonas*. Many commensal bacteria including *Cetobacterium*, *Methylobacterium*, *Sphingomonas*, and *Propionibacterium* (Suphoronski et al., 2019; Legrand et al., 2020; Silva et al., 2020) that colonise the fish gut are essential for the production of vitamin B12 and antimicrobial metabolites (Suphoronski et al., 2019; Legrand et al., 2020), protection against pathogens such as *Flavobacterium* (Boutin et al., 2014), and improving host health (Boutin et al., 2013). The differential ASV analysis revealed that the abundances of some of these opportunistic pathogens (*Psychrobacter*, *Pseudomonas*, and *Acinetobacter*) were more than 5-fold in the mouth of the outbred group compared to the inbred group. In the anterior and posterior intestine of the outbred group, although the opportunistic pathogens belonging to the genera *Acinetobacter*, *Aeromonas*, *Pleisomonas*, *Psychrobacter*, *Pseudomonas*, and *Flavobacterium* were differentially abundant,

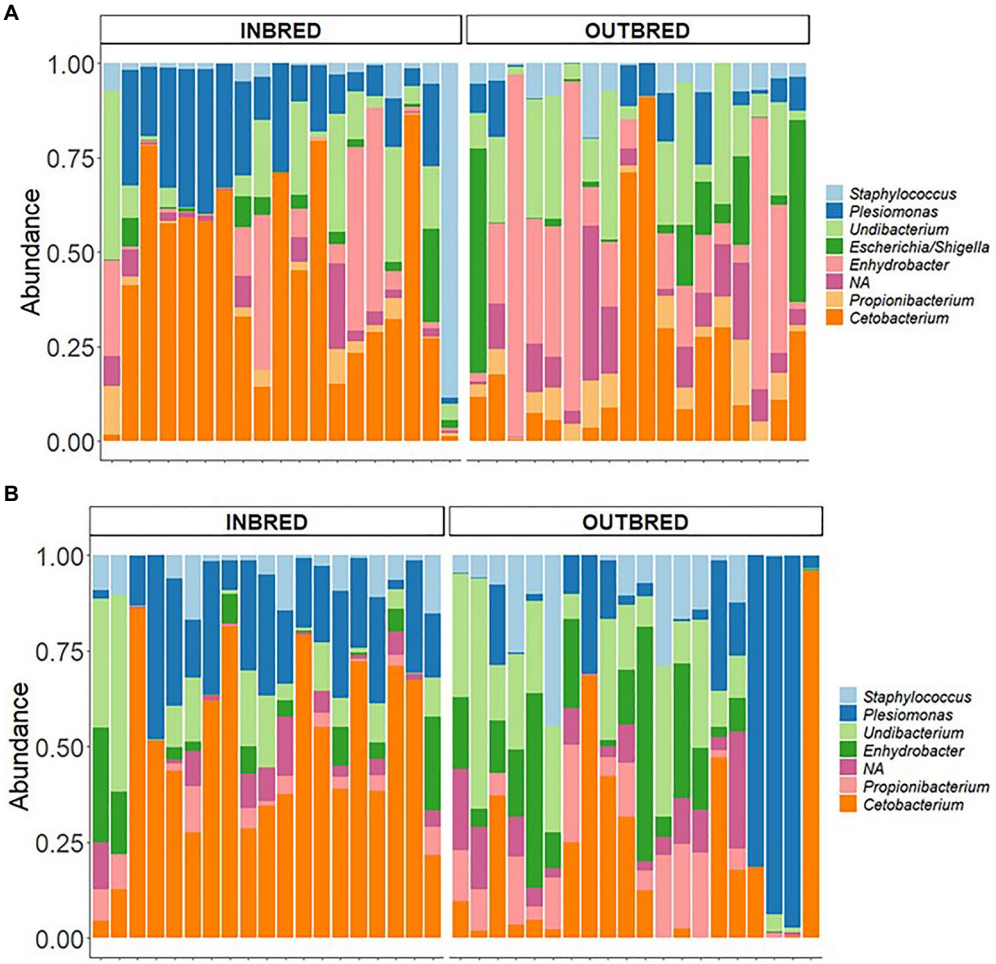

FIGURE 7 | Core microbiota in the anterior and posterior intestine of the inbred and outbred groups of Nile tilapia. **(A)** anterior intestine and **(B)** posterior intestine. NA: at the order level is classified as *Actinomycetales*.

their fold changes were less than 5-fold. The bacterial community in the mouth is extensively exposed to the external environment, and we found that the opportunistic pathogens in the mouth are more abundant in the outbred group. On the other hand, the abundance of potential pathogens was lower in the intestine of the inbred group. *Pseudomonas* sp. are opportunistic pathogens and they cause high mortality in farmed fishes (Oh et al., 2019). Moreover, bacteria belonging to *Flavobacterium* were reported to cause acute bacteremia primarily in small fishes or more chronic disease in larger fishes (Semple et al., 2020). Although the outbred fish had a more diverse microbiome, they appear to harbor potential opportunistic bacteria also.

Interestingly, the abundance of potential beneficial bacteria (*Cetobacterium*, *Methylobacterium*, *Sphingomonas*, and *Propionibacterium*; Boutin et al., 2013, 2014; Suphoronski et al., 2019; Legrand et al., 2020) was higher in the inbred group. Many studies report that commensal microbiota in the gut plays an important role in regulating the growth of other microbes by competing for space and nutrition. The mouth of the inbred fish had higher abundance of *Aeromonas* sp. which was found to compete for nutrients and play a negative role during infection (Wiles et al., 2016; Legrand et al., 2020). On the other hand, the bacteria that had higher abundance in the posterior intestine of the inbred tilapia, namely *Enhydrobacter* sp., is a commensal microbe in rainbow trout (*Oncorhynchus mykiss*), which is known to produce entericidin, and this antitoxin peptide inhibits the growth of certain pathogens such as those belonging to *Flavobacterium* (Legrand et al., 2020). Furthermore, *Pediococcus* and *Bifidobacterium* which were found to be more abundant in the anterior and posterior intestine of the inbred groups compared to the outbred group are known to outcompete some invasive pathogens, associated with tilapia intestinal mucosa (Ferguson et al., 2010; Standen et al., 2013) and promote fish growth (Ayyat et al., 2014). Thus, the inbred group had a higher abundance of potential beneficial commensal bacteria.

Changes in Core Microbiome

The transient allochthonous microbiome of fish is associated with digesta and is usually expelled after some period as they are predominantly influenced by diet. On the other hand, the

resident microbes that belong to the autochthonous microbiome colonise the mucus surface in the gut and make up the core microbiome (Egerton et al., 2018). These microbial communities, which are known to be vertically transmitted (Risely, 2020), associate with the host's cells (Egerton et al., 2018; Legrand et al., 2020). In the present study, the core microbiome in each body site was determined based on the ASVs present in all samples in each group. However, the inter-individual variation in abundance that we observed is similar to the learning from studies on zebrafish (Burns et al., 2016) and mice (Pang et al., 2012). In mice, inbreeding was found to reduce the inter-individual variation (Pang et al., 2012). The inter-individual variation in the core microbiome in the intestine of the inbred group is much lesser compared to the outbred group. In contrast, such similarity was not observed in the mouth of the inbred fish; this was attributed to the effect of external environment in other studies (Lokesh and Kiron, 2016; Krotman et al., 2020). However, in the present study, environmental factors were kept constant throughout the study period. In humans, the initial oral colonizers from the vagina and mother's milk and mouth can be perturbed by environmental factors (Kilian, 2018).

The most dominant bacterial phylum in the two study groups was *Proteobacteria*. Nevertheless, *Cetobacterium* (phylum *Fusobacteria)* was found to be dominant in the anterior and posterior intestine of the inbred group, while its proportion was reduced in the outbred group. Previous studies conducted on Nile tilapia showed that the composition of *Cetobacterium* spp., the most prevalent genera in tilapia gut, was not affected by diets (Ray et al., 2017) or presence of pathogens (Suphoronski et al., 2019; Silva et al., 2020). Other reports that studied the influence of factors including rearing environment (Giatsis et al., 2015), and salinity (Zhang et al., 2016) on the gut microbial composition substantiates our finding that *Cetobacterium* is a core member of the bacterial community. Based on the present study, it appears that the crossbreeding strategy does not impact the presence of this core member in the mouth and intestine of Nile tilapia.

Some of the commonly reported bacteria in the intestine of Nile tilapia (*Staphylococcus*, *Cetobacterium*, *Plesiomonas*, *Enhydrobacter*, *Undibacterium*, and *Propionibacterium*) were present in both groups. However, some core microbiome members such as *Pseudomonas* and *Curvibacter* were present only in the mouth of both groups. A study employing turbot (*Scophthalmus maximus*) showed that a similar microbiome community was present in the intestine of different breeds fed with different diets and reared in different water environments. In addition, it was reported that core microbiome could colonize fish gut for a long term and it could have a vital physiological significance to the host (Zhang et al., 2020). This suggests that fishes preserve their core microbiome community despite differences in environmental factors.

Host Genetics and Intestine Microbiome

Growing evidence shows that host genetics plays a key role in shaping the gut microbiome of mammals (Hufeldt et al., 2010; Miller et al., 2018; Alessandri et al., 2019), but not to the same degree as that of environmental factors (Davenport, 2016). While there are many reports on diet-based microbiota differences in fish, evidences of fish genetics-associated microbiota are sparse (Li et al., 2014; Kokou et al., 2018).

Our genetic diversity analysis indicated a small but significant difference between the inbred and outbred fish. Unexpectedly, the observed heterozygosity was slightly higher than the expected heterozygosity, probably arising from the low genetic diversity values in both the inbred and outbred groups. The Ho, He, and F_{st} results that we obtained are likely due to small number of founders with a similar genetic background since the F0 generation of the fish were caught from the same area. The F0 itself may have lost considerable genetic diversity, as noted for birds; a small number of founders in a population increased the probability of inbreeding and associated gene diversity loss (Jamieson, 2011).

Wild Nile tilapia populations in West Africa are reported to have low diversity, especially, the species within a particular region; for example in Gambia River and the far western region of the Niger River (Lind et al., 2019). Nile tilapia is seen as a range-limited species in these areas, and founder effect was reported to be the reason for their genetic diversity reduction (Lind et al., 2019). In addition, F_{st} results also indicated the low genetic differentiation within the inbred groups as well as the outbred groups.

Anthropogenic needs not only alter species behavior, feeding habits, rearing environment, and traits within the host genotype but also reshape the gut microbiota of domesticated/captivated animals (Li et al., 2014; Alessandri et al., 2019). A study on blue tilapia, which was selectively bred to retain a host genotype, has reported that gut microbiome was linked to host genotype as well as specific bacteria such as *Cetobacterium somerae* (Kokou et al., 2018). This bacterium is a cobalamin producer (Tsuchiya et al., 2008; Degnan et al., 2014) and fishes with high abundance of *C. somerae* do not require dietary vitamin B12 (Sugita et al., 1991; Tsuchiya et al., 2008).

In order to analyse the genetic effect (by controlling the mating strategy) on the mouth and gut microbiota, the fish were kept in the same environmental conditions and fed the same diet, since both these factors are determinants of host microbial communities. Thus, crossing strategy influenced the microbial alpha diversity and composition in Nile tilapia. A similar effect on the midgut microbiota composition was observed in selectively bred trout (Brown et al., 2019). In addition, a study conducted on mice suggested that the alpha diversity of the gastrointestinal tract microbiota is slightly decreased in the inbred individuals (Kreisinger et al., 2014). Thus, the differences in the diversities of the microbial communities of the two groups could be attributed to crossbreeding strategy.

The differences in abundance of the microbial composition of the core microbiome in the individual samples from the mouth of the inbred fish were more pronounced compared to the outbred groups. In the mouth, influence of an external environmental factor (water) appears to surpass that of the host genetics. On the other hand, there was more similarity in the abundance of the bacterial communities in the individual intestine samples of the inbred group compared to the outbred group of Nile tilapia.

Host genetics is known to have a long-lasting effect on the gut microbial communities and this is due to maternal transfer during early development (Kreisinger et al., 2014). A core microbiota is heritable in several species (Hauffe and Barelli, 2019), including cichlids (Baldo et al., 2017). The similarities in the abundances of the taxa in the inbred group of Nile tilapia, which is also a cichlid fish, suggest that the microbial composition in the gut is more established without being affected by the external environment. A study conducted in mice showed that the inter-individual variation in the gut microbiome of the inbred group is lower compared to the outbred animals (Hufeldt et al., 2010). Furthermore, in humans the similarity of the gut microbiome is higher among closer relatives in families (Zoetendal et al., 2001). Therefore, this finding suggests that the genetic factor is more prominent in the intestine of the inbred groups and the effect is likely the inheritance of the microbial profile to the offspring of the fish, especially the core microbiome.

We report for the first time the effect of inbreeding and outbreeding on the mouth and intestine microbiome in Nile tilapia. The genetic relationship and structure analysis indicated the genetic differentiation between the inbred and outbred groups. Differential ASV analysis revealed the abundance of the potential opportunistic pathogens such as *Flavobacterium* in the outbred group and beneficial bacteria like *Bifidobacterium* and *Pediococcus* in the inbred group. We also found that *Cetobacterium* is the core member in both groups, but its abundance was higher in the intestine of the inbred group. The inbred fish which has less inter-individual microbiome variability, could be a better choice for controlled studies that examine the maternal transfer of intestine microbiome to offspring. We highlight that crossbreeding can influence Nile tilapia bacterial communities.

DATA AVAILABILITY STATEMENT

The data used in this study is available at European Nucleotide Archive (ENA) with accession no PRJEB40093. Whole-genome data of the host are available at Sequence Read Archive (SRA) with accession no PRJNA719847.

ETHICS STATEMENT

The animal study was reviewed and approved by Norwegian Animal Research Authority, FOTS ID 1042.

AUTHOR CONTRIBUTIONS

VK, JF, and YA designed the study. YA carried out the sampling and lab work, analysed the data, and wrote the manuscript. CD also analysed the data. SL helped in sequencing and data generation. DA was involved in initial data analyses. OJ and AN prepared the whole genome shotgun sequencing libraries. OJ performed the SNPs analysis of the host. YA, JF, CD, and VK interpreted the data. VK, JF, and CD reviewed and edited the manuscript. All authors contributed to the article and approved the submitted version.

FUNDING

This study was funded by the European Research Council (ERC) under the European Union's Horizon 2020 Research and Innovation Programme (grant agreement no. 683210), the Research Council of Norway under the Toppforsk Programme (grant agreement no. 250548/F20), and the Faculty of Biosciences and Aquaculture (Nord University, Norway).

ACKNOWLEDGMENTS

We are grateful to Hilde Ribe, Steinar Johnsen, Øivind Torslett, particularly to Kaspar Klaudiussen at Nord University's research station (Bodø, Norway) for their assistance with fish husbandry and welfare of the fish. The authors are thankful to Massimo Pindo (Edmund Mach Foundation, San Michele, Italy) who performed formal analysis and data curation. We also thank Erika Stefani and Stefano Piazza at the sequencing platform of Edmund Mach Foundation for their significant assistance in library preparation and sequencing. Lastly, we express our gratitude to Bisa Saraswathy for her assistance in data analysis, scientific input and preparation of the manuscript.

SUPPLEMENTARY MATERIAL

The Supplementary Material for this article can be found online at: https://www.frontiersin.org/articles/10.3389/fmicb.2021.709611/full#supplementary-material

REFERENCES

Albanese, D., Fontana, P., De Filippo, C., Cavalieri, D., and Donati, C. (2015). MICCA: a complete and accurate software for taxonomic profiling of metagenomic data. *Sci. Rep.* 5:9743. doi: 10.1038/srep09743

Alessandri, G., Milani, C., Mancabelli, L., Mangifesta, M., Lugli, G. A., Viappiani, A., et al. (2019). The impact of human-facilitated selection on the gut microbiota of domesticated mammals. *FEMS Microbiol. Ecol.* 95:fiz121. doi: 10.1093/femsec/fiz121

Anderson, M. J. (2001). A new method for non-parametric multivariate analysis of variance. *Austral. Ecol.* 26, 32–46. doi: 10.1111/j.1442-9993.2001.01070.pp.x

Ayyat, M., Labib, H. M., and Mahmoud, H. K. (2014). A probiotic cocktail as a growth promoter in Nile tilapia (*Oreochromis niloticus*). *J. Appl. Aquac.* 26, 208–215. doi: 10.1080/10454438.2014.934164

Baldo, L., Pretus, J. L., Riera, J. L., Musilova, Z., Nyom, A. R. B., and Salzburger, W. (2017). Convergence of gut microbiotas in the adaptive radiations of African cichlid fishes. *ISME J.* 11, 1975–1987. doi: 10.1038/ismej.2017.62

Bolivar, R. B., and Newkirk, G. F. (2002). Response to within family selection for body weight in Nile tilapia (*Oreochromis niloticus*) using a single-trait animal model. *Aquaculture* 204, 371–381. doi: 10.1016/S0044-8486(01)00824-9

Boutin, S., Bernatchez, L., Audet, C., and Derôme, N. (2013). Network analysis highlights complex interactions between pathogen, host and commensal microbiota. *PLoS One* 8:e84772. doi: 10.1371/journal.pone.0084772

Boutin, S., Sauvage, C., Bernatchez, L., Audet, C., and Derome, N. (2014). Inter individual variations of the fish skin microbiota: host genetics basis of mutualism? *PLoS One* 9:e102649. doi: 10.1371/journal.pone.0102649

Brown, R. M., Wiens, G. D., and Salinas, I. (2019). Analysis of the gut and gill microbiome of resistant and susceptible lines of rainbow trout (*Oncorhynchus mykiss*). *Fish Shellfish Immunol.* 86, 497–506. doi: 10.1016/j.fsi.2018.11.079

Browning, B. L., and Browning, S. R. (2016). Genotype imputation with millions of reference samples. *Am. J. Hum. Genet.* 98, 116–126. doi: 10.1016/j.ajhg.2015.11.020

Burns, A. R., Stephens, W. Z., Stagaman, K., Wong, S., Rawls, J. F., Guillemin, K., et al. (2016). Contribution of neutral processes to the assembly of gut microbial communities in the zebrafish over host development. *ISME J.* 10, 655–664. doi: 10.1038/ismej.2015.142

Conte, M. A., Gammerdinger, W. J., Bartie, K. L., Penman, D. J., and Kocher, T. D. (2017). A high quality assembly of the Nile tilapia (*Oreochromis niloticus*) genome reveals the structure of two sex determination regions. *BMC Genomics* 18:341. doi: 10.1186/s12864-017-3723-5

D'ambrosio, J., Phocas, F., Haffray, P., Bestin, A., Brard-Fudulea, S., Poncet, C., et al. (2019). Genome-wide estimates of genetic diversity, inbreeding and effective size of experimental and commercial rainbow trout lines undergoing selective breeding. *Genet. Sel. Evol.* 51:26. doi: 10.1186/s12711-019-0468-4

Danecek, P., Auton, A., Abecasis, G., Albers, C. A., Banks, E., Depristo, M. A., et al. (2011). The variant call format and VCFtools. *Bioinformatics* 27, 2156–2158. doi: 10.1093/bioinformatics/btr330

Davenport, E. R. (2016). Elucidating the role of the host genome in shaping microbiome composition. *Gut Microbes* 7, 178–184. doi: 10.1080/19490976.2016.1155022

Degnan, P. H., Taga, M. E., and Goodman, A. L. (2014). Vitamin B12 as a modulator of gut microbial ecology. *Cell Metab.* 20, 769–778. doi: 10.1016/j.cmet.2014.10.002

Deng, F., Li, Y., and Zhao, J. (2019). The gut microbiome of healthy long-living people. *Aging (Albany NY)* 11, 289–290. doi: 10.18632/aging.101771

Desantis, T., Hugenholtz, P., Keller, K., Brodie, E., Larsen, N., Piceno, Y., et al. (2006). NAST: a multiple sequence alignment server for comparative analysis of 16S rRNA genes. *Nucleic Acids Res.* 34, W394–W399. doi: 10.1093/nar/gkl244

Edgar, R. C. (2016). UNOISE2: improved error-correction for Illumina 16S and ITS amplicon sequencing. bioRxiv [Preprint]. doi: 10.1101/081257

Edgar, R. C., and Flyvbjerg, H. (2015). Error filtering, pair assembly and error correction for next-generation sequencing reads. *Bioinformatics* 31, 3476–3482. doi: 10.1093/bioinformatics/btv401

Egerton, S., Culloty, S., Whooley, J., Stanton, C., and Ross, R. P. (2018). The gut microbiota of marine fish. *Front. Microbiol.* 9:873. doi: 10.3389/fmicb.2018.00873

Ericsson, A. C., Davis, J. W., Spollen, W., Bivens, N., Givan, S., Hagan, C. E., et al. (2015). Effects of vendor and genetic background on the composition of the fecal microbiota of inbred mice. *PLoS One* 10:e0116704. doi: 10.1371/journal.pone.0116704

Ferguson, R., Merrifield, D. L., Harper, G. M., Rawling, M. D., Mustafa, S., Picchietti, S., et al. (2010). The effect of *Pediococcus acidilactici* on the gut microbiota and immune status of on-growing red tilapia (*Oreochromis niloticus*). *J. Appl. Microbiol.* 109, 851–862. doi: 10.1111/j.1365-2672.2010.04713.x

Ferretti, P., Pasolli, E., Tett, A., Asnicar, F., Gorfer, V., Fedi, S., et al. (2018). Mother-to-infant microbial transmission from different body sites shapes the developing infant gut microbiome. *Cell Host Microbe* 24, 133.e135–145.e135. doi: 10.1016/j.chom.2018.06.005

Flint, A., and Woolliams, J. (2008). Precision animal breeding. *Philos. Trans. R. Soc. B Biol. Sci.* 363, 573–590. doi: 10.1098/rstb.2007.2171

Giatsis, C., Sipkema, D., Smidt, H., Heilig, H., Benvenuti, G., Verreth, J., et al. (2015). The impact of rearing environment on the development of gut microbiota in tilapia larvae. *Sci. Rep.* 5:18206. doi: 10.1038/srep18206

Gjedrem, T., Robinson, N., and Rye, M. (2012). The importance of selective breeding in aquaculture to meet future demands for animal protein: a review. *Aquaculture* 350, 117–129. doi: 10.1016/j.aquaculture.2012.04.008

Gjedrem, T., and Rye, M. (2018). Selection response in fish and shellfish: a review. *Rev. Aquac.* 10, 168–179. doi: 10.1111/raq.12154

Gratacap, R. L., Wargelius, A., Edvardsen, R. B., and Houston, R. D. (2019). Potential of genome editing to improve aquaculture breeding and production. *Trends Genet.* 35, 672–684. doi: 10.1016/j.tig.2019.06.006

Hallali, E., Kokou, F., Chourasia, T. K., Nitzan, T., Con, P., Harpaz, S., et al. (2018). Dietary salt levels affect digestibility, intestinal gene expression, and the microbiome, in Nile tilapia (*Oreochromis niloticus*). *PLoS One* 13:e0202351. doi: 10.1371/journal.pone.0202351

Hart, M. L., Ericsson, A. C., Lloyd, K. K., Grimsrud, K. N., Rogala, A. R., Godfrey, V. L., et al. (2018). Development of outbred CD1 mouse colonies with distinct standardized gut microbiota profiles for use in complex microbiota targeted studies. *Sci. Rep.* 8:10107. doi: 10.1038/s41598-018-28448-0

Hauffe, H. C., and Barelli, C. (2019). Conserve the germs: the gut microbiota and adaptive potential. *Conserv. Genet.* 20, 19–27. doi: 10.1007/s10592-019-01150-y

Hill, W. G. (2014). Applications of population genetics to animal breeding, from wright, fisher and lush to genomic prediction. *Genetics* 196, 1–16. doi: 10.1534/genetics.112.147850

Hill, W. G. (2016). Is continued genetic improvement of livestock sustainable? *Genetics* 202, 877–881. doi: 10.1534/genetics.115.186650

Hsieh, T., Ma, K., and Chao, A. (2016). iNEXT: an R package for rarefaction and extrapolation of species diversity (Hill numbers). *Methods Ecol. Evol.* 7, 1451–1456. doi: 10.1111/2041-210X.12613

Hufeldt, M. R., Nielsen, D. S., Vogensen, F. K., Midtvedt, T., and Hansen, A. K. (2010). Variation in the gut microbiota of laboratory mice is related to both genetic and environmental factors. *Comp. Med.* 60, 336–347.

Ina-Salwany, M. Y., Al-Saari, N., Mohamad, A., Mursidi, F.-A., Mohd-Aris, A., Amal, M. N. A., et al. (2019). Vibriosis in fish: a review on disease development and prevention. *J. Aquat. Anim. Health* 31, 3–22. doi: 10.1002/aah.10045

Jamieson, I. G. (2011). Founder effects, inbreeding, and loss of genetic diversity in four avian reintroduction programs. *Conserv. Biol.* 25, 115–123. doi: 10.1111/j.1523-1739.2010.01574.x

Jantrakajorn, S., Maisak, H., and Wongtavatchai, J. (2014). Comprehensive investigation of Streptococcosis outbreaks in cultured Nile tilapia, *Oreochromis niloticus*, and red tilapia, *Oreochromis* sp., of Thailand. *J. World Aquacult. Soc.* 45, 392–402. doi: 10.1111/jwas.12131

Jombart, T. (2008). Adegenet: a R package for the multivariate analysis of genetic markers. *Bioinformatics* 24, 1403–1405. doi: 10.1093/bioinformatics/btn129

Kamvar, Z. N., Brooks, J. C., and Grünwald, N. J. (2015). Novel R tools for analysis of genome-wide population genetic data with emphasis on clonality. *Front. Gent.* 6:208. doi: 10.3389/fgene.2015.00208

Kilian, M. (2018). The oral microbiome–friend or foe? *Eur. J. Oral Sci.* 126, 5–12. doi: 10.1111/eos.12527

Klindworth, A., Pruesse, E., Schweer, T., Peplies, J., Quast, C., Horn, M., et al. (2013). Evaluation of general 16S ribosomal RNA gene PCR primers for classical and next-generation sequencing-based diversity studies. *Nucleic Acids Res.* 41:e1. doi: 10.1093/nar/gks808

Knaus, B. J., and Grünwald, N. J. (2017). vcfr: a package to manipulate and visualize variant call format data in R. *Mol. Ecol.* 17, 44–53. doi: 10.1111/1755-0998.12549

Kokou, F., Sasson, G., Nitzan, T., Doron-Faigenboim, A., Harpaz, S., Cnaani, A., et al. (2018). Host genetic selection for cold tolerance shapes microbiome composition and modulates its response to temperature. *eLife* 7:e36398. doi: 10.7554/eLife.36398

Kolde, R., and Kolde, M. R. (2015). Package 'pheatmap'. R package 1, 790.

Konstantinidis, I., Sætrom, P., Mjelle, R., Nedoluzhko, A. V., Robledo, D., and Fernandes, J. M. (2020). Major gene expression changes and epigenetic remodelling in Nile tilapia muscle after just one generation of domestication. *Epigenetics* 15, 1052–1067. doi: 10.1080/15592294.2020.1748914

Kreisinger, J., Čížková, D., Vohánka, J., and Piálek, J. (2014). Gastrointestinal microbiota of wild and inbred individuals of two house mouse subspecies assessed using high-throughput parallel pyrosequencing. *Mol. Ecol.* 23, 5048–5060. doi: 10.1111/mec.12909

Krotman, Y., Yergaliyev, T. M., Shani, R. A., Avrahami, Y., and Szitenberg, A. (2020). Dissecting the factors shaping fish skin microbiomes in a heterogeneous inland water system. *Microbiome* 8:9. doi: 10.1186/s40168-020-0784-5

Langmead, B., and Salzberg, S. L. (2012). Fast gapped-read alignment with Bowtie 2. *Nat. Methods* 9:357. doi: 10.1038/nmeth.1923

Legrand, T. P., Wynne, J. W., Weyrich, L. S., and Oxley, A. P. (2020). A microbial sea of possibilities: current knowledge and prospects for an improved understanding of the fish microbiome. *Rev. Aquac.* 12, 1101–1134. doi: 10.1111/raq.12375

Li, H. (2011). A statistical framework for SNP calling, mutation discovery, association mapping and population genetical parameter estimation from sequencing data. *Bioinformatics* 27, 2987–2993. doi: 10.1093/bioinformatics/btr509

Li, J., Ni, J., Li, J., Wang, C., Li, X., Wu, S., et al. (2014). Comparative study on gastrointestinal microbiota of eight fish species with different feeding habits. *J. Appl. Microbiol.* 117, 1750–1760. doi: 10.1111/jam.12663

Lind, C. E., Agyakwah, S. K., Attipoe, F. Y., Nugent, C., Crooijmans, R. P., and Toguyeni, A. (2019). Genetic diversity of Nile tilapia (*Oreochromis niloticus*) throughout West Africa. *Sci. Rep.* 9:16767. doi: 10.1038/s41598-019-53295-y

Lind, C., Ponzoni, R., Nguyen, N., and Khaw, H. (2012). Selective breeding in fish and conservation of genetic resources for aquaculture. *Reprod. Domest. Anim.* 47, 255–263. doi: 10.1111/j.1439-0531.2012.02084.x

Lokesh, J., and Kiron, V. (2016). Transition from freshwater to seawater reshapes the skin-associated microbiota of Atlantic salmon. *Sci. Rep.* 6:19707. doi: 10.1038/srep19707

Love, M. I., Huber, W., and Anders, S. (2014). Moderated estimation of fold change and dispersion for RNA-seq data with DESeq2. *Genome Biol.* 15:550. doi: 10.1186/s13059-014-0550-8

Lozupone, C., and Knight, R. (2005). UniFrac: a new phylogenetic method for comparing microbial communities. *Appl. Environ. Microbiol.* 71, 8228–8235. doi: 10.1128/AEM.71.12.8228-8235.2005

Marcon, E., and Hérault, B. (2015). entropart: an R package to measure and partition diversity. *J. Stat. Softw.* 67, 1–26. doi: 10.18637/jss.v067.i08

McMurdie, P. J., and Holmes, S. (2013). phyloseq: an R package for reproducible interactive analysis and graphics of microbiome census data. *PLoS One* 8:e61217. doi: 10.1371/journal.pone.0061217

McMurdie, P. J., and Holmes, S. (2014). Waste not, want not: why rarefying microbiome data is inadmissible. *PLoS Comput. Biol.* 10:e1003531. doi: 10.1371/journal.pcbi.1003531

Mehar, M., Mekkawy, W., Mcdougall, C., and Benzie, J. A. (2019). Fish trait preferences: a review of existing knowledge and implications for breeding programmes. *Rev. Aquac.* 12, 1273–1296. doi: 10.1111/raq.12382

Miller, E. T., Svanbäck, R., and Bohannan, B. J. (2018). Microbiomes as metacommunities: understanding host-associated microbes through metacommunity ecology. *Trends Ecol. Evol.* 33, 926–935. doi: 10.1016/j.tree.2018.09.002

Oh, W. T., Kim, J. H., Jun, J. W., Giri, S. S., Yun, S., Kim, H. J., et al. (2019). Genetic characterization and pathological analysis of a novel bacterial pathogen, *Pseudomonas fructae*, in rainbow trout (*Oncorhynchus mykiss*). *Microorganisms* 7:432. doi: 10.3390/microorganisms7100432

Oksanen, J., Blanchet, F. G., Kindt, R., Legendre, P., Minchin, P., O'hara, R., et al. (2013). Community ecology package. R package version, 2.0–2.

Oriá, R. B., Malva, J. O., Foley, P. L., Freitas, R. S., Bolick, D. T., and Guerrant, R. L. (2018). Revisiting inbred mouse models to study the developing brain: the potential role of intestinal microbiota. *Front. Hum. Neurosci.* 12:358. doi: 10.3389/fnhum.2018.00358

Pang, W., Stradiotto, D., Krych, L., Karlskov-Mortensen, P., Vogensen, F. K., Nielsen, D. S., et al. (2012). Selective inbreeding does not increase gut microbiota similarity in BALB/c mice. *Lab. Anim.* 46, 335–337. doi: 10.1258/la.2012.012040

Paradis, E., and Schliep, K. (2019). ape 5.0: an environment for modern phylogenetics and evolutionary analyses in R. *Bioinformatics* 35, 526–528. doi: 10.1093/bioinformatics/bty633

Pembleton, L. W., Cogan, N. O., and Forster, J. W. (2013). St AMPP: an R package for calculation of genetic differentiation and structure of mixed-ploidy level populations. *Mol. Ecol.* 13, 946–952. doi: 10.1111/1755-0998.12129

Piazzon, M. C., Naya-Català, F., Perera, E., Palenzuela, O., Sitjà-Bobadilla, A., and Pérez-Sánchez, J. (2020). Genetic selection for growth drives differences in intestinal microbiota composition and parasite disease resistance in gilthead sea bream. *Microbiome* 8:168. doi: 10.1186/s40168-020-00922-w

Ray, C., Bujan, N., Tarnecki, A., Davis, A. D., Browdy, C., and Arias, C. (2017). Analysis of the gut microbiome of Nile tilapia *Oreochromis niloticus* L. fed diets supplemented with Previda® and saponin. *J. Fishscicom* 11:36. doi: 10.21767/1307-234X.1000116

Reese, A. T., and Dunn, R. R. (2018). Drivers of microbiome biodiversity: a review of general rules, feces, and ignorance. *MBio* 9:e01294–18. doi: 10.1128/mBio.01294-18

Risely, A. (2020). Applying the core microbiome to understand host–microbe systems. *J. Anim. Ecol.* 89, 1549–1558. doi: 10.1111/1365-2656.13229

Rognes, T., Flouri, T., Nichols, B., Quince, C., and Mahé, F. (2016). VSEARCH: a versatile open source tool for metagenomics. *PeerJ* 4:e2584. doi: 10.7717/peerj.2584

Romana-Eguia, M. R. R., Ikeda, M., Basiao, Z. U., and Taniguchi, N. (2005). Genetic changes during mass selection for growth in Nile tilapia, *Oreochromis niloticus* (L.), assessed by microsatellites. *Aquac. Res.* 36, 69–78. doi: 10.1111/j.1365-2109.2004.01185.x

Santos, V. B. D., Mareco, E. A., and Dal Pai Silva, M. (2013). Growth curves of Nile tilapia (*Oreochromis niloticus*) strains cultivated at different temperatures. *Acta Sci. Anim. Sci.* 35, 235–242. doi: 10.4025/actascianimsci.v35i3.19443

Schultz, B., Serão, N., and Ross, J. W. (2020). "Genetic improvement of livestock, from conventional breeding to biotechnological approaches," in *Animal Agriculture*. eds. F. W. Bazer, G. C. Lamb and G. Wu (London, UK: Elsevier), 393–405.

Semple, S. L., Bols, N. C., Lumsden, J. S., and Dixon, B. (2020). Understanding the pathogenesis of *Flavobacterium psychrophilum* using the rainbow trout monocyte/macrophage-like cell line, RTS11, as an infection model. *Microb. Pathog.* 139:103910. doi: 10.1016/j.micpath.2019.103910

Shin, N.-R., Whon, T. W., and Bae, J.-W. (2015). *Proteobacteria*: microbial signature of dysbiosis in gut microbiota. *Trends Biotechnol.* 33, 496–503. doi: 10.1016/j.tibtech.2015.06.011

Silva, B. R. D. S., Derami, M. S., Paixão, D. A., Persinoti, G. F., Dias Da Silveira, W., and Maluta, R. P. (2020). Comparison between the intestinal microbiome of healthy fish and fish experimentally infected with *Streptococcus agalactiae*. *Aquac. Res.* 51, 3412–3420. doi: 10.1111/are.14676

Simões, L. N., Lombardi, D. C., Gomide, A. T. M., and Gomes, L. C. (2011). Efficacy of clove oil as anesthetic in handling and transportation of Nile tilapia, *Oreochromis niloticus* (Actinopterygii: Cichlidae) juveniles. *Zoologia* 28, 285–290. doi: 10.1590/S1984-46702011000300001

Souza, F. P. D., Lima, E. C. S. D., Urrea-Rojas, A. M., Suphoronski, S. A., Facimoto, C. T., Bezerra Júnior, J. D. S., et al. (2020). Effects of dietary supplementation with a microalga (*Schizochytrium* sp.) on the hemato-immunological, and intestinal histological parameters and gut microbiota of Nile tilapia in net cages. *PLoS One* 15:e0226977. doi: 10.1371/journal.pone.0226977

Standen, B., Rawling, M., Davies, S., Castex, M., Foey, A., Gioacchini, G., et al. (2013). Probiotic *Pediococcus acidilactici* modulates both localised intestinal-and peripheral-immunity in tilapia (*Oreochromis niloticus*). *Fish Shellfish Immunol.* 35, 1097–1104. doi: 10.1016/j.fsi.2013.07.018

Sugita, H., Miyajima, C., and Deguchi, Y. (1991). The vitamin B12-producing ability of the intestinal microflora of freshwater fish. *Aquaculture* 92, 267–276. doi: 10.1016/0044-8486(91)90028-6

Suphoronski, S., Chideroli, R., Facimoto, C., Mainardi, R., Souza, F., Lopera-Barrero, N., et al. (2019). Effects of a phytogenic, alone and associated with potassium diformate, on tilapia growth, immunity, gut microbiome and resistance against Francisellosis. *Sci. Rep.* 9:6045. doi: 10.1038/s41598-019-42480-8

Sylvain, F.-É., and Derome, N. (2017). Vertically and horizontally transmitted microbial symbionts shape the gut microbiota ontogenesis of a skin-mucus feeding discus fish progeny. *Sci. Rep.* 7:5263. doi: 10.1038/s41598-017-05662-w

Tsuchiya, C., Sakata, T., and Sugita, H. (2008). Novel ecological niche of *Cetobacterium somerae*, an anaerobic bacterium in the intestinal tracts of freshwater fish. *Lett. Appl. Microbiol.* 46, 43–48. doi: 10.1111/j.1472-765X.2007.02258.x

Wagner, M. R., Roberts, J. H., Balint-Kurti, P. J., and Holland, J. B. (2020). Microbiome composition differs in hybrid and inbred maize. bioRxiv [Preprint]. doi: 10.1101/2020.01.13.904979

Wei, T., and Simko, V. (2017). R package "corrplot": Visualization of a correlation matrix (Version 0.84). Available at: https://github.com/taiyun/corrplot (Accessed April 28, 2021).

Wein, T., Dagan, T., Fraune, S., Bosch, T. C., Reusch, T. B., and Hülter, N. F. (2018). Carrying capacity and colonization dynamics of *Curvibacter* in the hydra host habitat. *Front. Microbiol.* 9:443. doi: 10.3389/fmicb.2018.00443

Wickham, H. (2011). ggplot2. *Wiley Interdiscip. Rev. Comput. Stat.* 3, 180–185. doi: 10.1002/wics.147

Wiles, T. J., Jemielita, M., Baker, R. P., Schlomann, B. H., Logan, S. L., Ganz, J., et al. (2016). Host gut motility promotes competitive exclusion within a model intestinal microbiota. *PLoS Biol.* 14:e1002517. doi: 10.1371/journal.pbio.1002517

Wynne, J. W., Thakur, K. K., Slinger, J., Samsing, F., Milligan, B., Powell, J. F. F., et al. (2020). Microbiome profiling reveals a microbial dysbiosis during a natural outbreak of Tenacibaculosis (yellow mouth) in Atlantic Salmon. *Front. Microbiol.* 11:586387. doi: 10.3389/fmicb.2020.586387

Yukgehnaish, K., Kumar, P., Sivachandran, P., Marimuthu, K., Arshad, A., Paray, B. A., et al. (2020). Gut microbiota metagenomics in aquaculture: factors influencing gut microbiome and its physiological role in fish. *Rev. Aquac.* 12, 1903–1927. doi: 10.1111/raq.12416

Zar, J. H. (2014). Spearman rank correlation: overview. Wiley StatsRef: Statistics Reference Online.

Zhang, M., Sun, Y., Liu, Y., Qiao, F., Chen, L., Liu, W.-T., et al. (2016). Response of gut microbiota to salinity change in two euryhaline aquatic animals with reverse salinity preference. *Aquaculture* 454, 72–80. doi: 10.1016/j.aquaculture.2015.12.014

Zhang, Z., Yu, Y., Jiang, Y., Wang, Y., Liao, M., Rong, X., et al. (2020). The intestine of artificially bred larval turbot (*Scophthalmus maximus*) contains a stable core group of microbiota. *Arch. Microbiol.* 202, 2619–2628. doi: 10.1007/s00203-020-01984-y

Zoetendal, E. G., Akkermans, A. D., Akkermans-Van Vliet, W. M., De Visser, J. A. G., and De Vos, W. M. (2001). The host genotype affects the bacterial community in the human gastronintestinal tract. *Microb. Ecol. Health Dis.* 13, 129–134. doi: 10.3402/mehd.v13i3.8013

Conflict of Interest: The authors declare that the research was conducted in the absence of any commercial or financial relationships that could be construed as a potential conflict of interest.

Publisher's Note: All claims expressed in this article are solely those of the authors and do not necessarily represent those of their affiliated organizations, or those of the publisher, the editors and the reviewers. Any product that may be evaluated in this article, or claim that may be made by its manufacturer, is not guaranteed or endorsed by the publisher.

frontiers in Microbiology

ORIGINAL RESEARCH
published: 20 September 2021
doi: 10.3389/fmicb.2021.700704

Metagenomics Reveals That Proper Placement After Long-Distance Transportation Significantly Affects Calf Nasopharyngeal Microbiota and Is Critical for the Prevention of Respiratory Diseases

Yaocheng Cui[1†], Jiancheng Qi[1†], Dongjie Cai[1], Jing Fang[1], Yue Xie[1], Hongrui Guo[1], Shiyi Chen[2], Xiaoping Ma[1], Liping Gou[1], Hengmin Cui[1], Yi Geng[1], Gang Ye[1], Zhijun Zhong[1], Zhihua Ren[1], Yanchun Hu[1], Ya Wang[1], Junliang Deng[1], Shuming Yu[1], Suizhong Cao[1], Huawei Zou[3], Zhisheng Wang[3] and Zhicai Zuo[1]**

[1] Key Laboratory of Animal Disease and Human Health of Sichuan Province, College of Veterinary Medicine, Sichuan Agricultural University, Chengdu, China, [2] College of Animal Science and Technology, Sichuan Agricultural University, Chengdu, China, [3] Animal Nutrition Institute, Sichuan Agricultural University, Chengdu, China

Transportation is an inevitable phase for the cattle industry, and its effect on the respiratory system of transported cattle remains controversial. To reveal cattle's nasopharyngeal microbiota dynamics, we tracked a batch of beef calves purchased from an auction market, transported to a farm by vehicle within 3 days, and adaptively fed for 7 days. Before and after the transport and after the placement, a total of 18 nasopharyngeal mucosal samples were collected, and microbial profiles were obtained using a metagenomic shotgun sequencing approach. The diversity, composition, structure, and function of the microbiota were collected at each time point, and their difference was analyzed. The results showed that, before the transportation, there were a great abundance of potential bovine respiratory disease (BRD)-related pathogens, and the transportation did not significantly change their abundance. After the transportation, 7 days of placement significantly decreased the risk of BRD by decreasing the abundance of potential BRD-related pathogens even if the diversity was decreased. We also discussed the controversial results of transportation's effect in previous works and the decrease in diversity induced by placement. Our work provided more accurate information about the effect of transportation and the followed placement on the calf nasopharyngeal microbial community, indicated the importance of adaptive placement after long-distance transport, and is helpful to prevent BRD induced by transportation stress.

Keywords: beef calf, transportation, nasopharyngeal microbial community, metagenomic shot-gun sequencing, adaptive placement, microbiota

OPEN ACCESS

Edited by:
Xudong Sun,
Heilongjiang Bayi Agricultural University, China

Reviewed by:
Mohamed Ghanem,
Benha University, Egypt
Xiliang Du,
Jilin University, China

***Correspondence:**
Zhisheng Wang
wangzs67@163.com
Zhicai Zuo
zzcjl@126.com

† These authors have contributed equally to this work

Specialty section:
This article was submitted to Systems Microbiology, a section of the journal Frontiers in Microbiology

Received: *26 April 2021*
Accepted: *20 August 2021*
Published: *20 September 2021*

Citation:
Cui Y, Qi J, Cai D, Fang J, Xie Y, Guo H, Chen S, Ma X, Gou L, Cui H, Geng Y, Ye G, Zhong Z, Ren Z, Hu Y, Wang Y, Deng J, Yu S, Cao S, Zou H, Wang Z and Zuo Z (2021) Metagenomics Reveals That Proper Placement After Long-Distance Transportation Significantly Affects Calf Nasopharyngeal Microbiota and Is Critical for the Prevention of Respiratory Diseases. Front. Microbiol. 12:700704. doi: 10.3389/fmicb.2021.700704

INTRODUCTION

The homeostasis of microflora colonized in the respiratory tract plays a vital role in maintaining airway health (Man et al., 2017). Emerging evidence indicated that, in cattle, the lung microbial community was more familiar with those in the nasopharynx than other upper respiratory niches (Mcmullen et al., 2020). Losing the balance of beef cattle's nasopharyngeal microorganisms contributes to the morbidity and mortality associated with bovine respiratory diseases (BRDs) (Holman et al., 2015; Zeineldin et al., 2017). Hence, the nasopharynx microbial community is regarded as the respiratory health situation indicator, especially BRD (Qi et al., 2021; Zeineldin et al., 2020).

The composition and diversity of cattle's nasopharynx microbial community are affected by many factors, including diet (Qi et al., 2021), vaccination and environment (Mcmullen et al., 2018), and transport (Pratelli et al., 2021). In China and North America, long-distance transport was an inevitable phase for the cattle industry (Cirone et al., 2019). Besides affecting the nervous, endocrine, immune, and energy supply systems (Van Engen and Coetzee, 2018), the latest research found that transportation also affected cattle's blood transcriptome, indicating that transport affected B cells' activity (Zhao et al., 2021). It is not surprising that transport was widely considered an intense BRD trigger (Earley et al., 2017; Zeineldin et al., 2019). Hence, exploring the effect of transport on the cattle's nasopharynx microbial community is of great value in cattle farming.

To date, there is limited research regarding the cattle's nasopharynx microbial community during transportation. Utilizing 16S rRNA sequencing technology, Holman et al. (2017) found that 2 days of transportation significantly decreased the diversity and richness of cattle's nasopharynx microbial community, and the decrease of diversity and richness recovered after a few days of adaptive feeding. Their team also implied a connection between the diversity of transported cattle's nasopharynx microbial community, especially lactic acid-producing bacteria and BRD (Amat et al., 2019). It is accepted that the susceptibility of BRD significantly increased in the first week after transport (Holman et al., 2017; Zeineldin et al., 2017), and selenium-biofortified alfalfa hay treatment in this period was found to benefit the recovery of microbial diversity and to help prevent BRD (Hall et al., 2017). However, these limited references are not enough to draw a convincing conclusion.

Besides the lack of references, technologies such as traditional bacterial culture technology and 16S rRNA sequencing also weaken the drawn conclusion. Although they are widely used to study respiratory tract microflora, they have their disadvantages. For example, many important bacteria are uncultivable, and the depth of 16S rRNA sequencing is not enough to identify microorganisms at the species level. In the past years, with the progress in the next-generation sequencing technologies, metagenomics-based studies are being widely applied to determine the composition of various microbiomes and analyze their functions at the DNA and RNA levels (Wang et al., 2015; Gilbert et al., 2016; Qi et al., 2021).

Therefore, to access the longitudinal dynamics of the transported beef calf nasopharynx microbial community before and after long-distance transport and the following adaptive placement, we collected the nasopharynx swab samples of 18 healthy beef calf before and after 3 days of transportation and 1 week after transportation. The nasopharyngeal microbiome profiles were obtained by the Whole Genome Shotgun (WGS) sequencing approach, and the dynamics in composition, diversity, structure, and function of these nasopharynx microbial communities were analyzed. As far as we know, this is the first time that a metagenomic shotgun sequencing approach is used in studying the dynamics of the nasopharynx microbial community during long-distance transportation. Our study will help understand the effect of transport and the followed adaptive placement on calf respiratory tract microflora and provide a reference for preventing respiratory system diseases related to transportation.

MATERIALS AND METHODS

All protocols used in the study referred to the Guidelines for the Care and Use of Laboratory Animals (National Institutes of Health, Bethesda, MD, United States) and were approved by the Ethics Committee of Sichuan Agricultural University (Chengdu, China). All methods were carried out following relevant guidelines and regulations.

Animals

In the auction market of Qiqihaer, 112 clinical healthy male Simmental calves (0.5 years old and 206 $\pm$ 9 kg) were purchased and then transported to a farm in Guangan for fattening by vehicles through the expressway. The criteria of clinical healthy are based on previous studies (Mcguirk and Peek, 2014), and the specific criteria are as follows: the mental outlook and appetite for food and water must be good; the shape of feces and the color of urine must be normal; and the secretion of eyes, mouth, and nose must be normal. The distance was approximately 3,000 km, and the transportation took three consecutive days, and all the calves were restricted from eating and drinking. As soon as the vehicles arrived at the farm, the calves were unloaded and then housed in a single pen for adaptive feeding for 1 week. All the calves were supplied with 3 L of drinking water, which contained brown sugar (0.5 kg/10 L) and ginger (0.3 kg/10 L) for the first three consecutive days and with regular drinking water for the other 4 days. The fodders were free to access in all 7 days. All these adaptive placement measures are conducted according to the farm management manual.

Sample Collection, DNA Extraction, Sequencing, and Quality Control

Eighteen calves were randomly selected and marked for sampling. Nasopharynx swabs of each selected calf were collected at three respective points: 6 h before loading, named group A, unloading, named group B, and the last day of the adaptive feeding, named group C. The nasopharyngeal swabs samples were collected using a 20-cm DNA-free sterile

swab (Meiruikelin Technology, China) from the nasopharynx mucosa and immediately stored in a dry icebox. Swab samples were kept in a dry ice box and were sent to Chengdu Beisibaier Biotechnology Co., Ltd. (Chengdu, China) for subsequent progress. Every three swab samples were combined into one sample to eliminate the difference induced by individual sampling and reduce sequencing cost by cutting down samples size.

According to Earth Microbiome Project standard protocols (Marotz et al., 2017), DNA was extracted using the MO BIO PowerSoil^{TM} DNA Isolation Kit (MO BIO Laboratories, United States). DNA concentration of all samples was detected by NanoDrop (Thermo Scientific, United States), and the results ranged from 15.2 to 75.4 ng/μl. The qualities of extracted DNA samples were estimated on agarose gel electrophoresis, and only samples that meet the following criteria were used for library construction: (1) DNA concentration was $>$ 15 ng/μl; (2) the total weight of DNA was $>$ 6 μg; and (3) the DNA band that was visualized on agarose gel electrophoresis must be clear and of good quality. Finally, 1 μg DNA of each qualified DNA sample was pooled to an equimolar concentration to construct the DNA libraries (DNA was sheared to 350 bp) using the Illumina DNA Sample Preparation Kit according to the manufacturer's instructions. Eighteen libraries were constructed, and the amplified libraries were then sequenced on Illumina HiSeq 2500 platform (2 bp × 250 bp). The adaptor contamination was removed using Cutadapt 1.3 (Martin, 2011) with parameters "-o 4 -e 0.1." Quality control was performed using a sliding window (5 bp bases) in Trimmomatic (Bolger et al., 2014) with the following criteria: (1) cutting once the average quality within the window falls below Q 20; (2) clean reads do not contain any N-bases; (3) trimming is applied to the 3′ end of reads, dropping those reads that were below 50 bp length; (4) only paired-end reads were retained for subsequent analyses. The obtained paired-end clean reads of each sample were performed by *de novo* assembly using Megahit (Li et al., 2010) with the parameter "K-mer ∼ [27, 127]" to contig and scaffold.

Species and Function Annotation and Analyzation

The species and function annotation procedures were the same as we described in our previous work (Qi et al., 2021). Briefly, the scaffolds/scaftigs sequence of each sample was subjected to BLASTN against bacterial, archaeal, fungal, and viral sequences in the NCBI-NT database (Nucleotide Collection, [1], v2016-6-19, E value was set to $<$ 0.00001). The "Lowest Common Ancestor" algorithm (Huson et al., 2018) in the MEGAN (MEta Genome Analyzer) software (Huson et al., 2011) was used to distinguish the reference sequence as the last level of a different species before branching and as classification annotation information of the target sequence species. Principal Component Analysis (PCA, Euclidean Distance) (Ramette, 2007) was used to determine whether there was a significant difference between the composition of samples from the same experimental group. A two-tailed *t*-test against the average relative abundance was performed using the SciPy database (Virtanen et al., 2020) in Python software, and the false discovery rate (FDR) was controlled using the Benjamini–Hochberg method (Benjamini and Hochberg, 1995). Only those functional groups with both |Log2 (fold change value)| $>$ 1 and $p < 0.05$ were considered having a significant difference. The species with the significant difference among groups and the top 50 most abundant species were clustered and analyzed using R software. We visualized each sample's composition structure at each classification level and their relative abundance in heat maps using R software. The linear discriminant analysis (LDA) effect size (LEfSe) (Segata et al., 2011) analysis was performed by submitting the composition spectrum data at the species level to Galaxy online analysis platform[2]. Mothur (Schloss et al., 2009) software was used to calculate Spearman's grade correlation coefficients (Faust and Raes, 2012) among the 50 most abundant species. The related dominant species with | rho $>$ 0.8| and $p < 0.01$ were used to construct the association network, and the networks were visualized by Cytoscape software (Shannon et al., 2003). The proteins predicted by the MetaGeneMark database (Zhu et al., 2010) were annotated and classified by comparing the protein sequence sets with the Kyoto Encyclopedia of Genes and Genomes (KEGG) Pathway Database (Kanehisa et al., 2004). The non-redundant protein sequence set was uploaded to the KEGG Automatic Annotation Server for functional annotation (parameters: "GENES data set" partially selected "for prokaryotes"; the rest of the parameters were default). The returned annotation results were summarized so that each level's annotation results and the corresponding abundance information were obtained. Detailed information about the analysis methods we used could be found in our previous paper (Qi et al., 2021).

Statistical Analysis

The Non-eukaryotic KEGG Orthology (KO) gene's relative abundances were calculated by normalizing all the KOs of each sample to sum to 1. Observation matrix tables that contain relative abundance information of KOs were used to calculate the Euclidean Distance (Ramette, 2007) based on the UPGMA algorithm (Hua et al., 2017), and the Principal Coordinate Analysis (PCoA) plot was built using the R data analysis package. All figures were drawn by R software and modification by Adobe Illustrator cc (United States). The *p*-value was calculated based on ANOVA and was used to determine whether there was a significant difference in the gene's abundance between different groups using R software packages and GraphPad Prism 8.0 (United States).

RESULTS

Quality Analysis of Sequencing Data

Eighteen libraries were conducted, and a total of 1.23×10^{11} bases and 819,054,624 reads were generated. The average base

[1] ftp://ftp.ncbi.bih.gov/blast/db/

[2] huttenhower.sph.harvard.edu/galaxy/

number and reads were 6,825,455,200 and 45,503,035. The average proportion of fuzzy bases (N %) was 0.00423%, and the average percentage of bases with 99.9% accuracy (Q30) was 92.02%. After quality control, 121.38 Mb of high-quality sequencing data were generated for all samples, with averages of 6.21, 7.11, and 6.9 Mb for group A, B, and C samples, respectively. The detailed statistical table of sequencing data is shown in **Supplementary Table 1**.

To estimate whether our sample size was big enough to reflect the difference in microbial communities' composition between samples and estimate microbial communities' richness, we draw a Specaccum species accumulation curve (Bevilacqua et al., 2018) according to the total number of taxa of each sample at the species level. The curve was flattened when the sample size was 18, which indicated that our sample size was big enough. The curve also implied that the upper limit of the sample species number was approximately 1,300 (**Figure 1A**). Besides, to determine whether the sequencing depth was deep enough to identify all species, all samples' rarefaction curves at the species level were drawn. When the sequencing depth reached 20,000 sequences per sample, all the curves trended to flat, which indicated that the sequencing depth was deep enough (**Figure 1B**).

Species Composition Analysis

In all 18 samples, a total of 1,301 species from 39 phyla were identified. In group A, the most dominant phylum was Proteobacteria (45.5%), followed by Firmicutes (13.1%), Tenericutes (2.1%), Actinobacteria (1.3%), and Deinococcus-Thermus (1.26%). In group B, the top five phyla were, respectively, Proteobacteria (47.5%), followed by Firmicutes (12.2%), Tenericutes (3.04%), Actinobacteria (0.92%), and Bacteroidetes (0.61%). In group C, they were, respectively, Firmicutes (17.6%), Proteobacteria (10.7%), Tenericutes (9.76%), Actinobacteria (4.18%), and Bacteroidetes (0.52%) (**Figure 1C** and **Supplementary Table 2**). In group A, the top five genera were *Moraxella* (17.6%), *Clostridium* (11.8%), *Mannheimia* (9.86%), *Acinetobacter* (4.41%), and *Psychrobacter* (2.95%). In group B, they were, respectively, *Moraxella* (19.3%), *Clostridium* (11.1%), *Mannheimia* (10.6%), *Acinetobacter* (3.92%), and *Mycoplasma* (3.01%). In group C, they were, respectively, *Clostridium* (15.3%), *Mycoplasma* (9.73%), *Acinetobacter* (3.92%), *Corynebacterium* (3.39%), and *Moraxella* (1.61%) (**Figure 1D** and **Supplementary Table 2**). The top 30 species with the highest average abundance of each group are, respectively, visualized in **Figure 1E**. As shown, 1,301 taxa were identified at the species level. In group A, the top five species were, respectively, *Clostridium botulinum* (11.8%), *Moraxella bovoculi* (5.13%), *Moraxella catarrhalis* (3.60%), *Moraxella osloensis* (3.41%), and *M. haemolytica* (2.81%). In group B, they were, respectively, *C. botulinum* (11.1%), *M. bovoculi* (5.68%), *M. catarrhalis* (3.71%), *M. osloensis* (3.56%), and *M. haemolytica* (3.15%). In group C, they were, respectively, *C. botulinum* (15.3%), *Mycoplasma bovoculi* (9.32%), *Acinetobacter pittii* (3.51%), *Corynebacterium maris* (1.40%), and *Psychrobacter* sp. *PRwf-1* (0.586%) (**Supplementary Table 2**). The detailed species annotation data for each sample are shown in **Supplementary Figure 1** and **Supplementary Table 3**.

Function Composition Analysis

To analyze the function composition of each sample and each group, the predicted non-redundant protein sets were compared with the KEGG protein database, and a total of 17,120 KEGG orthologs (KOs) and their abundance were identified (**Supplementary Table 4**). Then, the enrichment analysis of these KOs was performed at the third, second, and first levels among the groups (**Supplementary Table 5**). **Figure 1F** visualized the enrichment analysis at the first level for each group. As shown, in group A, the relative abundances of six first-level pathways were, respectively, 57.86% for Metabolism, 12.79% for Genetic Information Processing, 8.07% for Environmental Information Processing, 5.95% for Human Diseases, 4.80% for Cellular Processes, and 3.53% for Organismal Systems. In group B, the relative abundances were 53.9% for Metabolism, 12.9% for Genetic Information Processing, 8.93% for Environmental Information Processing, 7.44% for Human Diseases, 5.38% for Cellular Processes, and 4.17% for Organismal Systems. In group C, they were 63.7% for Metabolism, 14.3% for Genetic Information Processing, 5.28% for Environmental Information Processing, 5.18% for Human Diseases, 3.57% for Cellular Processes, and 3.26% for Organismal Systems.

Analysis of Interconnection Network of Dominant Species

To investigate the interconnection of the dominant species in each group, we calculated the correlation coefficient of Spearman grade of the top 50 species in each group based on the species abundance composition and visualized the conducted co-correlation networks using Cytoscape. In group A, a network containing 25 kinds of species was obtained. In this network, 22 of them had positive interconnection with each other, except *A. pittii*, *C. botulinum*, and *Eimeria necatrix*, which had negative interconnections with other (**Figure 2A**). In group B, a smaller network containing 14 kinds of species and three micro-networks were obtained. *C. botulinum* and *A. pittii* also had negative interconnections with others (**Figure 2B**). In group C, two dominant networks and a micro-network were obtained, which contained less *Moraxella* or *Acinetobacter* (**Figure 2C**).

Difference Analysis in Species Composition

To compare the differences in species composition among groups, firstly, we compared the abundance differences of each taxon among the three groups, and the statistical test was used to evaluate whether the differences were significant. The statistics data of abundance difference results are shown in **Table 1**. The detailed statistics data are shown in **Supplementary Table 6**. Then, using the R script, we conducted a cluster analysis on the top 50 taxa with significant differences among groups at the species level, and the results were shown in heat map form (**Figures 3A–C**). As shown, there were dominant populations for both groups A and B, but the relative abundance of populations in group C was almost significantly lower than that in group A or B, which indicated that the richness of the microflora of group C was lower than groups A and B. The cluster analysis results at

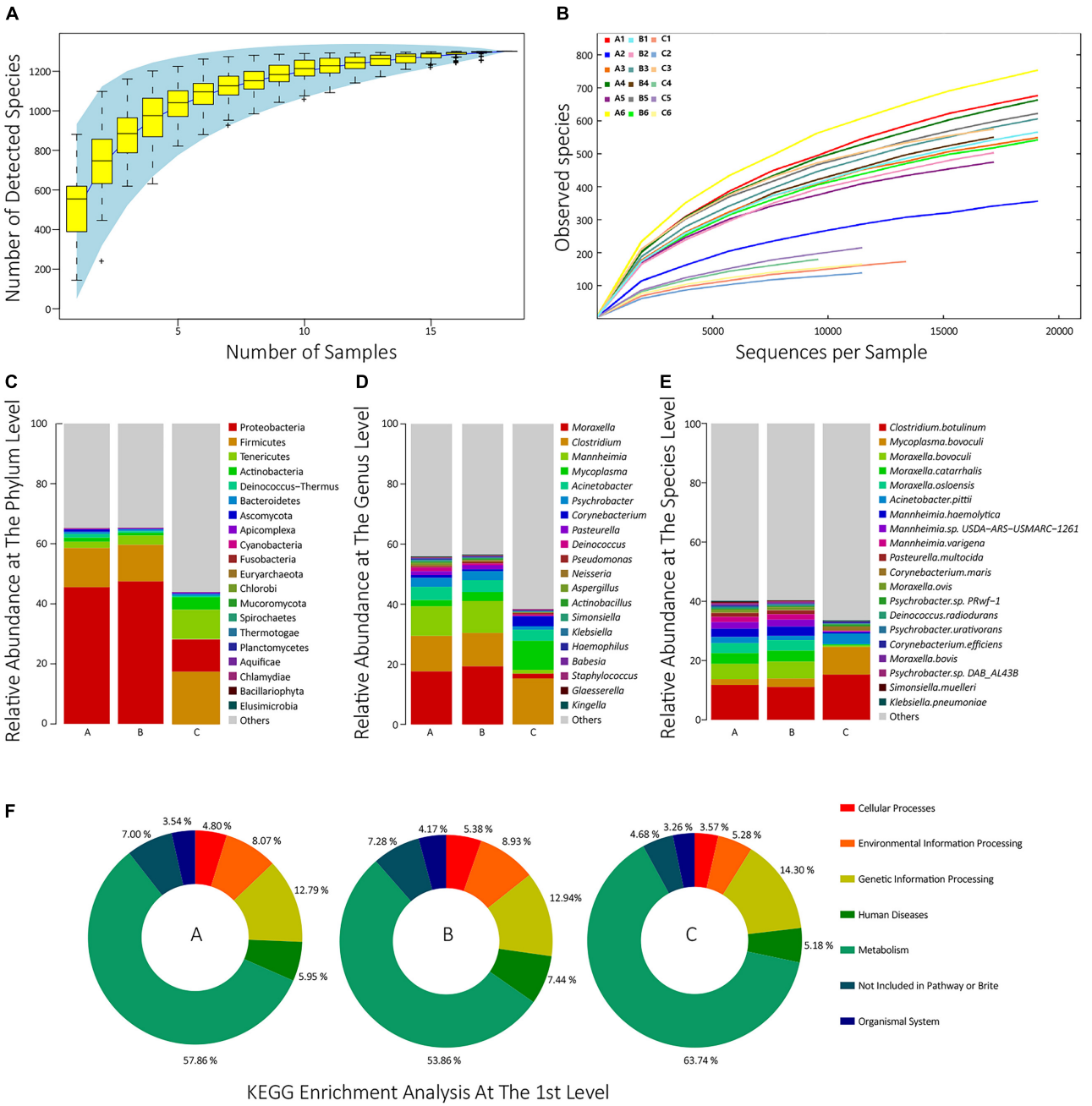

FIGURE 1 | (A) The Specaccum species accumulation curve at the species level. The horizontal axis represents the sequencing sample size; the longitudinal axis represents the detected species number at the species level; the blue shadow reflects the curve's confidence interval; the slope of the curve represents the rate of newly discovered species with expanding samples size. **(B)** Rarefaction curves at the species level of all samples. The horizontal axis represents the number of randomly selected sequences; the longitudinal axis represents the number of detected species in a sequencing depth; the length of the curves represents sequencing depth. If the curve is longer, the sequencing is more deep, and the possibility of detecting new species is higher; the slope of the curve represents the strength of the effect of sample size on the sequencing result, and if the curve is gentler, the sequencing result is more credible for reflecting the composition of the sample. **(C–E)** The top 20 taxon composition with the highest relative abundance of each group at the phylum, genus, and species level, respectively. **(F)** The relative abundances of the first KEGG pathways for each group.

the genus level are shown in **Supplementary Figure 2**, showing a similar phenotype. Considering that most of these significantly changed species had an extremely low relative abundance, we counted the significance of differences in those species and genus, which possessed the top 10 relative abundance between groups. At the species level, the differences in the relative abundance of the top 10 species were all non-significant between groups A and B, but between groups B and C and between groups A and C,

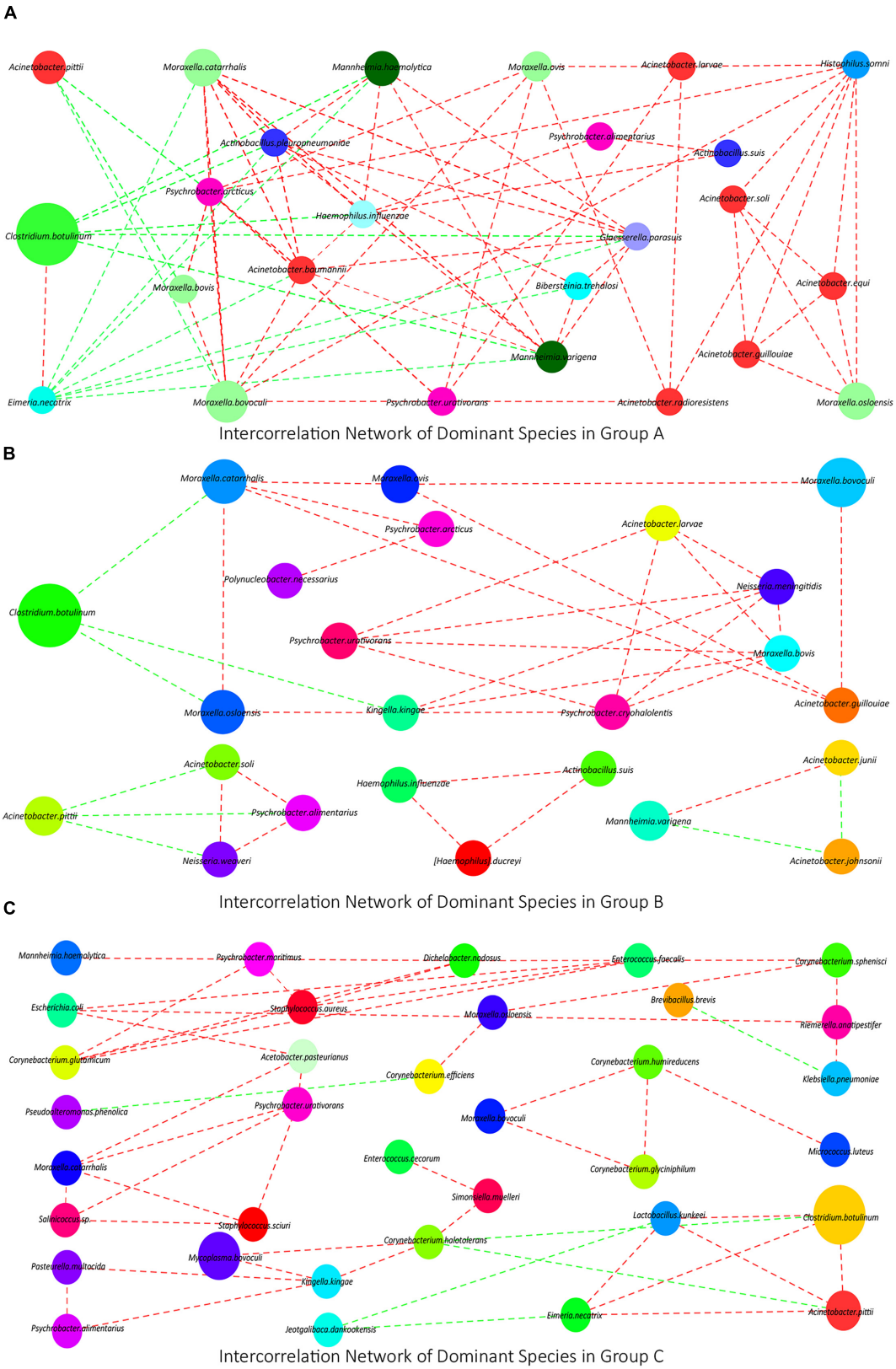

FIGURE 2 | (A–C) The interconnection networks of the top 50 species in groups A, B, and C, respectively. Red lines mean positive correlations, green lines mean negative correlations, and the size of circles represents the relative abundance of the corresponding species.

TABLE 1 | Statistical table of abundance difference analysis.

Group	Phylum	Genus	Species
A vs. B	5	31	48
B vs. C	13	190	378
A vs. C	11	166	330

A vs. B denotes that the comparison was performed in groups A and B; the number means the size of phylum/genus/species with a significant difference.

the differences were almost all significant (**Figure 3D**). At the genus level, except *Aspergillus*, the relative abundances of all other nine genera had non-significant changes between groups A and B. However, between groups B and C and between groups A and C, the relative abundances of *Moraxella*, *Clostridium*, *Mannheimia*, and *Mycoplasma* were significantly changed (**Figure 3E**).

Difference Analysis in Function Composition

To compare the differences in function composition among groups, we compared the abundance differences of each functional taxon among the three groups. The *p*-value and FDR were used to evaluate whether the differences were significant, and it was found that 64, 905, and 1,008 KOs were significantly changed between groups A and B, B and C, and A and C, respectively. The detailed data are shown in **Supplementary Table 7**. We also conducted a cluster analysis on the top 50 taxa with significant differences in KOs among groups, and the results are shown in **Supplementary Figures 2D–F**. Then, we performed a KEGG pathway enrichment analysis for the significantly changed KOs among groups, and the results are shown in **Table 2**. The KOs related to the Immune system, Immune diseases, and Infectious diseases were significantly enriched ($p < 0.05$) in group A against group B. The KOs related to Lipid metabolism and Carbohydrate metabolism were significantly enriched in group B against group C ($p < 0.05$). The KOs related to the Amino acid metabolism and Glycan biosynthesis and metabolism were significantly enriched in group C against group B ($p < 0.05$). The KOs related to Ribosome and Starch and sucrose metabolism were significantly enriched in group C against group A ($p < 0.05$).

Diversity Analysis

To compare the α diversity of each group, using QIIME software, we calculated the diversity indexes of Chao l, ACE, Simpson, and Shannon based on the abundance spectrum of bottom functional groups and species groups. All these four indexes of group C were significantly lower ($p < 0.05$) than groups A and B (**Figure 4A**). The detailed statistical data of α diversity indexes are shown in **Supplementary Table 8**. The unsupervised β diversity analysis was also performed. PCA of species and KOs were performed, and the results are shown in **Figures 4B,C**, respectively. Both species and KO PCA results showed no significant difference between groups A and B ($p > 0.05$) and that the differences between groups B and C or between groups A and C were highly significant ($p < 0.01$). To further evaluate whether the patterns of differences in the functional and species levels among groups are correlated, we also performed a Pearson correlation analysis to the Shannon indexes of species and function (**Figure 4D**). The results showed that the function difference among groups was highly correlated with the species difference ($R = 0.96$, $p < 0.01$).

DISCUSSION

In the present study, the dynamics of nasopharyngeal microflora of 3 days of transportation and 7 days of adaptive feeding was studied by a metagenomic shotgun sequencing approach. We analyzed the composition of a taxon at the species and genus level, the composition of function at different KO levels, and the α diversities for both samples and groups. Then, to investigate whether the influence of transportation and adaptive feeding on the nasopharynx microflora was significant, we calculated the difference based on the species and functional composition using multiple statistical methods. The structure of beef cattle's nasopharyngeal microflora has been clarified in previous work (Zeineldin et al., 2017; Amat et al., 2019; Mcmullen et al., 2020). Here, we focused on the dynamic variation induced by transportation or placement.

Tracking Sampling Without Interference and Metagenomic Shotgun Sequencing Allow Us to Analyze the Dynamics More Precisely

In the experiment, we never take part in the transportation or placement, and the farmer determined all the processes as he usually did. This study's transportation and placement procedures might represent a widely used process in Southwest China, including choosing the auction market and calves, the uninterrupted vehicle transportation, and the brown sugar and ginger in the water during the placement. Holman et al. (2017) performed a very similar experiment in which they specified the source of cattle and excluded cattle with specific pathogens, which might affect its results. Hence, the dynamics we observed could be more similar to the actual situation. Besides, the sequencing approach we used was a recently developed next-generation sequencing approach with higher accuracy than 16S rRNA sequencing technology. For example, Timsit and colleagues observed 963 taxa in the nasopharynx sample (Mcmullen et al., 2018) while identifying 1,301 species. For now, metagenomic shotgun sequencing has been widely used to explore the respiratory system (Qi et al., 2021) or the digestive system microorganism communities (Wang et al., 2015). In our study, the taxonomic level we identified even reached subspecies, which allowed us to analyze the composition and dynamics of the microorganism community more precisely. With these advantages, our results could be a more valuable reference.

Three Days of Transportation From an Auction Market to a Feedlot Did Not Significantly Change the Calves' Nasopharyngeal Microflora Community

In species PCA and KOs PCA (**Figures 4B,C**), there was no significant difference observed between groups A and B,

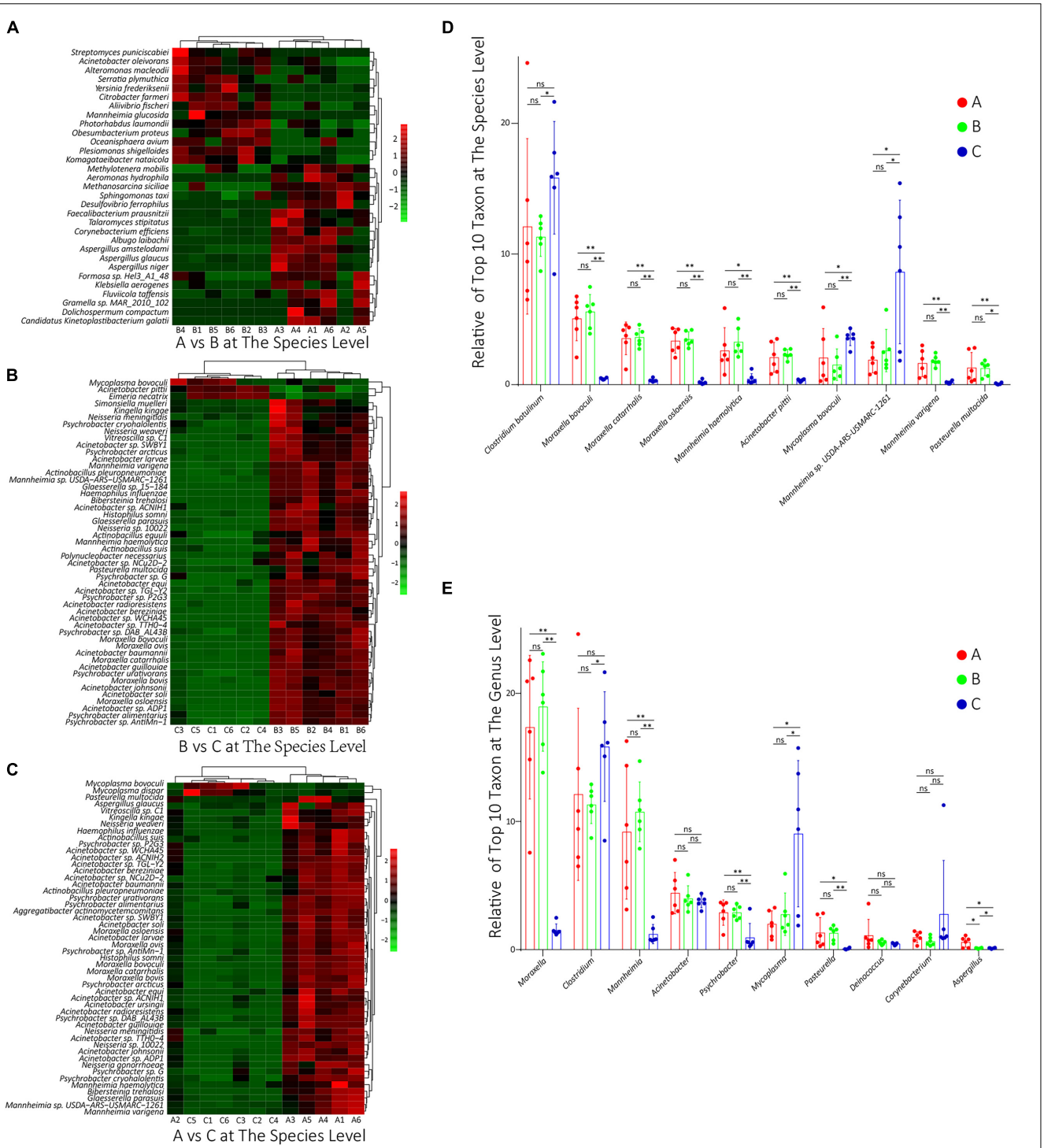

FIGURE 3 | (A–C) The results of cluster analysis on the top 50 taxa with significant differences between groups A and B, between groups B and C, and between groups A and C, respectively, at the species level. The red box denotes that the relative abundance was higher, and the green box indicates that the relative abundance was lower. **(D,E)** The relative abundance of these top 10 species and genus, respectively, in all groups. ns: non-significant; *$0.01 < p < 0.05$; **$p < 0.01$.

and the α diversity of groups A and B had no significant difference either (**Figure 4A**). Besides, there were no significant differences in the relative abundances of the top 10 species or genus between groups A and B (**Figures 3D,E**). Therefore, our results generally showed that 3 days of transportation had no significant effect on the structure or function of the

TABLE 2 | Results of KEGG enrichment analysis on significantly changed KOs among groups.

Group	Pathway	Pathway name	KO level 2
A vs. B	ko04650	Natural killer cell-mediated cytotoxicity	Immune system
	ko04144	Endocytosis	Transport and catabolism
	ko05170	Human immunodeficiency virus 1 infection	Infectious diseases: Viral
	ko04970	Salivary secretion	Digestive system
	ko04664	Fc epsilon RI signaling pathway	Immune system
	ko04662	B cell receptor signaling pathway	Immune system
	ko04666	Fc gamma R-mediated phagocytosis	Immune system
	ko05322	Systemic lupus erythematosus	Immune diseases
	ko05320	Autoimmune thyroid disease	Immune diseases
	ko00627	Aminobenzoate degradation	Xenobiotics biodegradation and metabolism
	ko04672	Intestinal immune network for IgA production	Immune system
	ko05330	Allograft rejection	Immune diseases
	ko04145	Phagosome	Transport and catabolism
	ko05146	Amoebiasis	Infectious diseases: Parasitic
	ko04612	Antigen processing and presentation	Immune system
	ko05150	*Staphylococcus aureus* infection	Infectious diseases: Bacterial
	ko05414	Dilated cardiomyopathy (DCM)	Cardiovascular diseases
	ko05416	Viral myocarditis	Cardiovascular diseases
	ko05166	Human T-cell leukemia virus 1 infection	Infectious diseases: Viral
	ko05163	Human cytomegalovirus infection	Infectious diseases: Viral
	ko05162	Measles	Infectious diseases: Viral
	ko05169	Epstein–Barr virus infection	Infectious diseases: Viral
B vs. C	ko00760	Nicotinate and nicotinamide metabolism	Metabolism of cofactors and vitamins
	ko00750	Vitamin B6 metabolism	Metabolism of cofactors and vitamins
	ko00500	Starch and sucrose metabolism	Carbohydrate metabolism
	ko00071	Fatty acid degradation	Lipid metabolism
	ko02010	ABC transporters	Membrane transport
	ko00400	Phenylalanine, tyrosine and tryptophan biosynthesis	Amino acid metabolism
	ko00350	Tyrosine metabolism	Amino acid metabolism
	ko00340	Histidine metabolism	Amino acid metabolism
	ko00540	Lipopolysaccharide biosynthesis	Glycan biosynthesis and metabolism
	ko00770	Pantothenate and CoA biosynthesis	Metabolism of cofactors and vitamins
A vs. C	ko00300	Lysine biosynthesis	Amino acid metabolism
	ko00750	Vitamin B6 metabolism	Metabolism of cofactors and vitamins
	ko00500	Starch and sucrose metabolism	Carbohydrate metabolism
	ko00364	Fluorobenzoate degradation	Xenobiotics biodegradation and metabolism
	ko02010	ABC transporters	Membrane transport
	ko03013	RNA transport	Translation
	ko04626	Plant–pathogen interaction	Environmental adaptation
	ko01502	Vancomycin resistance	Drug resistance: Antimicrobial
	ko00400	Phenylalanine, tyrosine, and tryptophan biosynthesis	Amino acid metabolism
	ko00480	Glutathione metabolism	Metabolism of other amino acids
	ko00340	Histidine metabolism	Amino acid metabolism
	ko00785	Lipoic acid metabolism	Metabolism of cofactors and vitamins
	ko00550	Peptidoglycan biosynthesis	Glycan biosynthesis and metabolism
	ko00540	Lipopolysaccharide biosynthesis	Glycan biosynthesis and metabolism
	ko03010	Ribosome	Translation

Red pathways mean that the pathway was enriched in the front group; green pathways mean that the pathway was enriched in the back group.

nasopharyngeal microorganism community of beef calves. The same conclusion was also shared by some previous works. For example, Ribble et al. (1995) found that the transport distance did not affect the risk of developing fatal fibrinous pneumonia by observing the pathological features of 45,243 spring-born steer calves purchased from auction markets. Timsit's team also found that the transportation from a feedlot to another feedlot directly or 24 h of co-mingling at an auction market did not significantly change cattle's nasopharyngeal microbial community (Stroebel et al., 2018). However, it cannot be ignored that we did not know how long these calves had been in this market, which means that we did not have the baseline information of the nasopharyngeal microbial community. It is unclear whether long-term exposure in the auction market has a significant effect on the microbial community, because the structure and diversity could have already been significantly affected before transportation, which weakened the influence of transportation and resulted in the non-significance. The difference of baseline might explain why some other works found that transportation significantly altered the composition

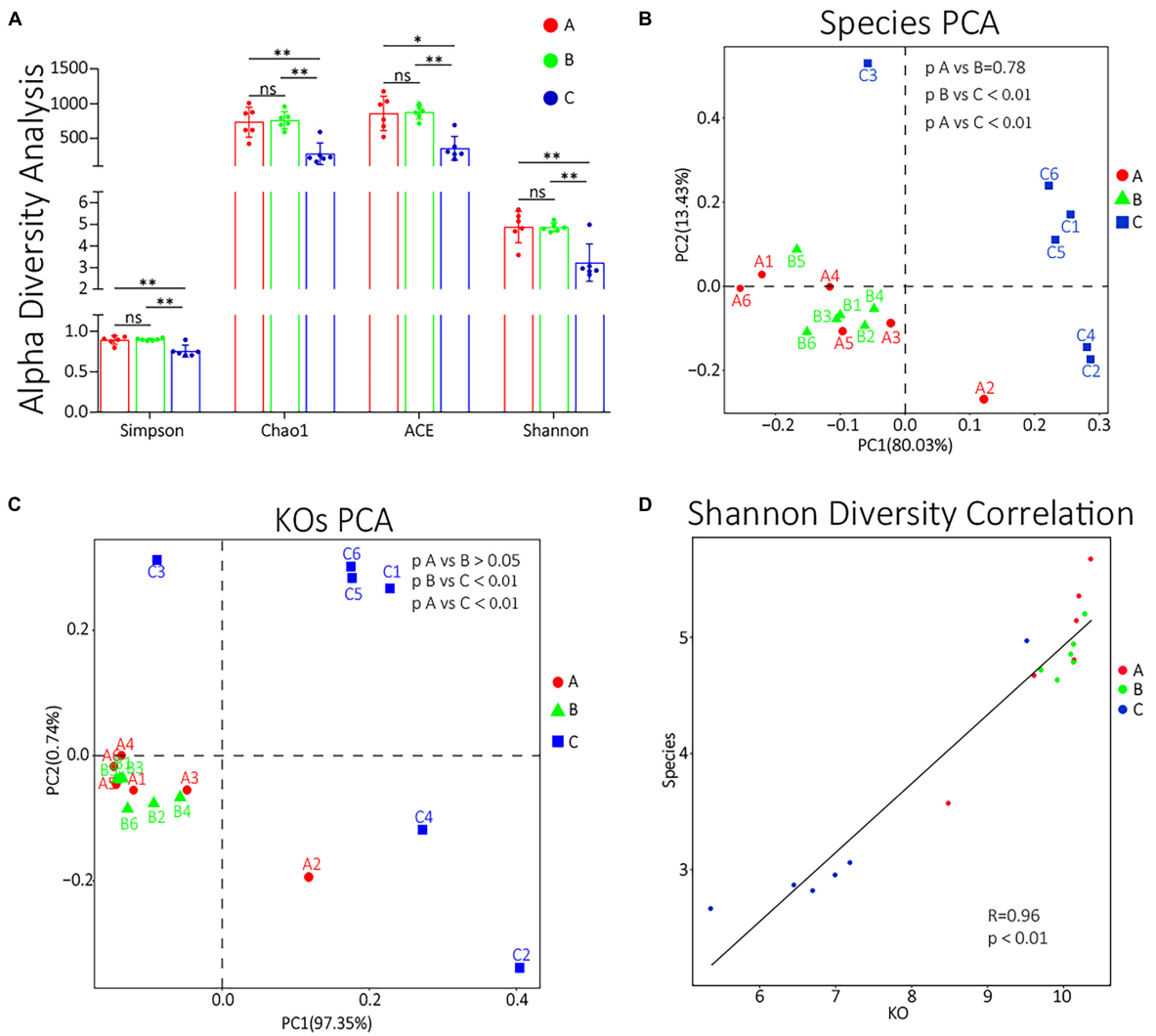

FIGURE 4 | (A) α diversity indexes of each group. ns, non-significant; *0.01 < p < 0.05; **p < 0.01. **(B,C)** The species PCA and KOs PCA, respectively, of each sample. **(D)** The Pearson correlation analysis of the Shannon diversity indexes of KOs and species. The abscissa represents the Shannon diversity index corresponding to the KO abundance spectrum of each sample, and the ordinate represents the Shannon index corresponding to the composition spectrum of each sample at the species level. The straight line represents the fitting results by Pearson correlation analysis.

and structure of the microbial community (Holman et al., 2017; Pratelli et al., 2021). The baseline they used was in the sourced feedlot, and the calves were healthy, while the baseline we used (group A) was in the market, and the calves were probably not as healthy as they were, and the nasopharynx microbiota might have been significantly altered already. However, this hypothesis needs to be verified. In groups A and B, we noticed a high abundance of *Moraxella*, *Mannheimia*, and *Acinetobacter*, which were considered potential pathogenic bacteria of BRD (Holman et al., 2015; Zeineldin et al., 2017) (**Figures 3D,E**), forming an interconnection network (**Figures 2A,B**), and this microbial community structure was similar to those cattle with BRD (Holman et al., 2015; Zeineldin et al., 2017). This structure might be a certification that the microbial community of these calves were already affected before transportation. In short, based on our results, 3 days of transportation from an auction market to a feedlot did not significantly change the calves' nasopharyngeal microflora community, probably because these calves' nasopharynx microbiota was already significantly altered in the auction market.

Transportation Affected the Interaction Between the Nasopharyngeal Microbial Community and the Host

Though our results showed that transportation had no significant effect on microbial community, some of these changes in species and KOs might provide us detailed information during the transport. Firstly, we noticed that the relative abundance of *M. haemolytica*, *Pasteurella multocida*, *Haemophilus somni*, *M. bovoculi*, etc., which are widely considered BRD pathogens (Holman et al., 2015; Amat et al., 2019), increased

after transportation (**Figure 3D**), though the increase was non-significant. Besides, the relative abundance of *C. botulinum* decreased, though the decrease was non-significant either (**Figure 3D**). *C. botulinum* is the most dominant species in cattle's nasopharynx (Mcmullen et al., 2020; Qi et al., 2021), which negatively correlated with most of the other dominant species in the network consisting of many BRD pathogens (**Figure 2A**). Furthermore, the interconnection among the top 50 species is more tight in group A than in group B (**Figures 2A,B**). Hence, from the perspective of species, the decrease of *C. botulinum* and the increase of BRD pathogens implied that if the exposure in the market altered the baseline, the transportation probably increased the risk of BRD. From the perspective of KOs, in the KEGG enrichment analysis, we noticed that many KOs that associated with the Immune system, Immune diseases, and Infectious diseases were enriched in group A compared with group B (**Table 2**), which implied that the microbial community after transportation had less connection with the host's immune system. The balance between the microflora and host was broken up by the 3 days of transportation, which also means the higher risk of BRD (Zeineldin et al., 2019). Considering these results, though the 3 days of transportation did not significantly change the composition or structure of the microbial community, it affected the interaction between the nasopharyngeal microbial community and the host and increased the risk of BRD.

Proper Adaptive Placement Is Necessary for the Health of Transported Calf

In the present study, the adaptive feeding with brown sugar and ginger after transportation significantly altered the diversity, structure, and composition of the transported calf's nasopharynx microbial community. In the PCA, the species and KOs of group C were both significantly ($p < 0.05$) different from groups A and B (**Figures 4B,C**). The α diversity indexes of group C were extremely different ($p < 0.01$) from groups A and B (**Figure 4A**). The relative abundances of the top 10 species and genus in group C were almost all significantly different ($p < 0.05$) from groups A and B (**Figures 3D,E**). The size of significantly changed species/genus/phylum between groups A and C or between groups B and C was much bigger than between groups A and B (**Table 1**). All these results indicated that an adaptive placement significantly affected the microbial community, supported by previous works (Hall et al., 2017; Schuetze et al., 2017; Amat et al., 2019). However, the consequence of this alteration seemed to be incomprehensible. Normally, the α diversity is positively related to the health of the cattle's respiratory system (Man et al., 2017; Zeineldin et al., 2019), but our results showed that the α diversity was extremely ($p < 0.01$) decreased after 7 days of placement (**Figure 4A**), which was contrary to previous work (Hall et al., 2017; Pratelli et al., 2021) and seemed to be harmful to the transported calves. We concluded the following reasons for the significant decrease in α diversity. Firstly, ginger was found to possess antimicrobial activity (Noori et al., 2018; Beristain-Bauza et al., 2019), so 3 days of ginger supply might inhibit the growth of some high abundant microorganisms, most of which were potential BRD-related pathogens. We noticed that the significantly decreased species (*M. bovoculi*, *M. catarrhalis*, *M. osloensis*, *M. haemolytica*, *P. multocida*, etc.) and genus (*Moraxella*, *Mannheimia*, and *Pasteurella*) were widely accepted to be related to the progress of BRD (Holman et al., 2015; Cirone et al., 2019; Mcmullen et al., 2019). Secondly, the recovered immune function inhibited the growth of pathogens. During the placement, calves were released from transport stress and were free to drink and eat, which supplied the deficiency in energy and enhanced the immune function (Earley et al., 2017; Qi et al., 2021). Besides, the relative abundance of Peptidoglycan biosynthesis (Bouhss et al., 2008) and Lipopolysaccharide biosynthesis (Heinrichs et al., 1998) in group A was enriched, implying that the synthesis level of the cell wall in group C was lower than that in group A and that the renewal of bacteria was inhibited. Furthermore, brown sugar is widely used in Chinese livestock's breeding industry, such as chicken and calf, which is thought to quickly replenish energy and contribute to the recovery of calf immune function (State Pharmacopoeia Commission of the PRC, 2005). However, there are few studies regarding the beneficial influence of brown sugar on the calf and these default roles of brown sugar are not confirmed and need to be investigated. Thirdly, as discussed in previous work (Qi et al., 2021), because of the supply of fodder, the absolute abundance of oral bacteria significantly increased, and they would compete for living resources (ecological locus, energy, etc.) with pathogens in the nasopharynx, which resulted in the decrease of pathogens. Moreover, the interconnection among group C was tighter and diversified. Hence, although the α diversity of the microbial community was decreased, the risk of BRD was also decreased. We speculated that the development of symbiotic bacteria needs to remove the existing pathogens, and 7 days of placement of brown sugar and ginger supply were not long enough to reestablish the balance between host and microbiota. This hypothesis explained why the α diversity of our microbial community decreased while it was increased in previous work (Hall et al., 2017; Pratelli et al., 2021) and enlightened us that this placement might not be appropriate. Nevertheless, further evidence is still needed.

CONCLUSION

In summary, after long-distance transportation, in the nasopharynx, the most abundant phylum was Proteobacteria (45.5%), followed by Firmicutes (13.1%), and the most dominant genus was *Moraxella* (17.6%), followed by *Clostridium* (11.8%) and *Mannheimia* (9.86%). Like previous works, the nasopharyngeal microbial community of transported calves was of a great abundance of potential BRD-related pathogens, which was closed to the cattle diagnosed with BRD. Probably because of the difference in baseline, our results showed that 3 days of transportation had no significant effect on the nasopharyngeal microbial community, which some other researchers also observed. The placement of brown sugar and ginger significantly decreased the relative abundance of those potential BRD-related pathogens and altered the functional composition of

the microbial community, which confirmed that the adaptive placement had a stronger influence on the calf nasopharynx microbiome than transportation itself and indicated that the risk of BRD was decreased and that proper adaptive placement was critical for the transported calf respiratory system's health. Interestingly, the α diversity of the microbial community was significantly decreased after the placement, which is contrary to previous work. The reason for this phenotype was hypothesized, but it needs to be further verified. Because of the lack of physiological data, sample size limitation, and the lack of baseline information, further experiments are still needed.

DATA AVAILABILITY STATEMENT

The datasets presented in this study can be found in online repositories. The names of the repository/repositories and accession number(s) can be found below: https://www.ncbi.nlm.nih.gov/bioproject/PRJNA724913/.

ETHICS STATEMENT

The animal study was reviewed and approved by Ethics Committee of Sichuan Agricultural University (Chengdu, China). Written informed consent was obtained from the owners for the participation of their animals in this study.

AUTHOR CONTRIBUTIONS

ZcZ and ZW designed the experiment. YC and JQ wrote the manuscript. All authors reviewed and revised the manuscript.

FUNDING

This study was supported by the National Key Research and Development Program of China (2018YFD0501800), the Sichuan Science and Technology Program (2018NZ0002 and 2019YFQ0012), and the Sichuan Beef Cattle Innovation Team of the National Modern Agricultural Industry Technology System (SCCXTD-2020-13).

ACKNOWLEDGMENTS

We would like to thank all the co-authors for their contributions to this work.

SUPPLEMENTARY MATERIAL

The Supplementary Material for this article can be found online at: https://www.frontiersin.org/articles/10.3389/fmicb.2021.700704/full#supplementary-material

Supplementary Figure 1 | (A–C) The top 20 taxon composition with the highest relative abundance of each sample at the phylum, genus, and species level, respectively.

Supplementary Figure 2 | (A–C) The results of cluster analysis on the top 50 taxa with significant differences between group A and B, B and C, and A and C, respectively, at the genus level. **(D–F)** The results of cluster analysis on the top 50 KOs with significant differences between groups A and B, B and C, and A and C, respectively, at the 3rd level. The red box represents that the relative abundance was higher, the green box represents that the relative abundance was lower.

Supplementary Table 1 | Statistical table of raw data and clean data.

Supplementary Table 2 | The species annotation data of each group at the phylum, genus, and species level, respectively.

Supplementary Table 3 | The detailed species annotation data for each sample.

Supplementary Table 4 | The detailed information of 17,120 KEGG orthologs (KOs) and their abundance.

Supplementary Table 5 | The KO enrichment analysis among groups at the 1st, 2nd, and 3rd, respectively.

Supplementary Table 6 | The detailed statistics data of abundance differences among groups at phylum/genus/species level, respectively.

Supplementary Table 7 | The detailed statistics data of relative abundance differences in KOs among groups.

Supplementary Table 8 | Statistical table of alpha diversity for each sample.

REFERENCES

Amat, S., Holman, D. B., Timsit, E., Schwinghamer, T., and Alexander, T. W. (2019). Evaluation of the nasopharyngeal microbiota in beef cattle transported to a feedlot, with a focus on lactic acid-producing bacteria. *Front. Microbiol.* 10:1988. doi: 10.3389/fmicb.2019.01988

Benjamini, Y., and Hochberg, Y. (1995). Controlling the false discovery rate-a practical and powerful approach to multiple testing. *J. R. Stat. Soc. Series. B (Methodol.)* 57, 289–300. doi: 10.1111/j.2517-6161.1995.tb02031.x

Beristain-Bauza, S. D. C., Hernández-Carranza, P., Cid-Pérez, T. S., Ávila-Sosa, R., Ruiz-López, I. I., Ochoa-Velasco, C. E., et al. (2019). Antimicrobial activity of ginger (*Zingiber Officinale*) and its application in food products. *Food Rev. Int.* 35, 407–426. doi: 10.1080/87559129.2019.1573829

Bevilacqua, S., Ugland, K. I., Plicanti, A., Scuderi, D., and Terlizzi, A. (2018). An approach based on the total-species accumulation curve and higher taxon richness to estimate realistic upper limits in regional species richness. *Ecol. Evol.* 8, 405–415. doi: 10.1002/ece3.3570

Bolger, A. M., Lohse, M., and Usadel, B. (2014). Trimmomatic: a flexible trimmer for Illumina sequence data. *Bioinformatics* 30, 2114–2120. doi: 10.1093/bioinformatics/btu170

Bouhss, A., Trunkfield, A. E., Bugg, T. D. H., and Mengin-Lecreulx, D. (2008). The biosynthesis of peptidoglycan lipid-linked intermediates. *FEMS Microbiol. Rev.* 32, 208–233. doi: 10.1111/j.1574-6976.2007.00089.x

Cirone, F., Padalino, B., Tullio, D., Capozza, P., Lo Surdo, M., Lanave, G., et al. (2019). Prevalence of pathogens related to bovine respiratory disease before and after transportation in beef steers: preliminary results. *Animals (Basel)* 9:1093. doi: 10.3390/ani9121093

Earley, B., Buckham Sporer, K., and Gupta, S. (2017). Invited review: relationship between cattle transport, immunity and respiratory disease. *Animal* 11, 486–492. doi: 10.1017/s1751731116001622

Faust, K., and Raes, J. (2012). Microbial interactions: from networks to models. *Nat. Rev. Microbiol.* 10, 538–550. doi: 10.1038/nrmicro2832

Gilbert, J. A., Quinn, R. A., Debelius, J., Xu, Z. Z., Morton, J., Garg, N., et al. (2016). Microbiome-wide association studies link dynamic

microbial consortia to disease. *Nature* 535, 94–103. doi: 10.1038/nature18850

Hall, J. A., Isaiah, A., Estill, C. T., Pirelli, G. J., and Suchodolski, J. S. (2017). Weaned beef calves fed selenium-biofortified alfalfa hay have an enriched nasal microbiota compared with healthy controls. *PLoS One* 12:e0179215. doi: 10.1371/journal.pone.0179215

Heinrichs, D. E., Yethon, J. A., and Whitfield, C. (1998). Molecular basis for structural diversity in the core regions of the lipopolysaccharides ofEscherichia coliandSalmonella enterica. *Mol. Microbiol.* 30, 221–232. doi: 10.1046/j.1365-2958.1998.01063.x

Holman, D. B., Mcallister, T. A., Topp, E., Wright, A. D., and Alexander, T. W. (2015). The nasopharyngeal microbiota of feedlot cattle that develop bovine respiratory disease. *Vet. Microbiol.* 180, 90–95. doi: 10.1016/j.vetmic.2015.07.031

Holman, D. B., Timsit, E., Amat, S., Abbott, D. W., Buret, A. G., and Alexander, T. W. (2017). The nasopharyngeal microbiota of beef cattle before and after transport to a feedlot. *BMC Microbiol.* 17:70. doi: 10.1186/s12866-017-0978-6

Hua, G.-J., Hung, C.-L., Lin, C.-Y., Wu, F. C., Chan, Y. W., Tang, C. Y., et al. (2017). MGUPGMA: a fast UPGMA algorithm with multiple graphics processing units using NCCL. *Evol. Bioinform.* 13:117693431773422. doi: 10.1177/1176934317734220

Huson, D. H., Albrecht, B., Bagci, C., Bessarab, I., Górska, A., Jolic, D., et al. (2018). MEGAN-LR: new algorithms allow accurate binning and easy interactive exploration of metagenomic long reads and contigs. *Biol. Direct* 13:6.

Huson, D. H., Mitra, S., Ruscheweyh, H. J., Weber, N., and Schuster, S. C. (2011). Integrative analysis of environmental sequences using MEGAN4. *Genome Res.* 21, 1552–1560. doi: 10.1101/gr.120618.111

Kanehisa, M., Goto, S., Kawashima, S., Okuno, Y., and Hattori, M. (2004). The KEGG resource for deciphering the genome. *Nucleic Acids Res.* 32, D277–D280.

Li, R., Zhu, H., Ruan, J., Qian, W., Fang, X., Shi, Z., et al. (2010). De novo assembly of human genomes with massively parallel short read sequencing. *Genome Res.* 20, 265–272. doi: 10.1101/gr.097261.109

Man, W. H., De Steenhuijsen Piters, W. A., and Bogaert, D. (2017). The microbiota of the respiratory tract: gatekeeper to respiratory health. *Nat. Rev. Microbiol.* 15, 259–270. doi: 10.1038/nrmicro.2017.14

Marotz, C., Amir, A., Humphrey, G., Gaffney, J., Gogul, G., Knight, R., et al. (2017). DNA extraction for streamlined metagenomics of diverse environmental samples. *Biotechniques* 62, 290–293.

Martin, M. (2011). Cutadapt removes adapter sequences from high-throughput sequencing reads. *EMBnet. J.* 17:3.

Mcguirk, S. M., and Peek, S. F. (2014). Timely diagnosis of dairy calf respiratory disease using a standardized scoring system. *Anim. Health Res. Rev.* 15, 145–147. doi: 10.1017/s1466252314000267

Mcmullen, C., Alexander, T. W., Leguillette, R., Workentine, M., and Timsit, E. (2020). Topography of the respiratory tract bacterial microbiota in cattle. *Microbiome* 8:91.

Mcmullen, C., Orsel, K., Alexander, T. W., van der Meer, F., Plastow, G., Timsit, E., et al. (2018). Evolution of the nasopharyngeal bacterial microbiota of beef calves from spring processing to 40 days after feedlot arrival. *Vet. Microbiol.* 225, 139–148. doi: 10.1016/j.vetmic.2018.09.019

Mcmullen, C., Orsel, K., Alexander, T. W., van der Meer, F., Plastow, G., Timsit, E., et al. (2019). Comparison of the nasopharyngeal bacterial microbiota of beef calves raised without the use of antimicrobials between healthy calves and those diagnosed with bovine respiratory disease. *Vet. Microbiol.* 231, 56–62. doi: 10.1016/j.vetmic.2019.02.030

Noori, S., Zeynali, F., and Almasi, H. (2018). Antimicrobial and antioxidant efficiency of nanoemulsion-based edible coating containing ginger (*Zingiber officinale*) essential oil and its effect on safety and quality attributes of chicken breast fillets. *Food Control* 84, 312–320. doi: 10.1016/j.foodcont.2017.08.015

Pratelli, A., Cirone, F., Capozza, P., Trotta, A., Corrente, M., Balestrieri, A., et al. (2021). Bovine respiratory disease in beef calves supported long transport stress: an epidemiological study and strategies for control and prevention. *Res. Vet. Sci.* 135, 450–455. doi: 10.1016/j.rvsc.2020.11.002

Qi, J., Cai, D., Cui, Y., Tan, T., Zou, H., Guo, W., et al. (2021). Metagenomics Reveals That intravenous injection of Beta-Hydroxybutyric Acid (BHBA) disturbs the nasopharynx microflora and increases the risk of respiratory diseases. *Front. Microbiol.* 11:630280. doi: 10.3389/fmicb.2020.630280

Ramette, A. (2007). Multivariate analyses in microbial ecology. *FEMS Microbiol. Ecol.* 62, 142–160. doi: 10.1111/j.1574-6941.2007.00375.x

Ribble, C. S., Meek, A. H., Shewen, P. E., Jim, G. K., and Guichon, P. T. (1995). Effect of transportation on fatal fibrinous pneumonia and shrinkage in calves arriving at a large feedlot. *J. Am. Vet. Med. Assoc.* 207, 612–615.

Schloss, P. D., Westcott, S. L., Ryabin, T., Hall, J. R., Hartmann, M., Hollister, E. B., et al. (2009). Introducing mothur: open-source, platform-independent, community-supported software for describing and comparing microbial communities. *Appl. Environ. Microbiol.* 75, 7537–7541. doi: 10.1128/aem.01541-09

Schuetze, S. J., Schwandt, E. F., Maghirang, R. G., and Thomson, D. U. (2017). Review: transportation of commercial finished cattle and animal welfare considerations. *Prof. Anim. Sci.* 33, 509–519. doi: 10.15232/pas.2017-01620

Segata, N., Izard, J., Waldron, L., Gevers, D., Miropolsky, L., Garrett, W. S., et al. (2011). Metagenomic biomarker discovery and explanation. *Genome Biol.* 12:R60.

Shannon, P., Markiel, A., Ozier, O., Baliga, N. S., Wang, J. T., Ramage, D., et al. (2003). Cytoscape: a software environment for integrated models of biomolecular interaction networks. *Genome Res.* 13, 2498–2504. doi: 10.1101/gr.1239303

State Pharmacopoeia Commission of the PRC (2005). Pharmacopoeia of the People's Republic of China. Beijing: People's Medical Publishing House.

Stroebel, C., Alexander, T., Workentine, M. L., and Timsit, E. (2018). Effects of transportation to and co-mingling at an auction market on nasopharyngeal and tracheal bacterial communities of recently weaned beef cattle. *Vet. Microbiol.* 223, 126–133. doi: 10.1016/j.vetmic.2018.08.007

Van Engen, N. K., and Coetzee, J. F. (2018). Effects of transportation on cattle health and production: a review. *Anim. Health Res. Rev.* 19, 142–154. doi: 10.1017/s1466252318000075

Virtanen, P., Gommers, R., Oliphant, T. E., Haberland, M., Reddy, T., Cournapeau, D., et al. (2020). SciPy 1.0: fundamental algorithms for scientific computing in Python. *Nat. Methods* 17, 261–272.

Wang, W.-L., Xu, S.-Y., Ren, Z.-G., Tao, L., Jiang, J. W., and Zheng, S. S. (2015). Application of metagenomics in the human gut microbiome .*World J. Gastroenterol.* 21, 803–814. doi: 10.3748/wjg.v21.i3.803

Zeineldin, M., Lowe, J., and Aldridge, B. (2019). Contribution of the mucosal microbiota to bovine respiratory health. *Trends Microbiol.* 27, 753–770. doi: 10.1016/j.tim.2019.04.005

Zeineldin, M., Lowe, J., and Aldridge, B. (2020). Effects of tilmicosin treatment on the nasopharyngeal microbiota of feedlot cattle with respiratory disease during the first week of clinical recovery. *Front. Vet. Sci.* 7:115. doi: 10.3389/fvets.2020.00115

Zeineldin, M., Lowe, J., De Godoy, M., Maradiaga, N., Ramirez, C., Ghanem, M., et al. (2017). Disparity in the nasopharyngeal microbiota between healthy cattle on feed, at entry processing and with respiratory disease. *Vet. Microbiol.* 208, 30–37. doi: 10.1016/j.vetmic.2017.07.006

Zhao, H., Tang, X., Wu, M., Li, Q., Yi, X., Liu, S., et al. (2021). Transcriptome characterization of short distance transport stress in beef cattle blood .*Front. Genet.* 12:616388. doi: 10.3389/fgene.2021.616388

Zhu, W., Lomsadze, A., and Borodovsky, M. (2010). Ab initio gene identification in metagenomic sequences. *Nucleic Acids Res.* 38:e132. doi: 10.1093/nar/gkq275

Conflict of Interest: The authors declare that the research was conducted in the absence of any commercial or financial relationships that could be construed as a potential conflict of interest.

Publisher's Note: All claims expressed in this article are solely those of the authors and do not necessarily represent those of their affiliated organizations, or those of the publisher, the editors and the reviewers. Any product that may be evaluated in this article, or claim that may be made by its manufacturer, is not guaranteed or endorsed by the publisher.

frontiers in Microbiology

ORIGINAL RESEARCH
published: 03 December 2021
doi: 10.3389/fmicb.2021.711905

Multi-Enzyme Supplementation Modifies the Gut Microbiome and Metabolome in Breeding Hens

Yuchen Liu[1], Dan Zeng[2], Lujiang Qu[1], Zhong Wang[3] and Zhonghua Ning[1]**

[1] National Engineering Laboratory for Animal Breeding and Key Laboratory of Animal Genetics, Breeding and Reproduction, Ministry of Agriculture and Rural Affairs, College of Animal Science and Technology, China Agricultural University, Beijing, China, [2] Huayu Agricultural Science and Technology Co., Ltd., Handan, China, [3] State Key Laboratory of Animal Nutrition, College of Animal Science and Technology, China Agricultural University, Beijing, China

Laying and reproductive performance, egg quality, and disease resistance of hens decrease during the late laying period. Exogenous enzymes promote nutrient digestibility and utilization and improve the intestinal environment. However, the specific regulation of the gut microbiome and metabolome by exogenous enzymes remains unelucidated. This study was conducted to evaluate effects of dietary multi-enzyme supplementation on egg and reproductive performance, egg quality, ileum microbiome, and metabolome of breeders. Here, 224 Hy-Line Brown breeding hens (55 weeks old) were randomly allocated to two groups: dietary controls fed basal diet (DC), and test hens fed 0.2 g/kg corn enzyme diet (CE). Serum levels of total protein, globulin, immunoglobulin Y, and antibodies against the Newcastle disease virus and avian influenza H9 strain were significantly increased ($p < 0.05$). Egg albumen height, Haugh unit, and fertilization and hatching rates were also significantly increased ($p < 0.05$) in the CE-fed group. 16S rRNA sequence analysis showed that CE strongly affected both α- and β-diversity of the ileal microbiota. LEfSe analysis revealed that the potentially beneficial genera *Lactobacillus*, *Enterococcus*, *Faecalicoccus*, and *Streptococcus* were enriched as biomarkers in the CE-fed group. Microbial functional analysis revealed that the functional genes associated with harmful-substance biodegradation was significantly increased in the CE-fed group. Additionally, Spearman correlation analysis indicated that changes in microbial genera were correlated with differential metabolites. In summary, dietary multi-enzyme addition can improve egg quality, humoral immunity, and reproductive performance and regulate the intestinal microbiome and metabolome in breeders. Therefore, multi-enzymes could be used as feed additive to extend breeder service life.

Keywords: multi-enzyme, aged layers, immunity, reproduction performance, microbiome, metabolome

OPEN ACCESS

Edited by:
Haidong Yao,
Karolinska Institutet (KI), Sweden

Reviewed by:
Lisa Osborne,
University of British Columbia, Canada
Kellie Anne Watson,
University of Edinburgh, United Kingdom
Vahid Rezaeipour,
Islamic Azad University, Iran

****Correspondence:***
Zhong Wang
wangzh@cau.edu.cn
Zhonghua Ning
ningzhh@cau.edu.cn

Specialty section:
This article was submitted to Systems Microbiology, a section of the journal Frontiers in Microbiology

Received: *19 May 2021*
Accepted: *04 November 2021*
Published: *03 December 2021*

Citation:
Liu Y, Zeng D, Qu L, Wang Z and Ning Z (2021) Multi-Enzyme Supplementation Modifies the Gut Microbiome and Metabolome in Breeding Hens. Front. Microbiol. 12:711905. doi: 10.3389/fmicb.2021.711905

INTRODUCTION

With increasing age, physiological function and digestive enzyme activity decrease and are always accompanied by gut microbiota disorder after the peak laying period in breeding hens, causing significant economic loss (Liu et al., 2013; Jing et al., 2014; Gu et al., 2021). Exogenous addition of enzymes was considered to improve the degradation of harmful macromolecules and activity of endogenous enzymes to assist in the degradation of starch and protein (Gu et al., 2021).

Starch is a complex polysaccharide composed of amylose and amylopectin (AP). AP accounts for 70–80% of most starch sources and requires pullulanase for hydrolysis (Scott et al., 2013;

Yin et al., 2018). Pullulanase is an important debranching enzyme that originates from bacteria, plants, and less commonly, fungi. Specifically, it could often attack α-1,6 linkages, thereby efficiently converting branched polysaccharides into small molecular sugars (Hii et al., 2012; Tomasik and Horton, 2012). In contrast to pullulanase, α-amylases split the α-1,4 glycosidic linkages in amylose to yield maltose and glucose (Sarian et al., 2017). Studies have demonstrated that the addition of α-amylase to a corn-soybean diet can release more feed energy and significantly improve apparent nutrient digestibility, digestive enzyme activity, and production performance of poultry (Aderibigbe et al., 2020). Glucoamylase (also known as amyloglucosidase or AMG) is an important digestive enzyme that mainly saccharifies partially processed starch/dextrin to glucose, which helps poultry absorb nutrients (da Costa Luchiari et al., 2021). Previous research indicated that supplementation with glucoamylase or protease combined with amylase could improve starch digestibility and gut microbiota diversity and promote the growth of broilers (Yin et al., 2018). Proteases can enhance protein and amino acid digestibility and reduce the adverse effects of heat-stabilized trypsin inhibitors or lectins, thus improving forage quality (Cowieson et al., 2017; Walk et al., 2018). A significant increase in the ileal digestibility of protein and amino acids occurs with proteases in poultry diets (Romero et al., 2014). Overall, exogenous enzymes can communicate with the host by utilizing indigestible dietary components and providing nutrients to regulate digestive, immune, and antioxidant functions to facilitate production performance and benefit the host (Pan and Yu, 2014; Cowieson and Kluenter, 2019; Monier, 2020; Giacobbo et al., 2021).

The use of enzymes in poultry feed is not uncommon. However, the role of enzymes in feed digestibility, productivity, and health of chickens is influenced by several factors, including the source, type, characteristics, dosage, and composition of complex enzymes as well as the diet structure, composition, and physiological status of chickens. In this study, we first evaluated the effects of new multi-enzymes (proteases, pullulanase, α-amylase, and glucoamylases) on laying performance, egg quality, reproductive performance, and immunity of older breeding hens and investigated the underlying mechanism through in-depth microbiome and metabolome analyses. Our objective was to develop a new nutritional strategy to improve health and extend the service life of breeding hens in their later laying stage.

MATERIALS AND METHODS

Birds, Diets, and Management

The Animal Welfare Policy has approved the bird management and handling procedures. All animal procedures were performed according to the principles of the Animal Care and Use Committee of the China Agricultural University. A total of 224 Hy-Line Brown breeding hens (55-week-old) with similar production performances and weights were randomly divided into two treatment groups with seven replicates of 16 hens each (4 hens per cage, 40 cm wide, 62 cm long, and 45 cm high). One is the dietary control fed with basal diet (DC), and the other with 0.2 g/kg corn enzyme diet (CE). The CE diet contained 11,000 u/g proteases, 20 u/g pullulanase, 1,000 u/g α-amylase, and 1,000 u/g glucoamylases, and was provided by the Wuhan SunHY Biological Co., Ltd. All hens were handled following the Hy-Line Brown Laying Hens Management Guide, and the hens were housed at the HuaYu Poultry Breeding Co., Ltd. (Handan, Hebei). All experimental hens were vaccinated with inactivated Newcastle virus (NDV) plus avian influenza virus (H9 subtype) strain vaccine by intermuscular injection at 55 weeks of age. The essential diet is shown in **Table 1** and meets the Chinese standards of agricultural trade standardization (NY/T33-2004).

Laying Performance Parameters

Eggs were collected daily during the experiment. The number of eggs laid, abnormal eggs, broken eggs, and egg weights were recorded on a replicate basis. The feed intake for each repetition was counted every 2 weeks. The average egg production rate, average egg weight, broken egg rate, abnormal egg rate, and feed egg ratio were calculated for 1–4, 5–8, and 1–8 weeks. Mortality was recorded daily as it appeared.

Egg Quality Parameters

Ten eggs were randomly collected from each replicate (70 eggs/group) for internal and external quality analyses during the last 2 days of the experiment. An egg-shaped index tester was used to measure the egg length and shortest diameter. An eggshell color tester was used to measure the eggshell color value (Konicaminolta CM-2600d). A quasi-static compression device (Robotmation, Japan) was used to measure the eggshell breaking strength. After removing the inner shell membrane,

TABLE 1 | Ingredients and nutrient composition of basal diet.

Ingredients	Percent	Nutrient level[c]	Percent
Corn (CP 8.3%)	64.00	ME (MJ/Kg)	16.01
Soybean meal (CP 44.0%)	20.93	CP (%)	16.04
Soybean oil	0.70	CF (%)	3.24
Wheat bran	3.00	Methionine (%)	0.24
Limestone	9.50	Lysine (%)	0.70
Calcium hydrogen phosphate	1.00	Calcium (%)	3.49
Sodium chloride	0.30	Total P (%)	0.32
DL-Methionine (98%)	0.10		
L-Lysine HCL (78%)	0.07		
Vitamin premix[a]	0.03		
Mineral premix[b]	0.20		
Choline chloride (50%)	0.15		
Phytase	0.02		
Total	100.00		

[a] *Supplied per kilogram of complete diet: vitamin A, 13,500 IU; vitamin D3, 4,500 IU; vitamin E, 75 IU; vitamin K3, 3.6 mg; vitamin B1, 3.0 mg; vitamin B2, 9.24 mg; vitamin B6, 6.0 mg; nicotinic acid, 66 mg; pantothenic acid, 16.8 mg; biotin, 0.54 mg; folic acid, 2.10 mg; vitamin B12, 0.03 mg; vitamin C, 135 mg; choline, 675 mg; ethoxyquinoline, 15 mg.*

[b] *Mineral premix provided per kilogram of complete diet: iron, 80 mg; copper, 10 mg; manganese, 100 mg; zinc, 100 mg; iodine, 0.35 mg; selenium, 0.30 mg.*

[c] *CP and CF were measured values, and the other nutrients were calculated values.*

the eggshell thickness was measured using a micrometer screw gauge at three different locations (lower, middle, and upper ends). Egg weight, albumen height, Haugh units, and yolk color were measured using an automatic egg quality analysis device (EMT-5200, Japan).

Blood Biochemical Parameters

Blood samples were collected for analyzing blood biochemistry and detecting serum antibody titers for 1 day before the end of the experiment. After fasting for 8 h, one hen per replicate was randomly selected (a total of 7 hens/group), and whole blood was collected from the wing vein using sterile blood collection tubes. The blood was centrifuged at 3,000 rpm for 10 min. The serum was extracted into a sterile 2 mL centrifuge tube and stored at −20°C until detection. Serum was used to detect aspartate aminotransferase (AST), total protein (TP), albumin (ALB), globulin (GLB), albumin/globulin, high-density lipoprotein cholesterol (HDL-C), immunoglobulin Y (IgY), and total antioxidant capacity (T-AOC). All indexes were tested using kits purchased from the Nanjing Jiancheng Bioengineering Institute (Nanjing, China). Other serum samples were used to detect antibody titers of NDV and avian influenza H9 strains by hemagglutination and hemagglutination inhibition assays. The virus, antigen, and positive control sera were purchased from Qingdao Yebio Biological Engineering Co., Ltd.

Reproductive Performance

All hens were inseminated on days 49 and 50 for 2 consecutive days of the formal phase. The semen was mixed and came from the same 12 cocks to ensure consistent semen quality. Eggs were collected on the 53rd–54th days. The total number of eggs produced and eligible hatching eggs were recorded and placed into pre-fumigated incubators. On the 18th day of incubation, the number of fertilized eggs was recorded by candling, and the eggs of identical replicates were placed in one string bag. On the 21st day of incubation, the number of newborn chicks in each replicate was recorded. Lastly, the rates of fertilized eggs and hatch of fertile (HoF) were calculated.

Gut Microbiota Sequencing

One hen per replicate was randomly selected (a total of 6 hens/group, one sample less than the number of replicates was due to unqualified DNA amplification), and euthanasia was performed using carbon dioxide on the last day of this trial (56 days). The ileum contents from each bird were collected and immediately frozen in liquid nitrogen until DNA extraction. Microbial genomic DNA extraction was conducted according to the manufacturer's instructions using the QIAamp 96 Powerfecal Qiacube HT Kit (5) (CatNo. 51531). DNA purity and concentration were detected using a NanoDrop 2000 spectrophotometer (Thermo Fisher Scientific, Waltham, MA, United States) and agarose gel electrophoresis. The purified DNA targeted the V3–V4 region of the 16S rDNA gene according to PCR bar-coded primers (343F: 5′-TACGGRAGGCAGCAG-3′ and 798R: 5′-AGGGTATCTAATCCT-3′). PCR was conducted using the KAPA HiFi Hot Start Ready Mix (KAPA Biosystems, Wilmington, MA, United States). Both reverse primers included a barcode and an Illumina sequencing adapter. The PCR products were visualized using 1% agarose gel electrophoresis, purified, and quantified using Agencourt AMPure XP beads (Beckman Coulter Co., United States) and Qubit dsDNA HS assay kit (Thermo Fisher Scientific), respectively. Sequencing was performed using an Illumina MiSeq platform with two paired-end read cycles of 300 bases each (Illumina Inc., San Diego, CA; OE Biotech Company, Shanghai, China).

Bioinformatic Analysis of the Microbiome

Microbiota data were subjected to bioinformatics analysis using QIIME software (version 1.8.0) (Caporaso et al., 2010). Data quality filtering, ambiguous bases, low-quality sequence removal, paired-end read assembly, and detachment of chimeric sequences were conducted using QIIME (Caporaso et al., 2010), Trimmomatic (Bolger et al., 2014), FLASH (Reyon et al., 2012), and UCHIME algorithms (Edgar et al., 2011), respectively. Reads with a similarity threshold of $\geq$ 97% were assigned to the same operational taxonomic unit (OTU) using the Vsearch pipeline (Rognes et al., 2016). Taxonomy was assigned to the OTUs using the SILVA database (v.123) with the RDP classifier at a 70% confidence threshold (Quast et al., 2012). Alpha diversity (Chao1, Observed, Shannon, Simpson's diversity) and beta diversity (principal coordinate analysis; PCoA) were calculated using QIIME 1.8 scripts.

Linear discriminant analysis (LDA) effect size (LEfSe) (Segata et al., 2011)[1] was used to identify representative species. LDA was performed from the phylum to genus level, and LDA scores $\geq$ 4.0 and p-values < 0.05 were considered signature taxa and selected for plotting and further analysis. The predicted metagenomic functional content was determined using PICRUSt[2] software by combining 16s rRNA data against the Greengenes database and the normalized data were analyzed to predict metagenomes using the Kyoto Encyclopedia of Genes and Genomes (KEGG) Orthology database.[3] Pairwise statistical comparative analysis (Welch's t-test, storey FDR correction) of microbial function was performed using STAMP (V2.1.3) (Parks et al., 2014). The microbial co-occurrence network analysis was performed using the CCLasso, sparCC, and NAMAP with Spearman correlation inference algorithm to elucidate gut microbiota interactions by MetagenoNets with default parameters (Nagpal et al., 2020). Only significant correlations ($p < 0.05$) based on the bootstrapping of 100 iterations were plotted.

Untargeted Metabolomics by Liquid Chromatography-Mass Spectrometry

The ileal chyme (30 mg) was precisely weighed and transferred to 1.5 mL microcentrifuge tubes (Eppendorf), to which two 3 mm stainless steel beads were added. Then, 20 μL of L-2-chlorophenylalanine (0.3 mg/mL) and 17:0 Lyso PC (1-heptadecanoyl-sn-glycero-3-phosphocholine, 0.01 mg/mL) were used as the internal standard. Both were configured with methanol. An internal standard mixed with 400 μL of methanol

[1] http://huttenhower.sph.harvard.edu/galaxy/

[2] http://picrust.github.io/picrust/

[3] https://www.genome.jp/kegg/ko.html

aqueous solution (CH_3OH: H_2O, V: V = 4:1) was added to each sample and pre-cooled at −20°C for 2 min. The sample was then ground in a fully automatic sample fast grinding machine (60 Hz, 2 min; Shanghai Jingxin Industrial Development Co., Ltd., Shanghai, China) and placed in an ultrasonic bath with ice water for 10 min. The sample was placed in a −20°C refrigerator for 20 min before centrifugation at 13,000 rpm at 4°C for 10 min. The supernatant was removed with a syringe and filtered by passing through a 0.22 μm-membrane filter to an LC-MS vial and stored at −80°C for subsequent analysis by *LC-MS*. Water, acetonitrile, formic acid, and methanol were purchased from CNW Technologies GmbH (Düsseldorf, Germany). L-2-chlorophenylalanine was purchased from Shanghai Hengchuang Bio-Technology Co., Ltd. (Shanghai, China). LysoPC17:0 was purchased from Avanti (Avanti Polar Lipids Inc., United States). All solvents and chemicals were of analytical or high-performance LC grade.

Metabolomics analysis was conducted using the Dionex U3000 UHPLC system (Waltham, MA, United States) coupled to a high-resolution QE plus mass spectrometer (Thermo Fisher Scientific) to analyze the metabolic profiles of the positive and negative ion modes. The LC system was fitted with an ACQUITY UPLC BEH C18 (100 × 2.1 mm, 1.7 μm) and a binary gradient elution system consisting of A) water (containing 0.1% formic acid) and B) acetonitrile (containing 0.1% formic acid) by the following separation gradient: 0 min 5% B, 1 min 5% B, 11 min 100% B, 13 min 100% B, 13.1 min 5% B, and 15 min 5% B. The column temperature was 50°C, and the flow rate was 0.35 mL/min. The injection volume was 5 μL, and the samples were randomized to avoid systematic errors. The mass spectrometer conditions and parameters were as follows: spray voltage, 3,800 V in positive mode, and 3,000 V in negative mode; capillary temperature, 320°C; aux gas heater temperature, 350°C; sheath gas flow rate, 35 arbitrary units; Aux gas flow rate, 8 arbitrary units; mass range: 70–1,000 m/z; full ms resolution, 70,000; MS/MS resolution, 17,500; and NCE, 20 and 40.

LC-MS raw data were collected by UNIFI (version 1.8.1) and then processed using Progenesis QI (version 2.3) with the following threshold parameters: precursor tolerance of 5 ppm, product tolerance of 10 ppm, and production threshold of 5%. Metabolites were identified by retention time, exact mass, and tandem MS data against the Human Metabolome Project,[4] Lipidmaps (v2.3)[5] and METLIN[6] databases. All metabolites with a percentage of missing values > 50% and quality scores < 30 were discarded by qualitative screening.

Metabolome Bioinformatics Analysis

Metabolome data were subjected to bioinformatics analysis using the SIMCA software (version 14.0, Umetrics, Umeå, Sweden). Principal component analysis (PCA) and orthogonal partial least squares discriminant analysis (OPLS-DA) models and plots were constructed using SIMCA. Volcano plots were plotted using the R package ggplot2. The differential metabolites were converted from names to KEGG compound IDs using MetaboAnalyst software (version 5.0),[7] CTS (Wohlgemuth et al., 2010), and MBRole software (version 2.0).[8] These IDs were used as input files for metabolite set enrichment analysis using MetaboAnalyst 5.0 software [annotations: KEGG pathway; Organism: *Homo sapiens* (human)] and MBRole 2.0 software [annotations: KEGG pathway; Organism: *Gallus gallus* (chicken)]. We also applied the pathway topology analysis [annotations: KEGG pathway; Organism: *G. gallus* (chicken)] to verify our findings using MetaboAnalyst with the default setting. Considering the relative lack of lipid information in the KEGG database, the differential metabolites that were annotated in the LipidMaps database were enriched by LIPEA[9] [annotations: KEGG pathway; Organism: *G. gallus* (chicken)]. Spearman's correlation between the differential microbial biomarkers and metabolites and the three identified metabolites and six microbial biomarkers were analyzed using R software. Only correlation coefficients with an absolute value of $|r| > 0.6$ (Adj P-value < 0.05) were considered a significant relationship. Network visualizations were performed using Gephi software (version 0.9.2, The Gephi Consortium, Paris, France) (Dalcin and Jackson, 2018).

Statistical Analysis

All graphs and data calculations were generated using R software (version 4.0.2), Prism8 (GraphPad, United States) software, and SPSS 24.0 (SPSS Inc., Chicago, IL, United States) software. Measurement data are expressed as the mean and standard error. A normal distribution and homogeneity of variance were performed. Comparisons between the two groups were performed using Student's t-test when it conformed to normal distribution and homogeneity of variance; otherwise, the non-parametric Wilcoxon rank-sum test was performed. $P < 0.05$ were considered as significant and $0.05 < p < 0.1$ was considered a trend.

RESULTS

Production Performance and Egg Quality

The laying performance of breeding hens fed the CE diet is presented in **Table 2**. Egg production, egg weight ratio, damaged egg ratio, abnormal egg ratio, FCR, mortality, and feed intake were not affected by CE administration at 55–59, 59–63, and 55–63 weeks ($p > 0.05$). The egg quality results are presented in **Table 3**. CE administration significantly increased the egg albumen height and Haugh unit ($p < 0.05$) but weakened the yolk color ($p < 0.05$) compared with those in the DC-fed group at week 63.

Blood Biochemical Parameters

Serum biochemical and antibody levels are physiological indices commonly used to evaluate animal health and immunity.

[4]https://hmdb.ca/

[5]http://www.lipidmaps.org

[6]http://metlin.scripps.edu

[7]https://www.metaboanalyst.ca/

[8]http://csbg.cnb.csic.es/mbrole2/

[9]https://lipea.biotec.tu-dresden.de/home

TABLE 2 | Effect of supplemental multi-enzyme on the performance of aged breeding hens.

Item	Egg production (%)	Egg weight (g)	Damaged egg (%)	Abnormal egg (%)	FCR[a] (g feed/g egg)	Mortality (%)	Feed intake (g/d/hen)
55–59 weeks							
DC[b]	74.1	62.2	4.9	2.8	2.3	1.8	107.2
CE[c]	76.0	63.1	4.5	3.2	2.2	0.9	105.0
SEM	1.7	0.4	0.5	0.4	0.1	0.7	1.0
P-value	0.59	0.25	0.70	0.61	0.20	0.55	0.32
59–63 weeks							
DC[b]	76.5	62.6	4.4	5.2	2.4	0.9	115.3
CE[c]	77.2	63.8	4.7	4.3	2.4	3.6	115.4
SEM	1.8	0.3	0.7	0.4	0.1	0.8	1.2
P-value	0.86	0.08	0.83	0.33	0.52	0.11	0.95
55–63 weeks							
DC[b]	75.3	62.4	4.6	4.0	2.4	2.7	111.2
CE[c]	76.6	63.4	4.6	3.8	2.3	4.5	110.1
SEM	1.5	0.3	0.6	0.4	0.0	0.9	1.0
P-value	0.67	0.13	0.99	0.71	0.21	0.32	0.61

[a]*FCR, feed conversion ratio.*
[b]*DC, dietary control (basal diet).*
[c]*CE, basal diet + 0.2 g/kg complex enzymes.*

CE administration significantly increased serum TP, GLB, IgY, HDL-C, and T-AOC levels. Serum AST levels were also markedly reduced, and a non-significant trend of decreased A/G ($p = 0.055$) was observed after supplementation with CE (**Figure 1A**). Furthermore, CE administration could enhance humoral immunity in hens by increasing serum-specific antibody titers against NDV and avian influenza H9 strains (**Figure 1B**).

Reproductive Performance

Reproductive performance is a vital indicator in breeding poultry, which affects the economic effectiveness of breeder companies. Descriptive data on the reproductive performance of aged breeder hens are shown in **Figure 1C**. The rate of fertilization and hatching of fertile (HoF) value was significantly improved upon CE supplementation ($p < 0.05$).

TABLE 3 | Effect of supplemental multi-enzyme on the egg quality of aged breeding hens (n = 70/group).

Item	DC[1]	CE[2]	SEM	*P*-value
Egg index	1.3	1.3	0.0	0.36
L	59.2	59.2	0.3	0.93
a	18.7	18.5	0.2	0.53
b	30.1	29.6	0.1	0.07
Shell strength (kg/cm^2)	4.0	4.0	0.1	0.67
Egg weight (g)	61.1	61.7	0.4	0.48
Yolk color	7.7[a]	7.0[b]	0.1	0.00
Egg albumen height	5.9[b]	6.2[a]	0.1	0.02
Haugh Unit	75.0[b]	77.5[a]	0.6	0.03
Eggshell thickness	0.4	0.4	0.0	0.67

[a,b]*Different superscript within a row means significantly different ($P < 0.05$).*
[1]*DC, dietary control (basal diet).*
[2]*CE, basal diet + 0.2 g/kg complex enzymes.*

Intestinal Bacterial Richness, Diversity, and Similarity

After size filtering, quality control, and chimera removal, an average of 29,200 clean tags and 27,376 valid tags were harvested from each sample for subsequent analysis through 16S amplicon sequencing. The species accumulation curve (**Figure 2A**) and alpha diversity rarefaction curve (**Figure 2B**) reached a stable plateau under the sample size and sequencing depth. The alpha diversity index reflects the richness and uniformity of the species composition. The Chao1 and Observed species indices are estimators of phylotype richness, and Shannon and Simpson's diversity indices reflect both richness and community uniformity. In this study, Shannon and Simpson's diversity indices were significantly enhanced ($p < 0.05$), while Chao1 and Observed species had a minimal effect on the addition of CE (**Figure 2C**). The Venn diagram showed that 635 distinct OTUs were clustered based on 97% sequence similarity, among which 258 were shared by both groups (**Figure 2D**). PCoA based on weighted UniFrac similarity showed a separation of each group (**Figure 2E**), with 61.33, 19.76, and 10.34% variation explained by principal components: PC1, PC2, and PC3, respectively (Adonis, $p = 0.009$, $R^2 = 0.49$).

Ileal Microbial Community Structure

Firmicutes, Proteobacteria, and Bacteroidetes were the dominant phyla in the aged breeder hens (relative abundance>1%), accounting for more than 98% of the total bacterial community (**Figure 3A**). The relative abundance of Proteobacteria increased from 5.94 to 21.05%, and the proportion of Firmicutes decreased from 90.79 to 75.87% with CE supplementation.

At the family level, the phyla of Firmicutes mainly contained Lactobacillaceae, Peptostreptococcaceae, Enterococcaceae, Erysipelotrichaceae, and Lachnospiraceae. Proteobacteria consisted of Helicobacteraceae, Pasteurellaceae, and

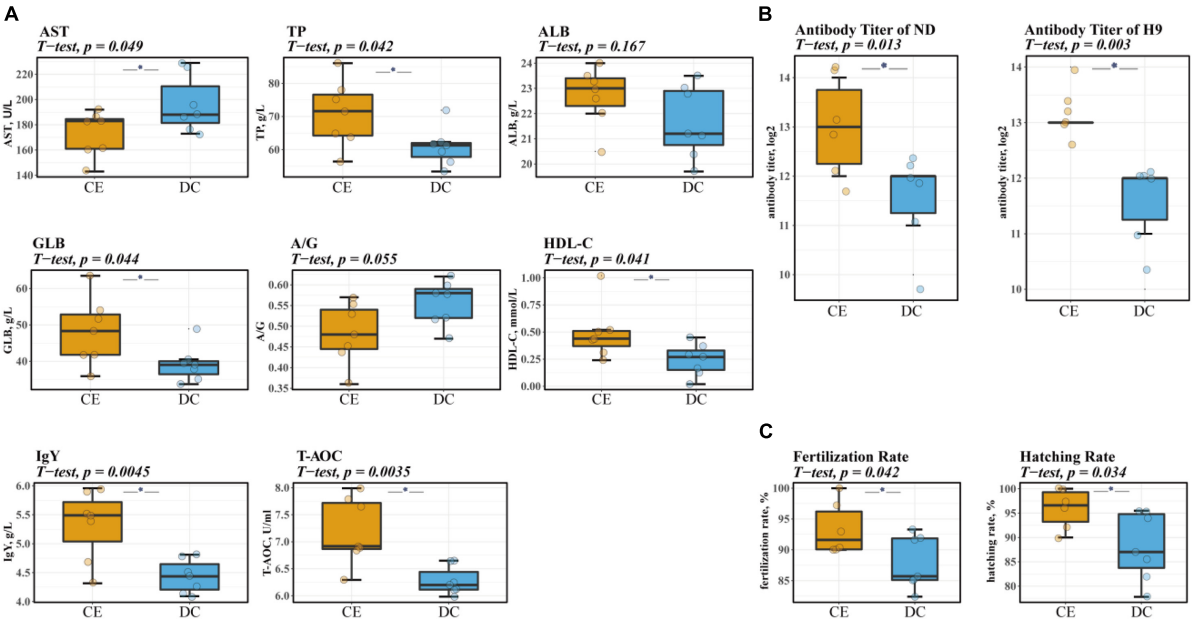

FIGURE 1 | CE can increase the level of serum immunity, antioxidant, and liver-related indicators and significantly improve breeding hens' reproduction performance (n = 7 hens/group). **(A)** The levels of biochemical parameters of breeding hens. **(B)** Serum antibody titers of NDV and avian influenza H9 strain of breeding hens. **(C)** The reproduction performance efficiency of breeding hens. Left: representative fertilized eggs rate; Right: representative the hatching of fertile (HoF) rate. ALB, Albumin; AST, Aspartate Aminotransferase; GLB, Globulin; HDL-C, High-density lipoprotein cholesterol; IgY, Immunoglobulin Y; ND, Newcastle disease. T-AOC, Total Antioxidant Capacity; TP, Total protein. *P < 0.05 compared to two groups.

mitochondria, while Bacteroidetes specifically included the Bacteroidales_S24_7_group (**Figure 3B**) (relative abundance> 1%). Lactobacillaceae and Peptostreptococcaceae were the dominant bacteria in the two groups, and their relative abundances in CE and DC were 44.42 vs. 14.38% and 25.07 vs. 70.57%, respectively.

At the genus level, *Romboutsia, Lactobacillus, Turicibacter, Enterococcus, Gallibacterium,* and *Helicobacter* were the predominant genera in the two groups (**Figure 3C**) (relative abundance> 1%). With the addition of CE, the relative abundance of *Lactobacillus* and *Enterococcus* increased, while the relative abundance of *Romboutsia* decreased.

Key Microbial Identification

LDA and effective size comparisons (LEfSe) were conducted to identify the core taxa most likely to explain the differences between the groups. The CE-treated samples appeared to be dominated by *Lactobacillus, Enterococcus, Faecalicoccus,* and *Streptococcus,* whereas DC samples showed *Romboutsia, Faecalibacterium,* and *Burkholderia* as the dominant genera (**Figure 4A**).

Predicted Functions of Ileal Bacterial Communities

Significant differences in the gut microbiota were observed between the two groups; however, their functions remain unknown. Hence, we performed a PICRUSt analysis to predict the potential functions of the gut microbiota. All functional genes were divided at level 3. When filtered for non-bacterial functional pathway, the predicted metabolic functional categories in the CE-fed group were related to pathways of biodegradation and metabolism of several xenobiotics, such as "polycyclic aromatic hydrocarbon degradation," "aminobenzoate degradation," and "ethylbenzene degradation." The CE group was also enriched for pathways such as "glycosyltransferases," "carbohydrate digestion and absorption," and "D-Arginine, and D-ornithine metabolism." Pathways such as "sporulation," "cyanoamino acid metabolism," "biosynthesis of ansamycins," "thiamin metabolism," and "methane metabolism" were enriched in the DC group (**Figure 4B**).

Response of Ileum Metabolomic Profiles to Corn Enzyme Diet

The ileal metabolome was analyzed in both groups to investigate the effect of multi-enzyme supplementation on the ileal chyme. LC-MS detected 23,595 untargeted peaks, and 4,884 metabolites were annotated. To reduce dimensionality, we applied PCA and OPLS-DA to leverage both unsupervised and supervised dimensionality reduction techniques to achieve this goal. Both PCA and OPLS-DA showed separation and discrimination (**Figures 5A,B**). The quality parameter values of the OPLS-DA model were predicted to be [R2X (cum) = 0.733, R2Y (cum) = 0.947] and fitness [Q2 (cum) = 0.698], which indicated that the model had good reliability and predictability (**Figure 5C**). The volcano plot indicated up-and downregulated differential metabolites based on statistical values ($p < 0.05$, $|\log_2 FC| > 1$),

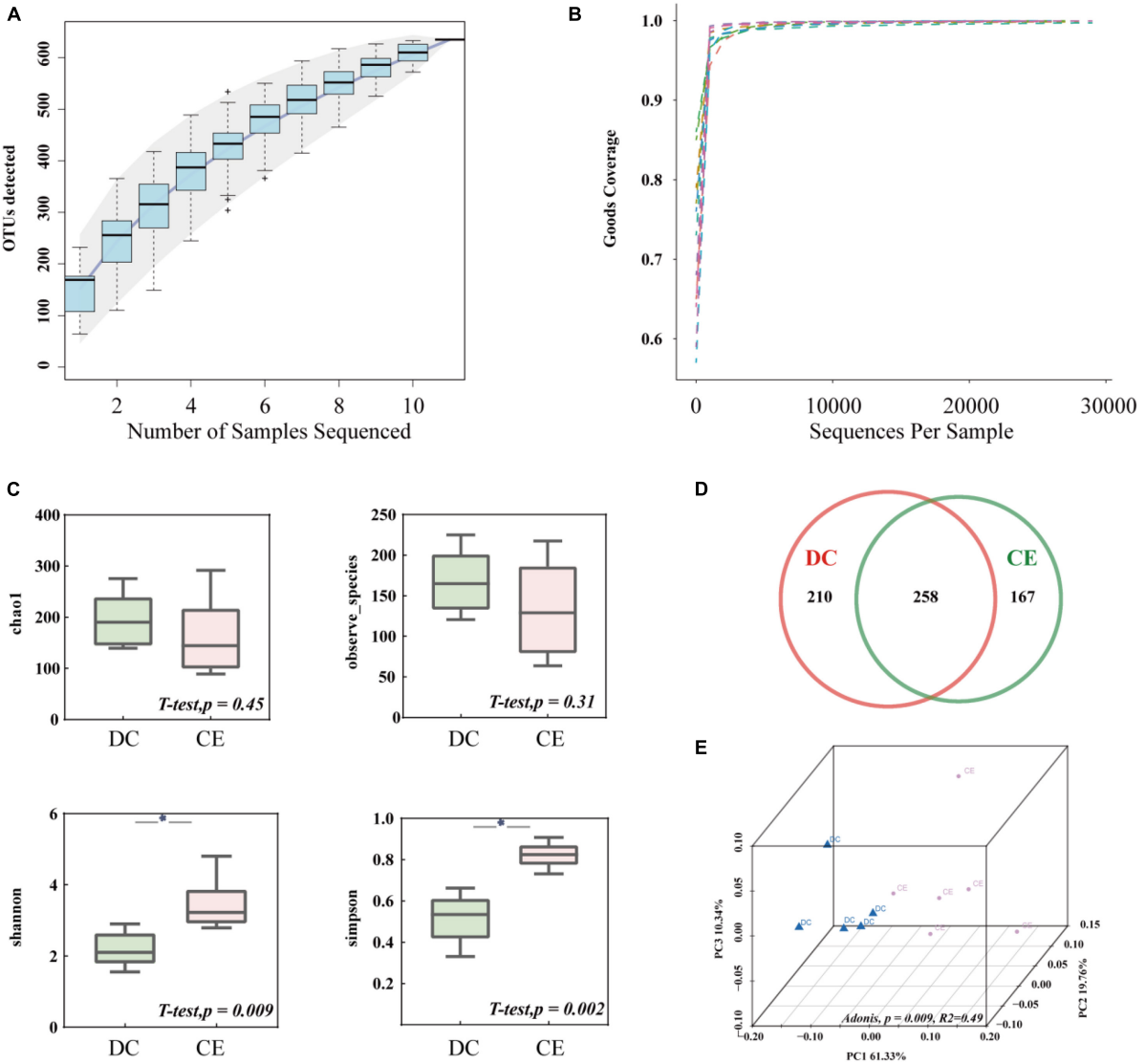

FIGURE 2 | The microbial community structure in the ileum was significantly altered by adding CE (n = 6 hens/group). **(A)** Species accumulation curve is used to estimate the rationality of sequencing sample quantity. **(B)** Alpha diversity Rarefaction curve based on Good's Coverage value, which reflects the rationale of sequencing depth. **(C)** Alpha-diversity evaluation of ileum microbial richness and evenness by measuring chao1, observe-species, Shannon, and Simpson's diversity indexes. **(D)** Venn diagram is used to represent the amount of shared and unique OTUs numbers. **(E)** Principal coordinate analysis (PCoA) is used to determine the similarities of microbial communities between different groups. *$P < 0.05$ compared to two groups.

and $p < 0.001$, $|\log_2 FC| > 2$ was considered to have higher significance (**Figure 5D**).

Identification of Differential Metabolites and Critical Metabolic Pathways

In total, 180 differential metabolites were assigned based on VIP values (VIP > 1) and p-values ($p < 0.05$). The results of MBRole and MetaboAnalyst (**Figure 6A**) showed that the differential metabolites were enriched in the "aminoacyl-tRNA biosynthesis," "ABC transporters," "D-glutamine and D-glutamate metabolism," and "arginine biosynthesis pathway." Moreover, the "arginine biosynthesis pathway" was the most prominent position in the topological analysis (**Figure 6B**). The LIPEA results (**Figure 6A**) indicated that the following pathways were significantly enriched by inputting differential lipid metabolites: "glycerophospholipid metabolism," "glycosylphosphatidylinositol (GPI)-anchor biosynthesis," "autophagy—other," "autophagy—animal," and "ferroptosis" pathways.

Co-occurrence Patterns of Microbial Communities

To further explore the complex microbial community structures in the DC and CE groups, we performed co-occurrence network analysis by calculating CCLasso (Fang et al., 2015), sparCC

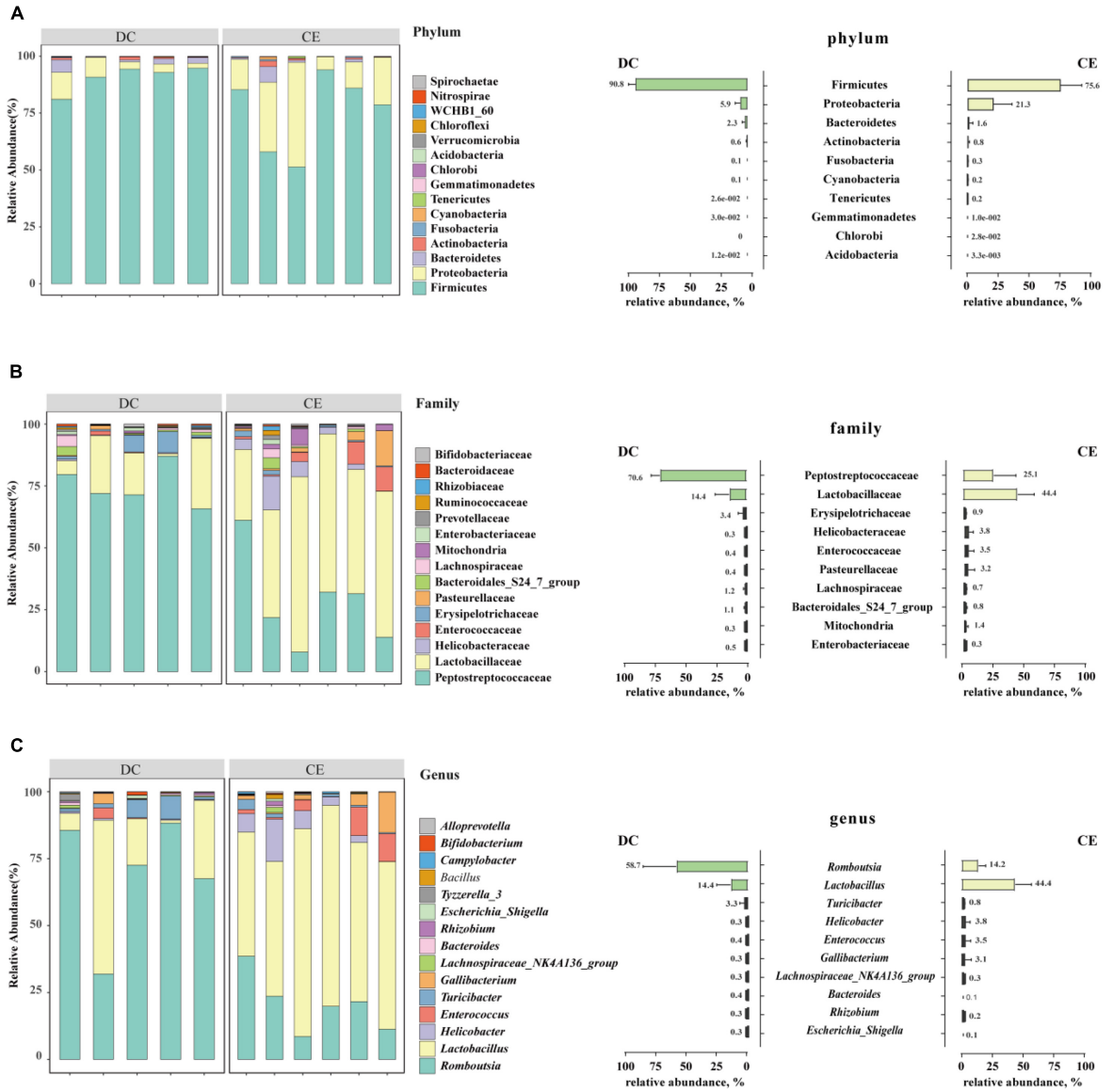

FIGURE 3 | The stacked graph of microbial community structure at **(A)** phylum level, **(B)** family level and **(C)** genus level (n = 6 hens/group). The bar chart on the right represents the relative abundance distribution of TOP 10 bacteria at different taxonomic levels, respectively.

(Friedman and Alm, 2012), and NAMAP with Spearman correlation inference algorithm *via* MetagenoNets between microbial taxa at the genus level based on 16S sequencing (Nagpal et al., 2020; **Figure 7A**). The results showed that the addition of CE significantly increased the interrelationship between bacteria under all three algorithms [edges: 2,541 vs. 954; 815 vs. 425; 137 vs. 33, CE vs. DC (CCLasson, SparCC, Spearman, respectively)], while the number of correlated nodes did not change significantly [nodes: 91 vs. 90; 88 vs. 89; 47 vs. 39, CE vs. DC (CCLasson, SparCC, Spearman, respectively)]. CCLasso obtained the highest number of interrelationships, followed by the SparCC and Spearman algorithms. All three algorithms indicated that CE activated the interactions between bacteria. Different algorithms have unique advantages and shortcomings. SparCC (Friedman and Alm, 2012) is a microbial network algorithm developed based on the log-ratio transformation of compositional data, which solves the problem of poor performance of the Spearman algorithm under the sparsity condition of bacterial communities; however, it did not consider the influence of errors in the compositional data (Fang et al., 2015). CCLasso made improvements based on such issues and had the characteristic of better edge recovery.

Correlations Among Differential Microbiota and Metabolites

Constructing a network between differential microbiota and metabolites is important for understanding their interaction

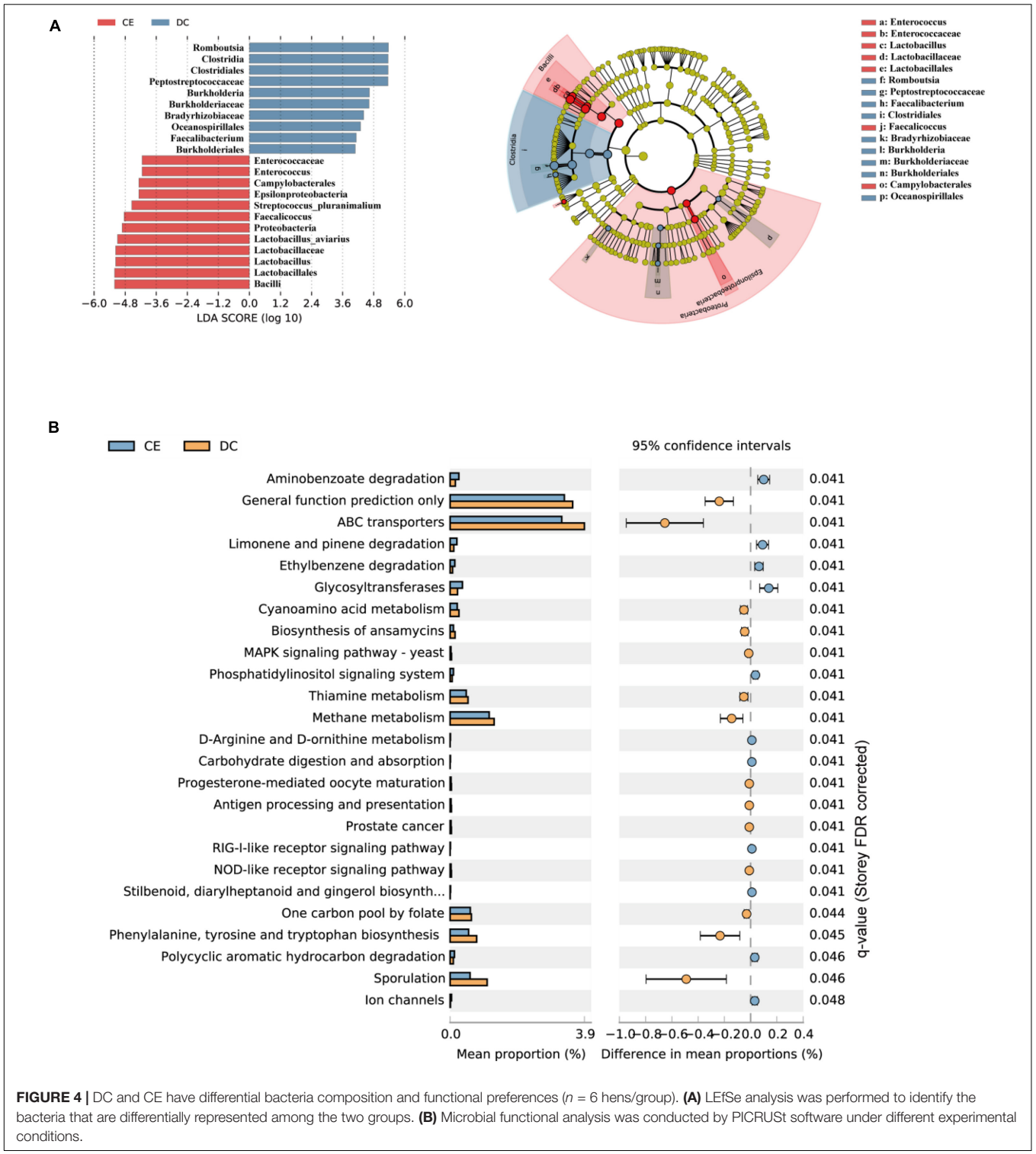

FIGURE 4 | DC and CE have differential bacteria composition and functional preferences (n = 6 hens/group). **(A)** LEfSe analysis was performed to identify the bacteria that are differentially represented among the two groups. **(B)** Microbial functional analysis was conducted by PICRUSt software under different experimental conditions.

relationships. Spearman correlation analysis of six microbiota (by LEfSe, LDA > 4, $p < 0.05$) and 180 metabolites (by $p < 0.05$, VIP > 1) was conducted (**Figure 7B**). The results showed that the bacteria enriched in CE were remarkably correlated with the upregulated metabolites. In contrast, the bacteria enriched in DCs were remarkably correlated with downregulated metabolites, reflecting a clear differential interaction pattern. This result further demonstrated a significant change in microbe-mediated metabolic patterns after the addition of CE.

To further identify more specific and sensitive markers of metabolites, we performed a more stringent threshold criteria ($p < 0.001$, | FC| > 4, VIP > 1) (**Figure 8A**). The top focus

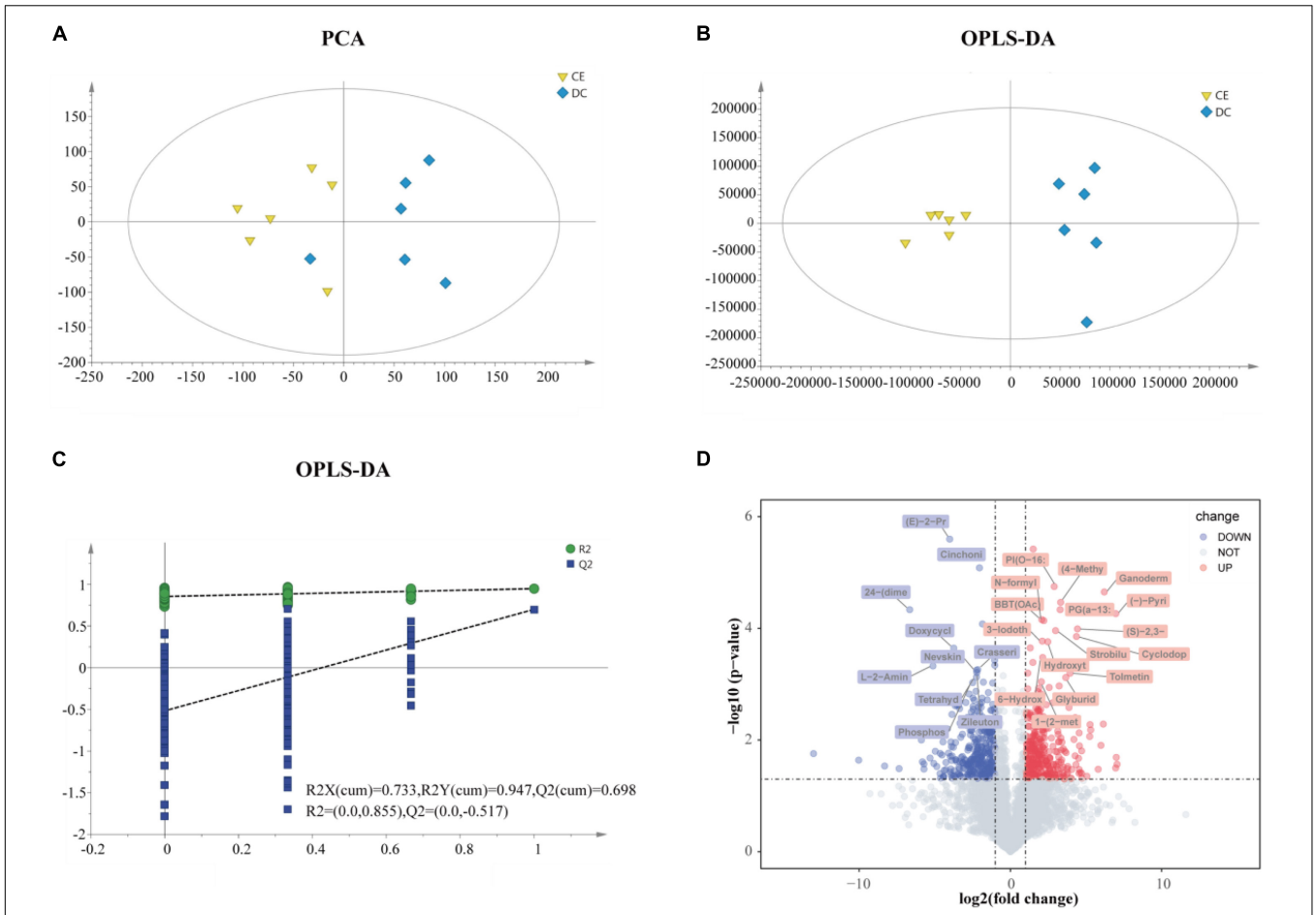

FIGURE 5 | The gut metabolites were remarkably perturbed by adding CE (n = 6 hens/group). **(A)** Principal component analyses (PCA) of ileum metabolome. **(B)** Orthogonal projections to latent structures-discriminate analysis (OPLS-DA) score plot was performed on ileum in DC and CE groups. In the permutation validation plot **(C)** (200 cycles) the Y-axis intercepts of R^2 and Q^2 are 0.855 and −0.517, respectively, indicating that the model is valid. **(D)** Volcano plots of ileum profiles showing $\log_2$(fold-change) and $-\log_{10}$(p-value) in metabolites levels induced by adding CE (up-regulated in red and down-regulated in green). The labeled metabolites were of particular interest (| fold change| > 4, $p < 0.001$).

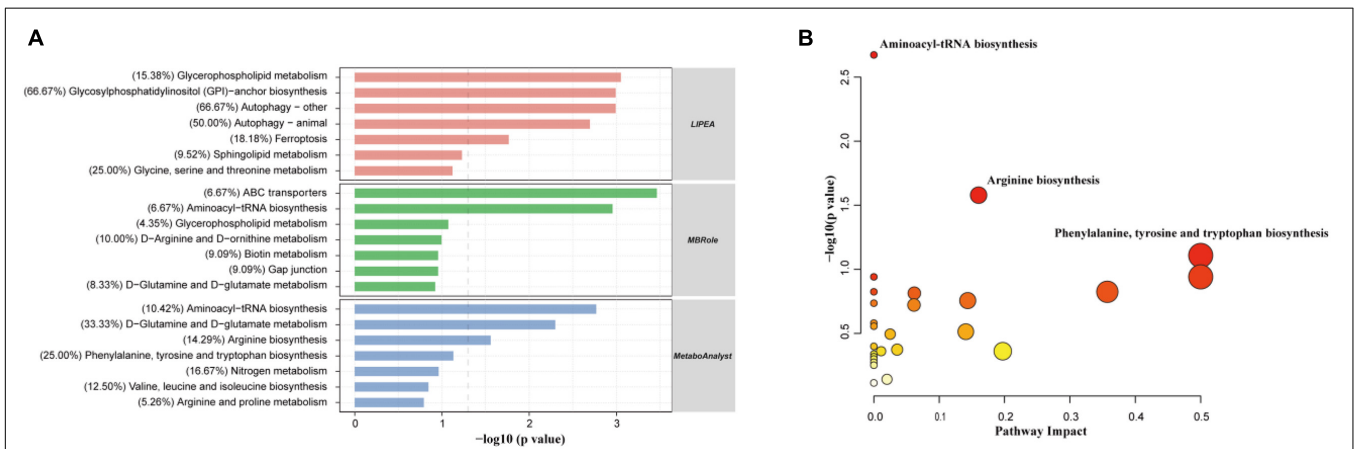

FIGURE 6 | Differential metabolites were significantly enriched in multiple pathways, suggesting that the addition of CE remarkably perturbed gut metabolic activities (n = 6 hens/group). **(A)** Functional KEGG pathway enrichment analysis of the differential expressed metabolites was carried out through three different platforms (LIPEA, MBRole, and MetaboAnalyst). **(B)** Analysis of metabolic pathways of DC and CE groups of differentially expressed metabolites was shown by bubble plot, each dot represents a metabolic pathway. X-axis and Y-axis stand for pathway impact and $-\log_{10}$(P-value), respectively.

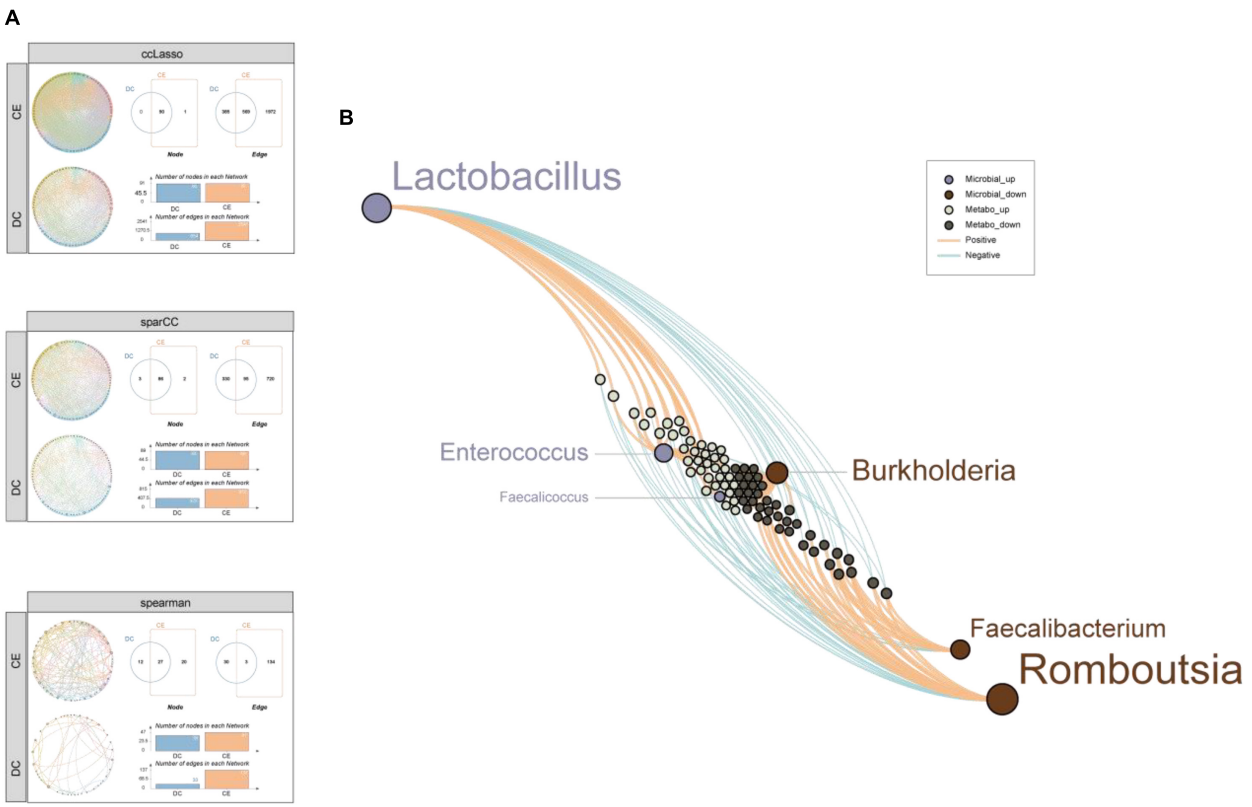

FIGURE 7 | CE enhanced co-expression correlation among the microbial community and the differential metabolites were tightly associated with the signature microbiota. **(A)** Microbial community co-expression network analysis explores the relationship between CE and DC groups through three standard algorithms. Different nodes represent different bacterial genera, colors represent phyla, and the dots size represent node degree. **(B)** A network diagram of differential microbiota-metabolites demonstrates that the up-regulated microbial were closely related with the up-regulated metabolites while down-regulated microbial were closely related with the down-regulated metabolites.

metabolites were used to perform correlation analysis with the signature microbiota (LDA $>$ 4, $p < 0.05$) (**Figure 8B**). The results showed that *Lactobacillus* was significantly positively correlated with 6-hydroxy-5-methoxyindole glucuronide and negatively correlated with doxycycline and cinchonidine, while *Romboutsia* and *Burkholderia* had the opposite regulation pattern to *Lactobacillus*. In addition, both *Enterococcus* and *Faecalicoccus* were negatively correlated with cinchonidine, and *Enterococcus* was also significantly positively correlated with 6-hydroxy-5-methoxyindole glucuronide.

DISCUSSION

Enzyme supplementation of poultry feed is of great significance in nutrition, economics, and the environment. Enzymes can improve the utilization of carbohydrates, proteins, lipids, and phytate phosphorus in feed to reduce the waste of fodder values and pollutant emissions (Douglas et al., 2000; Dosković et al., 2013). Our study showed that supplementation with multiple enzymes had no significant effect on laying performance, which contrasted with the results of previous studies. Studies by Khan et al. (2011) showed that adding 2.0 g/kg multi-enzyme preparation can increase egg production, egg weight, and egg mass; and improve the feed conversion ratio and bodyweight of layers without changing feed intake. Although enzymes have a significant impact on the performance of poultry, their application is greatly limited by the wide variety of enzymes and harsh application conditions. A previous study showed that the addition of complex enzymes (phytase, xylanase, cellulase, α-amylase, and acid-protease) had little effect on the production performance of aged hens (60–68 weeks old) but increased intestinal enzyme activity and nutrient retention (Wen et al., 2012). Interestingly, adding enzymes to low-protein and low-AME diets significantly improves hen and broiler performance and digestive enzyme activities (Zhou et al., 2009; Zhu et al., 2014; Rehman et al., 2018). Therefore, we supposed that adding multi-enzyme preparations has little impact on production performance, partly due to the balanced nutrition diet and the health status of breeding hens.

Blood biochemical indices reflect the health status of hens. CE administration increased the levels of TP and GLB in the serum. This was probably due to the adequate degradation of proteins promoted by the enzymes, which improve the absorption and utilization of amino acids in the small intestine (Al-Homidan et al., 2020). IgY is the primary serum antibody mainly distributed

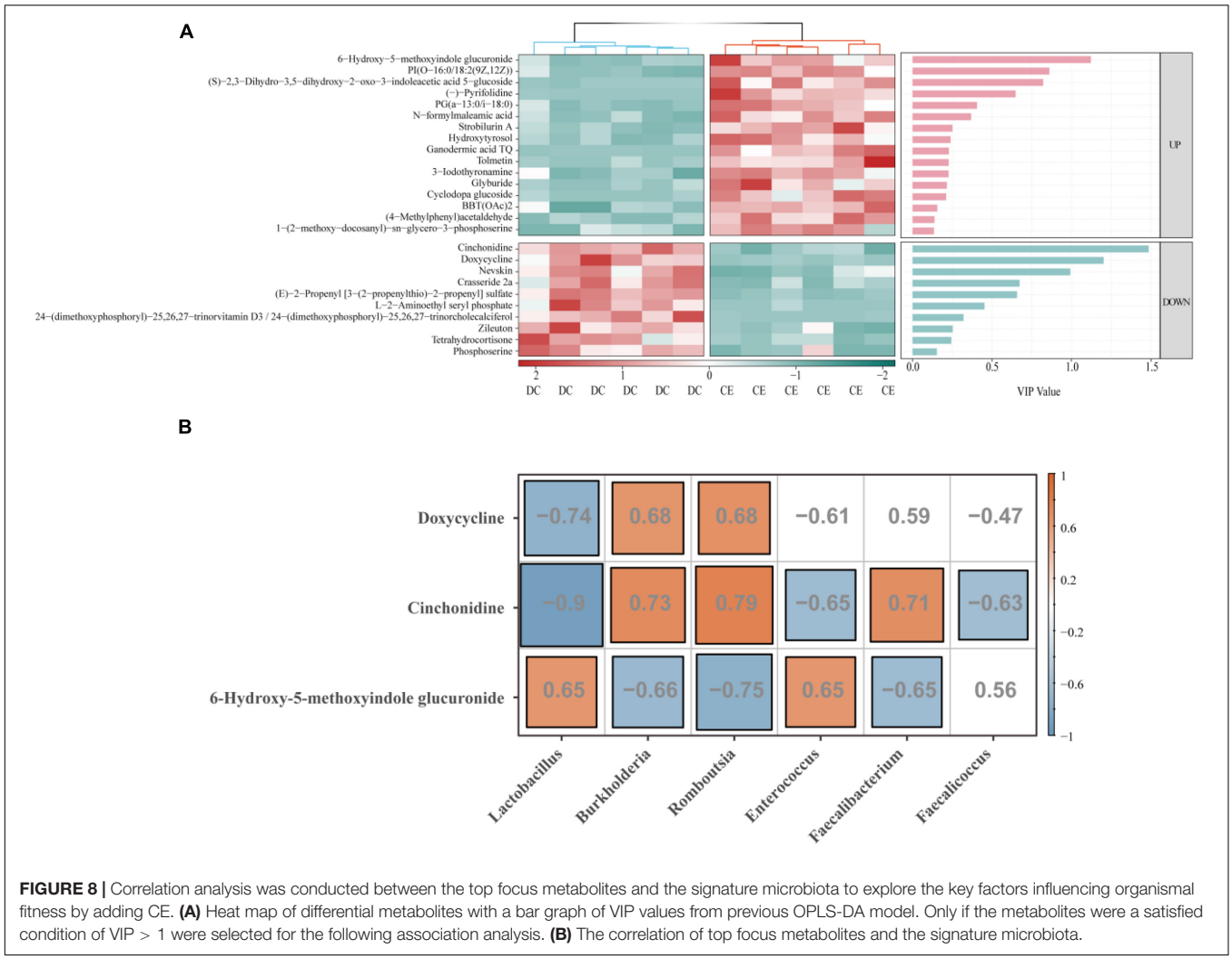

FIGURE 8 | Correlation analysis was conducted between the top focus metabolites and the signature microbiota to explore the key factors influencing organismal fitness by adding CE. **(A)** Heat map of differential metabolites with a bar graph of VIP values from previous OPLS-DA model. Only if the metabolites were a satisfied condition of VIP > 1 were selected for the following association analysis. **(B)** The correlation of top focus metabolites and the signature microbiota.

in poultry serum and egg yolk to protect the hens and their offspring from pathogens (Thirumalai et al., 2019). The improvement of in the titers of IgY and serum NDV and avian influenza H9 strain antibodies was associated with enhanced disease resistance. Enhanced humoral immunity was possibly related to the immune-regulatory effects of some oligosaccharides and beneficial microbiota in the gut after feeding with multiple enzymes. Additionally, CE administration significantly increased the serum HDL-C and T-AOC content and decreased the AST content. The T-AOC reflects the cumulative effect of all antioxidants in the blood and body fluids (Suresh et al., 2009; Liu et al., 2021). Breeding hens frequently face oxidative stress and ovarian aging problems in the later laying stage, which considerably affect their performance and physiology (Liu et al., 2018). AST is a sensitive marker for detecting liver injury, and high levels of AST indicate liver damage (Yousefi et al., 2005). HDL-C is considered "good cholesterol" and is associated with cardiovascular health. It can accelerate lipid migration from peripheral tissues to the liver, where cholesterol can be metabolized into bile acids (Li et al., 2018; Duan et al., 2019). Therefore, adding multiple enzymes to the diet enhances host systemic immunity, improves antioxidant capacity, and has no adverse effects on liver function.

Egg quality and reproductive performance, two important economic traits for breeding hens, tend to decrease rapidly because of the lower efficiency of absorption and immunity with age (Liu et al., 2001; Bain et al., 2016). We found that adding multiple enzymes can significantly increase albumen height and Haugh unit, indicating that the addition of multiple enzymes improves egg freshness. We then analyzed reproductive performance and found that CE administration also significantly enhanced the rate of fertilization and HoF value. The improvement of these two reproduction indexes may be related to the high-quality protein of the eggs and increased deposition of IgY in the yolk, thereby improving the reproductive performance of aged breeding hens (Thirumalai et al., 2019). In summary, CE supplementation can effectively enhance egg quality and reproductive performance of breeding hens.

To further discern the underlying mechanism of the enzyme on the productive performance and immune function of hens. The gut microbiota and metabolome after enzyme treatment were analyzed. Our results showed that adding CE had minimal

effect on Chao1 and Observed species, but significantly increased Shannon and Simpson's diversity indices. Meanwhile, the PCoA showed a clear separation between the CE and DC groups, which indicated that multiple enzymes could dramatically alter the gut microbiota with increasing microbial evenness without decreasing microbial richness (Zhang et al., 2017). Consistent with the results of previous studies, Firmicutes, Proteobacteria, and Bacteroidetes were the dominant phyla in the ileum of hens, accounting for more than 98% of the total bacteria (Pan and Yu, 2014; Liu et al., 2021). The genera *Lactobacillus*, *Enterococcus*, *Streptococcus*, and *Faecalicoccus* were the signature taxa of the CE group determined using LEfSe (LDA > 4, $p < 0.05$). *Lactobacillus* spp. contribute to intestinal health, immunity enhancement, nutrient absorption, and bile acid hydrolysis (Staley et al., 2017; Xiao et al., 2017). *Enterococcus* spp. are lactic acid bacteria that produce bacteriocins against pathogenic bacteria and regulate nutrient metabolism (Hanchi et al., 2018). *Streptococcus* spp. such as *S. thermophiles* and *S. salivarius* are often considered to have probiotic effects, which help establish intestinal immune homeostasis and regulate the inflammatory response of the host (Akpinar et al., 2011; Kaci et al., 2014). Analysis of microbial co-occurrence network patterns suggested that the addition of multi-enzymes remarkably increased the interactions between gut microbiota without affecting the number of interacting bacteria, illustrating that adding multiple enzymes enhanced the communication between bacteria. Correlation analysis of differential microbiota and metabolites demonstrated that the gut microbiota signature genera were strongly correlated with altered metabolites. Therefore, the addition of multi-enzyme modulated immune function and metabolism may be related to altering the intestinal microbiota, increasing the relative abundance of potentially beneficial bacteria, and enhancing the interaction between bacteria.

The gene function analysis of the predicted metagenomes from the DC group suggested that the microbial pathways were significantly enriched in the sporulation and biosynthesis of ansamycins. Spores can store the microbiota's hereditary material in a harmful or unsuitable environment so that their metabolism in this state is 10 million times slower than in normally growing bacteria (Huang and Hull, 2017; Bressuire-Isoard et al., 2018). Ansamycins are antibiotics produced by several *Actinomycetes* strains and have an inhibitory effect on the growth of many bacteria (Vardanyan and Hruby, 2016). Bacteria inhibit the growth of their surrounding bacteria by synthesizing antibiotics to compete for limited resources, leading to a vicious cycle in the gut environment. Metabolic pathway enrichment analysis showed significant enrichment of several pathways, including glycerophospholipid metabolism, autophagy, and ferroptosis. This could be because the bacteria in the DC group lacked genes related to the degradation of harmful substances and the higher concentration of antibiotics surrounding them. Hence, bacteria may degrade their components or excess proteins through autophagy to provide nutrition for survival or directly induce ferroptosis-like death in the DC group (Deretic and Levine, 2009; Xu et al., 2019; Shen et al., 2020). Spearman correlation analysis revealed that two top-focused metabolites, doxycycline, and cinchonidine, enriched in the DC group, were positively correlated with the DC signature bacteria *Romboutsia* spp. and *Burkholderia* spp. Doxycycline, a tetracycline, has a bacteriostatic effect by inhibiting the synthesis of bacterial proteins by destroying transfer RNA and messenger RNA at ribosomal sites (Raval et al., 2018). Because doxycycline is significant for maintaining animal health and controlling vertically transmitted diseases, it has been widely used in the breeding industry (Yan et al., 2018). Studies have shown that doxycycline mainly affects the relative abundance of Firmicutes and Proteobacteria and reduces the richness and evenness of the flora (Boynton et al., 2017; Stavroulaki et al., 2021). Cinchonidine is an alkaloid found in several foods such as fruits, herbs, spices, and olives (Olea europaea) (Eyal, 2018). However, the biosynthetic pathway of cinchonidine remains unclear (Maldonado et al., 2017). Overall, the bacteria in the DC group enriched genes related to sporulation and biosynthesis of ansamycins pathways and lacked communication. The intestinal environment had a higher doxycycline content than the CE group, which would affect the microbial community structure and reduce the evenness (Stavroulaki et al., 2021).

The gene function analysis of the predicted metagenomes from the CE group suggested that the microbial pathways were significantly enriched in the biodegradation and metabolism of multiple harmful substances. Polycyclic aromatic hydrocarbons (PAHs) are widely distributed organic pollutants with genetic toxicity and carcinogenicity that can significantly interfere with gut microbiota and are associated with harmful effects on host health (Ghosal et al., 2016; Redfern et al., 2021). Ethylbenzene is a toxic aromatic organic compound metabolized by the organism, and the accumulation of xenobiotics in an organism may cause tissue damage and harm the host (Pan et al., 2020). The addition of multiple enzymes significantly enriched microbial functional genes related to the degradation of the aforementioned harmful substances, which suggested that the microbes of the CE group may have a better ability to degrade toxic organic compounds and maintain homeostasis of the gut environment to create a better intestinal environment. Meanwhile, the ileum microbiota in the CE group also enriched "glycosyltransferases" pathways, which may promote bacterial surface antigen formation, thus stimulating the host immune system and improving humoral immunity (Hong et al., 2019). Spearman correlation analysis revealed that one top-focused metabolite, 6-hydroxy-5-methoxyindole glucuronide, enriched in the CE group, was positively correlated with the CE signature bacteria *Lactobacillus* spp., and *Enterococcus* spp. 6-Hydroxy-5-methoxyindole glucuronide, a member of the glucuronide family. It is a natural metabolite of 6-hydroxy-5-methoxyindole generated in the liver by UDP glucuronyltransferase, which assists with the excretion of toxic substances, drugs, or other substances that cannot be used as an energy source (Zhao et al., 2012; Liu et al., 2019). Collectively, the addition of multiple enzymes can improve the ability of microbes to degrade harmful substances, and the potentially beneficial bacteria enriched in the CE group are closely related to the metabolite 6-Hydroxy-5-methoxyindole glucuronide that facilitates the excretion of toxic substances. Thus, CE addition can benefit hen health, possibly by affecting the metabolic function of intestinal bacteria.

Taken together, the results showed that CE supplementation may provide a nutrient-rich environment for bacteria by improving the digestion and absorption of starch and protein, elevating the excretion of toxins and harmful substances, and reshaping the structure of the ileal microbial community such that *Lactobacillus* spp. are the dominant bacteria and the relative abundance of common potentially beneficial bacteria, such as *Enterococcus* and *Streptococcus*, is increased. Follow-up studies are needed to ascertain the changes in the gut microbiome and metabolome induced by complex enzymes on intestinal cell function.

CONCLUSION

Overall, administration of 0.2 g/kg of dietary multi-enzyme could enhance humoral immunity and improve egg quality and reproductive efficiency together with intestinal microbial community structure and metabolite composition of aged breeding hens. Multi-enzymes could be used to enhance the immunity and reproductive performance of old breeding hens and extend their service life.

DATA AVAILABILITY STATEMENT

The microbial raw sequencing data and the metabolome data were deposited into the NCBI Sequence Read Archive database (SRA accession: PRJNA728385).

ETHICS STATEMENT

The animal study was reviewed and approved by Animal care and Use Committee of China Agricultural University.

AUTHOR CONTRIBUTIONS

ZW and ZN conceptualized the project. YL performed experiments, collected data, analyzed data, and wrote the manuscript. LQ designed studies and made insightful edits. DZ performed experiments. All authors reviewed the manuscript and approved the final submission.

FUNDING

This work was supported by the China Agriculture Research System (CARS-40). Funders had no participation in the study design, analysis, or writing of this article.

ACKNOWLEDGMENTS

We would be deeply grateful to all of the participants involved in the study and all of the research staff and students working on the project. We would like to thank Editage (www.editage.cn) for English language editing.

REFERENCES

Aderibigbe, A., Cowieson, A. J., Sorbara, J. O., and Adeola, O. (2020). Growth phase and dietary α-amylase supplementation effects on nutrient digestibility and feedback enzyme secretion in broiler chickens. *Poult. Sci.* 99, 6867–6876. doi: 10.1016/j.psj.2020.09.007

Akpinar, A., Yerlikaya, O., and Kiliccedil, S. (2011). Antimicrobial activity and antibiotic resistance of *Lactobacillus delbrueckii* ssp. bulgaricus and *Streptococcus thermophilus* strains isolated from Turkish homemade yoghurts. *Afr. J. Microbiol. Res.* 5, 675–682. doi: 10.5897/AJMR10.835

Al-Homidan, I., Ebeid, T., Al-Muzaini, A., Abou-Emera, O., Mostafa, M., and Fathi, M. (2020). Impact of dietary fenugreek, mung bean, and garden cress on growth performance, carcass traits, blood measurements, and immune response in broiler chickens. *Livest. Sci.* 242:104318. doi: 10.1016/j.livsci.2020.104318

Bain, M. M., Nys, Y., and Dunn, I. C. (2016). Increasing persistency in lay and stabilising egg quality in longer laying cycles. What are the challenges? *Brit. Poult. Sci.* 57, 330–338. doi: 10.1080/00071668.2016.1161727

Bolger, A. M., Lohse, M., and Usadel, B. (2014). Trimmomatic: a flexible trimmer for Illumina sequence data. *Bioinformatics* 30, 2114–2120. doi: 10.1093/bioinformatics/btu170

Boynton, F. D. D., Ericsson, A. C., Uchihashi, M., Dunbar, M. L., and Wilkinson, J. E. (2017). Doxycycline induces dysbiosis in female C57BL/6NCrl mice. *BMC Res. Notes* 10:644. doi: 10.1186/s13104-017-2960-7

Bressuire-Isoard, C., Broussolle, V., and Carlin, F. (2018). Sporulation environment influences spore properties in Bacillus: evidence and insights on underlying molecular and physiological mechanisms. *FEMS Microbiol. Rev.* 42, 614–626. doi: 10.1093/femsre/fuy021

Caporaso, J. G., Kuczynski, J., Stombaugh, J., Bittinger, K., Bushman, F. D., Costello, E. K., et al. (2010). QIIME allows analysis of high-throughput community sequencing data. *Nat. Methods* 7, 335–336. doi: 10.1038/nmeth.f.303

Cowieson, A., Lu, H., Ajuwon, K., Knap, I., and Adeola, O. (2017). Interactive effects of dietary protein source and exogenous protease on growth performance, immune competence and jejunal health of broiler chickens. *Anim. Prod. Sci.* 57, 252–261. doi: 10.1071/AN15523

Cowieson, A. J., and Kluenter, A. M. (2019). Contribution of exogenous enzymes to potentiate the removal of antibiotic growth promoters in poultry production. *Anim. Feed Sci. Technol.* 250, 81–92. doi: 10.1016/j.anifeedsci.2018.04.026

da Costa Luchiari, I., Cedeno, F. R. P., de Macêdo Farias, T. A., Picheli, F. P., de Paula, A. V., Monti, R., et al. (2021). Glucoamylase immobilization in corncob powder: assessment of enzymatic hydrolysis of starch in the production of glucose. *Waste Biomass Valor.* 12, 5491–5504. doi: 10.1007/s12649-021-01379-0

Dalcin, E., and Jackson, P. W. (2018). A network-wide visualization of the implementation of the global strategy for plant conservation in Brazil. *Rodriguesia* 69, 1613–1639. doi: 10.1590/2175-7860201869411

Deretic, V., and Levine, B. (2009). Autophagy, immunity, and microbial adaptations. *Cell Host Microbe* 5, 527–549. doi: 10.1016/j.chom.2009.05.016

Dosković, V., Bogosavljević-Bosković, S., Pavlovski, Z., Milošević, B., Škrbić, Z., Rakonjac, S., et al. (2013). Enzymes in broiler diets with special reference to protease. *Worlds Poult. Sci. J.* 69, 343–360. doi: 10.1017/S0043933913000342

Douglas, M. W., Parsons, C. M., and Bedford, M. R. (2000). Effect of various soybean meal sources and Avizyme on chick growth performance and ileal digestible energy. *J. Appl. Poult. Res.* 9, 74–80. doi: 10.1093/japr/9.1.74

Duan, M., Sun, X., Ma, N., Liu, Y., Luo, T., Song, S., et al. (2019). Polysaccharides from *Laminaria japonica* alleviated metabolic syndrome in BALB/c mice by normalizing the gut microbiota. *Int. J. Biol. Macromol.* 121, 996–1004. doi: 10.1016/j.ijbiomac.2018.10.087

Edgar, R. C., Haas, B. J., Clemente, J. C., Quince, C., and Knight, R. (2011). UCHIME improves sensitivity and speed of chimera detection. *Bioinformatics* 27, 2194–2200. doi: 10.1093/bioinformatics/btr381

Eyal, S. (2018). The fever tree: from Malaria to neurological diseases. *Toxins* 10:491. doi: 10.3390/toxins10120491

Fang, H., Huang, C., Zhao, H., and Deng, M. (2015). CCLasso: correlation inference for compositional data through Lasso. *Bioinformatics* 31, 3172–3180. doi: 10.1093/bioinformatics/btv349

Friedman, J., and Alm, E. J. (2012). Inferring correlation networks from genomic survey data. *PLoS Comput. Biol.* 8:e1002687. doi: 10.1371/journal.pcbi.1002687

Ghosal, D., Ghosh, S., Dutta, T. K., and Ahn, Y. (2016). Current state of knowledge in microbial degradation of polycyclic aromatic hydrocarbons (PAHs): a review. *Front. Microbiol.* 7:1369. doi: 10.3389/fmicb.2016.01369

Giacobbo, F. C., Eyng, C., Nunes, R. V., de Souza, C., Teixeira, L. V., Pilla, R., et al. (2021). Different enzymatic associations in diets of broiler chickens formulated with corn dried at various temperatures. *Poult. Sci.* 100:101013. doi: 10.1016/j.psj.2021.01.035

Gu, Y., Chen, Y., Jin, R., Wang, C., Wen, C., and Zhou, Y. (2021). A comparison of intestinal integrity, digestive function, and egg quality in laying hens with different ages. *Poult. Sci.* 100:100949. doi: 10.1016/j.psj.2020.12.046

Hanchi, H., Mottawea, W., Sebei, K., and Hammami, R. (2018). The genus Enterococcus: between probiotic potential and safety concerns—an update. *Front. Microbiol.* 9:1791. doi: 10.3389/fmicb.2018.01791

Hii, S. L., Tan, J. S., Ling, T. C., and Ariff, A. B. (2012). Pullulanase: role in starch hydrolysis and potential industrial applications. *Enzyme. Res.* 2012:921362. doi: 10.1155/2012/921362

Hong, S., Shi, Y., Wu, N. C., Grande, G., Douthit, L., Wang, H., et al. (2019). Bacterial glycosyltransferase-mediated cell-surface chemoenzymatic glycan modification. *Nat. Commun.* 10:1799. doi: 10.1038/s41467-019-09608-w

Huang, M., and Hull, C. M. (2017). Sporulation: how to survive on planet Earth (and beyond). *Curr. Genet.* 63, 831–838. doi: 10.1007/s00294-017-0694-7

Jing, M., Munyaka, P., Tactacan, G., Rodriguez-Lecompte, J., and House, J. (2014). Performance, serum biochemical responses, and gene expression of intestinal folate transporters of young and older laying hens in response to dietary folic acid supplementation and challenge with *Escherichia coli* lipopolysaccharide. *Poult. Sci.* 93, 122–131. doi: 10.3382/ps.2013-03384

Kaci, G., Goudercourt, D., Dennin, V., Pot, B., Doré, J., Ehrlich, S. D., et al. (2014). Anti-inflammatory properties of Streptococcus salivarius, a commensal bacterium of the oral cavity and digestive tract. *Appl. Environ. Microbiol.* 80, 928–934. doi: 10.1128/AEM.03133-13

Khan, S. H., Atif, M., Mukhtar, N., Rehman, A., and Fareed, G. (2011). Effects of supplementation of multi-enzyme and multi-species probiotic on production performance, egg quality, cholesterol level and immune system in laying hens. *J. Appl. Anim. Res.* 39, 386–398. doi: 10.1080/09712119.2011.621538

Li, Z., Kim, H. J., Park, M. S., and Ji, G. E. (2018). Effects of fermented ginseng root and ginseng berry on obesity and lipid metabolism in mice fed a high-fat diet. *J. Ginseng Res.* 42, 312–319. doi: 10.1016/j.jgr.2017.04.001

Liu, H.-K., Long, D., and Bacon, W. (2001). Preovulatory luteinizing hormone surge interval in old and young laying turkey hens early in the egg production period. *Poult. Sci.* 80, 1364–1370. doi: 10.1093/ps/80.9.1364

Liu, X., Lin, X., Mi, Y., Li, J., and Zhang, C. (2018). Grape seed proanthocyanidin extract prevents ovarian aging by inhibiting oxidative stress in the hens. *Oxid. Med. Cell. Longev.* 2018:9390810. doi: 10.1155/2018/9390810

Liu, X., Wang, X., Sun, H., Guo, Z., Liu, X., Yuan, T., et al. (2019). Urinary metabolic variation analysis during pregnancy and application in gestational diabetes mellitus and spontaneous abortion biomarker discovery. *Sci. Rep.* 9:2605. doi: 10.1038/s41598-019-39259-2

Liu, Y., Cheng, X., Zhen, W., Zeng, D., Qu, L., Wang, Z., et al. (2021). Yeast culture improves egg quality and reproductive performance of aged breeder layers by regulating gut microbes. *Front. Microbiol.* 12:439. doi: 10.3389/fmicb.2021.633276

Liu, Y., Li, Y., Liu, H.-N., Suo, Y.-L., Hu, L.-L., Feng, X.-A., et al. (2013). Effect of quercetin on performance and egg quality during the late laying period of hens. *Br. Poult. Sci.* 54, 510–514. doi: 10.1080/00071668.2013.799758

Maldonado, C., Barnes, C. J., Cornett, C., Holmfred, E., Hansen, S. H., Persson, C., et al. (2017). Phylogeny predicts the quantity of antimalarial alkaloids within the iconic yellow *Cinchona* Bark (Rubiaceae: *Cinchona calisaya*). *Front. Plant. Sci.* 8:391. doi: 10.3389/fpls.2017.00391

Monier, M. N. (2020). Efficacy of dietary exogenous enzyme supplementation on growth performance, antioxidant activity, and digestive enzymes of common carp (*Cyprinus carpio*) fry. *Fish Physiol. Biochem.* 46, 713–723. doi: 10.1007/s10695-019-00745-z

Nagpal, S., Singh, R., Yadav, D., and Mande, S. S. (2020). MetagenoNets: comprehensive inference and meta-insights for microbial correlation networks. *Nucleic Acids Res.* 48, W572–W579. doi: 10.1093/nar/gkaa254

Pan, D., and Yu, Z. (2014). Intestinal microbiome of poultry and its interaction with host and diet. *Gut Microbes* 5, 108–119. doi: 10.4161/gmic.26945

Pan, F., Zhang, L.-L., Luo, H.-J., Chen, Y., Long, L., Wang, X., et al. (2020). Dietary riboflavin deficiency induces ariboflavinosis and esophageal epithelial atrophy in association with modification of gut microbiota in rats. *Eur. J. Nutr.* 60, 807–820. doi: 10.1007/s00394-020-02283-4

Parks, D. H., Tyson, G. W., Hugenholtz, P., and Beiko, R. G. (2014). STAMP: statistical analysis of taxonomic and functional profiles. *Bioinformatics* 30, 3123–3124. doi: 10.1093/bioinformatics/btu494

Quast, C., Pruesse, E., Yilmaz, P., Gerken, J., Schweer, T., Yarza, P., et al. (2012). The SILVA ribosomal RNA gene database project: improved data processing and web-based tools. *Nucleic Acids Res.* 41, D590–D596. doi: 10.1093/nar/gks1219

Raval, J. P., Chejara, D. R., Ranch, K., and Joshi, P. (2018). "Development of injectable *in situ* gelling systems of doxycycline hyclate for controlled drug delivery system," in *Applications of Nanocomposite Materials in Drug Delivery A volume in Woodhead Publishing Series in Biomaterials*, eds Inamuddin, A. M. Asiri, and A. Mohammad (Sawston: Woodhead Publishing), 149–162.

Redfern, L. K., Jayasundara, N., Singleton, D. R., Di Giulio, R. T., Carlson, J., Sumner, S. J., et al. (2021). The role of gut microbial community and metabolomic shifts in adaptive resistance of *Atlantic killifish* (*Fundulus heteroclitus*) to polycyclic aromatic hydrocarbons. *Sci. Total. Environ.* 776:145955. doi: 10.1016/j.scitotenv.2021.145955

Rehman, Z., Kamran, J., Abd El-Hack, M., Alagawany, M., Bhatti, S., Ahmad, G., et al. (2018). Influence of low-protein and low-amino acid diets with different sources of protease on performance, carcasses and nitrogen retention of broiler chickens. *Anim. Prod. Sci.* 58, 1625–1631. doi: 10.1071/AN16687

Reyon, D., Tsai, S. Q., Khayter, C., Foden, J. A., Sander, J. D., and Joung, J. K. (2012). FLASH assembly of TALENs for high-throughput genome editing. *Nat. Biotechnol.* 30:460. doi: 10.1038/nbt.2170

Rognes, T., Flouri, T., Nichols, B., Quince, C., and Mahé, F. (2016). VSEARCH: a versatile open source tool for metagenomics. *PeerJ* 4:e2584. doi: 10.7717/peerj.2584

Romero, L., Sands, J., Indrakumar, S., Plumstead, P., Dalsgaard, S., and Ravindran, V. (2014). Contribution of protein, starch, and fat to the apparent ileal digestible energy of corn-and wheat-based broiler diets in response to exogenous xylanase and amylase without or with protease. *Poult. Sci.* 93, 2501–2513. doi: 10.3382/ps.2013-03789

Sarian, F. D., Janeček, Š, Pijning, T., Ihsanawati, Nurachman, Z., Radjasa, O. K., et al. (2017). A new group of glycoside hydrolase family 13 α-amylases with an aberrant catalytic triad. *Sci. Rep.* 7:44230. doi: 10.1038/srep44230

Scott, K. P., Gratz, S. W., Sheridan, P. O., Flint, H. J., and Duncan, S. H. (2013). The influence of diet on the gut microbiota. *Pharmacol. Res.* 69, 52–60. doi: 10.1016/j.phrs.2012.10.020

Segata, N., Izard, J., Waldron, L., Gevers, D., Miropolsky, L., Garrett, W. S., et al. (2011). Metagenomic biomarker discovery and explanation. *Genome Biol.* 12:R60. doi: 10.1186/gb-2011-12-6-r60

Shen, X., Ma, R., Huang, Y., Chen, L., Xu, Z., Li, D., et al. (2020). Nano-decocted ferrous polysulfide coordinates ferroptosis-like death in bacteria for anti-infection therapy. *Nano Today* 35:100981. doi: 10.1016/j.nantod.2020.100981

Staley, C., Weingarden, A. R., Khoruts, A., and Sadowsky, M. J. (2017). Interaction of gut microbiota with bile acid metabolism and its influence on disease states. *Appl. Microbiol. Biotechnol.* 101, 47–64. doi: 10.1007/s00253-016-8006-6

Stavroulaki, E., Suchodolski, J. S., Pilla, R., Fosgate, G. T., Sung, C.-H., Lidbury, J. A., et al. (2021). Short-and long-term effects of amoxicillin/clavulanic acid or doxycycline on the gastrointestinal microbiome of growing cats. *bioRxiv* [Preprint]. doi: 10.1101/2021.05.28.446115

Suresh, D. R., Annam, V., Pratibha, K., and Prasad, B. V. M. (2009). Total antioxidant capacity – a novel early bio-chemical marker of oxidative stress in HIV infected individuals. *J. Biomed. Sci.* 16:61. doi: 10.1186/1423-0127-16-61

Thirumalai, D., Ambi, S. V., Vieira-Pires, R. S., Xiaoying, Z., Sekaran, S., and Krishnan, U. (2019). Chicken egg yolk antibody (IgY) as diagnostics and

therapeutics in parasitic infections–A review. *Int. J. Biol. Macromol.* 136, 755–763. doi: 10.1016/j.ijbiomac.2019.06.118

Tomasik, P., and Horton, D. (2012). Enzymatic conversions of starch. *Adv. Carbohydr. Chem. Biochem.* 68, 59–436. doi: 10.1016/b978-0-12-396523-3.00001-4

Vardanyan, R., and Hruby, V. (2016). "Chapter 30 – Antibiotics," in *Synthesis of Best-Seller Drugs*, eds R. Vardanyan and V. Hruby (Boston, MA: Academic Press), 573–643.

Walk, C., Pirgozliev, V., Juntunen, K., Paloheimo, M., and Ledoux, D. (2018). Evaluation of novel protease enzymes on growth performance and apparent ileal digestibility of amino acids in poultry: enzyme screening. *Poult. Sci.* 97, 2123–2138. doi: 10.3382/ps/pey080

Wen, C., Wang, L., Zhou, Y., Jiang, Z., and Wang, T. (2012). Effect of enzyme preparation on egg production, nutrient retention, digestive enzyme activities and pancreatic enzyme messenger RNA expression of late-phase laying hens. *Anim. Feed Sci. Technol.* 172, 180–186. doi: 10.1016/j.anifeedsci.2011.11.012

Wohlgemuth, G., Haldiya, P. K., Willighagen, E., Kind, T., and Fiehn, O. (2010). The CHEMICAL TRANSLATION SERVICE—a web-based tool to improve standardization of metabolomic reports. *Bioinformatics* 26, 2647–2648. doi: 10.1093/bioinformatics/btq476

Xiao, Y., Xiang, Y., Zhou, W., Chen, J., Li, K., and Yang, H. (2017). Microbial community mapping in intestinal tract of broiler chicken. *Poult. Sci.* 96, 1387–1393. doi: 10.3382/ps/pew372

Xu, Y., Zhou, P., Cheng, S., Lu, Q., Nowak, K., Hopp, A.-K., et al. (2019). A bacterial effector reveals the V-ATPase-ATG16L1 axis that initiates xenophagy. *Cell* 178, 552–566.e20. doi: 10.1016/j.cell.2019.06.007

Yan, Q., Li, X., Ma, B., Zou, Y., Wang, Y., Liao, X., et al. (2018). Different concentrations of doxycycline in swine manure affect the microbiome and degradation of doxycycline residue in soil. *Front. Microbiol.* 9:3129. doi: 10.3389/fmicb.2018.03129

Yin, D., Yin, X., Wang, X., Lei, Z., Wang, M., Guo, Y., et al. (2018). Supplementation of amylase combined with glucoamylase or protease changes intestinal microbiota diversity and benefits for broilers fed a diet of newly harvested corn. *J. Anim. Sci. Biotechnol.* 9:24. doi: 10.1186/s40104-018-0238-0

Yousefi, M., Shivazad, M., and Sohrabi-Haghdoost, I. (2005). Effect of dietary factors on induction of fatty liver-hemorrhagic syndrome and its diagnosis methods with use of serum and liver parameters in laying hens. *Int. J. Poult. Sci* 4, 568–572. doi: 10.3923/ijps.2005.568.572

Zhang, M., Liu, X., Li, Y., Wang, G., Wang, Z., and Wen, J. (2017). Microbial community and metabolic pathway succession driven by changed nutrient inputs in tailings: effects of different nutrients on tailing remediation. *Sci. Rep.* 7:474. doi: 10.1038/s41598-017-00580-3

Zhao, T., Zhang, H., Zhao, T., Zhang, X., Lu, J., Yin, T., et al. (2012). Intrarenal metabolomics reveals the association of local organic toxins with the progression of diabetic kidney disease. *J. Pharm. Biomed. Anal.* 60, 32–43. doi: 10.1016/j.jpba.2011.11.010

Zhou, Y., Jiang, Z., Lv, D., and Wang, T. (2009). Improved energy-utilizing efficiency by enzyme preparation supplement in broiler diets with different metabolizable energy levels. *Poult. Sci.* 88, 316–322. doi: 10.3382/ps.2008-00231

Zhu, H., Hu, L., Hou, Y., Zhang, J., and Ding, B. (2014). The effects of enzyme supplementation on performance and digestive parameters of broilers fed corn-soybean diets. *Poult. Sci.* 93, 1704–1712. doi: 10.3382/ps.2013-03626

Conflict of Interest: DZ was employed by company Huayu Agricultural Science and Technology Co., Ltd.

The remaining authors declare that the research was conducted in the absence of any commercial or financial relationships that could be construed as a potential conflict of interest.

Publisher's Note: All claims expressed in this article are solely those of the authors and do not necessarily represent those of their affiliated organizations, or those of the publisher, the editors and the reviewers. Any product that may be evaluated in this article, or claim that may be made by its manufacturer, is not guaranteed or endorsed by the publisher.

Advantages of publishing in Frontiers

OPEN ACCESS
Articles are free to read for greatest visibility and readership

FAST PUBLICATION
Around 90 days from submission to decision

HIGH QUALITY PEER-REVIEW
Rigorous, collaborative, and constructive peer-review

TRANSPARENT PEER-REVIEW
Editors and reviewers acknowledged by name on published articles

Frontiers
Avenue du Tribunal-Fédéral 34
1005 Lausanne | Switzerland

Visit us: www.frontiersin.org
Contact us: frontiersin.org/about/contact

REPRODUCIBILITY OF RESEARCH
Support open data and methods to enhance research reproducibility

DIGITAL PUBLISHING
Articles designed for optimal readership across devices

FOLLOW US
@frontiersin

IMPACT METRICS
Advanced article metrics track visibility across digital media

EXTENSIVE PROMOTION
Marketing and promotion of impactful research

LOOP RESEARCH NETWORK
Our network increases your article's readership